frontiers | Research Topics

Role of probiotics and probiotics' metabolites in food and intestine

Edited by
Rina Wu, Wenyi Zhang, Vincenzina Fusco and Qixiao Zhai

Published in
Frontiers in Microbiology

ISSN 1664-8714
ISBN 978-2-83252-127-4
DOI 10.3389/978-2-83252-127-4

About Frontiers

Frontiers is more than just an open access publisher of scholarly articles: it is a pioneering approach to the world of academia, radically improving the way scholarly research is managed. The grand vision of Frontiers is a world where all people have an equal opportunity to seek, share and generate knowledge. Frontiers provides immediate and permanent online open access to all its publications, but this alone is not enough to realize our grand goals.

Frontiers journal series

The Frontiers journal series is a multi-tier and interdisciplinary set of open-access, online journals, promising a paradigm shift from the current review, selection and dissemination processes in academic publishing. All Frontiers journals are driven by researchers for researchers; therefore, they constitute a service to the scholarly community. At the same time, the *Frontiers journal series* operates on a revolutionary invention, the tiered publishing system, initially addressing specific communities of scholars, and gradually climbing up to broader public understanding, thus serving the interests of the lay society, too.

Dedication to quality

Each Frontiers article is a landmark of the highest quality, thanks to genuinely collaborative interactions between authors and review editors, who include some of the world's best academicians. Research must be certified by peers before entering a stream of knowledge that may eventually reach the public - and shape society; therefore, Frontiers only applies the most rigorous and unbiased reviews. Frontiers revolutionizes research publishing by freely delivering the most outstanding research, evaluated with no bias from both the academic and social point of view. By applying the most advanced information technologies, Frontiers is catapulting scholarly publishing into a new generation.

What are Frontiers Research Topics?

Frontiers Research Topics are very popular trademarks of the *Frontiers journals series*: they are collections of at least ten articles, all centered on a particular subject. With their unique mix of varied contributions from Original Research to Review Articles, Frontiers Research Topics unify the most influential researchers, the latest key findings and historical advances in a hot research area.

Find out more on how to host your own Frontiers Research Topic or contribute to one as an author by contacting the Frontiers editorial office: frontiersin.org/about/contact

Role of probiotics and probiotics' metabolites in food and intestine

Topic editors

Rina Wu — Shenyang Agricultural University, China

Wenyi Zhang — Inner Mongolia Agricultural University, China

Vincenzina Fusco — Institute of Sciences of Food Production, National Research Council (CNR), Italy

Qixiao Zhai — Jiangnan University, China

Citation

Wu, R., Zhang, W., Fusco, V., Zhai, Q., eds. (2023). *Role of probiotics and probiotics' metabolites in food and intestine*. Lausanne: Frontiers Media SA.

doi: 10.3389/978-2-83252-127-4

Table of contents

frontiers | Frontiers in Microbiology

TYPE Editorial
PUBLISHED 24 March 2023
DOI 10.3389/fmicb.2023.1183550

OPEN ACCESS

EDITED AND REVIEWED BY
Giovanna Suzzi,
University of Teramo, Italy

*CORRESPONDENCE
Vincenzina Fusco
✉ vincenzina.fusco@ispa.cnr.it

SPECIALTY SECTION
This article was submitted to Food Microbiology, a section of the journal Frontiers in Microbiology

RECEIVED 10 March 2023
ACCEPTED 16 March 2023
PUBLISHED 24 March 2023

CITATION
Fusco V, Wu R, Zhang W and Zhai Q (2023) Editorial: Role of probiotics and probiotics' metabolites in food and intestine. *Front. Microbiol.* 14:1183550. doi: 10.3389/fmicb.2023.1183550

Editorial: Role of probiotics and probiotics' metabolites in food and intestine

Vincenzina Fusco[1]*, Rina Wu[2], Wenyi Zhang[3,4] and Qixiao Zhai[5]

[1]Institute of Sciences of Food Production of the National Research Council of Italy (CNR-ISPA), Bari, Italy, [2]Shenyang Agricultural University, Shenyang, China, [3]Key Laboratory of Dairy Biotechnology and Engineering, Ministry of Education, Hohhot, China, [4]Key Laboratory of Dairy Products Processing, Ministry of Agriculture and Rural Affairs, Inner Mongolia Agricultural University, Hohhot, China, [5]Jiangnan University, Wuxi, China

KEYWORDS

probiotics, prebiotics, food, intestine, metabolites

Editorial on the Research Topic
Role of probiotics and probiotics' metabolites in food and intestine

The emergence and exploration of new disciplines and technologies have provided new ideas and opportunities for probiotic science and industry development. The interaction between diet and intestinal flora has become a new target for human health regulation. Recently, probiotic supplements have received increasing attention as an important tool to modulate the gut microbiota (Brito Sampaio et al., 2022). Lactic acid bacteria (LAB) are powerful probiotics in the intestinal tract that can participate in metabolic regulation by directly or indirectly influencing the inhibition or activation of the signaling pathways. LAB can synthesize a variety of active metabolites, producing short-chain fatty acids, vitamins, enzymes, organic acids and antibacterial peptides. These metabolites can regulate the intestinal epithelium's barrier function and provide health benefits to the host.

Studies have found that probiotics have a variety of biological activities (Brito Sampaio et al., 2022; Leite de Souza et al., 2022). However, their application is still limited due to the poor colonization and the unclear mechanism of the induction of metabolites in the host involved in the interaction between pathogens and bacterial communities, etc. Therefore, this Research Topic aimed to collect new studies focused on probiotics and probiotics' metabolites in food and intestine with combined phenotyping, genotyping and targeting strategies as well as the multi-omics technologies.

Chen X. et al. assessed the effects of alkali stress on the growth and menaquinone-7 metabolism of *Bacillus subtilis natto*, whereas He et al. investigated the effects of *Akkermansia muciniphila* on gut microbiota and disease-related biomarkers in murine model, finding that this microorganism alters gut microbiota and immune system to improve cardiovascular diseases.

Li et al. demonstrated that autoinducer-2 exporters (AI-2E) family transporter protein in *Lactobacillus acidophilus* exhibits AI-2 exporter activity and relate with intestinal juice resistance of the strain.

Hu P. et al. isolated and identified *Rhodotorula mucilaginosa* TZR2014 and assessed its function as well as its effects on the growth and helath of weaned piglets.

Ke et al. demonstrated the inhibition of *Cronobacter sakazakii* in an infant simulator of the human intestinal microbial ecosystem using a potential synbiotic consisting of six lactic acid bacteria (LAB) strains and Vivinal GOS.

Hu Y. et al. demonstrated the alleviating effects of Selenium-enriched *Bifidobacterium longum* DD98 on dextran sulfate sodium-induced colitis in mice and explored the underlying mechanism.

Zhao et al. investigated the alleviating effects of gut micro-ecologically regulatory treatments on onstipation in mice.

Chen P. et al. investigated the regulations of lipid metabolism of broilers by *Bacillus amyloliquefaciens* TL both *in vivo* and *in vitro*, whereas Wang et al. demonstrated the exertion by *Lactobacillus mucosae* of different antiviral effects on respiratory syncytial virus infection in mice.

Sheng et al. discovered a novel exopolysaccharide derived from the probiotic *Lactobacillus pantheris* TCP102 strain exerting immune-enhancing and anticancer activities.

Finally, Liu et al. provided a review on antifungal mechanisms and application of Lactic Acid Bacteria in bakery products, whereas Shi et al., provided a review on the recent advances in the roles of microorganisms in fermented foods based on multi-omics data.

Author contributions

VF conceived and wrote the manuscript. All authors revised the manuscript. All authors contributed to the article and approved the submitted version.

Conflict of interest

The authors declare that the research was conducted in the absence of any commercial or financial relationships that could be construed as a potential conflict of interest.

Publisher's note

References

Brito Sampaio, K., Fusco V., de Brito Alves, J. L., and Leite de Souza, E. (2022). "Chapter 1—Probiotics: concepts, evolution, and applications," in *Probiotics for Human Nutrition in Health and Disease*, eds E. Leite de Souza, J. L. de Brito Alves, V. Fusco. Academic Press. *ISBN* 9780323899086.

Leite de Souza, E., de Brito Alves, J. L., Fusco V., eds. (2022). *Probiotics for Human Nutrition in Health and Disease*. Academic Press. ISBN: 978-0-323-89908-6.

frontiers | Frontiers in Microbiology

ORIGINAL RESEARCH
published: 28 April 2022
doi: 10.3389/fmicb.2022.899802

Effects of Alkali Stress on the Growth and Menaquinone-7 Metabolism of *Bacillus subtilis natto*

Xiaoqian Chen[1], Chao Shang[1], Huimin Zhang[1], Cuicui Sun[1], Guofang Zhang[1], Libo Liu[1], Chun Li[1,2]*, Aili Li[1,2] and Peng Du[1]*

[1] Key Laboratory of Dairy Science, College of Food Science, Northeast Agricultural University, Harbin, China, [2] Heilongjiang Green Food Science Research Institute, Harbin, China

Menaquinone-7 (MK-7) is an important vitamin K_2, synthesized from the menaquinone parent ring and seven isoprene side chains. Presently, the synthesis of MK-7 stimulated by environmental stress primarily focuses on oxygen stress, while the effect of alkali stress is rarely studied. Therefore, this study researched the effects of alkali stress on the fermentation performance and gene expression of *Bacillus subtilis natto*. The organism's growth characteristics, biomass, sporogenesis, MK-7 biosynthesis, and gene expression were analyzed. After a pH 8.5 stress adaptation treatment for 0.5 h and subsequent fermentation at pH 8.5, which promoted the growth of the strain and inhibited the spore formation rate. In addition, biomass was significantly increased ($P < 0.05$). The conversion rate of glycerol to MK-7 was 1.68 times higher than that of the control group, and the yield of MK-7 increased to 2.10 times. Transcriptomic analysis showed that the MK-7 high-yielding strain had enhanced carbon source utilization, increased glycerol and pyruvate metabolism, enhanced the Embden-Meyerhof pathway (EMP), tricarboxylic acid (TCA) circulation flux, and terpenoid biosynthesis pathway, and promoted the accumulation of acetyl-CoA, the side-chain precursor of isoprene. At the same time, the up-regulation of transketolase increased the metabolic flux of the pentose phosphate (HMP) pathway, which was conducive to the accumulation of D-erythrose 4-phosphate, the precursor of the menadione parent ring. This study's results contribute to a better understanding of the effects of environmental stress on MK-7 fermentation by *Bacillus subtilis natto* and the molecular regulatory mechanism of MK-7 biosynthesis.

Keywords: menaquinone-7, *Bacillus subtilis natto*, microbial fermentation, alkali stress, transcriptome

OPEN ACCESS

Edited by:
Wenyi Zhang,
Inner Mongolia Agricultural University, China

Reviewed by:
Huaxi Yi,
Ocean University of China, China
Guangqiang Wang,
University of Shanghai for Science and Technology, China

****Correspondence:***
Libo Liu
lbliu@neau.edu.cn
Chun Li
spxylch@126.com

Specialty section:
This article was submitted to Food Microbiology, a section of the journal Frontiers in Microbiology

Received: *19 March 2022*
Accepted: *08 April 2022*
Published: *28 April 2022*

Citation:
Chen X, Shang C, Zhang H, Sun C, Zhang G, Liu L, Li C, Li A and Du P (2022) Effects of Alkali Stress on the Growth and Menaquinone-7 Metabolism of Bacillus subtilis natto. Front. Microbiol. 13:899802. doi: 10.3389/fmicb.2022.899802

INTRODUCTION

Menaquinone-7 (MK-7) is a type of vitamin K_2 composed of a mother ring of menadione and seven isoprene side chains. MK-7 plays a role in respiratory chain transmission, coagulation function, and calcium homeostasis (Turck et al., 2017; Wilkens et al., 2021; Wu et al., 2021). In addition, MK-7 has more and more benefits in promoting bone healing, preventing cerebrovascular and cardiovascular diseases and fighting cancer cells, Alzheimer's disease and Parkinson's

disease (Halder et al., 2019; Mahdinia et al., 2019a; Tarkesh et al., 2020). However, the human body cannot synthesize MK-7, and the only channels to obtain it are food and dietary supplements (Bergeland et al., 2019; Brudzynski and Flick, 2019).

The content of MK-7 from natural food sources is too low to obtain preventive and therapeutic doses, such as pork liver oil, cheese and certain vegetables (kale and celery; Mahdinia et al., 2017). Therefore, it is mainly through nutritional supplements to achieve biomedical-level applications. Chemical synthesis has been the most common method of MK-7 production in the past (Łaszcz et al., 2018). However, chemical precursors for synthesis are of limited origin and produce both *cis* and *trans* isomers (Baj et al., 2016; Brudzynski and Maldonado-Alvarez, 2018; Vermeer et al., 2018), with only the latter being biologically active. So, MK-7 obtained by chemical synthesis has low biological activity and is prone to causing environmental pollution. In recent years, researchers have developed a biological fermentation method for the synthesis of MK-7 to obtain a more natural and active form of vitamin K_2 (Zhao et al., 2021; Bus et al., 2022), of which MK-7 accounts for about 97% (Mahdinia et al., 2019b; Zhao et al., 2021).

Menaquinone-7 contains some special structures, such as isoprene side chains and quinone skeleton, leading most bacteria to synthesize MK-7 in a complex way, increasing energy consumption and production costs. Hence, raising MK-7 production and reducing production costs is still a difficult problem (Berenjian et al., 2015). The key problems to be solved at present are to screen MK-7 producing strains efficiently and optimize fermentation conditions. Many researchers have used breeding (Song et al., 2014; Xu and Zhang, 2017), genetic modification (Liu et al., 2019; Yang et al., 2019), and optimized fermentation processes (Novin et al., 2020) to increase the yield of MK-7. With the development of metabolic (Xu et al., 2017; Chen T. et al., 2020) and genetic engineering technologies (Cui et al., 2019), related biotechnologies have been extensively studied to regulation MK-7 biosynthesis, while the study of abiotic stress methods to increase MK-7 production limited. *B. subtilis natto* is not only the main microorganism in the industrial production of MK-7, but also an excellent production source, which can be secreted intracellularly and extracellularly (Shih et al., 2005). In addition, the strain has some advantages, such as the high yield of MK-7, easy growth and culture, short fermentation time, resistance to environmental stress, and so on (Wu, 2019). Studies have found that environmental stress can induce changes in the metabolism of probiotics and secrete metabolites beneficial to their survival (Li et al., 2016). Our previous study confirmed that environmental stress can stimulate the production of metabolites and improve the stress tolerance of lactic acid bacteria (Chen X. et al., 2020; Zhang et al., 2020). In addition, Zeng et al. (2014) showed that heat stress promoted the synthesis of poly (γ-glutamic acid) and its precursors by *B. subtilis* GXA-28. And salt stress improved the poly (γ-glutamic acid) synthesis ability of *Bacillus licheniformis* WX-02 (Wei et al., 2010).

The omics technique is a method to explain how microorganisms respond to environmental changes at the level of molecular mechanism. Currently, technologies such as metabolomics, proteomics and transcriptomics have been used to explore the mechanisms of MK-7 metabolic changes under environmental stress (Priyadarshi et al., 2009; Ma Y. et al., 2019). Ma Y. et al. (2019) have found that under the condition of high oxygen supply at 200 rpm, the yield of MK-7 could be doubled through transcriptome research. Xu et al. (2017) found that overexpression of key enzymes in the metabolic pathway resulted in a 1.6-fold increase in MK-7 content through metabolomics studies. Therefore, omics technology can be applied to study the molecular mechanism of *B. subtilis natto* under environmental stress.

In this study, the aim was to study the effects of salt, acid, alkali, and temperature stress on the growth and MK-7 biosynthesis of *B. subtilis natto*, and analyze the optimal stress conditions to improve the biosynthesis of MK-7. In addition, transcriptome was used to study the effect of alkali stress on gene expression in the MK-7 enrichment pathway of *B. subtilis natto*. This study could provide a new perspective for extending techniques to increase MK-7 production and deepen understanding of the molecular mechanisms underlying MK-7 biosynthesis.

MATERIALS AND METHODS

Strain Culture Condition

The experimental strain was *B. subtilis natto* CICC10262. The cultivation conditions and methods were the same as described by Berenjian et al. (2011). The formula of the fermentation medium was glycerol 50 g/L, soybean peptone 150 g/L, yeast extract 50 g/L, K_2HPO_4 0.6 g/L. The passage medium and fermentation culture were carried out at speeds of 170 rpm and 200 rpm, respectively. Furthermore, we studied some of the intracellular reactions.

In order to determine the exact value of the optimal pH of *B. subtilis natto* CICC10262 growth medium, 3% (v/v) of seed culture in the exponential phase ($OD_{600} \sim 0.8$ or 10^8 CFU/mL) have been inoculated to 14 cultures with different initial pH (The pH of the medium was set to 3, 4, 4.5, 5, 5.5, 6, 6.5, 7, 7.5, 8, 8.5, 9, 9.5, and 10, respectively), and the number of viable bacteria was then monitored. All cultures were performed under aseptic conditions. The shaker incubator parameters were set to 170 rpm and 37°C.

Determination of Biomass and pH

Biomass and pH measurements have been slightly modified as described by Rincón Santamaría et al. (2019). The biomass was measured at 600 nm using a multifunctional enzyme reader [SpectraMax i3X, Molecular Devices (Shanghai, China) Co., Ltd.]. The pH-meter was calibrated at 25°C.

Determination of Adaptation Conditions to Stress

The activated thalli were inoculated into nutrient agar (NA) medium with 3% (v/v) inoculum for 10 h and cultured in NA medium, then 20 mL of bacterial solution was taken, centrifuged at 8000 rpm for 10 min to collect thalli. The cells were suspended in equal volumes of NA medium containing 1% (w/v), 3% (w/v), and 5% (w/v) NaCl and pH 4.0, 4.5, and 5.0, and incubated at

37°C for 0.5 h. In addition, incubated at 42°C, 45°C, and 48°C for 0.5 h to carry out high-temperature adaptation treatment. After the stress adaptation, the bacteria collected after treatment were washed twice with physiological saline, and the bacteria were centrifuged at 8000 rpm for 10 min to collect thalli. The thalli were suspended in 20 mL NA liquid medium, shaken well, and inoculated in NA medium with 3% (v/v) for 24 h, and the colonies were counted to determine the best suitable treatment conditions.

Determination of Number of Viable Bacteria

The number of viable bacteria in fermentation broth was determined by the dilution coating plate method described by Li et al. (2021). To measure the number of viable bacteria, each sample was diluted 10 times with physiological saline, and then the 100 μL diluted solution was coated on the nutrient agar plates in triplicate. The plates were incubated at 37°C for 24 h. The number of colonies on each plate ranged from 30 to 300, and the results were expressed in logarithmic form.

Determination of Residual Glycerol Analysis

Carbon source can affect the growth and metabolism of microorganisms, and glycerin has been proved to promote the production of MK-7 by *B. subtilis natto*, so glycerin was selected as the carbon source of this experiment. Carbon source content in fermentation broth was determined by the method described by Zhou et al. (2016), that was, the titration method was used to detect changes in glycerol concentration. Centrifuged 2.0 mL of fermentation broth at 8000 rpm for 3 min, sucked 1.0 mL of supernatant, added 10 mL of distilled water, added 2 drops of phenolphthalein as an indicator, and fixed with 0.05 mol/L NaOH standard drops until color changes. Recorded the NaOH dosage V_1. Then added 10 mL of 0.1 mol/L sodium periodate solution, reacted for 5 min in the absence of light, and then added 5.0 mL of 25% ethylene glycol, and continued to react in the absence of light for 5 min. Then used NaOH standard drops were used to fix to change color, recorded the amount of NaOH as V_2 at this time, and the formula was as follows.

$$\omega(\text{Glycerol}) = 92.1\text{c} \times (\text{V2} - \text{V1})/\text{M} \times 100\%$$

Among:

V_1: The volume of the NaOH standard solution used for the blank test, mL;

V_2: The volume of the NaOH standard solution used for the determination of sample, mL;

C: Concentration of the NaOH standard solution used, mol/L;

M: Mass of test sample, g;

92.1: Molar mass of glycerol, g/mol.

Determination of Spore Formation Rate

The sporulation rate of *B. subtilis natto* during fermentation was measured as described by Luo et al. (2016a). The cells were stained with ammonium oxalate crystal violet for 1 ∼ 2 min, washed to remove the floating color, and then randomly selected 5 fields under 100 × multiple oil microscope to count the number of transparent spores and the total number of cells. Detection was performed at the end of fermentation. The formula for calculating the sporulation rate was as follows.

$$\text{Sporulation rate}/\% = (\text{Number of spores})/(\text{Total number of cells}) \times 100$$

Menaquinone-7 Extraction and Analysis

The extraction and content of MK-7 in fermentation broth were measured as described by Sun et al. (2020). In our preliminary studies, *n*-hexane:2-propanol (2:1, v/v) with 1:4 (liquid: organic, v/v) was found to be the optimal mixture for MK-7 extractions. During each extraction, the mixture was shaken vigorously with a vortex mixer for 2 min and centrifuged at 3000 rpm for 10 min to separate two phases. The organic phase was then vaporized in the vacuum, and the extracted MK-7 was eventually recovered. High performance liquid chromatography (HPLC) Waters 2695-2420 (Nanchang Jiedao Scientific Instruments Co., Ltd., China) equipped with a UV detector and a C18 chromatographic column (5 μm, 250 × 4.6 mm, Hypersil ODS2, China), for analysis of MK-7 concentration at 40°C. Methanol: Dichloromethane (9:1, v/v) was the mobile phase at a flow rate of 1.0 mL/min and a wavelength of 254 nm for calibration and analysis.

RNA Isolation, Library Construction, and Sequencing

The fermentation broth was collected from the control group and the alkali stress group (pH 8.5), respectively. Immediately centrifuged at 8000 rpm for 10 min, stored at −80°C, and extracted with RNA lock Reagent. The specific procedures for RNA separation and sequencing were slightly modified by referring to Cheng et al. (2020).

RNA–Seq Data Analyses

Clean data was mapped to the reference sequence as described by Langmead and Salzberg (2012). The expression levels of genes and transcripts were estimated according to the method of Robinson et al. (2010). A mathematical statistical model was used to identify differentially expressed genes (DEG) in the control group and the alkali stress group as described by Kong et al. (2007). Finally, the DEGs were determined by the Log_2 ratio of ≥1 and FDR of ≤0.05. Then they were mapped to gene ontology (GO) and KEGG database for the functional and pathway analysis.

Statistical Analysis

Three biological replicates were performed, and three technical replicates were performed in each group. Data were analyzed using SPSS 20.0 (IBM SPSS Statistics, IBM Corp., Somers, NY, United States) for one-way analysis of variance (ANOVA). Results with $P < 0.05$ were considered statistically significant.

RESULTS AND DISCUSSION

The Optimum Growth and Fermentation Conditions of *Bacillus subtilis natto* CICC10262

The number of live bacteria of *B. subtilis natto* CICC10262 in the different treated groups is shown in **Figure 1A**. The optimum pH range for the growth of *B. subtilis natto* was wide, 5.0 ∼ 9.0, which was consistent with the findings of Luo et al. (2016b). However, after growing at pH 5.5 for 24 h, the number of viable bacteria was the highest, supporting the conclusion of Yang and Zhang (2011) that *Bacillus subtilis* grows vigorously in weak acid and neutral environments.

Figure 1B shows the number of viable *B. subtilis natto* after different stress adaptation treatments for 0.5 h and subsequent culturing in nutrient agar (NA) medium for 24 h at normal pH (the pH was not adjusted after sterilization and was between 5.5 and 6.0). Compared with the control group (without adaptation treatment), the number of viable bacteria in the treated group significantly decreased by 9.63% after incubation at 48°C for 0.5 h ($P < 0.05$), there was no significant change in the number of viable bacteria after other treatment. The number of viable bacteria increased significantly and reached the maximum after culturing for 0.5 h in NA medium with a pH 8.5 ($P < 0.05$), which was 1.14 times higher than that of the control group. Therefore, pH 8.5 adapted to 0.5 h was found to be the best adaptation treatment condition.

To study the effect of *B. subtilis natto* on the biosynthesis of MK-7 after the adaptation treatment, it was cultured for 0.5 h at pH 8.5. The treated bacteria were then placed into a normal beef extract peptone medium and cultured to the end of the logarithmic growth phase. After that, *B. subtilis natto* was inoculated into different alkaline pH fermentation mediums. The effects of the different alkaline pH conditions on the yield of MK-7 are shown in **Figure 1C**. Compared with untreated *B. subtilis natto*, the yield of MK-7 was significantly increased by the stress adaptation treatment and fermentation under alkali stress ($P < 0.05$). After stress adaptation treatment, the yield of MK-7 was highest at pH 8.5 (290.19 ± 1.12 mg/L), which was 2.10 times that of the control group. The results showed that the production of MK-7 could be significantly promoted by the alkaline environment of the fermentation medium and stress adaptation treatment of *B. subtilis natto* during its growth stage.

Fermentation Process of *Bacillus subtilis natto* CICC10262

Two different fermentation conditions were designed to understand the changes of the MK-7 biosynthesis process of *B. subtilis natto* after adaptation treatment and alkali stress. One fermentation medium had a normal pH was set as the control group; the other medium's pH was adjusted to pH 8.5. The changes in the number of live bacteria, sporulation rate, biomass, glycerol consumption, and MK-7 biosynthesis using the two different fermentation mediums are shown in **Figure 2**. After the *B. subtilis natto* was adapted to alkali stress, its growth was promoted, and the number of viable bacteria was 1.43

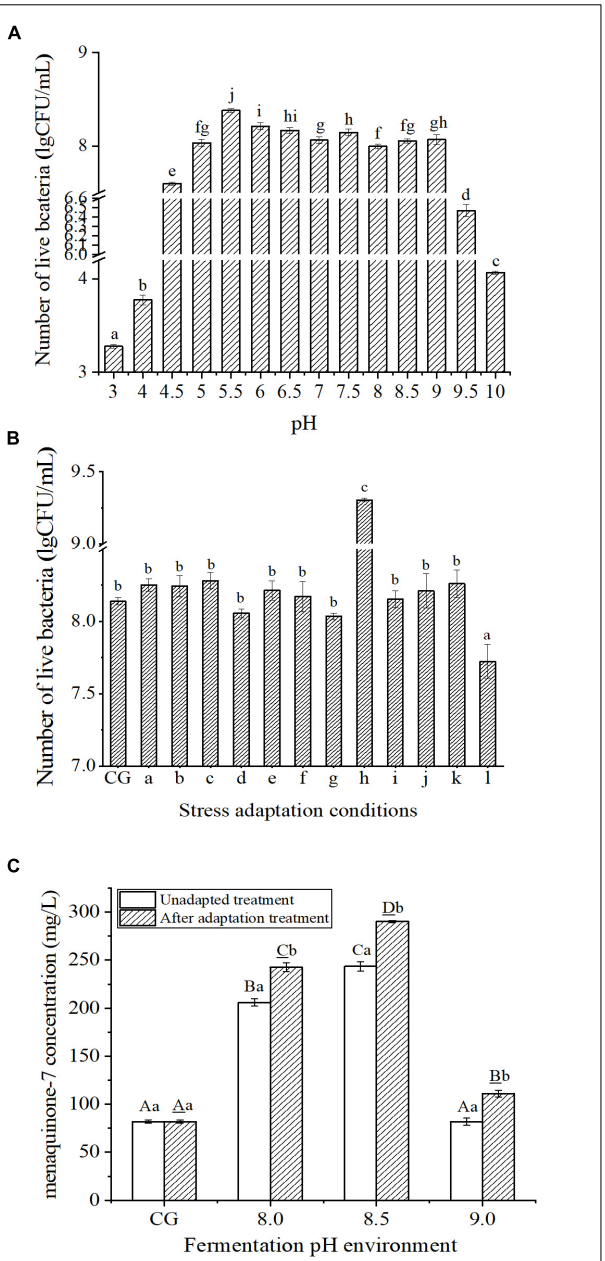

FIGURE 1 | (A) Growth of *Bacillus subtilis natto* CICC10262 at different pH. Different lowercase letters indicated that the values of each group were significantly different, $P < 0.05$. **(B)** Effects of different stress adaptation conditions on the growth of *Bacillus subtilis natto* CICC 10262. In group a, b, and c indicated that the strain was adapted to (nutrient agar) NA medium containing 1% (w/v), 3% (w/v), and 5% (w/v) NaCl for 0.5 h, d, e, f, g, h, i were strains adapted to NA medium at pH 4.5, 5.0, 6.0, 8.0, 8.5, 9.0 for 0.5 h, j, k, l were strains incubated at 42°C, 45°C, 48°C for 0.5 h, then inoculated into NA medium containing 3% (w/v) NaCl with normal pH and cultured at 37°C for 24 h. In the significance analysis, different lowercase letters indicated that the values of each group were significantly different, $P < 0.05$. **(C)** The yield of MK-7 fermented by strain under different pH conditions. Different lowercase letters indicated that there were significant differences between different stress intensities in the unadapted treatment group, $P < 0.05$. Different capital letters indicate that under the same pH condition, the difference between the unadapted treatment group and the adaptation treatment group is statistically significant, $P < 0.05$.

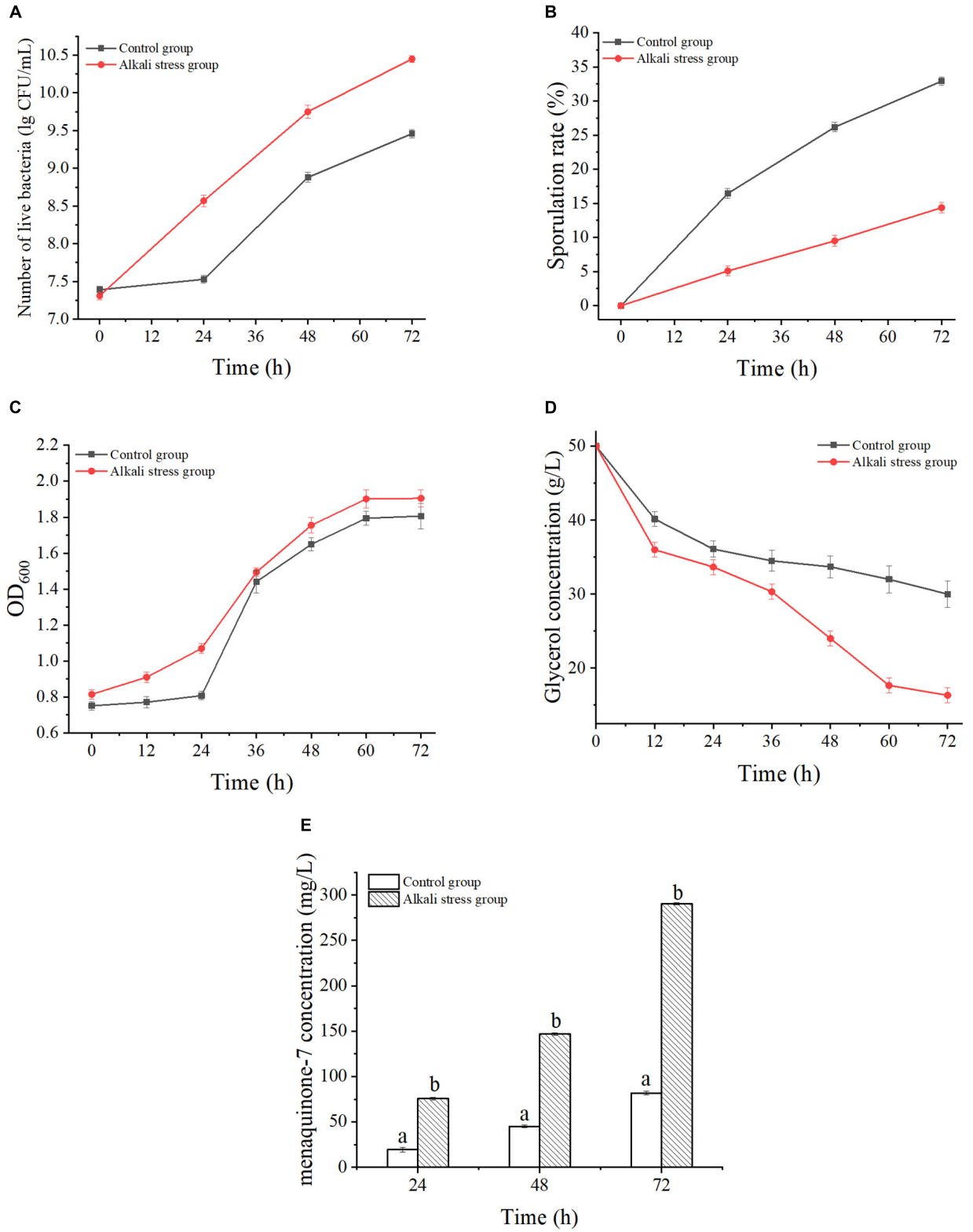

FIGURE 2 | Fermentation characteristics of *Bacillus subtilis natto* CICC10262 under alkali stress. **(A)** Live bacteria, **(B)** Sporulation rate, **(C)** Cellular biomass (OD_{600}), **(D)** Glycerol consumption, **(E)** MK-7 yield. Differences in lowercase letters indicate significant differences between the two groups of values at the same time, $P < 0.05$.

times that of the control group (**Figure 2A**); simultaneously, these conditions had an inhibitory effect on the rate of spore formation, and the spore rate decreased significantly by 56.32% ($P < 0.05$) (**Figure 2B**). Furthermore, the biomass in the two fermentation mediums entered the stable phase at 60 h. However, the biomass of the alkali stress group was always 3.68∼5.48% higher than that of the control group, indicating that the alkali stress adaptation treatment enhanced the biomass significantly ($P < 0.05$) (**Figure 2C**). The glycerol consumption under alkali stress conditions was faster than that of the control group, and the conversion rate of glycerol to MK-7 was 1.68 times that of the control group (**Figure 2D**). As MK-7 is a secondary metabolite and accumulates at the late stage of fermentation, significant accumulation of MK-7 was detected after 24 h. In addition, the yield of MK-7 was higher than that of the control group at all time points of fermentation after alkali stress treatment. The maximum yield was 290.19 ± 1.12 mg/L, which was 2.10 times that of the control group (**Figure 2E**). And, as shown in **Figures 2D,E**, the concentration of MK-7 in cells under alkali stress improved significantly with increasing consumption of glycerol as a carbon source and was positively correlated. These results were similar to those of previous studies: the substrate consumption increased under certain conditions of alkali stress and thus promoted the increase of metabolites (Ma Y. et al., 2019; Cheng et al., 2020). In addition, to evaluate the fermentation capacity of *B. subtilis natto* to produce MK-7, we studied the productivity change of MK-7. At the initial stage of fermentation, there was a significant difference in MK-7 yield between the two fermentation conditions ($P < 0.05$) and the difference continued to increase with the prolongation of fermentation time. Combined with **Figure 2A**, the alkali stress treatment increased the growth of *B. subtilis natto* by 12% compared to the control group. Therefore, alkali stress treatment could enhance the biosynthesis ability of *B. subtilis natto* to produce MK-7.

Transcriptome Analysis of Menaquinone-7 Production Gene Expression in *Bacillus subtilis natto* CICC1026

To better understand how alkali stress affects *B. subtilis natto* CICC 10262's production of MK-7, the differences in gene expression in the metabolic process under alkali stress were compared using transcriptome analysis. We identified a total of 820 differently expressed genes (DEGs) (**Figure 3**). Among these genes, 608 were found to be up-regulated and 212 down-regulated.

Gene Ontology and Kyoto Encyclopedia of Genes and Genomes Database Analysis

To understand the functional information of differential genes, Gene Ontology (GO) and Kyoto Encyclopedia of Genes and Genomes (KEGG) databases were used for gene annotation and functional classification of predicted protein-coding genes (CDSs). In **Figure 4**, we summarize three GO functional categories, including *biological processes*, *cellular component*, and *molecular function*. Each category was annotated with

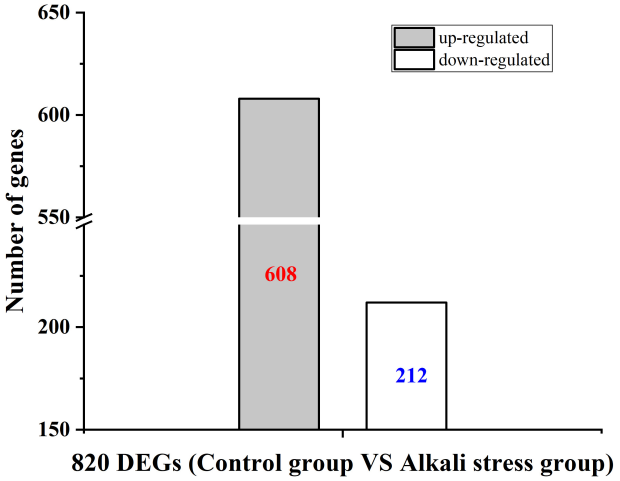

FIGURE 3 | Differential gene expression of control strain and strain after adaptation treatment in the fermentation process under alkali stress.

3,605, 1,031, and 2,106 genes, respectively. We found a large number of genes encoding catalytic activity (1035 genes), metabolic (989 genes), cellular (801 genes), single-organism (731 genes), and localization (325 genes) processes, and binding (673 genes), and membrane (460 genes) function. The KEGG database analysis revealed that these DEGs existed in three different enrichment pathways: cellular processes, environmental information processing, and metabolism. Of these pathways, metabolic changes were the most significant ($P < 0.05$) (**Figure 5**). A total of 1,679 CDSs were annotated to 65 KEGG functional categories, of which "carbohydrate metabolism" accounted for the largest proportion (24.36%, 409 genes) in the secondary classification, followed by "amino acid metabolism" (14.89%, 250 genes), "membrane transport" (9.77%, 164 genes), and "metabolism of cofactors and vitamins" (8.40%, 141 genes), as can be seen in **Figure 5**. These results show that the functions of the CDSs are mainly the metabolism and transportation of substances, which provide energy for the life activities of *B. subtilis natto* and also provide precursors for the synthesis of secondary metabolites (Wang et al., 2018). Explicitly, it included ATP-binding cassette (ABC) transporters, phosphotransferase system (PTS), purine, amino acid, glycerol and ketone body metabolism, peroxisome, and glycolysis/gluconeogenesis, and so on. The ABC transporters and PTS pathways were related to membrane transport (Zhou et al., 2020), which may affect the secretion of MK-7. These DEGs may be involved in alkali stress and MK-7 production.

Differentially Expressed Genes Related to Menaquinone-7 Biosynthesis

As shown in **Figure 6**, MK-7 consists of a menadione parent ring and seven isoprene side chains. The main synthetic pathways included the Embden-Meyerhof pathway (EMP), glycerol metabolism pathway, pentose phosphate pathway (HMP), 2-C-methyl-D-erythritol-4-phosphate (MEP) pathway, and menaquinone (MK) synthesis pathway (Bentley and

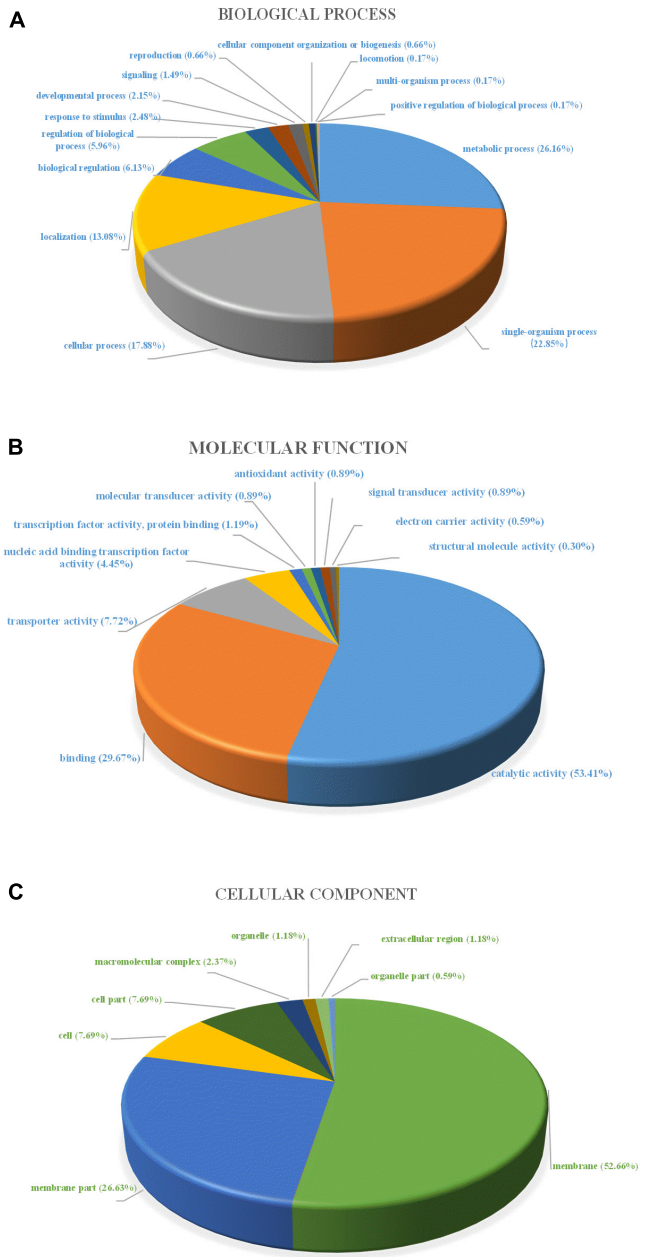

FIGURE 4 | Gene ontology (GO) functional analysis of unique sequences from control group and alkali stress group transcriptome. Unique sequences were assigned to three categories: **(A)** Biological process, **(B)** Molecular function, **(C)** Cellular component.

Meganathan, 1982; Ren et al., 2020). Comparison of the transcriptome results showed that alkali stress greatly influenced these pathways (**Supplementary Table 1**).

In glycerol metabolism and the EMP pathway, glycerol kinase (Glpk) was up-regulated 1.85-fold after alkali stress, which promoted glycerol consumption and utilization. Glyceraldehyde-3-phosphate dehydrogenase, enolase (Eno), and pyruvate kinase (PYK) were up-regulated by 1.16-, 0.92-, and 1.15-fold, respectively, and the EMP pathway flux increased. This result was consistent with that of Cheng et al. (2020), in which the expressions of Glpk, fructose bisphosphate aldolase (FBA), and phosphofructokinase (PFK) were up-regulated by 1.61, 0.91, and 2.31-fold, respectively, and the consumption of glycerol substrate increased. Eno and PYK were also up-regulated by a factor of 2.34 and 1.54, respectively, converting glyceraldehyde-3-phosphate to pyruvate, ultimately increasing MK-7 production (Cheng et al., 2020). Pyruvate is converted to acetyl-CoA by pyruvate dehydrogenases: dihydrolipoamide dehydrogenase (AcoL and AcoC). AcoL, AcoC, and citrate synthase (CS) were up-regulated by 6.08-, 5.70-, and 1.84-fold, respectively,

promoting the accumulation of the important precursor acetyl-CoA. The up-regulation of these enzymes was consistent with previous research results, that is, the expression of Eno and PYK were conducive to the accumulation of more pyruvate and the formation of acetyl-CoA, strengthening the metabolic flux of the tricarboxylic acid (TCA) cycle (Cheng et al., 2020), thus accumulating more pyruvate and generating more isoprene side chains (Xu et al., 2012). The enhancement of glycerin metabolism and the EMP pathway can provide higher energy for cell growth and produce more precursors for MK-7 biosynthesis (Ma X. et al., 2019).

In the process of entering the MEP pathway, 1-deoxyxylulose-5-phosphate synthase (Dxs), the first level of rate-limiting enzyme of the MEP pathway, was found to be up-regulated 2.21-fold. The enzymes 1-deoxy-D-xylulose 5-phosphate reductoisomerase (Dxr), 2-C-methyl-D-erythritol 4-phosphate cytidyltransferase (IspD), 2-C-methyl-D-erythritol-2,4-cyclodiphosphate synthase (IspF), 1-hydroxy-2-methyl-2-(E)-butenyl 4-diphosphate

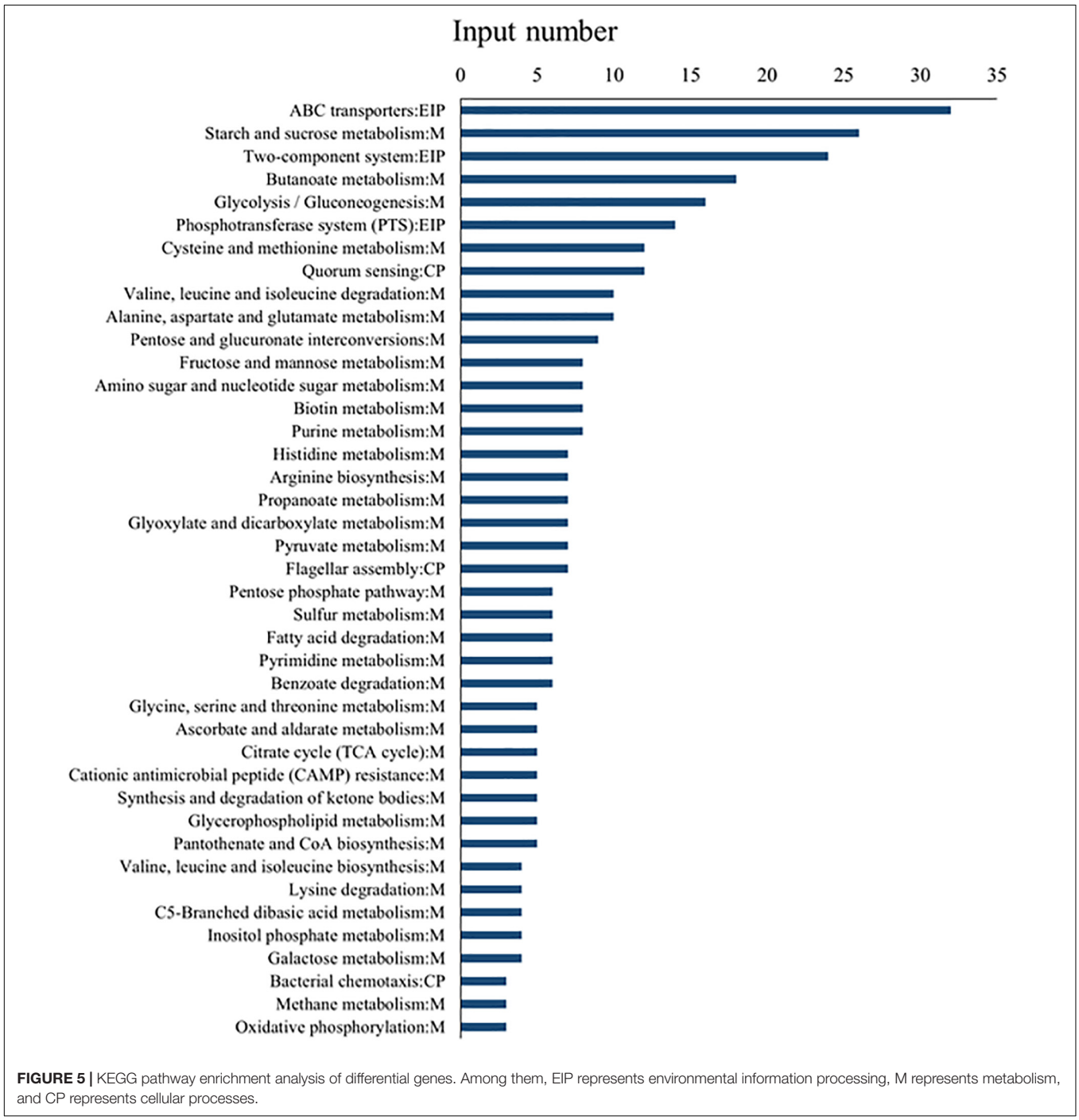

FIGURE 5 | KEGG pathway enrichment analysis of differential genes. Among them, EIP represents environmental information processing, M represents metabolism, and CP represents cellular processes.

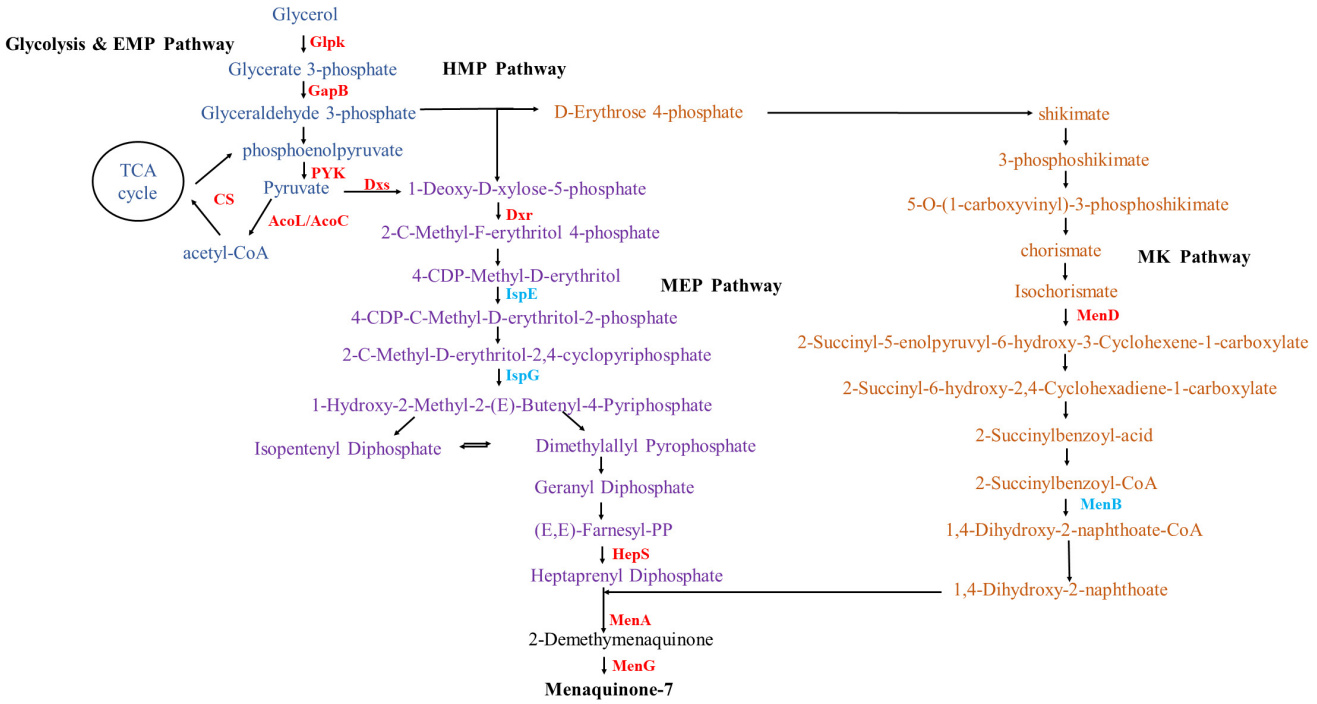

FIGURE 6 | Changes in transcript abundance of enzymes involved in menaquinone-7 metabolic pathway. Enzymes: GlpK, glycerol kinase; GapB, glyceraldehyde-3-phosphate dehydrogenase (NADP-dependent, gluconeogenesis); CS, citrate synthase; AcoL/AcoC, acetoin dehydrogenase E3/E2 component (dihydrolipoamide dehydrogenase); Dxs, 1-deoxyxylulose-5-phosphate synthase; Dxr, 1-deoxy-D-xylulose 5-phosphate reductoisomerase; IspE, 4-diphosphocytidyl-2-C-methyl-D-erythritol kinase; IspG, 4-hydroxy-3-methylbut-2-en-1-yl diphosphate synthase; IspA, farnesyl diphosphate synthase; HepS, heptaprenyl diphosphate synthase component I; MenD, 2-oxoglutarate decarboxylase and 2-succinyl-5-enolpyruvyl-6-hydroxy-3-cyclohexene-1-carboxylic-acid synthase; MenB, 1,4-dihydroxy-2-naphthoyl-CoA synthase; MenA, 1,4-dihydroxy-2-naphthoate octaprenyltransferase; MenG, demethylmenaquinone methyltransferase.

reductase (IspH), farnesyl diphosphate synthase (IspA), heptaprenyl diphosphate synthase component I (HepS), and heptaprenyl diphosphate synthase component II (HepT) were up-regulated 1.05-, 0.24-, 0.72-, 0.65-, 0.32-, 2.27-, and 0.56-fold, respectively. The enzymes Dxs and Dxr have been consistently identified as rate-limiting enzymes in the MEP pathway (Lv et al., 2013). Yang et al. (2019) showed that the over-expression of *dxs* and *dxr* genes in the EMP pathway increased the fermentation yield of MK-7 to 69.50 mg/L. In addition, these authors proved through genetic engineering that the over-expression of *dxs*, *dxr*, *ispD*, and *ispF* genes in the MEP pathway could increase the yield of MK-7 (Yang et al., 2020). Xu and Zhang (2017) studied a strain of *Bacillus amylolytica* Y-2 and found that *hepS* gene encoding heptapreny pyrophosphate synthase could make MK-7 expression higher than other enzymes, which also provided information on the rate-limiting steps of different MK-7 producing bacteria. The expression of 4-hydroxy-3-methylbut-2-en-1-yl diphosphate synthase (IspG) was reduced by 1.11-fold. The over-expression of IspG might have increased the content of β-carotene, a product of other pathways in the metabolic pathway, which may have inhibited MK-7 production (Yang and Guo, 2014). The enzyme 4-diphosphocytidyl-2-C-methyl-D-erythritol kinase (IspE) was down-regulated 1.53-fold, possibly because the expression intensity of the *ispE* gene is negatively correlated with MK-7 synthesis (Yu et al., 1995).

Erythrose 4-phosphate forms shikimate through synthesis, dehydration and dehydrogenation, and finally reacts to form chorismate, which enters the MK pathway. The genes *menF*, *D*, *H*, *C*, *E*, and *B* encode six key enzymes and hydrolases to form the quinone skeleton 1,4-dihydroxy-2-naphthoate, followed by decarboxylation and methylation with heptaprenyl diphosphate formed by the MEP pathway under the action of the transferases 1,4-dihydroxy-2-naphthoate octaprenyltransferase (MenA) and demethylmenaquinone methyltransferase (MenG) to form menaphthoquinone. In the MK pathway, except for the down-regulated expression level of 1,4-dihydroxy-2-naphthoyl-CoA synthase (MenB) and O-succinylbenzoate-CoA synthase (MenC), the other 6 genes were up-regulated. Menaquinone-specific isochorismate synthase (MenF), 2-succinyl-5-enolpyruvyl-6-hydroxy-3-cyclohexene-1-carboxylic-acid synthase (MenD), 2-succinyl-6-hydroxy-2,4-cyclohexadiene-1-carboxylate synthase (MenH), O-succinylbenzoic acid-CoA ligase (MenE), MenA, and MenG expression were increased 0.75-, 2.64-, 0.85-, 0.47-, 3.08-, and 4.53-fold, respectively. It has been reported that MenD is the only enzyme that adds the intermediate thiamine pyrophosphate to the secondary substrate

β-C (Dawson et al., 2008), the 1,4-dihydroxy-2-naphthoate octaprenyltransferase encoded by *menA*, polyisoprene pyrophosphate is used as the side chain to catalyze the formation of the water-soluble naphthalene compound 1,4-dihydroxy-2-naphthonic acid into membrane-bound 2-demethyl-menthoquinone, the precursor of MK (Suvarna et al., 1998; Hu et al., 2020). The results showed that enhancing the precursor supply and eliminating the by-product synthesis pathway were common methods to improve strain performance. MK-8 was the main menaquinone synthesized by *E. coli* (Kong and Lee, 2011). Over-expression of the menA or MenD, key enzymes associated with the supply of two precursors, increased the MK-8 content five times (Kong and Lee, 2011). Ma X. et al. (2019) found that over-expression of MenA in *Bacillus subtilis* increased MK-7 production three times. Using modular metabolic engineering design, Yang et al. (2019) also found that over-expression of the *menA* gene could increase the yield of MK-7 to 2.10 times that of the original strain *B. subtilis* 168. The over-expression of *menG* also increased the yield of MK-7 1.41 times by *Elizabethkingia meningoseptica* (Liu et al., 2018). These results might provide the impetus for further research on the transcriptional effects on MK-7 biosynthesis by *B. subtilis natto*.

CONCLUSION

This study systematically analyzed the effect of stress adaptation and gene expression on MK-7 biosynthesis by *B. subtilis natto* under alkali stress conditions. Our analysis identified 820 DEGs, of which 608 genes up-regulated and 212 genes down-regulated. Data analysis results showed that the glucose metabolic pathway and MK pathway associated with MK-7 synthesis were enhanced, which promoted the accumulation of acetyl CoA, an important precursor, and the formation of an isoprene side chain, thereby promoting the synthesis and accumulation of MK-7. This study's results provide a basis for improving the yield of MK-7 by *B. subtilis natto* under abiotic stress and valuable information to understand the molecular mechanism of MK-7 biosynthesis under environmental stress. In the future, the obtained *B. subtilis natto* with high MK-7 production will be applied to the production of MK-7-rich natto and other fermented products, which will also be important for health by preventing cardiovascular diseases, osteoporosis, cancer and nerve damage when consumed by people.

DATA AVAILABILITY STATEMENT

The original data on RNA sequencing have been uploaded to the NCBI Sequence Read Archive (SRA) under accession number PRJNA818476.

AUTHOR CONTRIBUTIONS

XC and LL contributed to conception and design of the study. CSh, HZ, and CSu performed the statistical analysis. XC wrote the first draft of the manuscript. CSh, HZ, CL, GZ, AL, and PD wrote sections of the manuscript. All authors contributed to manuscript revision, read, and approved the submitted version.

FUNDING

This research was supported by Distinguished Young Foundation of Heilongjiang Province of China (JQ2020C006); the research and development of high-quality milk protein base material and creation of nutritious and healthy food (CZKYF2021-2-B017); and the "Characteristic Probiotics and New Fermented Food" Team in Northeast Agricultural University.

ACKNOWLEDGMENTS

Special thanks to WORDVICE for its language polishing service.

SUPPLEMENTARY MATERIAL

The Supplementary Material for this article can be found online at: https://www.frontiersin.org/articles/10.3389/fmicb.2022.899802/full#supplementary-material

REFERENCES

Baj, A., Wałejko, P., Kutner, A., Kaczmarek, Ł, Morzycki, J. W., and Witkowski, S. (2016). Convergent synthesis of menaquinone-7 (MK-7). *Org. Process. Res. Dev.* 20, 1026–1033. doi: 10.1021/acs.oprd.6b00037

Bentley, R., and Meganathan, R. (1982). Biosynthesis of vitamin K (menaquinone) in bacteria. *Microbiol. Rev.* 46, 241–280. doi: 10.1128/mmbr.46.3.241-280.1982

Berenjian, A., Mahanama, R., Kavanagh, J., and Dehghani, F. (2015). Vitamin K series: current status and future prospects. *Crit. Rev. Biotechnol.* 35, 199–208. doi: 10.3109/07388551.2013.832142

Berenjian, A., Mahanama, R., Talbot, A., Biffin, R., Regtop, H., Valtchev, P., et al. (2011). Efficient media for high menaquinone-7 production: response surface methodology approach. *N. Biotechnol.* 28, 665–672. doi: 10.1016/j.nbt.2011.07.007

Bergeland, T., Nordstrand, S., and Aukrust, I. R. (2019). Commentary on method for detection of menaquinone-7 in dietary supplements. *Food Chem.* 292, 346–347. doi: 10.1016/j.foodchem.2018.12.001

Brudzynski, K., and Flick, R. (2019). Accumulation of soluble menaquinones MK-7 in honey coincides with death of *Bacillus spp.* present in honey. *Food Chem. X* 1:100008. doi: 10.1016/j.fochx.2019.100008

Brudzynski, K., and Maldonado-Alvarez, L. (2018). Identification of ubiquinones in honey: a new view on their potential contribution to honey's antioxidant state. *Molecules* 23:3067. doi: 10.3390/molecules23123067

Bus, K., Sitkowski, J., Bocian, W., Zmysłowski, A., Ofiara, K., and Szterk, A. (2022). Separation of menaquinone-7 geometric isomers by semipreparative high-performance liquid chromatography with silver complexation and identification by nuclear magnetic resonance. *Food Chem.* 368:130890. doi: 10.1016/j.foodchem.2021.130890

Chen, T., Xia, H., Cui, S., Lv, X., Li, X., Liu, Y., et al. (2020). Combinatorial methylerythritol phosphate pathway engineering and process optimization for increased menaquinone-7 synthesis in *Bacillus subtilis*. *J. Microbiol. Biotechnol.* 30, 762–769. doi: 10.4014/jmb.1912.12008

Chen, X., Wang, T., Jin, M., Tan, Y., Liu, L., Liu, L., et al. (2020). Metabolomics analysis of growth inhibition of *Lactobacillus plantarum* under ethanol stress. *Int. J. Food Sci. Technol.* 55, 3441–3454. doi: 10.1111/ijfs.14677

Cheng, P., Zhu, S., Lu, J., Hu, X., and Ren, L. (2020). Transcriptomic analysis of gene expression of menaquinone-7 in *Bacillus subtilis natto* toward different oxygen supply. *Food Res. Int.* 137:109700. doi: 10.1016/j.foodres.2020.109700

Cui, S., Lv, X., Wu, Y., Li, J., Du, G., Ledesma-Amaro, R., et al. (2019). Engineering a bifunctional Phr60-Rap60-Spo0A quorum-sensing molecular switch for dynamic fine-tuning of menaquinone-7 Synthesis in *Bacillus subtilis*. *ACS Synth. Biol.* 8, 1826–1837. doi: 10.1021/acssynbio.9b00140

Dawson, A., Fyfe, P. K., and Hunter, W. N. (2008). Specificity and reactivity in menaquinone biosynthesis: the structure of *Escherichia coli* MenD (2-Succinyl-5-Enolpyruvyl-6-Hydroxy-3-Cyclohexadiene-1-Carboxylate Synthase). *J. Mol. Biol.* 384, 1353–1368. doi: 10.1016/j.jmb.2008.10.048

Halder, M., Petsophonsakul, P., Akbulut, A. C., Pavlic, A., Bohan, F., Anderson, E., et al. (2019). Vitamin K: double bonds beyond coagulation insights into differences between vitamin K1 and K2 in health and disease. *Int. J. Mol. Sci.* 20:896. doi: 10.3390/ijms20040896

Hu, L., Feng, J., Wu, J., Li, W., Gningue, S. M., Yang, Z., et al. (2020). Identification of six important amino acid residues of MenA from *Bacillus subtilis natto* for enzyme activity and formation of menaquinone. *Enzyme Microb. Technol.* 138:109583. doi: 10.1016/j.enzmictec.2020.109583

Kong, L., Zhang, Y., Ye, Z. Q., Liu, X. Q., Zhao, S. Q., Wei, L., et al. (2007). CPC: assess the protein-coding potential of transcripts using sequence features and support vector machine. *Nucleic Acids Res.* 35, W345–W349. doi: 10.1093/nar/gkm391

Kong, M. K., and Lee, P. C. (2011). Metabolic engineering of menaquinone-8 pathway of *Escherichia coli* as a microbial platform for vitamin K production. *Biotechnol. Bioeng.* 108, 1997–2002. doi: 10.1002/bit.23142

Langmead, B., and Salzberg, S. L. (2012). Fast gapped-read alignment with Bowtie 2. *Nat. Methods* 9, 357–359. doi: 10.1038/nmeth.1923

Łaszcz, M., Trzcińska, K., Kubiszewski, M., and Krajewski, K. (2018). Structural and physicochemical studies of two key intermediates and the impurity in the new synthesis route of vitamin MK-7. *J. Mol. Struct.* 1160, 304–310. doi: 10.1016/j.molstruc.2018.02.018

Li, C., Chen, X., Jin, Z., Gu, Z., Rao, J., and Chen, B. (2021). Physicochemical property changes and aroma differences of fermented yellow pea flours: role of *Lactobacilli* and fermentation time. *Food Funct.* 12, 6950–6963. doi: 10.1039/d1fo00608h

Li, C., Sun, J. W., Zhang, G. F., and Liu, L. B. (2016). Effect of the absence of the CcpA gene on growth, metabolic production, and stress tolerance in *Lactobacillus delbrueckii ssp. bulgaricus*. *J. Dairy Sci.* 99, 104–111. doi: 10.3168/jds.2015-10321

Liu, C. L., Dong, H. G., Zhan, J., Liu, X., and Yang, Y. (2019). Multi-modular engineering for renewable production of isoprene via mevalonate pathway in *Escherichia coli*. *J. Appl. Microbiol.* 126, 1128–1139. doi: 10.1111/jam.14204

Liu, Y., Yang, Z., Xue, Z., Qian, S., Wang, Z., Hu, L., et al. (2018). Influence of site-directed mutagenesis of UbiA, overexpression of dxr, menA and ubiE, and supplementation with precursors on menaquinone production in *Elizabethkingia meningoseptica*. *Process Biochem.* 68, 64–72. doi: 10.1016/j.procbio.2018.01.022

Luo, M., Liu, B., and Ji, X. (2016a). Effect of fermentation with mixed carbon sources on the production of menadione-7 by *Bacillus natto*. *Food Ferment. Ind.* 11, 35–39.

Luo, M., Ren, L., Chen, S., Ji, X., and Huang, H. (2016b). Effect of media components and morphology of *Bacillus natto* on menaquinone-7 synthesis in submerged fermentation. *Biotechnol. Bioprocess. Eng.* 21, 777–786. doi: 10.1007/s12257-016-0202-9

Lv, X., Xu, H., and Yu, H. (2013). Significantly enhanced production of isoprene by ordered coexpression of genes dxs, dxr, and idi in *Escherichia coli*. *Appl. Microbiol. Biotechnol.* 97, 2357–2365. doi: 10.1007/s00253-012-4485-2

Ma, X., Zhu, S., Luo, M., Hu, X., Peng, C., Huang, H., et al. (2019). Intracellular response of *Bacillus natto* in response to different oxygen supply and its influence on menaquinone-7 biosynthesis. *Bioprocess Biosyst. Eng.* 42, 817–827. doi: 10.1007/s00449-019-02085-x

Ma, Y., McClure, D. D., Somerville, M. V., Proschogo, N. W., Dehghani, F., Kavanagh, J. M., et al. (2019). Metabolic engineering of the MEP pathway in *Bacillus subtilis* for increased biosynthesis of menaquinone-7. *ACS Synth. Biol.* 8, 1620–1630. doi: 10.1021/acssynbio.9b00077

Mahdinia, E., Demirci, A., and Berenjian, A. (2017). Production and application of menaquinone-7 (vitamin K2): a new perspective. *World J. Microbiol. Biotechnol.* 33:2. doi: 10.1007/s11274-016-2169-2

Mahdinia, E., Demirci, A., and Berenjian, A. (2019a). Biofilm reactors as a promising method for vitamin K (menaquinone-7) production. *Appl. Microbiol. Biotechnol.* 103, 5583–5592. doi: 10.1007/s00253-019-09913-w

Mahdinia, E., Demirci, A., and Berenjian, A. (2019b). Effects of medium components in a glycerol-based medium on vitamin K (menaquinone-7) production by *Bacillus subtilis natto* in biofilm reactors. *Bioprocess Biosyst. Eng.* 42, 223–232. doi: 10.1007/s00449-018-2027-8

Novin, D., van der Wel, J., Seifan, M., and Berenjian, A. (2020). The effect of aeration and mixing in developing a dairy-based functional food rich in menaquinone-7. *Bioprocess Biosyst. Eng.* 43, 1773–1780. doi: 10.1007/s00449-020-02366-w

Priyadarshi, A., Saleem, Y., Nam, K. H., Kim, K. S., Park, S. Y., Kim, E. E. K., et al. (2009). Structural insights of the MenD from *Escherichia coli* reveal ThDP affinity. *Biochem. Biophys. Res. Commun.* 380, 797–801. doi: 10.1016/j.bbrc.2009.01.168

Ren, L., Cheng, P., Hu, X., Han, Y., and Huang, H. (2020). Microbial production of vitamin K2: current status and future prospects. *Biotechnol. Adv.* 39:107453. doi: 10.1016/j.biotechadv.2019.107453

Rincón Santamaría, A., Cuellar Gil, J. A., Valencia Gil, L. F., and Sánchez Toro, O. J. (2019). Kinetics of gluconacetobacter diazotrophicus growth using cane molasses and sucrose: assessment of kinetic models. *Acta Biol. Colomb.* 24, 38–57. doi: 10.15446/abc.v24n1.70857

Robinson, M. D., McCarthy, D. J., and Smyth, G. K. (2010). edgeR: a Bioconductor package for differential expression analysis of digital gene expression data. *Bioinformatics* 26:139. doi: 10.1093/bioinformatics/btp616

Shih, I. L., Yu, Y. T., Shieh, C. J., and Hsieh, C. Y. (2005). Selective production and characterization of levan by *Bacillus subtilis* (*Natto*) Takahashi. *J. Agric. Food Chem.* 53, 8211–8215. doi: 10.1021/jf058084o

Song, J., Liu, H., Wang, L., Dai, J., Liu, Y., Liu, H., et al. (2014). Enhanced production of vitamin K2 from *Bacillus subtilis* (*natto*) by mutation and optimization of the fermentation medium. *Braz. Arch. Biol. Technol.* 57, 606–612. doi: 10.1590/S1516-8913201402126

Sun, X. F., Zhang, X. M., Gao, Y. J., Qiu, J., Liu, X., Li, S., et al. (2020). Determination of Vitamin K2 (MK-7) in nutrient supplements by high performance liquid chromatography-fluorescence spectrometry. *Mod. Food Sci. Technol.* 36:1209. doi: 10.13982/j.mfst.1673-9078.2020.6.1209

Suvarna, K., Stevenson, D., Meganathan, R., and Hudspeth, M. E. S. (1998). Menaquinone (vitamin K2) biosynthesis: Localization and characterization of the menA gene from *Escherichia coli*. *J .Bacteriol.* 180, 2782–2787. doi: 10.1128/jb.180.10.2782-2787.1998

Tarkesh, F., Namavar Jahromi, B., Hejazi, N., and Tabatabaee, H. (2020). Beneficial health effects of menaquinone-7 on body composition, glycemic indices, lipid profile, and endocrine markers in polycystic ovary syndrome patients. *Food Sci. Nutr.* 8, 5612–5621. doi: 10.1002/fsn3.1837

Turck, D., Bresson, J. L., Burlingame, B., Dean, T., Fairweather-Tait, S., Heinonen, M., et al. (2017). Dietary reference values for vitamin K. *EFSA J.* 15:e04780. doi: 10.2903/j.efsa.2017.4780

Vermeer, C., Raes, J., van 't Hoofd, C., Knapen, M. H. J., and Xanthoulea, S. (2018). Menaquinone content of cheese. *Nutrients* 10:446. doi: 10.3390/nu10040446

Wang, B., Lv, Y., Li, X., Lin, Y., Deng, H., and Pan, L. (2018). Profiling of secondary metabolite gene clusters regulated by LaeA in *Aspergillus niger* FGSC A1279 based on genome sequencing and transcriptome analysis. *Res. Microbiol.* 169, 67–77. doi: 10.1016/j.resmic.2017.10.002

Wei, X., Ji, Z., and Chen, S. (2010). Isolation of Halotolerant *Bacillus licheniformis* WX-02 and regulatory effects of sodium chloride on yield and molecular sizes of poly-γ-glutamic acid. *Appl. Biochem. Biotechnol.* 160, 1332–1340. doi: 10.1007/s12010-009-8681-1

Wilkens, D., Meusinger, R., Hein, S., and Simon, J. (2021). Sequence analysis and specificity of distinct types of menaquinone methyltransferases indicate the widespread potential of methylmenaquinone production in bacteria and archaea. *Environ. Microbiol.* 23, 1407–1421. doi: 10.1111/1462-2920.15344

Wu, D. (2019). Research progress in the mechanism of nattokinase. *Chin. J. Pharm. Biotechnol.* 26, 562–564. doi: 10.19526/j.cnki.1005-8915.20190622

Wu, J., Li, W., Zhao, S., Qian, S. H., Wang, Z., Zhou, M. J., et al. (2021). Site-directed mutagenesis of the quorum-sensing transcriptional regulator SinR affects the

biosynthesis of menaquinone in *Bacillus subtilis*. *Microb. Cell Fact.* 20:113. doi: 10.1186/s12934-021-01603-5

Xu, J., Yao, Z., Yang, X., Xie, K., and Liu, G. (2012). Breeding of High-yield strain of vitamin K2 by protoplast electro fusion. *Acad Biotechnol. Food Eng.* 33, 80–83.

Xu, J. Z., Yan, W. L., and Zhang, W. G. (2017). Enhancing menaquinone-7 production in recombinant: *Bacillus amyloliquefaciens* by metabolic pathway engineering. *RSC Adv.* 7, 28527–28534. doi: 10.1039/c7ra03388e

Xu, J. Z., and Zhang, W. G. (2017). Menaquinone-7 production from maize meal hydrolysate by *Bacillus* isolates with diphenylamine and analogue resistance. *J. Zhejiang Univ. Sci. B* 18, 462–473. doi: 10.1631/jzus.B1600127

Yang, F., and Zhang, T. (2011). Study on biological characteristics of *Bacillus subtilis*. *Feed Res.* 3, 34–36.

Yang, J., and Guo, L. (2014). Biosynthesis of β-carotene in engineered *E. coli* using the MEP and MVA pathways. *Microb. Cell Fact.* 13:160. doi: 10.1186/s12934-014-0160-x

Yang, S., Cao, Y., Sun, L., Li, C., Lin, X., Cai, Z., et al. (2019). Modular pathway engineering of *Bacillus subtilis* to promote de novo biosynthesis of menaquinone-7. *ACS Synth. Biol.* 8, 70–81. doi: 10.1021/acssynbio.8b00258

Yang, S., Wang, Y., Cai, Z., Zhang, G., and Song, H. (2020). Metabolic engineering of *Bacillus subtilis* for high-titer production of menaquinone-7. *AIChE J.* 66:e16754. doi: 10.1002/aic.16754

Yu, J., Hederstedt, L., and Piggot, P. J. (1995). The cytochrome bc complex (menaquinone:cytochrome c reductase) in *Bacillus subtilis* has a nontraditional subunit organization. *J. Bacteriol.* 177, 6751–6760. doi: 10.1128/jb.177.23.6751-6760.1995

Zeng, W., Chen, G., Wang, Q., Zheng, S., Shu, L., and Liang, Z. (2014). Metabolic studies of temperature control strategy on poly(γ-glutamic acid) production in a thermophilic strain *bacillus subtilis* GXA-28. *Bioresour. Technol.* 155, 104–110. doi: 10.1016/j.biortech.2013.12.086

Zhang, G., Liu, L., and Li, C. (2020). Effects of ccpA gene deficiency in *Lactobacillus delbrueckii subsp. bulgaricus* under aerobic conditions as assessed by proteomic analysis. *Microb. Cell Fact.* 19:9. doi: 10.1186/s12934-020-1278-7

Zhao, C., Wan, Y., Tang, G., Jin, Q., Zhang, H., and Xu, Z. (2021). Comparison of different fermentation processes for the vitamin K2 (Menaquinone-7) production by a novel *Bacillus velezensis* ND strain. *Process Biochem.* 102, 33–41. doi: 10.1016/j.procbio.2020.11.029

Zhou, A., Cao, Y., Zhou, D., Hu, S., Tan, W., Xiao, X., et al. (2020). Global transcriptomic analysis of *Cronobacter sakazakii* CICC 21544 by RNA-seq under inorganic acid and organic acid stresses. *Food Res. Int.* 130:108963. doi: 10.1016/j.foodres.2019.108963

Zhou, Z., Luo, M., and Qiu, H. (2016). Effects of carbon and nitrogen sources on the fermentation of vitamin K2 by *Bacillus natto* R127. *Biol Process* 14, 29–32.

Conflict of Interest: The authors declare that the research was conducted in the absence of any commercial or financial relationships that could be construed as a potential conflict of interest.

Publisher's Note: All claims expressed in this article are solely those of the authors and do not necessarily represent those of their affiliated organizations, or those of the publisher, the editors and the reviewers. Any product that may be evaluated in this article, or claim that may be made by its manufacturer, is not guaranteed or endorsed by the publisher.

frontiers | Frontiers in Microbiology

ORIGINAL RESEARCH
published: 12 May 2022
doi: 10.3389/fmicb.2022.908145

AI-2E Family Transporter Protein in *Lactobacillus acidophilus* Exhibits AI-2 Exporter Activity and Relate With Intestinal Juice Resistance of the Strain

Xiefei Li[1,2], *Xiankang Fan*[1,2], *Zihang Shi*[1,2], *Jue Xu*[1,2], *Yingying Cao*[1,2], *Tao Zhang*[1,2] *and Daodong Pan*[1,2]*

[1] State Key Laboratory for Managing Biotic and Chemical Threats to the Quality and Safety of Agro-Products, Ningbo University, Ningbo, China, [2] Key Laboratory of Animal Protein Deep Processing Technology of Zhejiang, Ningbo University, Ningbo, China

The function of the autoinducer-2 exporters (AI-2E) family transporter protein of *Lactobacillus acidophilus* is still unclear. The phylogenetic analysis was used to analyze the relationship between the AI-2E protein of the *L. acidophilus* CICC 6074 strain and other AI-2E family members. *Escherichia coli* KNabc strain was used to verify whether the protein has Na^+ (Li^+)/H^+ antiporter activity. The AI-2E protein overexpression strain was constructed by using the pMG36e expression vector, and the overexpression efficiency was determined by real-time quantitative PCR. The vitality and AI-2 activity of *L. acidophilus* CICC 6074 strains were determined. The results showed that the AI-2E protein of *Lactobacillus* formed a single branch on the phylogenetic tree and was closer to the AI-2E family members whose function was AI-2 exporter group I. The expression of AI-2E protein in the *E. coli* KNabc strain did not recover the resistance of the bacteria to the saline environment. Overexpression of AI-2E protein in *L. acidophilus* CICC 6074 could promote the AI-2 secretion of *L. acidophilus* CICC 6074 strain and enhance their survival ability in intestinal juice.

Keywords: AI-2E family transporter, *Lactobacillus acidophilus*, overexpression, intestinal juice, real-time quantitative PCR, AI-2

OPEN ACCESS

Edited by:
Rina Wu,
Shenyang Agricultural University, China

Reviewed by:
Hongfei Zhao,
Beijing Forestry University, China
Jixia Yang,
Southwest University, China

***Correspondence:**
Daodong Pan
daodongpan@163.com

Specialty section:
This article was submitted to Food Microbiology, a section of the journal Frontiers in Microbiology

Received: *30 March 2022*
Accepted: *12 April 2022*
Published: *12 May 2022*

Citation:
Li X, Fan X, Shi Z, Xu J, Cao Y, Zhang T and Pan D (2022) AI-2E Family Transporter Protein in Lactobacillus acidophilus Exhibits AI-2 Exporter Activity and Relate With Intestinal Juice Resistance of the Strain. Front. Microbiol. 13:908145. doi: 10.3389/fmicb.2022.908145

INTRODUCTION

The well-known probiotic effect of probiotics has made it widely accepted by consumers and has formed a massive market on a global scale (Nguyen et al., 2020). The health benefits of lactic acid bacteria (LAB) and their positive effects on food have led to their addition to various food products as a probiotic. As a representative of probiotics, the probiotic effects of LAB in maintaining the balance of the gastrointestinal tract, modulating the immune system, reducing lactose intolerance, and preventing diarrhea have been widely confirmed (Michael et al., 2001; Jin et al., 2010; Kostelac et al., 2021). *Lactobacillus* can only exert positive probiotic effects on the human body when sufficient amounts of live bacteria are ingested and safely pass through the digestive tract to reach the intestines and colonize. Studies have found that the viability of probiotic bacteria should be at least 10^7 CFU/g when consuming probiotic products (Ranadheera et al., 2010). The vitality of

probiotics is the key factor to play the probiotic effect, so the research to improve the vitality of probiotics is of great significance.

Factors affecting the viability of probiotics have been extensively studied, and researchers have thus proposed several methods to enhance the viability of LAB in the gastrointestinal tract. Among the common methods is the development of different probiotic food carriers, the screening of probiotic strains with good resistance, the optimization of probiotic production and storage conditions, and microencapsulation of bacterial cells. Compared to fermented milk, cheese has the advantages of higher pH, higher fat content, lower oxygen content, and a dense woven matrix, which is thought more effective in delivering probiotics into the human gut (Karimi et al., 2011). Sakamoto et al. (2001) screened 203 strains of *Lactobacilli* to select strains that exhibited high levels of resistance to gastric acidity, the *Lactobacillus gasseri* OLL2716 has been selected as the best strain, and a yogurt product that inhibits *Helicobacter pylori* was developed from this strain. Microencapsulation is a relatively effective method to improve the survival rate of LAB, which has been studied by many researchers (Damodharan et al., 2017; Ghibaudo et al., 2017; Chen et al., 2020).

Another way that could improve adaptation to the gastrointestinal fluid environment of LAB is to focus on the bacteria themselves and strain improvement. Several researchers have identified and confirmed that some genes or genetic factors are associated with the resistance of LAB (Azcarate-Peril et al., 2004; Fiocco et al., 2007; Bove et al., 2012). Patnaik et al. (2002) used the genomic recombination method to improve the acid tolerance of an industrial strain of *Lactobacillus* and obtained a mutant strain that grew on liquid and solid media at a much lower pH than the wild-type strain. Pfeiler et al. reported that deletion mutations in proteins such as transporter and *HPK* resulted in the loss of bile tolerance in *Lactobacillus acidophilus* NCFM strains, and mutations in an oxidoreductase and hypothetical protein genes resulted in a significant increase in bile tolerance in the strains (Pfeiler et al., 2007; Pfeiler and Klaenhammer, 2009). Goh et al. (2009) found that the Apf-like proteins may contribute to the survival of *L. acidophilus* during transit through the digestive tract and, potentially, participate in the interactions with the host intestinal mucosa.

Transmembrane transport is involved in nutrient uptake, metabolite excretion, energy production, and conversion in bacterial cells and is essential for bacteria to adapt to their environment (Lorca et al., 2007). The autoinducer-2 exporters (AI-2E) family homologs are widely distributed in various bacteria and archaea and are a common transporter protein encoded by genes on the bacterial chromosome (Rettner and Saier Jr, 2010). All members of AI-2E protein in the AI-2E family transporter have a uniform 8 transmembrane helices (TMHs), with the second 4 TMHs being more conserved than the first 4 TMHs. The functions of AI-2E have been identified mainly for two main categories, exporting autoinducer-2 (AI-2) molecules and acting as Na^+ (Li^+)/H^+ antiporter (Rettner and Saier Jr, 2010; Dong et al., 2017). These two functions of AI-2E are thought to be related to microbial lifestyle and environmental adaptability. Wang et al. (2020) used proteomics to find that AI-2E proteins were closely associated with the survival of *Acinetobacter johnsonii* and *Pseudomonas fluorescens* in the environment (Wang and Xie, 2020). Shao et al. (2018) found that the AI-2E protein with Na+/H+ antiporters activity was associated with *Halobacillus andaensis* resistance to high saline-alkaline stress (Shao et al., 2018).

The AI-2E proteins are present in almost all LAB strains, and the function and mechanism of action of AI-2E protein in LAB are rarely mentioned. Whether it is related to the adaptation of LAB to the environment has also been little studied. Lorca et al. (2007) identified the AI-2E protein as serving to export AI-2 in 11 bacterial species containing *L. casei* but not *L. acidophilus*. In one of our studies, we observed a significant upregulation of the LBA_RS00210 gene in *L. acidophilus* that had been exposed to intestinal juice (data unpublished). The effect of AI-2E protein on the ability of LAB to survive in the intestine has not yet been studied. Therefore, we verified the function of the AI-2E protein in *L. acidophilus* and found that this protein affects the viability of the bacteria cells in the intestinal juice.

MATERIALS AND METHODS

Bacteria Strains and Growth Conditions

The *E. coli* KNabc strain was grown in the KCl-modified Luria-Bertani (LBK) medium (Dong et al., 2017), and *E. coli* DH5α was cultured in the Luria–Bertani (LB) broth. *E. coli* competent cells were prepared with the Competent Cell Preparation Kit [Takara Biomedical Technology (Beijing) Co., Ltd., China], and the transformants were selected by ampicillin with a concentration of 100 μg/ml. Salt and alkaline pH tolerance of *E. coli* KNabc strain were tested as described in the studies of Shao et al. (2018). The *L. acidophilus* CICC 6074 strain was grown in the Man, Rogosa and Sharpe (MRS) medium. The mutant strain overexpressing the AI-2E protein was selectively grown in the MRS medium containing 5 μg/ml erythromycin. Intestinal juice tolerance experiments of *Lactobacillus* cells were performed as described in the studies of Maragkoudakis et al. (2006) and Ranadheera et al. (2014).

Bioinformatic Analyses

MEGA (Version 11.0.10) was used to construct the phylogenetic tree to analyze the functional and taxonomic information of the AI-2E protein of *Lactobacillus* (a neighbor-joining phylogenetic tree with a bootstrap analysis 1,000 replications). The AI-2E family transporter protein sequences of *Lactobacillus* were downloaded from the Identical Protein Groups (IPG) of NCBI, and the sequences of proteins belonging to the AI-2E family (TC #9.B.22) were downloaded from the transporter classification database (TCDB). The homolog protein of the AI-2E family transporter from *L. acidophilus* CICC 6074 was obtained by performed blastp and downloaded from NCBI. Topological analysis was carried out on SMART (http://smart.embl-heidelberg.de/), PredictProtein (https://predictprotein.org/), and Geneious. Weblogo was created with Geneious.

Construction of Recombinant Plasmid

To be able to express AI-2E protein in *E. coli* cells, we used the pUC19 plasmid to ligate the *AI-2E* gene fragment containing

the promoter sequence. To express the AI-2E protein with 6×His tag in *E. coli* cells and to take the strain ampicillin-resistant, we used the pET22b plasmid and replaced the pelB tag on the vector with the 6×His tag. And to overexpress AI-2E protein in cells of *L. acidophilus* CICC 6074, the pMG36e plasmid was used by us. This vector is known as a food-grade LAB expression vector with the advantages of simple structure, clean expression product, strong promoter, and no need to be induced. Many researchers have used this vector when expressing proteins in LAB strains. Geneious software was used to locate the AI-2E gene on the genome of *L. acidophilus*, and the TSSG program (http://www.softberry.com/berry.phtml?topic=tssg&group=programs&subgroup=promoter) and BDGP: Neural Network Promoter Prediction website (https://www.fruitfly.org/seq_tools/promoter.html) were used for promoter prediction. CE Design V1.04 software (Vazyme Biotech Co., Ltd., China) was used to design-specific primers for amplifying the AI-2E gene. The target gene was amplified using the 2× Phanta Max Master Mix (Vazyme Biotech Co., Ltd., China), and the amplification products were recovered and purified using the Ultra-Sep Gel Extraction Kit (Omega Biotek Inc., USA). The plasmids were extracted using the HP Plasmid DNA Midi Kit (Omega Biotek Inc., USA), and the Takara QuickCut restriction enzyme [Takara Biomedical Technology (Beijing) Co., Ltd., China] was used to digest the three vectors separately. The prepared target gene fragment and the linearized vector fragment were ligated using the ClonExpress® Ultra One Step Cloning Kit (Vazyme Biotech Co., Ltd., China). The constructed plasmids were sequenced to verify the ligation and ensure that the target gene was not mutated.

Transformation and Electrotransformation

The *E. coli* KNabc is a strain lacking the three major Na^+ (Li^+)/H^+ antiporters (Δ*nhaA*, Δ*nhaB*, and Δ*chaA*). The Na^+ (Li^+)/H^+ antiporter activity of the *AI-2E* genes can be verified by transferring and expressing these genes in *E. coli* KNabc strain to recover the resistance of strain cells to the saline environment (Majernik et al., 2001; Dong et al., 2017). Therefore, we used *E. coli* KNabc strain to verify the Na^+ (Li^+)/H^+ antiporter activity of AI-2E protein of *L. acidophilus*, and *L. acidophilus* CICC 6074 strain was used to overexpress AI-2E protein. For transformation, 100 μl of *E. coli* KNabc competent cells were melted on ice, 10 μl of recombinant plasmid was added to the competent cells. The mixture of competent cells with the recombinant plasmid was ice bathed for 30 min and then heat shock in hot water at 42°C for 45 s. Preparation of *L. acidophilus* competent cells and electroporation were carried out with some modifications of the method from Palomino et al. (2010). The MicroPulser Electroporator (Bio-Rad Laboratories, Inc., USA) was used to perform the electroporation with the parameters set to 12.5 kV/cm, 4 ms. We mixed 50 μl of *L. acidophilus* competent cells with 5 μl of the recombinant plasmid. The mixture was added to pre-cooled 0.2-cm electrode gap cuvettes and then performed electroporation according to the set parameters.

Na^+ (Li^+)/H^+ Antiporter Assay

The *E. coli* KNabc wild-type strain and the recombinant strains (*E. coli* KNabc/pUC19, *E. coli* KNabc/pET22b, *E. coli* KNabc/pUC19-AI-2E, and *E. coli* KNabc/pET22b-AI-2E) were streak cultured on fresh and 100 μg/ml ampicillin-added LBK agar plates, respectively. Single colonies were picked for the expansion. To determine the resistance of the *E. coli* KNabc strain to alkaline pH, Na^+ and Li^+; the *E. coli* KNabc strain and recombinant strains were activated, followed by 1% (v/v) subculture in the LBK medium at different pH (7.0, 7.5, 8.0, and 8.5) and the LBK medium at pH 7.0 but with different concentrations of NaCl (0.2, 0.3, and 0.4 M) or LiCl (5, 10, 25, and 30 mM). After incubation at 37°C for 24 h, the optical density (OD_{600}) values of the bacterial culture were measured by Infinite M200 PRO Multimode Microplate Reader (Tecan Group Ltd., Switzerland). Three replicates were done for each sample.

Real-Time Quantitative PCR

After being cultured at 37°C for 18 h, the total RNA of the *L. acidophilus* CICC 6074 wild-type strain and the recombinant strains (*L. acidophilus* CICC 6074/pMG36e and *L. acidophilus* CICC 6074/pMG36e-AI-2E) was extracted using E.Z.N.A.® Bacterial RNA Kit (Omega Biotek Inc., USA). The concentration of RNA was measured by NanoDrop ND-2000 Spectrophotometer (Thermo Fisher Scientific Inc. USA), and RNA integrity was observed by agarose gel electrophoresis. Genomic DNA removal and cDNA synthesis were accomplished using HiScript® III RT SuperMix for qPCR (+gDNA wiper) (Vazyme Biotech Co., Ltd, China). Real-time quantitative PCR (RT-qPCR) was performed using Taq Pro Universal SYBR qPCR Master Mix (Vazyme Biotech Co., Ltd, China) on LightCycler® 96 Instrument (Roche Molecular Systems, Inc., Switzerland). Primers used in RT-qPCR were designed using Primer premier 6, DNA polymerase III subunit delta gene was used as reference gene. The Livak ($2^{-\Delta\Delta CT}$) method was used to calculate the relative expression of the *AI-2E* gene.

AI-2 Detection

The detection of AI-2 is based on the method of Liu et al. (2018) with some modifications. Activated *L. acidophilus* CICC 6074 wild-type strain and recombinant strains (*L. acidophilus* CICC 6074/pMG36e and *L. acidophilus* CICC 6074/pMG36e-AI-2E) were added to 12% (w/w) skimmed milk medium without erythromycin. The *L. acidophilus* cells in cultures at 2, 4, 6, 8, 10, 12, 14, 16, 18, 20, 22, and 24 h were removed by centrifugation at 12,000 × *g* for 10 min at 4°C. The supernatant pH was adjusted to 7.0 and filtered by 0.22 μm Millex-GP Syringe Filter Unit (Merck KGaA, Germany). The obtained supernatant was added to *Vibrio harveyi* BB170 and the AB medium mixture in a ratio of 1:10 and incubated at 28°C for 5 h. Added 100 μl of culture solution to a 96-well white plate and determined luminescence values using the Infinite M200 PRO Multimode Microplate Reader (Tecan Group Ltd., Switzerland).

Stress Resistance Assay

To assess the effect of overexpressing AI-2E protein in *L. acidophilus* on the viability of cells in intestinal juice, we

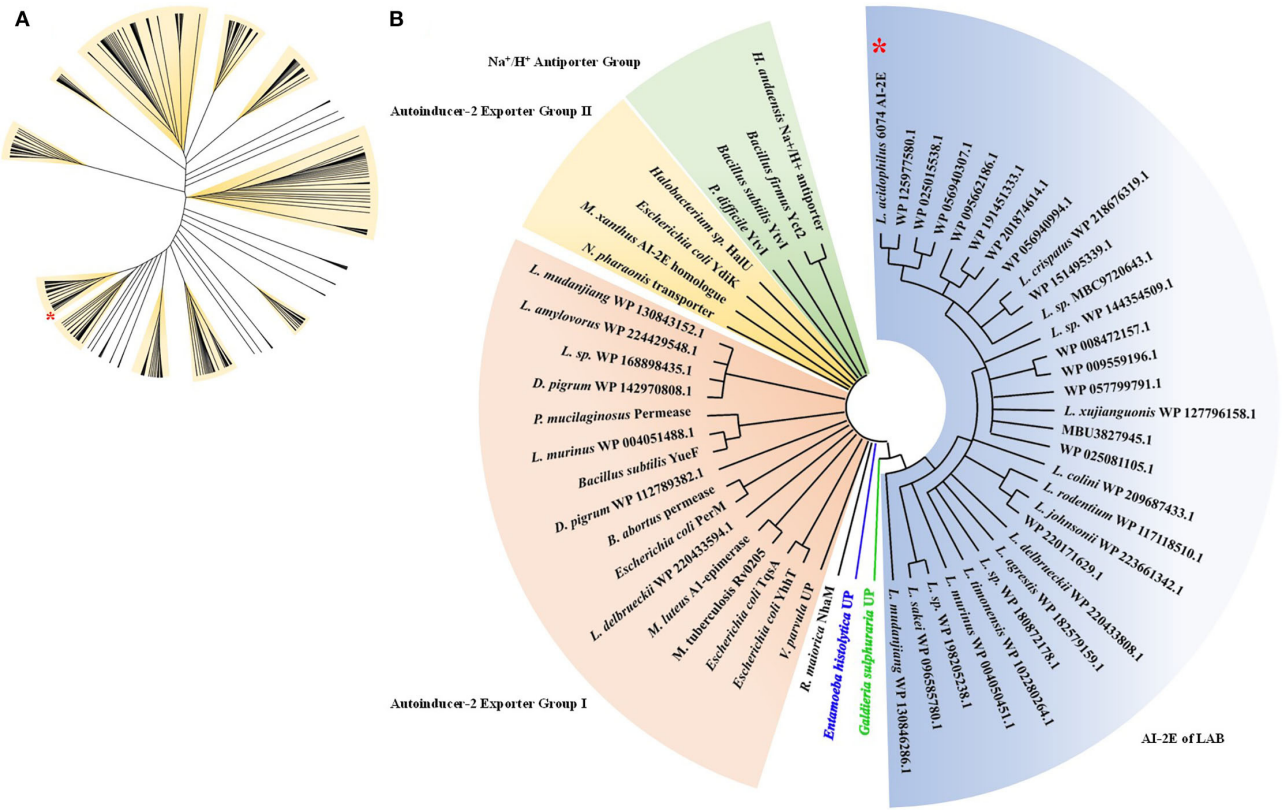

FIGURE 1 | Phylogenetic analysis of AI-2E family transporter protein of *Lactobacillus acidophilus* CICC 6074. Phylogenetic relationship between AI-2E proteins of *Lactobacillus* **(A)**, 530 AI-2E protein sequences of *Lactobacillus* were downloaded from IPG of NCBI, the AI-2E protein of *L. acidophilus* is marked with a red star. Phylogenetic relationship between AI-2E protein of *L. acidophilus* CICC 6074 and AI-2E family members **(B)**, phylogenetic analysis using the AI-2E protein of *L. acidophilus* with its homologous proteins, and the AI-2E protein of *L. acidophilus* is marked with a red star.

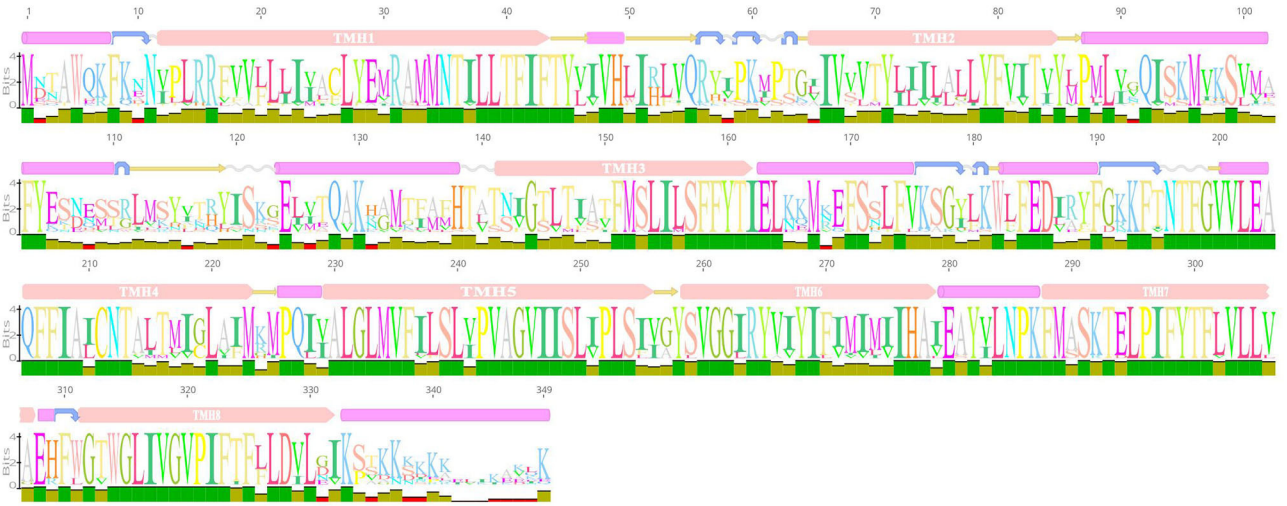

FIGURE 2 | Weblogo of AI-2E protein of *Lactobacillus acidophilus* CICC 6074 and its homologs. The first layer shows the predicted secondary structure and functional domains of AI-2E protein. The pink bars represent an α-helix, the blue arrows represent the corner, the yellow arrows represent the β-fold, and the pink bars marked with transmembrane helix (TMH) are the predicted transmembrane helices. The letters of different sizes in the second layer represent the size of similarity of homologous sequences at that locus, larger letter means higher similarity. The color block in the third layer represents the conservativeness of the sequence and the green color represents that the region is conserved.

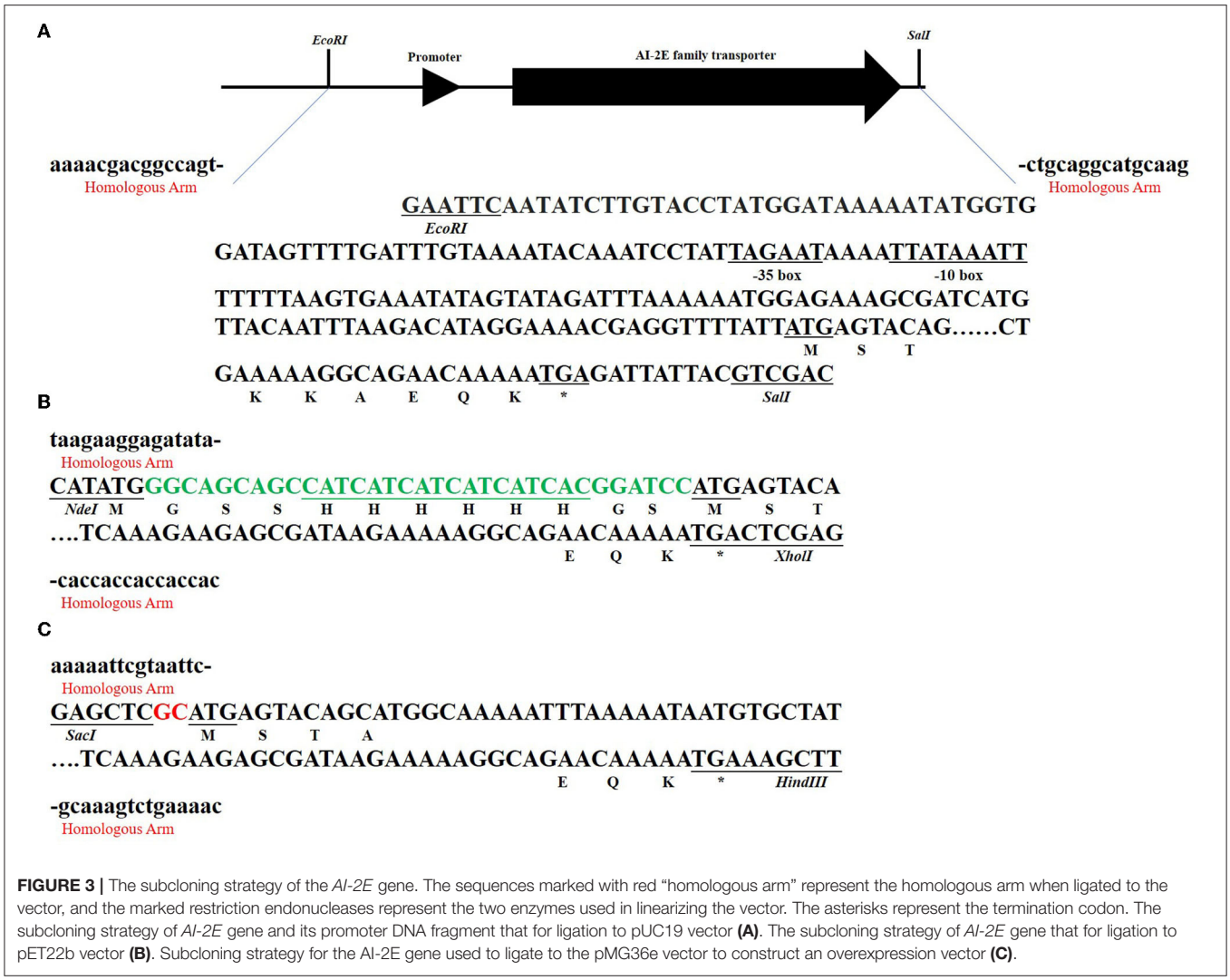

FIGURE 3 | The subcloning strategy of the *AI-2E* gene. The sequences marked with red "homologous arm" represent the homologous arm when ligated to the vector, and the marked restriction endonucleases represent the two enzymes used in linearizing the vector. The asterisks represent the termination codon. The subcloning strategy of *AI-2E* gene and its promoter DNA fragment that for ligation to pUC19 vector **(A)**. The subcloning strategy of *AI-2E* gene that for ligation to pET22b vector **(B)**. Subcloning strategy for the AI-2E gene used to ligate to the pMG36e vector to construct an overexpression vector **(C)**.

tested the survival of different strains during intestinal fluid tolerance. Injected 2% (v/v) activated *L. acidophilus* CICC 6074 wild-type strain and recombinant strains (*L. acidophilus* CICC 6074/pMG36e and *L. acidophilus* CICC 6074/pMG36e-AI-2E) into fresh MRS medium, incubated at 37°C for 18 h to logarithmic phase. The cells were centrifuged at 5,000 × *g* for 5 min at 4°C, washed three times with sterilized phosphate-buffered saline (PBS), and resuspended with the small intestine solution. The cultures were taken out at 0, 2, 4, and 6 h to count the number of viable bacteria by plate counting method. The survival rates were calculated as follows: the logarithm of survival cell number/the logarithm of initial cell number × 100%. The initial cell number was survival cell at 0 h.

Statistical Analysis

Statistical analysis was performed using IBM SPSS Statistics 26, and differences were considered statistically significant when the *p*-value was <0.05. One-way analysis of variance (ANOVA) was used for data analysis. Results are presented as the mean of three independent experiments.

RESULTS

Phylogenetic Analysis

To analyze the relationship between the AI-2E family transporter protein of *Lactobacillus*, 530 sequences were selected and downloaded for phylogenetic analysis, and phylogenetic trees were constructed by the neighbor-joining method. The result of the analysis is shown in **Figure 1A**. We can see that the sequences are divided into 11 branches and some minor branches, and the branch where the AI-2E family transporter protein of *L. acidophilus* CICC 6074 is marked with a red asterisk. There are 52 sequences in the branch where *L. acidophilus* CICC 6074 is, and these sequences mainly belong to four species (*L. acidophilus*, *L. helveticus*, *L. gigeriorum*, and *Lactobacillus* sp. A27). These results indicate that there is also some variability in AI-2E proteins of *Lactobacillus*, which also suggests that

TABLE 1 | Primers used in this study.

Purpose of primer	Forward primer (5′-3′)	Reverse primer (5′-3′)
Ligation to pUC19	AAAACGACGGCCAGTGAATTCAATATCTTGTACCTATGGATA AAAATATGGT	CTTGCATGCCTGCAGGTCGACGTAATAATCTCATTTTTGTT CTGCCTTT
Ligation to pET22b1	GGCAGCAGCCATCATCATCATCATCACGGATCCATGAGTACAGCA TGGCAAAAATTT	TCATTTTTGTTCTGCCTTTTTC
Ligation to pET22b2	TAAGAAGGAGATATACATATGGGCAGCAGCCATCATCATCA	GTGGTGGTGGTGGTGCTCGAGTCATTTTTGTTCTGCCTTTTTCTTA
Ligation to pMG36e	AAAAATTCGTAATTCGAGCTCGCATGAGTACAGCATGGCAAAAATTT	GTTTTCAGACTTTGCAAGCTTTCATTTTTGTTCTGCCTTTTTCTTA
MCS of pMG36e	CAATCTGCCTCCTCATCCT	CTGATCTCAACAATGTGAAGTC

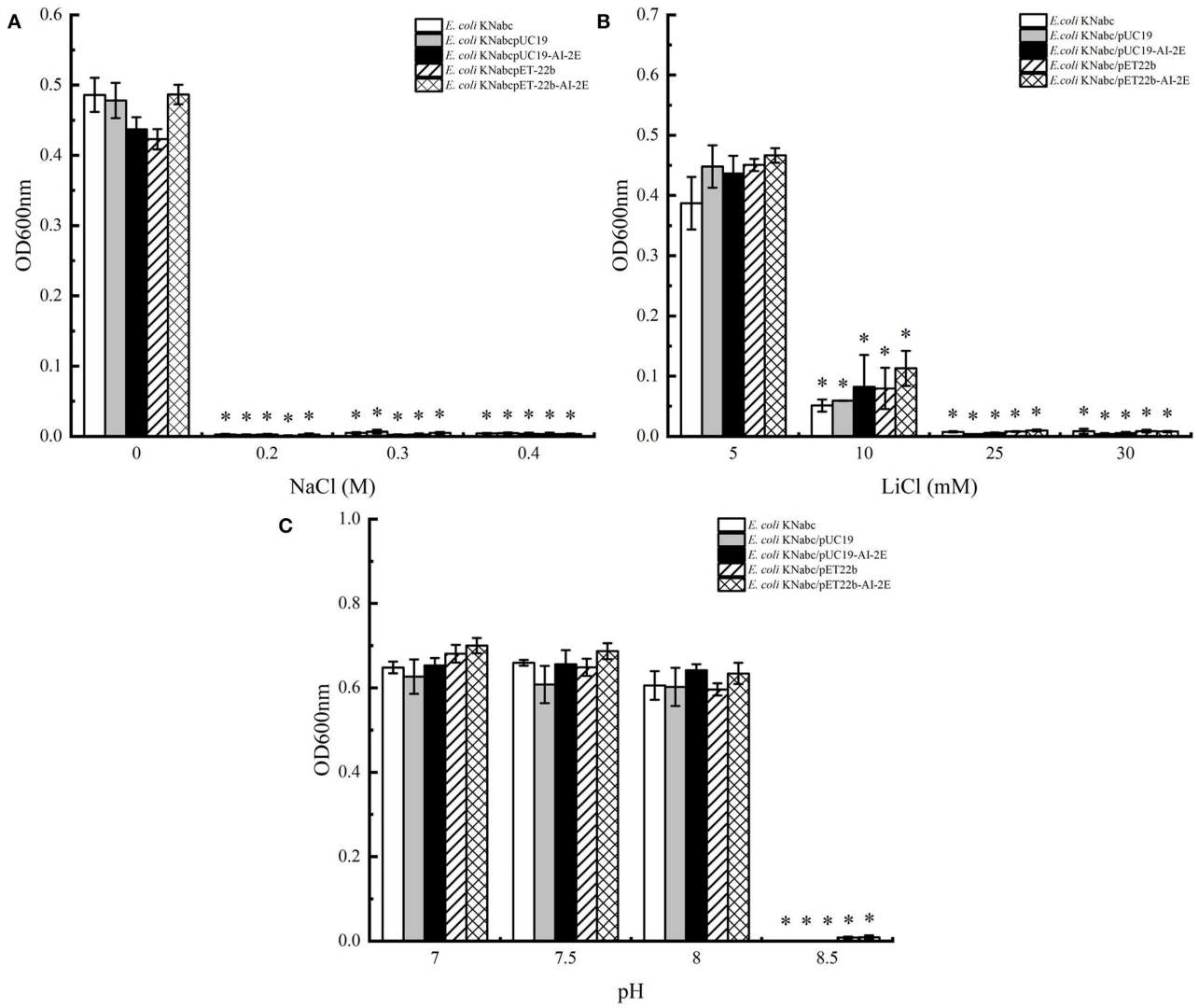

FIGURE 4 | Salinity tolerance of *Escherichia coli* KNabc strains. Growth tests were carried out in the LBK media containing 0.2, 0.3, and 0.4 M NaCl **(A)**, 5, 10, 25, and 30 mM LiCl **(B)**, or at pH 7.0, 7.5, 8.0, and 8.5 **(C)**. Data are presented as mean ± SEM; $n \geq 3$; $^*p < 0.05$ compared with the wild-type strain.

AI-2E protein of different LAB may have different functions. We constructed a neighbor-joining tree of representative AI-2E protein sequences in *Lactobacillus* with other AI-2E protein sequences from TCDB, results shown in **Figure 1B**. It shows that the functions of AI-2E family transporter proteins are divided into three categories, AI-2 exporter group I, AI-2 exporter group II, and Na^+ (Li^+)/H^+ antiporter group. Most of the AI-2E proteins from *Lactobacillus* on the phylogenetic tree are assigned to one branch and are closest to group I. There are also 6 AI-2E proteins from *Lactobacillus* assigned to AI-2 exporter group I.

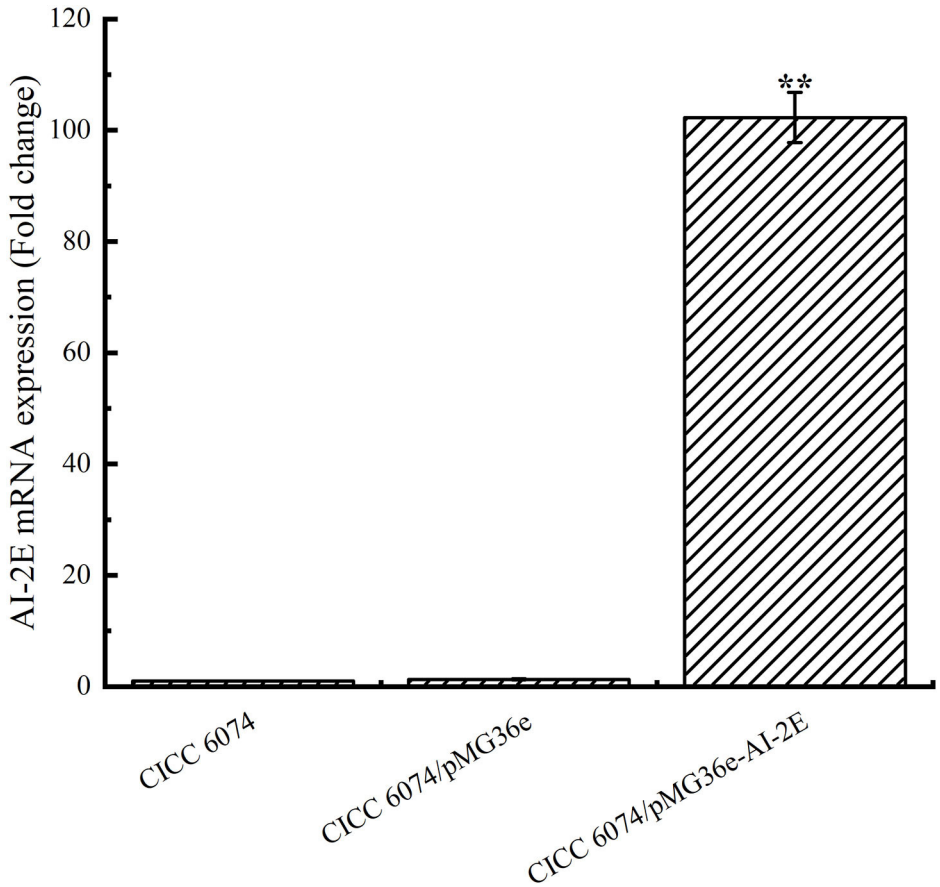

FIGURE 5 | *AI-2E* gene mRNA expressions of *Lactobacillus acidophilus* CICC 6074 wild-type strain, *L. acidophilus* CICC 6074/pMG36e recombinant strain, and *L. acidophilus* CICC 6074/pmG36e-AI-2E recombinant strain. Data are presented as mean ± SEM; $n \geq 3$; $^{**}p < 0.01$ compared with the wild-type strain.

These results suggest that the functions of AI-2E protein from *L. acidophilus* are most likely as AI-2 exporter, but further evidence is needed to prove this.

Structural Domain Prediction of AI-2E Protein of *L. acidophilus*

We predicted the secondary structure and domains of the AI-2E protein from *L. acidophilus* CICC 6074, and the results are shown in **Figure 2**. The results show that this protein sequence contains an AI-2E transport structural domain and has eight transmembrane regions. The AI-2E protein sequence of *L. acidophilus* was multiple alignments with 14 homologous proteins. A weblog plot was created to look at the conserved regions of the protein with the structure. It can be observed that the sequence is better conserved in the transmembrane regions, whereas the non-transmembrane region, especially the turn structure, is less conserved. In addition, we found that TMHs 5, 6, 7, and 8 were more conserved than TMHs 1, 2, 3, and 4.

Construction of Recombinant Plasmid

Figure 3 shows the sketch of the framework of the three recombinant plasmids we constructed. As can be seen in **Figure 3A**, we predicted the promoter sequence of AI-2E and ligated it into the pUC19 plasmid after complete amplification of the entire fragment of interest. In **Figure 3B**, we completely amplified the coding sequence (CDS) of AI-2E and ligated it into the multiple cloning sites of pET22b, which we replaced with a 6 × His tag as the pelB tag of pET22b vector. To overexpress AI-2E protein in *L. acidophilus*, we fully amplified the CDS of AI-2E into the pMG36e expression vector, and a slight adjustment was made to ensure the accuracy of the transcription process (**Figure 3C**). The sequences of primers used in this study are shown in **Table 1**.

Salinity Tolerance Test of *E. coli* Strains

The assay results of the resistance of *E. coli* KNabc wild-type strain and recombinant strains (*E. coli* KNabc/pUC19, *E. coli* KNabc/pUC19, *E. coli* KNabc/pET22b, and *E. coli* KNabc/pET22b-AI-2E) to salts and alkaline pH are shown in **Figure 4**. In the fresh LBK medium, all strains grew normally and were no significant difference in the OD_{600} values of all strains measured after 24 h, whereas the growth of all strains was inhibited by the addition of 0.2, 0.3, and 0.4 M NaCl to the LBK medium (**Figure 4A**). After adding 5 mM of LiCl to the fresh LBK medium, all strains grew normally or with low inhibition; all strains could grow slightly after adding 10 mM of LiCl and were inhibited completely after adding 25 and 30 mM of LiCl

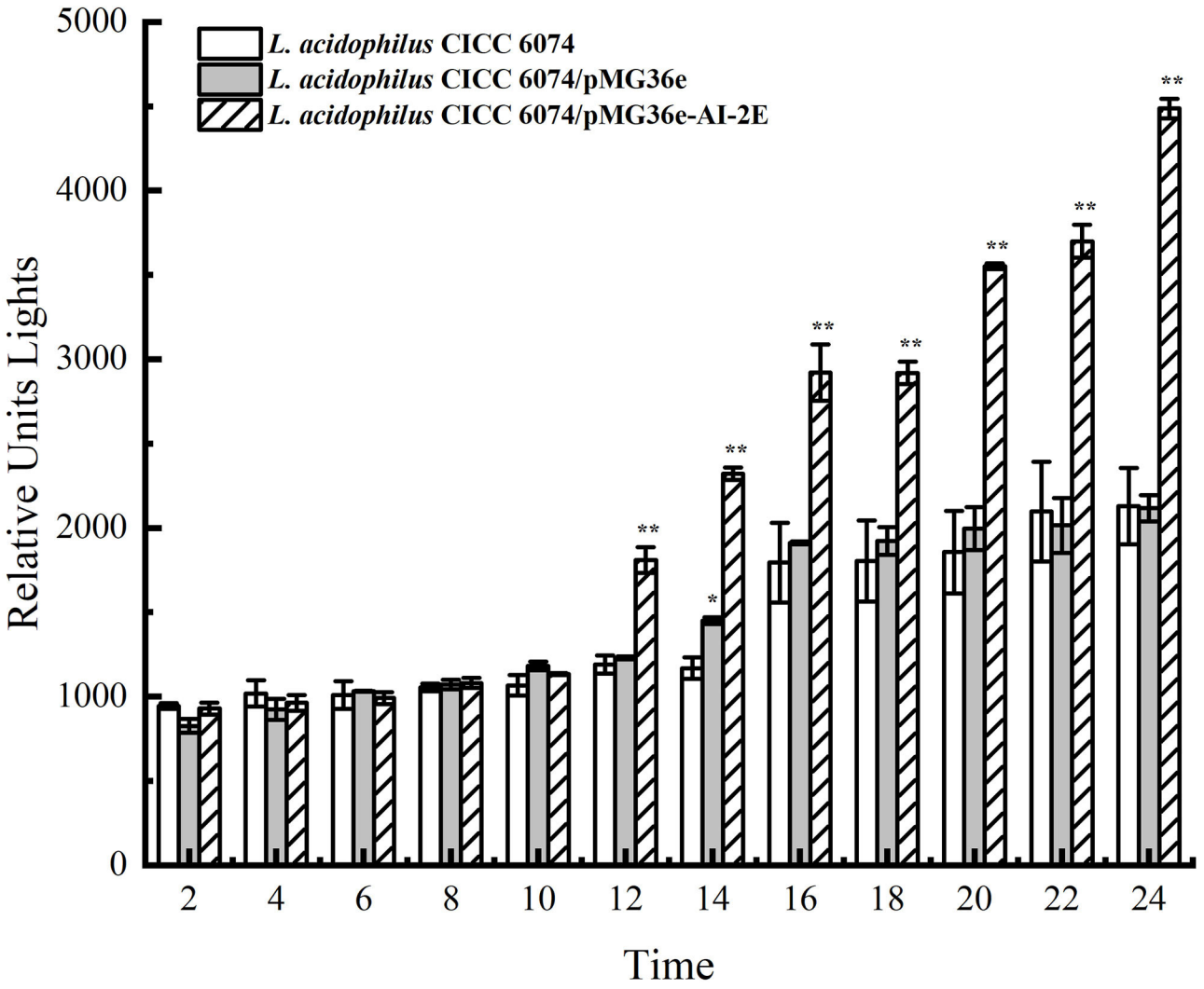

FIGURE 6 | AI-2 activity in culture supernatant with the bacterial cells removed of *Lactobacillus acidophilus* CICC 6074 wild-type strain, *L. acidophilus* CICC 6074/pMG36e recombinant strain, and *L. acidophilus* CICC 6074/pmG36e-AI-2E recombinant strain. Data are presented as mean ± SEM; $n \geq 3$; $^{*}p < 0.05$, $^{**}p < 0.01$ compared with the wild-type strain.

(**Figure 4B**). **Figure 4C** shows the growth of different strains in the LBK medium at different pH. We can see that all strains grew normally or were only very weakly inhibited in pH 7.0, 7.5, and 8.0, whereas the growth of all strains was inhibited completely in the LBK medium at pH 8.5. These phenomena suggest that the AI-2E protein of *L. acidophilus* does not recover the growth of the *E. coli* KNabc strains in saline environments. With the results we have observed so far, the AI-2E protein may not possess Na^+ (Li^+)/H^+ antiporter activity.

Overexpression of AI-2E Protein Promotes AI-2 Secretion in *L. acidophilus* CICC 6074

To verify whether the AI-2E gene was overexpressed in *L. acidophilus* CICC 6074 stain, RT-qPCR was used to detect the relative mRNA content of the AI-2E gene among different strains. As shown in **Figure 5**, the expression of the *AI-2E* gene was upregulated 102.29 times in the *L. acidophilus* CICC 6074/pMG36e-AI-2E relative to the wild-type strain, and no significant difference between the *L. acidophilus* CICC 6074/pMG36e strain and the wild-type strain was found.

Detection of AI-2

The AI-2E proteins are claimed to have the AI-2 exporter activity. To observe the effect of AI-2E overexpression on AI-2 secretion, we detected AI-2 activities in *L. acidophilus* CICC 6074 wild type strain and recombinant strains (*L. acidophilus* CICC 6074/pMG36e and *L. acidophilus* CICC 6074/pMG36e-AI-2E) over 24 h. As shown in **Figure 6**, AI-2 secretion by all strains increased slowly and did not differ significantly among strains in the first 10 h. *L. acidophilus* CICC 6074/pMG36e-AI-2E strain

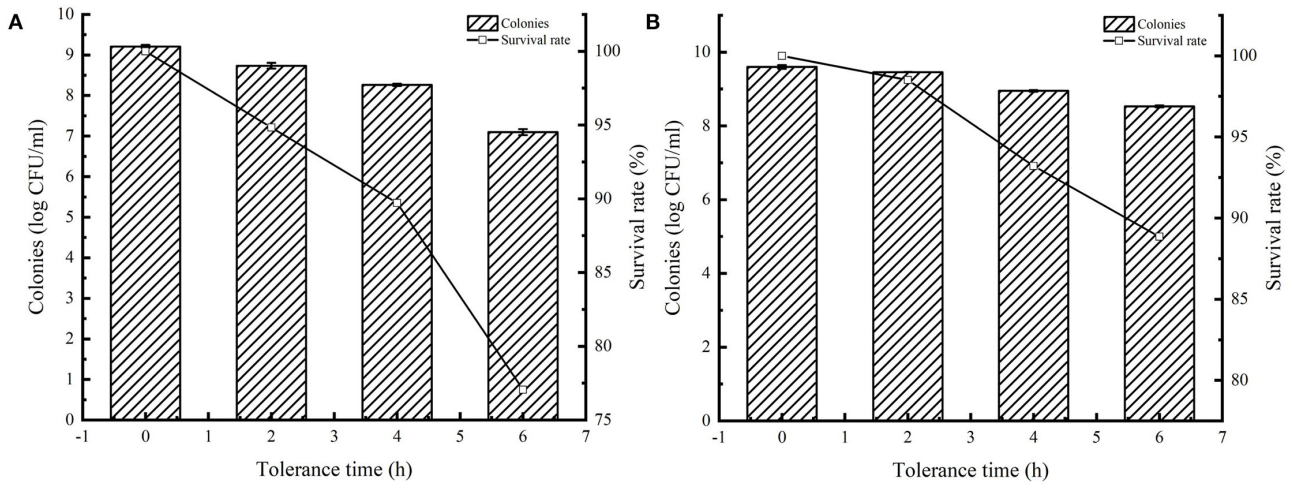

FIGURE 7 | Tolerance of *Lactobacillus acidophilus* CICC 6074 strains in artificial intestinal juice. Survival of *L. acidophilus* CICC 6074/pMG36e recombinant strain after tolerance in artificial intestinal juice **(A)**. Survival of *L. acidophilus* CICC 6074/pMG36e-AI-2E recombinant strain after tolerance in artificial intestinal juice **(B)**.

shows a rapid increase in AI-2 secretion between 12 and 24 h, which is significantly different from the other strains.

Overexpression of AI-2E Protein Improved Intestinal Juice Resistances of *L. acidophilus* CICC 6074

Many studies have reported that AI-2 facilitates bacterial tolerance to the environment. Overexpression of AI-2E enhances AI-2 secretion, and here we tested the tolerance of AI-2E protein overexpressing strain in simulated intestinal juice, and the results are shown in **Figure 7**. **Figure 7A** shows the survival status of the recombinant strain *L. acidophilus* CICC 6074 in simulated intestinal juice tolerated for 6 h. We can see that the viable count of *L. acidophilus* CICC 6074/pMG36e strain decreased from 9.21 log CFU/ml to 7.09 log CFU/ml, and the survival rate decreased to 77.06%. And **Figure 7B** shows that the viable count of AI-2E overexpression strain decreased from 9.42 to 8.89 log CFU/ml after 6 h of intestinal fluid tolerance, and the survival rate decreased to 94.35%. These results indicate that the overexpression of AI-2E protein can effectively enhance the viability of the *L. acidophilus* CICC 6074 strain in the intestinal juice.

DISCUSSION

In the study of Wang et al. (2020) and Shao et al. (2021), the AI-2E protein from the *H. andaensis* and their homolog proteins were also assigned to a single branch during phylogenetic analysis. The function of proteins in this branch was identified as the Na^+ (Li^+)/H^+ antiporter activity and is related to the salinity tolerance of microorganisms. During the phylogenetic analysis, we found that 530 AI-2E proteins belonging to *Lactobacillus* were divided into 11 large clades and some small clades, indicating that the AI-2E family transporter proteins of different species are not conserved. Proteins from different sources may have different functions, which is consistent with the findings of Wang et al. (2020). It was also found that proteins on the same branch tend to belong to several same species, which means that these AI-2E proteins may be relatively conserved within species. When the AI-2E protein of *Lactobacillus* and download from TCBD were used for phylogenetic analysis, it was found that most of the AI-2E proteins of *Lactobacillus* were allocated to one branch alone. The closest to this branch is AI-2 exporter group I. Interestingly, 6 other AI-2E proteins from *Lactobacillus* were assigned to AI-2 exporter group I. These suggest that the function of the AI-2E protein from *L. acidophilus* is most likely AI-2 exporter activity. In addition to protein amino acid sequence, protein structure is also a key point to consider when analyzing protein homology. We predicted the secondary structure and functional domains of AI-2E protein in *L. acidophilus* CICC 6074 strain cells, and the results show there are 8 transmembrane regions on the protein. In the study of Dong et al. (2017), 6 transmembrane domains were predicted in the UPF0118 protein with Na^+ (Li^+)/H^+ antiporter activity. Herzberg et al. (2006) reported that it predicted 8 transmembrane regions from the ydgG protein with AI-2 exporter activity in the *E. coli* K-12 strain, which indicates that the AI-2E protein of *L. acidophilus* is closer to the protein with AI-2 secretion function at least in terms of the number of transmembrane regions.

To verify the function of AI-2E protein in the *L. acidophilus* CICC6074 strain, we expressed it in the *E. coli* KNabc strain and overexpressed it in the *L. acidophilus* CICC6074 strain. The results show that the expressed AI-2E protein could not improve the salt-alkali resistance of *E. coli* KNabc. But could increase the secretion of AI-2 by overexpressing the AI-2E protein in the *L. acidophilus* CICC 6074 strain. All results indicate that the AI-2E in *L. acidophilus* CICC 6074 strain cells may have AI-2 exporter activity. LAB use quorum sensing (QS) to communicate with each other. AI-2 is a signaling molecule for intra-species

and inter-species communication. QS is closely related to the environmental adaptability, biofilm formation, and intestinal epithelial cell adhesion of LAB. The persistence of mutant strains in the gastrointestinal tract of mice was significantly reduced after the *LuxS* gene of *L. rhamnosus* GG was knocked out, and the resistance to gastric juice was recovered after gene backfilling (Lebeer et al., 2008). Jia et al. reported that LuxS/AI-2 is involved in the tolerance of LAB to the gastrointestinal environment. The survival rate of the *L. plantarum* KLDS1.0391 mutant strain with *LuxS* gene knockout in gastric acid and intestinal fluid was significantly lower than that of the wild-type strain (Jia et al., 2018).

Both Na^+ (Li^+)/H^+ antiporter activity and AI-2 exporter activity are related to the environmental adaptability of microorganisms. Dong et al. (2017) found that the AI-2E protein with Na+ (Li+)/H+ antiporter activity is important for the moderate halophile *H. andaensis* that to survive in saline environments. They also found that the expression of AI-2E protein in the *E. coli* KNabc strain could restore the resistance of this strain to salinity (Dong et al., 2017). Buck et al. (2009) reported that AI-2 could enhance the resistance of *L. acidophilus* NCFM to low pH and bile salts. Liu et al. (2018) demonstrated that overexpression of the LuxS protein could produce more AI-2, it could enhance the resistance of *L. paraplantarum* L-ZS9 strain to heat stress and bile salts. These studies indicate that AI-2 can improve the adaptability of LAB to these environments. In bad conditions, LAB can enhance the activity of the AI-2 by increasing the transcription level of the *LuxS* gene, and the presence of the AI-2/LuxS QS system in bacteria can help bacteria survive in the gastrointestinal tract. In our study, we overexpressed the AI-2E protein in the *L. acidophilus* CICC 6074 strain, and the AI-2 activity of this strain has also significantly increased. The results of intestinal juice tolerance show that more AI-2 can significantly improve the survival rate of *L. acidophilus* cells in intestinal juice.

CONCLUSION

In our study, we found that expressing the AI-2E protein in the *E. coli* KNabc strain did not recover the resistance of the bacteria to the saline environment, indicating that the AI-2E protein may not possess Na^+ (Li^+)/H^+ antiporter activity. Overexpression of AI-2E protein in *L. acidophilus* CICC 6074 strain resulted in more AI-2 secretion by the cells, which proves that the AI-2E protein of *L. acidophilus* may have the AI-2 exporter activity. The survival rate of the AI-2E protein overexpression strain is significantly higher than the wild-type strain when growing in intestinal juice. These results indicate that overexpression of AI-2E protein in *L. acidophilus* CICC 6074 strain could promote to secrete of more AI-2, thereby enhancing the viability of LAB cells in intestinal juice.

DATA AVAILABILITY STATEMENT

The original contributions presented in the study are included in the article/supplementary material, further inquiries can be directed to the corresponding author/s.

AUTHOR CONTRIBUTIONS

XL, ZS, and DP conceived and designed the experiments. XL, JX, and YC performed the experiments. XL, TZ, and XF performed bioinformatics analysis. XL wrote the manuscript. DP funded all the expenses for this article. All authors checked and approved the final version of this manuscript.

FUNDING

This work was supported by the Natural Science Foundation of China (31972048), the Science Technology Department of Ningbo (2019C10017 and 202002N3076), and the National Key R&D Program of China (2021YFD2100104).

REFERENCES

Azcarate-Peril, M. A., Altermann, E., Hoover-Fitzula, R. L., Cano, R. J., and Klaenhammer, T. R. (2004). Identification and inactivation of genetic loci involved with *Lactobacillus acidophilus* acid tolerance. *Appl. Environ. Microbiol.* 70, 5315–5322. doi: 10.1128/AEM.70.9.5315-5322.2004

Bove, P., Capozzi, V., Garofalo, C., Rieu, A., Spano, G., and Fiocco, D. (2012). Inactivation of the ftsH gene of *Lactobacillus plantarum* WCFS1: effects on growth, stress tolerance, cell surface properties and biofilm formation. *Microbiol. Res.* 167, 187–193. doi: 10.1016/j.micres.2011.07.001

Buck, B., Azcarate-Peril, M., and Klaenhammer, T. (2009). Role of autoinducer-2 on the adhesion ability of *Lactobacillus acidophilus*. *J. Appl. Microbiol.* 107, 269–279. doi: 10.1111/j.1365-2672.2009.04204.x

Chen, B., Lin, X., Lin, X., Li, W., Zheng, B., and He, Z. (2020). Pectin-microfibrillated cellulose microgel: Effects on survival of lactic acid bacteria in a simulated gastrointestinal tract. *Int. J. Biol. Macromol.* 158, 826–836. doi: 10.1016/j.ijbiomac.2020.04.161

Damodharan, K., Palaniyandi, S. A., Yang, S. H., and Suh, J. W. (2017). Co-encapsulation of lactic acid bacteria and prebiotic with alginate-fenugreek gum-locust bean gum matrix: viability of encapsulated bacteria under simulated gastrointestinal condition and during storage time. *Biotechnol. Bioprocess Eng.* 22, 265–271. doi: 10.1007/s12257-017-0096-1

Dong, P., Wang, L., Song, N., Yang, L., Chen, J., Yan, M., et al. (2017). A UPF0118 family protein with uncharacterized function from the moderate halophile *Halobacillus andaensis* represents a novel class of Na+ (Li+)/H+ antiporter. *Sci. Rep.* 7, 1–11. doi: 10.1038/srep45936

Fiocco, D., Capozzi, V., Goffin, P., Hols, P., and Spano, G. (2007). Improved adaptation to heat, cold, and solvent tolerance in *Lactobacillus plantarum*. *Appl. Microbiol. Biotechnol.* 77, 909–915. doi: 10.1007/s00253-007-1228-x

Ghibaudo, F., Gerbino, E., Dall'Orto, V. C., and Gómez-Zavaglia, A. (2017). Pectin-iron capsules: novel system to stabilise and deliver lactic acid bacteria. *J. Funct. Foods* 39, 299–305. doi: 10.1016/j.jff.2017.10.028

Goh, Y. J., Azcárate-Peril, M. A., O'Flaherty, S., Durmaz, E., Valence, F., Jardin, J., et al. (2009). Development and application of a upp-based counterselective gene replacement system for the study of the S-layer protein SlpX of *Lactobacillus acidophilus* NCFM. *Appl. Environ. Microbiol.* 75, 3093–3105. doi: 10.1128/AEM.02502-08

Herzberg, M., Kaye, I. K., Peti, W., and Wood, T. K. (2006). YdgG (TqsA) controls biofilm formation in *Escherichia coli* K-12 through autoinducer 2 transport. *J. Bacteriol.* 188, 587–598. doi: 10.1128/JB.188.2.587-598.2006

Jia, F.-F., Zheng, H.-Q., Sun, S.-R., Pang, X.-H., Liang, Y., Shang, J.-C., et al. (2018). Role of luxS in stress tolerance and adhesion ability in *Lactobacillus plantarum* KLDS1. 0391. *BioMed Res. Int.* 2018, 4506829. doi: 10.1155/2018/4506829

Jin, H., Higashikawa, F., Noda, M., Zhao, X., Matoba, Y., Kumagai, T., et al. (2010). Establishment of an in vitro Peyer's patch cell culture system correlative to in vivo study using intestine and screening of lactic acid bacteria enhancing intestinal immunity. *Biol. Pharm. Bull.* 33, 289–293. doi: 10.1248/bpb.33.289

Karimi, R., Mortazavian, A. M., and Da Cruz, A. G. (2011). Viability of probiotic microorganisms in cheese during production and storage: a review. *Dairy Sci. Technol.* 91, 283–308. doi: 10.1007/s13594-011-0005-x

Kostelac, D., Gerić, M., Gajski, G., Markov, K., Domijan, A. M., Canak, I., et al. (2021). Lactic acid bacteria isolated from equid milk and their extracellular metabolites show great probiotic properties and anti-inflammatory potential. *Int. Dairy J.* 112, 104828. doi: 10.1016/j.idairyj.2020.104828

Lebeer, S., Claes, I. J., Verhoeven, T. L., Shen, C., Lambrichts, I., Ceuppens, J. L., et al. (2008). Impact of luxS and suppressor mutations on the gastrointestinal transit of *Lactobacillus rhamnosus GG*. *Am. Soc. Microbiol.* 74, 4711–4718. doi: 10.1128/AEM.00133-08

Liu, L., Wu, R., Zhang, J., and Li, P. (2018). Overexpression of luxS promotes stress resistance and biofilm formation of *Lactobacillus paraplantarum* L-ZS9 by regulating the expression of multiple genes. *Front. Microbiol.* 9, 2628. doi: 10.3389/fmicb.2018.02628

Lorca, G. L., Barabote, R. D., Zlotopolski, V., Tran, C., Winnen, B., Hvorup, R. N., et al. (2007). Transport capabilities of eleven gram-positive bacteria: comparative genomic analyses. *Biochimica et Biophysica Acta Biomembranes* 1768, 1342–1366. doi: 10.1016/j.bbamem.2007.02.007

Majernik, A., Gottschalk, G., and Daniel, R. (2001). Screening of environmental DNA libraries for the presence of genes conferring $Na^+(Li^+)/H^+$ antiporter activity on *Escherichia coli*: characterization of the recovered genes and the corresponding gene products. *J. Bacteriol.* 183, 6645–6653. doi: 10.1128/JB.183.22.6645-6653.2001

Maragkoudakis, P. A., Zoumpopoulou, G., Miaris, C., Kalantzopoulos, G., Pot, B., and Tsakalidou, E. (2006). Probiotic potential of *Lactobacillus* strains isolated from dairy products. *Int. Dairy J.* 16, 189–199. doi: 10.1016/j.idairyj.2005.02.009

Michael, D. V., Anna, S., Bernd, R., Susanne, F., Christiane, L., and Jürgen, S. (2001). Probiotics—compensation for lactase insufficiency. *Am. J. Clin. Nutr.* 73, 421S. doi: 10.1093/ajcn/73.2.421s

Nguyen, T. H., Kim, Y., Kim, J.-S., Jeong, Y., Park, H. M., Kim, J. W., et al. (2020). Evaluating the cryoprotective encapsulation of the lactic acid bacteria in simulated gastrointestinal conditions. *Biotechnol. Bioprocess Eng.* 25, 287–292. doi: 10.1007/s12257-019-0406-x

Palomino, M. M., Allievi, M. C., Prado-Acosta, M., Sanchez-Rivas, C., and Ruzal, S. M. (2010). New method for electroporation of *Lactobacillus* species grown in high salt. *J. Microbiol. Methods* 83, 164–167. doi: 10.1016/j.mimet.2010.08.017

Patnaik, R., Louie, S., Gavrilovic, V., Perry, K., Stemmer, W. P., Ryan, C. M., et al. (2002). Genome shuffling of *Lactobacillus* for improved acid tolerance. *Nat. Biotechnol.* 20, 707–712. doi: 10.1038/nbt0702-707

Pfeiler, E. A., Azcarate-Peril, M. A., and Klaenhammer, T. R. (2007). Characterization of a novel bile-inducible operon encoding a two-component regulatory system in *Lactobacillus acidophilus*. *J. Bacteriol.* 189, 4624–4634. doi: 10.1128/JB.00337-07

Pfeiler, E. A., and Klaenhammer, T. R. (2009). Role of transporter proteins in bile tolerance of *Lactobacillus acidophilus*. *Appl. Environ. Microbiol.* 75, 6013–6016. doi: 10.1128/AEM.00495-09

Ranadheera, C. S., Evans, C. A., Adams, M. C., and Baines, S. K. (2014). Effect of dairy probiotic combinations on in vitro gastrointestinal tolerance, intestinal epithelial cell adhesion and cytokine secretion. *J. Funct. Foods* 8, 18–25. doi: 10.1016/j.jff.2014.02.022

Ranadheera, R., Baines, S., and Adams, M. (2010). Importance of food in probiotic efficacy. *Food Res. Int.* 43, 1–7. doi: 10.1016/j.foodres.2009.09.009

Rettner, R. E., and Saier Jr, M. H. (2010). The autoinducer-2 exporter superfamily. *Microbial Physiol.* 18, 195–205. doi: 10.1159/000316420

Sakamoto, I., Igarashi, M., Kimura, K., Takagi, A., Miwa, T., and Koga, Y. (2001). Suppressive effect of *Lactobacillus gasseri* OLL 2716 (LG21) on *Helicobacter pylori* infection in humans. *J. Antimicrob. Chemother.* 47, 709–710. doi: 10.1093/jac/47.5.709

Shao, L., Abdel-Motaal, H., Chen, J., Chen, H., Xu, T., Meng, L., et al. (2018). Characterization of a functionally unknown arginine–aspartate–aspartate family protein from *Halobacillus andaensis* and functional analysis of its conserved arginine/aspartate residues. *Front. Microbiol.* 9, 807. doi: 10.3389/fmicb.2018.00807

Shao, L., Xu, T., Zheng, X., Shao, D., Zhang, H., Chen, H., et al. (2021). A novel three-TMH Na^+/H^+ antiporter and the functional role of its oligomerization. *J. Mol. Biol.* 433, 166730. doi: 10.1016/j.jmb.2020.166730

Wang, L., Zou, Q., Yan, M., Wang, Y., Guo, S., Zhang, R., et al. (2020). Polar or charged residues located in four highly conserved motifs play a vital role in the function or pH response of a UPF0118 family $Na^+(Li^+)/H^+$ antiporter. *Front. Microbiol.* 11, 841. doi: 10.3389/fmicb.2020.00841

Wang, X.-Y., and Xie, J. (2020). Quorum sensing system-regulated proteins affect the spoilage potential of co-cultured *Acinetobacter johnsonii* and *Pseudomonas fluorescens* from spoiled bigeye tuna (*Thunnus obesus*) as determined by proteomic analysis. *Front. Microbiol.* 11, 940. doi: 10.3389/fmicb.2020.00940

Conflict of Interest: The authors declare that the research was conducted in the absence of any commercial or financial relationships that could be construed as a potential conflict of interest.

Publisher's Note: All claims expressed in this article are solely those of the authors and do not necessarily represent those of their affiliated organizations, or those of the publisher, the editors and the reviewers. Any product that may be evaluated in this article, or claim that may be made by its manufacturer, is not guaranteed or endorsed by the publisher.

frontiers | Frontiers in Microbiology

ORIGINAL RESEARCH
published: 14 June 2022
doi: 10.3389/fmicb.2022.906920

Akkermansia muciniphila Alters Gut Microbiota and Immune System to Improve Cardiovascular Diseases in Murine Model

*Xin He[1], Yang Bai[2], Haiyang Zhou[2] and Kemin Wu[2,3]**

[1] Department of Anesthesiology, Xiangya Hospital, Central South University, Changsha, China, [2] Department of General and Vascular Surgery, Xiangya Hospital, Central South University, Changsha, China, [3] National Clinical Research Center for Geriatric Disorders, Xiangya Hospital, Changsha, China

The gut microbiota plays an important role in a variety of cardiovascular diseases. The probiotics screened based on microbiota can effectively improve metabolism and immune function of the body, which is of great value in the field of cardiovascular disease treatment. Abdominal aortic aneurysms (AAA) refer to the lesion or injury of the abdominal aortic wall resulting in a localized bulge, which is one of the cardiovascular diseases with pulsing mass as the main clinical symptom. Previous studies have confirmed that *A. muciniphila* was depleted in the guts of AAA patients or mice. *A. muciniphila* is a potential probiotic for the treatment of intestinal microbiome-related diseases. Therefore, this study aims to investigate the effects of *A. muciniphila* on gut microbiota and disease-related biomarkers in AAA mice. C57BL/6J mice were used to construct the AAA model and treated with *A. muciniphila*. Aortic aneurysm formation in the AAA group is associated with the increased diameter of the abdominal aorta and inflammatory infiltration. *A. muciniphila* inhibited the formation of AAA and repaired tissue damage. The number of gut microbiota and α diversity index were decreased in the model group. *A. muciniphila* increased the number of gut microbiota and α diversity in AAA mice. The abundance of *uncultured bacterium* and *Lactobacillus* were increased, while the abundance of the *Lachnospiraceae NK4A136 group* was reduced in the AAA group. Compared with the control group, the levels of MMP-1, MMP-9, IL-33, CTSB, and CTSL in tissue and the levels of IL-6, IFN-γ, and CRP in blood were significantly increased, and the levels of IL-4, IL-10, and IL-17A in blood were significantly decreased in the AAA group. The intervention of *A. muciniphila* reversed these changes. The gut microbiota function prediction showed changes in *E. coli*, *Clostridium*, and *Lactobacillus* metabolism-related functional pathways. *Akkermansia* was negatively correlated with *Helicobacter* and *Lactobacillus* and positively correlated with *Clostridium_sensu_stricto_1* and *Escherichia shigella* at the genus level. In conclusion, *A. muciniphila* inhibited the formation of AAA by restoring gut microbiota diversity, altering the expression of peripheral immune factors, and the functions of *E. coli*, *Clostridium*, and *Lactobacillus*, which may provide a new theoretical basis for the application of probiotics in cardiovascular diseases.

Keywords: *Akkermansia muciniphila*, intestinal microbiology, microbial structure, abdominal aortic aneurysm, microbial physiology

OPEN ACCESS

Edited by:
Rina Wu,
Shenyang Agricultural University, China

Reviewed by:
Zuheng Liu,
The First Affiliated Hospital of Xiamen University, China
Walaa K. Mousa,
Mansoura University, Egypt

***Correspondence:**
Kemin Wu
wkmcsu2021@163.com

Specialty section:
This article was submitted to Food Microbiology, a section of the journal Frontiers in Microbiology

Received: *29 March 2022*
Accepted: *19 May 2022*
Published: *14 June 2022*

Citation:
He X, Bai Y, Zhou H and Wu K (2022) Akkermansia muciniphila Alters Gut Microbiota and Immune System to Improve Cardiovascular Diseases in Murine Model. Front. Microbiol. 13:906920. doi: 10.3389/fmicb.2022.906920

INTRODUCTION

Abdominal aortic aneurysm (AAA) is one of many diseases associated with inflammatory cell infiltration, matrix protein degradation, and smooth muscle cell apoptosis (Liu et al., 2019). AAA is the most commonly defined as having a maximum diameter of the abdominal aorta greater than 3 cm in anteriorly or cross-section, or having a focal dilation greater than 1.5 times the diameter of a normal adjacent artery segment (Wang et al., 2018). The pathological manifestations of AAA in human and animal models showed obvious immune cell infiltration and upregulated expression of pro-inflammatory cytokines, suggesting that inflammation plays an important role in the formation of AAA (Li Y. et al., 2019; Tsai and Xian, 2019). Functional enrichment analysis showed the level of granulocyte colony-stimulating factor (G-CSF), milk fat globule-EGF factor 8 protein (MFG-E8), macrophage inflammatory protein 1 g (MIP-1g), and cardiotrophin 1 (CT-1) were positively correlated with IL-33, periostin, matrix metalloproteinase-1 (MMP-1), matrix metalloproteinase-9 (MMP-9), cathepsin B (CTSB), and cathepsin L (CTSL) in AAA mice (Li Y. et al., 2019). IL-33 is a pliotropic cytokine with multiple immunomodulatory effects (Li J. et al., 2019). Exogenous IL-33 (daily intraperitoneal administration of recombinant IL-33 or transgenic IL-33 expression) protected mice from the effects of AAA formation by enhancing ST2-dependent aortic and systemic regulatory T-cell amplification (Li J. et al., 2019). These studies suggest that these cytokines may be involved in the formation of AAA by affecting protease activity, providing a series of meaningful targets for the study of biomarkers and molecular mechanisms of AAA.

Coronary artery disease is the most common health problem worldwide and remains a leading cause for morbidity and mortality (Kazemian et al., 2020). The gut microbiota plays an important role in a variety of cardiovascular diseases, such as atherosclerosis and hypertension associated with AAA (Jie et al., 2017; Peng et al., 2018). The 16S rRNA gene sequence analysis of the gut microbiota of AAA mice revealed that the gut microbiota was different between the normal and AAA mice, and the changes of *Akkermansia*, *Odoribacter*, *Helicobacter*, and *Ruminococcus* may participate in the development of AAA (Lindskog Jonsson et al., 2018; Xie et al., 2020). The relative abundance of *A. muciniphila* in the gut of AAA mice was significantly decreased, and the diameter of the abdominal aorta was negatively correlated with *A. muciniphila* in AAA mice (Xie et al., 2020). *A. muciniphila* is a kind of intestinal symbiotic bacteria stably colonized in the intestinal mucus layer, which is considered as one of the candidate strains for the next generation of probiotics (Geerlings et al., 2018). *A. muciniphila* can effectively improve the metabolism and immune function of the body in its host (Zhang et al., 2019). *A. muciniphila* may be used as one of the new probiotics for the treatment of AAA.

Since *A. muciniphila* was first described in 2004, many studies have been conducted (Hagi and Belzer, 2021). A number of studies have shown that *A. muciniphila* is a promising target for the treatment of gut microbiota-related diseases, such as colitis, metabolic syndrome, and immune diseases (Zhou, 2017). Oral administration of *A. muciniphila* in diabetic Sprague–Dawley rats has been shown to improve liver function, reduce glucose/lipid toxicity, reduce oxidative stress, inhibit inflammation, normalize gut microbiota, and improve type 2 diabetes (Zhang et al., 2018). *A. muciniphila* combined with cisplatin (CDDP) can enhance immune regulation by regulating the differentiation of Th17 cells in mice (Chen et al., 2020). Amuc_1100, a specific protein isolated from *A. muciniphila*'s outer membrane, can interact with Toll-like receptor 2 to improve the intestinal barrier and play a probiotic role (Plovier et al., 2017). *A. muciniphila* secretes an 84 kDa protein (P9) that increases thermogenesis and glucagon-like peptide-1 (GLP-1) secretion by inducing uncoupling protein 1 in brown adipose tissue and throughout the body in high-fat diet (HFD) induced C57BL/6J mice (Yoon et al., 2021). The above studies have proved that *A. muciniphila* can regulate the gene function and intestinal homeostasis of the host through autocrine or probiotic effects and improve the disease characterization.

Akkermansia muciniphila ameliorates inflammation caused by metabolic endotoxemia by restoring the intestinal barrier, thereby reducing atherosclerotic lesions (Li et al., 2016). Treatment with active *A. muciniphila* reversed metabolic disorders associated with a high-fat diet, including increased fat mass, metabolic endotoxemia, adipose tissue inflammation, and insulin resistance, while heat-killing *A. muciniphila* treatment did not improve metabolic characteristics or mucous layer thickness (Everard et al., 2013). Clinical data suggest that oral administration of *A. muciniphila* is safe, but its effect needs to be further verified in a larger sample size clinical trial (Zhou, 2017; Depommier et al., 2020). However, as a new probiotic, the role of *A. muciniphila* in the occurrence of AAA disease is still unknown. In this study, *A. muciniphila* was used to treat AAA mice, and 16S rRNA gene sequence was used to analyze the gut microbiota function and cytokine expression in order to clarify the potential mechanism of *A. muciniphila* in the treatment of AAA.

MATERIALS AND METHODS

Culture and Preparation of *A. muciniphila*

Akkermansia muciniphila (ATCC-BAA-865, DSM 22959) was purchased from BioVector NTCC Inc., Anaerobic culture of *A. muciniphila* (DSM 22959) in the culture medium of brain and heart infusion containing 1‰ L-cysteine for 48 h. The culture was centrifuged at 6,680 × *g* for 10 min. Then, the supernatant was discarded. The *A. muciniphila* were heavily suspended in a sterile mercaptoacetate/phosphate buffer (PBS) solution containing 25% (v/v) glycerol under anaerobic conditions. The concentration of the oral solution of *A. muciniphila* was adjusted to 1×10^8 CFU mL^{-1}, and the same concentration of the oral solution was inactivated by pasteurization at 70°C for 30 min. Bacterial concentrations were determined by plate counting using brain and heart extract agar (Land Bridge Technology Corporation, Beijing, China). Inactivated *A. muciniphila* suspension was stored at –80°C.

Animal Experiments and Grouping

A total of 50 male C57BL/6J mice aged 5–6 months were used in this study. All mice were kept in cages and raised

in a temperature-controlled room at 22–26°C with relative humidity of 45%–60% and standard food and water on a 12/12 h light and dark cycle. Mice were randomly divided into five groups, including the control group, sham group, AAA group, AAA + Am group, and AAA + Inactivated Am group, 10/group/squirrel cage. The mice in the AAA group and sham group were anesthetized by intraperitoneal injection of pentobarbital (40 mg kg^{-1}), and induced by $CaCl_2$ and NaCl (0.9%), respectively (Zhong et al., 2019). The mice in the AAA + Am group and AAA + Inactivated Am group were given 2×10^8 CFU/180 μl of *A. muciniphila* by oral gavage. The mice in the AAA group and sham group were given the same dose of sterile PBS by oral gavage. There was no treatment in the control group. On the 28th day of the experiment, fecal samples were collected and stored at −80°C. The experimental design flowchart is shown in the **Figure 1A**. Of note, 5 fecal samples were collected from each group in the squirrel cage with 10 mice/group. Mice were sacrificed with an overdose of pentobarbital (500 mg kg^{-1}), then 0.9% normal saline was injected into the left ventricle at a slow and uniform rate, and the right atrial appendage was cut. The blood flowed out of the right atrial appendage until no blood color was found. The PBS injection was stopped, and the aorta (from the aortic arch to the iliac abdominal aorta bifurcation) was taken. The aorta was dissected under an anatomical microscope (the aorta was placed in a petri dish filled with 0.9% normal saline). Fat and connective tissues attached to the outer membrane of the aorta were removed. The aorta was photographed, and the diameter of the abdominal aorta was measured.

Abdominal Aortic Aneurysms Model Construction

Male C57BL/6J mice were anesthetized by an intraperitoneal injection of pentobarbital (40 mg kg^{-1}) before laparotomy. The abdominal aortic passages below the renal artery and above the bifurcation of the artery were isolated from the surrounding retroperitoneal structures. Then, cotton gauze containing 0.5 mol L^{-1} $CaCl_2$ was spread on the outer surface of the aortic passage for 15 min. The aorta was then rinsed with 0.9% sterile saline and the incision was closed. All model mice were euthanized 28 days after $CaCl_2$ stimulation under different treatment groups.

16S rRNA Gene Sequencing and Analysis

On the 28th day of the experiment, fecal samples were collected and stored at −80°C. DNA was extracted from 200 mg fecal sample using the fecal genomic DNA extraction kit (tiangen.cat.# dp328-02) as per the manufacturer's instructions. The dsDNA HS Assay Kit for Qubit (Shanghai Yishen Biotechnology Co., Ltd., CAT.12640ES76) was used for concentration detection. Phusion enzyme (ApexBio K1031) and primers in the V3-V4 region of the 16S rRNA gene (357F 5′-ACTCCTACGGRAGGCAGCAG-3′ and 806R 5′-GGACTACHVGGGTWTCTCATAT-3′) were used for PCR amplification and adaptor addition. The magnetic beads were sorted using BMSX-200 kit (Wuxi Baimag Biotechnology Co., Ltd.). Agarose Gel DNA Recovery Kit (Tiangen.cat.# dp209-03) was used for DNA recovery. Mixed samples were sequenced by Illumina NovaseQ6000 PE250 to obtain raw data. QIIME 2 (version 2020.2) and DADA2 were used for quality control of raw data to obtain clean data that could be used for subsequent analysis (Caporaso et al., 2010). Qiime2 was used to train the classifier in the silva-132-99 representative sequence database for species annotation and representative sequence alignment for each ASV/OTU sequence (Pruesse et al., 2007). QIIME 2 (version 2020.2) and R software (version 4.0.2) were used for sequence data analysis (Caporaso et al., 2010). QIIME2 software was used to calculate the alpha diversity index (e.g., Chao1, ACE, Shannon, and Simpson evenness index) and draw the ranked abundance curve based on ASV and a dilution curve based on alpha diversity. R software (version 4.0.2) was used to draw the histogram of relative species abundance (R ggplot2 package), the heatmap of genus abundance (R reshape2/ggplot2 package), the box plot of alpha diversity difference (R phyloseq package), the principal component analysis (PCA) and non-metric multidimensional scaling (NMDS) based on the Bray-Curtis distance (phyloseq/vegan package), and the phylogenetic diversity analysis based on the Wald test (R DESeq2 package). Venn diagrams first used R software (Venn diagram package) to generate the list of ASVs owned by samples or groups and then used jvenn[1] web pages to visualize common and specific ASVs between samples or groups. Phylogenetic investigation of communities by reconstruction of unobserved states (PICRUSt[2]) and the MetaCyc database[3] were used for microbial function prediction (Klindworth et al., 2013). Linear discriminant analysis (LDA) effect size (LefSe[4]) was used to analyze the MetaCyc pathways (Li et al., 2020).

ELISA Assay

The samples of abdominal aorta tissues were collected and washed with precooled PBS (0.02 mol L^{-1}, pH 7.0–7.2). The abdominal aorta tissues were cut into small pieces and put into a tissue grinder (homogenate tube). Then, 500 μl PBS was added to prepare a homogenate. The tissue homogenate was freeze-thawed 1–2 times overnight and centrifuged at 5,000 × *g* at 2–8°C for 5 min to get the supernatant. The whole blood samples were placed at room temperature for 2 h, centrifuged at 1,000 × *g* at 2–8°C for 15 min. After that, the supernatant was taken for detection. According to the manufacturer's instructions, the levels of MMP-1 (ml037721, Shanghai Meilian, Shanghai, China), MMP-9 (CSB-E08007m, CUSABIO, Wuhan, China), CTSB (CSB-EL006185MO, CUSABIO, Wuhan, China), CTSL (E-EL-M0251c, Elabscience, Wuhan, China), IL-4 (CSB-E04634m, CUSABIO, Wuhan, China), IL-6 (CSB-E04639m, CUSABIO, Wuhan, China), IL-10 (CSB-E04594m, CUSABIO, Wuhan, China), IL-17A (CSB-E04608m, CUSABIO, Wuhan, China), IFN-γ (CSB-E04578m, CUSABIO, Wuhan, China), and C-reactive protein (CRP, CSB-E07922r, CUSABIO, Wuhan, China) were analyzed by ELISA assay.

[1]http://www.bioinformatics.com.cn/static/others/jvenn/example.html
[2]https://github.com/picrust/picrust2
[3]https://metacyc.org/
[4]https://github.com/SegataLab/lefse

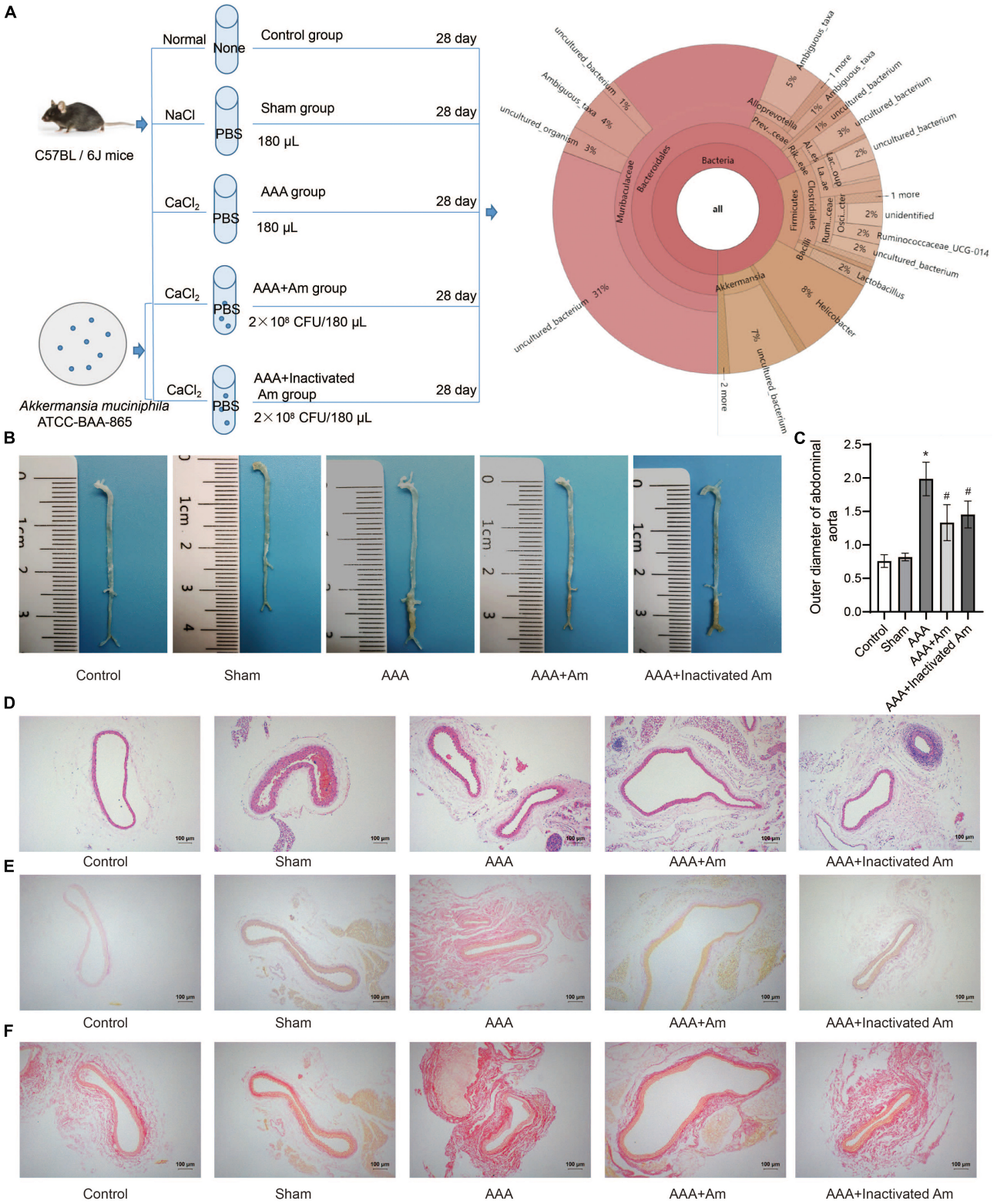

FIGURE 1 | *A. muciniphila* inhibit the formation of AAA. **(A)** The experimental design flowchart. **(B)** The distribution of abdominal aortic aneurysms in mice under different treatments. **(C)** The abdominal aortic dilatation degree of rats in different treatment groups. **(D)** HE staining was used to observe the pathological changes of abdominal aorta. **(E,F)** The distribution of collagen fibers was observed by picrosirius red staining and Van Gieson staining. Data were shown as means ± SD and analyzed by two-way ANOVA ($n = 10$ mice/group). *Compared with the control group, $P < 0.05$; #compared with the AAA group, $P < 0.05$.

Hematoxylin-Eosin Staining

The abdominal aortic tissue samples of mice were taken and fixed in 4% paraformaldehyde for 24 h, followed by gradient dehydration with 20% and 30% sucrose solutions. The abdominal aortic tissue was sliced, dehydrated, embedded in paraffin, successively sliced with a paraffin slicer, connected to the treated glass slides, and baked at 60°C for 12 h. The slices were placed in xylene for 20 min × 3 times. Then, the slices were placed in 100%, 95%, 85%, and 75% ethanol successively for 5 min at each stage for dewaxing to water. Hematoxylin (Wellbio, Changsha, China) was dyed for 3 min, washed with distilled water, and PBS was returned to blue. The slices were dyed with eosin (Wellbio, Changsha, China) for 5 s and rinsed with distilled water. The slices were soaked in gradient alcohol (95–100%) and dehydrated for 5 min per grade. After removal, the slices were placed in xylene for 10 min × 2 times, sealed with neutral gum, and observed under a microscope (BA210T, Motic).

Picrosirius Red and Van Gieson Staining

The slices were baked at 160°C for 12 h. The slices were placed in xylene for 20 min × 3 times. Then, the slices were placed in 100, 95, 85, and 75% ethanol successively for 5 min at each stage for dewaxing to water. Picrosirius red staining solution (Wellbio, Changsha, China) was dyed for 10 min. After that, the slices were rinsed with distilled water and then rinsed with running water for 5 s. Van Gieson staining solution (Wellbio, Changsha, China) was also dyed for 2 min. After that, the slices were rinsed with distilled water and then with tap water for 5 s. The slices were soaked with gradient alcohol (95–100%) and dehydrated for 5 min per grade. After removal, the slices were placed in xylene for 10 min × 2 times, sealed with neutral gum, and observed under a microscope (BA210T, Motic).

Immunohistochemistry

The slices were immersed in 0.01 M citrate buffer (pH 6.0), heated continuously in an electric furnace or microwave oven for 20 min for thermal repair of antigen. The endogenous enzyme was inactivated by adding 1% periodate acid at room temperature for 10 min. Primary antibody IL-33 (12372-1-AP, 1:200, Proteintech, United States) was incubated overnight at 4°C, followed by the secondary antibody anti-rabbit-IgG-HRP polymer at 37°C. Finally, the slices were visualized with diaminobenzidine (DAB, ZSGB-Bio, Peking, China) substrate, re-dyed with hematoxylin, gradient dehydration with all levels of alcohol (60–100%), neutral gum seal, and microscopically observed. The IPP (Image-Pro-Plus) software was used for image analysis and processing.

Real-Time Reverse Transcription-PCR Assay

The abdominal aorta tissues of mice in different treatment groups were collected. Total RNA in tissues was extracted by Trizol reagent (Thermo Fisher Scientific, MA, United States). The Hifiscript cDNA Synthesis Kit (Covin Biosciences, Changsha, China) was used for cDNA synthesis. Then quantitative real-time PCR was carried out by using an UltraSYBR mixture (Covin Biosciences, Changsha, China). The primers for IL-33 were designed by using Primer 5 software after searching for the target gene mRNA sequences on NCBI. The sequences for primers were listed as follows: IL-33, sense 5′-ATTCTTGGCTTACGATGTTGT-3′; antisense 5′-TCCTTCAGTTTCTTTACCAACGC-3′. GAPDH, sense 5′-GC GACTTCAACAGCAACTCCC-3′; antisense 5′-CACCCTGTT GCTGTAGCCGTA-3′. GAPDH was used as an internal control to calculate the target genes expression by using the $2^{-\Delta\Delta Ct}$ method.

Western Blot

After the experiment, the abdominal aorta tissues of mice in different treatment groups were collected. The proteins were extracted and determined by radioimmunoprecipitation analysis (RIPA), lysis buffer, and BCA (bicinchoninic acid) method. A total of 200 μg protein samples were separated by 12% sodium dodecyl sulfate polyacrylamide gel electrophoresis (SDS-PAGE). The isolated proteins were transferred to a polyvinylidene fluoride membrane that had been activated by methanol and blocked by 5% skim milk, and dried at room temperature for at least 1 h. Then, membranes were incubated with primary antibodies anti-IL-33 (1:1,000, ab187060, Abcam, United States), anti-PCNA (1:5,000, 10205-2-AP, proteintech, United States), anti-OPN (1:2,000, 22952-1-AP, proteintech, United States), anti-α-SMA (1:1,000, 14395-1-AP, proteintech, United States), and anti-β-actin (1:5,000, 60008-1-Ig, Proteintech, United States) for overnight at 4°C. After being washed with cold TBST, the membranes were incubated with horseradish peroxidase-conjugated secondary antibodies anti-IgG (1:5,000, SA00001-1; 1:6,000, SA00001-2, Proteintech, United States). Finally, the specific proteins were visualized with enhanced chemiluminescence detection reagent (Thermofisher, United States). The quantification was performed by dividing the intensity of each target protein with the intensity of total β-actin on the blot.

Analysis and Statistics

The statistical software SPSS 21.0 (IBM, United States) was used to analyze the data in this study. All the data were presented as means ± SD. Statistical significance between two groups within experiments was determined by unpaired two-tailed Student's *t*-tests and among more than two groups using ANOVA; $N = 5$ samples/group; P-value < 0.05 was considered statistically significant.

RESULTS

Akkermansia muciniphila Inhibited the Formation of Abdominal Aortic Aneurysms in Mice

The experimental design flowchart is shown in **Figure 1A**. After the experiment, the observation of aortic aneurysm showed that compared with the control group, aortic aneurysm was formed in the AAA group, indicating that the model construction was successful (**Figure 1B**). Compared with the

AAA group, the distribution of aortic aneurysm was reduced in the AAA + Am and AAA + Inactivated Am groups, indicating that *A. muciniphila* inhibited the formation of aortic aneurysm in AAA mice (**Figure 1B**). The measurement of the maximum diameter of the abdominal aorta showed that the AAA group had the largest diameter, and the diameter of the abdominal aorta decreased significantly after *A. muciniphila* intervention (**Figure 1C**). Hematoxylin-eosin (HE) staining showed thinning of the middle membrane of the abdominal aorta tissue and an obvious accumulation of inflammatory cells in the middle and outer membrane in AAA mice (**Figure 1D**). Picrosirius red and van Gieson staining showed that the elastic fibers of the vascular wall were degraded, continuity was interrupted, and a large number of inflammatory cells invaded the septum (**Figures 1E,F**). The intervention of *A. muciniphila* improved the injury of elastic fibers in the vascular wall, inhibited the infiltration of inflammatory cells, and protected the integrity of the septum media in the abdominal aorta of AAA mice (**Figures 1D–F**). The above results indicated that *A. muciniphila* could inhibit the formation of aortic aneurysms in AAA mice.

Akkermansia muciniphila Affected the Diversity and Composition of the Gut Microbiota in Abdominal Aortic Aneurysms Mice

The rank abundance curve showed that with the increase of sequencing depth, the read abundance of each sample increased exponentially and reached the plateau stage, indicating that the sequencing depth was sufficient (**Figure 2A**). Based on the analysis of α diversity index, compared with the control group, the microbial diversity of gut microbiota in the AAA group was decreased (**Figure 2B**). The intervention of *A. muciniphila* increased the α diversity index of gut microbiota in AAA mice (**Figure 2B**). Venn plot analysis showed 118, 98, 101, 134, and 132 microbiota were annotated in the control group, sham group, AAA group, AAA + Am group, and AAA + Inactivated Am group, respectively (**Figure 2C**). The Bacteroidetes, Firmicutes, Verrucomicrobia, Epsilonbacteraeota, Proteobacteria, Patescibacteria, Cyanobacteria, Tenericutes, and Actinobacteria were annotated at phylum level (**Figure 2D**). The heatmap showed the top 20 genera-phylum, which mainly belong to Bacteroidetes, Verrucomicrobia, Firmicutes, and Proteobacteria (**Figure 3A**). The *Lachnospiraceae NK4A136 group*, *Lactobacillus*, *Akkermansia*, *Alloprevotella*, *Helicobacter*, *Allobaculum*, *Prevotella_9*, *Alistipes*, *Muribaculum*, *Ruminiclostridium*, *Prevotellaceae UCG_001*, *Desulfovibrio*, *[Eubacterium] xylanophilum group*, and *Parabacteroides* were annotated at the genus level (**Figure 3B**). The results showed that the intervention of *A. muciniphila* increased the diversity of gut microbiota in AAA mice.

Akkermansia muciniphila Changed the Gut Microbiota Structure

A principal component analysis (PCA) showed PC1 = 34.2% and PC2 = 24.6%, indicating that *A. muciniphila* explained 58.8% of the difference in microbiota composition (**Figure 4A**). The non-metric multidimensional scaling (NMDS) analysis showed that the stress value is equal to 0.151 and less than 0.2, and the degree of difference between groups was significant (**Figure 4B**). Compared with the control group, Bacteroidetes and Patescibacteria were increased in the AAA group, whereas Firmicutes, Verrucomicrobia, and Proteobacteria were decreased (**Figure 4C**). Compared with the AAA group, the abundance of Bacteroidetes and Patescibacteria was decreased, while the abundance of Firmicutes and Verrucomicrobia was increased in the AAA + Am group (**Figure 4C**). The results of the AAA + Inactivated Am group were consistent with those of the AAA + Am group (**Figure 4C**). Compared with the control group, the relative abundance of *Akkermansia* was decreased in the AAA group at the genus level (**Figure 4D**). The intervention of *A. muciniphila* improved the relative abundance of *Akkermansia* in the AAA + Am and AAA + Inactivated Am groups (**Figure 4D**). Bacteroidetes-*uncultured bacterium* and Firmicutes-*Lactobacillus* abundances were increased, while Firmicutes–*Lachnospiraceae NK4A136 group* abundance was decreased in the AAA group compared to the control group (**Figure 4E**). Bacteroidetes-*uncultured bacterium* and Firmicutes-*Lactobacillus* abundances were decreased, while Firmicutes–*Lachnospiraceae NK4A136 group* abundance was increased after being treated with *A. muciniphila* in the AAA mice (**Figure 4E**). A. muciniphila changed the structure of gut microbiota and might be associated with the abundance of uncultured bacterium, Lactobacillus, and Lachnospiraceae NK4A136 group.

Akkermansia muciniphila Regulated Immune Factors' Expression in Abdominal Aortic Aneurysms Mice

Compared with the control group, the levels of MMP-1, MMP-9, CTSB, and CTSL in the abdominal aorta tissue of the AAA group were significantly increased (**Figure 5A**). After the intervention of *A. muciniphila*, the levels of MMP-1, MMP-9, CTSB, and CTSL were significantly decreased in the abdominal aorta tissue (**Figure 5A**). Immunohistochemistry (IHC) analysis of the distribution of IL-33 in the abdominal aorta tissue showed that compared with the control group, the expression of IL-33 was significantly increased in the AAA group (**Figures 5B,C**). After the intervention of *A. muciniphila*, the expression of IL-33 was significantly decreased compared to the AAA group (**Figures 5B,C**). The results of IL-33 expression were analyzed by real-time reverse transcription-PCR assay (qRT-PCR) and Western blot in the abdominal aorta tissue were consistent with those of IHC (**Figures 5D,E**). ELISA was used to detect inflammatory factors in peripheral blood, and the results showed that compared with the control group, the levels of IL-4, IL-10, and IL-17A were significantly decreased, while the levels of IL-6, IFN-γ, and CRP were significantly increased in the AAA group (**Figure 5F**). After the intervention of *A. muciniphila*, the levels of IL-4, IL-10, and IL-17A were significantly increased, while the levels of IL-6, IFN-γ, and CRP were significantly decreased compared to the AAA group (**Figure 5F**). Compared with the control group, the expression of PCNA and OPN was significantly decreased, while the expression of α-SMA was

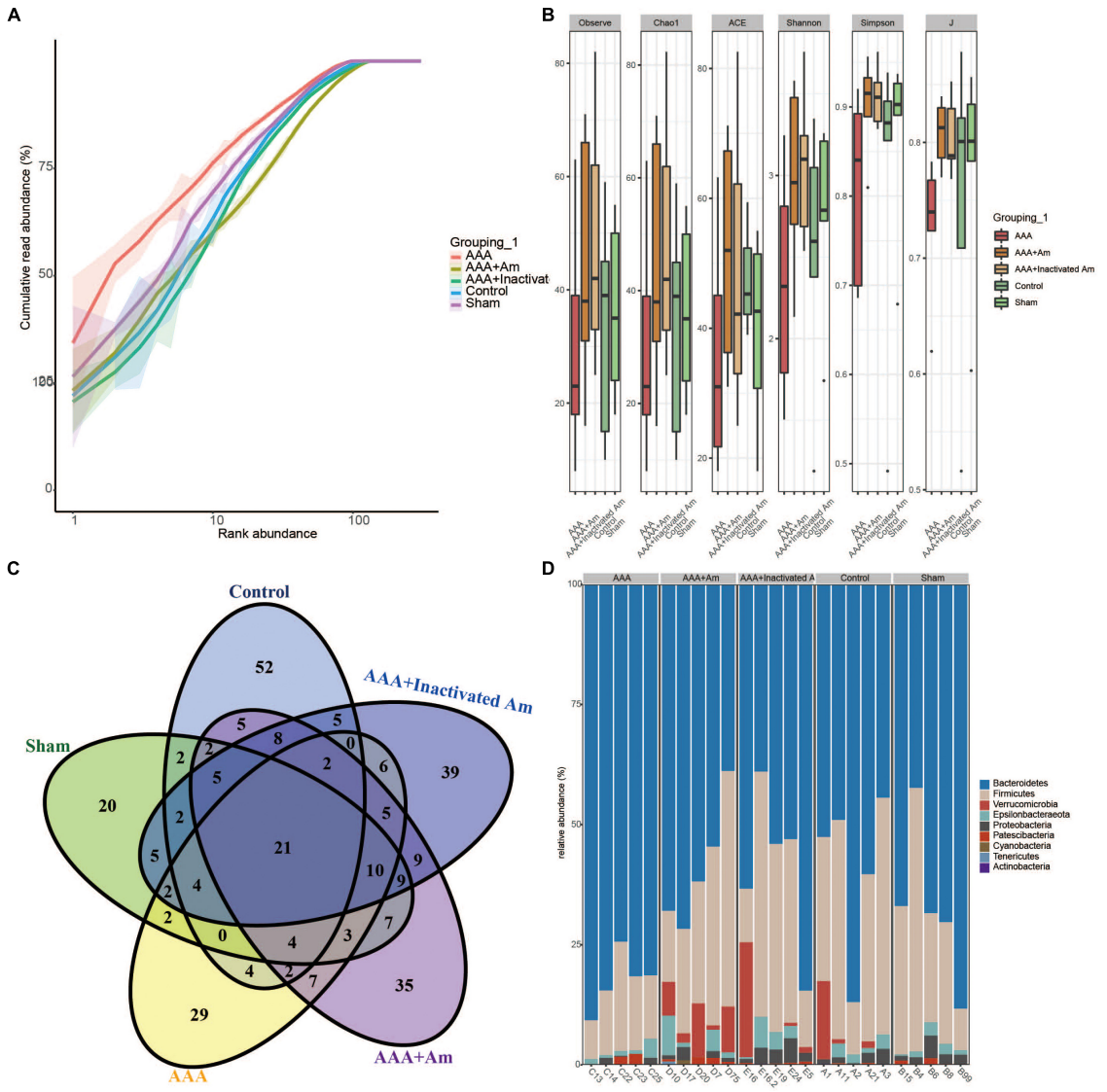

FIGURE 2 | *A. muciniphila* affects the diversity of gut microbiota. **(A)** Rank abundance curve was used to evaluate sequencing depth. **(B)** The α diversity analysis of gut microbiota. **(C)** Venn diagram showed changes in the number of microbiota in the gut. **(D)** The relative abundance of gut microbiota at the phylum level.

significantly increased in the AAA group (**Figure 5G**). Compared with the AAA group, the expression of PCNA and OPN was significantly increased, while the expression of α-SMA was significantly decreased after treated with *A. muciniphila* in the AAA mice (**Figure 5G**). It was proved that *A. muciniphila* might inhibit the formation of AAA by regulating the expression of IL-33 and immune factors in the abdominal aorta of AAA mice.

Akkermansia muciniphila Regulated the Function of Gut Microbiota to Inhibit the Formation of Abdominal Aortic Aneurysms

Akkermansia muciniphila could regulate the structure of the intestinal flora of AAA mice and the expression of IL-33 in the abdominal aorta tissues, but its functional impact on the intestinal flora was not yet known. Based on the lefSe analysis, it was found that some signal pathways related to bacterial metabolism were significantly enriched in the control group, AAA group, and AAA + Am group ($P < 0.05$, LDA ≥ 2.5). The palmitate biosynthesis II (bacteria and plants, LDA = 3.15), stearate biosynthesis II (bacteria and plants, LDA = 3.15), Kdo transfer to lipid IVA III (*Chlamydia*, LDA = 3.13), 6-hydroxymethyl-dihydropterin diphosphate biosynthesis III (*Chlamydia*, LDA = 3.10), thiazole biosynthesis I (*E. coli*, LDA = 3.00), polyisoprenoid biosynthesis (*E. coli*, LDA = 2.99), flavin biosynthesis I (bacteria and plants, LDA = 2.94), peptidoglycan biosynthesis III (*mycobacteria*, LDA = 2.88), and dTDP-L-rhamnose biosynthesis I (LDA = 2.91) were significantly enriched in the AAA group (Revised **Figures 6**, **7**).

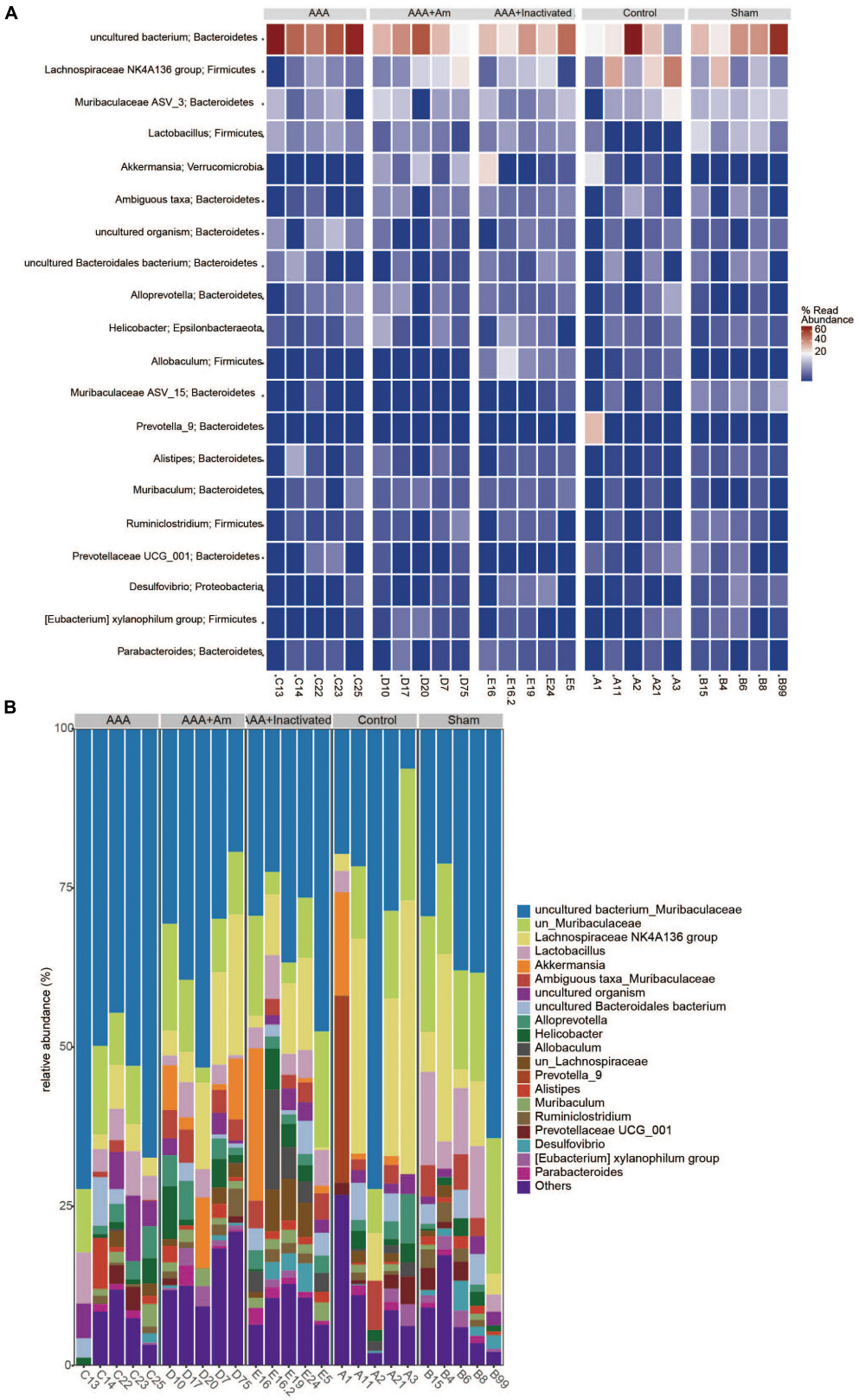

FIGURE 3 | *A. muciniphila* affects the composition of gut microbiota. **(A)** Heatmap showed the relative abundance of top 20 genera in gut. **(B)** The relative abundance of gut microbiota at the genus level ($n = 5$ samples, 10 mice/group).

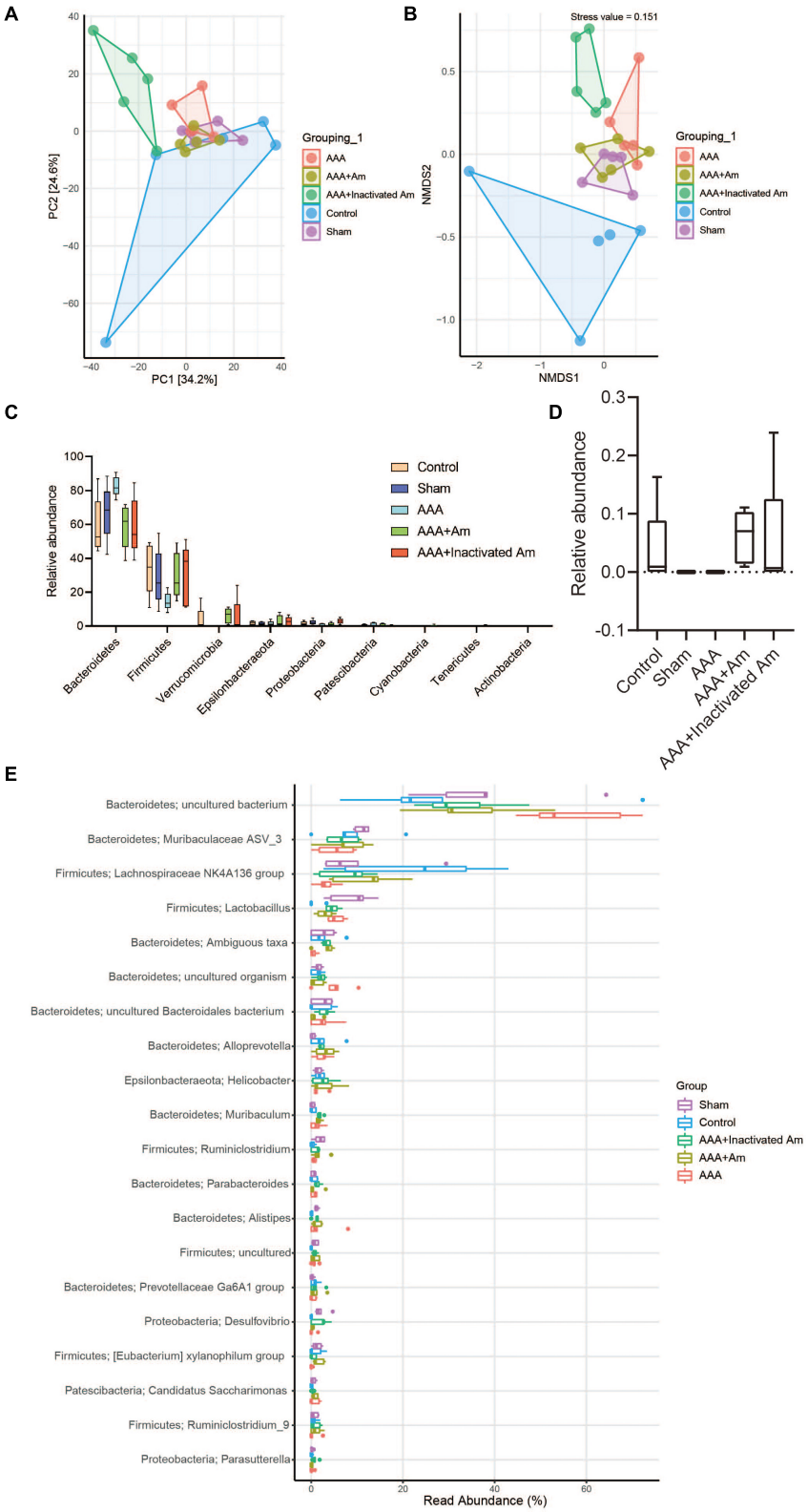

FIGURE 4 | *A. muciniphila* alters the structure of gut microbiota. **(A)** PCA was used to analyze the diversity of gut microbiota. **(B)** NMDS was used to analyze the differences between groups. **(C)** The abundance of gut microbiota changes at the phylum level. **(D)** The relative abundance of *Akkermansia* at the genus level. **(E)** The relative abundance of gut microbiota changes at the genus level ($n = 5$ samples, 10 mice/group).

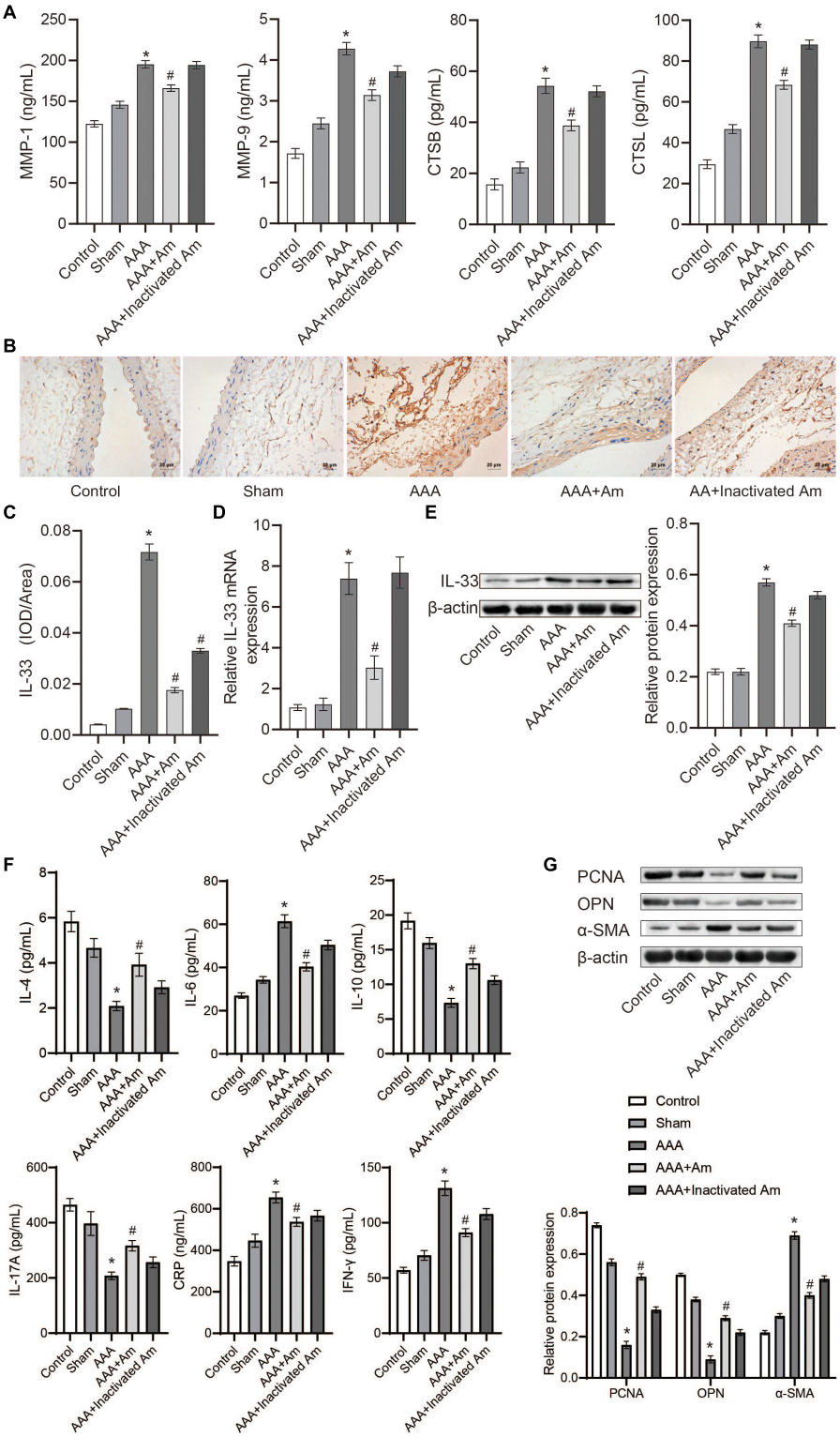

FIGURE 5 | *A. muciniphila* regulates the expression of immune factors. **(A)** The levels of MMP-1, MMP-9, CTSB, and CTSL in abdominal aortic tissue were analyzed by ELISA. **(B,C)** The expression of IL-33 in abdominal aortic tissue was analyzed by IHC (scale bar = 25 μm; the magnification is 400×). **(D)** qRT-PCR was used to analyze IL-33 gene expression in abdominal aortic tissue. **(E)** The expression of IL-33 protein in abdominal aortic tissue was analyzed by Western blot. **(F)** The levels of IL-4, IL-6, IL-10, IL-17A, IFN-γ, and C-reactive protein (CRP) in peripheral blood were determined by ELISA. **(G)** The expression of PCNA, OPN, and α-SMA protein in abdominal aortic aneurysm tissue were detected by Western blot. Data were shown as means ± SD and analyzed by two-way ANOVA ($n = 10$ mice/group). *Compared with the control group, $P < 0.05$; #compared with the AAA group, $P < 0.05$.

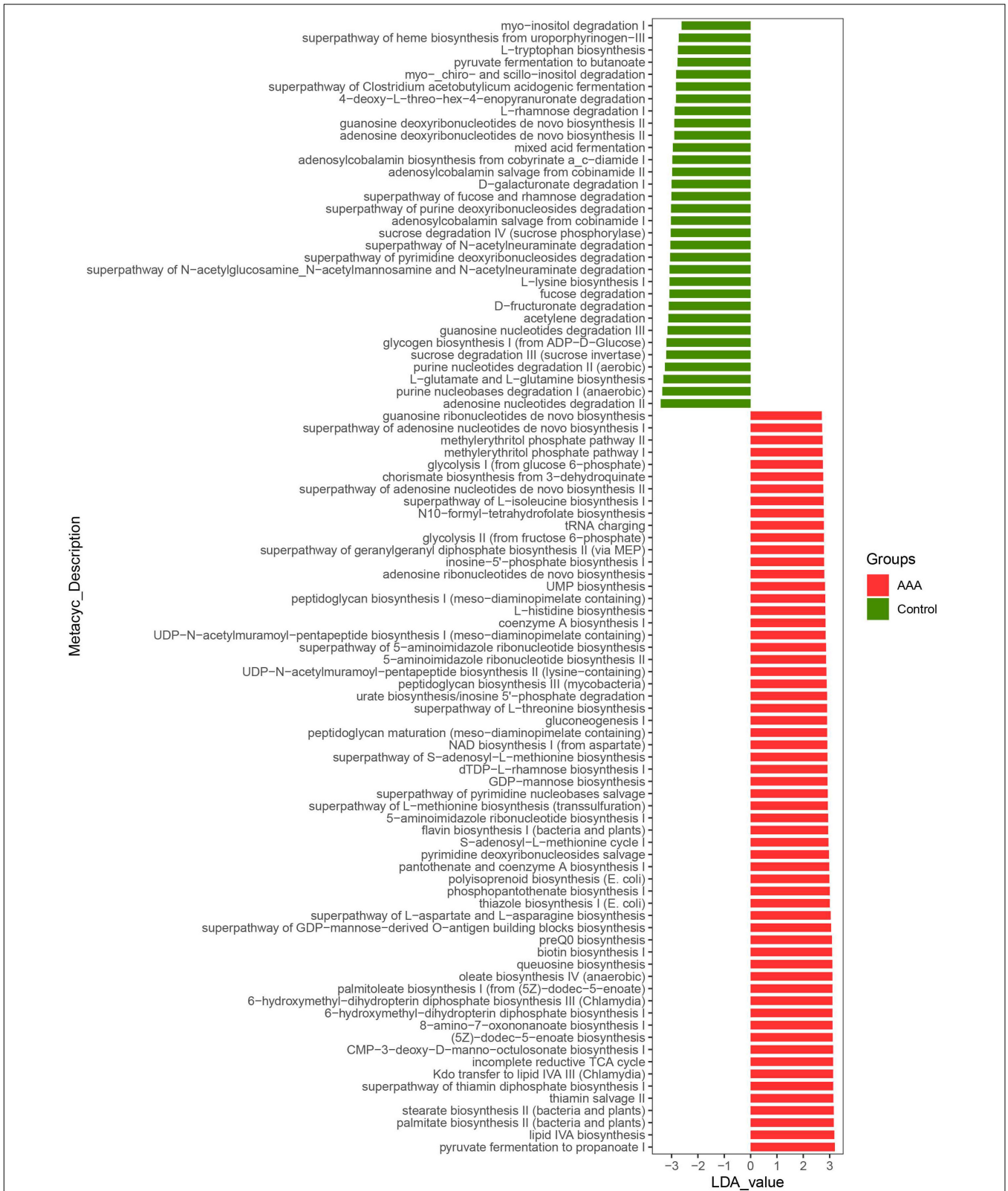

FIGURE 6 | LefSe analyzed the effect of *A. muciniphila* on gut microbiota function in the control group and AAA group. The red and green represented the AAA group and control group, respectively. The prediction of gene function profile using the PICRUSt2 software and MetaCyc database. Data were analyzed by LefSe ($n = 5$ samples, 10 mice/group).

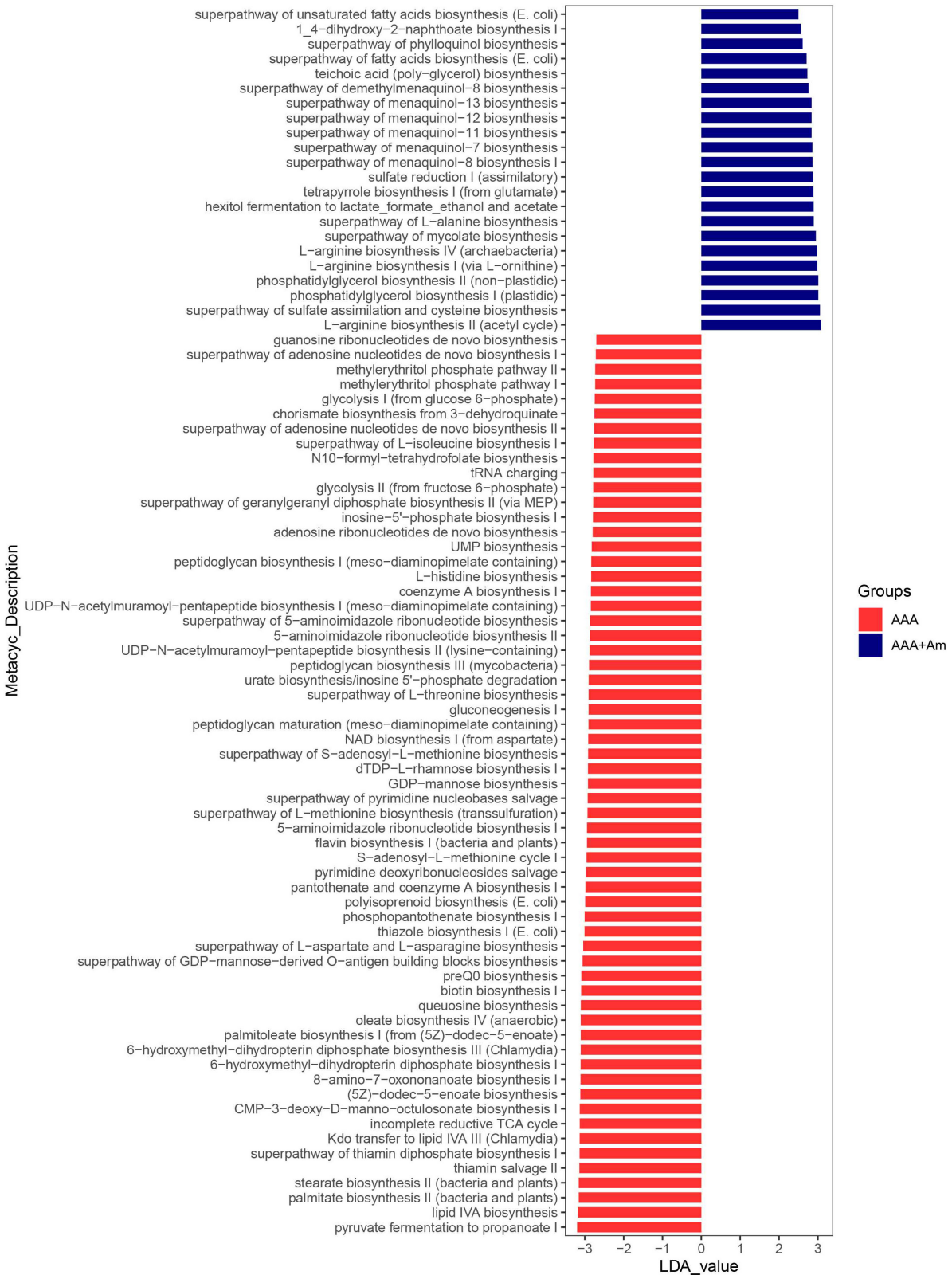

FIGURE 7 | LefSe analyzed the effect of *A. muciniphila* on gut microbiota function in the AAA group and AAA + Am group. The red and blue represented the AAA group and AAA + Am group, respectively. The prediction of gene function profile using the PICRUSt2 software and MetaCyc database. Data were analyzed by LefSe ($n = 5$ samples, 10 mice/group).

The L-arginine biosynthesis IV (*archaebacteria*, LDA = 2.97), superpathway of mycolate biosynthesis (LDA = 2.94), superpathway of fatty acid biosynthesis (*E. coli*, LDA = 2.71), and superpathway of unsaturated fatty acid biosynthesis (*E. coli*, LDA = 2.50) pathways were significantly enriched in the AAA + Am group (Revised **Figures 7**, **8**). The superpathway of Clostridium acetobutylicum acidogenic fermentation (LDA = 2.83), superpathway of fucose and rhamnose degradation (LDA = 3.00), and L-rhamnose degradation I (LDA = 2.88) pathways were significantly enriched in the control group (Revised **Figures 6**, **8**). These results suggest that a variety of microbial-related metabolic pathways are enriched in abdominal aortic aneurysm disease and treatment, or the potential mechanism of *A. muciniphila*'s inhibition of AAA formation through distal regulation of intestinal microorganisms.

The Correlation Between *Akkermansia* and Gut Microbiota at Genus Level

Finally, we used the Spearman's correlation to analyze the correlation between *Akkermansia* and gut microbiota at the genus level. The *Akkermansia* was positively correlated with *Bifidobacterium*, *Enterorhabdus*, *Bacteroides*, *Muribaculum*, *Alloprevotella*, *Prevotella_9*, *Prevotellaceae Ga6A1 group*, *Rikenella*, *Parabacteroides*, *Clostridium sensu stricto_1*, *Family XIII UCG_001*, *Eubacterium nodatum group*, *ASF356*, *Anaerostipes*, *Peptococcus*, *Coprococcus_2*, *Lachnoclostridium*, *Lachnospiraceae NC2004 group*, *Roseburia*, *Lachnospiraceae NK4A136 group*, *Marvinbryantia*, *Lachnospiraceae UCG_001*, *Eubacterium fissicatena group*, *Eubacterium ventriosum group*, *Romboutsia*, *Intestinimonas*, *Oscillibacter*, *Ruminiclostridium_5*, *Ruminiclostridium_6*, *Quinella*, *Ruminococcaceae UCG_004*, *Ruminococcaceae UCG_005*, *Allobaculum*, *Candidatus Saccharimonas*, *Ruminococcaceae UCG_010*, *Ruminococcus_1*, *Ruminococcaceae UCG_013*, *Ruminococcaceae UCG_014*, *Erysipelatoclostridium*, *Dubosiella*, *Ruminococcus_2*, *Eubacterium coprostanoligenes group*, *Parasutterella*, *Escherichia Shigella*, and *Anaeroplasma* at the genus level (Revised **Figure 9**).

The *Akkermansia* was negatively correlated with *Odoribacter*, *Prevotellaceae NK3B31 group*, *Prevotellaceae UCG_001*, *Alistipes*, *Helicobacter*, *Lactobacillus*, *Candidatus Arthromitus*, *A2*, *Blautia*, *GCA_900066575*, *Lachnospiraceae UCG_006*, *Eubacterium oxidoreducens group*, *Angelakisella*, *Butyricicoccus*, *Harryflintia*, *Ruminiclostridium*, *Ruminiclostridium_9*, *Ruminococcaceae NK4A214 group*, and *Desulfovibrio* at the genus level (Revised **Figure 9**).

DISCUSSION

Abdominal aortic aneurysms is a life-threatening disease, and there are still no drugs to treat it in clinical practice (Raffort et al., 2020). The risk factors for AAA included age, smoking, gender, and family history (Clancy et al., 2019). Symptoms associated with AAA may include abdominal or back pain, thromboembolism, atherosclerotic embolism, aortic rupture, or the development of an arteriovenous or aortic fistula (Ullery et al., 2018). Currently, early screening and treatment for AAA disease include one-time abdominal ultrasound screening and conventional open surgical repair or intravascular aortic stent implantation repair (Calero and Illig, 2016), but there is still a lack of effective adjuvant drugs. Studies of animal model construction of AAA showed that measurements of the aortic cross-section confirmed dilation of the lumen in AAA tissue, as well as thinning of the intermediate layer and enlargement of the outer membrane, and degeneration and destruction of the elastic layer (Yue et al., 2020). Matrix metalloproteinases (MMPs) were associated with the pathogenesis of aortic aneurysms because the histological characteristics of thoracic aortic aneurysms and AAA were loss of smooth muscle cells in the aortic middle membrane and destruction of the extracellular matrix (ECM) (Rabkin, 2017). Classic features of human AAA include ECM degeneration, MMP upregulation, and macrophage infiltration (Krishna et al., 2020). Clinical studies have shown that cathepsin is associated with collagen I degradation and inflammatory cells, and the mRNA levels of cathepsin B, D, L, and S were significantly increased in AAA compared with control aorta (Klaus et al., 2018). All these studies are consistent with the model characterization of mice in our AAA group, proving that our constructed AAA mice were consistent with the clinical characterization of AAA disease.

The role of probiotics *A. muciniphila* is known to include metabolic regulation, immune regulation, and intestinal health protection, and its abundance has been associated with various diseases such as metabolic syndrome and autoimmune diseases (Zhai et al., 2019). Recent studies have reported that *A. muciniphila* can play an important role in immunotherapy (Chen et al., 2020; Shi et al., 2020; Luo et al., 2021). Metagenomics based on stool samples from cancer patients at the time of diagnosis reveals a correlation between clinical response to immune checkpoint inhibitors and the relative abundance of *A. muciniphila* recruitment of CCR9 + CXCR3 + CD4 + T lymphocytes into the mouse tumor bed (Routy et al., 2018). *A. muciniphila* was an intestinal symbiotic bacterium with anti-inflammatory properties in the intestine and other organs, which enhanced intestinal barrier function and increased IL-10 release stimulated by whole blood lipopolysaccharide *in vitro* (Hiippala et al., 2018). *A. muciniphila* also affected the composition of immune cells in mesenteric lymph nodes, which could be seen from the increased total B cell population while reducing the total T cell and neutrophil populations (Katiraei et al., 2020). In this study, the oral administration of *A. muciniphila* in AAA mice showed that the aneurysm formation of abdominal aorta tissue was significantly inhibited, and the intestinal flora diversity and function of AAA mice were restored. Our study confirmed that *A. muciniphila* could inhibit aneurysm formation during the occurrence of AAA disease, but the specific mechanism of action still needs to be studied.

IL-33 is a member of a recently described family of IL-1 cytokines with multipotent pro-inflammatory and anti-inflammatory effects (Miller, 2011). Unlike most other cytokines, IL-33 was not secreted and was expressed constitutively in the nucleus of different cell types, where it functions as a chromatin-associated nuclear cytokine (Liew et al., 2016). During cell injury,

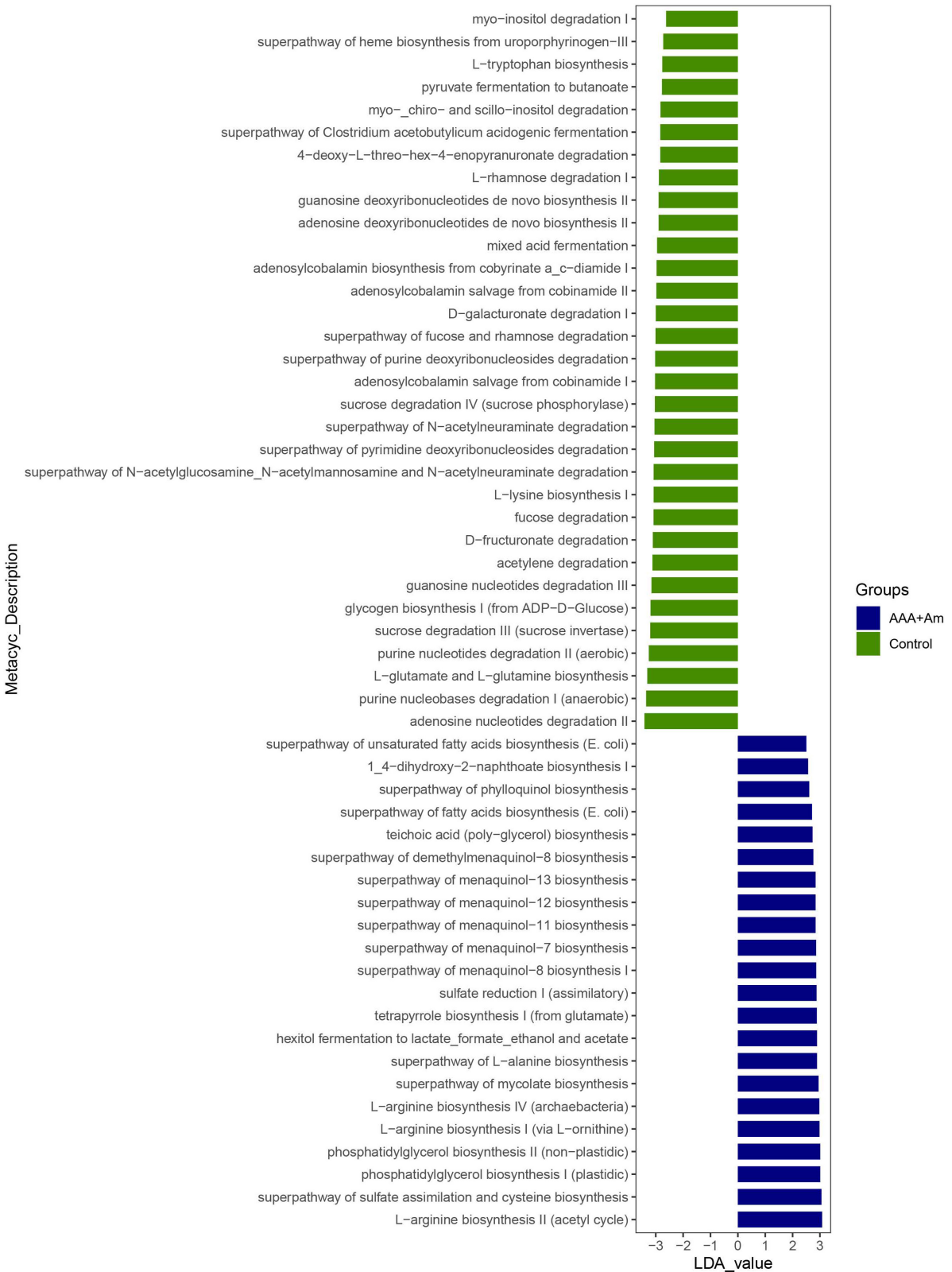

FIGURE 8 | LefSe analyzed the effect of *A. muciniphila* on gut microbiota function in the Control group and AAA + Am group. The green and blue represented the control group and AAA + Am group, respectively. The prediction of gene function profile using the PICRUSt2 software and MetaCyc database. Data were analyzed by LefSe ($n = 5$ samples, 10 mice/group).

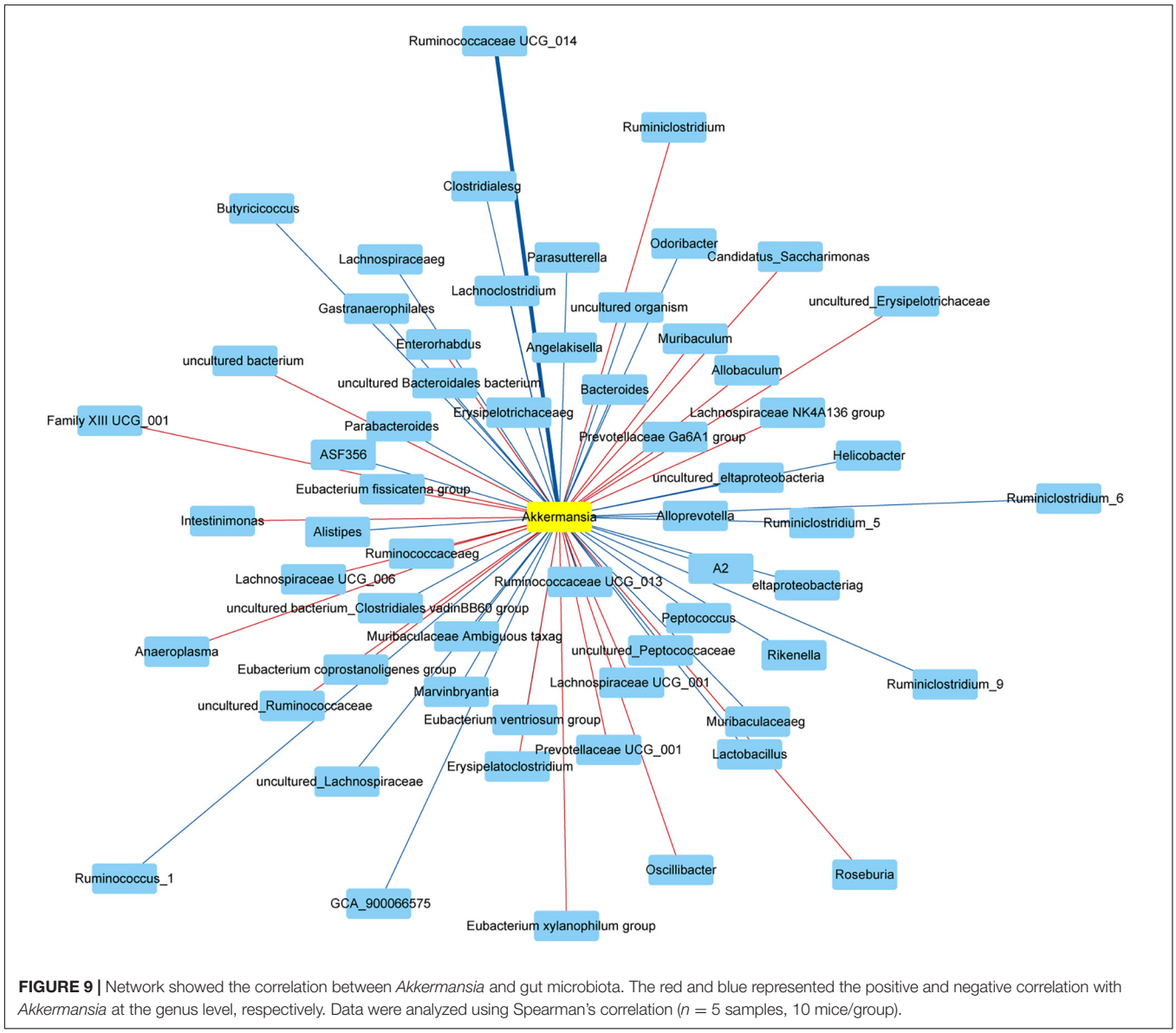

FIGURE 9 | Network showed the correlation between *Akkermansia* and gut microbiota. The red and blue represented the positive and negative correlation with *Akkermansia* at the genus level, respectively. Data were analyzed using Spearman's correlation ($n = 5$ samples, 10 mice/group).

IL-33 was released into the extracellular space and interacted with its receptor ST2, which was mainly expressed in Th2 cells, Treg cells, macrophages, and neutrophils, leading to the formation of heterodimer signaling complexes (De la Fuente et al., 2015; Tsai and Xian, 2019). The complexes included the connector protein myeloid differentiation primary reactive protein 88 (MyD88) and IL-1 receptor helper protein (IL1RAP), leading to the activation of the MAPK and NF-κB pathways (De la Fuente et al., 2015; Tsai and Xian, 2019). Less is known about IL-33 cross talk with the intestinal flora, but some studies suggest a potential interaction. Studies conducted in SAMP mice have shown that transplantation of common feces induces IL-33 expression in ex-GF mice (De Salvo et al., 2016). Furthermore, IL-33 expression had many known interactions with microbial-sensing Toll-like receptors (TLRs), and was indeed induced by pathogen-associated molecular patterns (PAMPs), perhaps as a protective mechanism in the host (Natarajan et al., 2016). Our study found that the expression of IL-33 was increased in the abdominal aorta tissues of AAA mice, and the expression of IL-33 was decreased after treatment with *A. muciniphila*. We speculated that the inhibitory effect of *A. muciniphila* on the formation of abdominal aortic aneurysms might be related to the molecular immunity of distal IL-33 through gut microbiota, but it still needs further study. It is unknown whether the Akk-reduced lesion was caused by an increase in bacterial diversity or Akk-reduced IL-33. In addition, we have not found a suitable method for quantitative analysis of *A. muciniphila* in the fecal sample except for the 16S rRNA gene sequencing. This is the limitation of our study. We also failed to show a cause-effect relationship, such as the reconstitution of IL-33-reversed Akk-reduced lesion. The highly personalized microbiome and its complex and multidirectional interactions with host metabolism and

immunity present potential opportunities for the development of the next generation of microbiome-based drugs and diagnostic biomarkers (Mousa et al., 2022). We will continue to explore this in the subsequent scientific research.

Lactobacillus casei cell wall extract (LCWE) induced systemic arterial dilation and aneurysm development, including AAA, in a mouse model of Kawasaki disease (KD) vasculitis (Wakita et al., 2016). Both IL-1α and IL-1β played a key role in KD disease, and the use of IL-1R blockers that inhibited both pathways might be a therapeutic target not only for KD coronary arteritis but also for other systemic aneurysms, including AAA (Lee et al., 2015; Wakita et al., 2016). There was a study that showed species from *Akkermansia muciniphila* and *Lachnospiraceae bacterium A2* were significantly higher in the control group than that in the AAA group, while six species, namely, *Lachnospiraceae bacterium*, *COE1*, *Corynebacterium stationis*, *Firmicutes Bacterium ASF500*, *Helicobacter bilis*, and *Clostridium leptum*, were increased in the AAA group (Xie et al., 2020). Our study found that Firmicutes-*Lactobacillus* increased in AAA mice and decreased after treatment with *A. muciniphila*. In addition, the effects of *Helicobacter pylori* and *Lactobacillus acidophilus* on peripheral blood mononuclear cell (PBMC) cytokine profiles showed changes in IL-10, Th1, and Th2 cytokines, but there were inherent differences between patients and healthy people (Aria et al., 2020). In addition, *Helicobacter pylori* and *Lactobacillus acidophilus* also affected the changes in miRNA expression profiles in CD4 + memory T cells in AAA patients and healthy controls, participating in the development and prevention of AAA (Kalani et al., 2021). In our study, we found that the *Akkermansia* was negatively correlated with *Helicobacter* and *Lactobacillus* at the genus level. These studies suggest that the mechanism of *A. muciniphila* inhibiting AAA formation might be related to the changes in the abundance of intestinal *Lactobacillus*.

L-Rhamnose could be used by the thermophilic bacterium *Clostridium stercorarium* to produce D-allose from D-allulose (Seo et al., 2018). L-Rhamnose could also be used as a carbon source and energy source for the growth of *E. coli* (Chen and Lin, 1984). L-Rhamnose inhibited phage adsorption to cells without inactivating free phages (Watanabe and Takesue, 1975). The inhibition of L-rhamnose on phage adsorption was competitive against host cells (Watanabe and Takesue, 1975). The function prediction based on the MetaCyc database showed the superpathway of fucose and rhamnose degradation (LDA = 3.00, $P = 0.007$) and L-rhamnose degradation I (LDA = 2.88, $P = 0.021$) pathways were enriched in the control group, whereas the dTDP-L-rhamnose biosynthesis I (LDA = 2.91, $P = 0.004$) pathway was enriched in the AAA group. In addition, the degradation of L-rhamnose in the intestinal microbiota metagenomic functional pathway during immunotherapy in melanoma patients was associated with progression-free survival (Peters et al., 2019). In our study, we found that the *Akkermansia* was positively correlated with *Clostridium sensu stricto_1* and *Escherichia shigella* at genus level. The above studies have proved that intestinal microbial-related L-rhamnose degradation and biosynthesis pathways are reversed in AAA disease, which may be the target of *A. muciniphila* to regulate the function of gut microbiota.

CONCLUSION

The occurrence of AAA disease might be accompanied by increased expression of inflammatory cytokines, decreased gut microbiota diversity, severe local immune infiltration, and elastic fiber degradation in the abdominal aorta. Oral administration of *A. muciniphila* could inhibit the expansion and inflammation of the abdominal aorta, restore the gut microbiota diversity, promote peripheral blood immunity and IL-33 expression, and regulate the functional pathways related to *Lactobacillus* and L-rhamnose degradation/synthesis to inhibit the formation of AAA.

DATA AVAILABILITY STATEMENT

The datasets presented in this study can be found in online repositories. The names of the repository/repositories and accession number(s) can be found in the article/supplementary material.

ETHICS STATEMENT

This study was approved by the Medical Ethics Committee of Xiangya Hospital of Central South University (202104809), Changsha, Hunan, China.

AUTHOR CONTRIBUTIONS

KW and XH designed and performed the study. YB and HZ analyzed the data. All authors contributed to the writing and revisions and reviewed the manuscript.

REFERENCES

Aria, H., Kalani, M., Hodjati, H., and Doroudchi, M. (2020). Different cytokine patterns induced by *Helicobacter* pylori and Lactobacillus acidophilus extracts in PBMCs of patients with abdominal aortic aneurysm. *Comp. Immunol. Microbiol. Infect. Dis.* 70:101449. doi: 10.1016/j.cimid.2020.101449

Calero, A., and Illig, K. A. (2016). Overview of aortic aneurysm management in the endovascular era. *Semin. Vasc. Surg.* 29, 3–17. doi: 10.1053/j.semvascsurg.2016.07.003

Caporaso, J. G., Kuczynski, J., Stombaugh, J., Bittinger, K., Bushman, F. D., Costello, E. K., et al. (2010). QIIME allows analysis of high-throughput community sequencing data. *Nat. Methods* 7, 335–336. doi: 10.1038/nmeth.f.303

Chen, Y. M., and Lin, E. C. (1984). Dual control of a common L-1,2-propanediol oxidoreductase by L-fucose and L-rhamnose in *Escherichia coli*. *J. Bacteriol.* 157, 828–832. doi: 10.1128/jb.157.3.828-832.1984

Chen, Z., Qian, X., Chen, S., Fu, X., Ma, G., and Zhang, A. (2020). Akkermansia muciniphila Enhances the antitumor effect of cisplatin in

lewis lung cancer mice. *J. Immunol. Res.* 2020:2969287. doi: 10.1155/2020/2969287

Clancy, K., Wong, J., and Spicher, A. (2019). Abdominal aortic aneurysm: a case report and literature review. *Perm. J.* 23:218. doi: 10.7812/tpp/18.218

De la Fuente, M., MacDonald, T. T., and Hermoso, M. A. (2015). The IL-33/ST2 axis: role in health and disease. *Cytokine Growth Fact. Rev.* 26, 615–623. doi: 10.1016/j.cytogfr.2015.07.017

De Salvo, C., Wang, X. M., Pastorelli, L., Mattioli, B., Omenetti, S., Buela, K. A., et al. (2016). IL-33 drives eosinophil infiltration and pathogenic type 2 Helper T-Cell immune responses leading to chronic experimental Ileitis. *Am. J. Pathol.* 186, 885–898. doi: 10.1016/j.ajpath.2015.11.028

Depommier, C., Van Hul, M., Everard, A., Delzenne, N. M., De Vos, W. M., and Cani, P. D. (2020). Pasteurized Akkermansia muciniphila increases whole-body energy expenditure and fecal energy excretion in diet-induced obese mice. *Gut. Microb.* 11, 1231–1245. doi: 10.1080/19490976.2020.1737307

Everard, A., Belzer, C., Geurts, L., Ouwerkerk, J. P., Druart, C., Bindels, L. B., et al. (2013). Cross-talk between Akkermansia muciniphila and intestinal epithelium controls diet-induced obesity. *Proc. Natl. Acad. Sci. USA* 110, 9066–9071. doi: 10.1073/pnas.1219451110

Geerlings, S. Y., Kostopoulos, I., de Vos, W. M., and Belzer, C. (2018). Akkermansia muciniphila in the human gastrointestinal tract: when, where, and how? *Microorganisms* 6:75. doi: 10.3390/microorganisms6030075

Hagi, T., and Belzer, C. (2021). The interaction of Akkermansia muciniphila with host-derived substances, bacteria and diets. *Appl. Microbiol. Biotechnol.* 105, 4833–4841. doi: 10.1007/s00253-021-11362-3

Hiippala, K., Jouhten, H., Ronkainen, A., Hartikainen, A., and Kainulainen, V. (2018). The Potential of gut commensals in reinforcing intestinal barrier function and alleviating inflammation. *Nutrients* 10:988. doi: 10.3390/nu10080988

Jie, Z., Xia, H., Zhong, S. L., Feng, Q., Li, S., Liang, S., et al. (2017). The gut microbiome in atherosclerotic cardiovascular disease. *Nat. Commun.* 8:845. doi: 10.1038/s41467-017-00900-1

Kalani, M., Hodjati, H., Ghoddusi Johari, H., and Doroudchi, M. (2021). Memory T cells of patients with abdominal aortic aneurysm differentially expressed micro RNAs 21, 92a, 146a, 155, 326 and 663 in response to *Helicobacter* pylori and Lactobacillus acidophilus. *Mol. Immunol.* 130, 77–84. doi: 10.1016/j.molimm.2020.11.007

Katiraei, S., de Vries, M. R., Costain, A. H., Thiem, K., Hoving, L. R., van Diepen, J. A., et al. (2020). Akkermansia muciniphila exerts lipid-lowering and immunomodulatory effects without affecting neointima formation in hyperlipidemic APOE*3-Leiden.CETP Mice. *Mol. Nutr. Food Res.* 64:e1900732. doi: 10.1002/mnfr.201900732

Kazemian, N., Mahmoudi, M., Halperin, F., Wu, J. C., and Pakpour, S. (2020). Gut microbiota and cardiovascular disease: opportunities and challenges. *Microbiome* 8:36. doi: 10.1186/s40168-020-00821-0

Klaus, V., Schmies, F., Reeps, C., Trenner, M., Geisbüsch, S., Lohoefer, F., et al. (2018). Cathepsin S is associated with degradation of collagen I in abdominal aortic aneurysm. *Vasa* 47, 285–293. doi: 10.1024/0301-1526/a000701

Klindworth, A., Pruesse, E., Schweer, T., Peplies, J., Quast, C., Horn, M., et al. (2013). Evaluation of general 16S ribosomal RNA gene PCR primers for classical and next-generation sequencing-based diversity studies. *Nucleic Acids Res.* 41:808. doi: 10.1093/nar/gks808

Krishna, S. M., Morton, S. K., Li, J., and Golledge, J. (2020). Risk factors and mouse models of abdominal aortic aneurysm rupture. *Int. J. Mol. Sci.* 21:250. doi: 10.3390/ijms21197250

Lee, Y., Wakita, D., Dagvadorj, J., Shimada, K., Chen, S., Huang, G., et al. (2015). IL-1 Signaling Is critically required in stromal cells in kawasaki disease vasculitis mouse model: role of both IL-1α and IL-1β. *Arterioscler. Thromb Vasc. Biol.* 35, 2605–2616. doi: 10.1161/atvbaha.115.306475

Li, J., Lin, S., Vanhoutte, P. M., Woo, C. W., and Xu, A. (2016). Akkermansia Muciniphila Protects against atherosclerosis by preventing metabolic endotoxemia-induced inflammation in apoe-/- mice. *Circulation* 133, 2434–2446. doi: 10.1161/circulationaha.115.019645

Li, J., Xia, N., Wen, S., Li, D., Lu, Y., Gu, M., et al. (2019). IL (Interleukin)-33 Suppresses abdominal aortic aneurysm by enhancing regulatory T-Cell Expansion and Activity. *Arterioscler. Thromb Vasc. Biol.* 39, 446–458. doi: 10.1161/atvbaha.118.312023

Li, Y., Yang, D., Sun, B., Zhang, X., Li, F., Liu, Z., et al. (2019). Discovery of crucial cytokines associated with abdominal aortic aneurysm formation by protein array analysis. *Exp. Biol. Med.* 244, 1648–1657. doi: 10.1177/1535370219885101

Li, Z., Ni, M., Yu, H., Wang, L., Zhou, X., Chen, T., et al. (2020). Gut microbiota and liver fibrosis: one potential biomarker for predicting liver fibrosis. *Biomed. Res. Int.* 2020:3905130. doi: 10.1155/2020/3905130

Liew, F. Y., Girard, J. P., and Turnquist, H. R. (2016). Interleukin-33 in health and disease. *Nat. Rev. Immunol.* 16, 676–689. doi: 10.1038/nri.2016.95

Lindskog Jonsson, A., Caesar, R., Akrami, R., Reinhardt, C., Fåk Hållenius, F., Borén, J., et al. (2018). Impact of gut microbiota and diet on the development of atherosclerosis in Apoe(−/−) Mice. *Arterioscler. Thromb. Vasc. Biol.* 38, 2318–2326. doi: 10.1161/atvbaha.118.311233

Liu, Z., Fitzgerald, M., Meisinger, T., Batra, R., Suh, M., Greene, H., et al. (2019). CD95-ligand contributes to abdominal aortic aneurysm progression by modulating inflammation. *Cardiovasc. Res.* 115, 807–818. doi: 10.1093/cvr/cvy264

Luo, Z. W., Xia, K., Liu, Y. W., Liu, J. H., Rao, S. S., Hu, X. K., et al. (2021). Extracellular vesicles from akkermansia muciniphila elicit antitumor immunity against prostate cancer via modulation of CD8(+) T Cells and Macrophages. *Int. J. Nanomed.* 16, 2949–2963. doi: 10.2147/ijn.S304515

Miller, A. M. (2011). Role of IL-33 in inflammation and disease. *J. Inflamm.* 8:22. doi: 10.1186/1476-9255-8-22

Mousa, W. K., Chehadeh, F., and Husband, S. (2022). Recent advances in understanding the structure and function of the human microbiome. *Front. Microbiol.* 13:825338. doi: 10.3389/fmicb.2022.825338

Natarajan, C., Yao, S. Y., and Sriram, S. (2016). TLR3 Agonist Poly-IC Induces IL-33 and promotes myelin repair. *PLoS One* 11:e0152163. doi: 10.1371/journal.pone.0152163

Peng, J., Xiao, X., Hu, M., and Zhang, X. (2018). Interaction between gut microbiome and cardiovascular disease. *Life Sci.* 214, 153–157. doi: 10.1016/j.lfs.2018.10.063

Peters, B. A., Wilson, M., Moran, U., Pavlick, A., Izsak, A., Wechter, T., et al. (2019). Relating the gut metagenome and metatranscriptome to immunotherapy responses in melanoma patients. *Genome Med.* 11:61. doi: 10.1186/s13073-019-0672-4

Plovier, H., Everard, A., Druart, C., Depommier, C., Van Hul, M., Geurts, L., et al. (2017). A purified membrane protein from Akkermansia muciniphila or the pasteurized bacterium improves metabolism in obese and diabetic mice. *Nat. Med.* 23, 107–113. doi: 10.1038/nm.4236

Pruesse, E., Quast, C., Knittel, K., Fuchs, B. M., Ludwig, W., Peplies, J., et al. (2007). SILVA: a comprehensive online resource for quality checked and aligned ribosomal RNA sequence data compatible with ARB. *Nucleic Acids Res.* 35, 7188–7196. doi: 10.1093/nar/gkm864

Rabkin, S. W. (2017). The role matrix metalloproteinases in the production of aortic aneurysm. *Prog. Mol. Biol. Transl. Sci.* 147, 239–265. doi: 10.1016/bs.pmbts.2017.02.002

Raffort, J., Hassen-Khodja, R., Jean-Baptiste, E., and Lareyre, F. (2020). Relationship between metformin and abdominal aortic aneurysm. *J. Vasc. Surg.* 71, 1056–1062. doi: 10.1016/j.jvs.2019.08.270

Routy, B., Le Chatelier, E., Derosa, L., Duong, C. P. M., Alou, M. T., Daillère, R., et al. (2018). Gut microbiome influences efficacy of PD-1-based immunotherapy against epithelial tumors. *Science* 359, 91–97. doi: 10.1126/science.aan3706

Seo, M. J., Choi, J. H., Kang, S. H., Shin, K. C., and Oh, D. K. (2018). Characterization of L-rhamnose isomerase from Clostridium stercorarium and its application to the production of D-allose from D-allulose (D-psicose). *Biotechnol. Lett.* 40, 325–334. doi: 10.1007/s10529-017-2468-1

Shi, L., Sheng, J., Chen, G., Zhu, P., Shi, C., Li, B., et al. (2020). Combining IL-2-based immunotherapy with commensal probiotics produces enhanced antitumor immune response and tumor clearance. *J. Immunother. Cancer* 8:973. doi: 10.1136/jitc-2020-000973

Tsai, S., and Xian, X. (2019). IL-33 in murine abdominal aortic aneurysm: a novel inflammatory mediator awaiting clinical translation. *J. Thorac. Dis.* 11, 2181–2184. doi: 10.21037/jtd.2019.06.20

Ullery, B. W., Hallett, R. L., and Fleischmann, D. (2018). Epidemiology and contemporary management of abdominal aortic aneurysms. *Abdom. Radiol.* 43, 1032–1043. doi: 10.1007/s00261-017-1450-7

Wakita, D., Kurashima, Y., Crother, T. R., Noval Rivas, M., Lee, Y., Chen, S., et al. (2016). Role of interleukin-1 signaling in a mouse model of kawasaki disease-associated abdominal aortic aneurysm. *Arterioscler. Thromb. Vasc. Biol.* 36, 886–897. doi: 10.1161/atvbaha.115.307072

Wang, Y. D., Liu, Z. J., Ren, J., and Xiang, M. X. (2018). Pharmacological therapy of abdominal aortic aneurysm: an update. *Curr. Vasc. Pharmacol.* 16, 114–124. doi: 10.2174/1570161115666170413145705

Watanabe, K., and Takesue, S. (1975). Use of L-rhamnose to study irreversible adsorption of bacteriophage PL-1 to a strain of Lactobacillus casei. *J. Gen. Virol.* 28, 29–35. doi: 10.1099/0022-1317-28-1-29

Xie, J., Lu, W., Zhong, L., Hu, Y., Li, Q., Ding, R., et al. (2020). Alterations in gut microbiota of abdominal aortic aneurysm mice. *BMC Cardiovasc. Disord.* 20:32. doi: 10.1186/s12872-020-01334-2

Yoon, H. S., Cho, C. H., Yun, M. S., Jang, S. J., You, H. J., Kim, J. H., et al. (2021). Akkermansia muciniphila secretes a glucagon-like peptide-1-inducing protein that improves glucose homeostasis and ameliorates metabolic disease in mice. *Nat. Microbiol.* 6, 563–573. doi: 10.1038/s41564-021-00880-5

Yue, J., Yin, L., Shen, J., and Liu, Z. (2020). A modified murine abdominal aortic aneurysm rupture model using elastase perfusion and angiotensin II Infusion. *Ann. Vasc. Surg.* 67, 474–481. doi: 10.1016/j.avsg.2020.03.002

Zhai, Q., Feng, S., Arjan, N., and Chen, W. (2019). A next generation probiotic, Akkermansia muciniphila. *Crit. Rev. Food Sci. Nutr.* 59, 3227–3236. doi: 10.1080/10408398.2018.1517725

Zhang, L., Qin, Q., Liu, M., Zhang, X., He, F., and Wang, G. (2018). Akkermansia muciniphila can reduce the damage of gluco/lipotoxicity, oxidative stress and inflammation, and normalize intestine microbiota in streptozotocin-induced diabetic rats. *Pathog. Dis.* 76:28. doi: 10.1093/femspd/fty028

Zhang, T., Li, Q., Cheng, L., Buch, H., and Zhang, F. (2019). Akkermansia muciniphila is a promising probiotic. *Microb. Biotechnol.* 12, 1109–1125. doi: 10.1111/1751-7915.13410

Zhong, L., He, X., Si, X., Wang, H., Li, B., Hu, Y., et al. (2019). SM22α (Smooth Muscle 22α) Prevents aortic aneurysm formation by inhibiting smooth muscle cell phenotypic switching through suppressing reactive oxygen Species/NF-κB (Nuclear Factor-κB). *Arterioscler. Thromb. Vasc. Biol.* 39, e10–e25. doi: 10.1161/atvbaha.118.311917

Zhou, K. (2017). Strategies to promote abundance of Akkermansia muciniphila, an emerging probiotics in the gut, evidence from dietary intervention studies. *J. Funct. Foods* 33, 194–201. doi: 10.1016/j.jff.2017.03.045

Conflict of Interest: The authors declare that the research was conducted in the absence of any commercial or financial relationships that could be construed as a potential conflict of interest.

Publisher's Note: All claims expressed in this article are solely those of the authors and do not necessarily represent those of their affiliated organizations, or those of the publisher, the editors and the reviewers. Any product that may be evaluated in this article, or claim that may be made by its manufacturer, is not guaranteed or endorsed by the publisher.

frontiers | Frontiers in Microbiology

REVIEW
published: 16 June 2022
doi: 10.3389/fmicb.2022.924398

Antifungal Mechanisms and Application of Lactic Acid Bacteria in Bakery Products: A Review

Aiping Liu†, Ruixia Xu†, Shun Zhang, Yuting Wang, Bin Hu*, Xiaolin Ao, Qin Li, Jianlong Li, Kaidi Hu, Yong Yang and Shuliang Liu*

College of Food Science, Sichuan Agricultural University, Ya'an, China

Bakery products are nutritious, but they are susceptible to fungal contamination, which leads to a decline in quality and safety. Chemical preservatives are often used to extend the shelf-life of bakery products, but long-term consumption of these preservatives may increase the risk of chronic diseases. Consumers increasingly demand food with fewer chemical preservatives. The application of lactic acid bacteria (LAB) as a novel biological preservative not only prolongs the shelf-life of bakery products but also improves the baking properties of bakery products. This review summarizes different types and action mechanisms of antifungal compounds produced by LAB, factors affecting the production of antifungal compounds, and the effects of antifungal LAB on bakery products, providing a reference for future applications of antifungal LAB in bakery products.

Keywords: lactic acid bacteria, antifungal mechanisms, bakery products, biological preservative, fungal contamination

OPEN ACCESS

Edited by:
Rina Wu,
Shenyang Agricultural University, China

Reviewed by:
Francesca Valerio,
Italian National Research Council, Italy
Qiya Yang,
Jiangsu University, China

***Correspondence:**
Bin Hu
hubin2555@sina.com
Aiping Liu
lapfood@126.com

†*These authors have contributed equally to this work and share first authorship*

Specialty section:
This article was submitted to Food Microbiology, a section of the journal Frontiers in Microbiology

Received: *20 April 2022*
Accepted: *25 May 2022*
Published: *16 June 2022*

Citation:
Liu A, Xu R, Zhang S, Wang Y, Hu B, Ao X, Li Q, Li J, Hu K, Yang Y and Liu S (2022) Antifungal Mechanisms and Application of Lactic Acid Bacteria in Bakery Products: A Review. Front. Microbiol. 13:924398. doi: 10.3389/fmicb.2022.924398

INTRODUCTION

Bakery products are among the most popular foods consumed daily by people throughout the world (ReportLinker, 2020). However, bakery products are susceptible to fungal contamination that greatly reduces their shelf-life, resulting in food waste and economic loss. Fungal contamination can also become a serious food safety issue due to the potential production and ingestion of toxic aflatoxins and other mycotoxins (Mahato et al., 2021). Inhibition of fungal growth on bakery products therefore offers significant economic and health benefits. The primary methods of inhibition that are being explored to extend the shelf-life of bakery products currently focus on physical methods (radio frequency sterilization, microwave sterilization, drying, pulsed-light, and low-pressure mercury lamp treatment) and chemical preservatives (calcium propionate, sorbate, benzoates, EDTA, nitrites, and sulfites; Salaheen et al., 2014). Although physical methods are better at maintaining taste, they simultaneously destroy the nutritional value of bakery products and are often costly. Calcium propionate and other chemical preservatives can be added directly to bakery products; however, long-term consumption of these preservatives may increase the risk of chronic disease (Qian et al., 2021). Food companies are interested in reducing the use of chemical preservatives because of the need of consumers for preservative-free foods (Sadeghi et al., 2019). Biological preservatives, on the other hand, are more consumer-friendly, ecologically sustainable, and have prospectively broad applications in controlling fungal contamination. Lactic acid bacteria (LAB) have gained attention as a potential biological preservative option since they are generally recognized as safe, and produce metabolites that

can inhibit fungal growth. For example, Korcari et al. (2021) found that *Pediococcus pentosaceus* MB33 and *Weissella cibaria* CM32 exhibited high antifungal activity, enhancing the shelf-life of emmer bread. LAB also improve baking properties of bakery products including texture, specific volume, and flavors of bakery products (Ma et al., 2021). Several antifungal compounds produced by *Leuconostoc citreum* HO12 and *Weissella koreensis* HO20 improved the flavor and texture of bakery products (Choi et al., 2012). Therefore, investigating the application of antifungal LAB in bakery products has substantial value. While there are reviews on the application of antifungal LAB in foods, and mechanisms of antifungal substances, few of them have comprehensively focused on the application of LAB as biopreservatives in bakery products, and the antifungal mechanism of exopolysaccharides (EPS; Crowley et al., 2013a; Chen et al., 2021b; Nasrollahzadeh et al., 2022). The present review seeks to present an update on the antifungal compounds produced by LAB and their mechanism of action toward target fungi, factors affecting the production of antifungal compounds by LAB, and the application of LAB in bakery products.

HEALTH PROBLEMS CAUSED BY FUNGAL CONTAMINATION

The most common fungi related to spoilage of bakery products include *Aspergillus*, *Penicillium*, *Fusarium*, *Mucor*, *Rhizopus*, *Candida*, and *Endopyrrhiza* (Mohamad Asri et al., 2020). Fungal contamination not only reduces the quality of bakery products but also results in huge economic losses to both consumers and the bakery industry. In addition, some fungi (*Aspergillus*, *Penicillium*, *Fusarium*, etc.) may produce mycotoxins such as aflatoxin, ochratoxin, and zearalenone (Krnjaja et al., 2019; Drakopoulos et al., 2021). Aflatoxins are difuran ring toxoids mainly produced by certain strains of *Aspergillus flavus* and *Aspergillus parasitica* (Wang et al., 2022a). Aflatoxins are carcinogenic, teratogenic, and mutagenic and can damage the liver of animals (Ben Taheur et al., 2019). Aflatoxin B1 (AFB1) is the most toxic type of aflatoxin and is a significant risk factor for the development of hepatocellular carcinoma (HCC) in humans and animals (Fang et al., 2022). Ochratoxins are mycotoxins derived from *Aspergillus* and *Penicillium*, and their toxic effects include hepatotoxicity, carcinogenicity, nephrotoxicity, immunotoxicity, teratogenicity, mutagenicity, genotoxicity, embryotoxicity, as well as testicular toxicity (Amézqueta et al., 2012; Wang et al., 2022b). Zearalenone-producing fungi are mainly *Fusarium*. Zearalenone causes obvious estrogenic effects in both humans and animals, as well as serious malignant alterations and lesions in the female reproductive system (Sanad et al., 2022).

OVERVIEW OF LAB

LAB are Gram-positive, non-spore-forming, facultatively anaerobic bacteria that produce a large amount of lactic acid during carbohydrate metabolism. LAB are widely distributed in nature, and include genus such as *Aerococcus*, *Carnobacterium*, *Enterococcus*, *Lactobacillus*, *Lactococcus*, *Leuconostoc*, *Pediococcus*, *Streptococcus*, *Tetragonococcus*, *Oenococcus*, *Weissella*, and *Vagococcus* (Stiles and Holzapfel, 1997). LAB play a critical role in food fermentation to enhance food shelf-life (Pontonio and Rizzello, 2021). LAB induce rapid acidification of raw materials during fermentation, producing organic acids, CO_2, H_2O_2, fatty acids, antifungal peptides, volatile compounds, and other antifungal compounds that inhibit fungal growth (Sadeghi et al., 2019). Moreover, mycotoxins can be detoxified by LAB with the help of one or more mechanisms. For instance, the utilization of metabolites and enzymes produced by LAB strains, adsorption of mycotoxins by LAB, or competitive relationship between LAB and other mycotoxin producing fungi (Ahlberg et al., 2015). LAB produce a variety of proteolytic enzymes, including cell-wall proteinases, peptide transporters, and ample intracellular peptidases, which are capable of biodegradation of mycotoxins to less toxic and less harmful compounds (Bangar et al., 2021). Citric acid and other organic acids produced by LAB also have a great effect on degrading aflatoxins. The results from Mendez-Albores et al. (2008) showed that the aflatoxin reduction was more effective when adding aqueous citric acid in the extrusion-cooking process. Ademola et al. (2021) found that lactic acid fermentation also reduced aflatoxin and fumonisin levels in maize. LAB cell wall including peptidoglycon and polysaccharides can adsorb mycotoxin, which also caused the toxin removal (Shetty and Jespersen, 2006). As a biological preservative, LAB significantly reduce the usage of chemical preservatives in bakery food. In addition, LAB also produce exopolysaccharides, ethanol, and volatile flavor substances during fermentation, which bring balanced bread sensory profiles. The α-glucan-producing *Lactobacillus reuteri* E81 was used in bread making, which improved the rheological properties, elasticity, and microstructure of bread dough, and the texture of bread (İspirli et al., 2020). Wu et al. (2022) found that sourdough fermented with *Lactococcus lactis* FCP1921 had improved volatile flavor substance abundance in bread when compared with ordinary wheat bread.

ANTIFUNGAL COMPOUNDS PRODUCED BY LAB

Metabolism of carbohydrates, proteins, lipids, and amino acids by LAB produces a variety of antifungal compounds discussed further here (**Figure 1**).

Organic Acids

LAB produce lactic acid, acetic acid, propionic acid, citric acid, phenyllactic acid, benzoic acid, and other organic acids. Most of these organic acids have antifungal properties; however, action mechanisms of some organic acids are still unclear. Studies have shown that acetic acid's inhibition of the growth of pathogenic and spoilage bacteria and fungi may be due to its low pKa. The higher concentration of undissociated acids can traverse the cell membrane, then dissociate in the cell, resulting in acid stress (Jin et al., 2021). Relative to other

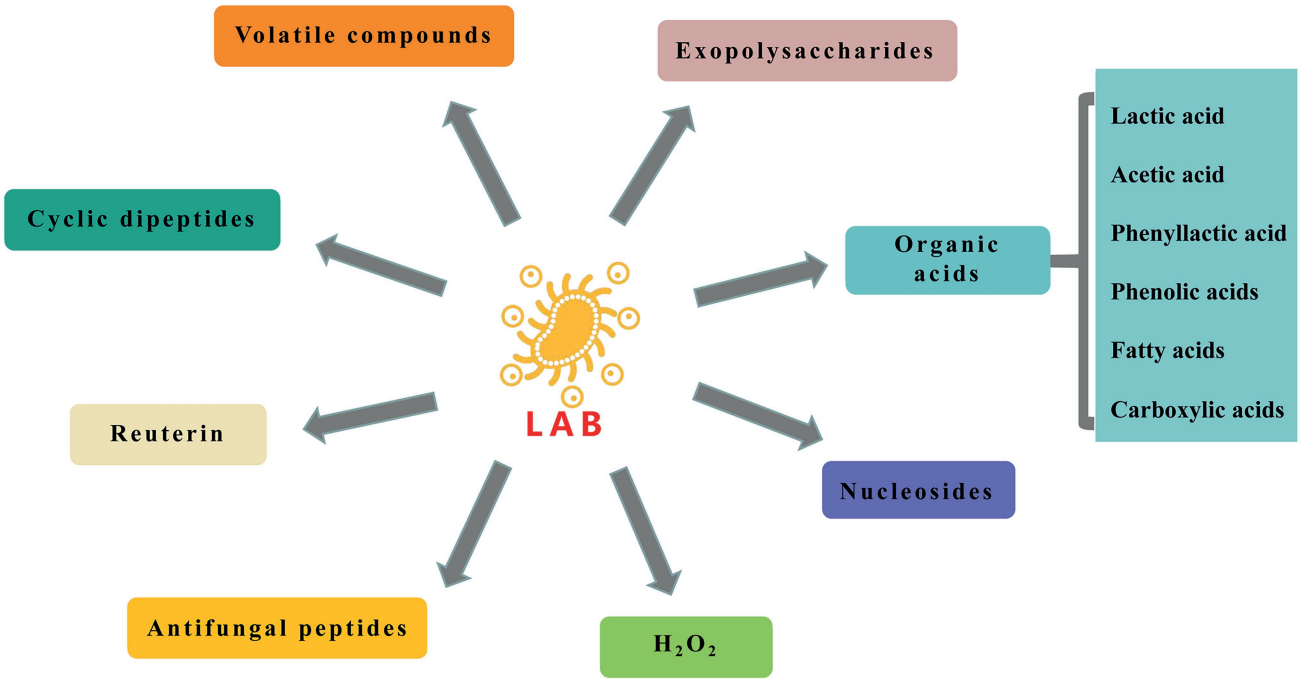

FIGURE 1 | Antifungal compounds produced by lactic acid bacteria (LAB).

organic acids, lactic acid demonstrated weaker inhibitory effects (Crowley et al., 2013a). With increased fermentation time, the lactic acid content of cell-free supernatants was positively correlated with antifungal activity, and lactic acid frequently played a synergistic role with other organic acids to ultimately enhance antifungal activity (Russo et al., 2017). Phenolic acids isolated from quinoa dough, including derivatives of cinnamic acid (p-coumaric acid, caffeic acid, and ferulic acid) and benzoic acid (vanillic acid, 4-hydroxybenzoic acid), also showed antifungal activity (Axel et al., 2016). Phenolic acids often exist in an insoluble form, or in a more complex cross-linked polymer, which can exert antioxidant and antifungal effects (John, 2008). Furthermore, some carboxylic acids produced by LAB, including 3-phenylpropionic acid, hydroxyphenyllactic acid, 3-(4-hydroxyphenyl) propionic acid, and 5-oxypyrroliden-2-carboxylic acid, showed inhibitory effects on *Mucor ractosum* and *Penicillium* (Leyva Salas et al., 2019). Honoré et al. (2016) isolated metabolites, such as 2-hydroxy-4-methylpentanoic acid, 2-hydroxy-3-phenylpropionic acid, and 2-hydroxy-3-(4-hydroxyphenylpropionic) propionic acid, from the cell-free supernatant of *Lacticaseibacillus paracasei*, which was positively correlated with inhibition of mold growth.

Phenyllactic Acid

Phenyllactic acid is derived from the catabolism of phenylalanine (Phe), which transfers its amino group to the ketoic acid receptor and then reduces the synthesized phenylpyruvate to phenyllactic acid (PLA) through dehydrogenase action (Vermeulen et al., 2006). PLA harbors broad spectrum antibacterial activity, which can destroy biofilm structures and inhibit the growth of pathogenic and spoilage bacteria and fungi. Dal Bello et al. (2007) isolated PLA, lactic acid, and two cyclic dipeptides from the cell-free supernatant of *Lactobacillus plantarum* FST1.7, all of which showed antifungal activity. Meanwhile, Gerez et al. (2009) obtained LAB with antifungal activity against *Aspergillus*, *Fusarium*, and *Penicillium* and also isolated PLA and acetic acid from these LAB. Le Lay et al. (2016a) detected PLA (22.04 mg/L) in the cell-free supernatant of *Lactobacillus spicheri* O15 with demonstrated antifungal activity. Like other organic acids, the antifungal activity of PLA is pH-dependent. At low pH, the undissociated form can easily pass through the cell membrane and accumulate within the cytoplasm, thereby causing loss of cell activity (Lambert and Stratford, 1999). At pH 3.5, the minimum concentration of PLA needed to inhibit 50% of the germination of different fungal spores was 0.03–0.07 mmol/L, while lactic acid and acetic acid were 80–180 and 0.9–18 mmol/L, respectively. Although PLA had higher antifungal activity than lactic acid and acetic acid, this was only true at high PLA concentrations and low pH (Gerez et al., 2009; Debonne et al., 2020). In addition, the minimum inhibitory concentration of PLA is different on different fungi. For example, PLA possesses MIC value of 2.5 mg/ml against *Aspergillus fumigatus*, in contrast to 20 mg/ml against *Aspergillus niger* (Lavermicocca et al., 2003; Ryan et al., 2011).

Fatty Acids

Fatty acids produced by LAB also have strong antifungal activity, and hexadecanoic acid, oleic acid, hexadecanoic acid, decanoic acid, and lauric acid isolated from antifungal LAB were confirmed

to show inhibitory effects against *Mucor ractosum* and *Penicillium common* (Leyva Salas et al., 2019). In addition, 3-hydroxy-5-dodecenoic acid purified from *Lactobacillus plantarum* EM culture using solid-phase extraction and recycling preparative HPLC also exhibited a strong antifungal activity, with MIC of 0.21 g/L and 0.25 g/L against *Aspergillus fumigatus* and *Bacillus cereus*, respectively (Mun et al., 2019). Liang et al. (2017) extracted two kinds of fatty acids from cultures of *Lactobacillus hammesii* and *Lactiplantibacillus plantarum* and found that HUFA (unsaturated fatty acids with hydroxyl groups) effectively inhibited *Aspergillus niger* and *Penicillum roqueforti* but had poor inhibitory effects on *Candida* and other yeasts. Studies have shown that the antifungal activity of fatty acids is related to their structure; while unsaturated monohydroxy fatty acids have antifungal activity, saturated hydroxy fatty acids and unsaturated fatty acids do not (Black et al., 2013). Studies by Pohl et al. (2008) showed that the MICs of 13-HOE against *Aspergillus niger* and *Penicillum roqueforti* were 0.25 and 0.38 g/L, respectively. The MICs of 10-HOE against *Aspergillus niger* and *Penicillum roqueforti* were 0.42 and 0.38 g/l, respectively. The antifungal activity of hydroxy fatty acids might be due to their interaction with the cell membrane since distribution of hydroxy fatty acids into the fungal membrane increased membrane permeability (Sjogren et al., 2003).

H_2O_2

Some LAB produce H_2O_2, which has been proven to affect the growth and metabolism of foodborne pathogenic bacteria and fungi. As a strong oxidizer, H_2O_2 plunders electrons and molecules of nearby microorganisms and thus sterilizes by destroying protein molecular structure. Since LAB do not produce catalase, H_2O_2 cannot be decomposed, and therefore accumulates in the cell, preventing fungal growth (Nes et al., 1996). Bundgaard-Nielsen and Nielsen (1996) found that 3% H_2O_2 solution exhibited low antifungal activity against *Penicillium*, *Cladosporium*, *Scopulariopsis*, *Aspergillus*, and *Eurotium* but damaged conidia of seven fungal species. Martin and Maris (2012) tested the antifungal effect of H_2O_2 and 17 kinds of acids on fungi. The results showed that formic acid, acetic acid, propionic acid, oxalic acid, and lactic acid had synergistic effects with H_2O_2, resulting in stronger antifungal activity.

Antifungal Peptides

Antifungal peptides are the main antifungal compounds produced by LAB. Arulrajah et al. (2021) used *Lactobacillus pentosus* RK3 to ferment kenaf seeds to produce antifungal peptides, and eight cationic peptides were identified in the kenaf seed mixture, which showed inhibitory effects on *Fusarium* and *Aspergillus niger*. Among them, four peptides were shown to be similar to *Gossypium mustelinum* (cotton), two peptides corresponded to *Gossypium barbadense* (Sea-island cotton), and two were novel cationic *de novo* peptides. Similarly, Nionelli et al. (2020) identified nine peptides from bread hydrolysates fermented by *Lactobacillus brevis*, and these peptides prevented growth of *Penicillium roqueforti*. The inhibitory effect of antifungal peptides on fungi is mainly due to the interaction between negatively charged molecules of the fungal membrane and positively charged polypeptides, which destroys the membrane structure resulting in cell death (Rai et al., 2016). In addition, the activity of antifungal peptides produced by plant substrate fermentation was significantly affected by molecular weight, chemical structure, net charge, and hydrophobic ratio (Jakubczyk et al., 2020). Most of the antifungal peptides have low molecular weights, cationic charges, and low hydrophobicity (Muhialdin et al., 2016). Muhialdin et al. (2020) confirmed the above views, and they isolated a component targeting *Aspergillus flavus* from the cell-free supernatant of *Lactiplantibacillus plantarum* TE10 and 37 peptides identified from the isolated component—22 were cationic peptides.

Antifungal peptides also inhibited conidial germination, potentially through the inhibition of germ tube elongation after conidial wall breakdown (Puig et al., 2016). Leon et al. (2020) observed that the antifungal peptides AMPs LR14 produced by *Lactiplantibacillus plantarum* inhibit conidial germination. Fungal mycelia treated with antifungal peptides were wrinkled with no conidia detected, and the expression levels of *brlA*, a transcription factor involved in fungal meristem, were also significantly decreased.

Volatile Compounds

LAB produce several volatile compounds in the fermentation process, which not only improves the aroma profile but also inhibits fungal growth. Leyva Salas et al. (2019) isolated 35 volatile compounds from dairy products fermented by antifungal LAB, among which diacetyl and acetoin had antifungal activity and exhibited significant antifungal effects against *Penicillium common* and *Mucor ractosum*. Diacetyl, lactic acid, acetic acid, and acetoin were reported to be produced by catabolism of the two main carbon substrates present in dairy products, lactose and citrate (Urbach, 1995). Thus, acetoin and diacetyl with antifungal activity may be produced by lactic acid bacteria fermentation. Aunsbjerg et al. (2015) isolated diacetyl, the main volatile compound, from *Lacticaseibacillus paracasei* DGCC2132, which slowed down the growth of *Penicillium* for 5 days at concentrations above 75 μg/ml. The antifungal mechanisms of diacetyl may be due to the induction of ROS accumulation, which destroys the membrane structure resulting in the leakage of cellular materials and cell death (Shi and Knøchel, 2021). In addition, Coda et al. (2011) found that soluble extract of *Lactiplantibacillus plantarum* by Tris-HCI buffer contained ethyl acetate and ethanol, and confirmed that the conidia germination of *Penicillium roqueforti* was completely inhibited when ethyl acetate and ethanol concentrations were 6.81 and 1.69 mg/ml, respectively.

Cyclic Dipeptides

Cyclic dipeptides (CDPs) are metabolites widely synthesized by cyclodipeptide synthases or non-ribosomal peptide synthetases, by both prokaryotic and eukaryotic cells. CDPs are minimal cyclic peptides formed by inner cyclization of two amino acids amides and have various bioactive properties including anticancer, immunomodulatory, and antifungal activities (Rhee, 2004).

Ström et al. (2002) reported for the first time that the production of antifungal cyclic dipeptides cyclo(L-Phe-L-Pro) and cyclo(L-Phe-trans-4-OH-L-Pro) by LAB, and MIC value of cyclo(L-Phe-L-Pro) against *Penicillium roqueforti* and *Aspergillus fumigatus* was 20 mg/ml. Cyclo(L-His-L-Pro), Cyclo(L-Pro-L-Pro), Cyclo(L-Met-L-Pro), Cyclo(L-Leu-L-Pro), and Cyclo(L-Tyr-L-Pro) were isolated from the cell-free supernatant of *Lactobacillus amylovorus* LA 19280, and these cyclic dipeptides all showed antifungal activity, with MICs between 25 and 50 mg/ml against *Aspergillus fumigatus* (Ryan et al., 2011). In addition, cis-cyclo(L-Tyr-L-Pro), cis-cyclo(L-Val-L-Pro), cis-cyclo(L-Ser-L-Pro), cis-cyclo(L-Leu-L-Pro), and cis-cyclo(L-Phe-LPro) isolated from the cell-free supernatant of LAB with antifungal activity, had inhibitory effects on *Ganoderma boninense*, with MICs of 8.2, 8.1, 9.0, 8.4, 6.8 mmol/L, respectively (Kwak et al., 2014). Furthermore, Kwak et al. (2018) isolated 15 cyclic dipeptides containing proline and a single cyclic dipeptide without proline from *Lactiplantibacillus plantarum* LBP-K10, all of which exhibited antifungal activity. Combinations of multiple cyclic dipeptides showed higher antifungal activity than single cyclic dipeptides, with MICs between 18.6 and 22.7 mg/L against *Candida albicans*. Cyclic dipeptides can also inhibit fungal biofilm formation. Li et al. (2022b) isolated cyclo (leu-pro) and cyclo (phe-pro) from the cell-free supernatant of *Lactiplantibacillus plantarum* CCFM8724 and found that these two cyclic dipeptides decreased the expression of virulence genes in *C. albicans* (*ALS3* and *HWP1* genes), achieving a reduction of biofilm formation. Notably, cyclic dipeptides isolated by Ebrahimi et al. (2020) from the cell-free supernatant of *P. pentosaceus* also reduced aflatoxin content, and exhibited the most antifungal activity, reducing aflatoxin G1 and G2 by 82.06% and 87.32%, respectively.

Reuterin

Reuterin is a non-protein, broad-spectrum antimicrobial agent secreted by *Limosilactobacillus reuteri*, which controls growth of Gram-positive and Gram-negative bacteria, and fungi. It is water-soluble, heat-resistant, and highly stable (Cleusix et al., 2007). The mechanism of reuterin's inhibition of fungi may be oxidative stress induced by modification of thiol groups in proteins and small molecules (Schaefer et al., 2010). The growth of *Fusarium culmorum*, *Aspergillus niger*, and *Penicillium expansum* spores were inhibited by reuterin produced by *Limosilactobacillus reuteri* R29; the cell-free supernatant with the highest concentration of reuterin completely prevented the growth of all three fungal spores. The MIC_{90} of reuterin against *Fusarium culmorum* was 4 mmol/L, while its MIC_{90} against both *Aspergillus niger* and *Penicillium expansum* was 8 mmol/L (Schmidt et al., 2018). Reuterin produced by *Limosilactobacillus reuteri* completely inhibited the growth of *Penicillium expansum* at a concentration of 10 mmol/L, and the concentration of reuterin was positively correlated with antifungal effects, within a specific range (Ortiz-Rivera et al., 2017).

Nucleoside (Cytidine)

Nucleosides are the basic elements of biological cells that maintain life, participate in the metabolic processes of DNA, and have a variety of anti-tumor, anti-viral, and antifungal functions (Dan et al., 2021). Ryan et al. (2011) isolated and identified two nucleosides with antifungal activity, cytidine and 2′ -deoxycytidine, from the cell-free supernatant of *L. amylovorus* LA 19280, and observed that these nucleosides showed antifungal activity against *Aspergillus fumigatus*, with MIC values >200 mg/ml. Chen et al. (2021a) also detected cytidine and 2′ -deoxycytidine in the cell-free supernatant of *Lactobacillus kefiri* M4 and *Pediococcus acidilactici* MRS-7, which retarded the growth of *Penicillum expansum*. In addition, nucleosides were also detected in the cell-free supernatant of other types of LAB, such as *Lactiplantibacillus plantarun*, *Propionibacterium freudenreichii*, *Limosilactobacillus reuteri*, and *L. brevis* (Le Lay et al., 2016a; Yépez et al., 2017). However, the studies of cytidine produced by LAB are limited, and cytidine's antifungal mechanisms are still unclear.

Exopolysaccharides

Exopolysaccharides (EPSs) are biopolymers produced by LAB, mainly during their growth and metabolism period. EPS are secondary metabolites of microorganisms, can improve the texture and nutritional value of food, and inhibit growth of pathogens and fungi (Moradi et al., 2021). Rodrigues et al. (2005) reported that Kefiran, an edible, biodegradable, and water-soluble EPS produced by LAB, could prevent growth of bacteria and fungi, with MIC of 462 mg/L against *C. albicans*. Nehal et al. (2019) found that EPS produced by *L. lactis* F-MOU also exhibited significant antifungal effects against *C. albicans*, with MIC of 16 mg/ml. EPS inhibition of the growth of pathogenic and spoilage bacteria and fungi may be through the disordering of cell division, destruction of cell membrane and plasma membrane, and decomposition of DNA (Wu et al., 2010). EPS can interact with fungi, depending on their cell membrane permeability, then attack the respiratory chain and cell division machinery, leading to cell death (Abinaya et al., 2018). EPS can also act as a barrier, preventing the input of nutrients to pathogenic bacteria and fungi, thus slowing down their growth; this barrier effect might increase with increased polysaccharide concentration (Han et al., 2016). In addition, EPS could degrade the biofilm of *C. albicans* and reduce the adhesion of other fungi (Abinaya et al., 2018). Similarly, Wang et al. (2020) also found that EPS (composed of glucose, galactose, mannose, and arabinose) produced by *Lactobacillus fermentum* S1 showed activity against biofilms. EPS reduces hydrophobicity, zeta potential, and interactions between cells forming biofilms. The antibiofilm activity of EPS might be related to modifying the bacterial and fungal cell surfaces, inhibiting the attachment of pathogenic and fungal cells to the surface or downregulating the gene expression involved in biofilm formation (Wang et al., 2015).

FACTORS AFFECTING PRODUCTION OF ANTIFUNGAL COMPOUNDS BY LACTIC ACID BACTERIA

Different LAB produce different types of antifungal compounds. In addition to the species of LAB, parameters including

temperature, time of incubation, nutritional factors, and growth medium also affect the production of antifungal compounds by LAB (Oliveira et al., 2014).

Crowley et al. (2013b) studied the effect of temperature on the production of antifungal compounds using six antifungal LAB, and they reported that the highest antifungal activity was recorded at 30°C. Valerio (2004) reported the effect of time of incubation on the production of antifungal compounds by *Lactiplantibacillus plantarum* ITM21B, and it was found that the maximum production of PLA and OH-PLA was reached after 72 h of incubation.

Mu et al. (2009) optimized the medium components for the production of PLA by *Lactobacillus* sp. SK007. And maximal PLA was obtained when the medium included 30 g/L glucose, 3 g/L K_2HPO_4, 5 g/L phenylpyruvic acid (PPA), 30 g/L yeast powder, 3 g/L CH_3COONa, 47 g/L corn steep liquor, and 3 ml g/L Tween-80. Roy et al. (1996) found that compared to M17 and MRS growth media, the cell-free supernatant of *L. lactis* subsp. *lactis* CHD-28.3 in Elliker's broth showed optimum antifungal activity against *Aspergillus flavus*. Magnusson and Schnürer (2001) reported that PLA yield were increased by the addition of peptides, α-ketoglutarate, citric acid in growth medium. Similar results were also obtained by Schmidt et al. (2018). The production of PLA was significantly increased by the addition of 1.5% phenylalanine (w/v) to MRS broth. And, a maximum yield of reuterin and the highest fungal inhibition were achieved by supplementation of 500 mmol/L glycerol and a reduced glucose content (1.5%) in MRS broth. The synthesis of reuterin was also correlated with temperature, pH, microbial concentration, oxygen concentration, and culture time (Ortiz-Rivera et al., 2017).

APPLICATION OF ANTIFUNGAL LAB IN BAKERY PRODUCTS

Sourdough is a natural dough improver that can be used in making bakery products (Nionelli and Rizzello, 2016). Traditionally, the early sourdough (sourdough type I) is obtained after spontaneous fermentation of cereal flour using continuous backslopping. The microorganisms of spontaneous fermentation originate mainly from flours and processing equipment. However, sourdough type I has some disadvantages, including a long fermentation cycle and unstable properties. Therefore, the use of sourdough fermented with certain LAB species together with baker's yeast for dough leavening is more attractive (Drakula et al., 2021). Sourdough fermentation improves the rheological properties of the dough and the nutritional properties of bakery products. This technique also has the potential to inhibit growth of fungi and extend the shelf-life of bakery products.

LAB Used to Extend the Shelf-Life of Bakery Products

Sun et al. (2020) added *Lactiplantibacillus plantarum* LB-1 suspension, which had strong antifungal activity against *Aspergillus ochraceus*, *Aspergillus niger*, *Fusarium graminearum*, *Aspergillus flavus*, *Aspergillus fumigatus*, and *Penicillium citrinum*, into dough, and doubled the shelf-life of whole wheat bread, from 3 to 6 days. Sourdough inoculated with *Lactiplantibacillus plantarum* CH1 and *Leuconostoc mesenteroides* L1 showing antifungal activity was added to bread artificially contaminated with *Aspergillus tubingensis* or *Aspergillus flavus*, and the shelf-life of bread was extended by 1 day (Ouiddir et al., 2019). Bartkiene et al. (2018) confirmed that a combination of 15% antifungal *Lactiplantibacillus plantarum* LUHS135 sourdough, and cranberry coating increased the shelf-life of bread by 6 days, and the shelf-life increased with the amount of sourdough added. However, since excessive sourdough affected the quality of bread, the amount of sourdough added should be determined based on the specific strain selected.

Interestingly, LAB show different antifungal activity in sourdough made with different cereals. Axel et al. (2016) confirmed the above views, and they reported that *Limosilactobacillus reuteri* R29 and *L. brevis* R2 δ with antifungal activity were inoculated into quinoa and white rice flour, for bread making. However, the shelf-life of quinoa bread and white rice flour bread inoculated with the same LAB were different. The concentration of carboxylic acid in quinoa sourdough was much higher than that in rice sourdough, which indicated that the level of metabolites produced by LAB in different cereal sourdough varied. Quattrini et al. (2019) prepared wheat sourdough bread and flaxseed sourdough bread with antifungal LAB, and showed that wheat sourdough fermented with *L. hammesii* DSM16381, *Lactiplantibacillus plantarum* C264, and *L. brevis* C186 greatly extended the shelf-life of bread contaminated by *Aspergillus niger*; however, there was no significant effect on bread contaminated with *Penicillium roqueforti*. Furthermore, they also found that the combination of ricinoleic acid and wheat sourdough greatly extended the shelf-life of bread contaminated with *Aspergillus niger* or *Penicillium roqueforti*, compared with linseed sourdough fermented with the same LAB. More examples of using LAB to extend the shelf-life of bakery products can be found in **Table 1**.

LAB Used to Improve the Baking Characteristics of Bakery Products

Antifungal LAB not only prolong the shelf-life of bakery products but also improve the aroma profile and texture of bakery products (Moghaddam et al., 2020). Rizzello et al. (2011) baked using wheat germ sourdough, which not only produced bread with extended shelf-life but also with the lowest hardness and maximum specific volume. *L. brevis* AM7 with antifungal activity was inoculated into bread hydrolysate, and then the bread hydrolysate was employed for bread making. The specific volume of bread supplemented with 18% bread hydrolysate was improved compared to bread with lower percentages of bread hydrolysate (Nionelli et al., 2020). Bread containing hop extract (25%, vol/wt) sourdough also had a similar effect, prolonging the shelf-life of bread by 7 days, and enhancing its nutritional value, phytase activity, total phenolic content, and antioxidant activity. In addition, although bread with added hop extract had increased

TABLE 1 | Application of antifungal LAB in prolonging the shelf-life of bakery products.

Raw material of sourdough	Antifungal LAB	Activity spectrum	Impact on the shelf-life of bakery products	References
Wheat flour	*Lactobacillus sakei* KTU05-6, *Pediococcus acidilactici* KTU05-7, *Pediococcus pentosaceus* KTU05-8, *Pediococcus pentosaceus* KTU05-9, *Pediococcus pentosaceus* KTU05-10	*Penicillium expansum*, *Aspergillus versicolor*, *Penicillium chrysogenum*, *Fusarium culmorum*, *Aspergillus fumigatus*, *Candida parapsilosis*, *Debaryomyces hansenii*	Shelf-life extended by 0.5–4.5 days	Cizeikiene et al., 2013
Wheat flour	*Lactiplantibacillus plantarum* CRL 778	Fungi in the environment	Shelf-life enhanced by 14 days	Gerez et al., 2015
Peas, lentils, and broad bean flour	*Lactiplantibacillus plantarum* 1A7	*Penicillium roqueforti* DPPMAF1	7 Days extension in shelf-life	Rizzello et al., 2017
Wheat flour	*Pediococcus acidilactici* CRL 1753	*Aspergillus niger CH2*, *Aspergillus japonicas CH5*, *Penicillium roqueforti CH4*, *Penicillium digitatum CH10*, *Metschnikowia pulcherrima CH7*	Shelf-life enhanced by 6 days	Bustos et al., 2018
Whey	*Lactiplantibacillus plantarum* CECT 220, *Lactiplantibacillus plantarum* CECT 221, *Lactiplantibacillus plantarum* CECT 223, *Lactiplantibacillus plantarum* CECT 748	*Penicillium expansum* CECT 2278, *Penicillium brevicompactum* CECT 2316	Enhanced the shelf-life of bread by 1–3 days	Izzo et al., 2020
Rye and wheat	*Pediococcus pentosaceus* KCCM12515P	*Aspergillus flavus*	2 Days extension in shelf-life	Jin et al., 2021

TABLE 2 | Application of antifungal LAB in improving the baking characteristics of bakery products.

Antifungal LAB	Impact on the shelf-life of bakery products	Impact on the baking characteristics of bakery products	References
Pediococcus pentosaceus LUHS183, *Pediococcus acidilactici* LUHS29, *Lactococcus paracasei* LUHS244, *Lactococcus brevis* LUHS173, *Lactiplantibacillus plantarum* LUHS135, *Leuconostoc mesenteroides* LUHS242	Shelf-life extended by 2–7 days	Increased the specific volume of bread and reduced acrylamide content	Bartkiene et al., 2018
Lactiplantibacillus plantarum	2 Days extension in shelf-life	Increased the sensory score and specific volume of bread and decreased hardness	Karimi et al., 2020
Lactiplantibacillus plantarum FST 1.7	Shelf-life extended by 3 days	Decreased the hardness of bread and increased elasticity	Moore et al., 2008
Lactiplantibacillus plantarum L9	7 Days extension in shelf-life	Maintained global appreciation unchanged	Ran et al., 2022
Weissella confusa A16	Shelf-life extended by 1–4 days	Increased the specific volume, sensory score, and moister mouthfeel of bread and decreased hardness	Wang et al., 2022c

bitterness in taste and odor, and reduced sensory score, LAB fermentation overall improved the aroma profile and sensory acceptability of the bread (Nionelli et al., 2018).

The combination of antifungal LAB and fruit fermentation substrate also increased the shelf-life of bakery products and improved their texture, flavor, and nutritional value. The combination of LAB and pitaya inhibited growth of mold; LAB also promoted the release of phenolic acids from pitaya and the conversion of insoluble dietary fiber to soluble dietary fiber. These changes probably favored the formation of covalent and non-covalent linkages with S–S bonds in dough, helping to maintain the integrity of the gluten network structure (Omedi et al., 2021). After fermentation by LAB, the molecular properties of phenolic compounds in fruits can be changed to produce new derivative compounds with more bioactive potential, thereby increasing their antioxidative properties (Massot-Cladera et al., 2014; Septembre-Malaterre et al., 2018). In addition, LAB can use different kinds of fruit sugars to produce different types of EPS. EPS is a natural, high molecular weight polymer with high viscosity, which can be used as a stabilizer and thickener to improve the rheological properties, taste, porosity, and specific volume of bakery products (Li et al., 2022a). A comprehensive list of LAB with potential for improving the baking characteristics of bakery products is listed in **Table 2**.

LAB Used to Improve the Safety of Bakery Products

Grains, the raw material of bakery products, are prone to fungal contamination and may be contaminated by mycotoxins

TABLE 3 | Application of antifungal LAB in improving the safety of bakery products.

Antifungal LAB	Impact on the shelf-life of bakery products	Impact on the safety of bakery products	References
Limosilactobacillus reuteri 5529, *Lactobacillus spicheri* O15, *Lactobacillus citreum* L123	Delayed the growth of fungi in milk bread rolls	Compared with potassium sorbate, sodium benzoate, and calcium propionate, LAB had better preservative effect and reduced the addition of chemical preservatives	Le Lay et al., 2016b
Lactobacillus amylovorus DSM 19280	Enhanced the shelf-life of bread by 6–7 days	The preservative effect of bread combined with sourdough and low-salt was much better than bread added standard salt (without sourdough) and reduced the addition of salt	Belz et al., 2019
Lactobacillus coryniformis LUHS71, *Lactobacillus curvatus* LUHS51, *Lactobacillus farraginis* LUHS206, *Leuconostoc mesenteroide* LUHS225	Shelf-life extended by 3 days	Decreased the acrylamide content of bread	Bartkiene et al., 2019
Lactobacillus sanfranciscensis	Shelf-life extended by 1–35 days	The preservative effect of bread added 60 g sourdough/100 g dough was similar to bread added with calcium propionate and reduced the addition of chemical preservatives	Debonne et al., 2019
Limosilactobacillus fermentum IAL 4541, *Wickerhamomyces anomallus* IAL 4533	Shelf-life enhanced by 70 days	Compared with calcium propionate, LAB had better preservative effect and reduced the addition of chemical preservatives	Facco Stefanello et al., 2019

during the growing or storage period, potentially harming consumer health. LAB inhibit growth of fungi and reduce the contents of aflatoxins B1, B2, G1, and G2. LAB-induced degradation of mycotoxins is achieved with binding of the toxin to the bacterial cell wall (Sadeghi et al., 2019). Saladino et al. (2016) reported that *Lactiplantibacillus plantarum* strains used in fermentation of sourdough reduced bread Aflatoxin B1 levels by 99.9% as compared to the control.

In addition to mycotoxins, acrylamide, which is potentially carcinogenic and neurotoxic to human, is also a common contaminant of bakery products (Capuano and Fogliano, 2011). Fermentation with selected LAB strains can inhibit the growth of fungi and reduce acrylamide levels in bakery products, which improves the safety of bakery products. The addition of selected LAB, in combination with the antimicrobial cranberry-based coating, resulted in wheat bread with extended shelf-life and reduced acrylamide content. Moreover, the content of acrylamide gradually decreased with increasing amounts of sourdough (Bartkiene et al., 2018). The formation of acrylamide has primarily been related to reducing sugar content (Nguyen et al., 2016). LAB metabolize carbohydrates during fermentation, which reduces the reducing sugar content in dough, in turn leading to the reduction of acrylamide content in dough. In addition, the increase in organic acids also contributes to the reduction of acrylamide content in bakery products (Capuano and Fogliano, 2011).

Furthermore, the use of LAB as a biological preservative greatly reduces the addition of chemical preservatives. The results from Ryan et al. (2008) showed that the combination of sourdough and 0.1% calcium propionate effectively extended the shelf-life of bread, which was similar to bread supplemented with 0.3% calcium propionate alone. Luz et al. (2021) also found that relative to bread supplemented with 0.3% calcium propionate and 3 g/kg lactic acid, bread supplemented with 25 ml *Lactiplantibacillus plantarum* TR7 fermented whey had its shelf-life extended by 1 day, while the shelf-life of bread supplemented with 50 ml fermented whey was extended by 2 days. Ryan et al. (2011) also similarly found that 0.3% calcium propionate-supplemented bread had weaker antiseptic effects than bread fermented by *L. amylovorus* DSM 19280. The LAB-fermented bread also greatly reduced the addition of chemical preservatives and improved bakery products' safety. More examples of the use of LAB to improve the safety of bakery products can be found in **Table 3**.

SUMMARY AND PROSPECT

In conclusion, LAB have extensive application prospects in bakery products. As a new kind of biological preservative, LAB can inhibit the growth of fungi through the production of organic acids, antifungal peptides, hydrogen peroxide, diacetyl, and other antifungal compounds, which greatly extends the shelf-life of bakery products and improves the baking characteristics and safety of products. The inhibitory effects of LAB on fungi are closely linked to the presence of antifungal compounds, with synergistic effects between various compounds. Therefore, LAB capable of producing a variety of antifungal compounds should be screened for use in bakery products. Additionally, we should also pay attention to LAB with antifungal activity and other properties that enhance the flavor profile and texture of bakery products. Lastly, LAB may be incorporated into packaging of bakery products for better protective function.

AUTHOR CONTRIBUTIONS

RX: conceptualization and writing—original draft. SZ, YW, XA, QL, and JL: writing—original draft. BH: writing—original draft

and writing—review and editing. KH, YY, and SL: writing—review and editing. AL: funding acquisition, writing—review and editing, and supervision. All authors contributed to the article and approved the submitted version.

FUNDING

This work was financially supported by the Sichuan Agricultural University "Shuang-Zhi Plan" foundation.

REFERENCES

Abinaya, M., Vaseeharan, B., Divya, M., Vijayakumar, S., Govindarajan, M., Alharbi, N. S., et al. (2018). Structural characterization of *Bacillus licheniformis* Dahb1 exopolysaccharide-antimicrobial potential and larvicidal activity on malaria and Zika virus mosquito vectors. *Environ. Sci. Pollut. R.* 25, 18604–18619. doi: 10.1007/s11356-018-2002-6

Ademola, O., Saha Turna, N., Liverpool-Tasie, L. S. O., Obadina, A., and Wu, F. (2021). Mycotoxin reduction through lactic acid fermentation: evidence from commercial Ogi processors in Southwest Nigeria. *Food Control* 121:107620. doi: 10.1016/j.foodcont.2020.107620

Ahlberg, S. H., Joutsjoki, V., and Korhonen, H. J. (2015). Potential of lactic acid bacteria in aflatoxin risk mitigation. *Int. J. Food Microbiol.* 207, 87–102. doi: 10.1016/j.ijfoodmicro.2015.04.042

Amézqueta, S., Schorr-Galindo, S., Murillo-Arbizu, M., González-Peñas, E., López De Cerain, A., and Guiraud, J. P. (2012). OTA-producing fungi in foodstuffs: a review. *Food Control* 26, 259–268. doi: 10.1016/j.foodcont.2012.01.042

Arulrajah, B., Muhialdin, B. J., Qoms, M. S., Zarei, M., Hussin, A. S. M., Hasan, H., et al. (2021). Production of cationic antifungal peptides from kenaf seed protein as natural bio preservatives to prolong the shelf-life of tomato puree. *Int. J. Food Microbiol.* 359:109418. doi: 10.1016/j.ijfoodmicro.2021.109418

Aunsbjerg, S. D., Honoré, A. H., Marcussen, J., Ebrahimi, P., Vogensen, F. K., Benfeldt, C., et al. (2015). Contribution of volatiles to the antifungal effect of *Lactobacillus paracasei* in defined medium and yogurt. *Int. J. Food Microbiol.* 194, 46–53. doi: 10.1016/j.ijfoodmicro.2014.11.007

Axel, C., Brosnan, B., Zannini, E., Furey, A., Coffey, A., and Arendt, E. K. (2016). Antifungal sourdough lactic acid bacteria as biopreservation tool in quinoa and rice bread. *Int. J. Food Microbiol.* 239, 86–94. doi: 10.1016/j.ijfoodmicro.2016.05.006

Bangar, S. P., Sharma, N., Kumar, M., Ozogul, F., Purewal, S. S., and Trif, M. (2021). Recent developments in applications of lactic acid bacteria against mycotoxin production and fungal contamination. *Food Biosci.* 44:101444. doi: 10.1016/j.fbio.2021.101444

Bartkiene, E., Bartkevics, V., Lele, V., Pugajeva, I., Zavistanaviciute, P., Mickiene, R., et al. (2018). A concept of mould spoilage prevention and acrylamide reduction in wheat bread: application of lactobacilli in combination with a cranberry coating. *Food Control* 91, 284–293. doi: 10.1016/j.foodcont.2018.04.019

Bartkiene, E., Bartkevics, V., Lele, V., Pugajeva, I., Zavistanaviciute, P., Zadeike, D., et al. (2019). Application of antifungal lactobacilli in combination with coatings based on apple processing by-products as a bio-preservative in wheat bread production. *J. Food Sci. Technol.* 56, 2989–3000. doi: 10.1007/s13197-019-03775-w

Belz, M. C. E., Axel, C., Arendt, E. K., Lynch, K. M., Brosnan, B., Sheehan, E. M., et al. (2019). Improvement of taste and shelf life of yeasted low-salt bread containing functional sourdoughs using *Lactobacillus amylovorus* DSM 19280 and *Weisella cibaria* MG1. *Int. J. Food Microbiol.* 302, 69–79. doi: 10.1016/j.ijfoodmicro.2018.07.015

Ben Taheur, F., Mansour, C., Kouidhi, B., and Chaieb, K. (2019). Use of lactic acid bacteria for the inhibition of *Aspergillus flavus* and *Aspergillus carbonarius* growth and mycotoxin production. *Toxicon* 166, 15–23. doi: 10.1016/j.toxicon.2019.05.004

Black, B. A., Zannini, E., Curtis, J. M., and Ganzle, M. G. (2013). Antifungal hydroxy fatty acids produced during sourdough fermentation: microbial and enzymatic pathways, and antifungal activity in bread. *Appl. Environ. Microbiol.* 79, 1866–1873. doi: 10.1128/AEM.03784-12

Bundgaard-Nielsen, K., and Nielsen, P. V. (1996). Fungicidal effect of 15 disinfectants against 25 fungal contaminants commonly found in bread and cheese manufacturing. *J. Food Prot.* 59, 268–275. doi: 10.4315/0362-028x-59.3.268

Bustos, A. Y., Font de Valdez, G., and Gerez, C. L. (2018). Optimization of phenyllactic acid production by *Pediococcus acidilactici* CRL 1753. Application of the formulated bio-preserver culture in bread. *Biol. Control* 123, 137–143. doi: 10.1016/j.biocontrol.2018.05.017

Capuano, E., and Fogliano, V. (2011). Acrylamide and 5-hydroxymethylfurfural (HMF): a review on metabolism, toxicity, occurrence in food and mitigation strategies. *LWT* 44, 793–810. doi: 10.1016/j.lwt.2010.11.002

Chen, H., Ju, H., Wang, Y., Du, G., Yan, X., Cui, Y., et al. (2021a). Antifungal activity and mode of action of lactic acid bacteria isolated from kefir against *Penicillium expansum*. *Food Control* 130:108274. doi: 10.1016/j.foodcont.2021.108274

Chen, H., Yan, X., Du, G., Guo, Q., Shi, Y., Chang, J., et al. (2021b). Recent developments in antifungal lactic acid bacteria: application, screening methods, separation, purification of antifungal compounds and antifungal mechanisms. *Crit. Rev. Food Sci. Nutr.*, 1–15. doi: 10.1080/10408398.2021.1977610 [Epub ahead of print]

Choi, H., Kim, Y. W., Hwang, I., Kim, J., and Yoon, S. (2012). Evaluation of *Leuconostoc citreum* HO12 and *Weissella koreensis* HO20 isolated from kimchi as a starter culture for whole wheat sourdough. *Food Chem.* 134, 2208–2216. doi: 10.1016/j.foodchem.2012.04.047

Cizeikiene, D., Juodeikiene, G., Paskevicius, A., and Bartkiene, E. (2013). Antimicrobial activity of lactic acid bacteria against pathogenic and spoilage microorganism isolated from food and their control in wheat bread. *Food Control* 31, 539–545. doi: 10.1016/j.foodcont.2012.12.004

Cleusix, V., Lacroix, C., Vollenweider, S., Duboux, M., and Le Blay, G. (2007). Inhibitory activity spectrum of reuterin produced by *Lactobacillus reuteri* against intestinal bacteria. *BMC Microbiol.* 7:101. doi: 10.1186/1471-2180-7-101

Coda, R., Cassone, A., Rizzello, C. G., Nionelli, L., Cardinali, G., and Gobbetti, M. (2011). Antifungal activity of *Wickerhamomyces anomalus* and *Lactobacillus plantarum* during sourdough fermentation: identification of novel compounds and long-term effect during storage of wheat bread. *Appl. Environ. Microbiol.* 77, 3484–3492. doi: 10.1128/AEM.02669-10

Crowley, S., Mahony, J., and van Sinderen, D. (2013a). Current perspectives on antifungal lactic acid bacteria as natural bio-preservatives. *Trends Food Sci. Technol.* 33, 93–109. doi: 10.1016/j.tifs.2013.07.004

Crowley, S., Mahony, J., and van Sinderen, D. (2013b). Broad-spectrum antifungal-producing lactic acid bacteria and their application in fruit models. *Folia Microbiol.* 58, 291–299. doi: 10.1007/s12223-012-0209-3

Dal Bello, F., Clarke, C. I., Ryan, L. A. M., Ulmer, H., Schober, T. J., Ström, K., et al. (2007). Improvement of the quality and shelf life of wheat bread by fermentation with the antifungal strain *Lactobacillus plantarum* FST 1.7. *J. Cereal Sci.* 45, 309–318. doi: 10.1016/j.jcs.2006.09.004

Dan, A., Hu, Y., Chen, R., Lin, X., Tian, Y., and Wang, S. (2021). Advances in research on chemical constituents and pharmacological effects of *Paecilomyces hepiali*. *Food Sci. Human Wellness* 10, 401–407. doi: 10.1016/j.fshw.2021.04.002

Debonne, E., Baert, H., Eeckhout, M., Devlieghere, F., and Van Bockstaele, F. (2019). Optimization of composite dough for the enrichment of bread crust with antifungal active compounds. *LWT* 99, 417–422. doi: 10.1016/j.lwt.2018.10.020

Debonne, E., Vermeulen, A., Bouboutiefski, N., Ruyssen, T., Van Bockstaele, F., Eeckhout, M., et al. (2020). Modelling and validation of the antifungal activity of DL-3-phenyllactic acid and acetic acid on bread spoilage moulds. *Food Microbiol.* 88:103407. doi: 10.1016/j.fm.2019.103407

Drakopoulos, D., Sulyok, M., Krska, R., Logrieco, A. F., and Vogelgsang, S. (2021). Raised concerns about the safety of barley grains and straw: a Swiss survey reveals a high diversity of mycotoxins and other fungal metabolites. *Food Control* 125:107919. doi: 10.1016/j.foodcont.2021.107919

Drakula, S., Novotni, D., Čukelj Mustač, N., Voučko, B., Krpan, M., Hruškar, M., et al. (2021). Alteration of phenolics and antioxidant capacity of gluten-free bread by yellow pea flour addition and sourdough fermentation. *Food Biosci.* 44:101424. doi: 10.1016/j.fbio.2021.101424

Ebrahimi, M., Sadeghi, A., and Mortazavi, S. A. (2020). The use of cyclic dipeptide producing LAB with potent anti-aflatoxigenic capability to improve techno-functional properties of clean-label bread. *Ann. Microbiol.* 70:24. doi: 10.1186/s13213-020-01571-y

Facco Stefanello, R., Nabeshima, E. H., de Oliveira Garcia, A., Heck, R. T., Valle Garcia, M., Martins Fries, L. L., et al. (2019). Stability, sensory attributes and acceptance of panettones elaborated with *Lactobacillus fermentum* IAL 4541 and *Wickerhamomyces anomallus* IAL 4533. *Food Res. Int.* 116, 973–984. doi: 10.1016/j.foodres.2018.09.035

Fang, L., Zhao, B., Zhang, R., Wu, P., Zhao, D., Chen, J., et al. (2022). Occurrence and exposure assessment of aflatoxins in Zhejiang province, China. *Environ. Toxicol. Pharmacol.* 92:103847. doi: 10.1016/j.etap.2022.103847

Gerez, C. L., Fornaguera, M. J., Obregozo, M. D., Font De Valdez, G., and Torino, M. I. (2015). Antifungal starter culture for packed bread: influence of two storage conditions. *Rev. Argent. Microbiol.* 47, 118–124. doi: 10.1016/j.ram.2015.02.002

Gerez, C. L., Torino, M. I., Rollán, G., and Font de Valdez, G. (2009). Prevention of bread mould spoilage by using lactic acid bacteria with antifungal properties. *Food Control* 20, 144–148. doi: 10.1016/j.foodcont.2008.03.005

Han, Q., Wu, Z., Huang, B., Sun, L., Ding, C., Yuan, S., et al. (2016). Extraction, antioxidant and antibacterial activities of *Broussonetia papyrifera* fruits polysaccharides. *Int. J. Biol. Macromol.* 92, 116–124. doi: 10.1016/j.ijbiomac.2016.06.087

Honoré, A. H., Aunsbjerg, S. D., Ebrahimi, P., Thorsen, M., Benfeldt, C., Knochel, S., et al. (2016). Metabolic footprinting for investigation of antifungal properties of *Lactobacillus paracasei*. *Anal. Bioanal. Chem.* 408, 83–96. doi: 10.1007/s00216-015-9103-6

İspirli, H., Özmen, D., Yılmaz, M. T., Sağdıç, O., and Dertli, E. (2020). Impact of glucan type exopolysaccharide (EPS) production on technological characteristics of sourdough bread. *Food Control* 107:106812. doi: 10.1016/j.foodcont.2019.106812

Izzo, L., Luz, C., Ritieni, A., Manes, J., and Meca, G. (2020). Whey fermented by using *Lactobacillus plantarum* strains: a promising approach to increase the shelf life of pita bread. *J. Dairy Sci.* 103, 5906–5915. doi: 10.3168/jds.2019-17547

Jakubczyk, A., Karas, M., Rybczynska-Tkaczyk, K., Zielinska, E., and Zielinski, D. (2020). Current trends of bioactive peptides-new sources and therapeutic effect. *Foods* 9:846. doi: 10.3390/foods9070846

Jin, J., Nguyen, T. T. H., Humayun, S., Park, S., Oh, H., Lim, S., et al. (2021). Characteristics of sourdough bread fermented with *Pediococcus pentosaceus* and *Saccharomyces cerevisiae* and its bio-preservative effect against *Aspergillus flavus*. *Food Chem.* 345:128787. doi: 10.1016/j.foodchem.2020.128787

John, V. (2008). Unique aspects of the grass cell wall John Vogel. *Curr. Opin. Plant Biol.* 11, 301–307. doi: 10.1016/j.pbi.2008.03.002

Karimi, N., Nikoo, M., Ahmadi Gavlighi, H., Piri Gheshlaghi, S., Regenstein, J. M., and Xu, X. (2020). Effect of pacific white shrimp (*Litopenaeus vannamei*) protein hydrolysates (SPH) and (−)-epigallocatechin gallate (EGCG) on sourdough and bread quality. *LWT* 131:109800. doi: 10.1016/j.lwt.2020.109800

Korcari, D., Secchiero, R., Laureati, M., Marti, A., Cardone, G., Rabitti, N. S., et al. (2021). Technological properties, shelf life and consumer preference of spelt-based sourdough bread using novel, selected starter cultures. *LWT* 151:112097. doi: 10.1016/j.lwt.2021.112097

Krnjaja, V., Mandić, V., Stanković, S., Obradović, A., Vasić, T., Lukić, M., et al. (2019). Influence of plant density on toxigenic fungal and mycotoxin contamination of maize grains. *Crop Prot.* 116, 126–131. doi: 10.1016/j.cropro.2018.10.021

Kwak, M. K., Liu, R., and Kang, S. O. (2018). Antimicrobial activity of cyclic dipeptides produced by *Lactobacillus plantarum* LBP-K10 against multidrug-resistant bacteria, pathogenic fungi, and influenza A virus. *Food Control* 85, 223–234. doi: 10.1016/j.foodcont.2017.10.001

Kwak, M. K., Liu, R., Kim, M. K., Moon, D., Kim, A. H., Song, S. H., et al. (2014). Cyclic dipeptides from lactic acid bacteria inhibit the proliferation of pathogenic fungi. *J. Microbiol.* 52, 64–70. doi: 10.1007/s12275-014-3520-7

Lambert, R. J., and Stratford, M. (1999). Weak-acid preservatives: modelling microbial inhibition and response. *J. Appl. Microbiol.* 86, 157–164. doi: 10.1046/j.1365-2672.1999.00646.x

Lavermicocca, P., Valerio, F., and Visconti, A. (2003). Antifungal activity of phenyllactic acid against molds isolated from bakery products. *Appl. Environ. Microbiol.* 69, 634–640. doi: 10.1128/AEM.69.1.634-640.2003

Le Lay, C., Coton, E., Le Blay, G., Chobert, J. M., Haertle, T., Choiset, Y., et al. (2016a). Identification and quantification of antifungal compounds produced by lactic acid bacteria and propionibacteria. *Int. J. Food Microbiol.* 239, 79–85. doi: 10.1016/j.ijfoodmicro.2016.06.020

Le Lay, C., Mounier, J., Vasseur, V., Weill, A., Le Blay, G., Barbier, G., et al. (2016b). *In vitro* and *in situ* screening of lactic acid bacteria and propionibacteria antifungal activities against bakery product spoilage molds. *Food Control* 60, 247–255. doi: 10.1016/j.foodcont.2015.07.034

Leon, R., Ruiz, M., Valero, Y., Cardenas, C., Guzman, F., Vila, M., et al. (2020). Exploring small cationic peptides of different origin as potential antimicrobial agents in aquaculture. *Fish Shellfish Immunol.* 98, 720–727. doi: 10.1016/j.fsi.2019.11.019

Leyva Salas, M., Mounier, J., Maillard, M. B., Valence, F., Coton, E., and Thierry, A. (2019). Identification and quantification of natural compounds produced by antifungal bioprotective cultures in dairy products. *Food Chem.* 301:125260. doi: 10.1016/j.foodchem.2019.125260

Li, J., Ai, L., Xu, F., Hu, X., Yao, Y., and Wang, L. (2022a). Structural characterization of exopolysaccharides from *Weissella cibaria* NC516.11 in distiller grains and its improvement in gluten-free dough. *Int. J. Biol. Macromol.* 199, 17–23. doi: 10.1016/j.ijbiomac.2021.12.089

Li, J., Zhang, Q., Zhao, J., Zhang, H., and Chen, W. (2022b). *Streptococcus mutans* and *Candida albicans* biofilm inhibitors produced by *Lactiplantibacillus plantarum* CCFM8724. *Curr. Microbiol.* 79:143. doi: 10.1007/s00284-022-02833-5

Liang, N., Cai, P., Wu, D., Pan, Y., Curtis, J. M., and Gänzle, M. G. (2017). High-speed counter-current chromatography (HSCCC) purification of antifungal hydroxy unsaturated fatty acids from plant-seed oil and lactobacillus cultures. *J. Agric. Food Chem.* 65, 11229–11236. doi: 10.1021/acs.jafc.7b05658

Luz, C., Quiles, J. M., Romano, R., Blaiotta, G., Rodríguez, L., and Meca, G. (2021). Application of whey of mozzarella di Bufala Campana fermented by lactic acid bacteria as a bread biopreservative agent. *Int. J. Food Sci. Technol.* 56, 4585–4593. doi: 10.1111/ijfs.15092

Ma, S., Wang, Z., Guo, X., Wang, F., Huang, J., Sun, B., et al. (2021). Sourdough improves the quality of whole-wheat flour products: mechanisms and challenges—a review. *Food Chem.* 360:130038. doi: 10.1016/j.foodchem.2021.130038

Magnusson, J., and Schnürer, J. S. (2001). *Lactobacillus coryniformis* subsp. *coryniformis* strain Si3 produces a broad-spectrum proteinaceous antifungal compound. *Appl. Environ. Microbiol.* 67, 1–5. doi: 10.1128/AEM.67.1.1

Mahato, D. K., Kamle, M., Sharma, B., Pandhi, S., Devi, S., Dhawan, K., et al. (2021). Patulin in food: a mycotoxin concern for human health and its management strategies. *Toxicon* 198, 12–23. doi: 10.1016/j.toxicon.2021.04.027

Martin, H., and Maris, P. (2012). Synergism between hydrogen peroxide and seventeen acids against five Agri-food-borne fungi and one yeast strain. *J. Appl. Microbiol.* 113, 1451–1460. doi: 10.1111/jam.12016

Massot-Cladera, M., Abril-Gil, M., Torres, S., Franch, À., Castell, M., and Pérez-Cano, F. J. (2014). Impact of cocoa polyphenol extracts on the immune system and microbiota in two strains of young rats. *Br. J. Nutr.* 112, 1944–1954. doi: 10.1017/S0007114514003080

Mendez-Albores, A., Martinez-Bustos, F., Gaytan-Martinez, M., and Moreno-Martinez, E. (2008). Effect of lactic and citric acid on the stability of B-aflatoxins in extrusion-cooked sorghum. *Lett. Appl. Microbiol.* 47, 1–7. doi: 10.1111/j.1472-765X.2008.02376.x

Moghaddam, M. F. T., Jalali, H., Nafchi, A. M., and Nouri, L. (2020). Evaluating the effects of lactic acid bacteria and olive leaf extract on the quality of gluten-free bread. *Gene Rep.* 21:100771. doi: 10.1016/j.genrep.2020.100771

Mohamad Asri, N., Muhialdin, B. J., Zarei, M., and Saari, N. (2020). Low molecular weight peptides generated from palm kernel cake via solid state lacto-fermentation extend the shelf life of bread. *LWT* 134:110206. doi: 10.1016/j.lwt.2020.110206

Moore, M. M., Bello, F. D., and Arendt, E. K. (2008). Sourdough fermented by *Lactobacillus plantarum* FST 1.7 improves the quality and shelf life of gluten-free bread. *Eur. Food Res. Technol.* 226, 1309–1316. doi: 10.1007/s00217-007-0659-z

Moradi, M., Guimarães, J. T., and Sahin, S. (2021). Current applications of exopolysaccharides from lactic acid bacteria in the development of food active edible packaging. *Curr. Opin. Food Sci.* 40, 33–39. doi: 10.1016/j.cofs.2020.06.001

Mu, W., Chen, C., Li, X., Zhang, T., and Jiang, B. (2009). Optimization of culture medium for the production of phenyllactic acid by *Lactobacillus* sp. SK007. *Bioresour. Technol.* 100, 1366–1370. doi: 10.1016/j.biortech.2008.08.010

Muhialdin, B. J., Algboory, H. L., Kadum, H., Mohammed, N. K., Saari, N., Hassan, Z., et al. (2020). Antifungal activity determination for the peptides generated by *Lactobacillus plantarum* TE10 against *Aspergillus flavus* in maize seeds. *Food Control* 109:106898. doi: 10.1016/j.foodcont.2019.106898

Muhialdin, B. J., Hassan, Z., Bakar, F. A., and Saari, N. (2016). Identification of antifungal peptides produced by *Lactobacillus plantarum* IS10 grown in the MRS broth. *Food Control* 59, 27–30. doi: 10.1016/j.foodcont.2015.05.022

Mun, S. Y., Kim, S. K., Woo, E. R., and Chang, H. C. (2019). Purification and characterization of an antimicrobial compound produced by *Lactobacillus plantarum* EM showing both antifungal and antibacterial activities. *LWT* 114:108403. doi: 10.1016/j.lwt.2019.108403

Nasrollahzadeh, A., Mokhtari, S., Khomeiri, M., and Saris, P. E. J. (2022). Antifungal preservation of food by lactic acid bacteria. *Foods* 11:395. doi: 10.3390/foods11030395

Nehal, F., Sahnoun, M., Smaoui, S., Jaouadi, B., Bejar, S., and Mohammed, S. (2019). Characterization, high production and antimicrobial activity of exopolysaccharides from *Lactococcus lactis* F-mou. *Microb. Pathog.* 132, 10–19. doi: 10.1016/j.micpath.2019.04.018

Nes, I. E., Diep, D. B., Varstein, L. S. H., Brurberg, M. B., Eijsink, V., and Holo, H. (1996). Biosynthesis of bacteriocins in lactic acid bacteria. *Antonie Van Leeuwenhoek* 70, 113–128. doi: 10.1007/BF00395929

Nguyen, H. T., Van der Fels-Klerx, H. J., Peters, R. J., and Van Boekel, M. A. (2016). Acrylamide and 5-hydroxymethylfurfural formation during baking of biscuits: part I: effects of sugar type. *Food Chem.* 192, 575–585. doi: 10.1016/j.foodchem.2015.07.016

Nionelli, L., Pontonio, E., Gobbetti, M., and Rizzello, C. G. (2018). Use of hop extract as antifungal ingredient for bread making and selection of autochthonous resistant starters for sourdough fermentation. *Int. J. Food Microbiol.* 266, 173–182. doi: 10.1016/j.ijfoodmicro.2017.12.002

Nionelli, L., and Rizzello, C. G. (2016). Sourdough-based biotechnologies for the production of gluten-free foods. *Foods* 5:65. doi: 10.3390/foods5030065

Nionelli, L., Wang, Y., Pontonio, E., Immonen, M., Rizzello, C. G., Maina, H. N., et al. (2020). Antifungal effect of bioprocessed surplus bread as ingredient for bread-making: identification of active compounds and impact on shelf-life. *Food Control* 118:107437. doi: 10.1016/j.foodcont.2020.107437

Oliveira, P. M., Zannini, E., and Arendt, E. K. (2014). Cereal fungal infection, mycotoxins, and lactic acid bacteria mediated bioprotection: from crop farming to cereal products. *Food Microbiol.* 37, 78–95. doi: 10.1016/j.fm.2013.06.003

Omedi, J. O., Huang, J., Huang, W., Zheng, J., Zeng, Y., Zhang, B., et al. (2021). Suitability of pitaya fruit fermented by sourdough LAB strains for bread making: its impact on dough physicochemical, rheo-fermentation properties and antioxidant, antifungal and quality performance of bread. *Heliyon* 7:e08290. doi: 10.1016/j.heliyon.2021.e08290

Ortiz-Rivera, Y., Sanchez-Vega, R., Gutierrez-Mendez, N., León-Félix, J., Acosta-Muñiz, C., and Sepulveda, D. R. (2017). Production of reuterin in a fermented milk product by *Lactobacillus reuteri*: inhibition of pathogens, spoilage microorganisms, and lactic acid bacteria. *J. Dairy Sci.* 100, 4258–4268. doi: 10.3168/jds.2016-11534

Ouiddir, M., Bettache, G., Leyva Salas, M., Pawtowski, A., Donot, C., Brahimi, S., et al. (2019). Selection of Algerian lactic acid bacteria for use as antifungal bioprotective cultures and application in dairy and bakery products. *Food Microbiol.* 82, 160–170. doi: 10.1016/j.fm.2019.01.020

Pohl, E. E., Voltchenko, A. M., and Rupprecht, A. (2008). Flip-flop of hydroxy fatty acids across the membrane as monitored by proton-sensitive microelectrodes. *Biochim. Biophys. Acta Biomembr.* 1778, 1292–1297. doi: 10.1016/j.bbamem.2008.01.025

Pontonio, E., and Rizzello, C. G. (2021). Editorial: ad-hoc selection of lactic acid bacteria for non-conventional food matrices fermentations: Agri-food perspectives. *Front. Microbiol.* 12:681830. doi: 10.3389/fmicb.2021.681830

Puig, M., Moragrega, C., Ruz, L., Calderon, C. E., Cazorla, F. M., Montesinos, E., et al. (2016). Interaction of antifungal peptide BP15 with *Stemphylium vesicarium*, the causal agent of brown spot of pear. *Fungal Biol.* 120, 61–71. doi: 10.1016/j.funbio.2015.10.007

Qian, M., Liu, D., Zhang, X., Yin, Z., Ismail, B. B., Ye, X., et al. (2021). A review of active packaging in bakery products: applications and future trends. *Trends Food Sci. Technol.* 114, 459–471. doi: 10.1016/j.tifs.2021.06.009

Quattrini, M., Liang, N., Fortina, M. G., Xiang, S., Curtis, J. M., and Ganzle, M. (2019). Exploiting synergies of sourdough and antifungal organic acids to delay fungal spoilage of bread. *Int. J. Food Microbiol.* 302, 8–14. doi: 10.1016/j.ijfoodmicro.2018.09.007

Rai, M., Pandit, R., Gaikwad, S., and Kovics, G. (2016). Antimicrobial peptides as natural bio-preservative to enhance the shelf-life of food. *J. Food Sci. Technol.* 53, 3381–3394. doi: 10.1007/s13197-016-2318-5

Ran, Q., Yang, F., Geng, M., Qin, L., Chang, Z., Gao, H., et al. (2022). A mixed culture of *Propionibacterium freudenreichii* and *Lactiplantibacillus plantarum* as antifungal biopreservatives in bakery product. *Food Biosci.* 47:101456. doi: 10.1016/j.fbio.2021.101456

ReportLinker. (2020). Global bakery products industry. https://www.reportlinker.com/p05069906/Global-Bakery-Products-Industry.html?utm_source=GNW (Accessed 10 May 2022).

Rhee, K. (2004). Cyclic dipeptides exhibit synergistic, broad spectrum antimicrobial effects and have anti-mutagenic properties. *Int. J. Antimicrob. Agents* 24, 423–427. doi: 10.1016/j.ijantimicag.2004.05.005

Rizzello, C. G., Cassone, A., Coda, R., and Gobbetti, M. (2011). Antifungal activity of sourdough fermented wheat germ used as an ingredient for bread making. *Food Chem.* 127, 952–959. doi: 10.1016/j.foodchem.2011.01.063

Rizzello, C. G., Verni, M., Bordignon, S., Gramaglia, V., and Gobbetti, M. (2017). Hydrolysate from a mixture of legume flours with antifungal activity as an ingredient for prolonging the shelf-life of wheat bread. *Food Microbiol.* 64, 72–82. doi: 10.1016/j.fm.2016.12.003

Rodrigues, K. L., Caputo, L. R., Carvalho, J. C., Evangelista, J., and Schneedorf, J. M. (2005). Antimicrobial and healing activity of kefir and kefiran extract. *Int. J. Antimicrob. Agents* 25, 404–408. doi: 10.1016/j.ijantimicag.2004.09.020

Roy, U., Batish, V. K., Grover, S., and Neelakantan, S. (1996). Production of antifungal substance by *Lactococcus lactis* subsp. *lactis* CHD-28.3. *Int. J. Food Microbiol.* 32, 27–34. doi: 10.1016/0168-1605(96)01101-4

Russo, P., Arena, M. P., Fiocco, D., Capozzi, V., Drider, D., and Spano, G. (2017). *Lactobacillus plantarum* with broad antifungal activity: a promising approach to increase safety and shelf-life of cereal-based products. *Int. J. Food Microbiol.* 247, 48–54. doi: 10.1016/j.ijfoodmicro.2016.04.027

Ryan, L. A., Dal Bello, F., and Arendt, E. K. (2008). The use of sourdough fermented by antifungal LAB to reduce the amount of calcium propionate in bread. *Int. J. Food Microbiol.* 125, 274–278. doi: 10.1016/j.ijfoodmicro.2008.04.013

Ryan, L. A. M., Zannini, E., Dal Bello, F., Pawlowska, A., Koehler, P., and Arendt, E. K. (2011). *Lactobacillus amylovorus* DSM 19280 as a novel food-grade antifungal agent for bakery products. *Int. J. Food Microbiol.* 146, 276–283. doi: 10.1016/j.ijfoodmicro.2011.02.036

Sadeghi, A., Ebrahimi, M., Mortazavi, S. A., and Abedfar, A. (2019). Application of the selected antifungal LAB isolate as a protective starter culture in pan whole-wheat sourdough bread. *Food Control* 95, 298–307. doi: 10.1016/j.foodcont.2018.08.013

Saladino, F., Luz, C., Manyes, L., Fernández-Franzón, M., and Meca, G. (2016). In vitro antifungal activity of lactic acid bacteria against mycotoxigenic fungi and their application in loaf bread shelf life improvement. *Food Control* 67, 273–277. doi: 10.1016/j.foodcont.2016.03.012

Salaheen, S., Peng, M., and Biswas, X. D. X. (2014). *Microbial Food Safety and Preservation Techniques*. Boca Raton: CRC Press.

Sanad, M. H., Farag, A. B., Bassem, S. A., and Marzook, F. A. (2022). Radioiodination of zearalenone and determination of *Lactobacillus plantarum* effect of on zearalenone organ distribution: in silico study and preclinical evaluation. *Toxicol. Rep.* 9, 470–479. doi: 10.1016/j.toxrep.2022.02.003

Schaefer, L., Auchtung, T. A., Hermans, K. E., Whitehead, D., Borhan, B., and Britton, R. A. (2010). The antimicrobial compound reuterin (3-hydroxypropionaldehyde) induces oxidative stress via interaction with thiol groups. *Microbiology* 156, 1589–1599. doi: 10.1099/mic.0.035642-0

Schmidt, M., Lynch, K. M., Zannini, E., and Arendt, E. K. (2018). Fundamental study on the improvement of the antifungal activity of *Lactobacillus reuteri* R29 through increased production of phenyllactic acid and reuterin. *Food Control* 88, 139–148. doi: 10.1016/j.foodcont.2017.11.041

Septembre-Malaterre, A., Remize, F., and Poucheret, P. (2018). Fruits and vegetables, as a source of nutritional compounds and phytochemicals: changes in bioactive compounds during lactic fermentation. *Food Res. Int.* 104, 86–99. doi: 10.1016/j.foodres.2017.09.031

Shetty, P. H., and Jespersen, L. (2006). *Saccharomyces cerevisiae* and lactic acid bacteria as potential mycotoxin decontaminating agents. *Trends Food Sci. Technol.* 17, 48–55. doi: 10.1016/j.tifs.2005.10.004

Shi, C., and Knøchel, S. (2021). Susceptibility of dairy associated molds towards microbial metabolites with focus on the response to diacetyl. *Food Control* 121:107573. doi: 10.1016/j.foodcont.2020.107573

Sjogren, J., Magnusson, J., Broberg, A., Schnurer, J., and Kenne, L. (2003). Antifungal 3-hydroxy fatty acids from *Lactobacillus plantarum* MiLAB 14. *Appl. Environ. Microbiol.* 69, 7554–7557. doi: 10.1128/AEM.69.12.7554-7557.2003

Stiles, M. E., and Holzapfel, W. H. (1997). Lactic acid bacteria of foods and their current taxonomy. *Int. J. Food Microbiol.* 36, 1–29. doi: 10.1016/S0168-1605(96)01233-0

Ström, K., Sjögren, J., Broberg, A., and Schnürer, J. (2002). *Lactobacillus plantarum* MiLAB 393 produces the antifungal cyclic dipeptides cyclo(L-Phe–L-pro) and cyclo(L-Phe–trans-4-OH-L-pro) and 3-phenyllactic acid. *Appl. Environ. Microbiol.* 68, 4322–4327. doi: 10.1128/AEM.68.9.4322

Sun, L., Li, X., Zhang, Y., Yang, W., Ma, G., Ma, N., et al. (2020). A novel lactic acid bacterium for improving the quality and shelf life of whole wheat bread. *Food Control* 109:106914. doi: 10.1016/j.foodcont.2019.106914

Urbach, G. (1995). Contribution of lactic acid bacteria to flavour compound formation in dairy products. *Int. Dairy J.* 5, 877–903. doi: 10.1016/0958-6946(95)00037-2

Valerio, F. (2004). Production of phenyllactic acid by lactic acid bacteria: an approach to the selection of strains contributing to food quality and preservation. *FEMS Microbiol. Lett.* 233, 289–295. doi: 10.1016/j.femsle.2004.02.020

Vermeulen, N., Gánzle, M. G., and Vogel, R. F. (2006). Influence of peptide supply and cosubstrates on phenylalanine metabolism of *Lactobacillus sanfranciscensis* DSM20451T and *Lactobacillus plantarum* TMW1.468. *J. Agric. Food Chem.* 54, 3832–3839. doi: 10.1021/jf052733e

Wang, L., Hua, X., Shi, J., Jing, N., Ji, T., Lv, B., et al. (2022b). Ochratoxin A: occurrence and recent advances in detoxification. *Toxicon* 210, 11–18. doi: 10.1016/j.toxicon.2022.02.010

Wang, F., Li, Z., Jia, H., Lu, R., Zhang, S., Pan, C., et al. (2022a). An ultralow concentration of Al-MOFs for turn-on fluorescence detection of aflatoxin B1 in tea samples. *Food Chem.* 383:132389. doi: 10.1016/j.foodchem.2022.132389

Wang, K., Niu, M., Song, D., Song, X., Zhao, J., Wu, Y., et al. (2020). Preparation, partial characterization and biological activity of exopolysaccharides produced from *Lactobacillus fermentum* S1. *J. Biosci. Bioeng.* 129, 206–214. doi: 10.1016/j.jbiosc.2019.07.009

Wang, Y., Xie, C., Pulkkinen, M., Edelmann, M., Chamlagain, B., Coda, R., et al. (2022c). In situ production of vitamin B12 and dextran in soya flour and rice bran: a tool to improve flavour and texture of B12-fortified bread. *LWT* 161:113407. doi: 10.1016/j.lwt.2022.113407

Wang, J., Zhao, X., Yang, Y., Zhao, A., and Yang, Z. (2015). Characterization and bioactivities of an exopolysaccharide produced by *Lactobacillus plantarum* YW32. *Int. J. Biol. Macromol.* 74, 119–126. doi: 10.1016/j.ijbiomac.2014.12.006

Wu, M., Pan, T., Wu, Y., Chang, S., Chang, M., and Hu, C. (2010). Exopolysaccharide activities from probiotic bifidobacterium: immunomodulatory effects (on J774A.1 macrophages) and antimicrobial properties. *Int. J. Food Microbiol.* 144, 104–110. doi: 10.1016/j.ijfoodmicro.2010.09.003

Wu, S., Peng, Y., Xi, J., Zhao, Q., Xu, D., Jin, Z., et al. (2022). Effect of sourdough fermented with corn oil and lactic acid bacteria on bread flavor. *LWT* 155:112935. doi: 10.1016/j.lwt.2021.112935

Yépez, A., Luz, C., Meca, G., Vignolo, G., Mañes, J., and Aznar, R. (2017). Biopreservation potential of lactic acid bacteria from Andean fermented food of vegetal origin. *Food Control* 78, 393–400. doi: 10.1016/j.foodcont.2017.03.009

Conflict of Interest: The authors declare that the research was conducted in the absence of any commercial or financial relationships that could be construed as a potential conflict of interest.

Publisher's Note: All claims expressed in this article are solely those of the authors and do not necessarily represent those of their affiliated organizations, or those of the publisher, the editors and the reviewers. Any product that may be evaluated in this article, or claim that may be made by its manufacturer, is not guaranteed or endorsed by the publisher.

frontiers | Frontiers in Microbiology

ORIGINAL RESEARCH
published: 12 July 2022
doi: 10.3389/fmicb.2022.922136

Isolation, Identification, and Function of *Rhodotorula mucilaginosa* TZR_{2014} and Its Effects on the Growth and Health of Weaned Piglets

Ping Hu[1†], *Junxia Mao*[1†], *Yan Zeng*[2], *Zhihong Sun*[1], *Huan Deng*[1], *Chen Chen*[1], *Weizhong Sun*[1] *and Zhiru Tang*[1*]

[1] *Laboratory for Bio-Feed and Animal Nutrition, Chongqing Key Laboratory of Herbivore Science, College of Animal Science and Technology, Southwest University, Chongqing, China,* [2] *Fermentation Engineering Department, Hunan Institute of Microbiology, Changsha, China*

A red yeast isolated from orange and grape soil and identified by the 26S rDNA sequence analysis revealed that it was *Rhodotorula mucilaginosa* and named TZR_{2014}. Its biomass and carotenoid production reached a maximum when using the fermentation medium with pH 6.0, containing 5% glucose, 1% peptone, and 1.5% yeast powder. TZR_{2014} was resistant to 55°C for 15 min, 0.2% pig bile salts for 4 h, and artificial gastric and intestinal fluids. A total of thirty 28-day weaned pigs were divided into three groups, and the piglets were fed a basal diet (CON), a basal diet and orally administered 1 ml 1.0×10^{10} CFU/ml *Candida utilis* DSM 2361 three times (*C. utilis*), or a basal diet and orally administered 1 ml 1.0×10^{10} CFU/mL TZR_{2014} three times daily (*R. mucilaginosa*) for 4 weeks. Compared with the piglets in the CON group, those in the *C. utilis* or *R. mucilaginosa* group reported an increased average daily weight gain and average daily feed intake ($P < 0.05$) and a decreased feed/gain ($P < 0.05$). The diarrhea rate of piglets in the *R. mucilaginosa* group was lower than that in the CON and *C. utilis* groups ($P < 0.05$). Compared with that in the CON and *C. utilis* groups, the *R. mucilaginosa* group reported an increased ileum villus height ($P < 0.05$), serum concentration of total antioxidant content, total superoxide dismutase, and glutathione peroxidase and pepsin and lipase activities in the intestinal content, while it reported a decreased serum concentration of malondialdehyde and pH of the intestinal tract ($P < 0.05$). The relative abundances of *Proteobacteria* and *Megasphaera* of caecum in the *R. mucilaginosa* group were lower than those in the CON and *C. utilis* groups ($P < 0.05$). The relative abundances of *Prevotella*, *Ruminococcaceae*, *Succinivibrio*, *Rikenellaceae RC9 gut group*, and *Roseburia* of caecum in the *R. mucilaginosa* group were higher than those in the CON and *C. utilis* groups ($P < 0.05$). *R. mucilaginosa* TZR_{2014} can produce carotenoids and adapts to the animal's gastrointestinal environment. Oral *R. mucilaginosa* TZR_{2014} improved growth performance, enhanced antioxidant capacity, strengthened gastrointestinal digestion, and maintained the intestinal microbiological balance of piglets.

Keywords: ***Rhodotorula mucilaginosa*** **TZR_{2014}, isolation and identification, intestinal health, antioxidant capacity, weaned piglets**

OPEN ACCESS

Edited by:
Aldo Corsetti,
University of Teramo, Italy

Reviewed by:
Giovanna Suzzi,
University of Teramo, Italy
Jiashun Chen,
Hunan Agricultural University, China

***Correspondence:**
Zhiru Tang
tangzhiru2326@sina.com

[†]These authors have contributed equally to this work

Specialty section:
This article was submitted to Food Microbiology, a section of the journal Frontiers in Microbiology

Received: *17 April 2022*
Accepted: *31 May 2022*
Published: *12 July 2022*

Citation:
Hu P, Mao J, Zeng Y, Sun Z, Deng H, Chen C, Sun W and Tang Z (2022) Isolation, Identification, and Function of Rhodotorula mucilaginosa TZR_{2014} and Its Effects on the Growth and Health of Weaned Piglets. Front. Microbiol. 13:922136. doi: 10.3389/fmicb.2022.922136

INTRODUCTION

Based on the concept of healthy feeding, probiotics not only help avoid the adverse effects of antibiotics on weaned piglets but also promote intestinal health. Yeast is a common, safe microecological agent. As a saprophytic microbe, *Rhodotorula* widely exists in the soil, sea, animals, and plants. *Rhodotorula mucilaginosa* has high nutritional value and probiotic effects (Nelis and De Leenheer, 1991). Glucan and mannan in the cell wall of *R. mucilaginosa* can enhance the migration and phagocytosis of macrophages and neutrophils, reduce intestinal inflammatory reactions, enhance animal resistance, promote the reproduction of beneficial bacteria, and competitively inhibit the colonization of harmful bacteria (Sakai, 1999; Dalmo and Bogwald, 2008). *R. mucilaginosa* products contain many carotenoids and zymochromes (Aksu and Eren, 2005); previous studies have shown that carotenoids are beneficial to human and animal health (Mannazzu et al., 2015). As the precursor of vitamin A, carotenoids can resist cancer, inhibit gene mutations, and resist the side effects of environment-induced genotoxic agents by regulating cell signaling and gene expression. Carotenoids are also recognized as super antioxidants (Dalmo and Bogwald, 2008; Bhagavathy and Sumathi, 2012), which have various health functions, such as enhancing host immunity, demonstrating anti-oxidation and anti-tumor activity, and lowering blood pressure (Sharma and Ghoshal, 2020). However, there are few studies on the application of *R. mucilaginosa* in livestock production, and its safety has not yet been verified. In this study, *R. mucilaginosa* TZR_{2014} was isolated and identified from orchard soil, and its safety was tested to study the effects of *R. mucilaginosa* TZR_{2014} on weaned piglets.

MATERIALS AND METHODS

Isolation, Identification, and Physiological and Biochemical Characteristics of *R. mucilaginosa* TZR_{2014}

Microorganisms, Culture Media, and Reagents

Soil samples containing *R. mucilaginosa* TZR_{2014} were collected from the Jingguoyuan orchard (Jingyun Mountain, Chongqing, China) on 8 September 2014 (Tang et al., 2016). Jingguoyuan is a fruit garden located at 500 m a.s.l. on the east side of the Jingyun Mountain, Chongqing, China, where the summer and winter temperatures are ∼32 and 10°C, respectively. The enrichment culture medium comprised 0.1% (w/v) urea, 5% (w/v) glucose, 0.05% (w/v) yeast extract, 0.1% (w/v) $(NH_4)_2SO_4$, 0.1% (w/v) $MgSO_4$ $7H_2O$, 0.25% (w/v) KH_2PO_4, 0.01% (w/v) $FeSO_4$ $7H_2O$, and 0.003% (w/v) Bangladesh Red, adjusted to pH 4.5, and sterilized for 15 min at 115°C. The potato dextrose agar (PDA) medium comprised 200 g of potato, 20 g of glucose, 20 g of agar powder, and distilled water. A constant volume of 1 L was maintained at natural pH and sterilized for 15 min at 115°C. The yeast extract peptone dextrose (YPD) culture medium comprised 2% (w/v) glucose, 1% (w/v) yeast powder, 2% (w/v) peptone, and 2% (w/v) agar, adjusted to pH 6.0, and sterilized for 15 min at 115°C. Nutrient broth (NB) medium comprised 0.3% (w/v) beef extract, 0.5% (w/v) NaCl, and 1% (w/v) peptone, adjusted to pH 7.0, and sterilized for 20 min at 121°C. The seed culture medium comprised 1% (w/v) peptone, 2% (w/v) glucose, and 1% (w/v) yeast powder, adjusted to pH 6.0, and sterilized for 15 min at 115°C. The fermentation medium comprised 1% peptone (w/v), 5% glucose (w/v), and 1.5% yeast powder (w/v), adjusted to pH 6.0, and sterilized for 15 min at 115°C.

Isolation and Morphological, Physiological, and Biochemical Characterization

One gram of soil containing yeast was mixed with 100 ml of yeast liquid enrichment medium. The suspension (1 ml) was serially diluted 10 times to 10^{-6}. The 100 μl suspension from the diluted samples was plated on PDA solid medium and cultured at 28°C for 2–3 days. Three-day-old cultures on PDA agar were used for cellular and colony morphology analyses of yeast. The morphology of *R. mucilaginosa* cells was photographed using an Olympus BX40 microscope (Olympus, Tokyo, Japan). Routine physiological and biochemical tests were conducted according to the characteristics and identification described by Barnett et al. (1983).

26S rDNA D1/D2 Identification of *R. mucilaginosa* TZR_{2014}

Three-day-old cultures of yeast in PDA liquid medium were collected and directly used for DNA extraction, according to the instructions of the Power DNA Isolation Kit (Mobio, Carlsbad, CA, USA). DNA was quantified using a Nanodrop spectrophotometre (Nyxor Biotech, Paris, France), followed by staining with the Quant Pico Green dsDNA Kit (Invitrogen Ltd., Paisley, UK). PCR amplification of the D1/D2 region of yeast 26S rDNA was performed using the universal primers NL1 (5'-GCATATCAATAAGCG GAGGAAAAG-3') and NL4 (5'-GGTCCGTGTT TCAAGACGG-3'; Thanh et al., 2002). The cycling parameters were as follows: initial denaturation at 94°C for 4 min, 25 cycles of denaturation at 94°C (40 s), annealing at 55°C (45 s), elongation at 72°C (30 s), and final extension at 72°C for 10 min. PCR reaction system consisted of the following: DNA template (20–50 ng/μl) 0.5 μl; 10 × buffer (with Mg^{2+}) 2.5 μl; dNTP (2.5 mM) 1 μl; Taq polymerase 0.2 μl; primer F (10 μM) 0.5 μl; primer R (10 μM) 0.5 μl; and ddH_2O 25 μl. The PCR products were separated by 1.0% agarose gel electrophoresis (150 V, 100 mA, 20 min) and purified using a QIAquick Gel Extraction Kit (Qiagen, Dusseldorf, Germany). The PCR products were sequenced by Sangon Biotech Co. Ltd. (Shanghai, China) and blasted in the NCBI gene bank. A phylogenetic tree was constructed, and the species of the yeast was determined using the base sequence of the yeast. The BLAST analysis was carried out to obtain the known strains with high homology to yeast 26S rDNA sequence, and the gene sequences of the strains with high similarity were obtained from the GenBank library for the establishment of a phylogenetic tree. This yeast was named *Pichia anomola* AR_{2016} and was stored at the China Center for Type Culture Collection (No. CCTCC M2017594, http://cctcc.whu.edu.cn/).

Determination of Protein and Amino Acid Content in *R. mucilaginosa* TZR_{2014} Cell

Three-day cultures in the PDA liquid medium were collected, and dry matter (DM) was measured by drying to a constant mass in a forced-air oven at 95°C. The amino acids in the dry yeast were determined using a Hitachi L-8800 automatic amino acid analyser.

Optimization of the Fermentation Condition for Carotenoid Production by *R. mucilaginosa* TZR_{2014}

The fermentation condition for carotenoid production by *R. mucilaginosa* TZR_{2014} was optimized by a three-factor and three-level (3×3) experimental design, denoted as L9 (3^3). Factor A was glucose with 3, 4, or 5% glucose. Factor B was peptone at 1, 1.5, or 2, and factor C was yeast powder at 0.5, 1, or 1.5. The 10% *R. mucilaginosa* culture was inoculated into the 90% fermentation media and fermented at 28°C with shaking at 200 rpm for 96 h. After fermentation, the carotenoid content was measured according to the introduction of GB5413.35-2010 (Ministry of Agriculture and Rural Affairs, Beijing, China). The biomass of *R. mucilaginosa* was measured by the weight of *R. mucilaginosa* TZR_{2014} cells.

Resistance Tests of *R. mucilaginosa* TZR_{2014}

The logarithmic phase *R. mucilaginosa* TZR_{2014} was centrifuged and washed twice with 0.85% saline to obtain a suspension for later use. The suspension ($1 \times l0^9$ CFU/ml) was immersed in a water bath at 35, 45, 55, 65, or 75°C for 15 min and then cooled rapidly. Live bacteria were counted using a dilution plate, and three repetitions were performed. The suspension ($1 \times l0^8$ CFU/ml) was inoculated in the YPD liquid medium containing 0, 0.1, 0.2, 0.3, 0.4, or 0.5% (w/v) pig bile salt and then cultured at 37°C for 4 h. Live bacteria were counted using a dilution plate, and three repetitions were performed. The suspension ($1 \times l0^7$ CFU/ml) was inoculated in artificial gastric juice (100 ml hydrochloric acid (pH = 2) containing 1 g pepsin) and then cultured at 37°C for 0, 0.5, 1, 1.5, or 2 h. Live bacteria were counted using a dilution plate, and three repetitions were performed. The suspension ($1 \times l0^7$ CFU/ml) was inoculated into the artificial intestinal fluid (100 ml potassium dihydrogen phosphate solution (pH 6.8) containing 1 g trypsase) and then cultured at 37°C for 0, 1, 2, 3, 4, or 5 h. Live bacteria were counted using a dilution plate, and three repetitions were performed.

Effects on Growth and Health in Weaned Pigs fed *R. mucilaginosa* TZR_{2014}

Strain

R. mucilaginosa TZR_{2014} and *C. utilis* were purchased from Deutsche Sammlung von Mikroorganismen und Zellkulturen (No. DSM 2361).

Animal Use and Care

Thirty 28-day-old weaned pigs (Large White × Landrace × Rongchang) were randomly divided into three groups with 10 barrows each. The piglets were fed (1) a basal diet (CON), (2) a basal diet and orally administered 1 ml 1.0×10^{10} CFU/ml *Candida utilis* DSM 2361 three times (*C. utilis*), and (3) a basal diet and orally administrated 1 ml 1.0×10^{10} CFU/ml *R. mucilaginosa* TZR_{2014} three times daily (*R. mucilaginosa*); the experiment lasted for 4 weeks. All piglets were fed a diet formulated according to the National Research Council requirements (2012). The ingredients and compositions of the basal diet are presented in **Table 1**. The piglets were individually kept in pens in a mechanically ventilated and temperature-controlled room (22 ± 1.2°C). Food and water were provided *ad libitum*. All experimental procedures involving pigs were approved by the License of Experimental Animals (IACAU-20160322-02) of the Animal Experimentation Ethics Committee of the Southwest University, Chongqing, China.

TABLE 1 | The ingredients and nutritional levels of basal diets (DM basis, %).

Ingredients	Content	Nutrition level	Content
Corn	62.78	DE/(MJ/kg)[c]	13.81
Soybean meal	19.90	CP	16.50
Fish meal	2.30	Ca	0.73
Whey powder	6.03	CF	2.60
Wheat Bran	5.00	AP	0.37
Soybean oil	0.85	Lys	1.27
Limestone	0.77	Met	0.37
Salt	0.30	Thr	0.75
$CaHPO_4$	0.70	Trp	0.22
Sweetener	0.06		
Antioxidant	0.02		
Choline chloride	0.08		
Vitamin premix[a]	0.08		
Trace mineral premix[b]	0.30		
Threonine (Thr)	0.09		
Lysine Hydrochloride (Lys)	0.31		
Methionine (Met)	0.09		
Tryptophan (Trp)	0.34		
Total	100.00		

AP, available phosphorus.

[a] Vitamin premix provided the following per kg of the diet: vitamin A 2 017 IU, vitamin D 208 IU, vitamin E 14 IU, vitamin K 0.49 mg, pantothenic acid 10.1 mg, riboflavin 3.4 mg, folic acid 0.29 mg, nicotinic acid 29.1 mg, thiamine 1.1 mg, vitamin B_6 5.7 mg, biotin 0.06 mg, vitamin B_{12} 0.017 mg.

[b] Trace mineral premix provided the following per kg of the diet: $ZnSO_4 \cdot 7H_2O$ 268 mg, $FeSO_4 \cdot 7H_2O$ 323.33 mg, $MnSO_4 \cdot H_2O$ 11.54 mg, $CuSO_4 \cdot 5H_2O$ 22.86 mg, KI 14.21 mg, and Na_2SeO_3 28.37 mg.

[c] DE was a calculated value, whereas the others were measured.

Measurements and Sampling

The experimental period lasted for 4 weeks. Piglets were weighed on day 29 before the morning feed. The feed intake was recorded daily throughout the study period. Prior to the morning feed on day 29, a 10-ml blood sample of five piglets selected from each group was collected. The blood sample was undisturbed for 60 min and then centrifuged at 3,500 × *g* for 10 min at 4°C to harvest the serum. Serum was stored at −20°C for biochemical analysis and ELISA. After blood sampling, five piglets selected from each group were anesthetized with an intravenous injection of sodium pentobarbital (50 mg/kg body weight (BW)) and bled

by exsanguination. The jejunal mucosa was rinsed with cold saline, scraped gently with a scalpel blade, and collected. The harvested jejunal mucosa was immediately frozen in liquid N_2 and stored at −80°C.

Biochemical Analysis

The jejunal mucosa sample (1 g) was homogenized in 9 ml of 0.9% NaCl with a polytron (Brinkmann Instruments Inc., Westbury, NY, USA) and centrifuged at 6,500 × *g* for 20 min at 4°C. The supernatant was collected and stored at −80°C for later analysis. The concentrations of alkaline phosphatase (ALP), malondialdehyde (MDA), lysozyme, glutathione peroxidase (GSH-Px), nitrogen oxide synthase (NOS), total superoxide dismutase (T-SOD), and total antioxidant content (T-AOC) in the serum were determined by colorimetric methods using AKP, MDA, lysozyme, GSH-Px, NOS, T-SOD, and T-AOC reagent kits (Nanjing Jianchen Institute of Bioengineering, Nanjing, Jiangsu, China), according to the manufacturer's instructions. The concentrations of pepsin, lipase, and amylase in the jejunum were determined by colorimetric methods using pepsin, lipase, and amylase reagent kits (Nanjing Jianchen Institute of Bioengineering, Nanjing, Jiangsu, China), according to the manufacturer's instructions.

Hematoxylin and Eosin (H and E) Staining

The morphology of the jejunum and ileum was analyzed according to the hematoxylin and eosin (H&E) staining method described by Wang et al. (2009). The sliced samples were viewed under an optical microscope (Carl Zeiss Inc., Oberkochen, Germany). Digital images were captured using a color video camera Sony 3CCD-VX3 camcorder (Sony Corporation, Tokyo, Japan). Villus height and crypt depth were measured using the image analysis software (Intronic GmbH & Co., Rothenstein, Berlin, Germany).

Diarrhea Rate

Piglet fecal conditions were observed at 8:00 every day. Strip or granular feces were assessed to be 0; soft stool feces were assessed to be 1; thick and water feces were assessed to be 2; and liquid, unformed, and water feces were assessed to be 3. The formula of diarrhea rate was given as follows: diarrhea rate = fecal stool score/total number of test piglets × test days. The higher the value, the more severe the diarrhea.

Analysis of the MiSeq Data

Samples of caecum contents collected on day 28 were directly used for DNA extraction according to a bead-beating method using a minibead beater, followed by the introduction of the Power Fecal DNA Isolation Kit (Mobio), and DNA was quantified using a Nanodrop spectrophotometre (Nyxor Biotech), followed by staining with the Quant-it Pico Green dsDNA Kit (Invitrogen Ltd.). PCR amplification of the V4 region of bacterial 16S rDNA was performed using universal primers 515F (5'-GTGCCAGCMGCCGCGGTAA-3') and 806R (5'-GGACTACHVGGGTWTCTAAT-3') incorporating the FLX titanium adapters and a sample bar code sequence; the cycling parameters were as follows: 5 min initial denaturation at 95°C; 25 cycles of denaturation at 95°C (30 s), annealing at 55°C (30 s), elongation at 72°C (30 s), and final extension at 72°C for 5 min. Three separate PCR reactions for each sample were pooled for the MiSeq analysis. The PCR products were separated by 1.5% agarose gel electrophoresis and purified using a QIAquick Gel Extraction Kit (Qiagen). Amplicons were quantified using a Quant-iT Pico Green dsDNA Assay Kit (Invitrogen). Equal concentrations of the amplicons were pooled for each sample. Libraries were constructed using the TruSeq DNA PCR-Free Sample Prep Kit (Illumina), and MiSeq was performed using the MiSeq Reagent Kit v2 (Illumina).

In total, 747,166 raw reads were obtained from MiSeq. All reads were based on bar codes and primer sequences. The resulting sequences were further screened and filtered for quality and length analysis. Sequences that were less than 200 nucleotides in length, contained ambiguous characters, contained over two mismatches to the primers, or contained mononucleotide repeats of over six nucleotides were removed. High-quality sequences were assigned to samples according to bar codes. Sequences with a similarity level of 97% were clustered into operational clustering of taxonomic units (OTUs) using the UPARSE algorithm 7. The representative sequence from OTUs at a 0.03 distance was obtained and classified using the RDP Bayesian classifier. Any sequence annotations for chloroplast, mitochondrial, or archaeal OTUs not identified to be of bacterial origin were excluded from further analyses. We calculated diversity, bias-corrected Chao1 richness estimator, Faith's phylogenetic diversity (PD), and Shannon and Simpson diversity indices. All analyses were performed using the MOTHUR program (v1.24) (http://www.mothur.org). Based on the above results at the community composition (compositional), development, and system (phylogenetic) levels, the species-level differences in species analysis and correlation analysis, alpha diversity, and community structure diversity analysis of the samples were analyzed using the QIIME, Mothur, and R software, respectively.

Data Calculation and Statistical Analysis

All data are presented as mean ± SEM. The data were subjected to a one-way analysis of variance using the general linear model (GLM) procedure in the SAS statistical software (SAS Institute, Inc. Cary, NC, USA) according to a completely randomized factorial design. The SNK test was performed to identify differences between the groups. Statistical significance was set at $P < 0.05$.

RESULTS

Characteristics of *R. mucilaginosa* TZR_{2014}

Identification by physiological biochemical methods and 26S rDNA D1/D2 sequence analysis revealed that the red yeast was *R. mucilaginosa* (**Figure 1A**). This strain was named TZR_{2014} and was stored at the China Center for Type Culture Collection (CCTCC M2015574, CCTCC, Wuhan, China) on 24 September 2015. The conserved internal transcribed sequence (ITS) region of *R. mucilaginosa* TZR_{2014} was submitted to sequencing data from NCBI GenBank (accession number MT940480). The colonies of *R. mucilaginosa* TZR_{2014} were round, orange-red,

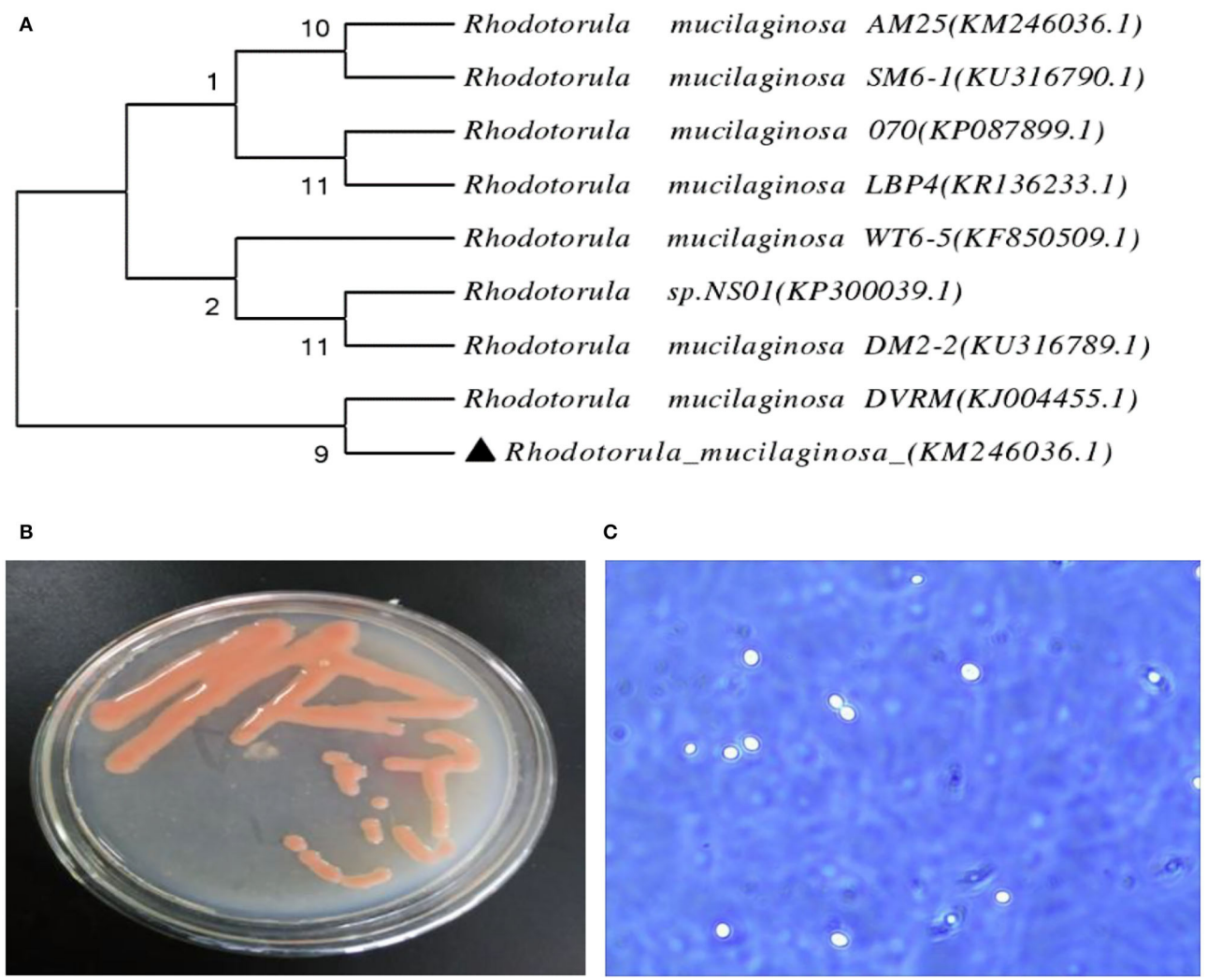

FIGURE 1 | The phylogenetic tree of *Rhodotorula mucilaginosa* TZR_{2014} **(A)**, the visual colony morphology **(B)**, and the cell morphology of *Rhodotorula mucilaginosa* TZR_{2014} **(C)**.

TABLE 2 | Carbon source assimilation of *Rhodotorula mucilaginosa* TZR_{2014}.

Carbon source assimilation	Results	Carbon source assimilation	Results
Galactose	+	Acetamide	–
Sucrose	+	Mannitol	+
Cellobiose	–	Rhamnose	–
Raffinose	+	Melibiose	–
Sorbitol	+	Xylose	+
Melezitose	+	Ribose	+
Inositol	–	Glycerol	+
Trehalose	+	Arabinose	+

"+" said positive; "-" means negative.

bulge, colloid sticky, with neat edges and smooth surfaces (**Figure 1B**). The cells of *R. mucilaginosa* TZR_{2014} were round and budded (**Figure 1C**). As shown in **Table 2**, *R. mucilaginosa* TZR_{2014} uses galactose, sucrose, raffinose, sorbitol, melezitose, trehalose, mannitol, xylose, ribose, glycerol, and arabinose as carbon sources for fermentation. *R. mucilaginosa* TZR_{2014} contained 17 amino acids. The contents of aspartic acid, glutamic acid, and alanine were relatively high, and the crude protein content was 37.8% ± 0.52 (**Table 3**).

Resistance of *R. mucilaginosa* TZR_{2014}

As shown in **Figure 2A**, there was no significant difference in the live cell number of *R. mucilaginosa* TZR_{2014} cultured at 35, 45, and 55°C. The number of live cells of *R. mucilaginosa* TZR_{2014} cultured at 65°C sharply decreased. *R. mucilaginosa* TZR_{2014} cultured at 75°C barely survived. As shown in **Figure 2B**, *R. mucilaginosa* TZR_{2014} grew well in a medium containing less than 0.2% pig bile salt. There was no significant difference in the live cell number of *R. mucilaginosa* TZR_{2014} in media containing 0, 0.1, and 0.2% pig bile salt ($P > 0.05$). The live cell number of *R.*

TABLE 3 | Protein content and amino acids composition of *Rhodotorula mucilaginosa* TZR_{2014} (DM basis, %).

Items	Content	Items	Content	Items	Content
Aspartic acid	2.03 ± 0.06	Cysteine	0.19 ± 0.01	Phenylalanine	1.05 ± 0.04
Threonine	1.14 ± 0.04	Valine	1.25 ± 0.03	Lysine	1.26 ± 0.01
Serine	1.14 ± 0.04	Methionine	0.39 ± 0.03	Histidine	0.58 ± 0.01
Glutamic acid	2.29 ± 0.05	Isoleucine	1.05 ± 0.04	Arginine	1.74 ± 0.04
Glycine	1.33 ± 0.03	Leucine	1.77 ± 0.02	Proline	1.16 ± 0.07
Alanine	2.02 ± 0.05	Tyrosine	0.65 ± 0.02	Crude protein	37.8 ± 0.52

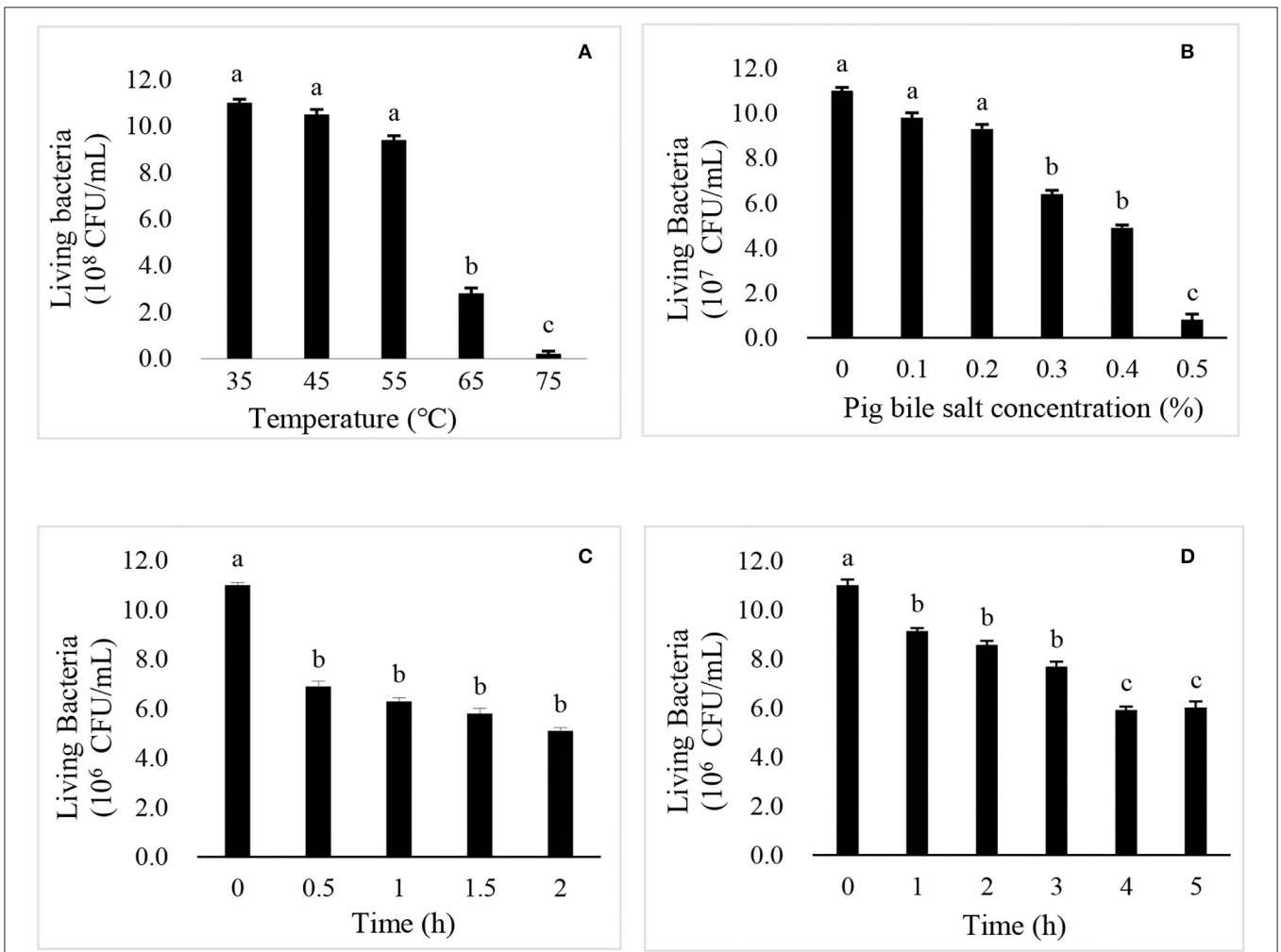

FIGURE 2 | The effects of temperature **(A)**, pig bile salts **(B)**, artificial gastric juice **(C)**, and artificial intestinal fluid **(D)** on the growth of *R. mucilaginosa* TZR_{2014}.

mucilaginosa TZR_{2014} in the medium with 0.3% and 0.4% pig bile salt decreased ($P < 0.05$). *R. mucilaginosa* TZR_{2014} in medium with more than 0.5% pig bile salt hardly grew.

As shown in **Figure 2C**, the live cell number of *R. mucilaginosa* TZR_{2014} in artificial gastric juice for 0.5 h significantly decreased ($P < 0.05$). There was no significant difference in the live cell number of *R. mucilaginosa* TZR_{2014} in artificial gastric juice at 0.5, 1, 1.5, and 2 h ($P > 0.05$). As shown in **Figure 2D**, the live cell number of *R. mucilaginosa* TZR_{2014} in artificial intestinal fluid for 0.5 h significantly decreased ($P < 0.05$). There was no significant difference in the number of live cells of *R. mucilaginosa* TZR_{2014} in artificial intestinal fluid at 1, 2, and 3 h ($P > 0.05$). The number of *R. mucilaginosa* TZR_{2014} cells in artificial intestinal fluid for 4 h significantly decreased ($P < 0.05$). There was no significant difference in the live cell number of *R. mucilaginosa* TZR_{2014} cultured in artificial intestinal fluid for 4 and 5 h ($P > 0.05$).

TABLE 4 | The result of the fermentation optimisation of *Rhodotorula mucilaginosa* TZR_{2014}.

Test number	A	B	C	Biomass (g/L)	Carotenoid content (μg/g)	Carotenoid yield (mg/L)
1	I	I	I	16.91	164.34 ± 26.12	2.74 ± 0.47
2	I	II	II	18.02	186.03 ± 26.14	3.35 ± 0.46
3	I	III	III	20.26	161.78 ± 15.75	3.27 ± 0.32
4	II	I	II	21.30	181.49 ± 13.26	3.86 ± 0.28
5	II	II	III	23.41	193.10 ± 48.02	4.50 ± 1.12
6	II	III	I	21.60	185.58 ± 24.77	4.00 ± 0.53
7	III	I	III	25.48	201.57 ± 54.98	15.44 ± 1.40
8	III	II	I	23.23	167.35 ± 12.99	11.83 ± 0.29
9	III	III	II	24.64	180.04 ± 12.93	4.43 ± 0.32
I/3				18.39	21.23	20.68
II/3				22.10	21.65	21.32
III/3				24.55	22.17	23.05
R				6.16	0.94	2.37
I/3				170.71	182.46	172.42
II/3				186.72	182.16	182.52
III/3				175.8	175.80	185.48
R				16.01	6.66	13.06
I/3				3.12	7.34	6.19
II/3				4.12	6.56	3.88
III/3				10.56	3.90	7.73
R				7.44	3.44	3.85

TABLE 5 | Effects of *C. utilis* DSM 2361 and *R. mucilaginosa* TZR_{2014} on the growth performance and diarrhea incidence in weaned piglets ($n = 10$).

Items	Treatments[a]			SEM[b]	*P*-value
	CON	*C. utilis*	*R. mucilaginosa*		
Intial BW (kg)	7.23	7.25	7.20	0.02	1.00
Final BW (kg)	11.9^{C}	13.5^{B}	14.5^{A}	0.09	0.01
Average daily gain (ADG) (g/d)	166^{C}	223^{B}	259^{A}	3.56	<0.01
Average daily feed intake (ADFI) (g/d)	382^{B}	438^{A}	449^{A}	4.51	0.036
Feed/gain (F/G)	2.3^{A}	1.96^{B}	1.73^{C}	0.03	<0.01
Diarrhea rate (%)	17.7^{A}	17.0^{A}	14.3^{B}	0.08	0.01

[a]*CON, piglets were fed a corn-and a soybean-based basal diet; C. utilis, piglets were fed a soybean-based basal diet and orally administrated 1 ml 1.0 × 10^{10} CFU/ml C. utilis DSM 2361 three times; R. mucilaginosa, piglets were fed a soybean-based basal diet and daily orally administrated 1 mL 1.0 × 10^{10} CFU/ml R. mucilaginosa TZR_{2014} three times daily.*

[b]*Standard error mean.*

[ABC]*Values in the same row with different superscript letters indicate significant differences ($P < 0.05$).*

Fermentation Optimisation of *R. mucilaginosa* TZR_{2014} and Biomass and Carotenoid Production Conditions

As shown in **Table 4**, the biomass (25.48 g/L), carotenoid content (201.57 ± 54.98 μg/g), and carotenoid yield (15.44 ± 1.40 mg/L) of *R. mucilaginosa* TZR_{2014} reached the maximum when the contents of each component of the optimized fermentation medium were 5% glucose, 1% peptone, and 1.5% yeast powder.

Effects of Orally Administered *C. utilis* and *R. mucilaginosa* TZR_{2014} on the Growth Performance and Diarrhea Incidence in Weaned Piglets

The final BW and average daily gain of pigs differed among the three groups ($P < 0.01$) (**Table 5**); that is, it was highest in the *R. mucilaginosa* group and lowest in the CON group ($P < 0.05$). Feed/gain and diarrhea rates of pigs differed among the three groups ($P < 0.01$) (**Table 5**); that is, they were the lowest in the *R. mucilaginosa* group and highest in the CON group ($P < 0.05$). Pigs orally administered *C. utilis* and *R. mucilaginosa* had a higher average daily food intake ($P < 0.05$) than pigs fed the basal diet. The average daily food intake did not differ between *C. utilis* and *R. mucilaginosa* groups ($P > 0.05$).

Effects of Orally Administered *C. utilis* and *R. mucilaginosa* TZR_{2014} on Intestinal Morphological Structure in Weaned Piglets

As shown in **Table 6**, there was no significant difference in jejunal or ileal length among the three groups ($P > 0.05$). Compared with the piglets in the CON and *C. utilis* groups, those in the orally administered *R. mucilaginosa* group had increased jejunum weight, ileum weight, and ileum villus height ($P < 0.05$). The jejunum weight, ileum weight, and ileum villus height did not

TABLE 6 | Effects of *C. utilis* DSM 2361 and *R. mucilaginosa* TZR_{2014} on intestinal structure in weaned piglets ($n = 5$).

Items	Treatments[a]			SEM[b]	*P*-value
	CON	*C. utilis*	*R. mucilaginosa*		
Jejunum length (cm)	344	363	420	32.5	0.28
Ileum length (cm)	533	561	580	25.5	0.45
Jejunum weight (g)	162^{B}	205^{B}	310^{A}	27.6	0.03
Ileum weight (g)	223^{B}	294^{B}	413^{A}	45.6	0.01
Ileum villus height (μm)	221^{B}	236^{B}	276^{A}	50.1	0.02
Ileum crypt depth (μm)	201^{A}	154^{B}	172^{B}	30.2	0.01

[a]*CON, piglets were fed a corn-and a soybean-based basal diet; C. utilis, piglets were fed a soybean-based basal diet and orally administrated 1 ml 1.0 × 10^{10} CFU/ml C. utilis DSM 2361 three times; R. mucilaginosa, piglets were fed a soybean-based basal diet and daily orally administrated 1 ml 1.0 × 10^{10} CFU/ml R. mucilaginosa TZR_{2014} three times daily.*
[b]*Standard error mean.*
[ABC]*Values in the same row with different superscript letters indicate significant differences ($P < 0.05$).*

differ between *C. utilis* and *R. mucilaginosa* groups ($P > 0.05$). Compared with the piglets in the CON group, those in the orally administered *R. mucilaginosa* and *C. utilis* groups had decreased ileal crypt depth. The ileum crypt depth did not differ between *C. utilis* and *R. mucilaginosa* groups ($P > 0.05$).

According to H&E-stained sections (**Figure 3**), some villi in the CON group were broken and missing. The villi in the *C. utilis* and *R. mucilaginosa* groups were clear and neatly arranged. Compared with that in the CON group, the villi in the *C. utilis* and *R. mucilaginosa* groups were more complete.

Effects of Orally Administered *C. utilis* and *R. mucilaginosa* TZR_{2014} on Blood Biochemical Indicators in Weaned Piglets

As shown in **Table 7**, there were no significant differences in serum ALP, NOS, or lysozyme concentrations among the three groups ($P > 0.05$). Compared with the piglets in the CON group, those in the orally administered *R. mucilaginosa* and *C. utilis* groups had increased serum T-AOC concentration. Serum T-AOC concentrations did not differ between *C. utilis* and *R. mucilaginosa* groups ($P > 0.05$). Serum T-SOD and GSH-Px concentrations differed among the three groups ($P < 0.01$) and were the highest in the *R. mucilaginosa* group and lowest in the CON group ($P < 0.05$). Serum MDA differed among the three groups ($P < 0.01$); that is, it was highest in the CON group and lowest in the *C. utilis* group ($P < 0.05$).

Effects of Orally Administered *C. utilis* and *R. mucilaginosa* TZR_{2014} on Digestive Enzyme Activities of Jejunal Contents and pH of Gastrointestinal Tract in Weaned Piglets

As shown in **Table 8**, compared with the piglets in the CON group, those in the orally administered *R. mucilaginosa* and *C. utilis* groups had increased pepsin activity in jejunal contents. The pepsin activity of jejunal contents did not differ between *C. utilis* and *R. mucilaginosa* groups ($P > 0.05$). There was no significant difference in the amylase activity of jejunal contents or stomach pH among the three groups ($P > 0.05$). The lipase activity of the jejunal contents differed among the three groups ($P < 0.01$); that is, the value was the highest in the *R. mucilaginosa* group and lowest in the CON group ($P < 0.05$). Compared with the piglets in the CON and *C. utilis* groups, those in the orally administered *R. mucilaginosa* group had increased jejunum pH. Jejunum pH values did not differ between the CON and *C. utilis* groups ($P > 0.05$). Compared with the piglets in the CON group, those in the orally administered *R. mucilaginosa* and *C. utilis* groups had increased pH in the ileum, colon, and caecum. The pH values of the ileum, colon, and caecum did not differ significantly between the *R. mucilaginosa* and *C. utilis* groups ($P > 0.05$).

Analysis of Colon Microbial Ecology in Weaned Piglets Orally Administered *R. mucilaginosa* TZR_{2014}

As shown in **Table 9**, the dominant bacteria in the colonic contents of the three groups were mainly Proteobacteria, Bacteriodetes, and Firmicutes, and the total number of microbes of the three types of bacteria reached more than 90%. Compared with the piglets in the CON and *C. utilis* groups, piglets in the orally administered *R. mucilaginosa* group showed an increasing trend in diversity, Chao1, Shannon, and Faith_ID indices ($P > 0.05$).

The relative abundances of seven phyla are shown in **Table 9**. Compared with that in the CON and *C. utilis* groups, the relative abundance of Bacteroidetes and Proteobacteria in the orally administered *R. mucilaginosa* TZR_{2014} group decreased ($P < 0.05$). The relative abundances of Bacteroidetes and Proteobacteria did not differ between the CON and *C. utilis* groups ($P > 0.05$). Compared with that in the CON group, the relative abundance of Actinobacteria in the orally administered *R. mucilaginosa* TZR_{2014} and *C. utilis* groups decreased ($P < 0.05$). The relative abundance of Actinobacteria did not differ between *R. mucilaginosa* and *C. utilis* groups ($P > 0.05$). Compared with that in the CON and *C. utilis* groups, the relative abundance of Firmicutes and Spirochaetae in the orally administered *R. mucilaginosa* TZR_{2014} group increased ($P < 0.05$). The relative abundances of Firmicutes and Spirochaetae did not differ between CON and *C. utilis* groups ($P > 0.05$). The

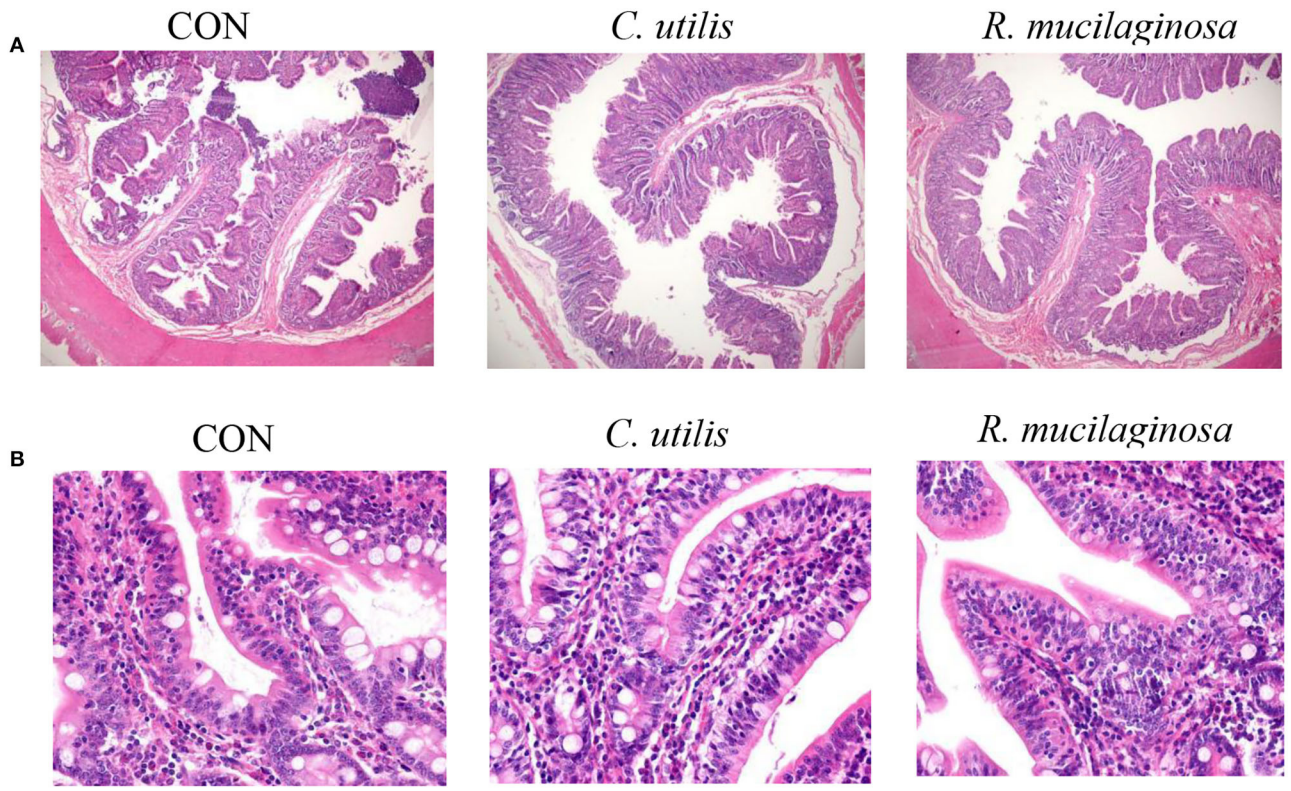

FIGURE 3 | Effects of *C. utilis* DSM 2361 and *R. mucilaginosa* on ileum morphology by magnification 40× **(A)** and 400× **(B)** in weaned piglets. CON, piglets were fed a corn-and a soybean-based basal diet; *C. utilis*, piglets were fed a soybean-based basal diet and orally administrated 1 ml 1.0×10^{10} CFU/ml *C. utilis* DSM 2361 three times; *R. mucilaginosa*, piglets were fed a soybean-based basal diet and daily orally administrated 1 ml 1.0×10^{10} CFU/ml *R. mucilaginosa* TZR_{2014} three times daily.

relative abundance of Verrucomicrobia differed among the three groups ($P < 0.01$); that is, it was the highest in the *R. mucilaginosa* group and lowest in the CON group ($P < 0.05$). There was no significant difference in the relative abundance of Acidobacteria in piglets among the groups ($P > 0.05$).

Sixteen genus groups with relative abundances greater than 1% are shown in **Table 9**. Compared with that in the CON and *C. utilis* groups, the relative abundance of Prevotella, Rikenellaceae RC9 gut group, and Roseburia in the orally administered *R. mucilaginosa* TZR_{2014} decreased ($P < 0.05$). The relative abundances of Prevotella, Rikenellaceae RC9 gut group, and Roseburia did not differ between the CON and *C. utilis* groups ($P > 0.05$). The relative abundance of Prevotellaceae *NK3B31 group* differed among the three groups ($P < 0.01$); that is, it was the highest in the *C. utilis* group and lowest in the CON group ($P < 0.05$). The relative abundance of Ruminococcaceae differed among the three groups ($P < 0.01$); that is, it was the highest in the *R. mucilaginosa* group and lowest in the CON group ($P < 0.05$). Compared with that in the CON group, the relative abundances of Alloprevotella, Succinivibrio, and Akkermansia in the orally administered *R. mucilaginosa* TZR_{2014} and *C. utilis* groups increased ($P < 0.05$). The relative abundance of Alloprevotella, Succinivibrio, and Akkermansia did not differ between *R. mucilaginosa* and *C. utilis* groups ($P > 0.05$). Compared with that in the CON group, the relative abundance of Lactobacillus and Megasphaera in the orally administered *R. mucilaginosa* TZR_{2014} and *C. utilis* decreased ($P < 0.05$). The relative abundances of Lactobacillus and Megasphaera did not differ between *R. mucilaginosa* and *C. utilis* groups ($P > 0.05$). There was no significant difference in the relative abundance of Bacteroidales S24-7 group, Lachnospiraceae, Anaerovibrio, Clostridium sensu stricto 1, Bacteroides, or Parabacteroides of piglets among the three groups ($P > 0.05$).

DISCUSSION

In this experiment, a red pigment-producing yeast strain was selected from the soil of a Chongqing orchard. The colonies it formed were orange-red, and the yield of carotenoids was very high. Through identification of its colony characteristics, individual morphology, and physiological and biochemical characteristics, it was determined to be a species of *Rhodotorula*. After further analysis of the 26S rDNA D1/D2 sequence, it was identified as *R. mucilaginosa*, which contains 17 amino acids and can utilize a variety of carbon sources. Through fermentation optimisation of *R. mucilaginosa* TZR_{2014}, we found that the

TABLE 7 | Effects of *C. utilis* DSM 2361 and *R. mucilaginosa* TZR_{2014} on serum blood biochemical indicators in weaned piglets ($n = 5$).

Items	Treatments[a]			SEM[b]	*P*-value
	CON	*C. utilis*	*R. mucilaginosa*		
Alkaline phosphatase (ALP) (King unit/100 mL)	16.9	17.1	17.4	0.1	0.21
Lysozyme (U/mL)	12.3	14.2	14.1	0.5	0.45
Nitricoxide synthase (NOS) (U/mL)	13.3	14.1	13.9	0.2	0.52
Total antioxidative capacity (T-AOC) (U/mL)	1.3^{B}	1.6^{A}	1.6^{A}	0.02	<0.01
Total superoxide dismutase (T-SOD) (U/mg prot)	52.5^{C}	58.2^{B}	60.7^{A}	0.77	0.03
Glutathione peroxidase (GSH-Px) (U/mg prot)	470^{C}	516^{B}	768^{A}	4.5	<0.01
Malondialdehyde (MDA) (nmol/mL)	4.9^{A}	2.3^{C}	2.6^{B}	0.07	<0.01

[a]*CON, piglets were fed a corn-and a soybean-based basal diet; C. utilis, piglets were fed a soybean-based basal diet and orally administrated 1 ml 1.0 × 10^{10} CFU/ml C. utilis DSM 2361 three times; R. mucilaginosa, piglets were fed a soybean-based basal diet and daily orally administrated 1 ml 1.0 × 10^{10} CFU/mL R. mucilaginosa TZR_{2014} three times daily.*
[b]*Standard error mean.*
[ABC]*Values in the same row with different superscript letters indicate significant differences ($P < 0.05$).*

TABLE 8 | Effects of *C. utilis* DSM 2361 and *R. mucilaginosa* TZR_{2014} on digestive enzyme activity of jejunal contents and pH of gastrointestinal tract in weaned piglets ($n = 5$).

Items	Treatments[a]			SEM[b]	*P*-value
	CON	*C. utilis*	*R. mucilaginosa*		
Pepsin (U/mg prot)	27.0^{B}	30.5^{A}	31.4^{A}	0.46	0.032
Amylase (U/mg prot)	0.047	0.070	0.193	0.08	0.41
Lipase (U/mg prot)	144^{C}	346^{B}	388^{A}	7.17	<0.01
Stomach pH	3.5	3.0	3.3	0.09	0.058
Jejunum pH	5.9^{A}	5.9^{A}	5.5^{B}	0.04	<0.01
Ileum pH	6.7^{A}	6.3^{B}	6.3^{B}	0.08	0.013
Colon pH	6.3^{A}	6.2^{B}	5.9^{B}	0.11	0.048
Cecum pH	6.2^{A}	5.8^{B}	5.8^{B}	0.06	<0.01

[a]*CON, piglets were fed a corn-and a soybean-based basal diet; C. utilis, piglets were fed a soybean-based basal diet and orally administrated 1 ml 1.0 × 10^{10} CFU/ml C. utilis DSM 2361 three times; R. mucilaginosa, piglets were fed a soybean-based basal diet and daily orally administrated 1 ml 1.0 × 10^{10} CFU/mL R. mucilaginosa TZR_{2014} three times daily.*
[b]*Standard error mean.*
[ABC]*Values in the same row with different superscript letters indicate significant differences ($P < 0.05$).*

ideal composition of the fermentation medium was 5% glucose, 1% peptone, and 1.5% yeast powder. In addition, the above results show that *R. mucilaginosa* TZR_{2014} has good tolerance to simulated gastric acid and porcine bile salt environments, indicating that *R. mucilaginosa* TZR_{2014} can be added as an additive to animal diets. This is similar to the results of Hamidi et al. (2020), who reported that *R. mucilaginosa* has high biocompatibility and low cytotoxicity.

In this study, *R. mucilaginosa* TZR_{2014} had a significant positive effect on the growth and performance of weaned piglets. The specific manifestation was that it significantly increased average daily gain and average daily feed intake in weaned piglets and significantly reduced feed/gain and diarrhea rates. The growth-promoting effect of *R. mucilaginosa* TZR_{2014} may be related to its effects on digestive enzymes, intestinal pH, and intestinal morphology. Studies have shown that feeding live yeast can promote the growth and development of fishes, increase the activity of pancreatic amylase, lipase, and protease (Tovar-RamiRez et al., 2004), and improve protein utilization and feed conversion rates (Lara-Flores et al., 2003). In addition, the metabolites of *R. mucilaginosa* TZR_{2014} include fatty acids, which can lower the pH of the intestinal tract. In this experiment, adding *R. mucilaginosa* TZR_{2014} to the diet significantly increased pepsin and lipase activities in the jejunum of weaned piglets and significantly reduced the pH value of the jejunum, ileum, colon, and caecum, similar to the above results. In terms of intestinal morphology, the ileal villus height and crypt depth of the *R. mucilaginosa* and *C. utilis* groups were greater than those of the CON group. The small intestine plays a major role in the digestion, absorption, and transport of nutrients and is the body's defense against harmful substances. This protective barrier against pathogenic microorganisms and good, intact intestinal morphology is important guarantees for maintaining the healthy growth of the body (El Aidy et al., 2015). The addition of *R. mucilaginosa* TZR_{2014} to the diet may alleviate the shortage of digestive enzymes and damage to intestinal morphology caused by weaning stress and improve feed utilization and growth performance.

Based on the serum biochemical indicators of weaned piglets, both the *R. mucilaginosa* and *C. utilis* groups showed

TABLE 9 | Effects of *C. utilis* DSM 2361 and *R. mucilaginosa* TZR_{2014} on alpha diversity and of phylum and genus level microbial composition in cecum of weaned piglets ($n = 5$).

Items	Treaments[a]			SEM[b]	*P-value*
	CON	***C.utilis***	***R.mucilaginosa***		
Diversity	845	967	1,056	55.4	0.09
Chao1	1,227	1,401	1,573	139.6	0.19
Simpson	0.96	0.98	0.98	0.11	0.33
Shannon	4.8	5.3	5.5	0.17	0.10
Faith_PD	70.9	77.1	79.4	2.11	0.07
Phylum (%)					
Bacteroidetes	61.9^{A}	60.1^{A}	52.3^{B}	1.43	0.007
Firmicutes	25.2^{B}	24.0^{B}	31.1^{A}	1.10	0.008
Proteobacteria	11.5^{A}	11.2^{A}	6.4^{B}	0.77	0.006
Verrucomicrobia	0.03^{C}	1.0^{B}	6.4^{A}	0.21	<0.01
Actinobacteria	2.4^{A}	1.1^{B}	1.2^{B}	0.14	0.001
Spirochaetae	0.07^{B}	0.4^{B}	1.8^{A}	0.18	0.001
Acidobacteria	0.07	0.03	0.07	0.03	0.73
Genus (%)					
Prevotella	16.86^{B}	18.10^{B}	22.01^{A}	0.905	0.016
Prevotellaceae NK3B31 group	2.15^{C}	19.56^{A}	9.16^{B}	0.517	<0.01
Bacteroidales S24-7 group	3.2	6.13	4.85	1.282	0.337
Ruminococcaceae	1.43^{C}	4.15^{B}	8.00^{A}	0.156	<0.01
Lachnospiraceae	2.13	4.48	6.06	0.904	0.057
Alloprevotella	3.19^{B}	4.18^{A}	4.03^{A}	0.189	0.021
Succinivibrio	2.08^{B}	4.31^{A}	4.42^{A}	0.157	<0.01
Rikenellaceae RC9 gut group	1.56^{B}	2.53^{B}	4.03^{A}	0.326	0.005
Roseburia	1.39^{B}	1.51^{B}	3.36^{A}	0.391	0.02
Anaerovibrio	1.01	3.03	1.78	1.137	0.492
Clostridium sensu stricto 1	1.41	1.1	2.31	0.783	0.557
Bacteroides	1.49	1.81	1.37	0.181	0.29
Lactobacillus	3.91^{A}	0.40^{B}	0.31^{B}	0.61	0.009
Parabacteroides	0.63	2.77	1.69	0.829	0.266
Akkermansia	0.03^{B}	1.5^{A}	1.44^{A}	0.174	0.002
Megasphaera	1.65^{A}	0.24^{B}	0.45^{B}	0.134	0.001

[a] *CON, piglets were fed a corn-and a soybean-based basal diet; C. utilis, piglets were fed a soybean-based basal diet and orally administrated 1 ml 1.0 × 10^{10} CFU/ml C. utilis DSM 2361 three times; R. mucilaginosa, piglets were fed a soybean-based basal diet and daily orally administrated 1 ml 1.0 × 10^{10} CFU/mL R. mucilaginosa TZR_{2014} three times daily.*

[b] *Standard error mean.*

[ABC] *Values in the same row with different superscript letters indicate significant differences ($P < 0.05$).*

strong antioxidant capacities, and the T-AOC, T-SOD, GSH-PX, and MDA indicators were better than those of the CON group. This may be due to the unique extracellular polysaccharide (EPS) of yeast. EPS may contain mannose, glucose, galactose, xylose, fucose, and rhamnose residues as the main chain or branch components (Ustyuzhanina et al., 2018). The EPS of *R. mucilaginosa* (composed of galactose, arabinose, glucose, and mannose with molar ratios of 63.1:0.2:18.3:18.3, respectively) has a strong free-radical scavenging ability [2,2-Diphenyl-1-picrylhydrazyl (DPPH) and 2, 2'-azino-bis(3-ethylbenzothiazoline-6-sulfonic acid) (ABTS)] and anti-tumor activity (Ma et al., 2018). Some researchers isolated linear mannan with ß-1,3 and ß-1,4 bonds produced by *R. mucilaginosa* and found that it can increase cholinesterase, α-amylase, aldolase, and red blood cell catalase in the liver and serum (Rahbar Saadat et al., 2021). The glucomannan produced by *C. utilis* is composed of D-mannose and D-glucose, which contain α-1,3, α-1,4, and α-1,6 glycosidic bonds and have strong antioxidant activity (Van Bogaert et al., 2009). Some *in vitro* experiments have shown that the isolated EPS is not cytotoxic to normal cell models, while it does exert antioxidant activity (Hamidi et al., 2020). Notably, *R. mucilaginosa* TZR_{2014} performed better than *C. utilis* in antioxidant indicators. This may be related to the unique metabolite of *R. mucilaginosa* TZR_{2014}, carotenoids. Carotenoids have a strong effect on the antioxidant and immune systems. Experiments have shown that carotenoids can improve disease resistance, antioxidant capacity, and growth performance of farmed fish without causing other

cytotoxicities or side effects (Nakano and Wiegertjes, 2020). Carotenoids can increase not only the activity of antioxidant enzymes (SOD and GPX) and endogenous antioxidants (GSH) but also the antioxidant capacity of cells by regenerating α-tocopherol and ascorbic acid from their corresponding free radical forms and cooperating with other antioxidants to protect lipoproteins from oxidation and reduce the body's oxidative stress (Nishida, 2012; Pisoschi and Pop, 2015; Lim et al., 2018). In addition, carotenoids can also inhibit the NF-κB signaling pathway (inflammatory response activation) and activate the Nrf2 signaling pathway (defense against ROS-induced cellular oxidative stress; Ambati et al., 2014; Gammone et al., 2015; Pisoschi and Pop, 2015; Ribeiro et al., 2018). Therefore, *R. mucilaginosa* TZR_{2014} is a promising feed additive for alleviating oxidative stress in weaned piglets.

Because the digestive and immune systems of weaned piglets have not yet fully developed, coupled with changes in diet, the number and structure of the intestinal flora have undergone great changes, which can easily lead to the proliferation of harmful bacteria and diarrhea. Studies have shown that mannan and β-glucan in the cell wall of yeast can adsorb intestinal pathogens and toxic metabolites. Their structure is similar to that of mannose residues on the surface of the intestinal epithelial cells. Mannose residues are the binding sites between pathogenic microorganisms and the intestinal tract. This yeast structure can competitively bind to pathogenic microorganisms and reduce the adhesion of these microorganisms in the intestinal tract. Because yeast is a passing visitor in the intestines, the yeast/pathogen complex can be quickly excreted from the digestive tract (Fuller, 1989; Spring et al., 2000; Li et al., 2005). In this study, orally administered *R. mucilaginosa* TZR_{2014} significantly reduced the relative abundance of Proteobacteria and Megasphaera. Proteobacteria contains many common pathogenic bacteria, such as *Escherichia coli*, *Salmonella*, and *Helicobacter pylori*, and harmful spoilage bacteria such as *Megasphaera*. These results were consistent with the above conclusions. In addition, orally administered *R. mucilaginosa* TZR_{2014} significantly increased the relative abundances of Prevotella, Ruminococcaceae, Succinivibrio, Rikenellaceae RC9 gut group, and Roseburia in this experiment. Prevotella is the dominant flora in the intestinal tract of weaned piglets. It can promote glucose metabolism and break down complex carbohydrates, such as polysaccharides and starch, into short-chain fatty acids (Kovatcheva-Datchary et al., 2015). Ruminococcaceae can not only decompose cellulose and carbohydrates but also synthesize secondary bile acids through 7α-dehydrogenation to reduce intestinal inflammation (Mullish et al., 2019). Succinivibrio is abundant in the rumen of high-yielding and multi-product dairy cows, and its growth is related to the activities of urease, glutamine synthase, glutamate dehydrogenase, and glutamate synthase, which can improve nitrogen utilization (Hailemariam et al., 2020). Studies have shown that the abundance of the Rikenellaceae RC9 gut group is negatively correlated with diarrhea rate and positively correlated with nutrient digestibility, similar to the results of this experiment (Tian et al., 2020). Roseburia is a saccharolytic, butyrate-producing bacterium from human feces that can decompose a variety of sugars (e.g., xylose, galactose, raffinose, maltose, cellobiose, sucrose, and starch), and also affects the activities of β-glucuronidase and β-glucosidase in *in vitro* experiments, which is conducive to improve feed utilization (Machiels et al., 2014). The number and structure of the intestinal flora are closely related to the host's nutrition and health. *R. mucilaginosa* TZR_{2014} can optimize the structure of the intestinal flora, inhibit the reproduction of harmful bacteria, and promote the utilization of nutrients and body health.

In general, this study found that *R. mucilaginosa* TZR_{2014} is safe and effective as an additive. Adding *R. mucilaginosa* TZR_{2014} to the diet can improve the growth performance of weaned piglets, promote the development of intestinal morphology, increase the activity of digestive enzymes, enhance antioxidant capacity, resist the invasion of harmful bacteria, and reduce the rate of diarrhea. However, before applying *R. mucilaginosa* TZR_{2014} to production practice, more experimental studies are needed to explore the probiotic mechanism of *R. mucilaginosa*, the best addition amount and form, and the possible side effects.

CONCLUSION

R. mucilaginosa was screened using traditional taxonomic and molecular biological classifications and identification methods and was named TZR_{2014}. *R. mucilaginosa* TZR_{2014} has a tolerance to gastric acid and bile salt environments. Oral administration of *R. mucilaginosa* TZR_{2014} improved the average daily gain and average daily feed intake of weaned piglets and reduced the feed/gain and diarrhea rates. *R. mucilaginosa* TZR_{2014} had a positive effect on improving the morphology of the small intestine, increasing the activities of digestive enzyme (pepsin and lipase), reducing gastrointestinal pH value, enhancing antioxidant performance (T-AOC, T-SOD, GSH-Px, and MDA), and improving the number and structure of intestinal flora in weaned piglets.

DATA AVAILABILITY STATEMENT

The 16sRNA sequencing raw data are available at NCBI under the accession number PRJNA827018 by web link (https://www.ncbi.nlm.nih.gov/sra/PRJNA827018). The rest of the raw data supporting the conclusions of this article will be made available by the authors without undue reservation.

ETHICS STATEMENT

The animal study was approved by the Animal Experimentation Ethics Committee of Southwest University, Chongqing, China (IACAU-20160322-02). All piglets were raised following the guidelines described by the Animal Care Committee of Chongqing, China. In addition, efforts were made to reduce

animal suffering and were carried out in compliance with the ARRIVE guidelines for reporting *in vivo* experiments in animal research.

AUTHOR CONTRIBUTIONS

PH and JM: investigation, data curation, methodology, formal analysis, and writing of the original draft. YZ and HD: investigation and methodology. ZS and CC: writing, review, and editing. WS: conceptualization and supervision. ZT: investigation, project administration, funding acquisition, and writing-reviewing and editing. All authors have contributed to the manuscript and approved the submitted version.

FUNDING

This study was funded by the Natural Science Foundation Project of Chongqing (cstc2021jcyj-msxmX0966), the Chongqing Key Innovation Project for Overseas Students (cx2017024), the Technical Service Cooperation (M2022002, FJ20202048, and FJ2021249), and the 2021-Research Topics in Committee of Agriculture and Forestry Discipline of Chinese Society of Degree and Graduate education (2021-NL2X-YB76).

ACKNOWLEDGMENTS

We would like to thank Editage (www.editage.cn) for English language editing.

REFERENCES

Aksu, Z., and Eren, A. T. (2005). Carotenoids production by the yeast *Rhodotorula mucilaginosa*: use of agricultural wastes as a carbon source. *Process Biochem.* 40, 2985–2991. doi: 10.1016/j.procbio.2005.01.011

Ambati, R. R., Phang, S. M., Ravi, S., and Aswathanarayana, R. G. (2014). Astaxanthin: sources, extraction, stability, biological activities and its commercial applications-a review. *Mar. Drugs* 12, 128–152. doi: 10.3390/md12010128

Barnett, J. A., Payne, R. W., Yarrow, D., and Barnett, P. (1983). *Yeasts: Characteristics and Identification*. Cambridge: Cambridge University Press.

Bhagavathy, S., and Sumathi, P. (2012). Evaluation of antigenotoxic effects of carotenoids from green algae Chlorococcum human lymphocytes. *Asian Pac J. Trop. Biomed.* 2, 109–117. doi: 10.1016/S2221-1691(11)60203-7

Dalmo, R. A., and Bogwald, J. (2008). β-glucan as conductors of immune symphonies. *Fish Shellfish Immunol.* 25, 384–396. doi: 10.1016/j.fsi.2008.04.008

El Aidy, S., Van Den Bogert, B., and Kleerebezem, M. (2015). The small intestine microbiota, nutritional modulation and relevance for health. *Curr. Opin. Biotechnol.* 32, 14–20. doi: 10.1016/j.copbio.2014.09.005

Fuller, R. (1989). Review probiotics in man and animals. *J. Appl. Bacteriol.* 66, 365–378. doi: 10.1111/j.1365-2672.1989.tb05105.x

Gammone, M. A., Riccioni, G., and D'Orazio, N. (2015). Marine carotenoids against oxidative stress: effects on human health. *Mar. Drugs* 13, 6226–6246. doi: 10.3390/md13106226

Hailemariam, S., Zhao, S., and Wang, J. (2020). Complete genome sequencing and transcriptome analysis of nitrogen metabolism of *Succinivibrio dextrinosolvens* strain Z6 isolated from dairy cow rumen. *Front. Microbiol.* 11:1826. doi: 10.3389/fmicb.2020.01826

Hamidi, M., Gholipour, A. R., Delattre, C., Sesdighi, F., Mirzaei Seveiri, R., Pasdaran, A., et al. (2020). Production, characterization and biological activities of exopolysaccharides from a new cold-adapted yeast: *Rhodotorula mucilaginosa* sp. GUMS16. *Int. J Biol. Macromol.* 151, 268–277. doi: 10.1016/j.ijbiomac.2020.02.206

Kovatcheva-Datchary, P., Nilsson, A., Akrami, R., Ying, F., Arora, T., Hallen, A., et al. (2015). Dietary fiber-induced improvement in glucose metabolism is associated with increased abundance of *Prevotella*. *Cell Metab.* 22, 971–982. doi: 10.1016/j.cmet.2015.10.001

Lara-Flores, M., Olvera-Novoa, M. A., Guzman-Mendez, B. E., and Lopez-Madrid, W. (2003). Use of the bacteria *Streptococcus faecium* and *Lactobacillus acidophilus*, and the yeast *Saccharomyces cerevisiae* as growth promoters in Nile tilapia (Oreochromis niloticus). *Aquaculture* 216, 193–201. doi: 10.1016/S0044-8486(02)00277-6

Li, J., Xing, J., Li, D. F., Wang, X., Zhao, L. D., Lv, S. Q., et al. (2005). Effect of β-glucan extracted from *Saccharomyces cerevisiae* on humoral and cellular immunity in weaned pigs. *Arch. Anim. Nutr.* 59: 303–312. doi: 10.1080/17450390500247832

Lim, K. C., Yusoff, F. M., Shariff, M., and Kamarudin, M. S. (2018). Astaxanthin as feed supplement in aquatic animals. *Rev. Aquac.* 10, 738–773. doi: 10.1111/raq.12200

Ma, W., Chen, X., Wang, B., Lou, W., Chen, X., Hua, J., et al. (2018). Characterization, antioxidativity, and anti-carcinoma activity of exopolysaccharide extract from *Rhodotorula mucilaginosa* CICC 33013. *Carbohydr. Polym.* 181, 768–777. doi: 10.1016/j.carbpol.2017.11.080

Machiels, K., Joossens, M., Sabino, J., De Preter, V., Arijs, I., Eeckhaut, V., et al. (2014). A decrease of the butyrate-producing species *Roseburia hominis* and *Faecalibacterium prausnitzii* defines dysbiosis in patients with ulcerative colitis. *Gut* 63, 1275–1283. doi: 10.1136/gutjnl-2013-304833

Mannazzu, I., Landolfo, S., Lopes da Silva, T., and Buzzini, P. (2015). Red yeasts and carotenoid production: outlining a future for non-conventional yeasts of biotechnological interest. *World J. Microbiol. Biotechnol.* 31, 1665–1673. doi: 10.1007/s11274-015-1927-x

Mullish, B. H., McDonald, J. A. K., Pechlivanis, A., Allegretti, J. R., Kao, D., Barker, G. F., et al. (2019). Microbial bile salt hydrolases mediate the efficacy of faecal microbiota transplant in the treatment of recurrent *Clostridioides difficile* infection. *Gut* 68, 1791–1800. doi: 10.1136/gutjnl-2018-317842

Nakano, T., and Wiegertjes, G. (2020). Properties of carotenoids in fish fitness: a review. *Mar. Drugs* 18:568. doi: 10.3390/md18110568

Nelis, H. J., and De Leenheer, A. P. (1991). Microbial sources of carotenoid pigments used in foods and feeds. *J. Appl. Bacteriol.* 70, 181–191. doi: 10.1111/j.1365-2672.1991.tb02922.x

Nishida, Y. (2012). Astaxanthin: commercial production and its potential health-promoting effects. *J. Oleo. Sci.* 12, 525–531. doi: 10.5650/oleoscience.12.525

Pisoschi, A. M., and Pop, A. (2015). The role of antioxidants in the chemistry of oxidative stress: a review. *Eur. J. Med. Chem.* 97, 55–74. doi: 10.1016/j.ejmech.2015.04.040

Rahbar Saadat, Y., Yari Khosroushahi, A., and Pourghassem Gargari, B. (2021). Yeast exopolysaccharides and their physiological functions. *Folia Microbiol.* 66, 171–182. doi: 10.1007/s12223-021-00856-2

Ribeiro, D., Freitas, M., Silva, A. M. S., Carvalho, F., and Fernandes, E. (2018). Antioxidant and pro-oxidant activities of carotenoids and their oxidation products. *Food Chem. Toxicol.* 120, 681–699. doi: 10.1016/j.fct.2018.07.060

Sakai, M. (1999). Current research status of fish immunostimulants. *Aquaculture* 172, 63–73. doi: 10.1016/S0044-8486(98)00436-0

Sharma, R., and Ghoshal, G. (2020). Optimization of carotenoids production by *Rhodotorula mucilaginosa* (MTCC-1403) using agro-industrial waste in bioreactor: a statistical approach. *Biotechnol. Rep.* 25, e00407. doi: 10.1016/j.btre.2019.e00407

Spring, P., Wenk, C., Dawson, K. A., and Newman, K. E. (2000). The effects of dietary mannaoligosaccharides on cecal parameters and the concentrations of enteric bacteria in the ceca of salmonella-challenged broiler chicks. *Poult. Sci.* 79, 205–211. doi: 10.1093/ps/79.2.205

Tang, Z. R., Mao, J. X., Sun, Z. H., and Li, M. (2016). *A Kind of Rhodotorula Mucilaginosa and its Fermentation Culture and Application*. CN106010990A.

Thanh, V. N., Van Dyk, M. S., and Wingfield, M. J. (2002). *Debaryomyces mycophilus* sp. nov. a siderophore-dependent yeast isolated from woodlice. *FEMS Yeast Res.* 2, 415–427. doi: 10.1111/j.1567-1364.2002.tb00112.x

Tian, H., Chen, Y., Zhu, N., Guo, Y., Deng, M., Liu, G., et al. (2020). Effect of *Broussonetia papyrifera* silage on the serum indicators, hindgut parameters and fecal bacterial community of holstein heifers. *AMB Expr.* 10:197. doi: 10.1186/s13568-020-01135-y

Tovar-RamiRez, D., Zambonino Infante, J., Cahu, C., Gatesoupe, F. J., and Vazquez-Juarez, R. (2004). Influence of dietary live yeast on European sea bass (*Dicentrarchus labrax*) larval development. *Aquaculture* 234, 415–427. doi: 10.1016/j.aquaculture.2004.01.028

Ustyuzhanina, N. E., Kulakovskaya, E. V., Kulakovskaya, T. V., Menshov, V. M., Dmitrenok, A. S., Shashkov, A. S., et al. (2018). Mannan and phosphomannan from *Kuraishia capsulata* yeast. *Carbohydr. Polym.* 181, 624–632. doi: 10.1016/j.carbpol.2017.11.103

Van Bogaert, I. N., De Maeseneire, S. L., and Vandamme, E. J. (2009). Extracellular polysaccharides produced by yeasts and yeast-like fungi. *Yeast Biotechnol.* 29, 651–671. doi: 10.1007/978-1-4020-8292-4_29

Wang, Y., Xu, M., Wang, F. N., Yu, Z. P., Yao, J. H., Zan, Z. S., et al. (2009). Effect of dietary starch on rumen and small intestine morphology and digesta pH in goats. *Livest. Sci.* 122, 48–52. doi: 10.1016/j.livsci.2008.07.024

Conflict of Interest: The authors declare that the research was conducted in the absence of any commercial or financial relationships that could be construed as a potential conflict of interest.

Publisher's Note: All claims expressed in this article are solely those of the authors and do not necessarily represent those of their affiliated organizations, or those of the publisher, the editors and the reviewers. Any product that may be evaluated in this article, or claim that may be made by its manufacturer, is not guaranteed or endorsed by the publisher.

frontiers | Frontiers in Microbiology

TYPE Original Research
PUBLISHED 15 July 2022
DOI 10.3389/fmicb.2022.947624

OPEN ACCESS

EDITED BY
Wenyi Zhang,
Inner Mongolia Agricultural University, China

REVIEWED BY
Peng Fei,
Nanyang Institute of Technology, China
Huai Lin,
Nankai University, China

*CORRESPONDENCE
Valeria R. Parreira
vparreir@uoguelph.ca

SPECIALTY SECTION
This article was submitted to Food Microbiology, a section of the journal Frontiers in Microbiology

RECEIVED 18 May 2022
ACCEPTED 27 June 2022
PUBLISHED 15 July 2022

CITATION
Ke A, Parreira VR, Farber JM and Goodridge L (2022) Inhibition of *Cronobacter sakazakii* in an infant simulator of the human intestinal microbial ecosystem using a potential synbiotic.
Front. Microbiol. 13:947624.
doi: 10.3389/fmicb.2022.947624

Inhibition of *Cronobacter sakazakii* in an infant simulator of the human intestinal microbial ecosystem using a potential synbiotic

Alfred Ke, Valeria R. Parreira*, Jeffrey M. Farber and Lawrence Goodridge

Canadian Research Institute for Food Safety, Department of Food Science, University of Guelph, Guelph, ON, Canada

Powdered infant formula (PIF) can be contaminated with *Cronobacter sakazakii*, which can cause severe illnesses in infants. Synbiotics, a combination of probiotics and prebiotics, could act as an alternative control measure for *C. sakazakii* contamination in PIF and within the infant gut, but synbiotics have not been well studied for their ability to inhibit *C. sakazakii*. Using a Simulator of the Human Intestinal Microbial Ecosystem (SHIME®) inoculated with infant fecal matter, we demonstrated that a potential synbiotic, consisting of six lactic acid bacteria (LAB) strains and Vivinal GOS, can inhibit the growth of *C. sakazakii* in an infant possibly through either the production of antimicrobial metabolites like acetate, increasing species diversity within the SHIME compartments to compete for nutrients or a combination of mechanisms. Using a triple SHIME set-up, i.e., three identical SHIME compartments, the first SHIME (SHIME 1) was designated as the control SHIME in the absence of a treatment, whereas SHIME 2 and 3 were the treated SHIME over 2, 1-week treatment periods. The addition of the potential synbiotic (LAB + VGOS) resulted in a significant decrease in *C. sakazakii* levels within 1 week ($p < 0.05$), but in the absence of a treatment the significant decline took 2 weeks ($p < 0.05$), and the LAB treatment did not decrease *C. sakazakii* levels ($p \geq 0.05$). The principal component analysis showed a distinction between metabolomic profiles for the control and LAB treatment, but similar profiles for the LAB + VGOS treatment. The addition of the potential synbiotic (LAB + VGOS) in the first treatment period slightly increased species diversity ($p \geq 0.05$) compared to the control and LAB, which may have had an effect on the survival of *C. sakazakii* throughout the treatment period. Our results also revealed that the relative abundance of *Bifidobacterium* was negatively correlated with *Cronobacter* when no treatments were added ($\rho = -0.96$; $p < 0.05$). These findings suggest that *C. sakazakii* could be inhibited by the native gut microbiota, and inhibition can be accelerated by the potential synbiotic treatment.

KEYWORDS

synbiotic, *Cronobacter sakazakii*, gut model, metabolomics, 16S sequencing

Introduction

Powdered infant formula (PIF) can be a vehicle of *Cronobacter sakazakii* infection in infants, which can cause the development of necrotizing enterocolitis (NEC), bacteremia, meningitis and neurological impairments, and the pathogen can be found in a wide variety of environments such as homes, hospitals, and manufacturing equipment (Kalyantanda et al., 2015; Centers for Disease Control and Prevention [CDC], 2020a,b). PIF contaminated with *C. sakazakii* poses a high risk of infection in infants, especially those that are pre-term (<37 weeks gestational age) and of low birth-weight (<2,500 g), and the consumption of PIF may not lead to the establishment of a diverse gut microbiota as compared to breast-fed infants (Le Doare et al., 2018). Despite recommendations from the World Health Organization (WHO) on best practices to rehydrate PIF, including using hot water (>70°C) to rehydrate PIF, *C. sakazakii* infections continue to occur and have resulted in a recent recall of PIF in addition to several hospitalizations and deaths in the United States and Canada (Centers for Disease Control and Prevention [CDC], 2022), so other mitigation strategies are needed. Probiotics, prebiotics, or a combination of both can be added to PIF to mimic the composition of breast milk (Ackerberg et al., 2012; Vandenplas et al., 2015), which is a challenge due to the various microbiota and oligosaccharides present.

A synbiotic is a combination of probiotics and prebiotic substrate(s) to confer a health benefit on the host (Swanson et al., 2020). Synbiotics can increase the populations of *Lactobacillus* and *Bifidobacterium* spp. in the gastrointestinal (GI) tract, improve immune compartment function and reduce the risk of bacterial infection in vulnerable patients (Pandey et al., 2015). However, interactions between the gut microbiota and probiotics can differ depending on the prebiotic. Therefore, compatibility between probiotics and prebiotic(s) is an important factor to consider when formulating synbiotics. The consumption of a synbiotic supplement in preterm infants can reduce the risk of infection by increasing the populations of beneficial gut microbiota, such as *Bifidobacteria*, and/or reducing the chances of pathogen adhesion to gut epithelial cells (Luoto et al., 2014; Kent et al., 2015), however, *in vivo* studies are rarely conducted due to ethical considerations. Furthermore, synbiotic supplementation in premature infants may have other benefits, including a decrease in NEC cases compared to the control group based on randomized clinical trials (Vongbhavit and Underwood, 2016).

An advanced approach to study *C. sakazakii* in the GI tract of humans is by using GI models to assess the pathogen's survival and changes in the gut microbiota and metabolome under controlled conditions. As compared to *in vivo* animal models, GI models can better mimic the human intestinal environment, e.g., pH variation in the GI tract and colonic metabolome. The Simulator of the Human Intestinal Microbial Ecosystem (SHIME) is a versatile, multi-compartment human GI simulator that can mimic the conditions of the stomach, small intestine and colon (Van den Abbeele et al., 2010). Using the SHIME, it is possible to evaluate the interactions between the gut microbiota, gut metabolome and foodborne pathogens by inoculating the colon vessels with fecal samples from a donor and assessing different experimental parameters such as pH and residence time (Sivieri et al., 2011; Van de Wiele et al., 2015). Given the highly dynamic and naïve nature of an infant gut microbiota and its association with protecting the host from colonization by a foodborne pathogen, such as the production of antimicrobial compounds and preventing pathogen adhesion to the gut epithelial cells, the SHIME may be a useful tool to study the interactions between *C. sakazakii* and the gut microbiota metabolome in a simulated infant GI tract.

Probiotics, prebiotics, and synbiotics have the potential to play a major role in preventing intestinal colonization of infants by pathogenic *Cronobacter* spp. or other enteropathogens. However, there has not been any research on the effect of synbiotics on *C. sakazakii*, although several studies have shown that the ingestion of synbiotics can reduce the morbidity or mortality of NEC (Dilli et al., 2015; Sreenivasa et al., 2015; Nandhini et al., 2016; Pehlevan et al., 2020), and other studies have shown the antimicrobial properties of synbiotics on other foodborne pathogens such as *Salmonella enterica*, *Shigella sonnei*, and enteropathogenic and enterohemorrhagic *E. coli* (Likotrafiti et al., 2016; Kusmivati and Wahyuningsih, 2018; Shanmugasundaram et al., 2019; Tabashsum et al., 2019; Piatek et al., 2020). Probiotics, prebiotics and synbiotics can reduce the risk of infection through various mechanisms including competitive exclusion, the production of antimicrobial compounds, or competition for nutrients, but further research is required to validate these hypotheses using more sophisticated *in vitro* models and clinical trials. The development of comprehensive *in vitro* models that simulate the human gut, such as the SHIME, provides an interesting opportunity to study the real-time interactions between *C. sakazakii* and the native infant gut microbiota *in vitro*. Here, we demonstrate that the SHIME can provide valuable evidence on the survival of *C. sakazakii* with and without a potential synbiotic treatment through the perspective of culture-based and bioinformatic methods. We also show that the inhibition of *C. sakazakii* in an infant SHIME may be due to the presence of the gut microbiota, the production of metabolites or multiple factors.

Materials and methods

Preparation of fecal slurry for the infant simulator of the human intestinal microbial ecosystem

Fecal samples were collected from a healthy 1-month old infant, as very young infants (<2 months) represent the

most vulnerable population to *C. sakazakii* The infant was of normal birth weight and gestational age, and was breast fed (but supplemented with formula) and had no history of sickness or antibiotic use. Fecal samples were collected in diapers at the donor's residence and frozen. The samples were kept frozen using ice packs in a Styrofoam box during transportation to the Canadian Research Institute for Food Safety (Guelph, ON, Canada) and immediately stored at −80°C prior to fecal extraction from the diapers. Fecal samples were extracted from the diapers aseptically and transferred into 50 mL Falcon tubes. Both the tubes and the samples were kept frozen throughout the extraction process to minimize thawing and potential loss of microbes in the fecal samples. The tubes were weighed before and after to obtain the net weight of the fecal samples in each tube.

On the day of the SHIME inoculation, the fecal slurry was mixed with sterilized phosphate buffer (0.1 M; pH 7) containing: K_2HP_{O4} (8.8; Alfa Aesar, Tewksbury, MA, United States), KH_2P_{O4} (6.8; Anachemia Science, Mississauga, ON, Canada), sodium thioglycolate (0.1; Sigma-Aldrich, Oakville, ON, Canada). Prior to use, 15 mg of sodium dithionite (Sigma-Aldrich, Oakville, ON, Canada) was added to the buffer solution. The buffer solution was added to the partially thawed tubes containing fecal samples at a volume of 20% (w/v) and homogenized by pipetting up and down in the tube. After homogenization, the proximal and distal colon vessels were inoculated with 5% (v/v) of the fecal inoculum.

Experimental design of the infant simulator of the human intestinal microbial ecosystem

This SHIME experiment was approved by the University of Guelph and conducted in accordance with the University guidelines and recommendations (REB# 20-12-004). The infant SHIME consisted of three parallel SHIME compartments. Each compartment was comprised of three double-jacketed glass vessels to simulate the stomach and small intestine (ST/SI), proximal colon, and distal colon and maintained at 37°C using a water bath. Anaerobic conditions were maintained by flushing all the SHIME vessels with nitrogen. The pH of each vessel representing the proximal and distal colon was monitored daily and adjusted to pH values of 6.0–6.2 and 6.0–6.5, respectively, using 0.5 M HCl and 0.5 M NaOH to simulate physiological conditions.

The proximal and distal colon vessels contained basal feed at a volume of 300 and 500 mL, respectively. The basal feed (ProDigest, Belgium) contained the following (g/L): pectin (1), starch (1), cellobiose (1), proteose peptone (2), mucin (6), lactose (2.1), casein (0.2), whey proteins lactalbumin (2.7) and L-cysteine-HCl (0.2). Prior to use, the basal feed was acidified to a pH value of 3 using concentrated HCl. Pancreatic juice was made in addition to the basal feed based on the following composition (g/L): NaHCO3 (2.5; Anachemia Science, Mississauga, ON, Canada), Oxgall (4; Difco, Detroit, MI, United States), pancreatin from porcine pancreas (0.9; Sigma-Aldrich, Oakville, ON, Canada). A volume of 60 mL of pancreatic juice and 140 mL basal feed was transferred to the ST/SI vessels three times every day and mixed before being transferred through the SHIME tubes simultaneously (**Figure 1**). After fecal inoculation, a stabilization period, which lasted approximately 3 weeks, began, followed by the treatment period (**Supplementary Figures 1, 2**).

Bacterial strains and culture conditions

Each SHIME compartment received two treatments spanning 1 week each, with SHIME 1 representing the control for the entire duration of the 2-week treatment period (**Table 1**). The lactic acid bacteria (LAB) and Vivinal GOS (VGOS), which is a commercial prebiotic substrate incorporated within infant formula, and used as the potential synbiotic in the infant SHIME, were formulated as previously described (Ke et al., 2022). The selected *C. sakazakii* and LAB strains (**Supplementary Table 1**) were grown in BHI or MRS broth, respectively, overnight at 37°C then diluted 1:100 the following day in fresh BHI or MRS broth and incubated for a further 24 h at 37°C. For the potential synbiotic, hereafter referred to as LAB + VGOS, the overnight cultures of LAB were centrifuged at 14,000 × *g* for 10 min at room temperature and resuspended in MRS, which did not contain any carbohydrates, containing 1% VGOS. The cultures, present at a level of approximately 9–10 log CFU/mL, were mixed in equal volumes (1:1) and inoculated at a volume of 1% (v/v) into the proximal colon vessels of each SHIME compartment to directly mimic the effects of the treatments on *C. sakazakii* in the large colon. Samples from the proximal and distal colon vessels were taken throughout the 2-week treatment period to enumerate *C. sakazakii* survival, metabolomic analysis and 16S rRNA gene sequencing. Samples were serially diluted in 0.1% PW (10^{-1} to 10^{-6}), plated on Brilliance *C. sakazakii* agar (Oxoid, Nepean, ON, Canada) in duplicate, and incubated for 24–72 h at 37°C.

Metabolomics

Metabolomic analysis of the triple SHIME was conducted using 1D ^{1}H nuclear magnetic (NMR) spectroscopy. Samples were taken from the proximal and distal colon SHIME vessels and passed through a sterile 1 μm pore size syringe filter (Fisher Scientific, Mississauga, ON, Canada), followed by a second filtration with a 0.8/0.2 μm pore size filter (VWR, Mississauga, ON, Canada). The internal standard (4,4-dimethyl-4-silapentane-1-sulfonic acid (DSS-d6) and sodium azide in

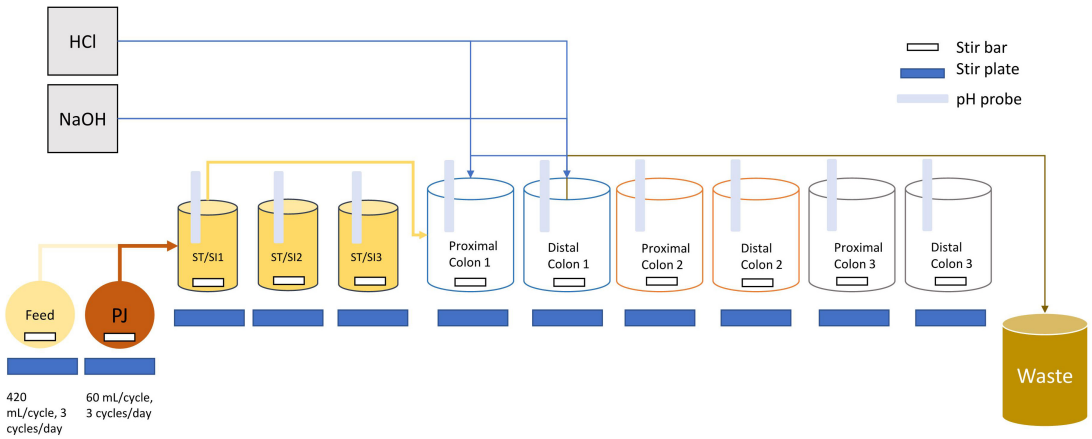

FIGURE 1
Schematic diagram of the infant triple SHIME. Tubing connections are only shown for SHIME 1 as an example, but SHIME 2 and 3 are connected in the same manner. Each SHIME compartment had one stomach/small intestine (ST/SI), proximal and distal colon vessel. Feed and contents from the proximal colon were transferred into each of the ST/SI vessels three times a day. Contents from the ST/SI vessels are then transferred into the proximal colon while contents from the proximal colon were transferred into the distal colon. HCl and NaOH were added into the vessels as needed to maintain a uniform pH range. Contents from the distal colon were transferred into a waste bucket for disposal. All vessels were kept at 37°C and consistently flushed with nitrogen to maintain an anaerobic environment. PJ refers to pancreatic juice.

D_2O, Chenomx Inc., Alberta, AB, Canada) was added to the final filtrate of each sample at a 1:10 (v/v) ratio to obtain a final concentration of 0.5 ± 0.005 mM DSS. Samples were scanned on a 600 MHz spectrometer at the Advanced Analysis Centre (University of Guelph, Guelph, ON, Canada) within 48 h of preparation. NMR spectra were analyzed using the Chenomx NMR Suite version 8.6 (Chenomx Inc., Alberta, AB, Canada) and exported to Microsoft Excel.

16S rRNA gene sequencing of the simulator of the human intestinal microbial ecosystem samples

Samples were taken from the SHIME and stored in a −80°C freezer prior to extraction for genomic DNA (gDNA). Thawed SHIME samples totaling 3 mL were collected and centrifuged at 14,000 × *g* for 2 min to pellet the bacterial cells and the supernatant was discarded. A volume of 1 mL of QIAGEN InhibitEx buffer and 0.2 g of 0.1 mm zirconia beads (Biospec Products Inc., Bartlesville, OK, United States) were added to the tubes containing the SHIME bacterial pellets and subjected to bead beating at 3,000 rpm for 4 min (Disruptor Genie, Scientific Industries Inc., NY, United States), followed by boiling for 15 min. The tubes were centrifuged at 14,000 × *g* for 2 min and the supernatant was used in subsequent extraction steps following the QiAamp Fast DNA Stool Mini Kit (Qiagen, Mississauga, ON, Canada) instructions with some modifications to the final elution step. DNA was eluted in 100 μL of warmed elution buffer and incubated for 5 min before centrifuging at 14,000 × *g* for 1 min. Eluted DNA was quantified and qualified using the Qubit (Thermofisher, Massachusetts, United States) and QIAxpert (Qiagen, Mississauga, ON, Canada), respectively. The gDNA was stored at −20°C for downstream applications.

TABLE 1 Treatment periods for each SHIME compartment spanning approximately 1 week each.

SHIME	Treatments	
	First treatment period	Second treatment period
1	*C. sakazakii* (~9 log CFU/mL)	Blank MRS[1]
2	*C. sakazakii* (~9 log CFU/mL) and LABs (~9–10 log CFU/mL)	LABs with 1% VGOS (~9–10 log CFU/mL)
3	*C. sakazakii* (~9 log CFU/mL) and LABs with 1% VGOS (~9–10 log CFU/mL)	LABs (~9–10 log CFU/mL)

[1]De Man, Rogosa, and sharpe media.

PCR amplification targeting the V4 region of the 16S rRNA gene was performed using the F515 (5′-GTGCCAGCMGCCGCGGTAA-3′) and R806 (5′-GGACTACHVGGGTWTCTAAT-3′) primers (Caporaso et al., 2011) in addition to Nextera XT Index v2 sequences (Illumina). The PCR reactions were conducted in a 96-well plate containing 2 μL of template DNA, 1 μL each forward and reverse primer sequences at 200 nM and 21 μL of Invitrogen Platinum PCR SuperMix High Fidelity (Fisher Scientific, Mississauga, ON, Canada) to make a total PCR reaction volume of 25 μL. Thermocycler conditions were as follows: an initial denaturation step at 94°C for 2 min; followed by 30 cycles of denaturation at 94°C for 30 s, annealing at 65°C for 30 s, elongation at 68°C for 30 s; and 10 cycles of the same parameters but with

annealing at 55°C, with a final extension step at 68°C for 5 min. The annealing temperature comprised of a 0.3°C increment touch-down starting at 65°C for 30 cycles, followed by 55°C for 10 cycles. PCR products were purified using AMPure XP beads (Fisher Scientific, Mississauga, ON, Canada) according to the Illumina 16S metagenomic sequencing library preparation guide and quantified on the Qubit. Purified libraries were normalized to 2 nM for each library and 8 μL of each library was pooled for sequencing at the Genomics Facility in the Advanced Analysis Center, University of Guelph, Guelph, ON, Canada. Sequencing data from the Miseq were processed using the QIIME2 (v2021.8) pipeline and the DADA2 plugin (Callahan et al., 2016). Classification of operational taxonomical units (OTUs) to the genus level was conducted using the pre-trained SILVA 138 99% OTUs from 515F/806R region of sequences (Quast et al., 2012; Bokulich et al., 2018). Validation of the *Cronobacter* genus from the SILVA classifier was done by comparing amplicon sequences to the National Center for Biotechnology Information (NCBI) database using the nucleotide BLAST, and the resulting hits allowed for confirmation of the genus and approximate speciation of *C. sakazakii* according to their closest match (≥97% identity match).

Statistical analysis

The results obtained from the proximal colon and distal colon samples were pooled together as two biological replicates for statistical analysis (n = 2). All statistical analyses were conducted using R (v4.0.4). Metabolites were analyzed based on the differences in metabolite profile between treatment periods for each SHIME compartment and combined were evaluated using a Principal Component Analysis (PCA) biplot based on the factoextra package on R (Kassambara, 2017). Correlations between metabolite concentration and *C. sakazakii* levels were evaluated using linear regression. Significant correlation between metabolite concentration and *C. sakazakii* levels were determined using a p-value of 0.05.

Sequencing results were analyzed for alpha- and beta-diversity on R using the phyloseq package (McMurdie and Holmes, 2013). The alpha-diversity metric was measured based on the Shannon and Gini-Simpson indices, which calculates the species diversity, considering species richness and evenness, within various metadata. Significant differences in alpha-diversity measures were calculated based on the non-parametric pairwise Wilcoxon Rank Sum test. The beta-diversity metric was calculated based on unweighted UniFrac and Bray-Curtis dissimilarity and visualized on a principal coordinate analysis (PCoA) using the phyloseq package. Significant differences between groups were calculated based on permutational multivariate analysis of variance (PERMANOVA) statistical tests. PERMANOVA was conducted using the adonis function (permutations = 10,000) on the vegan package (v2.5-7; Oksanen et al., 2020). Spearman's rank correlation was used to calculate correlations and p-values between and within metabolites and the microbial community. P-values obtained from the Wilcoxon Rank Sum test, PERMANOVA and Spearman's rank correlation were adjusted using the Benjamini-Hochberg false discovery rate.

Results

Survival of *Cronobacter sakazakii* in the infant simulator of the human intestinal microbial ecosystem

The change in *C. sakazakii* levels, based on the average of the plate counts from the proximal and distal colons of the SHIME, throughout the two treatment periods is shown in **Figure 2**. During the first treatment period and in the first 3 days, *C. sakazakii* decreased by 1–2 log CFU/mL for all SHIME compartments ($p \geq 0.05$). Between 5 and 7 days, there was approximately 2-log CFU/mL difference in *C. sakazakii* levels between the SHIME containing the LAB + VGOS treatment and the other SHIME compartments ($p < 0.05$). However, there were similar *C. sakazakii* levels between the LAB-treated SHIME and the control ($p \geq 0.05$).

During the second treatment period, there was no significant difference in *C. sakazakii* levels between all SHIME compartments between 9 and 12 days ($p \geq 0.05$). At 14 days, there was a significant difference in *C. sakazakii* levels between the LAB-treated SHIME and the other SHIMEs compartments ($p < 0.05$). At 16 days, the *C. sakazakii* levels in the control SHIME were significantly different than the treated SHIMEs ($p < 0.05$).

Despite the change in treatments between two SHIME compartments, similar patterns were observed with regards to the reduction in numbers of *C. sakazakii*. Overall, *C. sakazakii* levels in the LAB-treated SHIME decreased by up to 1.5 log CFU/mL throughout the 1-week treatment period. In contrast, in the SHIME containing LAB + VGOS, the levels of *C. sakazakii* decreased by approximately 3 log CFU/mL after 5 to 7 days of the treatment ($p < 0.05$), and the control steadily decreased throughout the entire 2-week treatment period. Compared to the control and the LAB + VGOS-treated SHIME, the LAB-treated SHIME showed the least reduction in numbers of *C. sakazakii*.

Metabolomic profile of the infant simulator of the human intestinal microbial ecosystem

A principal component analysis (PCA) revealed the general relationship between metabolites and treatment periods for

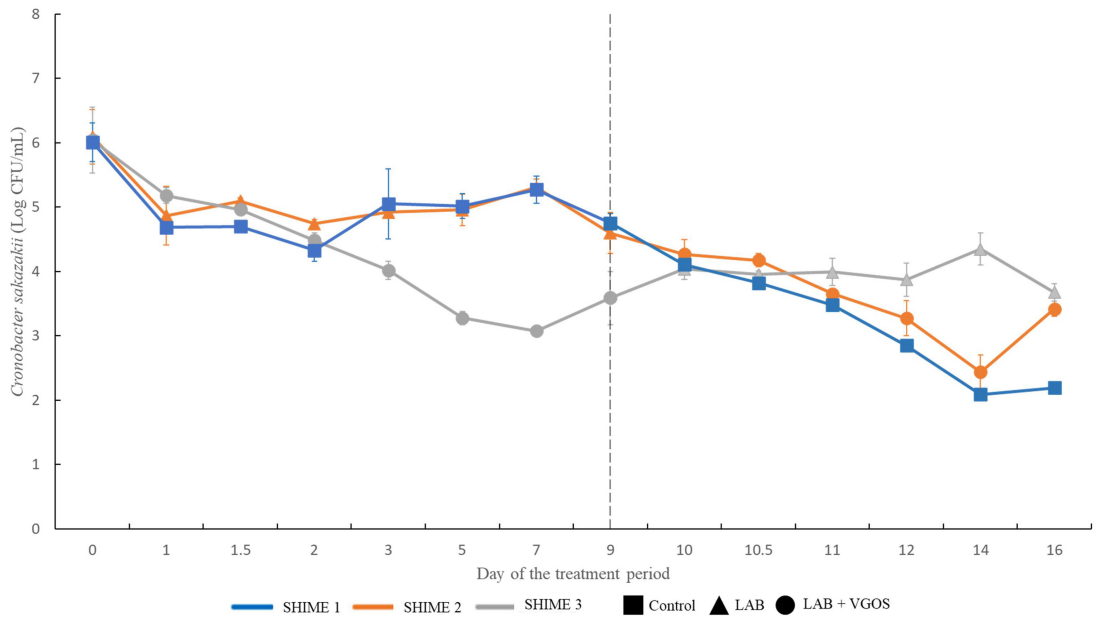

FIGURE 2
Survival of *C. sakazakii* in different SHIME compartments and under different treatment conditions (n = 2). At all time points, *C. sakazakii* was plated on Brilliance *C. sakazakii* agar. The gray dotted line indicates the start of the second treatment period. Values are the average of *C. sakazakii* plate counts from the proximal and distal colon vessels ± the standard deviation.

each SHIME (Figures 3, 4). The metabolite profile between the first and second treatment periods for SHIME 1 and 2 were different, but the profiles of SHIME 3 were similar (Figure 3). Based on the metabolite profiles of the SHIMEs, Principal Component 1 (PC1), accounting for 40.8% of the total variability of the data, may be associated between treatment periods as indicated with SHIME 1 and 2, and PC2, which accounts for 28.1% of the variability, may be associated with the metabolite concentrations.

The PCA biplot combining all SHIMEs and both treatment periods (Figure 4) also gave a different perspective on the overall relationship between SHIME compartments and treatment periods. In the first treatment period, the metabolite profiles of SHIME 1 and 2 (S1T1 and S2T1) were distinct from SHIME 3 (S3T1). A similar observation was observed in the second treatment period, as S3T2 was distinctly different than S1T2 and S2T2. Although we found a similar profile between treatment periods for SHIME 3, distinct metabolite profiles were found between treatment periods for SHIME 1 and 2. The PCA also indicated that the timing of the treatments may have had an effect on the metabolite profiles. S2T1 and S3T2, for example, were inoculated with the same types of LAB in similar concentrations, but yet the metabolite profiles for the two periods were distinct. When observed throughout the 2-week treatment period, however, no distinct metabolite profile was observed between the control and treatments (Supplementary Figure 3). During the first treatment period for SHIME 1 and 2, the change in *C. sakazakii* levels was similar ($p \geq 0.05$; Figure 2). In the PCA, this was also indicated based on the similar metabolic profile observed for S1T1 and S2T1 (Figure 4). In contrast, SHIME 3 had reduced levels of *C. sakazakii* in the first treatment period compared to SHIME 1 and 2, which was shown by the distinct metabolite profile of S3T1 on the PCA compared to S1T1 and S2T1. This observation continued into the second treatment period, as samples from SHIME 1 and 2 had similar levels of *C. sakazakii* and similar clusters in the PCA.

Based on the PCA analysis, some metabolites may be correlated with numbers of *C. sakazakii*, which were validated using a regression analysis. Acetate, ethanol, acetone and glycine concentrations were significantly correlated with *C. sakazakii* levels ($p < 0.05$; Figure 5). Acetate was negatively correlated with *C. sakazakii,* whereas the other metabolites were positively correlated. All of the other metabolites were not significantly correlated with *C. sakazakii* levels ($p \geq 0.05$; Supplementary Figure 4).

Microbial community compositions in the infant simulator of the human intestinal microbial ecosystem

There were 14 shared genera within 5 phyla identified across all SHIME compartments. Firmicutes and Bacteroidetes were the dominant phyla in all SHIMEs (Supplementary Figure 5), and within these phyla, *Veillonella* and *Bacteroides* were the most abundant genera accounting for approximately 80–90%

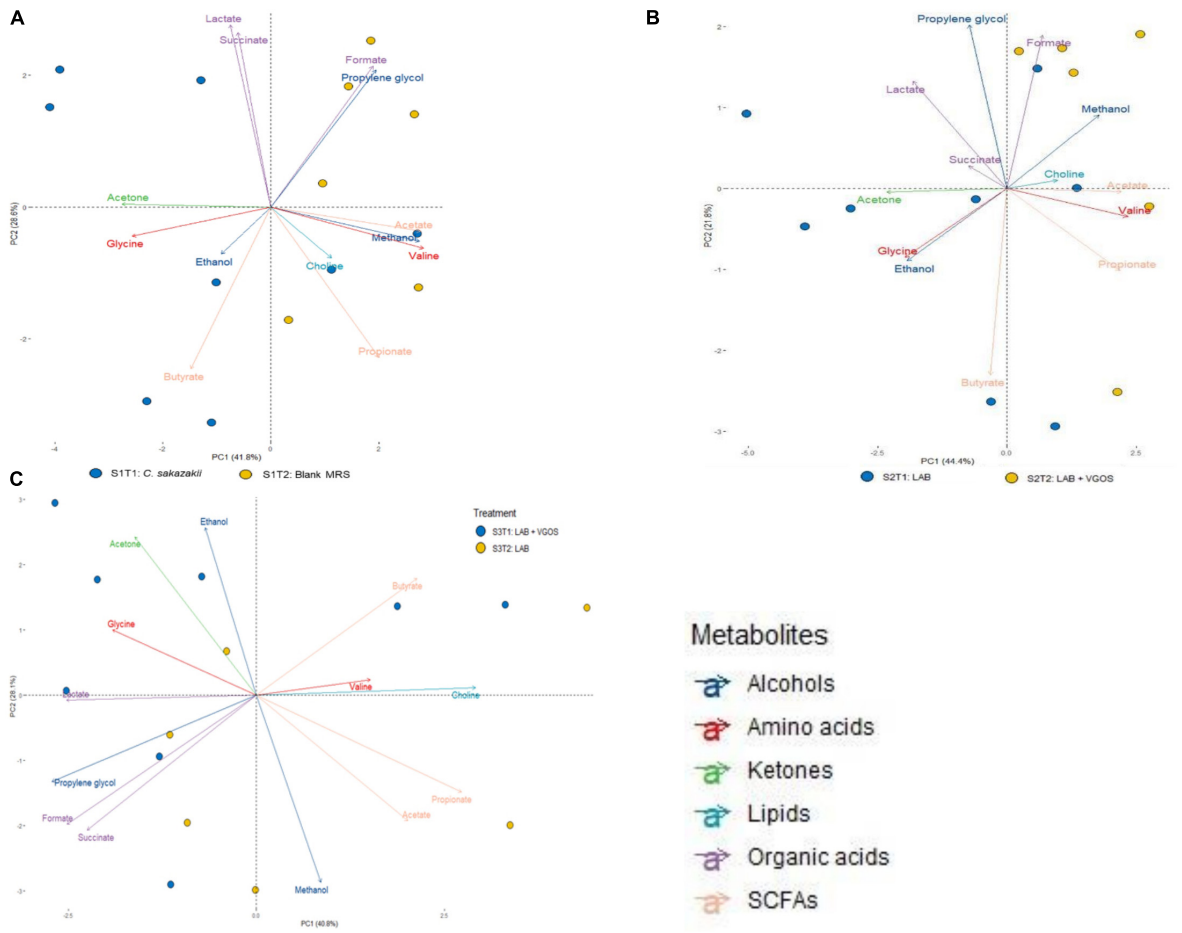

FIGURE 3
Principal Component Analysis (PCA) biplot of metabolite profiles from SHIME 1 **(A)**, SHIME 2 **(B)**, and SHIME 3 **(C)** over a 2-week treatment period. Each sample (bubble) represents a different day during the treatment period. The 2-week treatment period is separated with approximately 1 week for each treatment period and labeled accordingly based on color (i.e., blue for the first treatment period and yellow for the second). MRS represents de Man, Rogosa and Sharpe media, LAB represents lactic acid bacteria, VGOS represents Vivinal GOS, and SCFA represents short-chain fatty acids. Arrows represent the different metabolites profiled and colored based on the type of metabolite.

of the SHIME gut microorganisms (Figure 6). The species diversity across the three SHIME compartments remained fairly stable regardless of the treatment added. There was a slightly higher species diversity in the first treatment period across all SHIME compartments and during the LAB + VGOS treatment regardless of the SHIME compartment ($p \geq 0.05$; Figure 7). The first inoculation of the LAB + VGOS treatment into SHIME 3 also showed a slightly higher species diversity relative to the other SHIMEs and treatment periods ($p \geq 0.05$; Supplementary Figure 6). However, relative to the other SHIME compartments, SHIME 3 had the most diverse microbial community over the 2-week treatment period ($p < 0.05$; Figure 7). Furthermore, the presence of *C. sakazakii* did not alter the composition of the SHIME microbiota, even within the control SHIME in the absence of a treatment ($p \geq 0.05$; Supplementary Figure 6).

Beta-diversity metrics (i.e., unweighted UniFrac and Bray-Curtis dissimilarity) showed significantly different shared taxa during treatment periods ($p < 0.05$; Supplementary Figure 7). Furthermore, community abundance was significantly different between SHIME, treatments, and both SHIME and treatments ($p < 0.05$; Figure 8 and Supplementary Figures 8, 9). Sub-setting of the metadata revealed that the difference in community abundance was due to SHIME 3 across both treatment periods and the LAB + VGOS treatment between treatments ($p < 0.05$).

Metabolomic and gut microbiota associations in the simulator of the human intestinal microbial ecosystem

The relationships between metabolite-metabolite, metabolite-microbe and microbe-microbe pairs between the control and treatments (LAB and LAB + VGOS) were

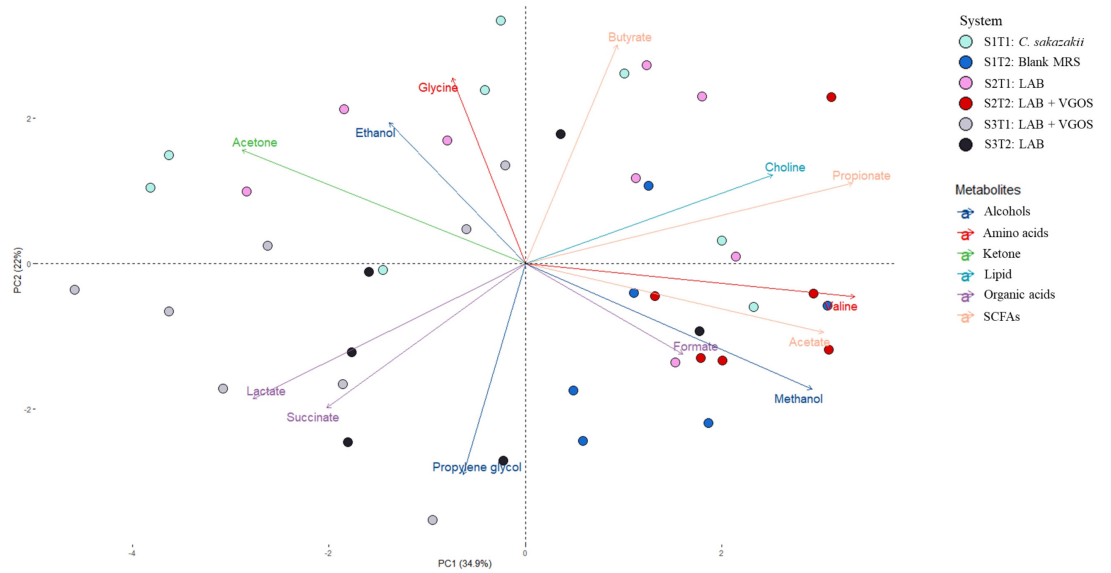

FIGURE 4
Principal Component Analysis (PCA) biplot of metabolite profiles from all SHIMEs across two treatment periods. The labels indicate the SHIME and treatment period. For example, S1T1 indicates that the light blue samples are for the first treatment period of SHIME 1. Each SHIME is represented by a different color and treatment periods are differentiated by the shade of the color, i.e., light or dark shade.

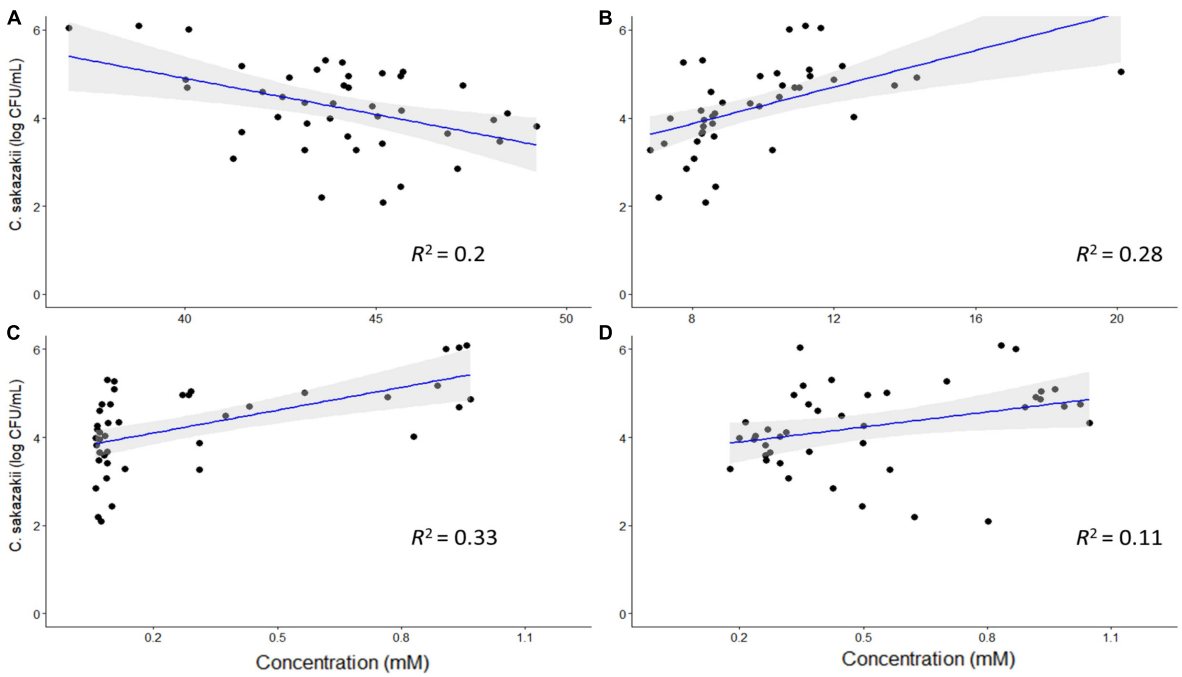

FIGURE 5
Regression analysis of *C. sakazakii* levels with concentrations (mM) of acetate **(A)**, ethanol **(B),** acetone **(C)**, and glycine **(D)**. There is a significant correlation between the concentrations of these metabolites and *C. sakazakii* levels ($p < 0.05$). Acetate is negatively correlated with *C. sakazakii*, whereas the other metabolites are positively correlated.

assessed using the Spearman's rank correlation to provide some insight into the *C. sakazakii* survival, metabolomics and gut microbiota trends as previously described. In general, there were similar positive correlations between formate, propionate, ethanol, methanol, and acetate between the treatments and the control (**Figure 9**). There was also a

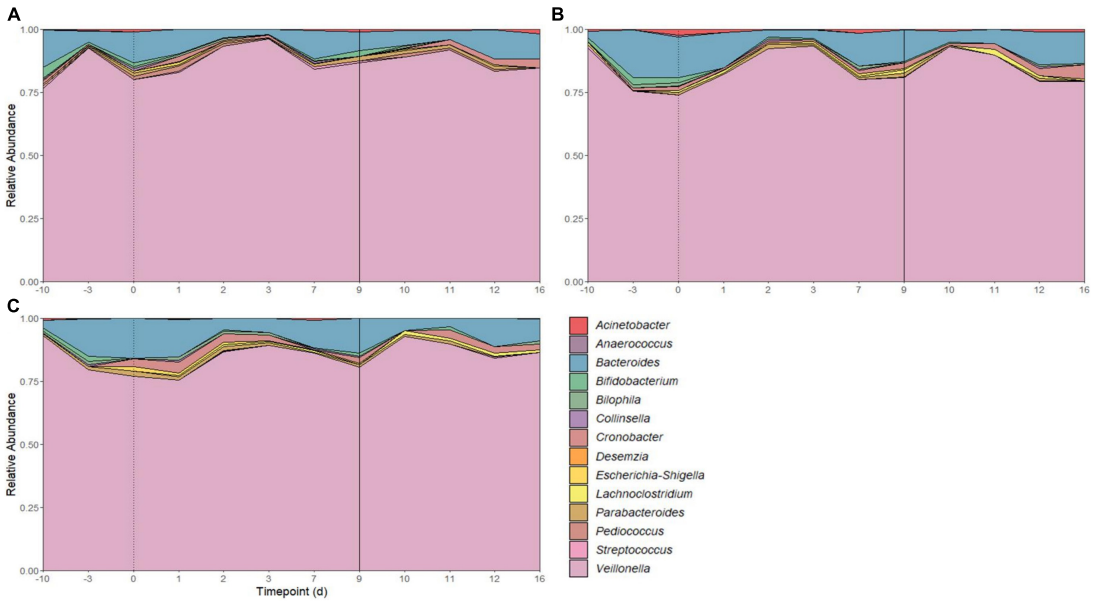

FIGURE 6
Microbial community composition of SHIME 1 **(A)**, SHIME 2 **(B)**, and SHIME 3 **(C)** before and throughout the treatment period. Microbial composition shown as average relative abundance and colored by genera. Relative abundances were based on 16S rRNA gene sequencing of SHIME samples from the distal colon vessels. Days −10 and −3 indicate the time points before the start of the first treatment period, as shown by a dotted line on day 0. Day 9 indicates the start of the second treatment period (solid line).

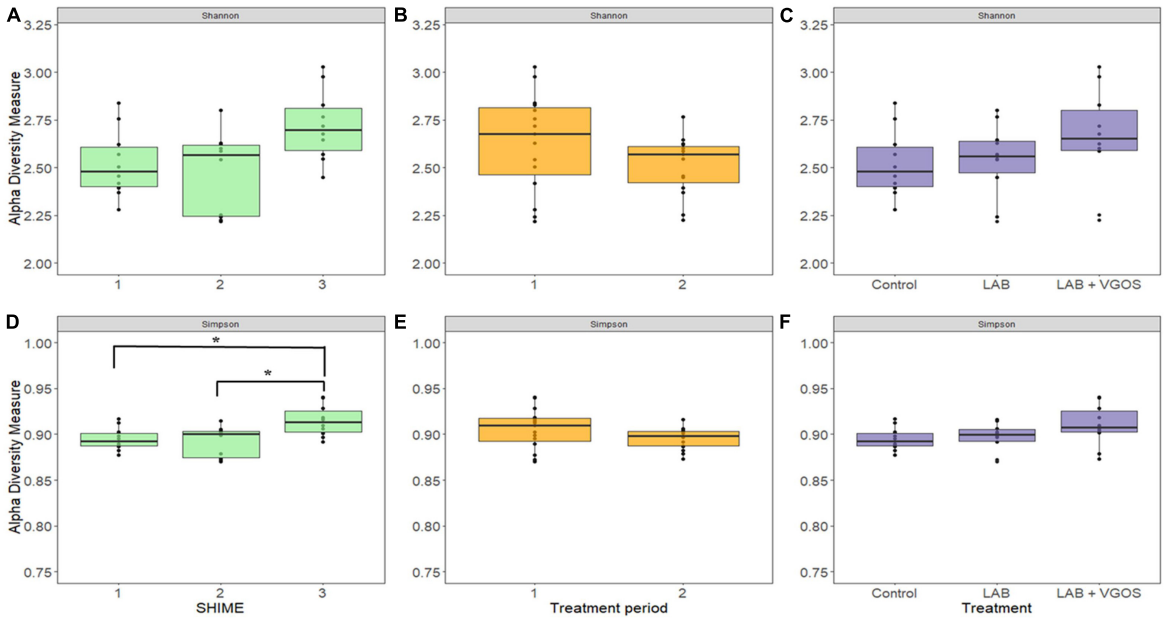

FIGURE 7
Shannon (top) and Gini-Simpson (bottom) indices for measurement of alpha diversity between SHIMEs **(A,D)**, treatment periods **(B,E)**, and treatments **(C,F)**. Significant differences in alpha diversity, as denoted by the asterisks in **(D)**, were calculated based on the Wilcoxon Rank Sum test and adjusted using the Benjamini-Hochberg false discovery rate ($p < 0.05$).

stronger metabolite-metabolite correlation in the LAB + VGOS treatment as compared to the LAB only treatment. In particular, there were strong correlations between propionate and acetate, formate and methanol ($\rho = > 0.73$; $p < 0.05$), which suggests that these metabolites were part of similar metabolic pathways that may have been strengthened due to the LAB + VGOS

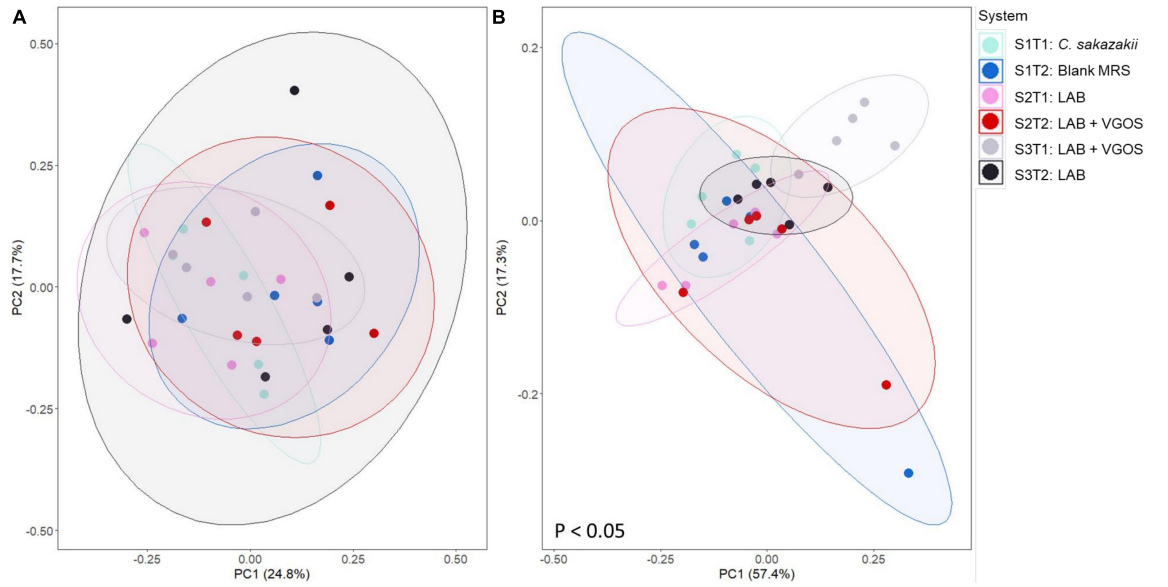

FIGURE 8
Principal coordinate analyses (PCoA) plots of unweighted UniFrac **(A)** and Bray-Curtis dissimilarity **(B)** based on operational taxonomical units from SHIME samples as visualized by treatment periods and SHIME, with ellipses indicating 80% confidence interval. The labels indicate the SHIME and treatment period. For example, S1T1 indicates that the light blue samples are for the first treatment period of SHIME 1. Each SHIME is represented by a different color and treatment periods are differentiated by the shade of the color, i.e., light or dark shade. Significant differences in groups were calculated based on PERMANOVA and adjusted using the Benjamini-Hochberg false discovery rate ($p < 0.05$).

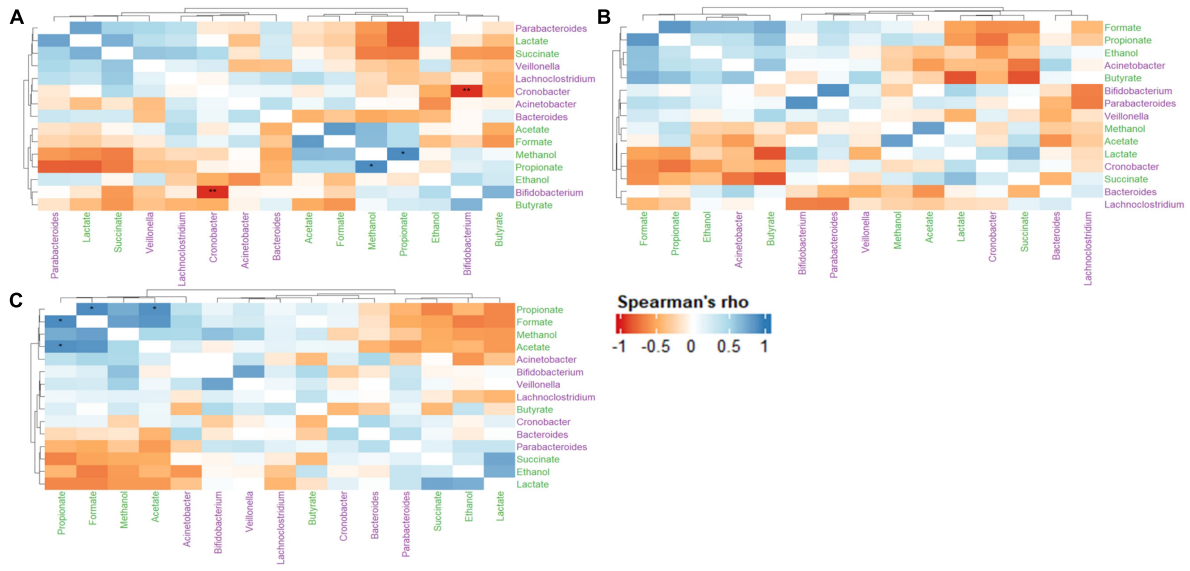

FIGURE 9
Heatmap of Spearman's rank correlation coefficients of select metabolites and microbial genera between the control **(A)**, LAB **(B)**, and LAB + VGOS **(C)** treatments. Microbial genera are colored in green, and metabolites are colored in purple. A positive correlation indicates that when a microbial genera or metabolite becomes more or less abundant, so does the other feature. Conversely, a negative correlation indicates that when a genera or metabolite becomes less abundant, the other feature increases in abundance. Statistical significance is indicated by the asterisks after correction with Benjamini-Hochberg false discovery rate, $*P < 0.05$, $**P < 0.01$.

treatment. Other trends in metabolite-metabolite correlation between different groups of metabolites were observed to be unique within the LAB + VGOS treatment, such as the negative correlation of the SCFAs with other organic acids, e.g., propionate with succinate and lactate, and the positive correlation between organic acids and ethanol. Between the

metabolite-microbe and microbe-microbe pairs, the relative abundance of *Bifidobacterium* and *Cronobacter* in the control SHIME was negatively correlated ($\rho = -0.96$; $p < 0.05$), which may indicate a potential role of *Bifidobacterium* in controlling *Cronobacter* in a healthy infant.

Discussion

Cronobacter sakazakii can pose a significant risk to infants when ingested, but the risk of illness may be reduced by ingesting probiotics or synbiotics which could inhibit the growth of *C. sakazakii*. Here, we demonstrated that a potential synbiotic consisting of LAB and VGOS can inhibit the growth of *C. sakazakii* in an infant SHIME model, but *C. sakazakii* levels also decreased, albeit slower, in the absence of a treatment. Metabolomics and 16S rRNA gene sequencing showed potential mechanisms of inhibition, such as the production of antimicrobial metabolites, or possibly through competition for nutrients due to a more diverse microbial community as a result of the potential synbiotic treatment.

In the infant SHIME, *C. sakazakii* levels significantly decreased after both applications of LAB + VGOS treatment and throughout the 2-week treatment period in the control SHIME. In contrast, both applications of the LAB treatment did not seem to have a significant effect on *C. sakazakii* levels regardless of the SHIME compartment. Synbiotics can increase *Lactobacillus* and *Bifidobacterium* levels and were found to be better at inhibiting foodborne pathogens than probiotics, as prebiotic substrates can be degraded by the probiotics or the gut microbiota into metabolites that could have antimicrobial properties (Likotrafiti et al., 2016; Markowiak and Śliżewska, 2017; Piatek et al., 2020; Sakr and Massoud, 2021).

The earliest colonizers of the infant gut are LAB and bifidobacteria, although the latter is generally more predominant (Martín et al., 2003; Solís et al., 2010). The numbers of LAB in infant feces range from 6 to 10 log CFU/g (Rubio et al., 2014; Murphy et al., 2017), which is in similar quantities to the concentration of LAB (9–10 log CFU/mL) used in the potential probiotic and synbiotic treatments. The LAB used in this study were not tested for acid or bile resistance, therefore their independent introduction into the SHIME may have reduced their survival rate as they were exposed to gastric and bile juices and other bacteria.

Probiotics and prebiotics, and by extension synbiotics, can influence the gut metabolome by modulating the gut microbiota (Abdulkadir et al., 2016; Chung et al., 2018; O'Connell, 2020). As a result, metabolomics, alone or in combination with 16S rRNA gene sequencing, can be used to evaluate changes in host health. In particular, short-chain fatty acids (SCFA) are regarded as some of the most important metabolites produced in the GI tract due to their association with host health (Koh et al., 2016; LeBlanc et al., 2017). Some of the key functions of SCFA are serving as energy sources for epithelial cells, inhibiting opportunistic pathogens and modulating the immune compartment (Koh et al., 2016).

In this study, metabolomic analyses revealed that the application of the LAB and LAB + VGOS in an infant SHIME affected the infant gut metabolome in a time-dependent manner. In general, there seems to be a time-dependent association between metabolomic profiles and treatments. Probiotics can influence the levels of SCFA and other metabolites, but the effects might be specific to the individual (Ghini et al., 2020; Markowiak-Kopeć and Śliżewska, 2020). Previous studies have also reported that metabolomic profiles are more stable than microbiota profiles (Abdulkadir et al., 2016; O'Connell, 2020), which may indicate that the beneficial effects of probiotics may not be revealed solely by metabolomics analyses. The infant diet, which includes prebiotics and breast milk, can alter the metabolomic profile of infants by shifting the composition of their gut microbiota (Stewart et al., 2017; Brink et al., 2020). A synbiotic consisting of *Lactobacillus paracasei* with GOS was found to increase the growth of lactobacilli and bifidobacteria, which subsequently increased the concentration of acetate in gnotobiotic mice inoculated with infant microbiota, as compared to the control (Martin et al., 2010). Synbiotic supplementation can also positively impact gut metabolic activities, as indicated by an increase in levels of SCFA, ketones, carbon disulfide and methyl acetate (Vitali et al., 2010). It is worthwhile to note that even in healthy, breast-fed infants, the metabolic profiles between infants can vary (Kirchberg et al., 2020), although this may be partially due to limitations in the studies' methodologies and analyses (Phan et al., 2019).

Organic acids and bacteriocins are produced by probiotics and synbiotics that can inhibit the growth of pathogens (Tomar et al., 2015; Markowiak and Śliżewska, 2017). In the infant SHIME, the pH is controlled to be between 6.0–6.2 and 6.0–6.5 for the proximal and distal colon vessels, respectively, which may have an effect on the ability of the organic acids to inhibit the growth of *C. sakazakii*. Likotrafiti et al. (2016) showed that the combination of *B. longum* or *L. fermentum* 907 and various prebiotics inhibited the growth of *E. coli* O157:H7 and *E. coli* O86 when the pH of the media was lower than the pKa values of the organic acids. The authors noted that the difference in pH of the media with *B. longum* containing either glucose or VGOS was a factor in whether the pathogens' growth was delayed or inhibited. Weak acids like organic acids can enter a bacterial cell through the cell membrane and acidify the cytoplasm, which in turn can damage enzymes and cell structures (Gao et al., 2019). Furthermore, organic acids can play a role in stabilizing the microbial population in the gut and stimulating the growth of commensal bacteria (Dittoe et al., 2018). Bacteriocins, unlike organic acids, are polypeptides produced by bacteria during ribosomal synthesis and can also have antimicrobial properties (Gao et al., 2019). Some LAB used in this study, e.g., *L. paracasei* and *P. acidilactici*, have been shown to produce bacteriocins

(Papagianni and Anastasiadou, 2009; Bendjeddou et al., 2012), but the particular strains used in this study have not been tested for bacteriocin production. Furthermore, due to the lack of an outer membrane, bacteriocins are more effective against Gram-positive than Gram-negative bacteria (Prudêncio et al., 2015; Simons et al., 2020), so they are unlikely to have been the causative factor that inhibited *C. sakazakii*.

Previous studies have shown that hydrogen peroxide (H_2O_2) is produced by LAB and can inhibit the growth of foodborne pathogens through oxidative stress (Tharrington and Sorrells, 1992; Kotsou et al., 2008). In the anaerobic conditions of the gut and the infant SHIME, the concentration of H_2O_2 may not be enough to inhibit the growth of pathogens (Knaus et al., 2017). Additionally, sub-lethal concentrations of H_2O_2 can increase the resistance of foodborne pathogens and their progeny (Rodríguez-Rojas et al., 2020), however, whether this occurs in the SHIME ecosystem is unclear.

An alternative mechanism by which probiotics and synbiotics inhibit foodborne pathogens is by competing for limited nutrients in the environment, which suggests that beneficial bacteria in the gut can use nutrients that would otherwise be used by opportunistic pathogens, thereby limiting their growth (Rolfe, 2000). There are more nutrients available in the proximal colon, as compared to the distal colon, due to its proximity to the stomach and small intestine, so increasing the levels of beneficial bacteria in the proximal colon can decrease nutrient availability for pathogens (Fooks and Gibson, 2002). Wilson and Perini (1988) found that fecal bacteria used glucose and other nutrients more efficiently than *Clostridium difficile*, which reduced its growth compared to the control without fecal bacteria. Furthermore, even bacteria within the same genera may compete for nutrients with opportunistic pathogens and each other as they have similar metabolic requirements (Fleming-Davies et al., 2017; Patnode et al., 2019). In contrast, depleted gut microbiota as a result of antibiotic treatment can lead to an increase in the amount of nutrients in the gut environment and limiting competition for nutrients with commensal gut microbiota, which can cause the proliferation of *Salmonella* Typhimurium and *C. difficile* (Ng et al., 2013). Similarly, Gillis et al. (2018) found that dysbiosis can cause the host metabolism to undergo lactate fermentation, which in turn facilitates the growth of *Salmonella*.

Metabolomics analyses gave some insight into the possible factors that could inhibit *C. sakazakii*. Untargeted metabolomics and PCA have been used to screen for potential bioactive molecules from plants and evaluate the metabolic changes of foodborne pathogens post-exposure to biochemical or physical treatments (Maifiah et al., 2017; Tian et al., 2018; Sieniawska and Georgiev, 2022). In this study, the PCA biplot revealed differences in metabolite profile within the SHIME compartments that may be generally associated with *C. sakazakii* levels. Additionally, there was no observed difference in metabolite profiles when comparing between the treatments and the control. Maifiah et al. (2017) used PCA to identify changes and similarities in the metabolite profile of *Acinetobacter baumannii* after antibiotic treatment at different time points. Additionally, Tian et al. (2018) used PCA to identify changes in the metabolomic response of *E. coli* after exposure to ohmic heating. This study found that some metabolites, such as valine, alcohols, acetate and other organic acids are generally associated with lower levels of *C. sakazakii*.

Regression analysis of the profiled metabolites revealed that acetate, ethanol, acetone and glycine were significantly correlated with *C. sakazakii* levels. However, of these metabolites, only acetate was negatively correlated with *C. sakazakii*. Acetate, in addition to propionate and butyrate, has been reported to reduce the growth and pathogenicity of foodborne pathogens (Peng and Biswas, 2017; Zhang et al., 2020). In this study, however, only acetate was shown to be a significant factor in reducing the levels of *C. sakazakii*. The efficacy of acetate as an antimicrobial compound could be affected by pH, where a lower pH would allow SCFAs and other organic acids to permeate bacterial cells and acidify the cytoplasm (Lawhon et al., 2002; Lund et al., 2020). For example, Zhang et al. (2020) reported that SCFAs in a broth medium with a pH of 6.5 were able to inhibit the growth of *E. coli*, whereas a neutral pH stimulated its growth. Foodborne pathogens, including *C. sakazakii*, can develop acid resistance when exposed to sub-lethal concentrations of acetate, although the adaptation is influenced by the acid concentration and the pH of the environment (Arnold et al., 2001; Álvarez-Ordóñez et al., 2012; Gavriil et al., 2020). *E. coli* can adapt to the acid stress induced by SCFAs at a neutral pH by regulating the expression of *rpoS* (Arnold et al., 2001). Changes in protein synthesis have been linked to an increase in resistance to salt and acid (pH value of 3.0) in *S.* Typhimurium after exposure to a > 100 mM SCFA mixture (Kwon et al., 2000), however, the concentration of SCFA used by Kwon et al. (2000) exceeded the concentration reported in our study. Similarly, *C. sakazakii* strains with high catalase activity and low *rpoS* expression can use acetate as a growth substrate in a nutrient-deprived environment (Álvarez-Ordóñez et al., 2012). The robust metabolism of *C. sakazakii*, in addition to the complex gut microbiota and metabolome, could indicate why, despite previous studies demonstrating the potent antimicrobial properties of acetate, there was a weak correlation between acetate concentration and *C. sakazakii* levels.

As with the other main SCFAs, propionate and butyrate have been reported to inhibit the growth of foodborne pathogens, despite these metabolites not being significantly correlated with the inhibition of *C. sakazakii* in this study. Butyrate has been noted to have the most consistent antimicrobial activity among the SCFAs, which may be attributed to stimulating the immune compartment and decreasing the expression of virulence genes in pathogens (Harrison et al., 2013). Additionally, propionate was also found to be better than acetate at inhibiting the growth of *C. sakazakii* in rehydrated infant formula, although it is not

an acceptable additive in powdered infant formula (Oshima et al., 2012). The minimum inhibitory concentration (MIC) of butyrate and propionate against *S. enterica* strains in culture media was found to be approximately 3,750 μg/mL or around 45 mM on average (Lamas et al., 2019), but these concentrations exceed the SCFA levels generated in the infant SHIME. Both breast-fed and formula-fed infants lack the predominant butyrate-producing bacteria, such as *Eubacterium rectale* and *Faecalibacterium prausnitzii*, until approximately 6 months of age (Appert et al., 2020; Nilsen et al., 2020). Although the concentration of propionate and butyrate in the SHIME may not directly contribute to the inhibition of *C. sakazakii*, the combination of SCFAs in the colon environment may have a synergistic effect in inhibiting the growth of foodborne pathogens (Peng and Biswas, 2017). On the other hand, SCFA at sub-lethal concentrations may also be used by foodborne pathogens as a carbon source, thereby stimulating their growth (Dittoe et al., 2018). Although it is recognized that SCFAs have some role in inhibiting the growth of foodborne pathogens, it is important to consider that their efficacy depends on various factors including environmental pH, concentration and other bacterial strains and metabolites.

The infant SHIME microbiota was dominated by *Veillonella* and *Bacteroides*, which is in contrast to the commonly reported genera of a breast-fed infant which includes *Bifidobacterium*, *Staphylococcus*, *Streptococcus*, and *Lactobacillus* (Bäckhed et al., 2015; Moore and Townsend, 2019; Turroni et al., 2020; Ding et al., 2021). Although the composition of the infant gut microbiota can vary depending on various factors including diet, environment and delivery method, in this study, the SHIME microbiota composition may have been influenced by the basal feed used in the SHIME compartment. *Bacteroides*, *Veillonella*, and *Lachnoclostridium*, which represent some of the most abundant genera in the SHIME compartments from our study, can degrade mucin, a main component of the infant SHIME feed, to produce SCFAs (Flynn et al., 2016; Venegas et al., 2019; Raimondi et al., 2021). The ability of *Veillonella* to degrade mucin may also be a reason for its high abundance (>75% of the community abundance) in all SHIME compartments, which indicates that *Veillonella* can potentially outcompete other microorganisms within the SHIME compartments.

Alpha and beta-diversity indices were used to assess the stability of the SHIME microbiota once the *C. sakazakii* cocktail, with and without the treatments, had been introduced. The results showed that the first addition of the LAB + VGOS slightly increased the species diversity of SHIME 3 compared to the control and LAB, which may be a factor in the decline of *C. sakazakii* in both treatment periods. The gut microbiota can compete with pathogenic bacteria for nutrients, thereby limiting growth (Kamada et al., 2013; Tomar et al., 2015), and it is possible that a more diverse environment can contain other bacteria which use the same nutrients as *C. sakazakii*. The production of metabolites may be a result of a higher species diversity after the LAB + VGOS treatment, as the VGOS may be an additional nutrient source that can be metabolized into antimicrobial metabolites (Martin et al., 2019). In fact, the reduction in levels of *C. sakazakii* in the control and LAB + VGOS treatments may be a result of multiple factors involving the SHIME microbiota and metabolites.

To the best of the author's knowledge, the impact of *C. sakazakii* on the infant gut microbiota has not been documented. In this study, the results suggest that the presence of *C. sakazakii* at 6 log CFU/mL, a concentration much higher than found in contaminated foods and in the environment, did not significantly affect the diversity of the infant SHIME microbiota. While some studies have shown that the presence of a foodborne pathogen can alter the gut microbiota in animal and *in vitro* gut models (Sannasiddappa et al., 2011; Iljazovic et al., 2021), others have highlighted the robustness of the human gut microbiota. Zhang et al. (2016) described a "like-to-like rule" for the human gut microbiota, which suggests that the native gut microbiota resists change to extraneous bacteria, such as foodborne pathogens and beneficial bacteria, that are ingested. The authors noted that a gut microbiota with a high abundance of native Enterobacteriaceae, which can include opportunistic pathogens like *Salmonella* and *Cronobacter* spp., can provide more favorable conditions for foodborne pathogens to grow. Conversely, another study by Stecher et al. (2010) found that *Lactobacillus reuteri* more effectively colonized a mouse microbiota containing a high abundance of lactobacilli compared to the ones with a lower abundance.

Despite previous studies reporting the efficacy of LAB to inhibit the growth of foodborne pathogens or the ability of probiotics to modulate the gut microbiota to exert a protective effect on the host (Sivieri et al., 2021), this study demonstrated the opposite. Species diversity and community abundance were similar between the LAB treatment and the control. Additionally, the metabolomic profiles of the SHIME suggest that the LAB treatment did not affect the SHIME metabolome. This may be due to the robustness of the microbiota as previously mentioned, where the lack of *Lactobacillus* and *Pediococcus* present in the SHIME prior to the treatment period resulted in poor colonization and/or adherence of the LAB within the vessels. However, the frequency of the LAB treatment should also be considered. Ren et al. (2018) found that the addition of a mixed LAB culture can not only prevent *Staphylococcus aureus* infection, but also maintain the gut microbiota in a mouse model. A key difference that may have minimized the efficacy of the LAB used in this study is the dosage or frequency of the LAB treatment. The study by Ren et al. (2018) used multiple feedings of the LAB throughout their experiment in an animal model, whereas in this study, the LAB was only introduced once in an *in vitro* gut model. The one-time inoculation of LAB may not have been sufficient to exhibit inhibitory effects on *C. sakazakii*, which would support the

notion that probiotics should be ingested in adequate amounts to exert a health benefit (Hill et al., 2014).

Despite the controlled environment of the SHIME compartment, the results suggest that there is a vast network of interactions between and within the gut microbiota and metabolome. In this study, the associations between select metabolites and microbial genera were evaluated using a Spearman's rank correlation and visualized on a heat map to provide insight into the reasons by which *C. sakazakii* levels decreased with and without any intervention. While the correlation matrix does not explicitly demonstrate the metabolic pathways within the infant SHIME, it does provide a statistical representation of several major interactions within the compartment based on the available data.

The correlation matrix of the control SHIME revealed a strong negative correlation between *Cronobacter* and *Bifidobacterium* spp., which is interesting as *Bifidobacterium* has been previously reported to inhibit the growth of enteropathogens (Servin, 2004; Vazquez-Gutierrez et al., 2016; Chichlowski et al., 2020). Infants that are premature or of low-birthweight may be more susceptible to *C. sakazakii* infection, as they may be missing some beneficial gut microbiota including *Bacteroides* and *Bifidobacterium* (Bäckhed et al., 2015; Yang et al., 2016; Cukrowska et al., 2020). Therefore, the findings of this study suggest that the presence of *Bifidobacterium* spp. could play a role in controlling *C. sakazakii* in a healthy infant gut. A possible mechanism of inhibition involves the production of organic acids, such as acetate, lactate and formate, which have a strong antagonistic effect against Gram-negative bacteria (Makras and De Vuyst, 2006). *Bifidobacterium* and other commensal gut microbiota can compete for nutrients with foodborne pathogens (Kamada et al., 2013; O'Callaghan and van Sinderen, 2016), which would further limit the ability for *C. sakazakii* to grow within the SHIME compartment. Despite the relatively low abundance of some gut microbiota, including *Bifidobacterium*, our results provide further evidence that the gut microbiota may play a significant biological role through synergistic interactions with other microorganisms (Claussen et al., 2017; Benjamino et al., 2018; Cena et al., 2021).

The Spearman's rank correlation of the treatments revealed a stronger metabolite-metabolite relationship in the LAB + VGOS treatment as compared to the LAB treatment. The correlation matrix of the LAB + VGOS showed more defined metabolite-metabolite clusters compared to the LAB only treatment, and the significant associations between some metabolites such as propionate-acetate and propionate-formate. These patterns of correlations between metabolites and significant interactions were less evident within the LAB only treatment. These results provide further evidence that the reduction of *C. sakazakii* as a result of the LAB + VGOS treatment may be metabolite-dependent, since the regression analysis of the profiled metabolites showed a significant, but weak, correlation between acetate and *C. sakazakii*. The most abundant bacteria in the SHIME, namely *Bacteroides* and *Veillonella*, can produce acetate and other metabolites by metabolizing VGOS through similar metabolic pathways (Oliphant and Allen-Vercoe, 2019). It is important to note, however, that other SHIME microbiota could play a role in the complex metabolome-microbiota network by creating intermediary metabolites, e.g., formate, succinate and lactate, which are later converted into SCFAs (Oliphant and Allen-Vercoe, 2019; Tang et al., 2019). For example, Hinton and Hume (1995) found that a synergistic interaction between *Veillonella,* lactate and succinate could inhibit the growth of *S.* Typhimurium and *Salmonella* Enteritidis through the production of volatile fatty acids and a reduction of pH in broth media. Other studies on the effects of prebiotics on the gut metabolome and microbiota typically include consistent consumption of the prebiotic by the participants lasting multiple weeks, however, this SHIME experiment lasted 2 weeks, separated by 1-week intervals, with only one addition of the VGOS. In such cases, Tang et al. (2019) found that short-term diets had a stronger effect on the gut metabolome, as recently consumed nutrients are quickly metabolized by the gut microbiota without influencing the microbial composition.

The infant SHIME focused on the luminal portion of the colon, but the mucosal environment of the colon may be able to better simulate the colonization of pathogens, probiotics and the commensal gut bacteria (Van den Abbeele et al., 2012). Furthermore, the SHIME does not have an absorption unit, which allows SCFA to accumulate in the distal colon and therefore may not accurately reflect *in vivo* concentrations, immune compartment and maternal antibodies (Van de Wiele et al., 2015). Physical constraints also exist when one uses the triple SHIME. For example, the control used in this study was inoculated with only *C. sakazakii* in the first treatment period and sterile MRS media in the second treatment period. In order to evaluate the natural changes in community composition within the infant SHIME, it would have been interesting to conduct a SHIME trial that was not inoculated with *C. sakazakii* or the treatments. Additionally, as the start of the second treatment period occurred only a week after the start of the first treatment period, there may not have been sufficient time for the gut microbiota and metabolome to stabilize (Van de Wiele et al., 2015). The effects of the first treatment period on the gut microbiota and metabolome could have lingered and subsequently affected the efficacy of the second treatments. Overall, this continuous SHIME experiment gives insight into the short-term effects of different treatment combinations on the survival of *C. sakazakii* in the infant gut.

The focus of this study was on the inhibitory properties of a potential probiotic and synbiotic treatment, however, probiotics and synbiotics can exert antagonistic effects on foodborne pathogens in other ways. Additionally, probiotics and synbiotics can have beneficial effects on the intestinal epithelial cells by mitigating the adhesion of pathogens and

promoting tight junction integrity (Collado et al., 2008; Piqué et al., 2019). Several factors, including the timing and dosage of probiotics and synbiotics should be considered when evaluating their beneficial effects on the host. The inconsistencies in methodology and reporting of the health benefits of probiotics, prebiotics and synbiotics, in addition to the wide selections of probiotics available, including *Bifidobacterium*, are a challenge in determining their optimal applications in infants (Van den Nieuwboer et al., 2014). The treatments used in this study were also directly applied to the colon in the absence of a food matrix such as PIF. Future experiments should also investigate the ability of probiotics and synbiotics to inhibit foodborne pathogens within a food matrix, such as PIF, the infant stomach/small intestine conditions, and a more thorough assessment on whether these LAB and LAB + VGOS treatments can be classified as probiotics or a synbiotic, respectively, and are safe to be added to PIF. Additionally, to better determine any symbiotic effects between the prebiotics and the LAB or probiotics, it may be worthwhile to test for the effects of only a prebiotic substrate on the inhibition of *C. sakazakii* as compared to the substrate in addition to LAB or other probiotics. The SHIME used in this study simulated the colonic conditions of a healthy infant, however, it would be beneficial for future studies to try and evaluate the efficacy of treatments in an *in vitro* model simulating the colonic conditions of low birth-weight and/or premature infants, as they are more vulnerable to infection by *C. sakazakii*.

To the best of our knowledge, this study is the first to evaluate the survival of *C. sakazakii* by using an *in vitro* gut model to mimic an infant's colonic conditions. Altogether, our results suggest that *C. sakazakii* can be inhibited in the colon of healthy infants through competition for nutrients, production of antimicrobial compounds or a combination of mechanisms. In a healthy infant, it is possible that the presence of *C. sakazakii* is self-limiting due to the native gut microbiota. However, ingesting a treatment, such as synbiotics, could reduce the levels of *C. sakazakii* due to the production of metabolites such as SCFAs or through interactions between metabolites and the native gut microbiota. Furthermore, we provide evidence regarding the robustness of a healthy infant gut microbiota, albeit within a controlled environment simulating the colonic conditions of an infant, and for the potential biological significance of microbial genera present in relatively low abundance in the gut. Overall, our study suggests that the use of a synbiotic could be helpful in controlling potential *C. sakazakii* infection in infants.

Data availability statement

The datasets presented in this study can be found in online repositories. The names of the repository/repositories and accession number(s) can be found in the article/**Supplementary Material**.

Ethics statement

The studies involving human participants were reviewed and approved by the University of Guelph, Research Ethics Board (REB). Application to Involve Human Participants in Research. Written informed consent to participate in this study was provided by the participants' legal guardian/next of kin.

Author contributions

AK planned, conducted, and analyzed the experiments and the associated data, in addition to writing and revising the manuscript. VP, JF, and LG planned the experiment and revised the manuscript. All authors contributed to the article and approved the submitted version.

Acknowledgments

We would like to acknowledge the financial support from the Canada First Research Excellence Fund (CFREF) through the Food for Thought Initiative (Grant #499114). We thank the following individuals for their assistance with the SHIME: Ceylon Simon, Ives Ivusic Polic, Yafei Liu, Grace Li, Devita Kireina, and Gabby Bui.

Conflict of interest

The authors declare that the research was conducted in the absence of any commercial or financial relationships that could be construed as a potential conflict of interest.

Publisher's note

Supplementary material

The Supplementary Material for this article can be found online at: https://www.frontiersin.org/articles/10.3389/fmicb.2022.947624/full#supplementary-material

References

Abdulkadir, B., Nelson, A., Skeath, T., Marrs, E. C., Perry, J. D., Cummings, S. P., et al. (2016). Routine use of probiotics in preterm infants: longitudinal impact on the microbiome and metabolome. *Neonatology* 109, 239–247. doi: 10.1159/000442936

Ackerberg, T. S., Labuschagne, L. I, and Lombard, M. J. (2012). The use of prebiotics and probiotics in infant formula. *S. Afr. Fam. Pract.* 54, 321–323. doi: 10.1080/20786204.2012.10874243

Álvarez-Ordóñez, A., Begley, M., and Hill, C. (2012). Polymorphisms in *rpoS* and stress tolerance heterogeneity in natural isolates of *Cronobacter sakazakii*. *Appl. Environ. Microbiol.* 78, 3975–3984. doi: 10.1128/AEM.07835-11

Appert, O., Garcia, A. R., Frei, R., Roduit, C., Constancias, F., Neuzil-Bunesova, V., et al. (2020). Initial butyrate producers during infant gut microbiota development are endospore formers. *Environ. Microbiol.* 22, 3909–3921. doi: 10.1111/1462-2920.15167

Arnold, C. N., McElhanon, J., Lee, A., Leonhart, R., and Siegele, D. A. (2001). Global analysis of *Escherichia coli* gene expression during the acetate-induced acid tolerance response. *J. Bacteriol.* 183, 2178–2186.

Bäckhed, F., Roswall, J., Peng, Y., Feng, Q., Jia, H., Kovatcheva-Datchary, P., et al. (2015). Dynamics and stabilization of the human gut microbiome during the first year of life. *Cell Host Microbe* 17, 690–703. doi: 10.1016/j.chom.2015.04.004

Bendjeddou, K., Fons, M., Strocker, P., and Sadoun, D. (2012). Characterization and purification of a bacteriocin from *Lactobacillus paracasei* subsp. *paracasei* BMK2005, an intestinal isolate active against multidrug-resistant pathogens. *World J. Microbiol. Biotechnol.* 28, 1543–1552. doi: 10.1007/s11274-011-0958-1

Benjamino, J., Lincoln, S., Srivastava, R., and Graf, J. (2018). Low-abundant bacteria drive compositional changes in the gut microbiota after dietary alteration. *Microbiome* 6, 1–13. doi: 10.1186/s40168-018-0469-5

Bokulich, N. A., Kaehler, B. D., Rideout, J. R., Dillon, M., Bolyen, E., Knight, R., et al. (2018). Optimizing taxonomic classification of marker gene amplicon sequences. *Microbiome* 6:90. doi: 10.1186/s40168-018-0470-z

Brink, L. R., Mercer, K. E., Piccolo, B. D., Chintapalli, S. V., Elolimy, A., Bowlin, A. K., et al. (2020). Neonatal diet alters fecal microbiota and metabolome profiles at different ages in infants fed breast milk or formula. *Am. J. Clin. Nutr.* 111, 1190–1202. doi: 10.1093/ajcn/nqaa076

Callahan, B. J., McMurdie, P. J., Rosen, M. J., Han, A. W., Johnson, A. J. A., and Holmes, S. P. (2016). DADA2: high-resolution sample inference from Illumina amplicon data. *Nat. Methods* 13, 581–583. doi: 10.1038/nmeth.3869

Caporaso, J. G., Lauber, C. L., Walters, W. A., Berg-Lyons, D., Lozupone, C. A., Turnbaugh, P. J., et al. (2011). Global patterns of 16S rRNA diversity at a depth of millions of sequences per sample. *Proc. Nat. Acad. Sci. U.S.A.* 108, 4516–4522. doi: 10.1073/pnas.1000080107

Cena, J., Zhang, J., Deng, D., Damé-Teixeira, N., and Do, T. (2021). Low-abundant microorganisms: the human microbiome's dark matter, a scoping review. *Front. Cell. Infect. Microbiol.* 11:689197. doi: 10.3389/fcimb.2021.689197

Centers for Disease Control and Prevention [CDC] (2020a). *Frequently Asked Questions*. Atlanta: Centers for Disease Control and Prevention.

Centers for Disease Control and Prevention [CDC] (2020b). *Cronobacter Infection and Infants*. Atlanta: Centers for Disease Control and Prevention.

Centers for Disease Control and Prevention [CDC] (2022). *Cronobacter and Powdered Infant* Formula Investigation. Atlanta: Centers for Disease Control and Prevention.

Chichlowski, M., Shah, N., Wampler, J. L., Wu, S. S., and Vanderhoof, J. A. (2020). *Bifidobacterium longum* subspecies *infantis* (*B. infantis*) in pediatric nutrition: current state of knowledge. *Nutrients* 12:1581. doi: 10.3390/nu12061581

Chung, H. J., Sim, J. H., Min, T. S., and Choi, H. K. (2018). Metabolomics and lipidomics approaches in the science of probiotics: a review. *J. Med. Food* 21, 1086–1095. doi: 10.1089/jmf.2017.4175

Claussen, J. C., Skiecevičienė, J., Wang, J., Rausch, P., Karlsen, T. H., Lieb, W., et al. (2017). Boolean analysis reveals systematic interactions among low-abundance species in the human gut microbiome. *PLoS Comput. Biol.* 13:e1005361. doi: 10.1371/journal.pcbi.1005361

Collado, M. C., Isolauri, E., and Salminen, S. (2008). Specific probiotic strains and their combinations counteract adhesion of *Enterobacter sakazakii* to intestinal mucus. *FEMS Microbiol. Lett.* 285, 58–64. doi: 10.1111/j.1574-6968.2008.01211.x

Cukrowska, B., Bierła, J. B., Zakrzewska, M., Klukowski, M., and Maciorkowska, E. (2020). The relationship between the infant gut microbiota and allergy. The role of *Bifidobacterium breve* and prebiotic oligosaccharides in the activation of anti-allergic mechanisms in early life. *Nutrients* 12:946. doi: 10.3390/nu12040946

Dilli, D., Aydin, B., Fettah, N. D., Özyazıcı, E., Beken, S., Zenciroğlu, A., et al. (2015). The ProPre-save study: effects of probiotics and prebiotics alone or combined on necrotizing enterocolitis in very low birth weight infants. *J. Pediatr.* 166, 545–551. doi: 10.1016/j.jpeds.2014.12.004

Ding, M., Yang, B., Khine, W. W. T., Lee, Y. K., Rahayu, E. S., Ross, R. P., et al. (2021). The species-level composition of the fecal *Bifidobacterium* and *Lactobacillus* Genera in Indonesian children differs from that of their mothers. *Microorganisms* 9:1995. doi: 10.3390/microorganisms9091995

Dittoe, D. K., Ricke, S. C., and Kiess, A. S. (2018). Organic acids and potential for modifying the avian gastrointestinal tract and reducing pathogens and disease. *Front. Vet. Sci.* 5:216. doi: 10.3389/fvets.2018.00216

Fleming-Davies, A., Jabbari, S., Robertson, S. L., Asih, T. S. N., Lanzas, C., Lenhart, S., et al. (2017). "Mathematical modeling of the effects of nutrient competition and bile acid metabolism by the gut microbiota on colonization resistance against *Clostridium difficile*," in *Women in Mathematical Biology*, eds A. Layton, and L. Miller (Cham: Springer), 137–161. doi: 10.1007/978-3-319-60304-9_8

Flynn, J. M., Niccum, D., Dunitz, J. M., and Hunter, R. C. (2016). Evidence and role for bacterial mucin degradation in cystic fibrosis airway disease. *PLoS Pathog.* 12:e1005846. doi: 10.1371/journal.ppat.1005846

Fooks, L. J., and Gibson, G. R. (2002). Probiotics as modulators of the gut flora. *Br. J. Nutr.* 88, S39–S49. doi: 10.1079/BJN2002628

Gao, Z., Daliri, E. B. M., Wang, J. U. N., Liu, D., Chen, S., Ye, X., et al. (2019). Inhibitory effect of lactic acid bacteria on foodborne pathogens: a review. *J. Food Prot.* 82, 441–453. doi: 10.4315/0362-028X.JFP-18-303

Gavriil, A., Thanasoulia, A., and Skandamis, P. N. (2020). Sublethal concentrations of undissociated acetic acid may not always stimulate acid resistance in *Salmonella enterica* sub. *enterica* serovar Enteritidis Phage Type 4: implications of challenge substrate associated factors. *PLoS One* 15:e0234999. doi: 10.1371/journal.pone.0234999

Ghini, V., Tenori, L., Pane, M., Amoruso, A., Marroncini, G., Squarzanti, D. F., et al. (2020). Effects of Probiotics Administration on Human Metabolic Phenotype. *Metabolites* 10:396. doi: 10.3390/metabo10100396

Gillis, C. C., Hughes, E. R., Spiga, L., Winter, M. G., Zhu, W., de Carvalho, T. F., et al. (2018). Dysbiosis-associated change in host metabolism generates lactate to support *Salmonella* growth. *Cell Host Microbe* 23, 54–64. doi: 10.1016/j.chom.2017.11.006

Harrison, L. M., Balan, K. V., and Babu, U. S. (2013). Dietary fatty acids and immune response to food-borne bacterial infections. *Nutrients* 5, 1801–1822. doi: 10.3390/nu5051801

Hill, C., Guarner, F., Reid, G., Gibson, G. R., Merenstein, D. J., Pot, B., et al. (2014). Expert consensus document: the international scientific association for probiotics and prebiotics consensus statement on the scope and appropriate use of the term probiotic. *Nat. Rev. Gastroenterol. Hepatol.* 11, 506–514. doi: 10.1038/nrgastro.2014.66

Hinton, A. Jr., and Hume, M. E. (1995). Synergism of lactate and succinate as metabolites utilized by *Veillonella* to inhibit the growth of *Salmonella* typhimurium and *Salmonella* enteritidis *in vitro*. *Avian Dis.* 39, 309–316. doi: 10.2307/1591872

Iljazovic, A., Roy, U., Gálvez, E. J., Lesker, T. R., Zhao, B., Gronow, A., et al. (2021). Perturbation of the gut microbiome by *Prevotella* spp. enhances host susceptibility to mucosal inflammation. *Mucosal Immunol.* 14, 113–124. doi: 10.1038/s41385-020-0296-4

Kalyantanda, G., Shumyak, L., and Archibald, L. K. (2015). Cronobacter species contamination of powdered infant formula and the implications for neonatal health. *Front. Pediatr.* 3:56. doi: 10.3389/fped.2015.00056

Kamada, N., Chen, G. Y., Inohara, N., and Núñez, G. (2013). Control of pathogens and pathobionts by the gut microbiota. *Nat. Immunol.* 14, 685–690. doi: 10.1038/ni.2608

Kassambara, A. (2017). *Practical Guide to Principal Component Methods in R: PCA, M (CA), FAMD, MFA, HCPC, Factoextra*, Vol. 2. STHDA. Available online at: http://www.sthda.com/english/wiki/practical-guide-to-principal-component-methods-in-r

Ke, A., Parreira, V., Farber, J. M., and Goodridge, L. (2022). Selection of a Potential Synbiotic against *Cronobacter sakazakii*. *J. Food Prot.* [Epub ahead of print]. doi: 10.4315/JFP-22-048

Kent, R. M., Fitzgerald, G. F., Hill, C., Stanton, C., and Paul Ross, R. (2015). Novel approaches to improve the intrinsic microbiological safety of

powdered infant milk formula. *Nutrients* 7, 1217–1244. doi: 10.3390/nu7021217

Kirchberg, F. F., Hellmuth, C., Totzauer, M., Uhl, O., Closa-Monasterolo, R., Escribano, J., et al. (2020). Impact of infant protein supply and other early life factors on plasma metabolome at 5.5 and 8 years of age: a randomized trial. *Int. J. Obes.* 44, 69–81. doi: 10.1038/s41366-019-0398-9

Knaus, U. G., Hertzberger, R., Pircalabioru, G. G., Yousefi, S. P. M., and Branco dos Santos, F. (2017). Pathogen control at the intestinal mucosa–H_2O_2 to the rescue. *Gut Microbes* 8, 67–74. doi: 10.1080/19490976.2017.1279378

Koh, A., De Vadder, F., Kovatcheva-Datchary, P., and Bäckhed, F. (2016). From dietary fiber to host physiology: short-chain fatty acids as key bacterial metabolites. *Cell* 165, 1332–1345. doi: 10.1016/j.cell.2016.05.041

Kotsou, M. G., Mitsou, E. K., Oikonomou, I. G., and Kyriacou, A. A. (2008). *In vitro* assessment of probiotic properties of *Lactobacillus* strains from infant gut microflora. *Food Biotechnol.* 22, 1–17. doi: 10.1080/08905430701707844

Kusmivati, N., and Wahyuningsih, T. D. (2018). "Effect of Synbiotics *Lactobacillus casei* AP and Inulin Extract Dahlia pinnata L. in Enteropathogenic *Escherichia coli*-Induced Diarrhea," in *2018 1st International Conference on Bioinformatics. Biotechnology, and Biomedical Engineering-Bioinformatics and Biomedical Engineering*, (Yogyakarta: IEEE), 1–6. doi: 10.1109/BIOMIC.2018.8610642

Kwon, Y. M., Park, S. Y., Birkhold, S. G., and Ricke, S. C. (2000). Induction of resistance of *Salmonella* Typhimurium to environmental stresses by exposure to short-chain fatty acids. *J. Food Sci.* 65, 1037–1040. doi: 10.1111/j.1365-2621.2000.tb09413.x

Lamas, A., Regal, P., Vázquez, B., Cepeda, A., and Franco, C. M. (2019). Short chain fatty acids commonly produced by gut microbiota influence *Salmonella enterica* motility, biofilm formation, and gene expression. *Antibiotics* 8:265. doi: 10.3390/antibiotics8040265

Lawhon, S. D., Maurer, R., Suyemoto, M., and Altier, C. (2002). Intestinal short-chain fatty acids alter *Salmonella* typhimurium invasion gene expression and virulence through BarA/SirA. *Mol. Microbiol.* 46, 1451–1464. doi: 10.1046/j.1365-2958.2002.03268.x

Le Doare, K., Holder, B., Bassett, A., and Pannaraj, P. S. (2018). Mother's Milk: a purposeful contribution to the development of the infant microbiota and immunity. *Front. Immunol.* 9:361. doi: 10.3389/fimmu.2018.00361

LeBlanc, J. G., Chain, F., Martín, R., Bermúdez-Humarán, L. G., Courau, S., and Langella, P. (2017). Beneficial effects on host energy metabolism of short-chain fatty acids and vitamins produced by commensal and probiotic bacteria. *Microb. Cell Fact.* 16, 1–10. doi: 10.1186/s12934-017-0691-z

Likotrafiti, E., Tuohy, K. M., Gibson, G. R., and Rastall, R. A. (2016). Antimicrobial activity of selected synbiotics targeted for the elderly against pathogenic *Escherichia coli* strains. *Int. J. Food Sci. Nutr.* 67, 83–91. doi: 10.3109/09637486.2015.1134444

Lund, P. A., De Biase, D., Liran, O., Scheler, O., Mira, N. P., Cetecioglu, Z., et al. (2020). Understanding how microorganisms respond to acid pH is central to their control and successful exploitation. *Front. Microbiol.* 11:556140. doi: 10.3389/fmicb.2020.556140

Luoto, R., Ruuskanen, O., Waris, M., Kalliomäki, M., Salminen, S., and Isolauri, E. (2014). Prebiotic and probiotic supplementation prevents rhinovirus infections in preterm infants: a randomized, placebo-controlled trial. *J. Allergy Clin. Immunol.* 133, 405–413. doi: 10.1016/j.jaci.2013.08.020

Maifiah, M. H. M., Creek, D. J., Nation, R. L., Forrest, A., Tsuji, B. T., Velkov, T., et al. (2017). Untargeted metabolomics analysis reveals key pathways responsible for the synergistic killing of colistin and doripenem combination against *Acinetobacter baumannii*. *Sci. Rep.* 7, 1–12. doi: 10.1038/srep45527

Makras, L., and De Vuyst, L. (2006). The *in vitro* inhibition of Gram-negative pathogenic bacteria by bifidobacteria is caused by the production of organic acids. *Int. Dairy J.* 16, 1049–1057. doi: 10.1016/j.idairyj.2005.09.006

Markowiak, P., and Śliżewska, K. (2017). Effects of probiotics, prebiotics, and synbiotics on human health. *Nutrients* 9:1021. doi: 10.3390/nu9091021

Markowiak-Kopeć, P., and Śliżewska, K. (2020). The effect of probiotics on the production of short-chain fatty acids by human intestinal microbiome. *Nutrients* 12:1107. doi: 10.3390/nu12041107

Martin, A. M., Sun, E. W., Rogers, G. B., and Keating, D. J. (2019). The influence of the gut microbiome on host metabolism through the regulation of gut hormone release. *Front. Physiol.* 10:428. doi: 10.3389/fphys.2019.00428

Martin, F. P. J., Sprenger, N., Montoliu, I., Rezzi, S., Kochhar, S., and Nicholson, J. K. (2010). Dietary modulation of gut functional ecology studied by fecal metabonomics. *J. Proteome Res.* 9, 5284–5295. doi: 10.1021/pr100554m

Martín, R., Langa, S., Reviriego, C., Jimínez, E., Marín, M. L., Xaus, J., et al. (2003). Human milk is a source of lactic acid bacteria for the infant gut. *J. Pediatr.* 143, 754–758. doi: 10.1016/j.jpeds.2003.09.028

McMurdie, P. J., and Holmes, S. (2013). phyloseq: an R package for reproducible interactive analysis and graphics of microbiome census data. *PLoS One* 8:e61217. doi: 10.1371/journal.pone.0061217

Moore, R. E., and Townsend, S. D. (2019). Temporal development of the infant gut microbiome. *Open Biol.* 9:190128. doi: 10.1098/rsob.190128

Murphy, J., Mahony, J., Fitzgerald, G. F., and van Sinderen, D. (2017). "Bacteriophages infecting lactic acid bacteria," in *Cheese*, eds M. P. C. P. P.F. Fox, and D. Everett (Cambridge: Academic Press), 249–272. doi: 10.1016/B978-0-12-417012-4.00010-7

Nandhini, L. P., Biswal, N., Adhisivam, B., Mandal, J., Bhat, B. V., and Mathai, B. (2016). Synbiotics for decreasing incidence of necrotizing enterocolitis among preterm neonates–a randomized controlled trial. *J. Matern.-Fetal Neonatal Med.* 29, 821–825. doi: 10.3109/14767058.2015.1019854

Ng, K. M., Ferreyra, J. A., Higginbottom, S. K., Lynch, J. B., Kashyap, P. C., Gopinath, S., et al. (2013). Microbiota-liberated host sugars facilitate post-antibiotic expansion of enteric pathogens. *Nature* 502, 96–99. doi: 10.1038/nature12503

Nilsen, M., Madelen Saunders, C., Leena Angell, I., Arntzen, M. Ø, Lødrup Carlsen, K. C., Carlsen, K. H., et al. (2020). Butyrate levels in the transition from an infant-to an adult-like gut microbiota correlate with bacterial networks associated with *Eubacterium rectale* and *Ruminococcus gnavus*. *Genes* 11:1245. doi: 10.3390/genes11111245

O'Callaghan, A., and van Sinderen, D. (2016). Bifidobacteria and their role as members of the human gut microbiota. *Front. Microbiol.* 7:925. doi: 10.3389/fmicb.2016.00925

O'Connell, T. M. (2020). The application of metabolomics to probiotic and prebiotic interventions in human clinical studies. *Metabolites* 10:120. doi: 10.3390/metabo10030120

Oksanen, J., Blanchet, F. G., Friendly, M., Kindt, R., Legendre, P., McGlinn, D., et al. (2020). *Vegan: Community Ecology Package*. Available Online at: https://CRAN.R-project.org/package=vegan (accessed November 6, 2021).

Oliphant, K., and Allen-Vercoe, E. (2019). Macronutrient metabolism by the human gut microbiome: major fermentation by-products and their impact on host health. *Microbiome* 7, 1–15. doi: 10.1186/s40168-019-0704-8

Oshima, S., Rea, M. C., Lothe, S., Morgan, S., Begley, M., O'Connor, P. M., et al. (2012). Efficacy of organic acids, bacteriocins, and the lactoperoxidase system in inhibiting the growth of *Cronobacter* spp. in rehydrated infant formula. *J. Food Prot.* 75, 1734–1742. doi: 10.4315/0362-028X.JFP-12-066

Pandey, K. R., Naik, S. R., and Vakil, B. V. (2015). Probiotics, prebiotics and synbiotics - a review. *J. Food Sci. Technol.* 52, 7577–7587. doi: 10.1007/s13197-015-1921-1

Papagianni, M., and Anastasiadou, S. (2009). Pediocins: the bacteriocins of *Pediococci*. Sources, production, properties and applications. *Microb. Cell Fact.* 8, 1–16. doi: 10.1186/1475-2859-8-3

Patnode, M. L., Beller, Z. W., Han, N. D., Cheng, J., Peters, S. L., Terrapon, N., et al. (2019). Interspecies competition impacts targeted manipulation of human gut bacteria by fiber-derived glycans. *Cell* 179, 59–73. doi: 10.1016/j.cell.2019.08.011

Pehlevan, O. S., Benzer, D., Gursoy, T., Karatekin, G., and Ovali, F. (2020). Synbiotics use for preventing sepsis and necrotizing enterocolitis in very low birth weight neonates: a randomized controlled trial. *Clin. Exp. Pediatr.* 63:226. doi: 10.3345/cep.2019.00381

Peng, M., and Biswas, D. (2017). Short chain and polyunsaturated fatty acids in host gut health and foodborne bacterial pathogen inhibition. *Crit. Rev. Food Sci. Nutr.* 57, 3987–4002. doi: 10.1080/10408398.2016.1203286

Phan, M., Momin, S. R., Senn, M. K., and Wood, A. C. (2019). Metabolomic insights into the effects of breast milk versus formula milk feeding in infants. *Curr. Nutr. Rep.* 8, 295–306. doi: 10.1007/s13668-019-00284-2

Piatek, J., Krauss, H., Ciechelska-Rybarczyk, A., Bernatek, M., Wojtyla-Buciora, P., and Sommermeyer, H. (2020). In-Vitro Growth Inhibition of Bacterial Pathogens by Probiotics and a Synbiotic: Product Composition Matters. *Int. J. Environ. Res. Public Health* 17:3332. doi: 10.3390/ijerph17093332

Piqué, N., Berlanga, M., and Miñana-Galbis, D. (2019). Health benefits of heat-killed (Tyndallized) probiotics: an overview. *Int. J. Mol. Sci.* 20:2534. doi: 10.3390/ijms20102534

Prudêncio, C. V., Dos Santos, M. T., and Vanetti, M. C. D. (2015). Strategies for the use of bacteriocins in Gram-negative bacteria: relevance in food microbiology. *J. Food Sci. Technol.* 52, 5408–5417. doi: 10.1007/s13197-014-1666-2

Quast, C., Pruesse, E., Yilmaz, P., Gerken, J., Schweer, T., Yarza, P., et al. (2012). The SILVA ribosomal RNA gene database project: improved data processing and web-based tools. *Nucleic Acids Res.* 41, D590–D596. doi: 10.1093/nar/gks1219

Raimondi, S., Musmeci, E., Candeliere, F., Amaretti, A., and Rossi, M. (2021). Identification of mucin degraders of the human gut microbiota. *Sci. Rep.* 11, 1–10. doi: 10.1038/s41598-021-90553-4

Ren, D., Gong, S., Shu, J., Zhu, J., Liu, H., and Chen, P. (2018). Effects of mixed lactic acid bacteria on intestinal microbiota of mice infected with *Staphylococcus aureus*. *BMC Microbiol.* 18:109. doi: 10.1186/s12866-018-1245-1

Rodríguez-Rojas, A., Kim, J. J., Johnston, P. R., Makarova, O., Eravci, M., Weise, C., et al. (2020). Non-lethal exposure to H2O2 boosts bacterial survival and evolvability against oxidative stress. *PLoS Genet.* 16:e1008649. doi: 10.1371/journal.pgen.1008649

Rolfe, R. D. (2000). The role of probiotic cultures in the control of gastrointestinal health. *J. Nutr.* 130, 396S–402S. doi: 10.1093/jn/130.2.396S

Rubio, R., Jofré, A., Martín, B., Aymerich, T., and Garriga, M. (2014). Characterization of lactic acid bacteria isolated from infant faeces as potential probiotic starter cultures for fermented sausages. *Food Microbiol.* 38, 303–311. doi: 10.1016/j.fm.2013.07.015

Sakr, E. A., and Massoud, M. I. (2021). Impact of prebiotic potential of stevia sweeteners-sugar used as synbiotic preparation on antimicrobial, antibiofilm, and antioxidant activities. *LWT* 144:111260. doi: 10.1016/j.lwt.2021.111260

Sannasiddappa, T. H., Costabile, A., Gibson, G. R., and Clarke, S. R. (2011). The influence of *Staphylococcus aureus* on gut microbial ecology in an *in vitro* continuous culture human colonic model system. *PLoS One* 6:e23227. doi: 10.1371/journal.pone.0023227

Servin, A. L. (2004). Antagonistic activities of lactobacilli and bifidobacteria against microbial pathogens. *FEMS Microbiol. Rev.* 28, 405–440. doi: 10.1016/j.femsre.2004.01.003

Shanmugasundaram, R., Mortada, M., Cosby, D. E., Singh, M., Applegate, T. J., Syed, B., et al. (2019). Synbiotic supplementation to decrease *Salmonella* colonization in the intestine and carcass contamination in broiler birds. *PLoS One* 14:e0223577. doi: 10.1371/journal.pone.0223577

Sieniawska, E., and Georgiev, M. I. (2022). Metabolomics: towards acceleration of antibacterial plant-based leads discovery. *Phytochem. Rev.* 21, 765–781. doi: 10.1007/s11101-021-09762-4

Simons, A., Alhanout, K., and Duval, R. E. (2020). Bacteriocins, antimicrobial peptides from bacterial origin: overview of their biology and their impact against multidrug-resistant bacteria. *Microorganisms* 8:639.

Sivieri, K., Bianchi, F., Tallarico, M. A., and Rossi, E. A. (2011). Fermentation by gut microbiota cultured in a simulator of the human intestinal microbial ecosystem is improved by probiotic *Enterococcus faecium* CRL 183. *Funct. Foods Health Dis.* 1, 389–402. doi: 10.31989/ffhd.v1i10.119

Sivieri, K., Sáyago-Ayerdi, S. G., and Binetti, A. G. (2021). Insights of Gut Microbiota: probiotics and Bioactive Compounds. *Front. Microbiol.* 12:780596. doi: 10.3389/fmicb.2021.780596

Solís, G., de Los Reyes-Gavilan, C. G., Fernández, N., Margolles, A., and Gueimonde, M. (2010). Establishment and development of lactic acid bacteria and bifidobacteria microbiota in breast-milk and the infant gut. *Anaerobe* 16, 307–310. doi: 10.1016/j.anaerobe.2010.02.004

Sreenivasa, B., Kumar, P. S., Suresh Babu, M. T., and Ragavendra, K. (2015). Role of synbiotics in the prevention of necrotizing enterocolitis in preterm neonates: a randomized controlled trial. *Int. J. Contemp. Pediatr.* 2, 127–130. doi: 10.5455/2349-3291.ijcp20150512

Stecher, B., Chaffron, S., Käppeli, R., Hapfelmeier, S., Freedrich, S., Weber, T. C., et al. (2010). Like will to like: abundances of closely related species can predict susceptibility to intestinal colonization by pathogenic and commensal bacteria. *PLoS Pathog.* 6:e1000711. doi: 10.1371/journal.ppat.1000711

Stewart, C. J., Embleton, N. D., Marrs, E. C., Smith, D. P., Fofanova, T., Nelson, A., et al. (2017). Longitudinal development of the gut microbiome and metabolome in preterm neonates with late onset sepsis and healthy controls. *Microbiome* 5, 1–11. doi: 10.1186/s40168-017-0295-1

Swanson, K. S., Gibson, G. R., Hutkins, R., Reimer, R. A., Reid, G., Verbeke, K., et al. (2020). The International Scientific Association for Probiotics and Prebiotics (ISAPP) consensus statement on the definition and scope of synbiotics. *Nat. Rev. Gastroenterol. Hepatol.* 17, 687–701. doi: 10.1038/s41575-020-0344-2

Tabashsum, Z., Peng, M., Bernhardt, C., Patel, P., Carrion, M., and Biswas, D. (2019). Synbiotic-like effect of linoleic acid overproducing *Lactobacillus casei* with berry phenolic extracts against pathogenesis of enterohemorrhagic *Escherichia coli*. *Gut Pathog.* 11:41. doi: 10.1186/s13099-019-0320-y

Tang, Z. Z., Chen, G., Hong, Q., Huang, S., Smith, H. M., Shah, R. D., et al. (2019). Multi-omic analysis of the microbiome and metabolome in healthy subjects reveals microbiome-dependent relationships between diet and metabolites. *Front. Genet.* 10:454. doi: 10.3389/fgene.2019.00454

Tharrington, G., and Sorrells, K. M. (1992). Inhibition of *Listeria monocytogenes* by milk culture filtrates from *Lactobacillus delbrueckii* subsp. *lactis*. *J. Food Prot.* 55, 542–544. doi: 10.4315/0362-028x-55.7.542

Tian, X., Yu, Q., Yao, D., Shao, L., Liang, Z., Jia, F., et al. (2018). New insights into the response of metabolome of *Escherichia coli* O157: H7 to ohmic heating. *Front. Microbiol.* 9:2936. doi: 10.3389/fmicb.2018.02936

Tomar, S. K., Anand, S., Sharma, P., Sangwan, V., and Mandal, S. (2015). "Role of probiotic, prebiotics, synbiotics and postbiotics in inhibition of pathogens," in *The Battle against Microbial Pathogens: Basic Science, Technological Advances and Educational Programs*, ed. A. Méndez-Vilas (Badajoz: Formatex Research Centre), 717–732.

Turroni, F., Milani, C., Duranti, S., Lugli, G. A., Bernasconi, S., Margolles, A., et al. (2020). The infant gut microbiome as a microbial organ influencing host well-being. *Ital. J. Pediatr.* 46, 1–13. doi: 10.1186/s13052-020-0781-0

Van de Wiele, T., Van den Abbeele, P., Ossieur, W., Possemiers, S., and Marzorati, M. (2015). "The simulator of the human intestinal microbial ecosystem (SHIME®)," in *The Impact of Food Bioactives on Health*, eds K. Verhoeckx, P. Cotter, I. L. ópez-Expósito, C. Kleiveland, T. Lea, A. Mackie, et al. (Cham: Springer), 305–317. doi: 10.1007/978-3-319-16104-4_27

Van den Abbeele, P., Grootaert, C., Marzorati, M., Possemiers, S., Verstraete, W., Gérard, P., et al. (2010). Microbial community development in a dynamic gut model is reproducible, colon region specific, and selective for Bacteroidetes and Clostridium cluster IX. *Appl. Environ. Microbiol.* 76, 5237–5246. doi: 10.1128/AEM.00759-10

Van den Abbeele, P., Roos, S., Eeckhaut, V., MacKenzie, D. A., Derde, M., Verstraete, W., et al. (2012). Incorporating a mucosal environment in a dynamic gut model results in a more representative colonization by lactobacilli. *Microb. Biotechnol.* 5, 106–115. doi: 10.1111/j.1751-7915.2011.00308.x

Van den Nieuwboer, M., Claassen, E., Morelli, L., Guarner, F., and Brummer, R. J. (2014). Probiotic and synbiotic safety in infants under two years of age. *Benef. Microbes* 5, 45–60. doi: 10.3920/BM2013.0046

Vandenplas, Y., Zakharova, I., and Dmitrieva, Y. (2015). Oligosaccharides in infant formula: more evidence to validate the role of prebiotics. *Br. J. Nutr.* 113, 1339–1344. doi: 10.1017/S0007114515000823

Vazquez-Gutierrez, P., de Wouters, T., Werder, J., Chassard, C., and Lacroix, C. (2016). High iron-sequestrating bifidobacteria inhibit enteropathogen growth and adhesion to intestinal epithelial cells *in vitro*. *Front. Microbiol.* 7:1480. doi: 10.3389/fmicb.2016.01480

Venegas, D. P., De La Fuente, M. K., Landskron, G., González, M. J., Quera, R., Dijkstra, G., et al. (2019). Short chain fatty acids (SCFAs) mediated gut epithelial and immune regulation and its relevance for inflammatory bowel diseases. *Front. Immunol.* 10:277. doi: 10.3389/fimmu.2019.00277

Vitali, B., Ndagijimana, M., Cruciani, F., Carnevali, P., Candela, M., Guerzoni, M. E., et al. (2010). Impact of a synbiotic food on the gut microbial ecology and metabolic profiles. *BMC Microbiol.* 10:4. doi: 10.1186/1471-2180-10-4

Vongbhavit, K., and Underwood, M. A. (2016). Prevention of Necrotizing Enterocolitis Through Manipulation of the Intestinal Microbiota of the Premature Infant. *Clin. Ther.* 38, 716–732. doi: 10.1016/j.clinthera.2016.01.006

Wilson, K. H., and Perini, F. (1988). Role of competition for nutrients in suppression of *Clostridium difficile* by the colonic microflora. *Infect. Immun.* 56, 2610–2614. doi: 10.1128/iai.56.10.2610-2614.1988

Yang, I., Corwin, E. J., Brennan, P. A., Jordan, S., Murphy, J. R., and Dunlop, A. (2016). The infant microbiome: implications for infant health and neurocognitive development. *Nurs. Res.* 65:76. doi: 10.1097/NNR.0000000000000133

Zhang, C., Derrien, M., Levenez, F., Brazeilles, R., Ballal, S. A., Kim, J., et al. (2016). Ecological robustness of the gut microbiota in response to ingestion of transient food-borne microbes. *ISME J.* 10, 2235–2245. doi: 10.1038/ismej.2016.13

Zhang, Y., Xie, Y., Tang, J., Wang, S., Wang, L., Zhu, G., et al. (2020). Thermal inactivation of *Cronobacter sakazakii* ATCC 29544 in powdered infant formula milk using thermostatic radio frequency. *Food Control* 114:107270. doi: 10.1016/j.foodcont.2020.1070

frontiers | Frontiers in Microbiology

TYPE Original Research
PUBLISHED 27 July 2022
DOI 10.3389/fmicb.2022.958112

OPEN ACCESS

EDITED BY
Qixiao Zhai,
Jiangnan University, China

REVIEWED BY
Fengjie Sun,
Georgia Gwinnett College, United States
Yiru Shen,
Poultry Institute (CAAS), China
Guohua Liu,
Feed Research Institute (CAAS), China
Zhongfang Tan,
Zhengzhou University, China

*CORRESPONDENCE
Yuncai Xiao
xyc88@mail.hzau.edu.cn

SPECIALTY SECTION
This article was submitted to Food Microbiology, a section of the journal Frontiers in Microbiology

RECEIVED 31 May 2022
ACCEPTED 30 June 2022
PUBLISHED 27 July 2022

CITATION
Chen P, Li S, Zhou Z, Wang X, Shi D, Li Z, Li X and Xiao Y (2022) Liver fat metabolism of broilers regulated by *Bacillus amyloliquefaciens* TL *via* stimulating IGF-1 secretion and regulating the IGF signaling pathway. *Front. Microbiol.* 13:958112. doi: 10.3389/fmicb.2022.958112

Liver fat metabolism of broilers regulated by *Bacillus amyloliquefaciens* TL *via* stimulating IGF-1 secretion and regulating the IGF signaling pathway

Pinpin Chen, Shijie Li, Zutao Zhou, Xu Wang, Deshi Shi, Zili Li, Xiaowen Li and Yuncai Xiao*

State Key Laboratory of Agricultural Microbiology, College of Veterinary Medicine, Huazhong Agricultural University, Wuhan, China

Bacillus amyloliquefaciens TL (B.A-TL) is well-known for its capability of promoting protein synthesis and lipid metabolism, in particular, the abdominal fat deposition in broilers. However, the underlying molecular mechanism remains unclear. In our study, the regulations of lipid metabolism of broilers by B.A-TL were explored both *in vivo* and *in vitro*. The metabolites of B.A-TL were used to simulate *in vitro* the effect of B.A-TL on liver metabolism based on the chicken hepatocellular carcinoma cell line (i.e., LMH cells). The effects of B.A-TL on lipid metabolism by regulating insulin/IGF signaling pathways were investigated by applying the signal pathway inhibitors *in vitro*. The results showed that the B.A-TL metabolites enhanced hepatic lipid synthesis and stimulated the secretion of IGF-1. The liver transcriptome analysis revealed the significantly upregulated expressions of four genes (*SI, AMY2A*, *PCK1*, and *FASN*) in the B.A-TL treatment group, mainly involved in carbohydrate digestion and absorption as well as biomacromolecule metabolism, with a particularly prominent effect on fatty acid synthase (FASN). Results of cellular assays showed that B.A-TL metabolites were involved in the insulin/IGF signaling pathway, regulating the expressions of lipid metabolism genes (e.g., *FASN, ACCα, LPIN*, and *ACOX*) and the FASN protein, ultimately regulating the lipid metabolism *via* the IGF/PI3K/FASN pathway in broilers.

KEYWORDS

***Bacillus amyloliquefaciens* TL, broilers, lipid metabolism, liver, insulin-like factor 1, IGF signaling pathway, fatty acid synthase**

Introduction

More than 60 years ago, Salmon and Daughaday (1957) first described a serum factor that was controlled by hormones to stimulate sulfate incorporation by cartilage *in vitro*. This serum factor was later identified as the insulin-like growth factor (IGF) (Daughaday et al., 1987). The IGF system consists of two ligands, i.e., IGF-1

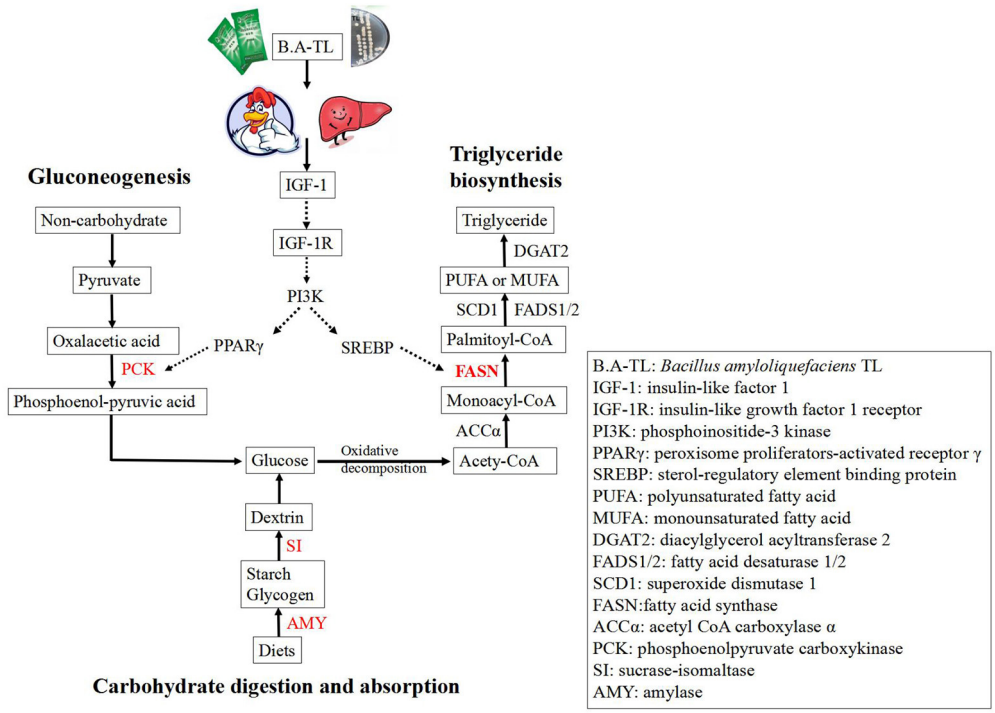

GRAPHICAL ABSTRACT |

and IGF-2 (Moerth et al., 2007; Poreba and Durzynska, 2020). The IGF-1 is a pleiotropic factor, expressed mainly in the liver (Poreba and Durzynska, 2020), and its physiological effects are to promote tissue growth and development and to regulate both lipid and carbohydrate metabolisms as well as the anti-inflammatory, antioxidant, and neuro- and hepato-protective properties (Liu et al., 2016; Halmos and Suba, 2019; Stanley et al., 2021). The IGF-2 is expressed in many tissues, in particular the placenta (Forbes et al., 2020). The IGF-2 plays an important role in follicular growth and in oocyte and embryonic development (Sirotkin et al., 2000; Chang et al., 2021), generally considered as a major growth factor involved in the early body development (Chang et al., 2021).

The growth hormone (GH)/IGF system, also known as the pituitary-liver axis, has shown somatotrophic effects *in vivo* (Li, 2022). However, both animal and clinical studies have revealed that IGF-2 is not a substitute for IGF-1 to stimulate normal postnatal body growth (Sjögren et al., 1999; Moerth et al., 2007), while animal weight growth is regulated by GH and IGF-1 (Sjögren et al., 1999; Anh et al., 2015; Jia et al., 2018). Although the effect of GH can be directly activated by tyrosine kinase *via* the GH receptor, more peripheral effects are mainly mediated by stimulating the expression of IGF-1 in the liver and peripheral tissues (Sjögren et al., 1999; Brooks and Waters, 2010; Sigalos and Pastuszak, 2018). Serum IGF-1 level is an indicator for GH level simply because IGF-1 is both a downstream effector and an upstream regulator of GH (Sigalos and Pastuszak, 2018). Several studies have shown that IGF-1 can stimulate physical growth in animal models with GH deficiency/GH receptor mutation (Sjögren et al., 1999; Laron, 2008; Castilla-Cortazar et al., 2017). In a study on LI-IGF-1/- mice with the *IGF-1* gene knocked out by the Cre/loxP recombinant system, Sjögren et al.

Abbreviations: B.A-TL, *Bacillus amyloliquefaciens* TL; IGF-1, insulin-like factor 1; FST, fermentation supernatant; EPS, exopolysaccharides; L-Tyr, L-tyrosine; LMH, chicken hepatocellular carcinoma cell line; IGF-1R, insulin-like growth factor 1 receptor; PI3Kα, phosphoinositide 3-kinase α; MEK, MAP kinase; GLU, glucose; TG, triglycerides; PCK1, phosphoenolpyruvate carboxykinase; FASN, fatty acid synthase; ACCα, acetyl CoA carboxylase α; GH, growth hormone; INS, insulin; CHO, cholesterol; VLDL, very low-density lipoprotein; ALT, alanine aminotransferase; AST, aspartate aminotransferase; MDA, malondialdehyde; CAT, catalase; SOD, superoxide dismutase; T-AOC, total antioxidant capacity; GSH-Px, glutathione peroxidase; IR, insulin receptor; RTK, receptor tyrosine kinases; FA, fatty acid; SREBP1, sterol regulatory element binding protein 1; SCD, stearoyl-CoA desaturase; ABW, average body weight; ADG, average daily gain; FCR feed conversion ratio; LXRα, liver X receptor α; LPIN1, lipid phosphate phosphohydrolase 1; CPT1A, carnitine palmitoyltransferase 1A; PPARα, peroxisome proliferators-activated receptors α; ACOX1, acyl-Coenzyme A oxidase 1; SDS-PAGE, sodium dodecyl sulfate-polyacrylamide gel electrophoresis; LC-MS, liquid chromatography and mass spectrometry; TPM, transcripts per million; DEGs, differentially expressed genes; GO, Gene Ontology; KEGG, Kyoto Encyclopedia of Genes and Genomes; AMY1, salivary amylase; AMY2, pancreatic amylase; SI, sucrase-isomaltase; MGAM, maltase-glucoamylase; LDs, lipid droplets; SOCE, store-operated calcium entry; DG, diacylglycerol.

(1999) reported that the liver-derived IGF-1 exerted a negative feedback regulation on the pulsatile secretion pattern of GH. Furthermore, studies showed that the Benha line chickens with improved growth performance, carcass characteristics, and meat quality traits showed the highest levels of hepatic *GH* and *IGF-1* as well as the muscle *IGF-1* gene expression compared to both Rhode Island Red and Golden Montazah chickens (El-Attrouny et al., 2021). Moreover, as the two major components in the somatotropic axis, the GH is the main regulator of growth rate, while the IGF-1 regulates both growth rate and body weight in broilers (Jia et al., 2018).

It is well known that the binding of IGF to its receptor leads to the activation of the insulin (INS)/IGF signaling cascade pathway, which contains two major downstream signaling pathways, including (1) the IRS-initiated PI3K-AKT/rapamycin pathway primarily involved in metabolism and (2) the SHC-initiated RAS/MAPK pathway controlling mitosis (Forbes et al., 2020). At the cellular level, the INS/IGF signaling pathway has been considered to contribute to cell division and glucose (GLU) metabolism (Perry and Shulman, 2020), whereas the current understanding of insulin signaling in chickens is rather inadequate compared to that in mammals (Dupont et al., 2009). Despite the lack of convincing evidence, it appears that the insulin signaling in the chicken liver is similar to that in mammals but different from that in chicken muscle (Dupont et al., 2009). Furthermore, it has been reported that the activation of insulin signaling in the liver during the early developmental stages of broiler chickens could cause the acceleration of lipogenesis, ultimately fattening fatty broilers (Dupont et al., 1999).

Previous studies revealed significantly increased body weight in broilers fed with *Bacillus amyloliquefaciens* TL (B.A-TL) in 21 days as well as improved feed efficiency and enhanced stress resistance of broilers (Hong et al., 2019). In particular, the results of the analysis of the cecum microbiota showed that the relative abundance of *Firmicutes* was increased, whereas the relative abundance of *Bacteroidetes* was decreased in the B.A-TL group (Hong et al., 2019). Furthermore, studies showed that a higher *Firmicutes/Bacteroidetes* ratio promoted not only body growth (Mancabelli et al., 2016; Salaheen et al., 2017) but also fat deposition (Ley et al., 2005; Hong et al., 2019) in various types of animal models. Moreover, the ileal transcriptome analysis showed that the treatment of B.A-TL reduced the levels of both intestinal inflammation and intestinal damage and facilitated the energy accumulation in broilers, with the upregulated differentially expressed genes (DEGs) significantly enriched in the "insulin signaling pathway" and both genes *FGF16* and *FGF10* expressed only in the B.A-TL group (Hong et al., 2021). This unique expression of the FGF family members in the B.A-TL group suggested enhanced glycogen and protein syntheses and lipid differentiation in the B.A-TL group (Hong et al., 2021).

In avian species, lipogenesis takes place primarily in the liver, accounting for 95% of *de novo* fatty acid (FA) synthesis (Han et al., 2015), while the gut-derived products exit the gut and enter the portal circulation to bath the liver and potentially regulate the hepatic metabolism and function (Kieffer et al., 2016; Arab et al., 2018; Albillos et al., 2020). Therefore, in this study, we performed liver transcriptome analysis, liver oil red O staining, and serum analysis of broilers at 21 days of age to elucidate the lipid metabolism changes in response to the probiotic treatment of B.A-TL. Since B.A-TL cannot but its metabolites can reach liver tissues through the gut-liver axis, the B.A-TL metabolites were used in this study to act on LMH cells to simulate the effect of B.A-TL entering broiler chickens on the liver. Furthermore, the quantitative real-time polymerase chain reaction (qRT-PCR) analysis and western blotting techniques as well as the cellular pathway blocking assays were performed to investigate the regulatory mechanism of B.A-TL underlying the INS/IGF signaling pathway and thus regulating the lipid metabolism.

Materials and methods

Bacterial strains and antibodies

As a facultative anaerobic bacterium closely related to *Bacillus subtilis* (Hong et al., 2019), the B.A-TL is an invention of a patented strain (Patent No. ZL 2015 1 0551645.9) obtained from the Hubei Huada Real Technology Co., Ltd. (Wuhan, China). Both the horseradish peroxidase (HRP)-conjugated goat anti-rabbit IgG and the rabbit β-Actin mAb antibody were purchased from ABclonal (Wuhan, China). Rabbit mAbs against FASN were purchased from the Hangzhou HuaAn Biotechnology Co., Ltd. (Hangzhou, China).

Extraction and analysis of metabolites of fermentation supernatant and exopolysaccharides of B.A-TL

The metabolomics analysis of B.A-TL fermentation supernatant (FST) was performed by liquid chromatography with tandem mass spectrometry (LC-MS/MS). The B.A-TL was transferred from petri dishes to LB medium and incubated at 37°C for 12 h. Then, a 5 mL seed medium was inoculated into a 500 mL sterile seed medium and cultured at 37°C and 180 rpm for 24 h to generate the FST.

A total of 5 mL seed medium was inoculated into a 500 mL sterile seed medium, cultured at 37°C and 180 rpm for 72 h. After fermentation, the broth was centrifuged at 8,000 rpm for 15 min to extract exopolysaccharides (EPS) for 12 h at 4°C under various pH values with 60–90% ethanol. The precipitate was collected by filtration and then dissolved in distilled water. After the removal of proteins by Sevag reagent, the polysaccharide was dialyzed using a dialysis bag (molecular weight cutoff =

7 kDa; Beijing Solarbio Technology Co., Ltd., Beijing, China) extensively against distilled water for 72 h and then lyophilized.

The FST sample (20 mL) was frozen into powder, dissolved with 10 mL of methanol solution, shaken to mix for 1 min, then centrifuged at 12,000 rpm and 4°C for 10 min, and with the supernatant transferred to a new centrifuge tube. Samples were vacuum dried to concentrate, then dissolved with 2-chlorobenzalanine (4 ppm) and 80% methanol solution and filtered through 0.22 μm membrane for the liquid chromatography and mass spectrometry (LC-MS) analysis (UltiMate 3000 and Q Exactive Focus, Thermo Fisher, Waltham, MA, USA). A total of 20 μL of each sample was used as the quality control, while the rest of each sample was used for LC-MS analysis.

The EPS sample of 5 mg (±0.05 mg) was added to a clean chromatography bottle with configured TFA acid solution, heated for 2 h at 121°C, and blow-dried with nitrogen. Then, the sample was cleaned with methanol, blow-dried again, and repeated twice. Finally, the sample was dissolved in aseptic water and transferred to the chromatography bottle for testing using the Thermo ICS5000 plus ion chromatography system (Thermo Fisher, Waltham, MA, USA) and the DynexTM CarboPacTM PA10 liquid chromatography column (250 × 4.0 mm, 10 μm) with a sample size of 5 μL, flow phase A (H_2O), and flow phase B (100 mM NaOH).

Laboratory animals

The present study was performed in strict accordance with the Guide for the Care and Use of Laboratory Animals Monitoring Committee of Hubei Province, China, with the protocol approved by the Committee on the Ethics of Animal Experiments of the College of Veterinary Medicine, Huazhong Agricultural University (approval No. HZAUCH-2020-0009). All chickens were reared in cages. A total of 108 3-day-old male Cobb broiler chickens were randomly and evenly divided into two groups, i.e., the control and the B.A-TL treatment groups, with six pens (9 chickens per pen) in each group. Chickens in the control group were fed with a basal diet (no drugs or additives added) and the B.A-TL group was fed with grain containing B.A-TL (4×10^6 CFU/g) for 21 days. The B.A-TL was added to the feed in the form of dry powder at a concentration of 200 g/ton and an effective viable number of 2×10^{10} CFU/g (Hong et al., 2019, 2021), as recommended by the manufacturer's instructions. Our previous studies have shown that the probiotics of B.A-TL were the most effective in promoting growth in broilers over a 21-day growth period (Hong et al., 2019, 2021).

The chicken coop, where the pens were housed, and the surrounding areas were thoroughly disinfected before the trial started, with the temperature of the chicken coop maintained at ∼33°C until the chickens were 7 days old. Then, the temperature was gradually reduced to and finally maintained at 23°C. All chickens were free to feed and drink and were weighed once a week with no antibiotics used during the entire experiment. Feed consumption by chickens in both groups was recorded daily. The broiler pellet feed formulation and nutrient compositions are provided in Supplementary Table 1.

Tissue sampling

A total of six chickens were sampled from each of the control and the B.A-TL groups on day 21, i.e., for a total of 12 chickens, with the pen number and weight of each individual chicken recorded before slaughter. The most representative chicken was selected based on the median weight of each pen for the liver transcriptomic analysis and the representative data were applied to predict the molecular patterns in the entire population (Supplementary Table 2). Blood samples (∼3 mL in each of the 2 tubes for each chicken) were taken from the wing vein, collected into the vacuum blood collection tubes, and centrifuged at 3,000 rpm and 4°C to obtain the serum sample. The chickens were euthanized with the liver tissues collected immediately for further analyses. One-half of the liver tissue was washed with phosphate buffer solution (PBS 0.01M pH 7.4; Biosharp Co., Ltd., Hefei, China), snap-frozen in liquid nitrogen, and stored at −80°C for further mRNA expression analysis. Simultaneously, the other half of the liver tissue was immediately fixed in 4% paraformaldehyde (Biosharp Co., Ltd., Hefei, China) for subsequent morphological analysis.

Serum analysis

The contents of glucose (GLU), triglycerides (TG), cholesterol (CHO), alanine aminotransferase (ALT), and aspartate aminotransferase (AST) were measured by a BK-280 automatic biochemical analyzer (Shandong Blobase Biotechnology Co., Ltd., Shandong, China). The contents of INS, GH, IGF-1, very low-density lipoprotein (VLDL), malondialdehyde (MDA), catalase (CAT), superoxide dismutase (SOD), total antioxidant capacity (T-AOC), and glutathione peroxidase (GSH-Px) were measured using the enzyme-linked immunosorbent assay (ELISA) kits (Wuhan Meimian Biotechnology Co., Ltd., Wuhan, China). All experiments were performed in strict accordance with the protocols and instructions recommended by the manufacturers.

Hematoxylin and eosin staining and oil red O staining

Liver samples were embedded in paraffin, sectioned (3-μm thickness), stained with hematoxylin and eosin (HE) for panoramic scanning, and imaged with a Panoramic MIDI slide scanner (3D HISTECH Co., Ltd., Budapest, Hungary). According to a previous protocol (Pinterić et al., 2020), 0.5% Oil Red O solution (Sigma Aldrich, St. Louis, MO, USA) was prepared. Tissues were embedded in Optimal Cutting Temperature medium (CRYOSTAR NX50, Thermo Fisher Scientific, Waltham, MA, USA), sectioned (8-μm thickness), air-dried for 1 h, and fixed in 10% formaldehyde for 5 min. The LMH cells (70–80% confluent) cultured on the six-well plates were stimulated by FST (10^{-4}), EPS (0.1 mg/mL), and L-Tyr (0.25 mmol/L) for 4 h, respectively, and washed thrice with PBS, and fixed in 10% formaldehyde for 30 min. All samples were briefly stained with 60% isopropanol, Oil Red O dye for 15 min, rinsed with 60% isopropanol, and incubated in ddH_2O for 5 min, then stained with Mayer hematoxylin (Wuhan Baichan Biotechnology Co., Ltd., Wuhan, China) for 1 min, washed with tap water and ddH_2O, and finally mounted in aqueous mounting solution (Wuhan Baichan Biotechnology Co., Ltd., Wuhan, China). Images were obtained using an Axiovert 40 CFL microscope (Olympus, Tokyo, Japan) and analyzed using Image-Pro plus 6.0 (Media Cybernetics, Rockville, MD, USA). All experiments were performed in triplicates.

RNA extraction, library preparation, and sequencing

Total RNA was extracted from the liver tissue using RNApure Tissue and Cell Kit according to the manufacturer's instructions (Cowin Biotech Co., Ltd., Taizhou, China). RNA concentration and quality were determined by NanoDrop 2000c (Thermo Fisher, Waltham, MA, USA). RNA samples (each of 1 μg) with high quality (i.e., based on $OD_{260/280}$ ratio $= 1.8\sim2.2$, $OD_{260/230}$ ratio ≥ 2.0, RIN ≥ 6.5, 28S:18S ratio ≥ 1.0, and weighed more than 1 μg) were submitted to Shanghai Majorbio Bio-pharm Technology Co., Ltd. (Shanghai, China) to construct RNA-Seq transcriptomic library using the TruSeq™ RNA sample preparation Kit from Illumina (San Diego, CA, USA). The mRNAs were isolated according to the polyA selection method by oligo(dT) beads and then fragmented by fragmentation buffer. Then, the double-stranded cDNA was synthesized using the SuperScript double-stranded cDNA synthesis kit (Invitrogen, CA, USA) with random hexamer primers (Illumina, CA, USA). The synthesized cDNA was subjected to end-repair, phosphorylation, and "A" base addition according to Illumina's library construction protocol. Libraries were size selected for cDNA target fragments of 300 bp on 2% low-range ultra agarose followed by PCR amplification of 15 cycles using Phusion DNA polymerase (NEB, Beijing, China). After quantified by TBS380, the paired-end RNA-Seq library was sequenced with the Illumina HiSeq xten/NovaSeq 6000 sequencer (with 2 × 150 bp read length).

RNA-Seq read mapping

The raw paired-end reads were trimmed, and quality controlled by SeqPrep and Sickle with default parameters. The clean reads of control and experimental groups were separately aligned to the reference genome with orientation mode using HISAT2 (Kim et al., 2015). The mapped reads of each sample were assembled by StringTie using a reference-based approach (Pertea et al., 2015).

Differential expression analysis and functional enrichment analysis

To identify the DEGs between two different samples, the expression level of each transcript was calculated according to the transcripts per million reads (TPM) method. RSEM (Li and Dewey, 2011) was used to quantify gene abundances. The differential expression analysis was performed using the DESeq2 (Love et al., 2014) with Q value ≤ 0.05. DEGs were identified based on fold change > 2 or < -2 and Q value ≤ 0.05. Functional enrichment analysis based on Gene Ontology (GO) and Kyoto Encyclopedia of Genes and Genomes (KEGG) databases were performed by Goatools and KOBAS, respectively (Xie et al., 2011), to identify the DEGs significantly enriched in GO terms and KEGG metabolic pathways based on the Bonferroni-corrected p-value ≤ 0.05 compared with the background of the entire transcriptome.

Quantitative real-time polymerase chain reaction analysis

In the validation experiments based on qRT-PCR analysis, a total of 12 genes were randomly selected to assess the reliability of RNA-Seq data (Supplementary Table 3). The RNA sample of 1 μg was reverse-transcribed into cDNA using the PrimeScript™ RT Reagent Kit with gDNA Eraser (TaKaRa, Dalian, China) according to the manufacturer's instructions. The cDNA was diluted 10-fold and used for qRT-PCR analyses with a Bio-Rad CFX96TM System and signal detection protocols in accordance with the manufacturer's instructions (TaKaRa, Dalian, China). The qRT-PCR experiments were performed in three replicates with the *β-Actin* used as the endogenous control and the expression of individual genes normalized to that of *β-Actin*

(Xiang et al., 2017). Primers used for qRT-PCR experiments are shown in Supplementary Table 3.

CCK8 cell viability and proliferation assays

The LMH cells (stored in the Microbiology and Immunology Laboratory of Huazhong Agricultural University, Wuhan, China) were cultured in Dulbecco's Modified Eagle Medium/Nutrient Mixture F-12 (DMEM/F12; Gibco, Waltham, MA, USA) supplemented with 10% fetal bovine serum (FBS; Gibco, Waltham, MA, USA). A total of 100 μL of the diluted cell culture was added into each well of a 96-well cell culture cluster (Biosharp Co., Ltd., Hefei, China), cultured for 12 h in DMEM/F12 at 37°C to achieve 70% of the cells of the full monolayer and then starved for 12 h in DMEM/F12 without FBS at 37°C. The cell cultures were washed with 100 μL PBS before the treatment with 100 μL DMEM/F12 containing FST (10^{-3}, 10^{-4}, 10^{-5}, and 10^{-6}, respectively), EPS (0.01, 0.1, 1, and 5 mg/mL, respectively), and L-Tyr (0.1, 0.25, 0.5, 0.75, and 1 mmol/L, respectively) for 2, 4, 8, and 12 h, respectively, while the control was treated with 100 μL DMEM/F12. Finally, the 10 μL Cell Counting Kit-8 (CCK8, Dojindo Molecular Technologies, Inc., USA) was added to the cell cultures and incubated for 1 h. The OD at 450 nm of the cultures was measured using a MULTISKAN MK3 (Thermo Electron Corporation, Waltham, MA, USA).

Cell RNA preparation and qRT-PCR analysis

The LMH cells (70–80% confluence) were stimulated with FST (10^{-4}), EPS (0.1 mg/mL), and L-Tyr (0.25 mmol/L), respectively. Total RNA was extracted using the Ultrapure RNA Kit (CW0581M, CoWin Biosciences, Beijing, China) and the reverse transcription reaction was performed using PrimeScript™ RT Reagent Kit with gDNA Eraser (TaKaRa, Dalian, China) following the manufacturer's protocol. After mixing the extracted RNA with ChamQ Universal SYBR qPCR Master Mix (Q711-02/03, Vazyme Biotech Co., Ltd., Nanjing, China) and specific primers, the qRT-PCR analyses were performed on a CFX96TM (Bio-Rad, Richmond, CA, USA). Primers used for the qRT-PCR analysis (Han et al., 2015) are shown in Supplementary Table 4.

Western blotting

The LMH cells (70–80% confluence) were stimulated with FST (10^{-4}), EPS (0.1 mg/mL), and L-Tyr (0.25 mmol/L), respectively. Cells were washed twice with PBS and incubated on ice with RIPA Lysis Buffer (Beyotime, Shanghai, China) containing a protease inhibitor cocktail (Roche, Basel, Switzerland). The cell lysates were separated with sodium dodecyl sulfate-polyacrylamide gel electrophoresis (SDS-PAGE) of 7.5% gel. The proteins were then transfer-embedded onto a polyvinylidene difluoride membrane (Bio-Rad, Richmond, CA, USA), which was blocked with TBST containing 5% skim milk (BD, San Jose, CA, USA) for 1 h and then incubated with the primary antibody overnight at 4°C, followed by the incubation with corresponding HRP-conjugated secondary antibody for 1 h. The antibodies used in the western blotting experiments included anti-FASN (1:1,000) and anti-β-Actin (1:10,000). β-Actin was employed as the loading standard. The protein bands were quantified with the ImageJ software. All western blotting analyses were performed as previously described (Guo et al., 2016).

Signaling pathway inhibition assays

The LMH cells (70–80% confluence) were treated with pathway inhibitor picropodophyllin (2.5 μM; MedChemexpress, NJ, USA) for 1 h and then either LY294002 (10 nM; MedChemexpress, NJ, USA) or PD98059 (10 nM; MedChemexpress, NJ, USA) for 24 h before being stimulated with FST (10^{-4}), EPS (0.1 mg/mL), and L-Tyr (0.25 mmol/L), respectively. The cells were harvested at the indicated time points (4 h) for RNA and protein extractions. The qRT-PCR was performed to detect the expression of specified genes (i.e., *FASN*, *ACCα*, *SREBP1*, *SCD1*, *LXRα*, *LPIN1*, *CPT1A*, *PPARα*, and *ACOX1*) (Han et al., 2015). Western blotting assays were performed to evaluate the expression of specified proteins (i.e., β-Actin and FASN).

Statistical analysis

Significant differences were determined with Student's *t*-test using GraphPad Prism 8.0 (GraphPad Software, Inc., San Diego, CA, USA). Unless indicated, data were shown as mean ± standard error of the mean (SEM). The significance levels for all statistical analyses were set to $p < 0.05$ (*), $p < 0.01$ (**), and $p < 0.001$ (***), respectively.

Results

Analysis of FST and EPS

The results of the metabolomics studies of B.A-TL FST showed that a total of 312 types of metabolites

TABLE 1 Effects of *Bacillus amyloliquefaciens* TL on the growth performance of broilers in the control and experimental groups.

Item	Time	Control group	B.A-TL group	*p*-value
Average body weight (g)	Initial	63.17 ± 0.09	63.20 ± 0.12	0.8050
	Week 1	175.40 ± 2.85^{b}	185.30 ± 1.87^{a}	0.0128
	Week 2	333.10 ± 6.62^{b}	363.50 ± 6.57^{a}	0.0117
	Week 3	696.80 ± 16.24^{B}	787.10 ± 15.29^{A}	< 0.001
Average daily gain (g)	Week 1	15.78 ± 0.43^{b}	17.12 ± 0.40^{a}	0.0385
	Week 2	22.79 ± 0.61^{B}	25.79 ± 0.62^{A}	0.0040
	Week 3	51.94 ± 2.48^{b}	60.51 ± 2.46^{a}	0.0280
Feed conversion ratio	Overall	1.84 ± 0.02^{A}	1.70 ± 0.03^{B}	0.0035

Data are expressed as mean ± SEM (n = 54 chickens per group). Means within a row with different superscripts differ significantly at $p < 0.01$ (A or B) and $p < 0.05$ (a or b), respectively.

TABLE 2 Effects of *Bacillus amyloliquefaciens* TL on the levels of serum biochemical indices in broilers at 21 days of age in both the control and experimental groups.

Biochemical index	Control group	B.A-TL group	*p*-value
INS (mL/L)	5.14 ± 0.24	5.58 ± 0.30	0.2830
GH (μg/L)	10.28 ± 0.20	10.04 ± 0.30	0.5260
IGF-1 (μg/L)	23.41 ± 0.35^{b}	27.04 ± 1.36^{a}	0.0275
GLU (mmol/L)	13.00 ± 0.55^{B}	17.67 ± 1.19^{A}	0.0051
TG (mmol/L)	0.37 ± 0.01^{b}	0.50 ± 0.052^{a}	0.0175
CHO (mmol/L)	4.09 ± 0.13	4.15 ± 0.27	0.9090
VLDL (mmol/L)	9.86 ± 1.73	9.94 ± 1.36	0.9725
ALT (U/L)	7.22 ± 0.48^{b}	13.22 ± 2.14^{a}	0.0211
AST (U/L)	341.10 ± 27.17	290.90 ± 3.98	0.1312
MDA (nmol/mL)	63.75 ± 9.16^{A}	23.50 ± 6.64^{B}	0.0081
CAT (U/mL)	1.72 ± 0.39^{b}	3.92 ± 0.67^{a}	0.0159
SOD (U/mL)	19.74 ± 0.14^{B}	20.89 ± 0.17^{A}	0.0004
T-AOC (U/mL)	0.16 ± 0.07^{B}	0.59 ± 0.08^{A}	0.0021
GSH-Px (μmol/L)	269.50 ± 29.20	277.80 ± 25.86	0.8360

Data are expressed as mean ± SEM (n = 6 chickens per group). Means within a row with different superscripts differ significantly at $p < 0.01$ (A or B) and $p < 0.05$ (a or b), respectively.

(Supplementary Table 5) were obtained and annotated in the samples with L-Tyr showing the highest content (29.02%) among all the identified components (supplementary figure 1C). Based on these results, L-Tyr was selected as the stimulant used in the following tests.

The EPS were acidified into monosaccharides with the monosaccharide compositions detected with an electrochemical detector (Supplementary Figure 2). The results showed that the EPS of B.A-TL contained mainly six types of sugars (Supplementary Table 6) with mannose, GLU, and galactose together accounting for 98.27% of the total EPS (Supplementary Figure 2B).

Growth performance

The average body weight (ABW), average daily gain (ADG) and overall feed conversion ratio (FCR) in broilers are shown in Table 1. The ABWs and ADGs of the B.A-TL group were significantly higher than those of the control group at 7, 14, and 21 days with the most significant difference in ABW observed at 21 days ($p < 0.001$), while the overall FCR ($p < 0.01$) of broilers in the B.A-TL group was lower than that in the control group.

Serum analysis

The results of the serum biochemical indices of Cobb broiler chickens treated with B.A-TL are shown in Table 2. No significant changes were observed in the contents of INS, GH, CHO, VLDL, AST, and GSH-Px between the B.A-TL and the control groups, while the other eight indices showed significant differences between the control and experimental groups. For example, in the B.A-TL group, the contents of GLU, IGF-1, and TG were increased by 35.92 ($p < 0.001$), 15.51 ($p < 0.05$), and 31.19% ($p < 0.01$), respectively, while the content of MDA was decreased by 63.15%, compared with those of the control group.

HE staining and oil red O staining

The observations of HE-stained sections showed that the liver tissue was not damaged by B.A-TL (Supplementary Figure 3). The results of the liver Oil Red O staining showed that the percentage of lipid droplets in the liver of broilers in the B.A-TL group was significantly higher than that in the control group ($p < 0.001$; Figure 1), indicating that B.A-TL accelerated the liver fat metabolism and promoted fat deposition in the liver tissue of the broiler chickens. The results of cellular Oil Red O staining (Figure 2) showed a significant increase in the percentage of lipid droplets in the FST ($p < 0.001$) and Tyr ($p < 0.05$) groups and a significant decrease in the EPS ($p < 0.05$) group, indicating that some metabolites of B.A-TL (i.e., FST and Tyr) could enhance the lipid synthesis activity of LMH cells and promote lipid droplet formation.

Transcriptome analysis

The results of transcriptomics analysis based on the 11 liver samples (6 in control and 5 in experimental groups; the sample TL6 was removed due to its significant deviation

10.3389/fmicb.2022.958112

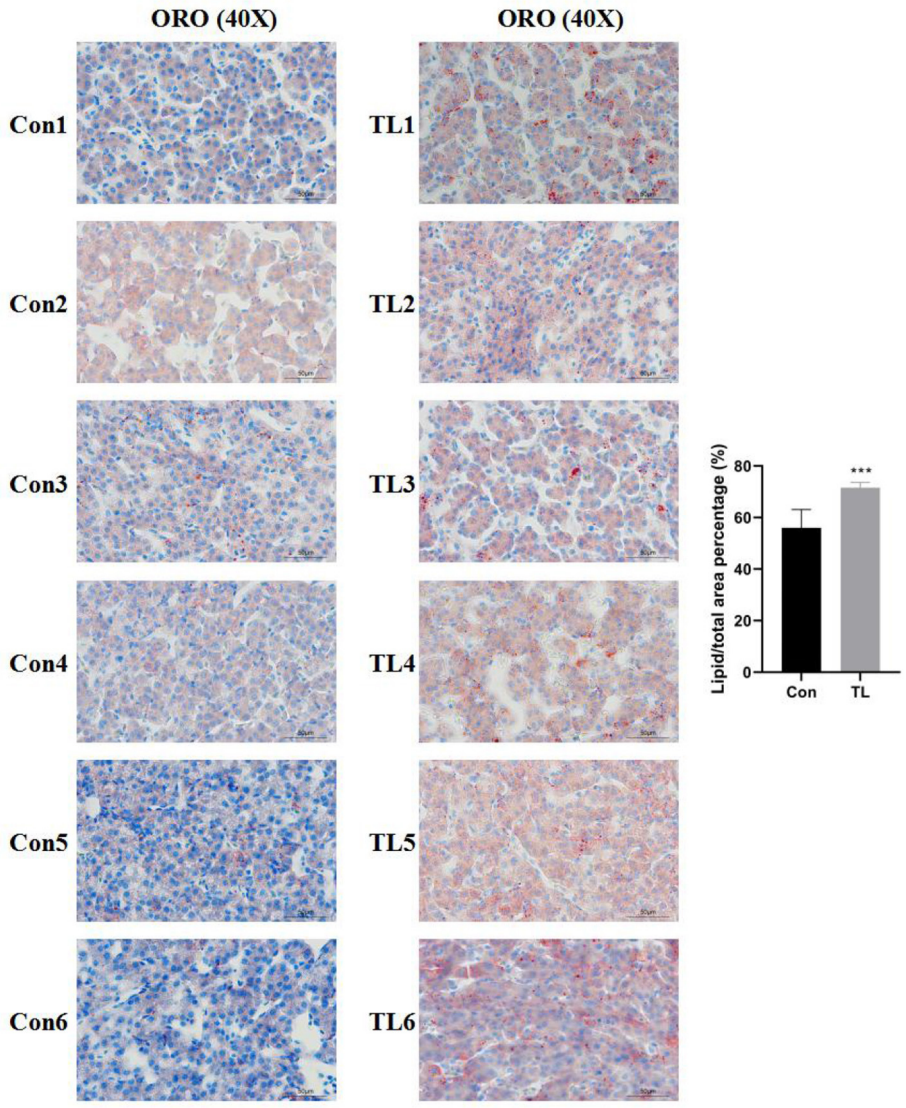

FIGURE 1
The liver tissues stained with Oil Red O of broilers in the control and experimental groups at 21 days of age. "Con" = control group; "TL" = Bacillus amyloliquefaciens TL experimental group. The significance level for all analyses is set to $p < 0.001$ (***).

from other samples) showed that after the removal of low-quality data, a total of 6.83–10.38 Gb of clean data were obtained for further analyses (Supplementary Table 7). The high Pearson correlation coefficients (R^2) of the biological repeats in the control and B.A-TL groups (Supplementary Figure 4A) indicated that the RNA-Seq data were suitable for subsequent analyses. The transcriptome profiles of the liver tissues from the B.A-TL group were clearly separated from those of the control group based on the principal component analysis (PCA; Supplementary Figure 4B).

Functional annotations of differentially expressed genes identified in the liver tissue of broilers

A total of 358 DEGs ($p < 0.05$) were identified in the liver with 145 upregulated (40.50%) and 213 downregulated (59.50%) in the B.A-TL group (Supplementary Table 8), including four genes (i.e., *AMY2A*, *SI*, *PCK1*, and *FASN*) significantly upregulated ($p < 0.001$). The functions of these DEGs were further explored by the KEGG pathway enrichment analyses (Figures 3A,B). The results showed that the "calcium

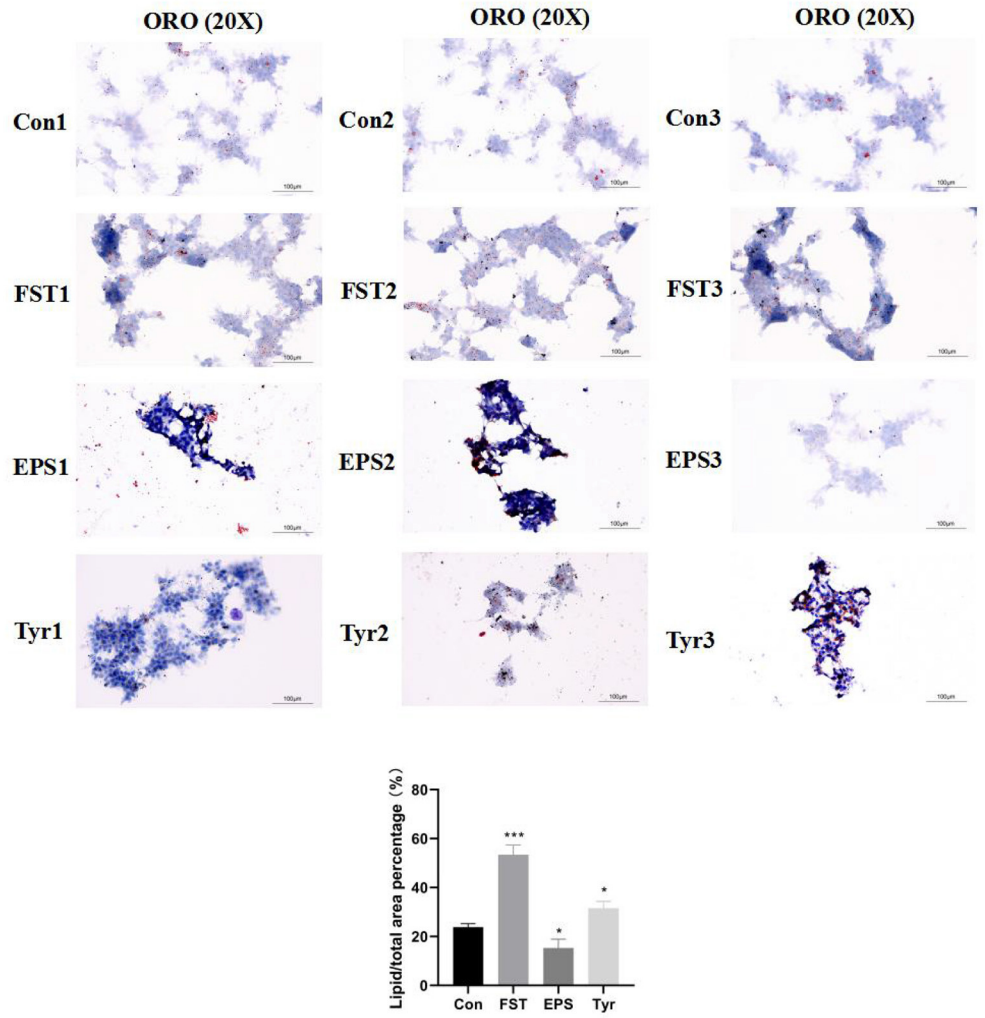

FIGURE 2
The Oil Red O staining of the LMH cells treated with Bacillus amyloliquefaciens TL fermentation supernatant, exopolysaccharide, and L-tyrosine, respectively. "Con" = control group; "FST" = fermentation supernatant group; "EPS" = exopolysaccharides group; "Tyr" = L-tyrosine group. The significance levels for all analyses were set at $p < 0.05$ (*), and $p < 0.001$ (***), respectively.

signaling pathway" was the most significantly enriched by the downregulated DEGs between the control and experimental groups, while the upregulated DEGs were significantly enriched in the metabolic pathways of "carbohydrate digestion and absorption," "starch and sucrose metabolism," and "PI3K-AKT signaling pathway" (Table 3).

Advanced transcriptome analysis of FASN

Results of the correlation analysis showed that *FASN* and FASN played critical roles in the broiler liver of the B.A-TL group (Figures 4A,B; Supplementary Tables 9A,B), closely correlated with the expression of 36 ($p < 0.05$) out of 358 DEGs and establishing interactions with a total of 7 proteins ($p < 0.05$), respectively. These complex network relationships and the strong connections (i.e., large nodes) of both *FASN* and FASN indicated the significant importance of both *FASN* and FASN in these networks. Therefore, we further investigated the expression changes of both *FASN* and FASN in cellular experiments (below).

Verification of gene expression patterns based on RNA-Seq by qRT-PCR analysis

To validate the DEGs identified in the liver tissue between the control and the experimental groups based on the RNA-Seq, a total of 12 DEGs ($p < 0.05$; Supplementary Table 3)

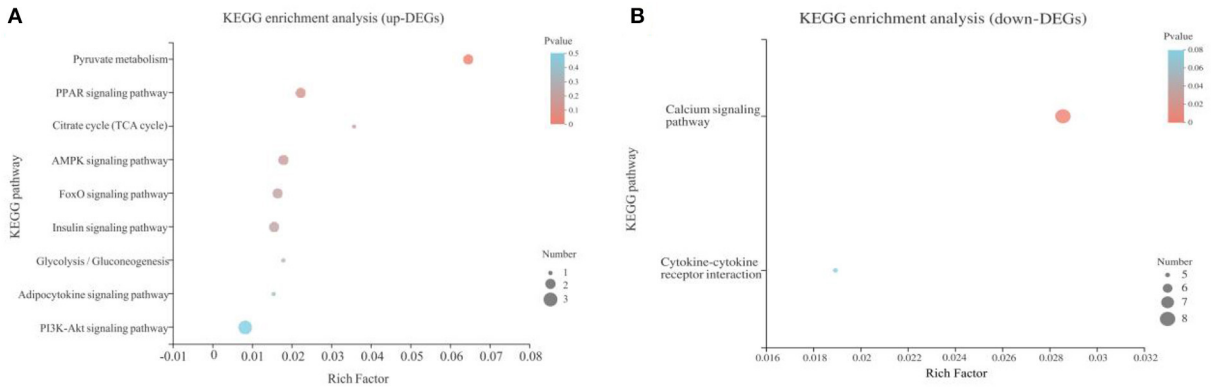

FIGURE 3
Functional annotation of differentially expressed genes (DEGs) identified in *Bacillus amyloliquefaciens* TL group of broilers in comparison to the control group. **(A)** Kyoto Encyclopedia of Genes and Genomes (KEGG) pathway enrichment analysis of upregulated DEGs. **(B)** KEGG pathway enrichment analysis of downregulated DEGs. The vertical axis represents the name of the pathways, and the horizontal axis represents the Rich factor. The size of the color dot proportionally indicates the number of DEGs enriched in the pathway, while the color dot corresponds to the Q value range.

were randomly selected for qRT-PCR verification. The results of both qRT-PCR and RNA-Seq analyses were consistent, showing similar trends of upregulation and downregulation, thereby validating the RNA-Seq results (Supplementary Figure 5).

Effects of FST, EPS, and Tyr on the viability and proliferation of LMH cells

The effects of FST, EPS, and Tyr on LMH cell proliferation are shown in Figure 5. The results showed that LMH cell proliferation was significantly enhanced by the treatments of FST, EPS, and Tyr with various concentrations and lengths of treatment time. The optimum conditions were observed at 10^{-4} FST ($p < 0.001$), 0.1 mg/mL EPS ($p < 0.01$), and 0.25 mmol/L Tyr ($p < 0.01$) for 4 h, respectively.

Effects of FST, EPS, and Tyr on the IGF-1 level of LMH cells

Treatments of LMH cells with 10^{-4} FST ($p < 0.05$) and 0.25 mmol/L Tyr ($p < 0.001$) for 4 h, respectively, significantly increased the IGF-1 secretion in LMH cells, while 0.1 mg/mL EPS ($p < 0.05$) significantly decreased the IGF-1 secretion in LMH cells, suggesting that some metabolites of B.A-TL regulated the IGF-1 secretion in liver cells, ultimately affecting the metabolic activities in the bodies of broilers (Figure 6).

TABLE 3 Kyoto Encyclopedia of Genes and Genomes (KEGG) pathway enrichment analysis of differentially expressed genes (DEGs) identified in the *Bacillus amyloliquefaciens* TL group of broilers.

DEGs	*p*-value	Number of gene	KEGG Pathway
Up-regulated		15	
CACNA1D, AMY2A, SI	0.002235	3	Carbohydrate digestion and absorption
LOC101750607, AMY2A, SI	0.002982	3	Starch and sucrose metabolism
PCK1, CDKN1A, HSP90AA1	0.463672	3	PI3K-AKT signaling pathway
PCK1, FASN	0.222832	2	Insulin signaling pathway
PCK1, FASN	0.180216	2	AMPK signaling pathway
FASN	0.117013	1	Fatty acid biosynthesis
PCK1	0.362511	1	Adipocytokine signaling pathway
Down-regulated		13	
PLCD4, GRIN2A, DRD5, P2RX7, CAMK1D, PGR2/3, LOC121109428, LOC121112155	0.002702	8	Calcium signaling pathway
CCR8L, TNFSF11, GDF7, GDF9, LOC121112225	0.075272	5	Cytokine-cytokine receptor interaction

FST, EPS, and Tyr stimulate lipid metabolism in LMH cells

Results of the relative expression levels of genes involved in fat metabolism showed that the B.A-TL metabolites of different

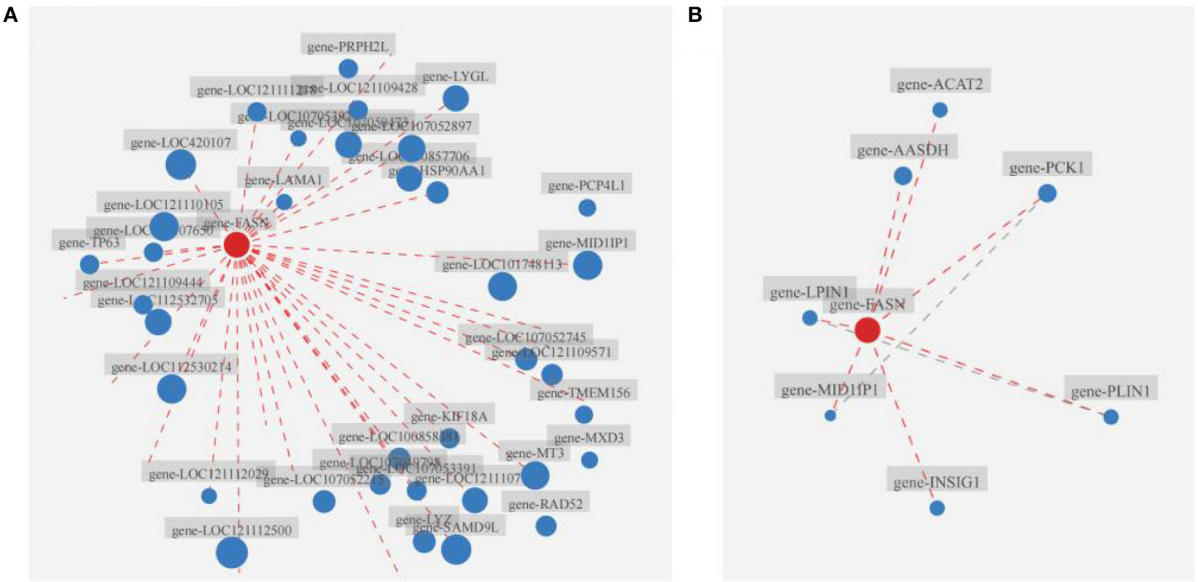

FIGURE 4
Correlation analysis of *FASN* with other genes and the relationships between FASN and other proteins. **(A)** Correlation analysis of *FASN* with other genes. **(B)** Interaction analysis of FASN with other proteins. Nodes (i.e., red and blue dots) indicate genes/transcripts, and dashed lines indicate the existence of the reciprocal relationship between two genes/transcripts. The size of a node is proportional to its connectivity (i.e., degree), i.e., the more edges connected to the node, the larger degree the node is, indicating the greater importance of the gene/transcript in the network.

components either upregulated or downregulated the genes involved in adipogenesis and fatty acid oxidation, indicating that B.A-TL affected the lipid metabolic activities, i.e., lipid synthesis and decomposition (Figures 7A,B). For example, FST significantly increased the expression of three adipogenesis genes ($p < 0.05$), i.e., *FASN*, *ACCα*, and *SCD1*, while the expressions of the fatty acid oxidation genes (e.g., *LPIN* and *ACOX*) were either upregulated or downregulated. It was noted that no significant changes were observed in the expression levels of *PPARα* in both control and experimental groups. Results showed that both FST ($p < 0.001$) and Tyr ($p < 0.05$) of B.A-TL enhanced the expression of FASN in LMH cells, while EPS inhibited the expression of FASN ($p < 0.01$; Figure 8). Therefore, it was speculated that the promotion of fat synthesis by B.A-TL was likely due to the enhanced expression of FASN in hepatocytes stimulated by metabolites of both FST and Tyr.

To verify the regulation of lipid metabolism by B.A-TL with the involvements of RTKs and their downstream signaling pathways, the lipid metabolism was evaluated in LMH cells treated with the metabolites of B.A-TL and IGF-1R signaling inhibitor, i.e., picropodophyllin (Figure 9). The results showed that compared to the inhibitor group, the inhibitory effect of inhibitors on *FASN* and *ACCα* was alleviated in all three experimental groups (i.e., FST, EPS, and Tyr) with *LPIN* downregulated ($p < 0.01$). *CPTA1* ($p < 0.05$) was downregulated in both FST and EPS groups, while both *PPARα* ($p < 0.05$) and *ACOX* ($p < 0.01$) were upregulated in the Tyr group. Furthermore, the expressions of *SREBP*, *SCD1*, and *LXRα* were not significantly altered between the control and experimental groups.

The effects of different stimulants on the protein expression level of FASN under the treatment of different inhibitors are shown in Figure 10. When the IGF-1R was blocked (Figure 10A), the inhibition of FASN by inhibitors was alleviated in both FST ($p < 0.01$) and Tyr ($p < 0.05$) groups. When the PI3K pathway was blocked (Figure 10B), the expression levels of FASN in all three groups ($p < 0.001$) of FST, EPS, and Tyr were decreased, indicating that the expression of FASN was mainly regulated by the PI3K pathway. Furthermore, when the MAPK pathway was blocked (Figure 10C), the expression of FASN in the FST group was not inhibited ($p < 0.01$) but was decreased in both EPS ($p < 0.001$) and Tyr ($p < 0.001$) groups, suggesting that there were other small molecules in the FST that played an important role in regulating the lipid metabolism. Further studies are needed to verify this speculation. These results suggested that the metabolite FST of B.A-TL mainly affected the PI3K pathway to regulate the expression of FASN, while Tyr played an important role in this regulation as well.

Overall, these results suggested that B.A-TL stimulated both the IGF-1 synthesis and the PI3K signaling pathway (i.e., the downstream of the IGF signaling pathway), promoted the FASN protein expression, and accelerated the lipid metabolism in liver tissue, ultimately promoting the fat deposition in broilers.

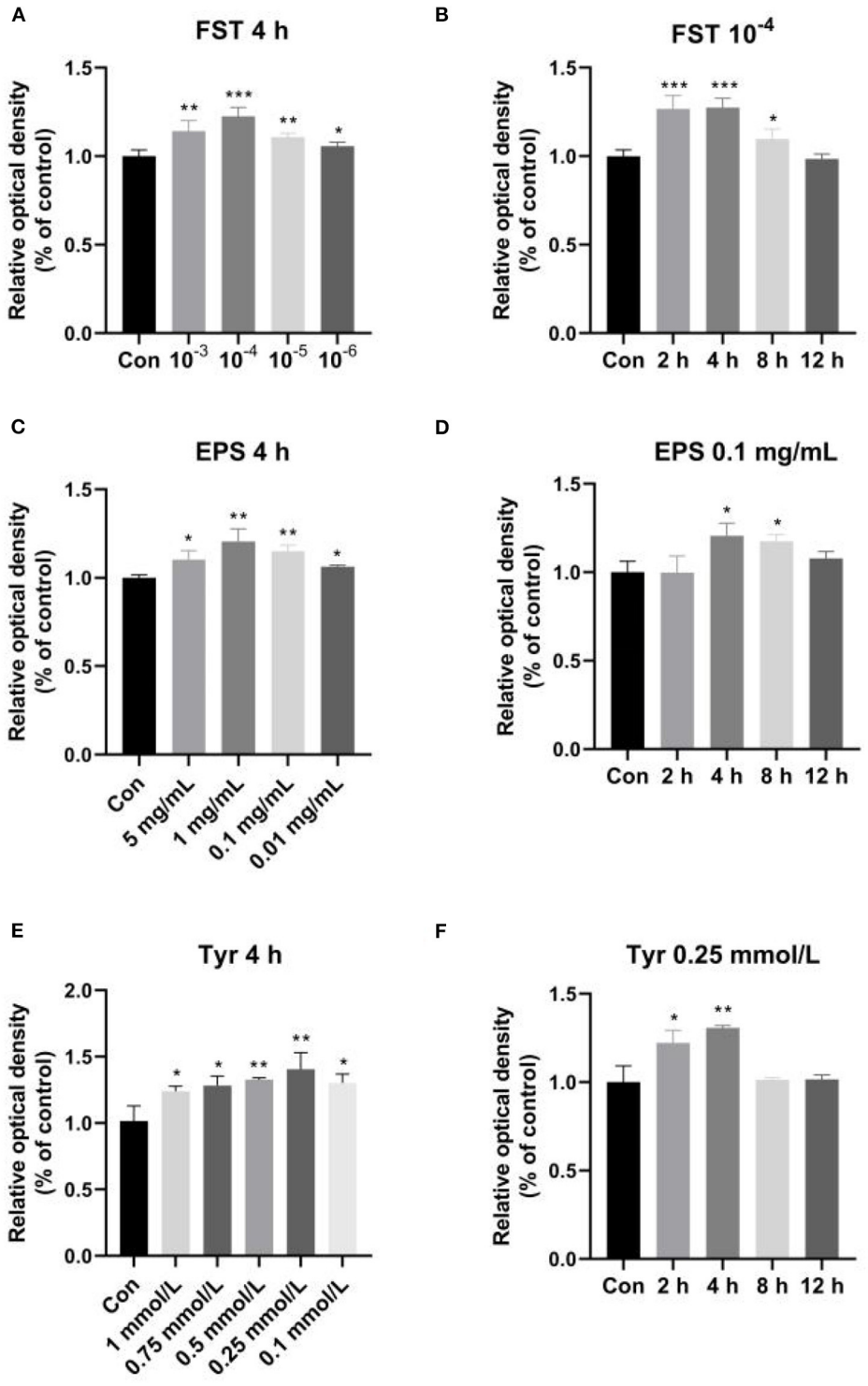

FIGURE 5
Effects of fermentation supernatant **(A,B)**, exopolysaccharides **(C,D)**, and L-tyrosine **(E,F)** of different concentrations with different lengths of treatment time on LMH cell proliferation. "Con" = control group; "'FST" = fermentation supernatant group; "EPS" = exopolysaccharides group; "Tyr" = L-tyrosine group. The significance levels for all analyses are set at $p < 0.05$ (*), $p < 0.01$ (**), and $p < 0.001$ (***), respectively.

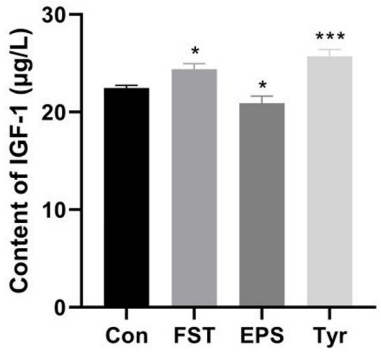

FIGURE 6
Effects of fermentation supernatant, exopolysaccharide, and L-tyrosine on the IGF-1 level of LMH cells. "Con" = control group; "FST" = fermentation supernatant group; "EPS" = exopolysaccharides group; "Tyr" = L-tyrosine group. The significance levels for all analyses are set at $p < 0.05$ (*), and $p < 0.001$ (***), respectively.

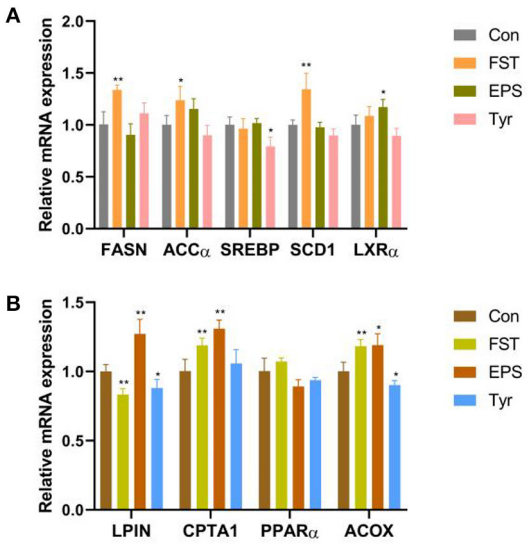

FIGURE 7
Relative mRNA levels of genes associated with fat synthesis (**A**) and fat oxidation (**B**) in LMH cells treated with fermentation supernatant, exopolysaccharide, and L-tyrosine, respectively. "Con" = control group; "FST" = fermentation supernatant group; "EPS" = exopolysaccharides group; "Tyr" = L-tyrosine group. The significance levels for all analyses are set at $p < 0.05$ (*), and $p < 0.01$ (***), respectively.

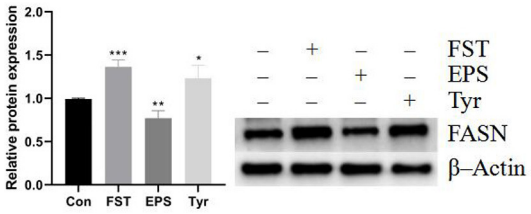

FIGURE 8
The FASN protein levels of LMH cells treated with fermentation supernatant, exopolysaccharide, and L-tyrosine, respectively. "Con" = control group; "FST" = fermentation supernatant group; "EPS" = exopolysaccharides group; "Tyr" = L-tyrosine group. FASN is used as a target protein; β-Actin is used as a loading standard. The significance levels for all analyses are set at $p < 0.05$ (*), $p < 0.01$ (**), and $p < 0.001$ (***), respectively.

Discussion

Variations of serum biochemical indices

It is well-known that serum parameters are reliable indicators of health status, reflecting many physiological, nutritional, and pathological changes in the organisms (Koronowicz et al., 2016). In general, the antioxidant enzymes, e.g., CAT, SOD, and T-AOC, are frequently used to assess oxidative damage and to scavenge excessive reactive oxygen species (ROS) from the body (Cecerska-Heryć et al., 2021). Furthermore, fast-growing commercial chickens are susceptible to high environmental temperatures due to their high growth rate (Habibian et al., 2016; Wan et al., 2018), while both oxidative and heat stresses could increase the ROS production and impair muscle quality in broilers (Wan et al., 2018). Numerous studies have shown that probiotics could improve both the antioxidant (Inatomi and Otomaru, 2018; Zhang et al., 2021) and heat stress resistance (Abd El-Hack et al., 2020; Wang et al., 2022) of the body. GLU is the main energy source (Gallenberger et al., 2012), while triglyceride represents another type of energy source (Pillutla et al., 2005). Total cholesterol is a building component of cell membranes (Zhang et al., 2019), while the VLDL is the principal vehicle for the transport of endogenous TG (Mason, 1998). The health status of the liver can be detected from the activity of liver enzymes, i.e., AST and ALT (Mollahosseini et al., 2017). Studies have shown that GH, IGF-1, and INS have significant growth-promoting and anabolic effects (Clayton et al., 2011). In our study, B.A-TL significantly improved the serum physiological indices in broilers, i.e., increasing the contents of CAT, SOD, and T-AOC, while the content of MDA was decreased. Although the ALT content was increased in the serum, no pathological lesions were observed in the livers of broiler chickens. Furthermore, the contents of IGF-1, GLU, and TG in the B.A-TL group were significantly higher than those of the control group, whereas no significant differences were observed in the contents of GH, INS, CHO, and VLDL between the control and the experimental groups. The high GLU content was consistent with the results reported previously, showing that B.A-TL reduced the lipid oxidation and glycolysis activities, suggesting that GLU anabolism (i.e., gluconeogenesis) was active in the B.A-TL group, as reported previously (Hong et al., 2021). The high TG content revealed

active lipid metabolism in the B.A-TL group. The results of our study evidently demonstrated that adding B.A-TL into the broiler diet could improve the ABW of the chickens, with the most significant effect observed on day 21, which was consistent with the results reported previously (Hong et al., 2019, 2021). Our results showed that B.A-TL enhanced both the synthesis of TG and the antioxidant and antistress capacities of the body, promoting the growth and improving the muscle quality of broilers.

Liver-derived IGF-1 was revealed with a negative feedback regulatory effect on the secretion of GH (Sjögren et al., 1999), suggesting that liver-derived IGF-1 would inhibit the secretion of GH. Interestingly, it was observed in our study that, without inhibiting the secretion of GH, the B.A-TL promoted the secretion of IGF-1 in the liver of broilers during the brooding period (i.e., younger than 21 days in age). Studies have shown that a large amount of IGF-1 was secreted into the circulation system to promote the rapid development of the muscle, fat, and other tissues, ultimately achieving a significant increase in body weight (Deng et al., 2017), while protein metabolism played a key role in the regulation of the mass of skeletal muscles (Deng et al., 2017; Yoshida and Delafontaine, 2020). Moreover, studies have shown that muscle growth is regulated by IGF-1 and GH *via* the GH/IGF-1 axis (Saleh et al., 2021). Our study showed that the content of IGF-1 in the B.A-TL group was increased by 15.5% compared with that in the control group ($p < 0.05$). These results were consistent with those reported previously, showing that the increased expressions of IGF-1 resulted in the enhanced growth performance of broilers (Deng et al., 2017).

Functions of probiotic metabolites of B.A-TL

Microbiota-derived metabolites include small molecules, such as amino acids, short-chain fatty acids (FAs) (Dong et al., 2019; Lavelle and Sokol, 2020), and biomolecules, such as peptides and polysaccharides (Kunishima et al., 2019; Hejdysz et al., 2020). It is worth noting that different microorganisms showed varied effects on the body weight, intestinal barrier, and biomolecule metabolism (Wieërs et al., 2020). Therefore, it is necessary to consider the metabolic effects of some bacteria as strain-specific (Wieërs et al., 2020). In our study, we extracted B.A-TL metabolites (i.e., FST) as well as isolated and purified EPS to perform the compositional assays of small molecules in the FST and EPS, and finally selected Tyr and extracellular polysaccharides for subsequent cellular assays. Tyr is a neutral amino acid involved in building essential proteins to provide energy (Dollins et al., 1995) and constitutes the precursor of the catecholamine neurotransmitters, norepinephrine, and dopamine (Lieberman et al., 2005) to effectively respond to acute stress (Lieberman et al., 2005) and enhance cognitive performance (Kühn et al., 2019). Our results showed that Tyr accounted for the highest proportion (29.02%) of the metabolites identified in B.A-TL. Chen et al. (2020) extracted the EPS of *Bacillus amyloliquefaciens* strain AMY-1 and found that the EPS may be involved in the hypoglycemic function of probiotics based on its regulation of blood GLU in mice, while the main components of EPS in strain AMY-1 identified by high-performance liquid chromatography, i.e., mannose, GLU, and galactose, were polymers larger than 1,000 kDa in molecular weight. Our results indicated that EPS of B.A-TL were composed mainly of six sugars, with mannose, GLU, and galactose together accounting for 98.27%, which were consistent with the main components of EPS in strain AMY-1. Furthermore, studies showed that the EPS of strain AMY-1 significantly reduced the blood GLU content of mice ($p < 0.001$) (Chen et al., 2020). Further studies are necessary to verify these explicitly shared regulatory functions of Tyr and EPS in chickens.

Functional analysis of the liver tissues based on enriched pathways in B.A-TL group

Starch is the most important nutrient in poultry diets (Svihus, 2014; Aderibigbe et al., 2020). On a dry matter basis, the poultry diets may contain up to 50% starch, which is the most important source of energy (Svihus, 2014). The enzymes involved in starch digestion include salivary amylase (AMY1), pancreatic amylase (AMY2), sucrase-isomaltase (SI), and maltase-glucoamylase (MGAM) (Brun et al., 2020; Wolever et al., 2021). Starch must be digested first to initiate a glycemic response, and then GLU is directly absorbed by the organisms. Therefore, differences in starch digestive enzymes may affect the rate and extent of starch digestion and change in the blood glucose levels in body, and consequently, affect the indicators of production performance (Svihus, 2014; Wolever et al., 2021). Studies have shown that the endogenous amylase secretion in broilers is not ideal for the complete digestion of dietary starch (Schramm et al., 2021). However, the prominent digestibility of native starch in chickens compared to other species, such as pigs may be due to the high secretion of amylase induced by the pancreatic juice of chickens (Svihus, 2014), thus increasing the level of amylase to enhance the starch digestion. In our study, it was clearly observed that the serum GLU content of B.A-TL group was significantly increased by 35.92% compared to the control group. Furthermore, the transcriptome results showed that the expressions of genes encoding AMY2A and SI were significantly upregulated, indicating that the increase in serum GLU was associated with the enhanced expression of these two enzymes, while the B.A-TL enhanced the digestion of the body and absorption of starch, ultimately significantly contributing to the fat synthesis in broilers.

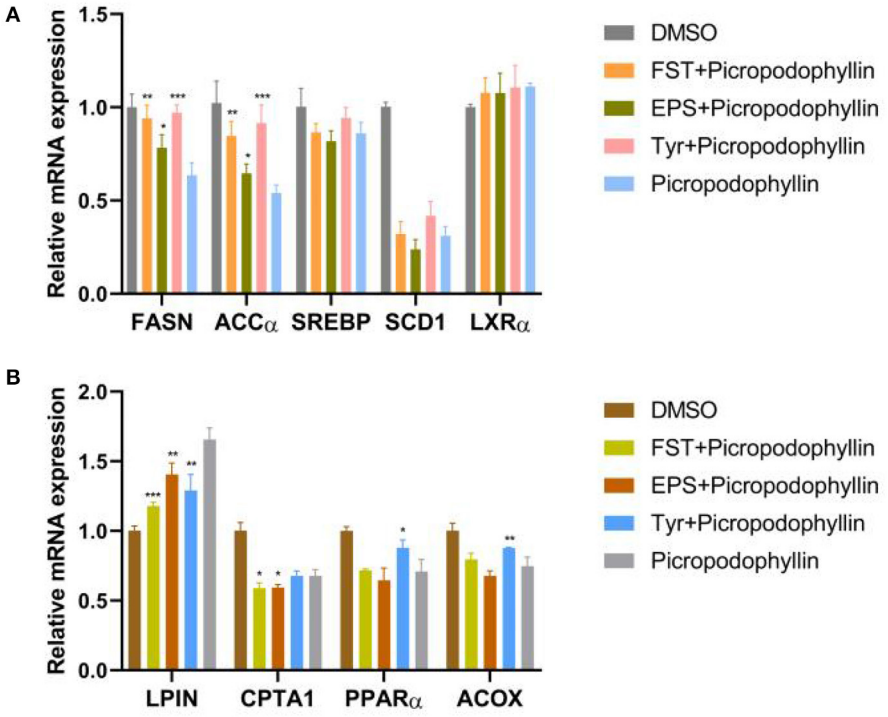

FIGURE 9
Relative mRNA levels of genes associated with fat synthesis **(A)** and fat oxidation **(B)** in LMH cells treated with fermentation supernatant and IGF-1R signaling inhibitor (i.e., picropodophyllin), exopolysaccharide and picropodophyllin, and L-tyrosine and picropodophyllin, respectively. DMSO is used as a toxicity control. "Con" = control group; "FST" = fermentation supernatant group; "EPS" = exopolysaccharides group; "Tyr" = L-tyrosine group. The significance levels for all analyses are set at $p < 0.05$ (*), $p < 0.01$ (**), and $p < 0.001$ (***), respectively.

Gluconeogenesis is the reverse process of glycolysis (Tang et al., 2018; Jiang et al., 2020), producing GLU from non-carbohydrates, such as pyruvate, lactic acid, and glycerol (Bhalla et al., 2014). Phosphoenolpyruvate carboxykinase 1 (PCK1) is one of the key enzymes of gluconeogenesis (Jiang et al., 2020). The overexpression of *PCK1* gene activated gluconeogenesis but inhibited the glycolysis pathway (Chong et al., 1994), revealing the key role of PCK1 protein kinase activity in SREBP-dependent lipid synthesis (Tang et al., 2018; Xu et al., 2020). As a complex, active, and dynamically changing multifunctional organelle, the lipid droplet is mainly composed of TG and sterol esters and is involved in lipid metabolism and storage as well as protein storage and degradation (Ploegh, 2007), membrane transport (Bartz et al., 2007), signal transduction, and other metabolic processes (Cohen et al., 2011). Generally, adipocytes grow and accumulate lipids with limits in order to avoid tissue damage lesions (Hirsch and Batchelor, 1976). Our results showed that serum IGF-1 content was increased and the expression of *PCK1* gene was upregulated in BA-TL group, and the results of liver Oil Red O staining showed that the B.A-TL promoted lipid droplet formation, indicating that B.A-TL enhanced gluconeogenesis to produce TG *via* IGF-1-regulated GLU internalization process.

Studies have shown that calcium regulates adipocyte metabolism by affecting intracellular calcium levels and fatty acid absorption in the gastrointestinal tract (Fleischman et al., 1966; Shi et al., 2001). He et al. (2012) found that an early low-calcium diet caused an increased fat mass and body weight, and ultimately became significant when rats were exposed to a late high-fat diet. Furthermore, Ca^{2+} in hepatocytes is an important regulator of GLU and lipid metabolism, bile secretion, mitochondrial activity, cell growth, and apoptosis (Berridge et al., 2000; Barritt et al., 2008; Amaya and Nathanson, 2013; Longo et al., 2019). The activity of hepatocytes is regulated by hormones and growth factors that utilize changes in Ca^{2+} concentration as intracellular signals (Amaya and Nathanson, 2013), while many of the cellular effects of Ca^{2+} are mediated by the Ca^{2+} binding protein calmodulin (CaM) (Zayzafoon, 2006). Although lipid metabolism in the liver is normally balanced without excessive lipid accumulation, when this homeostasis is disrupted, the lipid droplets are accumulated in hepatocytes, leading to cytotoxicity (Ali and Petrovsky, 2019). Excess lipid droplets may also impair the effects of IGF-1 (Petersen and Shulman, 2018), while the hepatic lipid accumulation may reflect increased hepatic lipid influx and hepatic lipogenesis (Maus et al., 2017). Recently, impaired calcium signaling was identified

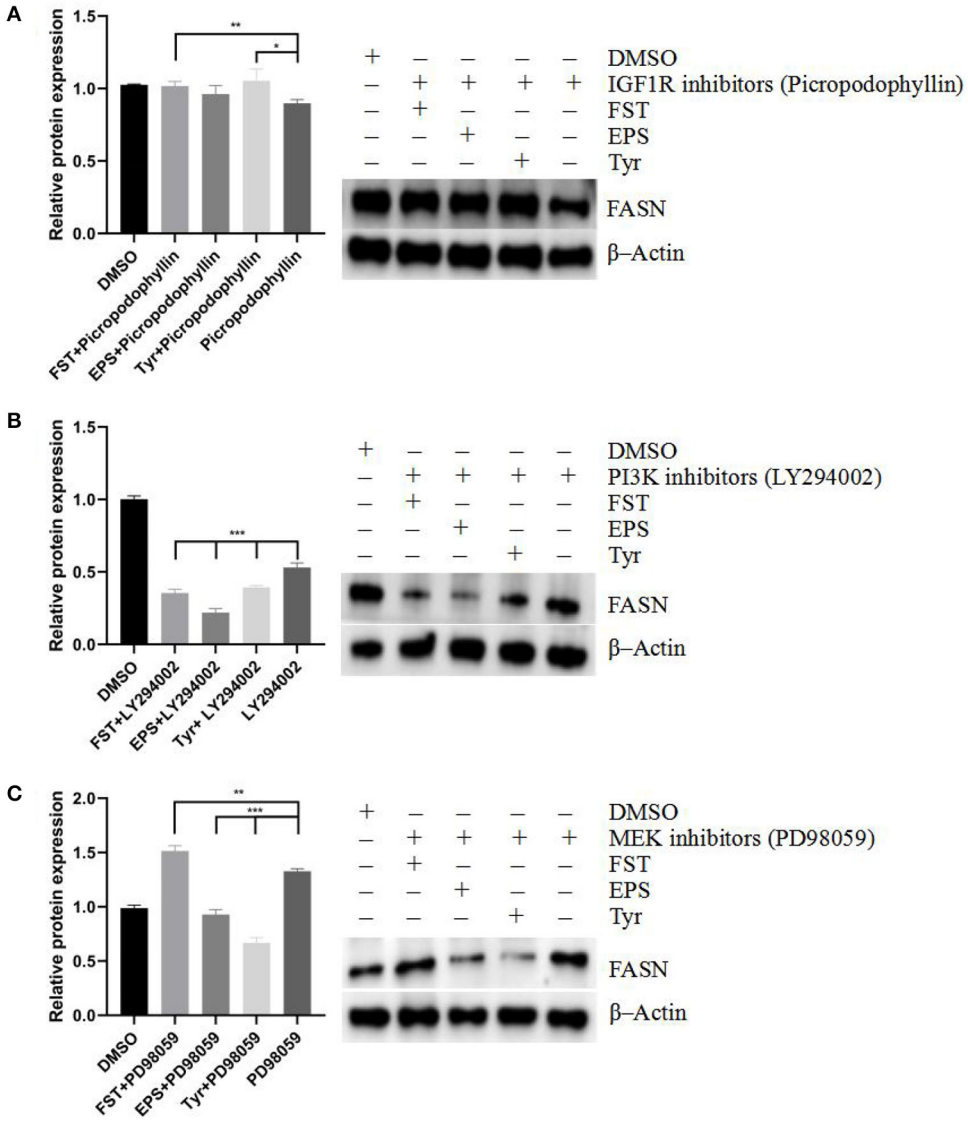

FIGURE 10
Effects of fermentation supernatant, exopolysaccharide, and L-tyrosine on LMH cells treated with different inhibitors including **(A)** IGF-1R inhibitor (picropodophyllin), **(B)** PI3K inhibitor (LY294002), and **(C)** MEK inhibitor (PD98059), respectively, at the FASN protein level. FASN is used as a target protein; β-Actin is used as a loading standard. "Con" = control group; "FST" = fermentation supernatant group; "EPS" = exopolysaccharides group; "Tyr" = L-tyrosine group. The signi?cance levels for all analyses are set at $p < 0.05$ (*), $p < 0.01$ (**), and $p < 0.001$ (***), respectively.

as a cause of increased endoplasmic reticulum (ER) stress, leading to hepatic lipid accumulation (Maus et al., 2017; Ali and Petrovsky, 2019). Studies have shown that the inhibition of store-operated calcium entry (SOCE) exacerbates the lipid accumulation, while the reduction of intracellular Ca^{2+} may cause lipid accumulation in fatty liver cells (Wilson et al., 2015) and fat storage cells (Baumbach et al., 2014). In turn, excessive lipid accumulation in hepatocytes also inhibits the SOCE (Wilson et al., 2015) and reduces the Ca^{2+} content in ER (Park et al., 2010; Baumbach et al., 2014; Wilson et al., 2015). The ER stress response initiated by low ER-Ca^{2+} stimulates the synthesis of both diacylglycerol and TG (Park et al., 2010; Arruda and Hotamisligil, 2015) utilizing these excess FAs, ultimately leading to the deposition of lipids in the cytoplasm (Ali and Petrovsky, 2019). Our study showed that the hepatic calcium pathway was downregulated in the B.A-TL group, which was consistent with the fact that low calcium caused hepatic lipid accumulation. However, our results of liver HE staining and serum biochemical indices showed that this downregulation of the hepatic calcium pathway was a reflection of the physiological

regulation without causing liver lesions or affecting the healthy growth of broilers, strongly indicating that B.A-TL could indeed promote liver lipid metabolism in broilers.

Regulations of IGF/PI3K/FASN pathway

In birds, lipogenesis occurs mainly in the liver, while the adipocytes function as a storage site for TG (Claire D'Andree et al., 2013). It is estimated that 80–85% of the FAs presented in TG stores of broiler adipose tissue are derived from hepatic lipogenesis or absorbed from the diet *via* the intestine (Richards et al., 2003), while the lipogenic activity in the liver is much greater than that in adipose tissue in chickens (Claire D'Andree et al., 2013). Studies showed that when the levels of saccharides exceeded the immediate energy requirements, GLU was converted into storage lipids (*via* lipogenesis) after the saturation of tissue glycogen deposition (Massari et al., 2016). Furthermore, fat is one of the factors affecting meat flavor, while the intermuscular fat affects the color, taste, and savory of meat (Claire D'Andree et al., 2013; Peña-Saldarriaga et al., 2020). Therefore, it is practically important to regulate the fat deposition in broiler production (Claire D'Andree et al., 2013). Hong et al. (2019) found an increase in the relative abundance of *Firmicutes* in the cecum microbiota ($p < 0.01$). It has been pointed out that a higher relative abundance of *Firmicutes* triggers energy storage, resulting in higher fat deposition (Wang et al., 2021), while fat deposition increases faster and earlier in fast-growing chickens compared to slow-growing chickens (Lilja, 1983; Carlborg et al., 2003). The liver is the major site for fatty acid biosynthesis regulated by a complex molecular network that controls the hepatic lipid composition and regulates systemic lipid metabolism (Liao et al., 2018). This molecular network contains various transcription factors, such as SREBP-1c, LXR, and PPAR, and pathways, such as PI3K/AKT (Wang et al., 2015; Titchenell et al., 2016). The positive effect of the PI3K/AKT signaling axis on lipid metabolism has been illustrated in hepatocytes and adipocytes, upregulating the key lipogenic enzymes, including FASN, SCD1, and ACCα (Wan et al., 2011; Liao et al., 2018). These results were consistent with those reported previously, showing that the interactions between the nutrients and the synthesis and activity of lipogenic enzymes were the possible causes of lipid deposition in adipose tissue (Peña-Saldarriaga et al., 2020).

FASN is a large multi-enzyme complex with a single protein of ∼270 kDa (Maier et al., 2006). FASN catalyzes the synthesis of palmitic acid based on both acetyl-CoA and malonyl-CoA and plays a role as a central regulator of lipid metabolism. It is considered to be an important protein in the liver under normal physiological conditions, controlling the mechanism of liver TG synthesis. As the carbohydrates become abundant, GLU is converted to FAs catalyzed by FASN, and the excess FAs are then assembled into TG and stored as fat droplets or secreted as VLDL (Ventura et al., 2015; Fhu and Ali, 2020). Studies showed that the G4928024A of the *FASN* gene is significantly correlated with fat bandwidth and abdominal fat percentage (Claire D'Andree et al., 2013). Furthermore, studies have shown that FASN expression is regulated by SREBP-1c, NF-Y, AZGP1, NAC1, and PKD1 (Chang et al., 2019; Li et al., 2021), which are in turn modulated by PI3K/AKT/mTOR (Li et al., 2012; Chang et al., 2019; Zhu et al., 2019), ERK/MAPK (Chang et al., 2019), and Wnt/β-catenin (Zhang et al., 2020) pathways. Moreover, the expression of FASN is downregulated after the PI3K/AKT/mTOR pathway is inhibited (Li et al., 2012; Han et al., 2015). Han et al. (2015) showed that INS mediated the lipid deposition in goose hepatocytes *via* the PI3K/AKT/mTOR signaling pathway. The results of Oil Red O staining reported in the previous studies revealed that lipid accumulation occurred in a dose-dependent manner following the addition of INS, and that 50, 100, or 150 nmol/L INS dose-dependently increased mRNA expression levels of lipogenesis-related genes (e.g., *SREBP-1, FASN,* and *ACCα*) and increased both FASN and ACCα protein levels (Han et al., 2015). Furthermore, the PI3K inhibitor treatment reduced insulin-induced increases in TG content, lipid content, mRNA levels of genes involved in adipogenesis (e.g., SREBP-1, FASN, and ACCα) and protein levels of FASN and ACCα (Han et al., 2015). Our study showed that both FST and Tyr in B.A-TL stimulated the expression of FASN in LMH cells, suggesting that B.A-TL promoted the synthesis of body fat which could be induced by the metabolic product stimulation of FASN protein expression, probably with both FST and Tyr involved and playing an important role. When IGF-1R was blocked, the treatments of FST, EPS, and Tyr on the LMH cells alleviated the inhibition of FASN by inhibitors. When the PI3K pathway was blocked, the expression levels of FASN in LMH cells treated with FST, EPS, and Tyr were significantly decreased, indicating that the expression of FASN was mainly regulated by the PI3K pathway. Furthermore, when the MAPK pathway was blocked, the expression of FASN in the FST group was not inhibited, suggesting that besides Tyr, other substances in the supernatant could also regulate FASN expression. Future studies are necessary to verify the existence of these substances and their functions in the expression of FASN.

In summary, these results showed that the FASN protein expression in the experimental groups was significantly downregulated with the treatment of the PI3K/AKT pathway inhibitor LY294002, suggesting that B.A-TL metabolites (Tyr and other components in the supernatant) stimulated the IGF-1 synthesis, activated the IGF/PI3K signaling pathway, promoted FASN protein expression, accelerated lipid metabolism in the liver tissue, and ultimately promoted fat deposition in broilers.

Conclusion

The results of our *in vivo* experiments indicated that B.A-TL changed the expression of relevant genes to stimulate the secretion of IGF-1 in the liver tissue of broilers without

affecting the secretion of GH and to enhance the antioxidant and antistress capacities of the organism. With the treatment of B.A-TL, a large amount of IGF-1 was secreted into the circulatory system to promote the rapid growth of muscle tissue, thus promoting the rapid weight gain of broilers during the brooding period (i.e., younger than 21 days in age). Our *in vitro* experiments showed that B.A-TL metabolites (i.e., FST and Tyr) stimulated the secretion of IGF-1 in LMH cells, altered the expression of fat metabolism genes, improved the expression of FASN protein, and promoted the synthesis of lipid substances in the liver. Our study is the first report demonstrating that probiotic B.A-TL promotes IGF-1 secretion by the liver of birds and its role in lipogenesis *via* IGF/PI3K/FASN pathway. These novel findings provide strong experimental evidence to support the application of B.A-TL in the regulatory studies of hepatic lipid metabolism in birds (i.e., fast-growing broilers) and to promote the commercial fatty liver production of poultry, such as Landes geese.

Data availability statement

The data presented in the study are deposited in the NCBI/Bioproject repository, accession number PRJNA835984 (https://www.ncbi.nlm.nih.gov/bioproject?term=PRJNA835984&cmd=DetailsSearch).

Ethics statement

The animal study was reviewed and approved by Animal Experiments at the College of Veterinary Medicine, Huazhong Agricultural University.

Author contributions

Conceptualization: PC, ZZ, DS, ZL, and YX. Methodology: PC, XW, XL, and YX. Software, formal analysis, data curation, and writing—original draft preparation: PC. Validation: PC and SL. Writing—review and editing: YX. All authors have read and agreed to the published version of the manuscript.

Funding

This research was funded by the National Key Research and Development Program of China (Grant number 2017YFD05010001) and the Innovative Job Funds of Agricultural Science and Technology of Hubei Province (Grant number 2019-620-000-001-30).

Acknowledgments

The authors would like to thank Ping Xu, Qiuyuan Li, Jie Wang, Fancong Meng, and Jingjing Zhou at the Huazhong Agricultural University for their assistance with broiler feeding.

Conflicts of interest

The authors declare that the research was conducted in the absence of any commercial or financial relationships that could be construed as a potential conflict of interest.

Publisher's note

Supplementary material

The Supplementary Material for this article can be found online at: https://www.frontiersin.org/articles/10.3389/fmicb.2022.958112/full#supplementary-material

References

Abd El-Hack, M. E., El-Saadony, M. T., Shafi, M. E., Qattan, S., Batiha, G. E., Khafaga, A. F., et al. (2020). Probiotics in poultry feed: a comprehensive review. *J. Anim. Physiol. Anim. Nutr.* 104, 1835–1850. doi: 10.1111/jpn.13454

Aderibigbe, A., Cowieson, A., Sorbara, J. O., and Adeola, O. (2020). Intestinal starch and energy digestibility in broiler chickens fed diets supplemented with α-amylase. *Poult. Sci.* 99, 5907–5914. doi: 10.1016/j.psj.2020.08.036

Albillos, A., de Gottardi, A., and Rescigno, M. (2020). The gut-liver axis in liver disease: pathophysiological basis for therapy. *J. Hepatol.* 72, 558–577. doi: 10.1016/j.jhep.2019.10.003

Ali, E. S., and Petrovsky, N. (2019). Calcium Signaling as a Therapeutic Target for Liver Steatosis. *Trends Endocrinol. Metab.* 30, 270–281. doi: 10.1016/j.tem.2019.02.005

Amaya, M. J., and Nathanson, M. H. (2013). Calcium signaling in the liver. *Compr. Physiol.* 3, 515–539. doi: 10.1002/cphy.c120013

Anh, N. T., Kunhareang, S., and Duangjinda, M. (2015). Association of chicken growth hormones and insulin-like growth factor gene polymorphisms with growth performance and carcass traits in Thai broilers. *Asian-australas. J. Anim. Sci.* 28, 1686–1695. doi: 10.5713/ajas.15.0028

Arab, J. P., Martin-Mateos, R. M., and Shah, V. H. (2018). Gut-liver axis, cirrhosis and portal hypertension: the chicken and the egg. *Hepatol. Int.* 12, 24–33. doi: 10.1007/s12072-017-9798-x

Arruda, A. P., and Hotamisligil, G. S. (2015). Calcium homeostasis and organelle function in the pathogenesis of obesity and diabetes. *Cell Metab.* 22, 381–397. doi: 10.1016/j.cmet.2015.06.010

Barritt, G. J., Chen, J., and Rychkov, G. Y. (2008). Ca^{2+}-permeable channels in the hepatocyte plasma membrane and their roles in hepatocyte physiology. *Biochim. Biophys. Acta* 1783, 651–672. doi: 10.1016/j.bbamcr.2008.01.016

Bartz, R., Zehmer, J. K., Zhu, M., Chen, Y., Serrero, G., Zhao, Y., et al. (2007). Dynamic activity of lipid droplets: protein phosphorylation and GTP-mediated protein translocation. *J. Proteome Res.* 6, 3256–3265. doi: 10.1021/pr070158j

Baumbach, J., Hummel, P., Bickmeyer, I., Kowalczyk, K. M., Frank, M., Knorr, K., et al. (2014). A Drosophila *in vivo* screen identifies store-operated calcium entry as a key regulator of adiposity. *Cell Metab.* 19, 331–343. doi: 10.1016/j.cmet.2013.12.004

Berridge, M. J., Lipp, P., and Bootman, M. D. (2000). The versatility and universality of calcium signalling. *Nat. Rev. Mol. Cell Biol.* 1, 11–21. doi: 10.1038/35036035

Bhalla, K., Liu, W. J., Thompson, K., Anders, L., Devarakonda, S., Dewi, R., et al. (2014). Cyclin D1 represses gluconeogenesis via inhibition of the transcriptional coactivator PGC1α. *Diabetes* 63, 3266–3278. doi: 10.2337/db13-1283

Brooks, A. J., and Waters, M. J. (2010). The growth hormone receptor: mechanism of activation and clinical implications. *Nat. Rev. Endocrinol.* 6, 515–525. doi: 10.1038/nrendo.2010.123

Brun, A., Mendez-Aranda, D., Magallanes, M. E., Karasov, W. H., Martínez Del Rio, C., Baldwin, M. W., et al. (2020). Duplications and functional convergence of intestinal carbohydrate-digesting enzymes. *Mol. Biol. Evol.* 37, 1657–1666. doi: 10.1093/molbev/msaa034

Carlborg, O., Kerje, S., Schütz, K., Jacobsson, L., Jensen, P., and Andersson, L. (2003). A global search reveals epistatic interaction between QTL for early growth in the chicken. *Genome Res.* 13, 413–421. doi: 10.1101/gr.528003

Castilla-Cortazar, I., de Ita, J. R., Aguirre, G. A., Castorena-Torres, F., Ortiz-Urbina, J., García-Magariño, M., et al. (2017). Fanconi anemia and laron syndrome. *Am. J. Med. Sci.* 353, 425–432. doi: 10.1016/j.amjms.2017.02.001

Cecerska-Heryć, E., Surowska, O., Heryć, R., Serwin, N., Napiontek-Balińska, S., and Dołegowska, B. (2021). Are antioxidant enzymes essential markers in the diagnosis and monitoring of cancer patients - a review. *Clin. Biochem.* 93, 1–8. doi: 10.1016/j.clinbiochem.2021.03.008

Chang, L., Fang, S., Chen, Y., Yang, Z., Yuan, Y., Zhang, J., et al. (2019). Inhibition of FASN suppresses the malignant biological behavior of non-small cell lung cancer cells via deregulating glucose metabolism and AKT/ERK pathway. *Lipids Health Dis.* 18, 118. doi: 10.1186/s12944-019-1058-8

Chang, T., Li, M., An, X., Bai, F., Wang, F., Yu, J., et al. (2021). Association analysis of *IGF2* gene polymorphisms with growth traits of Dezhou donkey. *Anim. Biotechnol.* 2021, 1–11. doi: 10.1080/10495398.2021.2013860

Chen, Y. C., Huang, S. D., Tu, J. H., Yu, J. S., Nurlatifah, A. O., Chiu, W. C., et al. (2020). Exopolysaccharides of Bacillus amyloliquefaciens modulate glycemic level in mice and promote glucose uptake of cells through the activation of AKT. *Int. J. Biol. Macromol.* 146, 202–211. doi: 10.1016/j.ijbiomac.2019.12.217

Chong, P. K., Jung, R. T., Scrimgeour, C. M., Rennie, M. J., and Paterson, C. R. (1994). Energy expenditure and body composition in growth hormone deficient adults on exogenous growth hormone. *Clin. Endocrinol.* 40, 103–110. doi: 10.1111/j.1365-2265.1994.tb02451.x

Claire D'Andree, H., Paul, W., Shen, X., Jia, X., Zhang, R., Sun, L., et al. (2013). Identification and characterization of genes that control fat deposition in chickens. *J. Anim. Sci. Biotechnol.* 4, 43. doi: 10.1186/2049-1891-4-43

Clayton, P. E., Banerjee, I., Murray, P. G., and Renehan, A. G. (2011). Growth hormone, the insulin-like growth factor axis, insulin and cancer risk. *Nat. Rev. Endocrinol.* 7, 11–24. doi: 10.1038/nrendo.2010.171

Cohen, J. C., Horton, J. D., and Hobbs, H. H. (2011). Human fatty liver disease: old questions and new insights. *Science* 332, 1519–1523. doi: 10.1126/science.1204265

Daughaday, W. H., Hall, K., Salmon, W. D. Jr, Van den Brande, J. L., and Van Wyk, J. J. (1987). On the nomenclature of the somatomedins and insulin-like growth factors. *Endocrinology* 121, 1911–1912. doi: 10.1210/jcem-65-5-1075

Deng, B., Zhang, F., Wen, J., Ye, S., Wang, L., Yang, Y., et al. (2017). The function of myostatin in the regulation of fat mass in mammals. *Nutr. Metab.* 14, 29. doi: 10.1186/s12986-017-0179-1

Dollins, A. B., Krock, L. P., Storm, W. F., Wurtman, R. J., and Lieberman, H. R. (1995). L-tyrosine ameliorates some effects of lower body negative pressure stress. *Physiol. Behav.* 57, 223–230. doi: 10.1016/0031-9384(94)00278-D

Dong, L. N., Wang, M., Guo, J., and Wang, J. P. (2019). Role of intestinal microbiota and metabolites in inflammatory bowel disease. *Chin. Med. J.* 132, 1610–1614. doi: 10.1097/CM9.0000000000000290

Dupont, J., Chen, J., Derouet, M., Simon, J., Leclercq, B., and Taouis, M. (1999). Metabolic differences between genetically lean and fat chickens are partly attributed to the alteration of insulin signaling in liver. *J. Nutr.* 129, 1937–1944. doi: 10.1093/jn/129.11.1937

Dupont, J., Tesseraud, S., and Simon, J. (2009). Insulin signaling in chicken liver and muscle. *Gen. Comp. Endocrinol.* 163, 52–57. doi: 10.1016/j.ygcen.2008.10.016

El-Attrouny, M. M., Iraqi, M. M., Sabike, I. I., Abdelatty, A. M., Moustafa, M. M., and Badr, O. A. (2021). Comparative evaluation of growth performance, carcass characteristics and timed series gene expression profile of GH and IGF-1 in two Egyptian indigenous chicken breeds versus Rhode Island Red. *J. Anim. Breed. Genet.* 138, 463–473. doi: 10.1111/jbg.12517

Fhu, C. W., and Ali, A. (2020). Fatty acid synthase: an emerging target in cancer. *Molecules* 25, 3935. doi: 10.3390/molecules25173935

Fleischman, A. I., Yacowitz, H., Hayton, T., and Bierenbaum, M. L. (1966). Effects of dietary calcium upon lipid metabolism in mature male rats fed beef tallow. *J. Nutr.* 88, 255–260. doi: 10.1093/jn/88.3.255

Forbes, B. E., Blyth, A. J., and Wit, J. M. (2020). Disorders of IGFs and IGF-1R signaling pathways. *Mol. Cell. Endocrinol.* 518, 111035. doi: 10.1016/j.mce.2020.111035

Gallenberger, M., zu Castell, W., Hense, B. A., and Kuttler, C. (2012). Dynamics of glucose and insulin concentration connected to the β-cell cycle: model development and analysis. *Theor. Biol. Med. Modell.* 9, 46. doi: 10.1186/1742-4682-9-46

Guo, J., Li, F., Qian, S., Bi, D., He, Q., Jin, H., et al. (2016). TGEV infection up-regulates FcRn expression via activation of NF-κB signaling. *Sci. Rep.* 6, 32154. doi: 10.1038/srep32154

Habibian, M., Ghazi, S., and Moeini, M. M. (2016). Effects of Dietary selenium and vitamin E on growth performance, meat yield, and selenium content and lipid oxidation of breast meat of broilers reared under heat stress. *Biol. Trace Elem. Res.* 169, 142–152. doi: 10.1007/s12011-015-0404-6

Halmos, T., and Suba, I. (2019). The physiological role of growth hormone and insulin-like growth factors. *Orv. Hetil.* 160, 1774–1783. doi: 10.1556/650.2019.31507

Han, C., Wei, S., He, F., Liu, D., Wan, H., Liu, H., et al. (2015). The regulation of lipid deposition by insulin in goose liver cells is mediated by the PI3K-AKT-mTOR signaling pathway. *PLoS ONE* 10, e0098759. doi: 10.1371/journal.pone.0098759

He, Y. H., Li, S. T., Wang, Y. Y., Wang, G., He, Y., Liao, X. L., et al. (2012). Postweaning low-calcium diet promotes later-life obesity induced by a high-fat diet. *J. Nutr. Biochem.* 23, 1238–1244. doi: 10.1016/j.jnutbio.2011.07.004

Hejdysz, M., Kaczmarek, S. A., Kubiś, M., Wiśniewska, Z., Peris, S., Budnik, S., et al. (2020). The effect of protease and *Bacillus licheniformis* on nutritional value of pea, faba bean, yellow lupin and narrow-leaved lupin in broiler chicken diets. *Br. Poult. Sci.* 61, 287–293. doi: 10.1080/00071668.2020.1716303

Hirsch, J., and Batchelor, B. (1976). Adipose tissue cellularity in human obesity. *Clin. Endocrinol. Metab.* 5, 299–311. doi: 10.1016/S0300-595X(76)80023-0

Hong, Y., Cheng, Y., Guan, L., Zhou, Z., Li, X., Shi, D., et al. (2021). *Bacillus amyloliquefaciens* TL downregulates the ileal expression of genes involved in immune responses in broiler chickens to improve growth performance. *Microorganisms* 9, 382. doi: 10.3390/microorganisms9020382

Hong, Y., Cheng, Y., Li, Y., Li, X., Zhou, Z., Shi, D., et al. (2019). Preliminary study on the effect of *Bacillus amyloliquefaciens* TL on cecal bacterial community structure of broiler chickens. *Biomed Res. Int.* 2019, 5431354. doi: 10.1155/2019/5431354

Inatomi, T., and Otomaru, K. (2018). Effect of dietary probiotics on the semen traits and antioxidative activity of male broiler breeders. *Sci. Rep.* 8, 5874. doi: 10.1038/s41598-018-24345-8

Jia, J., Ahmed, I., Liu, L., Liu, Y., Xu, Z., Duan, X., et al. (2018). Selection for growth rate and body size have altered the expression profiles of somatotropic axis genes in chickens. *PLoS ONE* 13, e0195378. doi: 10.1371/journal.pone.0195378

Jiang, H., Zhu, L., Xu, D., and Lu, Z. (2020). A newly discovered role of metabolic enzyme PCK1 as a protein kinase to promote cancer lipogenesis. *Cancer Commun.* 40, 389–394. doi: 10.1002/cac2.12084

Kieffer, D. A., Piccolo, B. D., Marco, M. L., Kim, E. B., Goodson, M. L., Keenan, M. J., et al. (2016). Mice fed a high-fat diet supplemented with resistant starch

display marked shifts in the liver metabolome concurrent with altered gut bacteria. *J. Nutr.* 146, 2476–2490. doi: 10.3945/jn.116.238931

Kim, D., Langmead, B., and Salzberg, S. L. (2015). HISAT: a fast spliced aligner with low memory requirements. *Nat. Methods* 12, 357–360. doi: 10.1038/nmeth.3317

Koronowicz, A. A., Banks, P., Szymczyk, B., Leszczyńska, T., Master, A., Piasna, E., et al. (2016). Dietary conjugated linoleic acid affects blood parameters, liver morphology and expression of selected hepatic genes in laying hens. *Br. Poult. Sci.* 57, 663–673. doi: 10.1080/00071668.2016.1192280

Kühn, S., Düzel, S., Colzato, L., Norman, K., Gallinat, J., Brandmaier, A. M., et al. (2019). Food for thought: association between dietary tyrosine and cognitive performance in younger and older adults. *Psychol. Res.* 83, 1097–1106. doi: 10.1007/s00426-017-0957-4

Kunishima, H., Ishibashi, N., Wada, K., Oka, K., Takahashi, M., Yamasaki, Y., et al. (2019). The effect of gut microbiota and probiotic organisms on the properties of extended spectrum beta-lactamase producing and carbapenem resistant enterobacteriaceae including growth, beta-lactamase activity and gene transmissibility. *J. Infection Chemother.* 25, 894–900. doi: 10.1016/j.jiac.2019.04.021

Laron, Z. (2008). Insulin-like growth factor-I treatment of children with Laron syndrome (primary growth hormone insensitivity). *Pediatr. Endocrinol. Rev.* 5, 766–771.

Lavelle, A., and Sokol, H. (2020). Gut microbiota-derived metabolites as key actors in inflammatory bowel disease. *Nat. Rev. Gastroenterol. Hepatol.* 17, 223–237. doi: 10.1038/s41575-019-0258-z

Ley, R. E., Bäckhed, F., Turnbaugh, P., Lozupone, C. A., Knight, R. D., and Gordon, J. I. (2005). Obesity alters gut microbial ecology. *Proc. Natl. Acad. Sci. U. S. A.* 102, 11070–11075. doi: 10.1073/pnas.0504978102

Li, B., and Dewey, C. N. (2011). RSEM: accurate transcript quantification from RNA-Seq data with or without a reference genome. *BMC Bioinformatics* 12, 323. doi: 10.1186/1471-2105-12-323

Li, G., Xing, Z., Wang, W., Luo, W., Ma, Z., Wu, Z., et al. (2021). Adipose-specific knockout of Protein Kinase D1 suppresses *de novo* lipogenesis in mice via SREBP1c-dependent signaling. *Exp. Cell Res.* 401, 112548. doi: 10.1016/j.yexcr.2021.112548

Li, M. (2022). The origination of growth hormone/insulin-like growth factor system: a story from ancient basal chordate amphioxus. *Front Endocrinol.* 13, 825722. doi: 10.3389/fendo.2022.825722

Li, N., Bu, X., Tian, X., Wu, P., Yang, L., and Huang, P. (2012). Fatty acid synthase regulates proliferation and migration of colorectal cancer cells via HER2-PI3K/AKT signaling pathway. *Nutr. Cancer* 64, 864–870. doi: 10.1080/01635581.2012.701704

Liao, X., Song, L., Zhang, L., Wang, H., Tong, Q., Xu, J., et al. (2018). LAMP3 regulates hepatic lipid metabolism through activating PI3K/AKT pathway. *Mol. Cell. Endocrinol.* 470, 160–167. doi: 10.1016/j.mce.2017.10.010

Lieberman, H. R., Georgelis, J. H., Maher, T. J., and Yeghiayan, S. K. (2005). Tyrosine prevents effects of hyperthermia on behavior and increases norepinephrine. *Physiol. Behav.* 84, 33–38. doi: 10.1016/j.physbeh.2004.10.023

Lilja, C. (1983). A comparative study of postnatal growth and organ development in some species of birds. *Growth* 47, 317–339. doi: 10.1002/mrd.1120070411

Liu, Z., Cordoba-Chacon, J., Kineman, R. D., Cronstein, B. N., Muzumdar, R., Gong, Z., et al. (2016). Growth hormone control of hepatic lipid metabolism. *Diabetes* 65, 3598–3609. doi: 10.2337/db16-0649

Longo, M., Zatterale, F., Naderi, J., Parrillo, L., Formisano, P., Raciti, G. A., et al. (2019). Adipose tissue dysfunction as determinant of obesity-associated metabolic complications. *Int. J. Mol. Sci.* 20, 2358. doi: 10.3390/ijms20092358

Love, M. I., Huber, W., and Anders, S. (2014). Moderated estimation of fold change and dispersion for RNA-seq data with DESeq2. *Genome Biol.* 15, 550. doi: 10.1186/s13059-014-0550-8

Maier, T., Jenni, S., and Ban, N. (2006). Architecture of mammalian fatty acid synthase at 4.5 A resolution. *Science* 311, 1258–1262. doi: 10.1126/science.1123248

Mancabelli, L., Ferrario, C., Milani, C., Mangifesta, M., Turroni, F., Duranti, S., et al. (2016). Insights into the biodiversity of the gut microbiota of broiler chickens. *Environ. Microbiol.* 18, 4727–4738. doi: 10.1111/1462-2920.13363

Mason, T. M. (1998). The role of factors that regulate the synthesis and secretion of very-low-density lipoprotein by hepatocytes. *Crit. Rev. Clin. Lab. Sci.* 35, 461–487. doi: 10.1080/10408369891234246

Massari, F., Ciccarese, C., Santoni, M., Iacovelli, R., Mazzucchelli, R., Piva, F., et al. (2016). Metabolic phenotype of bladder cancer. *Cancer Treat. Rev.* 45, 46–57. doi: 10.1016/j.ctrv.2016.03.005

Maus, M., Cuk, M., Patel, B., Lian, J., Ouimet, M., Kaufmann, U., et al. (2017). Store-operated Ca^{2+} entry controls induction of lipolysis and the transcriptional reprogramming to lipid metabolism. *Cell Metab.* 25, 698–712. doi: 10.1016/j.cmet.2016.12.021

Moerth, C., Schneider, M. R., Renner-Mueller, I., Blutke, A., Elmlinger, M. W., Erben, R. G., et al. (2007). Postnatally elevated levels of insulin-like growth factor (IGF)-II fail to rescue the dwarfism of IGF-I-deficient mice except kidney weight. *Endocrinology* 148, 441–451. doi: 10.1210/en.2006-0385

Mollahosseini, M., Daneshzad, E., Rahimi, M. H., Yekaninejad, M. S., Maghbooli, Z., and Mirzaei, K. (2017). The association between fruit and vegetable intake and liver enzymes (Aspartate and Alanine Transaminases) in Tehran, Iran. *Ethiop. J. Health Sci.* 27, 401–410. doi: 10.4314/ejhs.v27i4.11

Park, S. W., Zhou, Y., Lee, J., Lee, J., and Ozcan, U. (2010). Sarco(endo)plasmic reticulum Ca^{2+}-ATPase 2b is a major regulator of endoplasmic reticulum stress and glucose homeostasis in obesity. *Proc. Natl. Acad. Sci. U. S. A.* 107, 19320–19325. doi: 10.1073/pnas.1012044107

Peña-Saldarriaga, L. M., Fernández-López, J., and Pérez-Alvarez, J. A. (2020). Quality of chicken fat by-products: lipid profile and colour properties. *Foods* 9, 1046. doi: 10.3390/foods9081046

Perry, R. J., and Shulman, G. I. (2020). Mechanistic links between obesity, insulin, and cancer. *Trends Cancer* 6, 75–78. doi: 10.1016/j.trecan.2019.12.003

Pertea, M., Pertea, G. M., Antonescu, C. M., Chang, T. C., Mendell, J. T., and Salzberg, S. L. (2015). StringTie enables improved reconstruction of a transcriptome from RNA-seq reads. *Nat. Biotechnol.* 33, 290–295. doi: 10.1038/nbt.3122

Petersen, M. C., and Shulman, G. I. (2018). Mechanisms of insulin action and insulin resistance. *Physiol. Rev.* 98, 2133–2223. doi: 10.1152/physrev.00063.2017

Pillutla, P., Hwang, Y. C., Augustus, A., Yokoyama, M., Yagyu, H., Johnston, T. P., et al. (2005). Perfusion of hearts with triglyceride-rich particles reproduces the metabolic abnormalities in lipotoxic cardiomyopathy. *Am. J. Physiol. Endocrinol. Metab.* 288, 1229–1235. doi: 10.1152/ajpendo.00273.2004

Pinterić, M., Podgorski, I. I., HadŽija, M. P., Bujak, I. T., Dekanić, A., Bagarić, R., et al. (2020). Role of Sirt3 in differential sex-related responses to a high-fat diet in Mice. *Antioxidants* 9, 174. doi: 10.3390/antiox9020174

Ploegh, H. L. (2007). A lipid-based model for the creation of an escape hatch from the endoplasmic reticulum. *Nature* 448, 435–438. doi: 10.1038/nature06004

Poreba, E., and Durzynska, J. (2020). Nuclear localization and actions of the insulin-like growth factor 1 (IGF-1) system components: transcriptional regulation and DNA damage response. *Mutat. Res. Rev. Mutat. Res.* 784, 108307. doi: 10.1016/j.mrrev.2020.108307

Richards, M. P., Poch, S. M., Coon, C. N., Rosebrough, R. W., Ashwell, C. M., and McMurtry, J. P. (2003). Feed restriction significantly alters lipogenic gene expression in broiler breeder chickens. *J. Nutr.* 133, 707–715. doi: 10.1093/jn/133.3.707

Salaheen, S., Kim, S. W., Haley, B. J., Van Kessel, J., and Biswas, D. (2017). Alternative growth promoters modulate broiler gut microbiome and enhance body weight gain. *Front. Microbiol.* 8, 2088. doi: 10.3389/fmicb.2017.02088

Saleh, A. A., Shukry, M., Farrag, F., Soliman, M. M., and Abdel-Moneim, A. E. (2021). Effect of feeding wet feed or wet feed fermented by *Bacillus licheniformis* on growth performance, histopathology and growth and lipid metabolism marker genes in broiler chickens. *Animals* 11, 83. doi: 10.3390/ani11010083

Salmon, W. D. Jr., and Daughaday, W. H. (1957). A hormonally controlled serum factor which stimulates sulfate incorporation by cartilage *in vitro*. *J. Lab. Clin. Med.* 49, 825–836.

Schramm, V. G., Massuquetto, A., Bassi, L. S., Zavelinski, V., Sorbara, J., Cowieson, A. J., et al. (2021). Exogenous α-amylase improves the digestibility of corn and corn-soybean meal diets for broilers. *Poult. Sci.* 100, 101019. doi: 10.1016/j.psj.2021.101019

Shi, H., Dirienzo, D., and Zemel, M. B. (2001). Effects of dietary calcium on adipocyte lipid metabolism and body weight regulation in energy-restricted aP2-agouti transgenic mice. *FASEB J.* 15, 291–293. doi: 10.1096/fj.00-0584fje

Sigalos, J. T., and Pastuszak, A. W. (2018). The safety and efficacy of growth hormone secretagogues. *Sexual Med. Rev.* 6, 45–53. doi: 10.1016/j.sxmr.2017.02.004

Sirotkin, A. V., Dukesová, J., Makarevich, A. V., Kubek, A., and Bulla, J. (2000). Evidence that growth factors IGF-I, IGF-II and EGF can stimulate nuclear maturation of porcine oocytes via intracellular protein kinase A. *Reprod. Nutr. Dev.* 40, 559–569. doi: 10.1051/rnd:2000137

Sjögren, K., Liu, J. L., Blad, K., Skrtic, S., Vidal, O., Wallenius, V., et al. (1999). Liver-derived insulin-like growth factor I (IGF-I) is the principal source of IGF-I in blood but is not required for postnatal body growth in mice. *Proc. Natl. Acad. Sci. U. S. A.* 96, 7088–7092. doi: 10.1073/pnas.96.12.7088

Stanley, T. L., Fourman, L. T., Zheng, I., McClure, C. M., Feldpausch, M. N., Torriani, M., et al. (2021). Relationship of IGF-1 and IGF-Binding proteins to disease severity and glycemia in nonalcoholic fatty liver disease. *J. Clin. Endocrinol. Metab.* 106, e520–e533. doi: 10.1210/clinem/dgaa792

Svihus, B. (2014). Starch digestion capacity of poultry. *Poult. Sci.* 93, 2394–2399. doi: 10.3382/ps.2014-03905

Tang, Y., Zhang, Y., Wang, C., Sun, Z., Li, L., Cheng, S., et al. (2018). Overexpression of PCK1 gene antagonizes hepatocellular carcinoma through the activation of gluconeogenesis and suppression of glycolysis pathways. *Cell. Physiol. Biochem.* 47, 344–355. doi: 10.1159/000489811

Titchenell, P. M., Quinn, W. J., Lu, M., Chu, Q., Lu, W., Li, C., et al. (2016). Direct hepatocyte insulin signaling is required for lipogenesis but is dispensable for the suppression of glucose production. *Cell Metab.* 23, 1154–1166. doi: 10.1016/j.cmet.2016.04.022

Ventura, R., Mordec, K., Waszczuk, J., Wang, Z., Lai, J., Fridlib, M., et al. (2015). Inhibition of *de novo* palmitate synthesis by fatty acid synthase induces apoptosis in tumor cells by remodeling cell membranes, inhibiting signaling pathways, and reprogramming gene expression. *EBioMedicine* 2, 808–824. doi: 10.1016/j.ebiom.2015.06.020

Wan, M., Leavens, K. F., Saleh, D., Easton, R. M., Guertin, D. A., Peterson, T. R., et al. (2011). Postprandial hepatic lipid metabolism requires signaling through AKT2 independent of the transcription factors FoxA2, FoxO1, and SREBP1c. *Cell Metab.* 14, 516–527. doi: 10.1016/j.cmet.2011.09.001

Wan, X., Ahmad, H., Zhang, L., Wang, Z., and Wang, T. (2018). Dietary enzymatically treated *Artemisia annua* L. improves meat quality, antioxidant capacity and energy status of breast muscle in heat-stressed broilers. *J. Sci. Food Agric.* 98, 3715–3721. doi: 10.1002/jsfa.8879

Wang, J., Ishfaq, M., Miao, Y., Liu, Z., Hao, M., Wang, C., et al. (2022). Dietary administration of Bacillus subtilis KC1 improves growth performance, immune response, heat stress tolerance, and disease resistance of broiler chickens. *Poult. Sci.* 101, 101693. doi: 10.1016/j.psj.2021.101693

Wang, J., Wan, C., Shuju, Z., Yang, Z., Celi, P., Ding, X., et al. (2021). Differential analysis of gut microbiota and the effect of dietary *Enterococcus faecium* supplementation in broiler breeders with high or low laying performance. *Poult. Sci.* 100, 1109–1119. doi: 10.1016/j.psj.2020.10.024

Wang, Y., Viscarra, J., Kim, S. J., and Sul, H. S. (2015). Transcriptional regulation of hepatic lipogenesis. *Nat. Rev. Mol. Cell Biol.* 16, 678–689. doi: 10.1038/nrm4074

Wieërs, G., Belkhir, L., Enaud, R., Leclercq, S., Philippart de Foy, J. M., Dequenne, I., et al. (2020). How probiotics affect the microbiota. *Front. Cell. Infect. Microbiol.* 9, 454. doi: 10.3389/fcimb.2019.00454

Wilson, C. H., Ali, E. S., Scrimgeour, N., Martin, A. M., Hua, J., Tallis, G. A., et al. (2015). Steatosis inhibits liver cell store-operated Ca^{2}? entry and reduces ER Ca^{2}? through a protein kinase C-dependent mechanism. *Biochem. J.* 466, 379–390. doi: 10.1042/BJ20140881

Wolever, T., El-Sohemy, A., Ezatagha, A., Zurbau, A., and Jenkins, A. L. (2021). Neither low salivary amylase activity, cooling cooked white rice, nor single nucleotide polymorphisms in starch-digesting enzymes reduce glycemic index or starch digestibility: a randomized, crossover trial in healthy adults. *Am. J. Clin. Nutr.* 114, 1633–1645. doi: 10.1093/ajcn/nqab228

Xiang, W., Shang, Y., Wang, Q., Xu, Y., Zhu, P., Huang, K., et al. (2017). Identification of a chicken (*Gallus gallus*) endogenous reference gene (Actb) and its application in meat adulteration. *Food Chem.* 234, 472–478. doi: 10.1016/j.foodchem.2017.05.038

Xie, C., Mao, X., Huang, J., Ding, Y., Wu, J., Dong, S., et al. (2011). KOBAS 2.0: a web server for annotation and identification of enriched pathways and diseases. *Nucleic Acids Res.* 39, W316–W322. doi: 10.1093/nar/gkr483

Xu, D., Wang, Z., Xia, Y., Shao, F., Xia, W., Wei, Y., et al. (2020). The gluconeogenic enzyme PCK1 phosphorylates INSIG1/2 for lipogenesis. *Nature* 580, 530–535. doi: 10.1038/s41586-020-2183-2

Yoshida, T., and Delafontaine, P. (2020). Mechanisms of IGF-1-mediated regulation of skeletal muscle hypertrophy and atrophy. *Cells* 9, 1970. doi: 10.3390/cells9091970

Zayzafoon, M. (2006). Calcium/calmodulin signaling controls osteoblast growth and differentiation. *J. Cell. Biochem.* 97, 56–70. doi: 10.1002/jcb.20675

Zhang, J., Li, Q., Wu, Y., Wang, D., Xu, L., Zhang, Y., et al. (2019). Cholesterol content in cell membrane maintains surface levels of ErbB2 and confers a therapeutic vulnerability in ErbB2-positive breast cancer. *Cell Commun. Signal.* 17, 15. doi: 10.1186/s12964-019-0328-4

Zhang, L., Zhang, R., Jia, H., Zhu, Z., Li, H., and Ma, Y. (2021). Supplementation of probiotics in water beneficial growth performance, carcass traits, immune function, and antioxidant capacity in broiler chickens. *Open Life Sci.* 16, 311–322. doi: 10.1515/biol-2021-0031

Zhang, W. L., Wang, S. S., Jiang, Y. P., Liu, Y., Yu, X. H., Wu, J. B., et al. (2020). Fatty acid synthase contributes to epithelial-mesenchymal transition and invasion of salivary adenoid cystic carcinoma through PRRX1/Wnt/β-catenin pathway. *J. Cell. Mol. Med.* 24, 11465–11476. doi: 10.1111/jcmm.15760

Zhu, L., Du, W., Liu, Y., Cheng, M., Wang, X., Zhang, C., et al. (2019). Prolonged high-glucose exposure decreased SREBP-1/FASN/ACC in Schwann cells of diabetic mice via blocking PI3K/Akt pathway. *J Cell Biochem.* 120, 5777–5789. doi: 10.1002/jcb.27864

frontiers | Frontiers in Microbiology

TYPE Original Research
PUBLISHED 05 August 2022
DOI 10.3389/fmicb.2022.955112

OPEN ACCESS

EDITED BY
Rina Wu,
Shenyang Agricultural University, China

REVIEWED BY
Sabine Stegemann-Koniszewski,
University Hospital Magdeburg, Germany
Yuying Li,
Institute of Subtropical Agriculture (CAS), China

*CORRESPONDENCE
Daijie Chen
chen_lab@sjtu.edu.cn

SPECIALTY SECTION
This article was submitted to Food Microbiology, a section of the journal Frontiers in Microbiology

RECEIVED 28 May 2022
ACCEPTED 11 July 2022
PUBLISHED 05 August 2022

CITATION
Hu Y, Jin X, Gao F, Lin T, Zhu H, Hou X, Yin Y, Kan S and Chen D (2022) Selenium-enriched *Bifidobacterium longum* DD98 effectively ameliorates dextran sulfate sodium-induced ulcerative colitis in mice. *Front. Microbiol.* 13:955112. doi: 10.3389/fmicb.2022.955112

Selenium-enriched *Bifidobacterium longum* DD98 effectively ameliorates dextran sulfate sodium-induced ulcerative colitis in mice

Yongjia Hu[1,2], Xueli Jin[1], Fei Gao[1], Ting Lin[1], Hui Zhu[1], Xiao Hou[1], Yu Yin[1], Shidong Kan[1] and Daijie Chen[1,2]*

[1]School of Pharmacy, Shanghai Jiao Tong University, Shanghai, China, [2]State Key Laboratory of Microbial Metabolism, Shanghai Jiao Tong University, Shanghai, China

The pathogenesis of ulcerative colitis (UC) is complicated with impaired intestinal epithelial barrier and imbalanced gut microbiota. Both selenium and probiotics have shown effects in regulating intestinal flora and ameliorating UC. The objective of this study is to investigate the alleviating effects of Selenium-enriched *Bifidobacterium longum* DD98 (Se-*B. longum* DD98) on dextran sulfate sodium (DSS)-induced colitis in mice and explore the underlying mechanism. After treatment of *B. longum* DD98, Se-*B. longum* DD98, and sulfasalazine for 3 weeks, the disease severity of UC mice was decreased, with colon lengthened and pathological phenotype improved. The expression of pro-inflammatory cytokines and oxidative stress parameters were also decreased. Thus, Se-*B. longum* DD98 showed a stronger effect on relieving the aforementioned symptoms caused by DSS-induced colitis. Exploration of the potential mechanism demonstrated that Se-*B. longum* DD98 showed higher activities to suppress the inflammatory response by inhibiting the activation of the toll-like receptor 4 (TLR4), compared to *B. longum* DD98 and sulfasalazine. Se-*B. longum* DD98 also significantly improved the intestinal barrier integrity by increasing the expression of tight junction proteins including ZO-1 and occludin. 16S rDNA sequencing analyses showed that Se-*B. longum* DD98 improved the diversity of the intestinal flora and promoted the abundance of health-benefiting taxa including *Lachnospiraceae*, *Lactobacillaceae*, and *Prevotellaceae* in family level. In conclusion, compared to *B. longum* DD98 and sulfasalazine, Se-*B. longum* DD98 showed stronger therapeutic effects on DSS-induced colitis in mice and might be a promising candidate for the treatment of UC.

KEYWORDS

selenium-enriched *Bifidobacterium longum*, DD98, probiotic, IBD, DSS-induced colitis, gut microbiota

Introduction

Inflammatory bowel disease (IBD), comprising Crohn's disease (CD) and ulcerative colitis (UC), is characterized as a chronic and idiopathic inflammatory disease affecting the ileum, rectum, and colon (Ungaro et al., 2017). The pathogenesis of UC is not well-understood and usually complicated by multi-factors including genetic predisposition, intestinal flora dysbiosis, epithelial barrier defects, immune susceptibility, and environmental elements (Hindryckx et al., 2016). It is reported that the prevalence of IBD is increasing worldwide, posing a significant challenge to medical industries (Molodecky et al., 2012; Kaplan and Ng, 2017). Furthermore, as an incurable intestinal inflammation, IBD contributes to colorectal cancer development through a dysregulated form of tissue repair or aberrant activation of inflammatory pathways (Elinav et al., 2013). The application of therapeutic drugs for UC patients, such as aminosalicylic acids, corticosteroids, immunosuppressants, and biological agents, was limited for their poor efficacy and potential adverse drug reactions (Meier and Sturm, 2011).

In recent years, the correlation between compositional and metabolic changes in the gut microbiota and UC has been investigated. Multiple studies reported that the diversity of intestinal microbiota and the proportional abundance of *Firmicutes* to *Bacteroidetes* or *Proteobacteria* was decreased in UC patients (Sartor and Wu, 2017). Besides, the metabolites of gut microbiota such as short-chain fatty acids (SCFAs), bile acids, and tryptophan catabolites, which exert a protective function in maintaining the gut barrier integrity and immunity homeostasis, are significantly reduced during the development of UC (Ni et al., 2017; Agus et al., 2018). Probiotics refer to the live microorganisms that confer a health benefit on the host if taken in a sufficient amount (Hill et al., 2014). Nowadays, the application of probiotics such as *Bifidobacterium* were confirmed to exert an important role in UC (Sartor, 2004). For instance, probiotics increased intestinal biodiversity and restored gut microbiota dysbiosis in colitis mice (Bian et al., 2019). Administration of *Bifidobacterium longum* inhibited inflammatory pathway activation in lamina propria cells and downregulated inflammatory mediators expression (Bai et al., 2006). In addition, probiotics alleviated symptoms of UC in DSS-colitis rats by improving gut barrier integrity and increasing SCFAs content (Sanders et al., 2019; Li et al., 2022).

Selenium (Se) is an essential trace element for human health. Selenoproteins, the main active form of selenium in the human body, are famous for their anti-inflammatory properties and immunomodulatory effects. Therefore, Selenoproteins were used in the prevention and treatment of autoimmune, allergic, cardiovascular, and chronic inflammatory diseases (Huang et al., 2012; Kuria et al., 2022). It is demonstrated that the patients with IBD were commonly found with selenium deficiency (Han et al., 2017). Besides, the efficacy of selenium supplement on UC patients and DSS-induced colitis animal models has been proven by many studies (Zhai et al., 2018a; Khazdouz et al., 2020). Krehl et al. (2012) reported that selenium mitigated the severity of DSS colitis by enhancing GPX2 activity. Zhu et al. (2016) demonstrated that selenium-containing phycocyanin significantly decreased the level of inflammatory cytokines and oxidative stress. Furthermore, selenium also regulated the composition of gut microbiota, thus restoring the flora dysbiosis in colitis (Zhai et al., 2018a).

Taken together, previous studies have demonstrated that both probiotics and selenium have improvement effects on UC. Se-*B. longum* DD98, a selenium-enriched probiotic, obtained through applying Na_2SeO_3 into the process of *B. longum* DD98 fermentation, thus converting inorganic selenium to organic selenium. Our previous studies showed the efficacy of Se-*B. longum* DD98 in antibiotic-induced intestinal dysbacteriosis and type 2 diabetes (Zhu et al., 2019; Zhao et al., 2020b). In this study, we investigated the effect of Se-*B. longum* DD98 on the prevention and treatment in DSS-induced colitis mice. Because of the situation that the use of selenium is limited by its potential toxicity in excessive intake and wide employment of probiotics in UC treatment, we compared its effects with pure *B. longum* and sulfasalazine (one of the first-line aminosalicylic acid drugs) to find out whether the Se-*B. longum* DD98 would show superior functions in relieving DSS colitis. Furthermore, mechanisms related to the level of inflammatory response and oxidative stress, the expression levels of tight junction proteins, and gut microbiota composition were also evaluated to explore the prevention and therapeutic effects of Se-*B. longum* DD98 in DSS-induced colitis mice.

Materials and methods

Preparation of selenium-enriched *Bifidobacterium longum* DD98

Selenium-enriched *Bifidobacterium longum* DD98 was prepared in our laboratory. The origin of the DD98 strain and preparation procedure were described in our previous study (Zhu et al., 2019). In brief, a high-throughput screening approach was used to select the DD98 strain. Se-*B. longum* DD98 was enriched by applying DD98 strain in the 24 h fermentation of culture medium containing 8.5 $\mu g mL^{-1}$ Se (as Na_2SeO_3). At the end of fermentation, the bacterial cells were harvested, washed, and then freeze-dried for subsequent administration. The viable count of bacteria in the fermentation broth was determined by colony counting in reinforced clostridial medium (RCM) agar plates. The total selenium content

is determined by the iCAP-Q inductively coupled plasma mass spectrometer (ICP-MS, Thermo Fisher Scientific, MA, United States). In this study, the total Se concentration and CFU of Se-*B. longum* DD98 were 0.38 mg/g and 2×10^9 CFU/g, respectively.

Animal experiments

The animal experimental design is summarized in **Figure 1**. All animal experiments were performed by confirming to the relevant regulations and permitted by the Institutional Animal Care and Use Committee (IACUC) of Shanghai Jiao Tong University (NO. A2021046). Thirty male C57BL/6 mice (6–8 weeks, 20–22 g) were purchased from Beijing Vital River Laboratory Animal Technology Co., Ltd. (Beijing, China). All mice were acclimatized at 25 ± 2°C in a 12-h light/dark cycle with a standard mice chow diet and distilled water *ad libitum* for 7 days. Then, the mice were randomly divided into five groups (n = 6 per group): a normal control group (NC), a 3.5% DSS group (DSS, molecular weight: 36,000–50,000; MP Biomedicals), a 3.5% DSS + *B. longum* DD98 group (DD98), a 3.5% DSS + Se-*B. longum* DD98 (SeDD98), and a sulfasalazine group (SASP). Mice in the DSS group and treatment groups were treated with normal drinking water before DSS administration (day −14 to 0) followed by 3.5% DSS water for 7 days to induce colitis (day 0–7). Then, 3.5% DSS water was replaced by normal drinking water from day 7 to 9. In comparison, mice in the NC group were treated with normal drinking water throughout the whole experiment. For treatment, mice in the DD98 and SeDD98 groups were separately administered *B. longum* DD98 (1×10^{10} CFU/kg) and Se-*B. longum* DD98 (0.1 mg Se/kg, 1×10^{10} CFU/kg) once daily by oral gavage for 21 days (day −14 to day 7), while sulfasalazine was orally administered to mice at the dose of 300 mg/kg at the same time in the SASP group. By contrast, the NC group and DSS group were supplied with the same amount of normal saline. Besides, the body weight, stool consistency, and rectal bleeding were recorded daily from day 0 to day 9. At the end of the experiment (day 9), all mice were humanely euthanized. After that, the weight of the spleen and the length of the colon were measured. Feces and serum were stored at −80°C until analysis. Colon segments were either fixed with 4% paraformaldehyde or stored at −80°C for further procedures.

Disease activity index assessment

The severity of colitis was measured using DAI assessment, a scoring system that includes three parts: body weight loss (0–4), degree of intestinal bleeding (0–4), and stool consistency (0–4) (Wirtz et al., 2017). For observation of disease progression, the DAI scoring was performed daily from day 0 to day 9 of the experiment.

Histological analysis

Colon tissue was fixed with 4% paraformaldehyde solution and dehydrated by ethanol with different concentration gradients. Fixed tissue was embedded in paraffin and sections with a thickness of 4 μm were cut and stained with hematoxylin and eosin (H&E) followed by microscopic observations (Olympus Corporation, Tokyo, Japan). The colon damages were scored according to the criteria shown in **Supplementary Table 1** as previously described (Stillie and Stadnyk, 2009). Scores were calculated by summing the score for four parameters (extent of inflammation, crypt damage, ulceration, and edema).

Total RNA extraction and real-time quantitative PCR

Total RNA was extracted from tissues using TRIzol following manufacturer instructions. The concentrations of total RNA and the ratios of 260/280 and 260/230 were measured using Nanodrop (Thermo Fisher Scientific, MA, United States) to evaluate the quality of extracted RNA. The primers used to amplify the target genes were listed in **Supplementary Table 2**. The qPCR assays were performed using a StepOnePlus™ Real-Time PCR System (Thermo Fisher Scientific, MA, United States). The results were expressed as a relative value after normalization to the mRNA of GAPDH.

Measurement of oxidative stress parameters in serum and colon

Malondialdehyde (MDA) concentration, superoxide dismutase (SOD), and Catalase (CAT) activity in serum were quantified using commercial kits (Nanjing Jiancheng Bioengineering Institute, Nanjing, China). The level of Glutathione reductase (GR) activity in colon tissue samples was measured by a commercial kit (Beyotime Biotechnology, Shanghai, China). All operations followed the kit's instructions.

Western blot analysis

Tissues were lysed in RIPA buffer with the addition of protease and phosphatase inhibitor cocktail (200 mM AEBSF, 30 μM Aprotinin, 13 mM Bestatin, 1.4 mM E64, 1 mM Leupeptin in DMSO, and 0.1 M EDTA). The lysate was centrifuged at 12,000 g at 4°C for 30 min and the protein

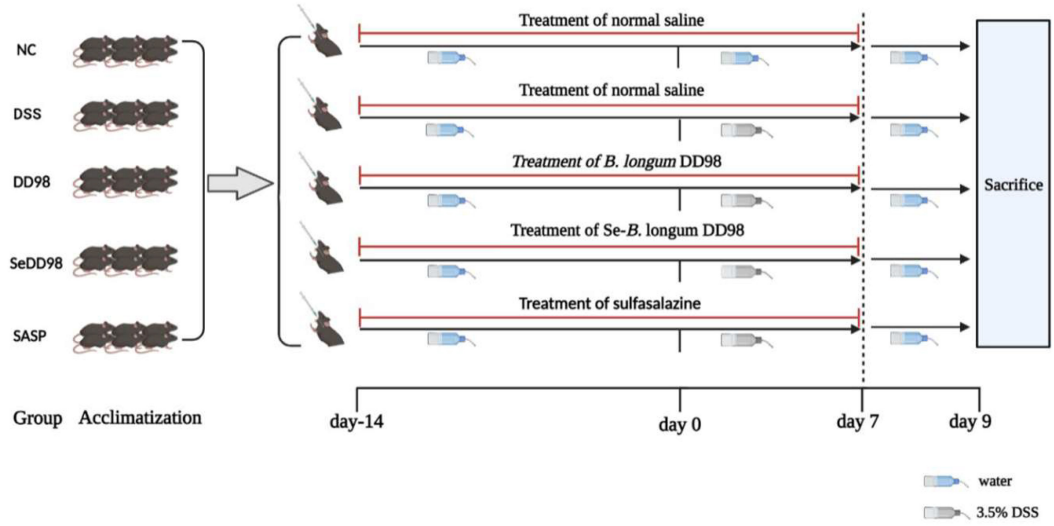

FIGURE 1
Scheme of the animal experimental design.

concentration was measured using a BCA protein quantitative reagent kit (Beyotime, Shanghai, China). An equal amount of protein from each sample was separated by 8% SDS-PAGE and transferred to a PVDF membrane (Millipore, MA, United States). After blocking the membrane with 5% skimmed milk in tris buffered saline with tween-20 (TBST), the membrane was incubated with primary antibody against occludin, ZO-1, and TLR4 (Proteintech Group Inc., IL, United States) overnight at 4°C. GAPDH was used as a control. The membranes were then washed three times with TBST before being probed with the horseradish peroxidase-conjugated secondary antibodies. Signals were detected using a chemiluminescence system (ECL; Bio-rad, CA, United States; Tanon 4600, China) and the intensities were quantified using the ImageJ software.

16S gut microbiota profiling

Samples of mice colon contents of all groups were taken out and three mice in DSS and five mice in other groups were sequenced. Total bacterial DNA was extracted from fecal samples using a QIAamp Fast DNA Stool Mini Kit (Qiagen, Hilden, Germany) following the manufacturer's procedures. The V3-V4 hypervariable region of the bacterial 16S rRNA gene was amplified for species classification by PCR using the specific primer. Illumina Miseq PE300 was used for sequencing after purification and library construction. Then, high-throughput sequencing was used to analyze the sample data. Alpha and beta-diversity were calculated to reflect the species richness in each group as well as to evaluate the similarity or difference of bacterial composition among groups. Linear discriminant analysis Effect Size (LEfSe) was analyzed to assay the species differences.

Statistical analysis

All data were presented as the mean ± standard error of the mean (SEM). Statistical analysis was performed by the SPSS 26.0 statistical software. The difference between groups was analyzed by the one-way analysis of variance (ANOVA) or Kruskal–Wallis tests, and $p < 0.05$ was considered to be statistically significant.

Results

Effect of selenium-enriched *Bifidobacterium longum* DD98 on symptoms of the dextran sulfate sodium-induced colitis

As reported previously, body weight, DAI, and colon length reflected the severity of inflammation in DSS-induced colitis. The average body weight of each group during this experiment can be seen in **Supplementary Table 3**. The body weight of each mouse was recorded daily after 3.5% DSS water administration. Compared to the initial weight on day 0, the body weight of mice in another four groups except the NC group was consistently reduced since day 5 (**Figure 2A**). Mice in the DSS model group exhibited significant weight loss relative to untreated controls. However, Se-*B. longum* DD98 treatment significantly alleviated weight loss (**Figure 2B**). Similarly, DSS treatment remarkably

increased the DAI scores and administration of Se-*B. longum* DD98 markedly decreased the DAI scores compared to the DSS, DD98, and SASP groups (**Figures 2C,D**). Following 7 days of DSS exposure, the colons of the mice were significantly shortened. Treatments of *B. longum* DD98, Se-*B. longum* DD98, and sulfasalazine significantly increased the length of colon and Se-*B. longum* DD98 exhibited a higher distinct effect ($p < 0.05$) (**Figures 2E,F**).

Of note are the spleens from mice that received DSS for 7 days which were significantly enlarged compared to untreated control. Mice from the DD98 displayed mild splenomegaly and the mice in SASP group suffered severe splenomegaly comparable to the DSS group. While, spleen weight of mice in SeDD98 group was significantly lighter than the other treatment (**Figure 2G**). Taken together, these data suggested that Se-*B. longum* DD98 treatment significantly improved UC-related parameters.

Selenium-enriched *Bifidobacterium longum* DD98 alleviated histopathological damage in colitis mice

To better evaluate the effect of Se-*B. longum* DD98 in reducing disease severity in DSS-colitis mice, histological examination of colon sections was also conducted. As shown in **Figure 3A**, the colon section of the DSS group exhibited extensive colonic damages, including neutrophilic infiltrates, ulceration, crypt abscess, and strong transmural inflammation with loss of crypt structure and depletion of goblet cells, while none of these pathological features were found in the NC group. Compared with the DSS group, the treatments of *B. longum* DD98, Se-*B. longum* DD98, and sulfasalazine could improve pathological injury to varying degrees. Furthermore, administration of *B. longum* DD98 and sulfasalazine induced less neutrophil infiltration and ulceration, partially preserved crypt structure and goblet cells in colon sections, and decreased scores in histological analysis although no significant difference. However, Se-*B. longum* DD98 treatment significantly improved these pathological damages and reduced histological scores ($p < 0.05$) (**Figure 3B**). Therefore, Se-*B. longum* DD98 could alleviate colon damage in mice with colitis, which was more effective than *B. longum* DD98 and sulfasalazine.

Effects of selenium-enriched *Bifidobacterium longum* DD98 on the inflammation-related gene expression

The effects of Se-*B. longum* DD98 on the expression of genes involved in inflammation in the colon is measured by RT-qPCR and shown in **Figure 4A**. The results showed that the expression of TNF-α, IFN-γ, IL-6, IL-1β, inducible nitric oxide synthases (iNOS), and cyclooxygenase-2 (COX-2) were significantly increased upon DSS administration, which indicated the severe inflammation of colon tissues in DSS mice. *B. longum* DD98 and sulfasalazine exerted different effects on these parameters compared to colitis mice in this study. For example, *B. longum* DD98 decreased the expression of IL-6, iNOS, and COX-2 in the colon significantly, while, sulfasalazine only exhibited a dramatically protective role in TNF-α and IL-6. Administration of Se-*B. longum* DD98 significantly reduced these six inflammatory genes expression and showed a stronger anti-inflammation action compared to *B. longum* DD98 and sulfasalazine. Something else we need to notice is that Se-*B. longum* DD98 reverted the gut inflammation to normal status, which was inferred from the expression of IFN-γ, IL-6, IL-1β, iNOs, and COX-2 in the SeDD98 group, which was in accordance with that in the NC group ($p > 0.05$). In general, Se-*B. longum* DD98 could regulate colon inflammation to the levels of the NC group and show a higher ability in decreasing inflammation parameters than *B. longum* DD98 and sulfasalazine.

Effects of selenium-enriched *Bifidobacterium longum* DD98 on oxidative stress in serum and colon

Oxidative stress plays an important role in the progression of colitis. To better understand the mechanism of the protection of Se-*B. longum* DD98 against oxidative stress, we determined the content of MDA as well as the activities of SOD and CAT in serum and the activity of GR in colon (**Figure 4B**). The results showed that the content of MDA, which reflects the degree of lipoperoxidation in the host, was significantly increased in the DSS group, indicating the elevated oxidative stress induced by colitis. Among all treatments, Se-*B. longum* DD98 exerted greater influence in bringing down the aberrant level of MDA to the same level as the NC group. What's more, the activities of SOD, CAT, and GR, mirroring the ability of scavenging oxygen-free radicals and resisting oxidative stress, were significantly decreased upon DSS administration. However, their activities could be restored by Se-*B. longum* DD98 treatment. In brief, Se-*B. longum* DD98 exerted significantly greater ability in maintaining the redox balance than *B. longum* DD98 and sulfasalazine.

The impact of selenium-enriched *Bifidobacterium longum* DD98 on intestinal barrier and TLR4 in mice

The impact of Se-*B. longum* DD98 on intestinal barrier function was further investigated. To evaluate the relationship

10.3389/fmicb.2022.955112

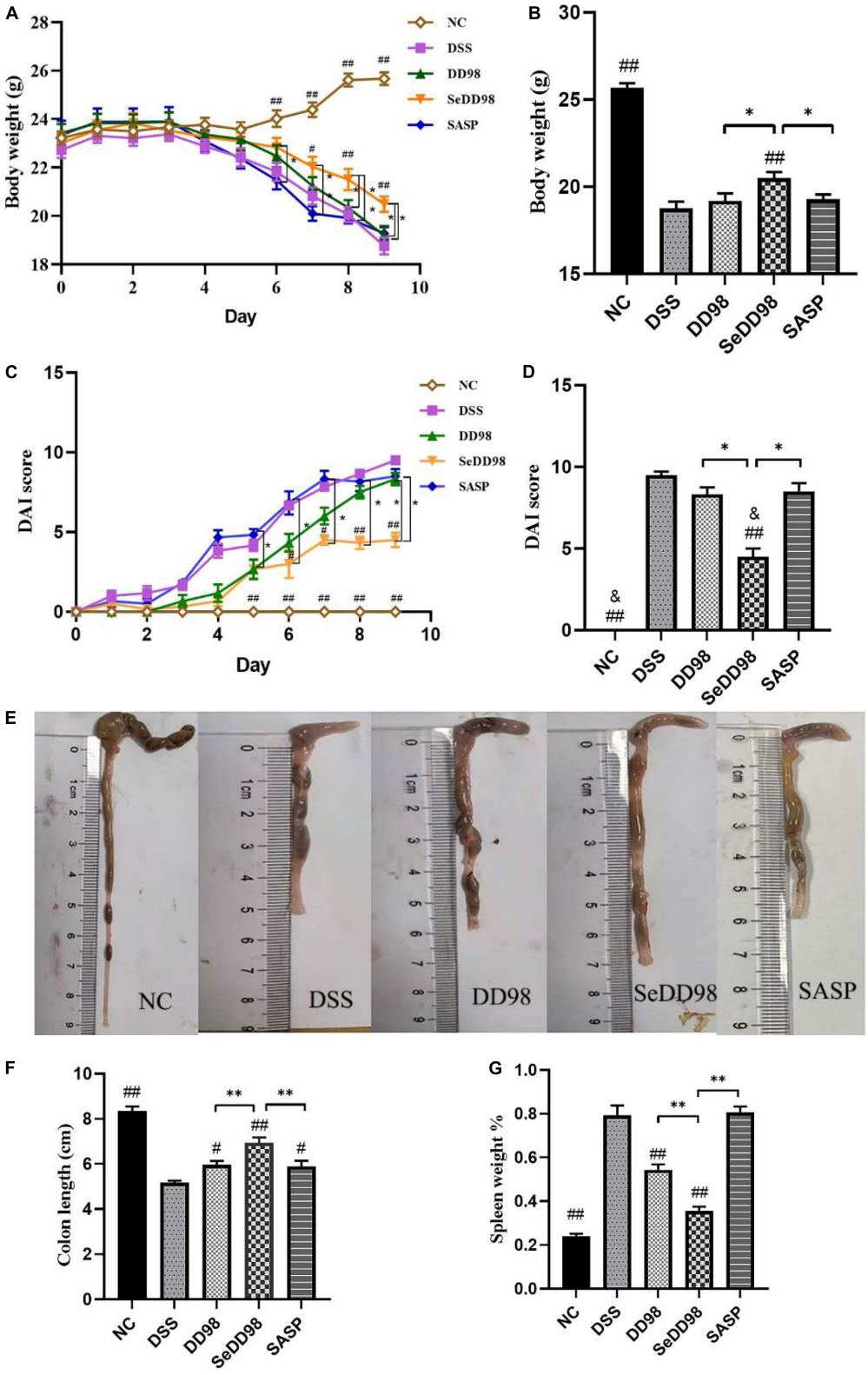

FIGURE 2
Effects of Se-*B. longum* DD98 on colitis symptoms in mice (n = 6). **(A)** Body weight change. **(B)** Body weight among the groups at day 9. **(C)** The disease activity index (DAI) scores calculated with time. **(D)** The DAI scores among the groups at day 9. **(E)** Representative images of colon tissues. **(F)** Data of the colon length. **(G)** The ratio of spleen weight to body weight. Data are shown as the mean ± SEM. $^{*}p < 0.05$, $^{**}p < 0.01$. $^{\#}p < 0.05$ compared to DSS group. $^{\#\#}p < 0.01$ compared to DSS group. $^{\&}p > 0.05$ compared to NC group. Body weight, colon length, and the percentage of spleen weight were analyzed by one-way ANOVA. DAI score was analyzed by Kruskal–Wallis tests.

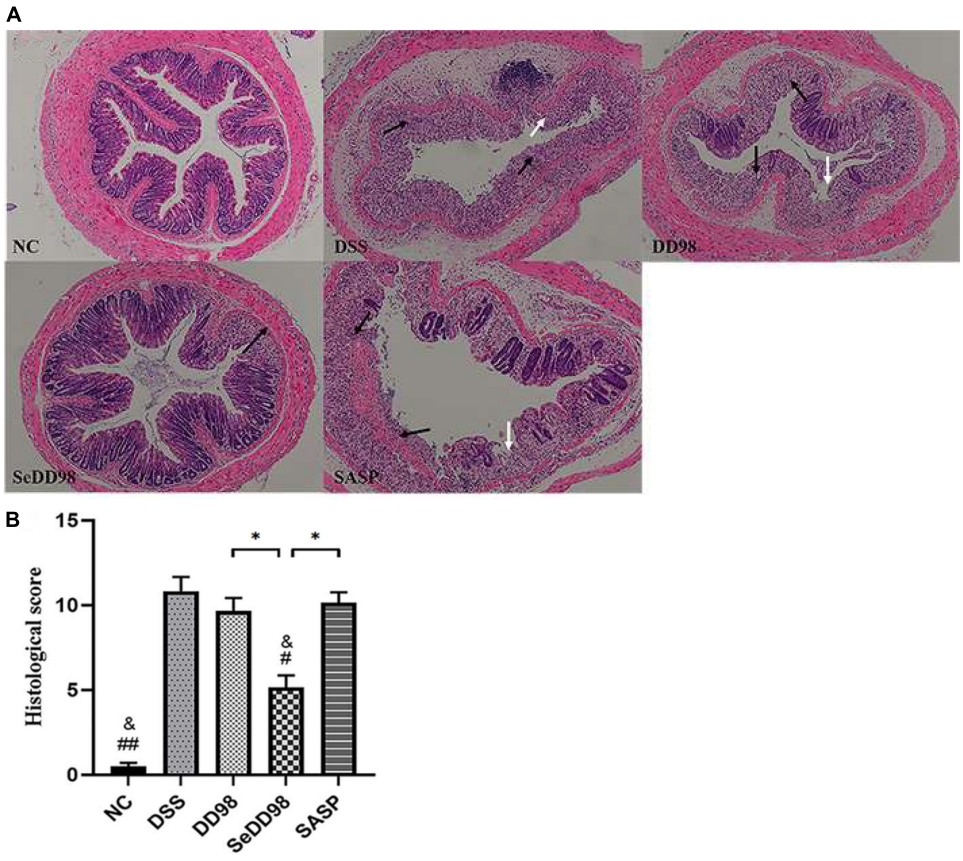

FIGURE 3
(A) Representative photomicrographs of H&E-stained sections of colons. Black arrow, area of strong transmural inflammation with loss of crypt structure and depletion of goblet cells; white arrow, ulceration. **(B)** Histopathology scores of colon tissues (n = 6). Data are shown as the mean ± SEM. $^{*}p < 0.05$. $^{\#}p < 0.05$ compared to DSS group. $^{\#\#}p < 0.01$ compared to DSS group. $^{\&}p > 0.05$ compared to NC group. Histological score was analyzed by Kruskal–Wallis tests.

between Se-*B. longum* DD98 treatment and tight junction integrity in the intestines, we adopted RT-qPCR and western blotting to assess the expression of genes and protein levels of occludin and ZO-1. As shown in **Figure 5**, both gene and protein expressions of occludin (**Figures 5A,C,D**) and ZO-1 (**Figures 5B,C,E**) in the DSS group were significantly decreased compared with that in the NC group. However, *B. longum* DD98, Se-*B. longum* DD98, and sulfasalazine treatments could increase their expression, especially for Se-*B. longum* DD98 (**Figures 5C–E**). These results may explain the reasons for Se-*B. longum* DD98 with higher activity.

Increasing studies suggested that activation of toll-like receptors (TLRs) leads to increased expression of inflammatory cytokines and chemokines, contributing to the inflammatory response in colitis (Kordjazy et al., 2018). We found that both mRNA and protein expression levels of TLR4 were elevated in DSS-induced colitis mice (**Figures 5F,G**), corresponding to the results of increased inflammation caused by DSS. Se-*B. longum* DD98 inhibited TLR4 expression to the normal level, showing a better property in decreasing inflammatory reaction compared to *B. longum* DD98 and sulfasalazine.

The effect of selenium-enriched *Bifidobacterium longum* DD98 on the gut microbiota in colitis mice

To characterize the changes in the gut microbiota composition, the 16S rDNA high-throughput sequencing approach was employed. Rank-abundance curve, reflecting both abundance and evenness of specie, is a way of analyzing diversity in intestinal flora analysis. As shown in **Figure 6A**, the curve revealed that Se-*B. longum* DD98 treatment showed an advantage in increasing the abundance and evenness of gut microbiota in colitis mice. According to the Venn diagram shown in **Figure 6B**, 172 gut microbial species were shared by the five groups of mice, and there were 200, 55, 19, 61, and 97 distinct microbes (ASVs) in the NC, DSS, DD98, SeDD98, and SASP groups, respectively. Analyses of α-diversity demonstrated

10.3389/fmicb.2022.955112

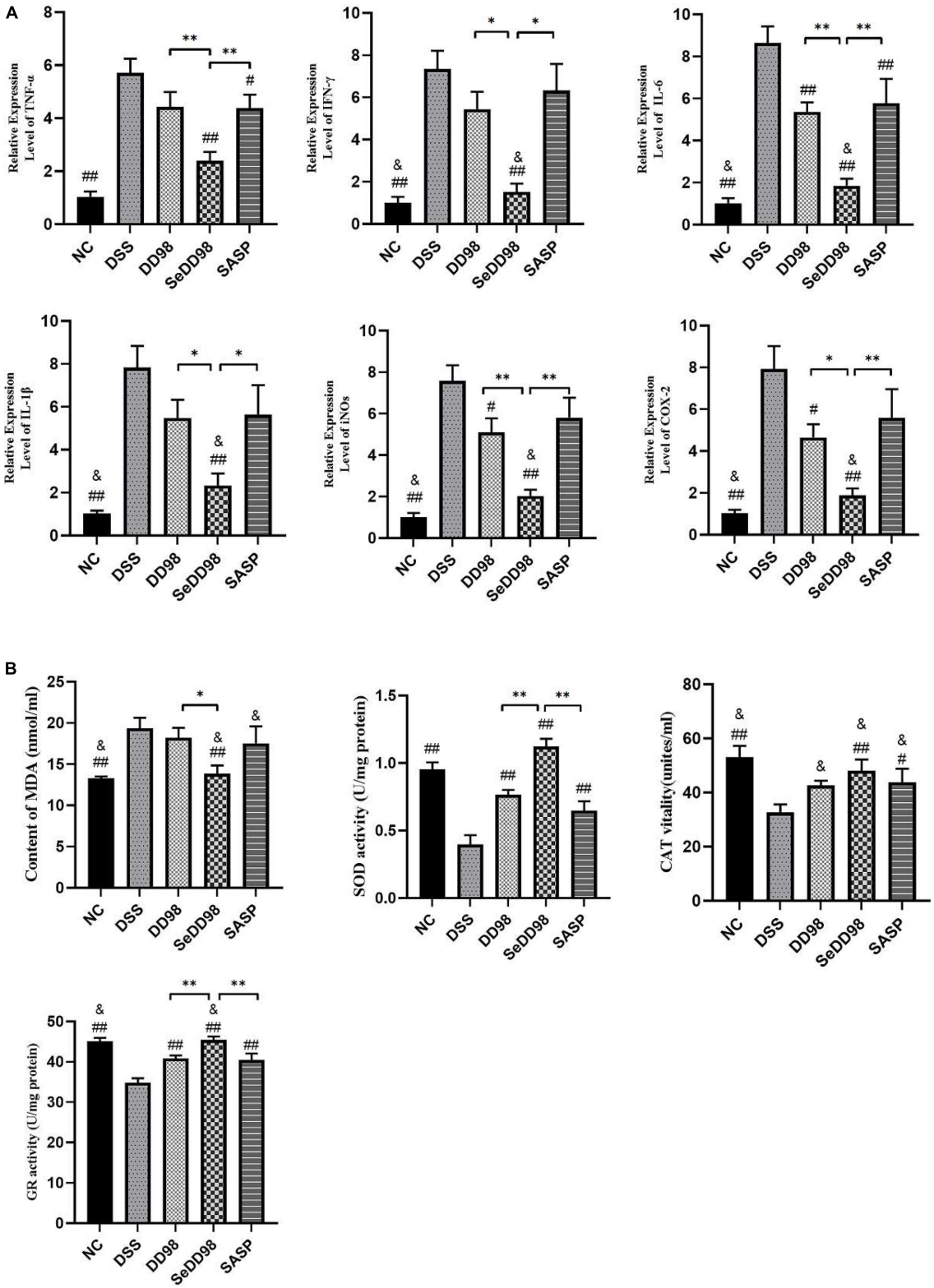

FIGURE 4
Effects of Se-*B. longum* DD98 on the relative expression levels of inflammation in the colon (n = 6) **(A)** and oxidative stress parameters in serum and colon (n = 6) **(B)**. Data are shown as the mean ± SEM. $^{*}p < 0.05$, $^{**}p < 0.01$. $^{\#}p < 0.05$ compared to DSS group. $^{\#\#}p < 0.01$ compared to DSS group. $^{\&}p > 0.05$ compared to NC group. TNF-α, IL-1β, and the activity of SOD, CAT, and GR were analyzed by one-way ANOVA. IFN-γ, IL-6, iNOs, COX-2, and MDA were analyzed by Kruskal–Wallis tests.

10.3389/fmicb.2022.955112

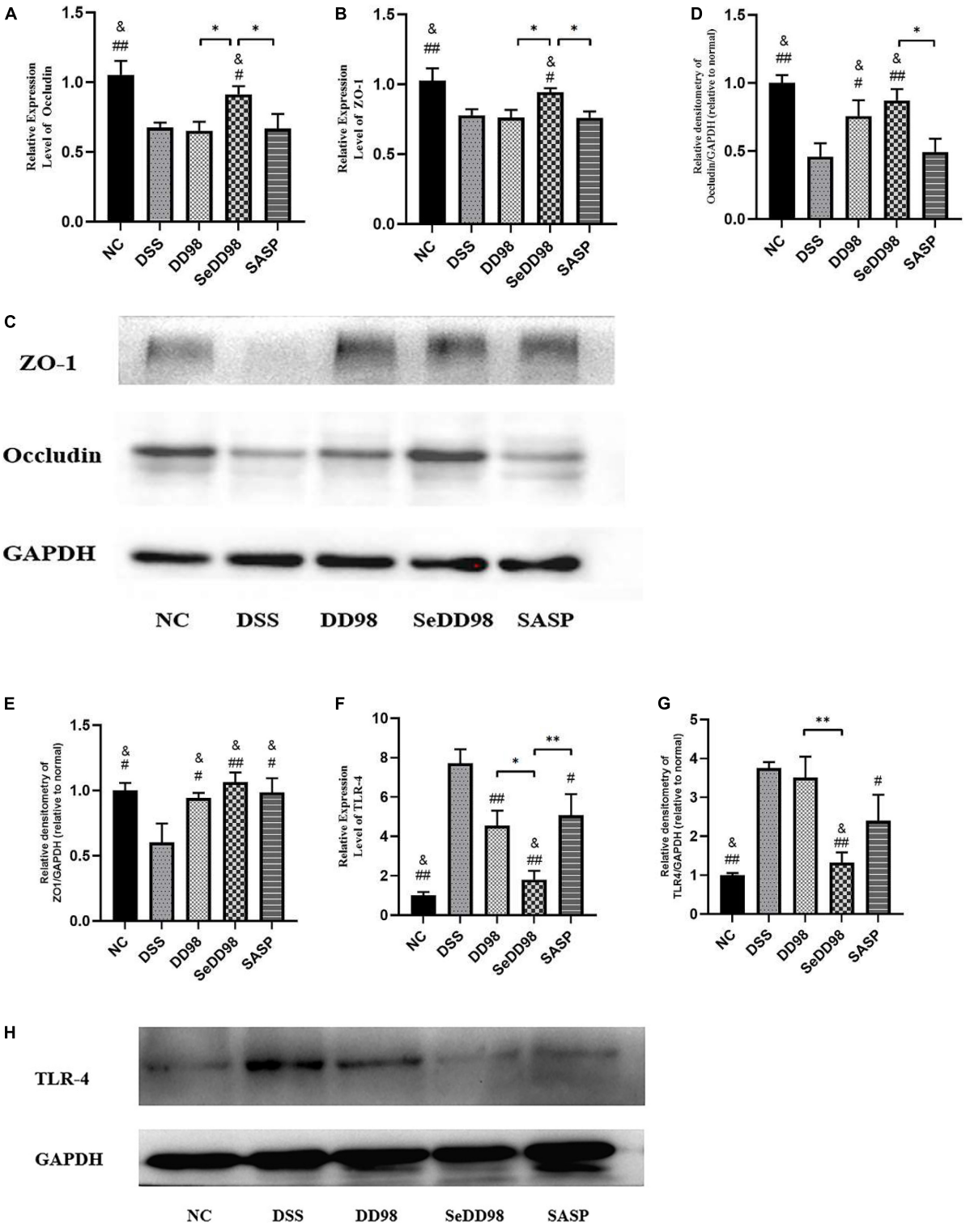

FIGURE 5
The impact of Se-*B. longum* DD98 on intestinal barrier function in DSS-treated mice. **(A,B)** Occludin and ZO-1 mRNA expression levels were assessed *via* RT-qPCR ($n = 6$). **(C–E)** Occludin and ZO-1 levels in colon tissues were assessed *via* western blotting ($n = 3$). **(F)** TLR4 mRNA expression level was assessed *via* RT-qPCR ($n = 6$). **(G,H)** TLR4 level in colon tissues was assessed *via* western blotting ($n = 3$). Data are shown as the mean ± SEM. $^{*}p < 0.05$, $^{**}p < 0.01$. $^{\#}p < 0.05$ compared to DSS group. $^{\#\#}p < 0.01$ compared to DSS group. $^{\&}p > 0.05$ compared to the NC group by one-way ANOVA.

that mice in the SeDD98 group exhibited increased intestinal flora richness and diversity compared with DSS, DD98, and SASP groups. However, it is worth noting that the diversity of microbiota in the DD98 group is the lowest among these groups (**Figure 6C**). β-diversity represents the similarity of microbial composition among different groups, and the β-diversity analysis showed that the similarity of microbial composition between the NC group and the SASP group was good. While, there is a great difference in microbial composition between the NC group and the DSS group and the difference was reduced after Se-*B. longum* DD98 administration (**Figures 6D,E**).

As shown in **Figure 7A**, the phylum of *Bacteroidetes* decreased and the phylum of *Firmicutes* increased after Se-*B. longum* DD98 administration compared with the DSS group. At a family level (**Figure 7B**), an increase in *Akkermansiaceae*, *Bacteroidaceae*, and *Muribaculaceae* and a decrease in *Clostridia-UCG014*, *Lachnospiraceae*, *Lactobacillaceae*, and *Prevotellaceae* in DSS group was observed, and this dysbiosis was altered after Se-*B. longum* DD98 treatment. The LEfSe analysis was also conducted to identify groups of bacteria that differed significantly among groups (**Figures 7C,D**). *Bacteroidaceae* in the DSS group and *Christensenellaceae* and *Lachnospiraceae* in the SeDD98 group were specifically abundant. Spearman's correlation analysis was employed to investigate the correlation of gut microbiota at a genus level with colitis parameters. It was found that 10 genera were at least negatively or positively correlated with one parameter of IBD, including DAI score, transcriptional expression of inflammatory factors, oxidative stress indicators, colon length, the percentage of spleen weight, histopathological score, and intestinal integrity-related genes in intestinal tissue (**Figure 7E**). For instance, *Lactobacillus*, *Erysipelatoclostridium*, and *Colidextribacter* was significantly positively correlated with SOD activity. *Romboutsia* was negatively correlated with ZO1 expression. *Gastranaerophilales* have a very significant positive correlation with MDA, iNOS, IL-6, histopathological score, and DAI score and a significant negative correlation with colon length, GR, and SOD activity.

Discussion

Ulcerative colitis is characterized by a non-specific chronic intestinal inflammation, generally occurring in the distal colon and rectum. The pathogenesis is not entirely understood and is usually caused by multi-factors including genetic predisposition, intestinal flora dysbiosis, epithelial barrier defects, immune susceptibility, and environmental elements (Ungaro et al., 2017). Therapeutic drugs for UC are not effective enough and associate with many adverse reactions. Probiotics such as *Lactobacillus* and *Bifidobacterium* are safe and proven effective in the treatment of UC by mediating microbiota dysbiosis, enhancing intestinal integrity and generating functional metabolites (Sanders et al., 2019). Additionally, as an essential trace element, selenium, especially the organic selenium, is famous for its antioxidative properties and effect on regulating immune systems, thus playing a positive role in UC treatment (Ala and Kheyri, 2021). In this report, we found that Se-*B. longum* DD98, which combines the properties of probiotics and organic selenium, was able to efficiently alleviate symptoms caused by DSS-induced colitis. As **Figure 8** showed, Se-*B. longum* DD98 functioned as the gut microbiota regulator, which was proven to increase the diversity and richness of gut microbiota in DSS-treated mice. Se-*B. longum* DD98 could also enhance tight junction protein expression, such as ZO-1 and Occludin, thus improving the intestinal barrier integrity in colitis mice. Besides, we found that Se-*B. longum* DD98 significantly inhibited the TLR4 expression in colon tissues of UC mice, which was deemed to be a key factor in decreasing pro-inflammatory cytokines. Furthermore, the selenoproteins, that Se-*B. longum* DD98 contains, were famous for its anti-oxidation effect, which was certified by enhanced activity of SOD, CAT, and GR, and decreased MDA content induced by Se-*B. longum* DD98 in this text.

It is reported that DSS colitis caused severe symptoms characterized by weight loss, bloody diarrhea, and abdominal pain that resemble typical features in UC patients (Wirtz et al., 2017). Of note is that although sulfasalazine is one of the first-line drugs in IBD treatment, its effectiveness is just modest and approximately 20% of UC patients are intolerant to this treatment due to its adverse effects (Ye and van Langenberg, 2015; Cai et al., 2021). Besides, lifelong medication was recommended for relapse prevention in mild-to-moderate UC patients (Ko et al., 2019). It also has been reported that the application of sulfasalazine exerted protective effects in DSS-induced colitis mice, whereas there was little significance (Shin et al., 2017). In this study, sulfasalazine showed a modest therapeutic effect on body weight and DAI. Whereas, treatment of sulfasalazine significantly improved the colon length, the activity of SOD, CAT, and GR, and the expression of ZO-1 in colitis mice. What's more, sulfasalazine significantly decreased the expression of pro-inflammatory cytokines, such as TNF-α and IL-6, as well as TLR4 activation in colon tissue compared with DSS-treated mice, indicating the effective but not satisfactory enough effect of sulfasalazine in UC treatment, which was consistent with the utilization status of sulfasalazine in IBD patients. Our findings were in the accordance with related reports, which called for a more efficient treatment both in colitis mice and UC patients. Herein, we demonstrated that Se-*B. longum* DD98 treatment significantly reduced weight loss, colon shortening, splenomegaly, and improved DAI scores and histological scores induced by DSS colitis. Se-*B. longum* DD98 showed a greater advantage in treatment compared with *B. longum* DD98 and sulfasalazine.

It has been pointed out that proinflammatory cytokines and oxidative stress play an important role in the initiation and

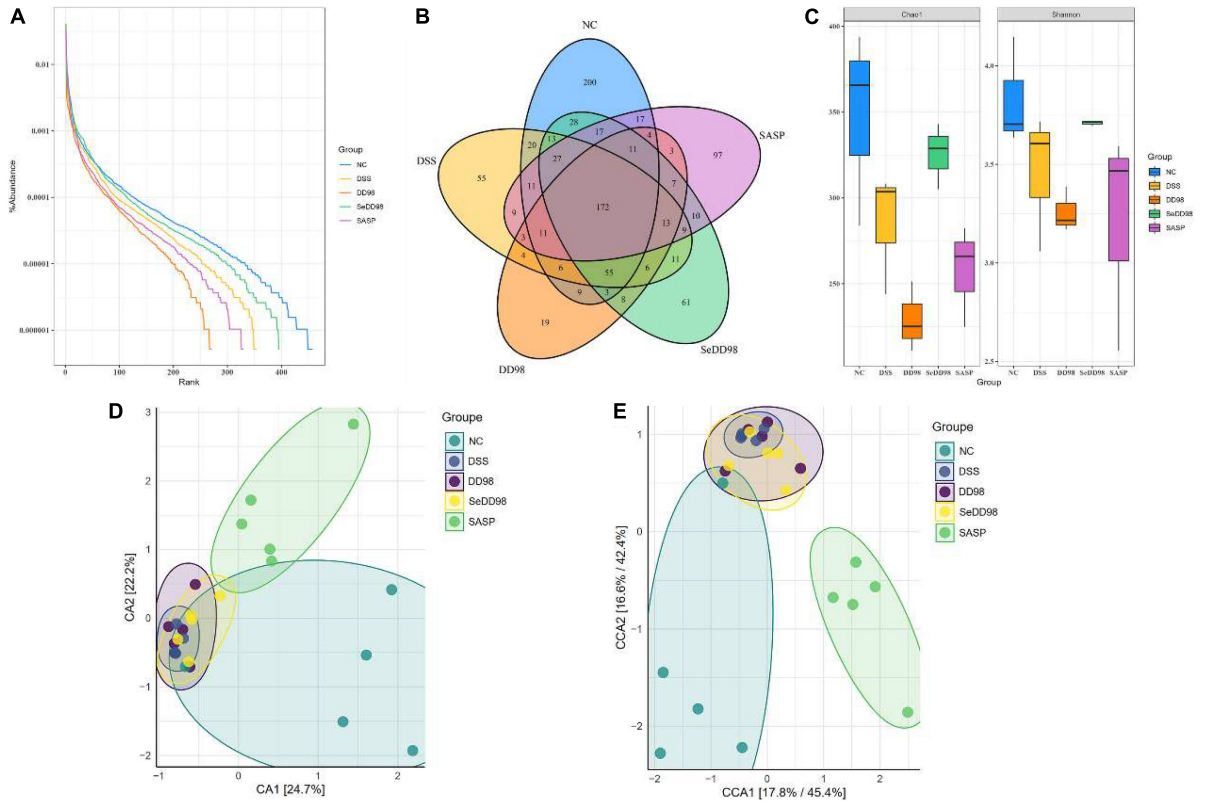

FIGURE 6
The effect of Se-*B. longum* DD98 on the intestinal microbiota (n = 3–5). **(A)** Rank-abundance curve. **(B)** Venn diagram. Totally 172 gut microbial species were shared by the five groups of mice, and there were 200, 55, 19, 61, and 97 distinct microbes (ASVs) in the NC, DSS, DD98, SeDD98, and SASP groups, respectively. **(C)** Chao and Shannon index. **(D,E)** CA and CCA analysis.

evolution of IBD (Strober and Fuss, 2011; Wang et al., 2016). And the supplement of selenium or probiotics could alleviate inflammatory cytokines and preserve the microstructure of colon (Kaur et al., 2018; Bian et al., 2019). TNF-α is the major meditator of inflammation and specific blockade of TNF-α with drugs such as infliximab and etanercept were demonstrated to have great efficacy in the treatment of IBD patients (Yao et al., 2019). IFN-γ, IL-1β, and IL-6 also play a crucial role in the development of colitis. Peng et al. reported that anthocyanins from the fruits of *Lycium ruthenicum* Murray decreased mRNA of TNF-α, IL-6, IFN-γ, and IL-1β in DSS-induced colitis in mice (Peng et al., 2019). Our study was in line with this research and demonstrated that the inhibitory effect of Se-*B. longum* DD98 on mRNA expression of proinflammatory cytokines was better than *B. longum* DD98 and sulfasalazine in colitis mice. NO is also an important pro-inflammatory initiator generated by iNOS in damaging tissue cells and leading to inflammation. A reduction of expression of iNOS is beneficial to alleviate oxidative stress and inflammation. A recent study demonstrated that enhanced COX-2 expression was observed in colonic epithelial tissues of UC patients and selenium decreased COX-2 expression by activating AMP-activated protein kinase (Hwang et al., 2006; Lin et al., 2018). Therefore, the change of COX-2, which was decreased to a normal level after Se-*B. longum* DD98 treatment, was detected by expression at the mRNA level in the present study. Besides, UC is complicated with a large amount of generation of reactive oxygen species (ROS), leading to lipid peroxidation and MDA production. So, MDA reflects the degree of lipid peroxidation and cell injury. The endogenous antioxidant system such as SOD, CAT, and GR can reduce oxidative stress and ROS production directly or indirectly. It is widely recognized that selenoproteins exert an antioxidant effect by participating in the synthesis of antioxidant enzymes (Ala and Kheyri, 2021). In the present study, the results showed that the content of MDA was significantly increased after DSS administration. At the same time, SOD, CAT, and GR activities were significantly inhibited in the DSS group. Administration of Se-*B. longum* DD98 exerted greater ability in regulating the aberrant level of the aforementioned parameters to the same level as the NC group, indicating a better inhibition effect on oxidative stress than probiotic *B. longum* DD98 and sulfasalazine.

Furthermore, IBD is complicated with a reduced intestinal barrier and an impaired intestinal barrier precedes symptoms

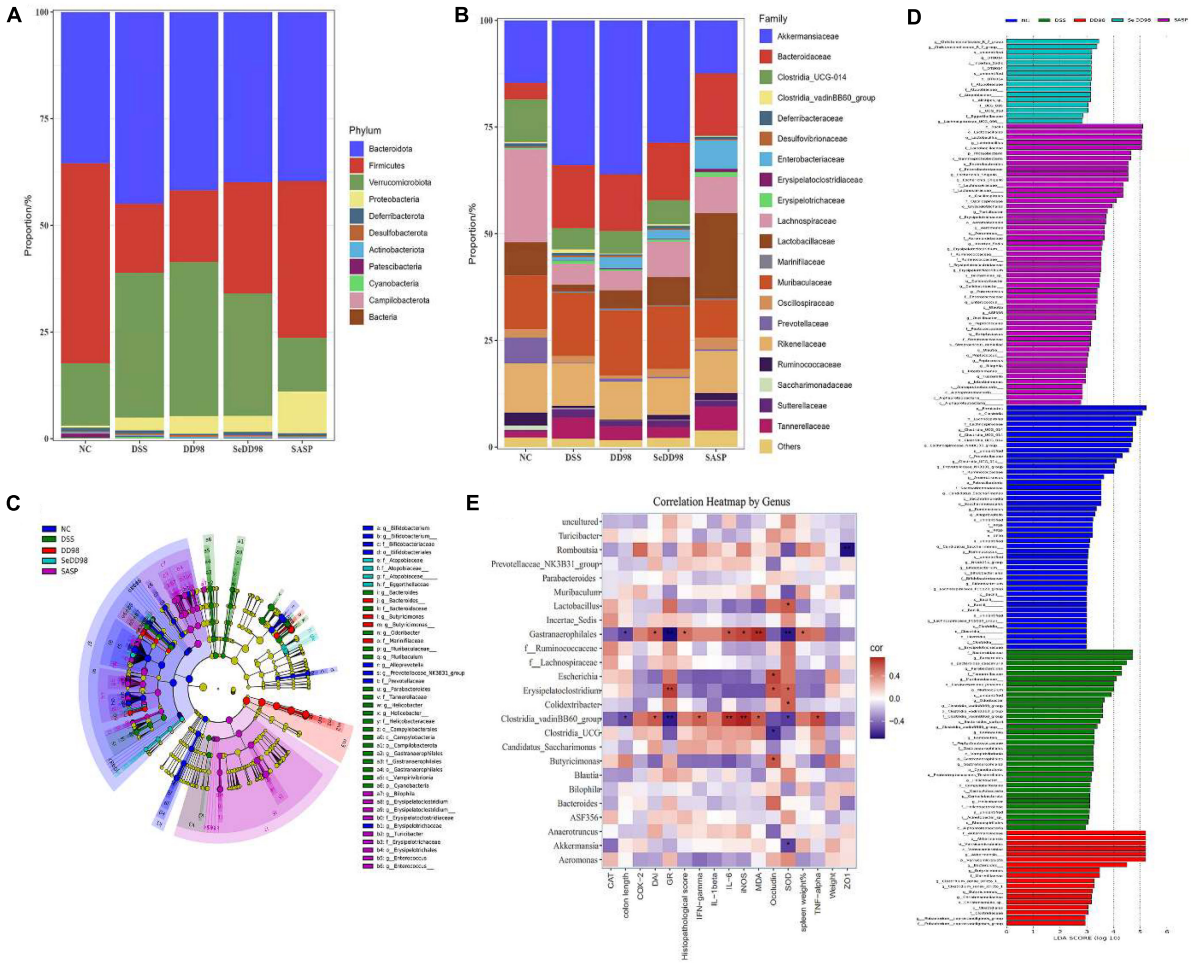

FIGURE 7
Relative abundance of taxa at the phylum **(A)** and family **(B)** levels; Cladogram of LEfSe analysis **(C)** and Histogram of the LDA scores **(D)**; Correlation between gut microbiota and colitis parameters by Spearman correlation analysis. *Spearman's correlation is significant at a level of 0.05; **Spearman's correlation is significant at a level of 0.01 **(E)** (n = 3–5).

for years, indicating that an impaired intestinal barrier contributed to the progression of this disease (Mehandru and Colombel, 2021). As a vital component of the intestinal barrier, tight junction (TJ) proteins play crucial roles in maintaining barrier integrity. The abnormal function of colonic TJ proteins, including the downregulation of ZO-1 and occludin, increases colon permeability and leads to the destruction of the intestinal barrier (Zeisel et al., 2019). *In vitro* and *in vivo* studies showed that supplementation of probiotics formed the microscopic scaffolds of the intestinal barrier, and enhanced intestinal barrier integrity and expression of tight junction proteins (Resta–Lenert and Barrett, 2006; Rose et al., 2021). Besides, Zhai et al. (2018b) reported that dietary selenium supplementation promoted the mRNA expression levels of TJ proteins in normal mice, which was confirmed by FMT to DSS-treated mice. In this study, DSS induced a dramatic reduction on the expression of occludin and ZO-1 in colon tissues, while Se-*B. longum* DD98 treatment significantly increased mRNA expression of TJ protein levels, which was ascertained by western-blotting results.

In DSS colitis mice, DSS exerted toxicity to the intestinal barrier and caused epithelial injury in the colon, giving opportunistic pathogens and luminal antigens a chance to pass through the impaired barrier and induce a rapid and profound inflammatory immune response (Wirtz et al., 2017). Therefore, TLR4, a receptor expressed in intestinal epithelial cells, recognized pathogen-associated molecular patterns (PAMPs) such as flagellin and lipopolysaccharide (LPS) and becomes activated, which leads to the over-generation of inflammatory cytokines and IBD (Kordjazy et al., 2018). Besides, the activation of TLR4 is known to induce NF-κB to transfer from cytoplasm to nucleus through MyD88-dependent or MyD88-independent pathways, thus initiating pro-inflammatory gene transcription and aggravating inflammation severity. It was also reported

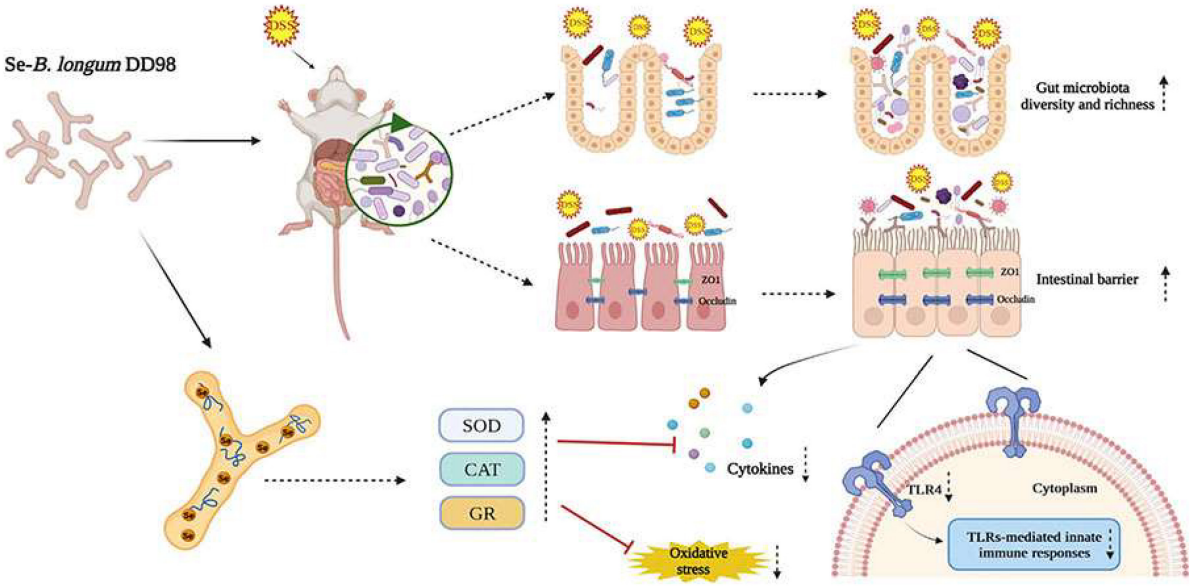

FIGURE 8
Proposed mechanisms of Se-*B. longum* DD98 in the inhibition of DSS-induced colitis in mice.

that TLR4 activation both had advantages and disadvantages. On one hand, minor activation of TLR4 is essential for immune homeostasis. While, over-expression of TLR4 can lead to the induction of host inflammatory responses, such as IBD (Luo et al., 2020). Therefore, decreasing the over-expression of TLR4 is an important target for the treatment of IBD. In the present study, the mRNA and protein levels of TLR4 were elevated in the intestines after DSS treatment. All interventions reversed the increased TLR4 level to a different degree, while mice in the SeDD98 group possessed the significantly lowest TLR4 level in the colon. Probiotics or selenium supplements have been reported to decrease the level of TLR4 expression (Bian et al., 2019; Chen et al., 2020), which is in line with our results that Se-*B. longum* DD98 exhibited a priority in decreasing the activation of TLR4 and related proinflammatory cytokines compared with probiotic *B. longum* DD98 and sulfasalazine.

Recent evidence showed that the pathogenesis of IBD was complicated by gut microbiota dysbiosis, an undesirable change in the composition of gut microbiota, which includes a reduction in the abundance of *Firmicutes* as well as increases in the abundance of *Proteobacteria* and *Bacteroidetes* (Ni et al., 2017; Nishida et al., 2018). Probiotics and selenium supplements are widely used to regulate intestinal flora in experimental colitis models (Bian et al., 2019; Ala and Kheyri, 2021). Furthermore, the intestinal microbiome is also associated with the integrity of the intestinal barrier and stable immune function. Herein, the composition of intestinal flora in mice among different treatment groups was investigated. We found that the community of composition of the microbiota from the DSS group is significantly different from the NC group. The Chao and Shannon index are important indicators of community richness and diversity. The results showed that after Se-*B. longum* DD98 treatment, the richness and diversity of gut microbiota were elevated. At the phylum level, the ratio of *Firmicutes* to *Bacteroidetes*, an index inversely related to the severity of IBD symptoms (Sartor and Wu, 2017), was increased after Se-*B. longum* DD98 treatment. At the family level, the administration of Se-*B. longum* DD98 altered the flora composition in DSS-treated mice, including a decrease in *Akkermansiaceae* and an increase in *Clostridia-UCG014*, *Lachnospiraceae*, *Lactobacillaceae*, and *Prevotellaceae*. A recent study pointed out that some enzymes secreted by *Akkermansiaceae* broke down the mucus in the lining of the large intestine, posing a risk to the intestinal barrier in the gut (Khan et al., 2020). *Clostridia-UCG014* is a probiotic associated with tryptophan metabolism. Its tryptophan catabolite indole-3-acetic acid (IAA) can activate the aryl hydrocarbon receptor (AhR), which was thought to exert a protective role in the gut barrier (Chengcheng et al., 2021). Besides, *Lactobacillaceae* has been widely recognized as a probiotic and used for the prevention of IBD for many years. *Prevotellaceae* was thought to participate in short chain fatty acid (SCFA) generation, which protected the intestinal barrier in IBD patients (Shen et al., 2017). Therefore, Se-*B. longum* DD98 may play a protective role in DSS-induced mice by upregulating the abundance of *Clostridia-UCG014*, *Lachnospiraceae*, *Lactobacillaceae*, and *Prevotellaceae*. It is interesting to note that the abundance and diversity of gut microbiota in the DD98 group were the lowest in these groups,

which may be related to the relatively small sequencing samples. However, at the phylum level, the ratio of *Firmicutes* to *Bacteroidetes* was increased in the DD98 group compared with the DSS group. What's more, supplement of *B. longum* DD98 upregulated the proportion of *Lactobacillaceae*, which could be connected with colitis improvement in mice. Additionally, LEFSe analysis was employed to identify the community with statistical differences between groups. Herein, we found that *Christensenellaceae* and *Lachnospiraceae* in the SeDD98 group were specifically abundant. *Lachnospiraceae* is a kind of SCFA-producing probiotic, which regulates the immune response and inflammatory response in the host. Furthermore, *Lachnospiraceae* was demonstrated to protect the colon barrier and is inversely related to diarrhea in patients (Guo et al., 2020). It is reported that *Christensenellaceae* is very important for host health and was a significantly negative correlation with inflammation, although the exact mechanism was unknown (Waters and Ley, 2019). What's more, Spearman's correlation analysis was employed to investigate the correlation of gut microbiota at a genus level with colitis parameters in our study. It is worth noting that *Gastranaerophilales* had a significant positive correlation with MDA, iNOS, IL-6, histopathological score, and DAI score and a significant negative correlation with colon length, GR, and SOD activity. However, little is known about this microorganism. There was also a study indicating that *Gastranaerophilales* is capable of converting glucose, mannose, starch, or glycogen into lactate, ethanol, and formate (Soo et al., 2014). Besides, one analysis of the correlation between gut microbiota and six common autoimmune diseases revealed that the family *Peptostreptococcaceae*, order *Gastranaerophilales*, and genus *Romboutsia* shared the most enriched taxa among five autoimmune diseases (Cao et al., 2021). Our research was in line with this and a relevant study should be the carrier to investigate the exact function of *Gastranaerophilales*. Although, Khattab et al. (2022) demonstrated the protective effect of selenium-enriched *Bifidobacterium longum* mutants on piroxicam-induced UC. However, there were many differences between these two studies. In all, Se-*B. longum* DD98 showed a better alleviation of symptoms, inflammation level, and oxidative stress, as well as a priority in protecting the intestinal barrier integrity and regulating the composition of gut microbiota in DSS-treated mice. We have compared the efficacy of Se-*B. longum* DD98 with Na_2SeO_3 (inorganic selenium), SeMet (organic selenium), or the combination of *B. longum* DD98 and SeMet during many experiments, and found that Se-*B. longum* DD98 exerted a superior effect than selenium or the combination in these different symptoms or diseases (Zhao et al., 2020a,b; Zhu et al., 2021). What's more, in this study, Se-*B. longum* DD98 was treated as a whole, independent enhanced probiotic product. Meanwhile, the applications of probiotic or sulfasalazine are dominant in UC treatment, and selenium is seldom used in UC prevention alone due to its potential toxicity. So, we did not adopt selenium-treated group as a comparison in this study. Many studies have confirmed the protective effect of probiotics in UC *via* regulating gut microbiota dysbiosis. Lu et al. (2022) demonstrated that *Eurotium cristatum*, a probiotic, ameliorated DSS-Induced UC in mice by modulating the gut microbiota, and fecal bacteria transplantation (FMT) from probiotic-treated mice showed a similar protective effect in colitis mice, indicating that the microbiome changes result from probiotic supplement cause the alleviated inflammation in UC. What's more, selenium was also determined to balance the gut microbiota avoiding health damage associated with dysbiosis (Ferreira et al., 2021). However, whether the restoration of gut microbiota after Se-*B. longum* DD98 administration is the cause or consequence of the alleviated inflammation in UC needs to be further confirmed. Germ-free mice and FMT should be adopted to investigate the role that gut microbiota plays in the alleviation of UC after Se-*B. longum* DD98 supplement. Further studies should be carried out to investigate the exact mechanism of how selenium strengthened the efficacy of probiotic *B. longum* DD98.

Conclusion

In this study, we found that Se-*B. longum* DD98 effectively ameliorates DDS-induced colitis in mice. The effects were mainly due to alleviating symptoms caused by DSS, inhibiting the expression of the pro-inflammatory cytokines, decreasing the level of oxidative stress, promoting the expression of tight junction proteins, inhibiting the activation of TLR4, and regulating the gut microbiota. Furthermore, Se-*B. longum* DD98 presented greater protective effects than *B. longum* DD98 or sulfasalazine. In summary, Se-*B. longum* DD98 effectively attenuated DSS-induced colitis in mice, providing a potential therapeutic strategy for the treatment of IBD patients in the future.

Data availability statement

The datasets for this study can be found in online repositories. The name of the repositories and accession number can be found below: NCBI BioProject accession no: PRJNA842916.

Ethics statement

The animal study was reviewed and approved by Institutional Animal Care and Use Committee (IACUC) of Shanghai Jiao Tong University.

Author contributions

YH: investigation, methodology, writing-original draft, and writing-review and editing. XJ: investigation and methodology. FG: investigation and software. TL: visualization and software. HZ: methodology. XH: investigation. YY: resources and project administration. SK: writing-review and editing. DC: supervision, project administration, and funding acquisition. All authors contributed to the article and approved the submitted version.

Funding

This work was supported by grants from the National Key Research and Development Program of China (No. 2018YFA0901904), the Science and Technology Talent Project of Shanghai (No. 17XD1423200), the National Natural Science Foundation of China (No. 81872775), and funding from the Consumer Products Group of Ministry of Industry and Information Technology of China (No. CEIEC-2020-ZM02-0165).

Conflict of interest

The authors declare that the research was conducted in the absence of any commercial or financial relationships that could be construed as a potential conflict of interest.

Publisher's note

All claims expressed in this article are solely those of the authors and do not necessarily represent those of their affiliated organizations, or those of the publisher, the editors and the reviewers. Any product that may be evaluated in this article, or claim that may be made by its manufacturer, is not guaranteed or endorsed by the publisher.

Supplementary material

The Supplementary Material for this article can be found online at: https://www.frontiersin.org/articles/10.3389/fmicb.2022.955112/full#supplementary-material

References

Agus, A., Planchais, J., and Sokol, H. (2018). Gut Microbiota Regulation of Tryptophan Metabolism in Health and Disease. *Cell Host Microbe* 23, 716–724. doi: 10.1016/j.chom.2018.05.003

Ala, M., and Kheyri, Z. (2021). The rationale for selenium supplementation in inflammatory bowel disease: A mechanism-based point of view. *Nutrition* 85:111153. doi: 10.1016/j.nut.2021.111153

Bai, A. P., Ouyang, Q., Xiao, X. R., and Li, S. F. (2006). Probiotics modulate inflammatory cytokine secretion from inflamed mucosa in active ulcerative colitis. *Int. J. Clin. Pract.* 60, 284–288. doi: 10.1111/j.1368-5031.2006.00833.x

Bian, X., Wu, W., Yang, L., Lv, L., Wang, Q., Li, Y., et al. (2019). Administration of Akkermansia muciniphila Ameliorates Dextran Sulfate Sodium-Induced Ulcerative Colitis in Mice. *Front. Microbiol.* 10:2259. doi: 10.3389/fmicb.2019.02259

Cai, Z., Wang, S., and Li, J. (2021). Treatment of Inflammatory Bowel Disease: A Comprehensive Review. *Front. Med.* 8:765474. doi: 10.3389/fmed.2021.765474

Cao, R. R., He, P., and Lei, S. F. (2021). Novel microbiota-related gene set enrichment analysis identified osteoporosis associated gut microbiota from autoimmune diseases. *J. Bone Miner. Metab.* 39, 984–996. doi: 10.1007/s00774-021-01247-w

Chen, Y., Zhao, Y.-F., Yang, J., Jing, H.-Y., Liang, W., Chen, M.-Y., et al. (2020). Selenium alleviates lipopolysaccharide-induced endometritisviaregulating the recruitment of TLR4 into lipid rafts in mice. *Food Funct.* 11, 200–210. doi: 10.1039/c9fo02415h

Chengcheng, Y., Yao, D., Daoyuan, R., Xingbin, Y., and Yan, Z. (2021). Gut microbiota-dependent catabolites of tryptophan play a predominant role in the protective effects of turmeric polysaccharides against DSS-induced ulcerative colitis. *Food Funct.* 12, 9793–9807. doi: 10.1039/d1fo01468d

Elinav, E., Nowarski, R., Thaiss, C. A., Hu, B., Jin, C. C., and Flavell, R. A. (2013). Inflammation-induced cancer: Crosstalk between tumours, immune cells and microorganisms. *Nat. Rev. Cancer* 13, 759–771. doi: 10.1038/nrc3611

Ferreira, R. L. U., Sena-Evangelista, K. C. M., De Azevedo, E. P., Pinheiro, F. I., Cobucci, R. N., and Pedrosa, L. F. C. (2021). Selenium in Human Health and Gut Microflora: Bioavailability of Selenocompounds and Relationship With Diseases. *Front. Nutr.* 8:685317. doi: 10.3389/fnut.2021.685317

Guo, H., Chou, W. C., Lai, Y. J., Liang, K. X., Tam, J. W., Brickey, W. J., et al. (2020). Multi-omics analyses of radiation survivors identify radioprotective microbes and metabolites. *Science* 370:eaay9097. doi: 10.1126/science.aay9097

Han, Y. M., Yoon, H., Lim, S., Sung, M.-K., Shin, C. M., Park, Y. S., et al. (2017). Risk Factors for Vitamin D, Zinc, and Selenium Deficiencies in Korean Patients with Inflammatory Bowel Disease. *Gut Liver* 11, 363–369. doi: 10.5009/gnl16333

Hill, C., Guarner, F., Reid, G., Gibson, G. R., Merenstein, D. J., Pot, B., et al. (2014). The International Scientific Association for Probiotics and Prebiotics consensus statement on the scope and appropriate use of the term probiotic. *Nat. Rev. Gastroenterol. Hepatol.* 11, 506–514. doi: 10.1038/nrgastro.2014.66

Hindryckx, P., Jairath, V., and D'Haens, G. (2016). Acute severe ulcerative colitis: From pathophysiology to clinical management. *Nat. Rev. Gastroenterol. Hepatol.* 13, 654–664. doi: 10.1038/nrgastro.2016.116

Huang, Z., Rose, A. H., and Hoffmann, P. R. (2012). The Role of Selenium in Inflammation and Immunity: From Molecular Mechanisms to Therapeutic Opportunities. *Antioxid. Redox Signal.* 16, 705–743. doi: 10.1089/ars.2011.4145

Hwang, J. T., Kim, Y. M., Surh, Y. J., Baik, H. W., Lee, S. K., Ha, J., et al. (2006). Selenium regulates cyclooxygenase-2 and extracellular signal-regulated kinase signaling pathways by activating AMP-activated protein kinase in colon cancer cells. *Cancer Res.* 66, 10057–10063. doi: 10.1158/0008-5472.CAN-06-1814

Kaplan, G. G., and Ng, S. C. (2017). Understanding and Preventing the Global Increase of Inflammatory Bowel Disease. *Gastroenterology* 152, 313–321.e2. doi: 10.1053/j.gastro.2016.10.020

Kaur, R., Thakur, S., Rastogi, P., and Kaushal, N. (2018). Resolution of Cox mediated inflammation by Se supplementation in mouse experimental model of colitis. *PLoS One* 13:e0201356. doi: 10.1371/journal.pone.0201356

Khan, S., Waliullah, S., Godfrey, V., Khan, M. A. W., Ramachandran, R. A., Cantarel, B. L., et al. (2020). Dietary simple sugars alter microbial ecology in the gut and promote colitis in mice. *Sci. Transl. Med.* 12:eaay6218. doi: 10.1126/scitranslmed.aay6218

Khattab, A. N., Darwish, A. M., Othman, S. I., Allam, A. A., and Alqhtani, H. A. (2022). Anti-inflammatory and Immunomodulatory Potency of Selenium-Enriched Probiotic Mutants in Mice with Induced Ulcerative Colitis. *Biol. Trace Elem. Res.* [Epub ahead of print]. doi: 10.1007/s12011-022-03154-1

Khazdouz, M., Daryani, N. E., Alborzi, F., Jazayeri, M. H., Farsi, F., Hasani, M., et al. (2020). Effect of Selenium Supplementation on Expression of SIRT1 and PGC-1alpha Genes in Ulcerative Colitis Patients: A Double Blind Randomized Clinical Trial. *Clin. Nutr. Res.* 9, 284–295. doi: 10.7762/cnr.2020.9.4.284

Ko, C. W., Singh, S., Feuerstein, J. D., Falck-Ytter, C., Falck-Ytter, Y., Cross, R. K., et al. (2019). AGA Clinical Practice Guidelines on the Management of Mild-to-Moderate Ulcerative Colitis. *Gastroenterology* 156, 748–764. doi: 10.1053/j.gastro.2018.12.009

Kordjazy, N., Haj-Mirzaian, A., Haj-Mirzaian, A., Rohani, M. M., Gelfand, E. W., Rezaei, N., et al. (2018). Role of toll-like receptors in inflammatory bowel disease. *Pharmacol. Res.* 129, 204–215. doi: 10.1016/j.phrs.2017.11.017

Krehl, S., Loewinger, M., Florian, S., Kipp, A. P., Banning, A., Wessjohann, L. A., et al. (2012). Glutathione peroxidase-2 and selenium decreased inflammation and tumors in a mouse model of inflammation-associated carcinogenesis whereas sulforaphane effects differed with selenium supply. *Carcinogenesis* 33, 620–628. doi: 10.1093/carcin/bgr288

Kuria, A., Tian, H. D., Li, M., Wang, Y. H., Aaseth, J. O., Zang, J. J., et al. (2022). Selenium status in the body and cardiovascular disease: A systematic review and meta-analysis. *Crit. Rev. Food Sci. Nutr.* 62, 282–283. doi: 10.1080/10408398.2020.1815964

Li, P., Chen, G., Zhang, J., Pei, C., Chen, Y., Gong, J., et al. (2022). Live Lactobacillus acidophilus alleviates ulcerative colitis *via* the SCFAs/mitophagy/NLRP3 inflammasome axis. *Food Funct.* 13, 2985–2997. doi: 10.1039/d1fo03360c

Lin, X., Sun, Q., Zhou, L., He, M., Dong, X., Lai, M., et al. (2018). Colonic epithelial mTORC1 promotes ulcerative colitis through COX-2-mediated Th17 responses. *Mucosal Immunol.* 11, 1663–1673. doi: 10.1038/s41385-018-0018-3

Lu, X. J., Jing, Y., Zhang, N. S., and Cao, Y. G. (2022). Eurotium cristatum, a Probiotic Fungus from Fuzhuan Brick Tea, and Its Polysaccharides Ameliorated DSS-Induced Ulcerative Colitis in Mice by Modulating the Gut Microbiota. *J. Agric. Food Chem.* 70, 2957–2967. doi: 10.1021/acs.jafc.1c08301

Luo, X., Yue, B., Yu, Z., Ren, Y., Zhang, J., Ren, J., et al. (2020). Obacunone Protects Against Ulcerative Colitis in Mice by Modulating Gut Microbiota, Attenuating TLR4/NF-kappaB Signaling Cascades, and Improving Disrupted Epithelial Barriers. *Front. Microbiol.* 11:497. doi: 10.3389/fmicb.2020.00497

Mehandru, S., and Colombel, J. F. (2021). The intestinal barrier, an arbitrator turned provocateur in IBD. *Nat. Rev. Gastroenterol. Hepatol.* 18, 83–84. doi: 10.1038/s41575-020-00399-w

Meier, J., and Sturm, A. (2011). Current treatment of ulcerative colitis. *World J. Gastroenterol.* 17, 3204–3212. doi: 10.3748/wjg.v17.i27.3204

Molodecky, N. A., Soon, I. S., Rabi, D. M., Ghali, W. A., Ferris, M., Chernoff, G., et al. (2012). Increasing Incidence and Prevalence of the Inflammatory Bowel Diseases With Time, Based on Systematic Review. *Gastroenterology* 142, 46–54. doi: 10.1053/j.gastro.2011.10.001

Ni, J., Wu, G. D., Albenberg, L., and Tomov, V. T. (2017). Gut microbiota and IBD: Causation or correlation? *Nat. Rev. Gastroenterol. Hepatol.* 14, 573–584. doi: 10.1038/nrgastro.2017.88

Nishida, A., Inoue, R., Inatomi, O., Bamba, S., Naito, Y., and Andoh, A. (2018). Gut microbiota in the pathogenesis of inflammatory bowel disease. *Clin. J. Gastroenterol.* 11, 1–10. doi: 10.1007/s12328-017-0813-5

Peng, Y., Yan, Y., Wan, P., Chen, D., Ding, Y., Ran, L., et al. (2019). Gut microbiota modulation and anti-inflammatory properties of anthocyanins from the fruits of Lycium ruthenicum Murray in dextran sodium sulfate-induced colitis in mice. *Free Radic. Biol. Med.* 136, 96–108. doi: 10.1016/j.freeradbiomed.2019.04.005

Resta–Lenert, S., and Barrett, K. E. (2006). Probiotics and Commensals Reverse TNF-α– and IFN-γ–Induced Dysfunction in Human Intestinal Epithelial Cells. *Gastroenterology* 130, 731–746. doi: 10.1053/j.gastro.2005.12.015

Rose, E. C., Odle, J., Blikslager, A. T., and Ziegler, A. L. (2021). Probiotics, Prebiotics and Epithelial Tight Junctions: A Promising Approach to Modulate Intestinal Barrier Function. *Int. J. Mol. Sci.* 22:6729. doi: 10.3390/ijms22136729

Sanders, M. E., Merenstein, D. J., Reid, G., Gibson, G. R., and Rastall, R. A. (2019). Probiotics and prebiotics in intestinal health and disease: From biology to the clinic. *Nat. Rev. Gastroenterol. Hepatol.* 16, 605–616. doi: 10.1038/s41575-019-0173-3

Sartor, R. B. (2004). Therapeutic manipulation of the enteric microflora in inflammatory bowel diseases: Antibiotics, probiotics, and prebiotics. *Gastroenterology* 126, 1620–1633. doi: 10.1053/j.gastro.2004.03.024

Sartor, R. B., and Wu, G. D. (2017). Roles for Intestinal Bacteria, Viruses, and Fungi in Pathogenesis of Inflammatory Bowel Diseases and Therapeutic Approaches. *Gastroenterology* 152, 327–339.e4. doi: 10.1053/j.gastro.2016.10.012

Shen, F., Zheng, R. D., Sun, X. Q., Ding, W. J., Wang, X. Y., and Fan, J. G. (2017). Gut microbiota dysbiosis in patients with non-alcoholic fatty liver disease. *Hepatobiliary Pancreat. Dis. Int.* 16, 375–381. doi: 10.1016/s1499-3872(17)60019-5

Shin, M.-R., Kim, K. J., Kim, S. H., Kim, S. J., Seo, B.-I., An, H.-J., et al. (2017). Comparative Evaluation between Sulfasalazine Alone and in Combination with Herbal Medicine on DSS-Induced Ulcerative Colitis Mice. *Biomed Res. Int.* 2017, 1–10. doi: 10.1155/2017/6742652

Soo, R. M., Skennerton, C. T., Sekiguchi, Y., Imelfort, M., Paech, S. J., Dennis, P. G., et al. (2014). An Expanded Genomic Representation of the Phylum Cyanobacteria. *Genome Biol. Evol.* 6, 1031–1045. doi: 10.1093/gbe/evu073

Stillie, R., and Stadnyk, A. W. (2009). Role of TNF receptors, TNFR1 and TNFR2, in dextran sodium sulfate-induced colitis. *Inflamm. Bowel Dis.* 15, 1515–1525. doi: 10.1002/ibd.20951

Strober, W., and Fuss, I. J. (2011). Proinflammatory cytokines in the pathogenesis of inflammatory bowel diseases. *Gastroenterology* 140, 1756–1767. doi: 10.1053/j.gastro.2011.02.016

Ungaro, R., Mehandru, S., Allen, P. B., Peyrin-Biroulet, L., and Colombel, J.-F. (2017). Ulcerative colitis. *Lancet* 389, 1756–1770. doi: 10.1016/s0140-6736(16)32126-2

Wang, Z., Li, S., Cao, Y., Tian, X., Zeng, R., Liao, D. F., et al. (2016). Oxidative Stress and Carbonyl Lesions in Ulcerative Colitis and Associated Colorectal Cancer. *Oxid. Med. Cell. Longev.* 2016:9875298. doi: 10.1155/2016/9875298

Waters, J. L., and Ley, R. E. (2019). The human gut bacteria Christensenellaceae are widespread, heritable, and associated with health. *BMC Biol.* 17:83. doi: 10.1186/s12915-019-0699-4

Wirtz, S., Popp, V., Kindermann, M., Gerlach, K., Weigmann, B., Fichtner-Feigl, S., et al. (2017). Chemically induced mouse models of acute and chronic intestinal inflammation. *Nat. Protoc.* 12, 1295–1309. doi: 10.1038/nprot.2017.044

Yao, D., Dong, M., Dai, C., and Wu, S. (2019). Inflammation and Inflammatory Cytokine Contribute to the Initiation and Development of Ulcerative Colitis and Its Associated Cancer. *Inflamm. Bowel Dis.* 25, 1595–1602. doi: 10.1093/ibd/izz149

Ye, B., and van Langenberg, D. R. (2015). Mesalazine preparations for the treatment of ulcerative colitis: Are all created equal? *World J. Gastrointest. Pharmacol. Ther.* 6, 137–144. doi: 10.4292/wjgpt.v6.i4.137

Zeisel, M. B., Dhawan, P., and Baumert, T. F. (2019). Tight junction proteins in gastrointestinal and liver disease. *Gut* 68, 547–561. doi: 10.1136/gutjnl-2018-316906

Zhai, Q. X., Cen, S., Li, P., Tian, F. W., Zhao, J. X., Zhang, H., et al. (2018a). Effects of Dietary Selenium Supplementation on Intestinal Barrier and Immune Responses Associated with Its Modulation of Gut Microbiota. *Environ. Sci. Technol. Lett.* 5, 724–730. doi: 10.1021/acs.estlett.8b00563

Zhai, Q., Cen, S., Li, P., Tian, F., Zhao, J., Zhang, H., et al. (2018b). Effects of Dietary Selenium Supplementation on Intestinal Barrier and Immune Responses Associated with Its Modulation of Gut Microbiota. *Environ. Sci. Technol. Lett.* 5, 724–730.

Zhao, D., Zhu, H., Gao, F., Qian, Z., Mao, W., Yin, Y., et al. (2020b). Antidiabetic effects of selenium-enriched Bifidobacterium longum DD98 in type 2 diabetes model of mice. *Food Funct.* 11, 6528–6541. doi: 10.1039/d0fo00180e

Zhao, D., Gao, F., Zhu, H., Qian, Z., Mao, W., Yin, Y., et al. (2020a). Selenium-enriched Bifidobacterium longum DD98 relieves metabolic alterations and liver injuries associated with obesity in high-fat diet-fed mice. *J. Funct. Foods* 72:104051. doi: 10.1016/j.jff.2020.104051

Zhu, C., Ling, Q., Cai, Z., Wang, Y., Zhang, Y., Hoffmann, P. R., et al. (2016). Selenium-Containing Phycocyanin from Se-Enriched Spirulina platensis Reduces Inflammation in Dextran Sulfate Sodium-Induced Colitis by Inhibiting NF-κB Activation. *J. Agric. Food Chem.* 64, 5060–5070. doi: 10.1021/acs.jafc.6b01308

Zhu, H., Lu, C., Gao, F., Qian, Z., Yin, Y., Kan, S., et al. (2021). Selenium-enriched Bifidobacterium longum DD98 attenuates irinotecan-induced intestinal and hepatic toxicity *in vitro* and *in vivo*. *Biomed. Pharmacother.* 143:112192. doi: 10.1016/j.biopha.2021.112192

Zhu, H., Zhou, Y., Qi, Y., Ji, R., Zhang, J., Qian, Z., et al. (2019). Preparation and characterization of selenium enriched-Bifidobacterium longum DD98, and its repairing effects on antibiotic-induced intestinal dysbacteriosis in mice. *Food Funct.* 10, 4975–4984. doi: 10.1039/c9fo00960d

frontiers | Frontiers in Microbiology

TYPE Original Research
PUBLISHED 09 August 2022
DOI 10.3389/fmicb.2022.956438

OPEN ACCESS

EDITED BY
Vincenzina Fusco,
Italian National Research Council, Italy

REVIEWED BY
Laura Mitrea,
University of Agricultural Sciences and Veterinary Medicine of Cluj-Napoca, Romania
Wenyi Zhang,
Inner Mongolia Agricultural University, China

*CORRESPONDENCE
Yiqing Zhao
yiqing.zhao@hyproca.com

SPECIALTY SECTION
This article was submitted to Food Microbiology, a section of the journal Frontiers in Microbiology

RECEIVED 30 May 2022
ACCEPTED 18 July 2022
PUBLISHED 09 August 2022

CITATION
Zhao Y, Liu Q, Hou Y and Zhao Y (2022) Alleviating effects of gut micro-ecologically regulatory treatments on mice with constipation. *Front. Microbiol.* 13:956438. doi: 10.3389/fmicb.2022.956438

Alleviating effects of gut micro-ecologically regulatory treatments on mice with constipation

Yueming Zhao[1,2], Qingjing Liu[2], Yanmei Hou[2,3] and Yiqing Zhao[2]*

[1]Key Laboratory of Dairy Science, Ministry of Education, Department of Food Science, Northeast Agricultural University, Harbin, China, [2]Hyproca Nutrition Co., Ltd., Changsha, China, [3]Hunan Provincial Key Laboratory of Food Science and Biotechnology, Changsha, China

Treatments targeted for gut microbial regulation are newly developed strategies in constipation management. In this study, the alleviating effects of gut micro-ecologically regulatory treatments on constipation in mice were investigated. Male BALB/c mice were treated with loperamide to induce constipation, and then the corresponding intervention was administered in each group, respectively. The results showed that administration of mixed probiotics (MP), a 5-fold dose of postbiotics (P5), both synbiotics (S and S2), as well as mixed probiotics and postbiotics (MPP) blend for 8 days shortened the time to the first black stool, raised fecal water content, promoted intestinal motility, and increased serum motilin level in loperamide-treated mice. Furthermore, these treatments altered gut microbial composition and metabolism of short-chain fatty acids (SCFA). Based on linear regression analysis, SCFA was positively correlated with serum motilin except for isobutyrate. It suggested gut microbial metabolites affected secretion of motilin to increase gastrointestinal movement and transportation function and thus improved pathological symptoms of mice with constipation. In conclusion, the alteration of gut micro-ecology is closely associated with gastrointestinal function, and it is an effective way to improve constipation *via* probiotic, prebiotic, and postbiotic treatment.

KEYWORDS

constipation, probiotics, postbiotics, synbiotics, gut microbial regulation, short-chain fatty acids

Introduction

Constipation, a worldwide digestive disorder, impacts around 14% of people in different regions (Black and Ford, 2018). Patients with constipation usually show symptoms like reduced frequency of defecation, hard or lumpy stools, a sensation of incomplete evacuation, and abdominal bloating and pain (Mearin et al., 2016).

Chronic constipation not only hurts patients' health but also increases the burden on the social health care system (Sharma and Rao, 2017). Conventionally, laxative drugs are widely used for the treatment of astriction, which can prompt defecation soon after administration, but the effects are less likely to exist when the drug use is ceased (Smith, 1973; Corazziari, 1999; Wang et al., 2020). Thus, laxative abuse probably leads to drug dependence and may deteriorate the symptom of constipation. Understanding the mechanisms of astriction has become the key aspect of developing new therapies.

Studies in recent years have shown the role of the gut microbiome in the pathogenesis of constipation. Zoppi et al. (1998) compared the composition of the fecal sample from children with constipation as well as their healthy counterparts and found that clostridia were more abundant in the constipated subjects (Zoppi et al., 1998). *Clostridium difficile* is the main cause to induce nosocomial diarrhea in children (Sadeghifard et al., 2010). Furthermore, in a children cohort with autism spectrum disorder (ASD), the proportion of *Clostridium* spp. including *Clostridium paraputri*, *Clostridium bolteae*, and *Clostridium perfringens* in the feces of was significantly higher than in neurotypical children, and especially *Clostridium diffiicile* and *Clostridium clostridiioforme* were not found in neurotypical children (Kandeel et al., 2020). This suggests that *Clostridium* spp. play an important role in affecting the development of diseases including neurological and intestinal disorders during childhood. Adult patients with functional constipation presented lower abundances of *Bacteroides*, *Roseburia*, and *Coprococcus* compared with healthy volunteers (Shin et al., 2019), and a pediatric study showed that the genus *Prevotella* decreased in constipated obese children compared with non-constipated obese children, while *Blautia*, *Coprococcus*, and *Ruminococcus* increased (Zhu et al., 2014). Animal experiments reported a reduced abundance of *Bacteroides*, *Lactobacillus*, *Desulfovibrio, and Methylobacterium*, and enriched *Clostridium* and *Akkermansia* (Cao et al., 2017; Wang et al., 2017a; Yi et al., 2019). Cao et al. transferred the feces of constipated patients to the intestine of germ-free mice and the recipient formed constipation-like symptoms, including reduced intestinal peristalsis and fecal water content (Cao et al., 2017). Although the character of the gut microbiome in constipated subjects differs across different researches, gut microbial dysbiosis probably contributes to the pathogenesis of constipation.

Intestinal health lays a great reliance on the gut microbiome (Sekirov et al., 2010). Gut microbiota affects the development of constipation *via* modulating the intestinal functions and communication with the central nervous system (Simon et al., 2021). Regulating gut microecology has been a newly developed strategy for constipation treatment. Probiotics, prebiotics, and synbiotics have been reported as dietary supplements to regulate immune responses, gut microbial composition, and metabolisms (Ştefănuţ et al., 2015; Kamiński et al., 2020), and especially microbial metabolites contribute to the improvement of gastrointestinal functions and interaction between the gut and central system *via* cell signaling pathways (Mitrea et al., 2022). Probiotics supplement is one of the most effective measures to regulate gut microbiota. Many studies have concluded that probiotic consumption helps to change the gut microbial structure and alleviate constipation in humans (Dimidi et al., 2014; Martinez-Martinez et al., 2017; Huang et al., 2018) and animal models (Wang et al., 2017a, 2020; Inatomi and Honma, 2021; Wang R. et al., 2021). Meanwhile, prebiotics, which can promote the growth of beneficial bacteria in the intestine, has been reported to improve constipation-associated disorders and partly change the gut microbial composition in adults (Yu et al., 2017; Chu et al., 2019). Present literature has demonstrated postbiotics consist of cell corpses, cell components, cell-wall fractions, cellular secretions, and metabolites, that are from probiotics and if received in sufficient quantity possess health effects on the host (Sabahi et al., 2022). In this research, the effects of mixed probiotics, postbiotics, synbiotics, and probiotics plus postbiotics on loperamide-induced constipation in BALB/c mice were compared, and their influence on the hormonal level, fecal short-chain fatty acids (SCFA), as well as gut microbial composition were sequenced to explore the potential targets of their constipation-alleviating function.

Materials and methods

Preparation of experimental formulation

The experimental formulation used in this study was a mixture of probiotics, prebiotics, postbiotics, and other nutritional components. Probiotics, prebiotics, and postbiotics were all purchased from Aunulife Biotechnology Co., Ltd. (Changsha, China). All these powdered products were resuspended or dissolved in saline before use. MP consisted of 6 strains (*Bifidobacterium animalis* subsp. *animalis* BB-115, *B. longum* subsp. *infantis* BLI-02, *Lacticaseibacillus rhamnosus* MP108, *Ligilactobacillus salivarius* AP-32, *L. rhamnosus* F-1, and *Lactiplantibacillus plantarum* LPL28) with a total colony-forming unit of 2.0×10^{10}. The prebiotics contained lactitol, fructooligosaccharides, inulin, and stachyose, and postbiotics consisted of isolated soy protein and 4 strains including *L. plantarum* LPL28, *L. salivarius* AP-32, *B. longum* subsp. *infantis* BLI-02, and *Lactobacillus acidophilus* TYCA06. After fermentation, the supernatant of 4 strains was extracted *via* centrifuging, and then it was mixed with isolated soy protein after heat-kill sterilization. The mixture was made with postbiotics after heat-kill sterilization and spay-drying. Other components used as nutritional supplements were lactose, vitamin C, psyllium seed husk, and some fruit and vegetable powder.

TABLE 1 Experimental design of the animal trail.

Groups	Treatment	Dose (mg/day)	Volume (μL/day)	Vehicle
Control	Saline	–	200	Saline
Model	Saline	–	200	Saline
MP	Mixed probiotics	–	200	Saline
P	Postbiotics	2.5	200	Saline
P5	Postbiotics	0.5	200	Saline
MPP	Mixed probiotics plus postbiotics	1.5	200	Saline
S	Synbiotics	12.3	200	Saline
S2	Synbiotics	24.6	200	Saline

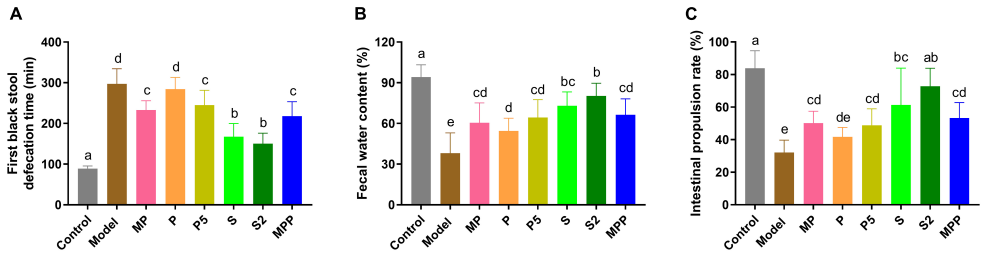

FIGURE 1
The differences in **(A)** time to the first black stool, **(B)** fecal water content, and **(C)** intestinal propulsion rate among groups. Values are expressed as mean ± SEM (n = 8). Results were compared by one-way ANOVA followed Duncan's multiple comparison test. Different letters represent significant differences ($p < 0.05$).

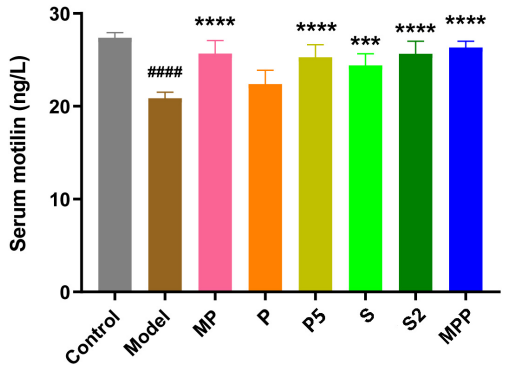

FIGURE 2
The differences in serum motilin level among groups. Values are expressed as mean ± SEM (n = 8). Results were compared by one-way ANOVA and Dunnett's multiple comparison test: ***$p < 0.001$, ****$p < 0.0001$ compared with the model group; ####$p < 0.0001$ compared with the control group.

Animals and experimental design

Eight-week-old male BALB/c mice (n = 64) were purchased from Vital River Laboratory Animal Technology Co., Ltd. (Beijing, China). Mice were fed in a specific pathogen-free environment at a room temperature of 25°C ± 2°C and humidity of 50% ± 5% with a 12-h light–dark cycle, having free access to drinking water and standard chow. After 1 week of adaptation, mice were randomly divided into 8 groups (n = 8/group), containing the control group (control), model group (model), six constipated groups treated with mixed probiotics (MP), postbiotics (P and a 5-fold dose of P, P5), synbiotics (S and a 2-fold dose of S, S2), and probiotics plus postbiotics (MPP), and details of the experimental design were listed in Table 1. The Control group was orally treated only with saline per day during the experimental period by gavage, while the other groups were treated every day with loperamide (10 mg/kg body weight), and with corresponding products 1 h after loperamide administration. The treatments were carried out by gavage and lasted for 8 days. After the intervention period, animals were anesthetized with pentobarbital (50 mg/kg body weight) (Wang et al., 2010) and were then sacrificed by exsanguination. All protocols for the animal experiment were approved by the Ethics Committee of Jiangnan University [JN. No20201130b0720301(355)] and were in accord with the European Community guidelines (directive 2010/63/EU).

Defecation test

Defecation status was represented by first defecation time and fecal water content. Mice were treated with activated

TABLE 2 Serum cytokine concentration in different groups (ng/L).

Groups	IL-6	IL-10	IL-17A	TNF-α	IFN-α	TGF-β 1	IL-1β
Control	15.21 ± 2.34	70.82 ± 7.02	1.00 ± 0.16	70.87 ± 10.99	3.42 ± 0.46	22.44 ± 2.21	10.23 ± 0.84
Model	13.80 ± 0.92	69.10 ± 10.50	1.17 ± 0.20	67.06 ± 4.04	4.04 ± 0.41	23.36 ± 4.10	11.49 ± 1.94
MP	13.85 ± 1.49	70.50 ± 8.84	1.11 ± 0.17	71.52 ± 7.74	3.82 ± 0.64	24.94 ± 5.01	11.28 ± 1.66
P	13.58 ± 1.34	70.39 ± 9.56	1.10 ± 0.18	70.91 ± 8.33	3.82 ± 0.58	22.64 ± 1.21	10.57 ± 0.98
P5	13.50 ± 1.96	70.31 ± 7.72	1.18 ± 0.13	67.04 ± 8.53	4.28 ± 0.49	21.94 ± 2.85	10.28 ± 1.78
MPP	14.64 ± 1.66	67.94 ± 8.65	1.20 ± 0.25	65.25 ± 7.01	4.12 ± 0.32	22.93 ± 3.83	10.65 ± 0.90
S	13.87 ± 2.32	70.34 ± 6.62	1.16 ± 0.14	71.34 ± 5.69	4.14 ± 0.17	22.78 ± 2.58	10.29 ± 1.16
S2	13.26 ± 1.64	71.80 ± 7.24	1.18 ± 0.24	68.56 ± 6.66	4.17 ± 0.23	24.50 ± 2.49	10.99 ± 1.55

Values were expressed as mean ± SD. Results were compared by one-way ANOVA and Dunnett's multiple comparison test.

TABLE 3 Fecal SCFA concentration in different groups (pmol/mg).

	Acetate	Propionate	Butyrate	Isobutyrate	Valerate	Isovalerate
Control	89.568 ± 22.712	15.094 ± 1.767	15.958 ± 3.020	3.354 ± 0.772	2.446 ± 0.228	2.262 ± 0.347
Model	54.733 ± 15.559$^{\#}$	8.133 ± 1.368$^{\#}$	6.271 ± 3.423$^{\#}$	2.488 ± 0.464	1.511 ± 0.169$^{\#}$	1.632 ± 0.381
MP	103.986 ± 18.477**	13.912 ± 2.841*	15.066 ± 4.123*	3.487 ± 0.806	3.140 ± 0.492***	3.042 ± 0.974**
P	54.706 ± 11.628	8.449 ± 1.303	7.616 ± 3.335	2.278 ± 0.493	1.506 ± 0.429	1.511 ± 0.226
P5	76.496 ± 11.071*	16.669 ± 3.743*	17.247 ± 6.501*	2.597 ± 0.334	2.322 ± 0.418	1.764 ± 0.485
MPP	106.951 ± 19.109**	19.486 ± 6.669**	19.129 ± 7.339*	3.608 ± 0.569	2.354 ± 0.847	2.803 ± 0.501*
S	116.413 ± 16.732***	22.318 ± 10.578**	20.168 ± 6.779**	3.664 ± 0.616	2.695 ± 0.427**	3.193 ± 0.631*
S2	100.315 ± 15.478**	17.006 ± 3.752*	16.817 ± 8.198	3.262 ± 0.948	2.703 ± 0.607**	2.407 ± 0.323

Values are expressed as mean ± SD. Results were compared by one-way ANOVA and Dunnett's multiple comparison test: *$p < 0.05$, **$p < 0.01$, ***$p < 0.001$ compared with the model group; $^{\#}p < 0.05$ compared with the control group.

carbon meal 1 h after treatments on the eighth day, and then the time to the first black stool of each mouse was measured according to Wang et al. (Cao et al., 2017). Feces were then collected in individual sterile EP tubes on ice and the water content was determined as described by Lee et al. (2012).

Determination of intestinal propulsion rate

Gastrointestinal (GI) motility was determined as previously described with a modification (Verdu et al., 2009). Mice were fasted from 6:00 p.m. for 18 h on the eighth day and were then treated with loperamide (treated groups) or saline (control group), and activated carbo meal, after which mice were anesthetized with pentobarbital (50 mg/kg body weight) and executed by exsanguination (Wang et al., 2010). The blood sample was collected immediately centrifuged at 3000 × *g*, 4°C for 15 min to obtain serum. The entire intestine was carefully removed out of the abdomen and put on blotting paper. The distance from the pylorus to the end of the darkened intestine as well as the entire length of the intestine was measured. The intestinal propulsion rate was calculated by the ratio of the length of the black intestine to the entire intestinal length.

Serum cytokine detection

Serum samples were divided into 2 to 3 individual sterile EP tubes and then stored at −80°C. Cytokines containing IFN-α, TGF-β1, TNF-α, IL-1β, IL-6, IL-10, and IL-17A were determined using a MILLIPLEX MAP Kit Mouse Cytokine/Chemokine Magnetic Bead Panel (EMD Millipore Corporation, Billerica, MA, United States) according to the manufacturer's instruction and performed with a Luminex MAGPIX System (Luminex, Austin, TX, United States).

Quantification of fecal short-chain fatty acids

Fecal samples (∼50 mg) were soaked with saturated NaCl solution and acidified with sulfuric acid (10%). Total SCFAs extracted with diethyl ether. Determination of the concentration of SCFA was carried out through a gas chromatography-mass spectrometry system (GCMS-QP2010 Ultra system, Shimadzu Corporation, Japan) according to Wang et al. (2017a). The concentration of total SCFA was calculated as the sum of

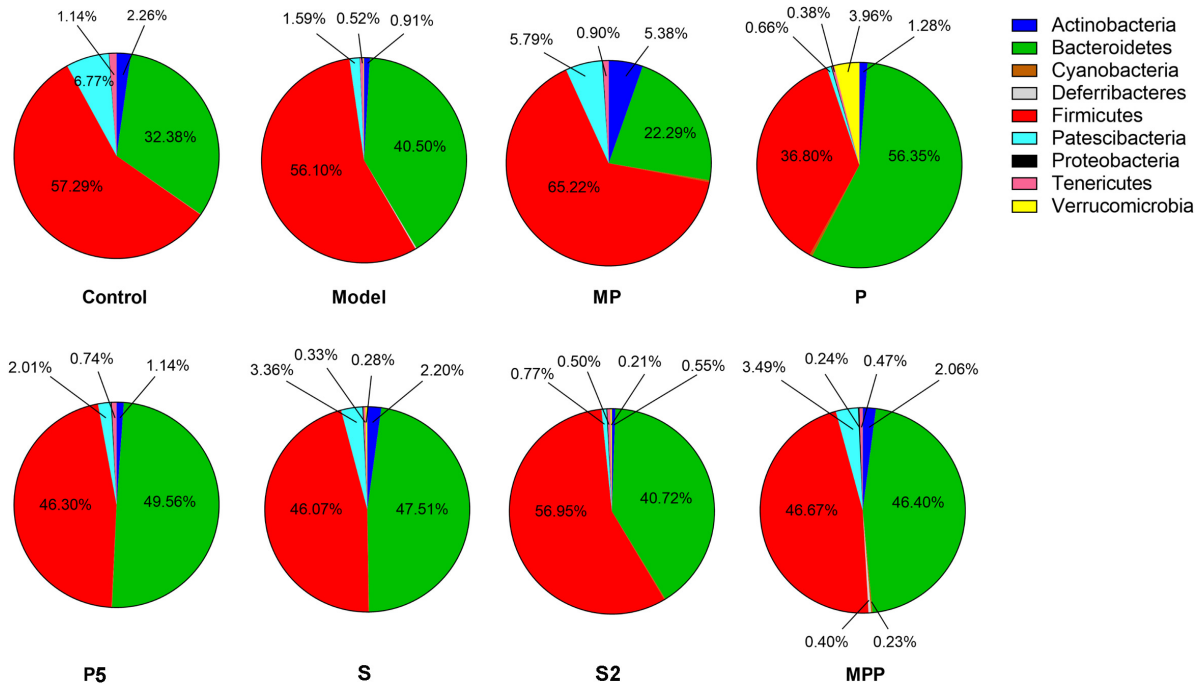

FIGURE 3
The differences in the relevant abundance of gut microbial phyla among groups.

acetic, propionic, butyric, isobutyric, valeric, and isovaleric acids.

Analysis of fecal microbiome

Total DNA was extracted from fecal samples with a FastDNA Spin Kit for Soil (MP Biomedicals, catalog no. 6560-200) following the manufacturer's instructions. The V4 region of the 16S rRNA gene was amplified using a specific primer (forward primer, 5′-AYT GGG YDT AAA GNG-3′; reverse primer, 5′-TAC NVG GGT ATC TAA TCC-3′) by polymerase chain reaction (PCR) as previously described. Then the PCR products were purified, quantified, and sequenced as previously described by Zhao et al. (2018). Afterward, the 16S rRNA sequence data were analyzed using the QIIME2 pipeline as previously described (Zhao et al., 2018).

Statistical analysis

Results were all expressed as mean ± SD. One-way ANOVA and Dunnett's multiple comparison test were applied for the comparison between groups. Comparisons and linear regression analysis were carried out using GraphPad Prism version 8.0.2 (GraphPad Software Inc., United States). Values with $p < 0.05$ were considered significantly different. Pearson's correlation analysis was conducted in MetaboAnalyst 5.0.[1]

Results

The synbiotics improved defecation status and gastrointestinal transit

As shown in **Figure 1A**, compared with the control group, a 2.3-fold increase in the time to the first black stool was observed in the model group ($p < 0.0001$), suggesting the formation of constipation due to loperamide treatment. The figure for S and S2 treatments decreased to approximately 50% of that of the model group. MP, P5, and MPP treatments partly shortened the defecation time, while P treatment showed little effect on it. Fecal water content in the model group decreased in comparison with the control group, which was nearly restored in S and S2 groups (**Figure 1B**). MP, P5, and MPP partly raised fecal water content, while the effect of P treatment was less significant than other treatments (**Figure 1B**). As shown in **Figure 1C**, the intestinal propulsion rate in the model group was significantly lower than that in the control group. Administration of S2 restored the decrease in intestinal propulsion rate, while the

1 https://www.metaboanalyst.ca/

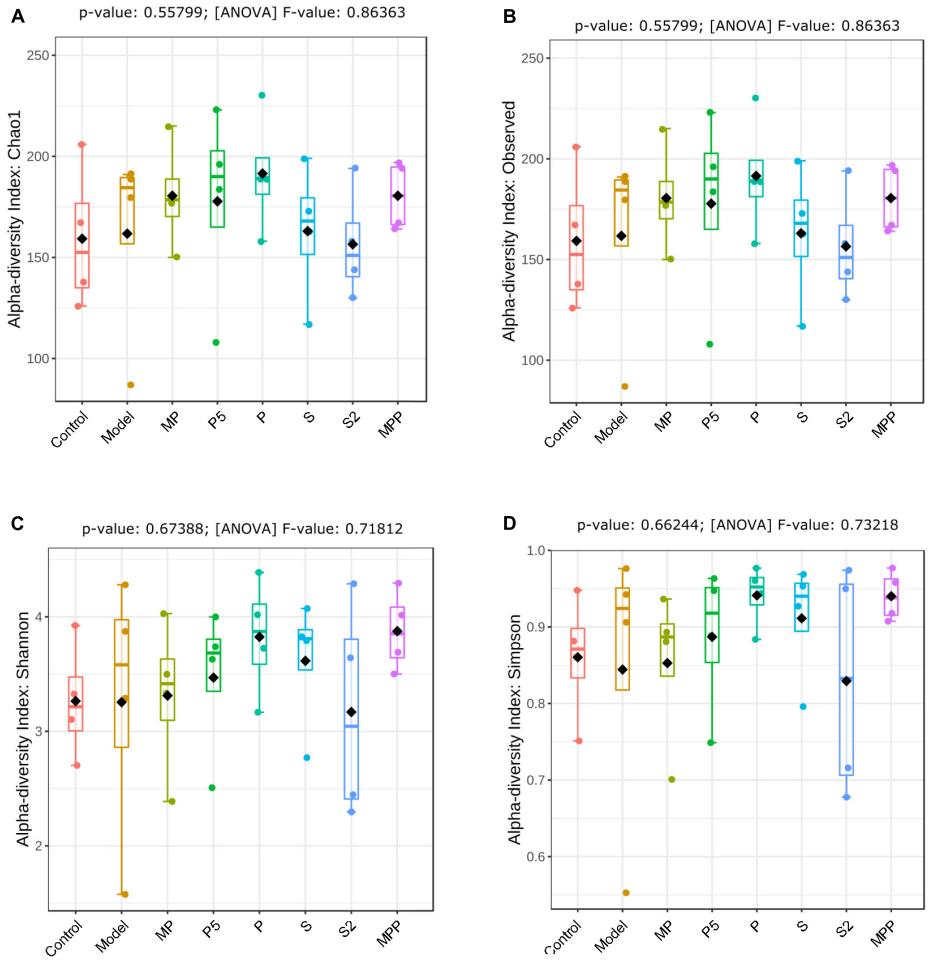

FIGURE 4
The differences in **(A)** Chao1 index, **(B)** observed OTUs, **(C)** Shannon index, and **(D)** Simpson index of fecal microbiome among groups. Results were compared by one-way ANOVA and Dunnett's multiple comparison test.

treatment with S partly inverted the decrease. MP, P5, and MPP slightly promoted the intestinal propulsion rate. In contrast, P treatment did not affect the intestinal propulsion rate in constipated mice.

The synbiotics changed serum hormones relevant to gastrointestinal motility

Motilin, a peptide hormone released from enterochromaffin cells, promotes GI contraction and digestive motility (Kamerling et al., 2003). A lack of motilin is associated with both normal transit constipation and slow transit constipation (Wang Y. Y. et al., 2021). As shown in **Figure 2**, compared with the control group, a significant decrease in serum motilin level was recorded in the model group ($p < 0.0001$). All the interventions except for P restored the serum motilin level in constipated mice. Furthermore, all the interventions did not change the level of proinflammatory cytokines in serum, including IFN-α, TGF-β1, TNF-α, IL-1β, IL-6, IL-10, and IL-17A (**Table 2**).

The synbiotics changed gut microbial composition in mice

16S rRNA sequencing results showed that Firmicutes and Bacteroidetes were the two dominating phyla in fecal samples. As shown in **Figure 3**, after loperamide treatment, the relative abundance of Actinobacteria decreased from 2.26 to 0.91%, and the figure for Patescibacteria dropped from 6.77 to 1.59%, while Bacteroidetes increased from 32.38 to 40.50%. MP administration upregulated Actinobacteria, Patescibacteria, and Firmicutes in constipated mice, and down-regulated Bacteroidetes. The proportion of Verrucomicrobia and Bacteroidetes increased in the P group compared with the

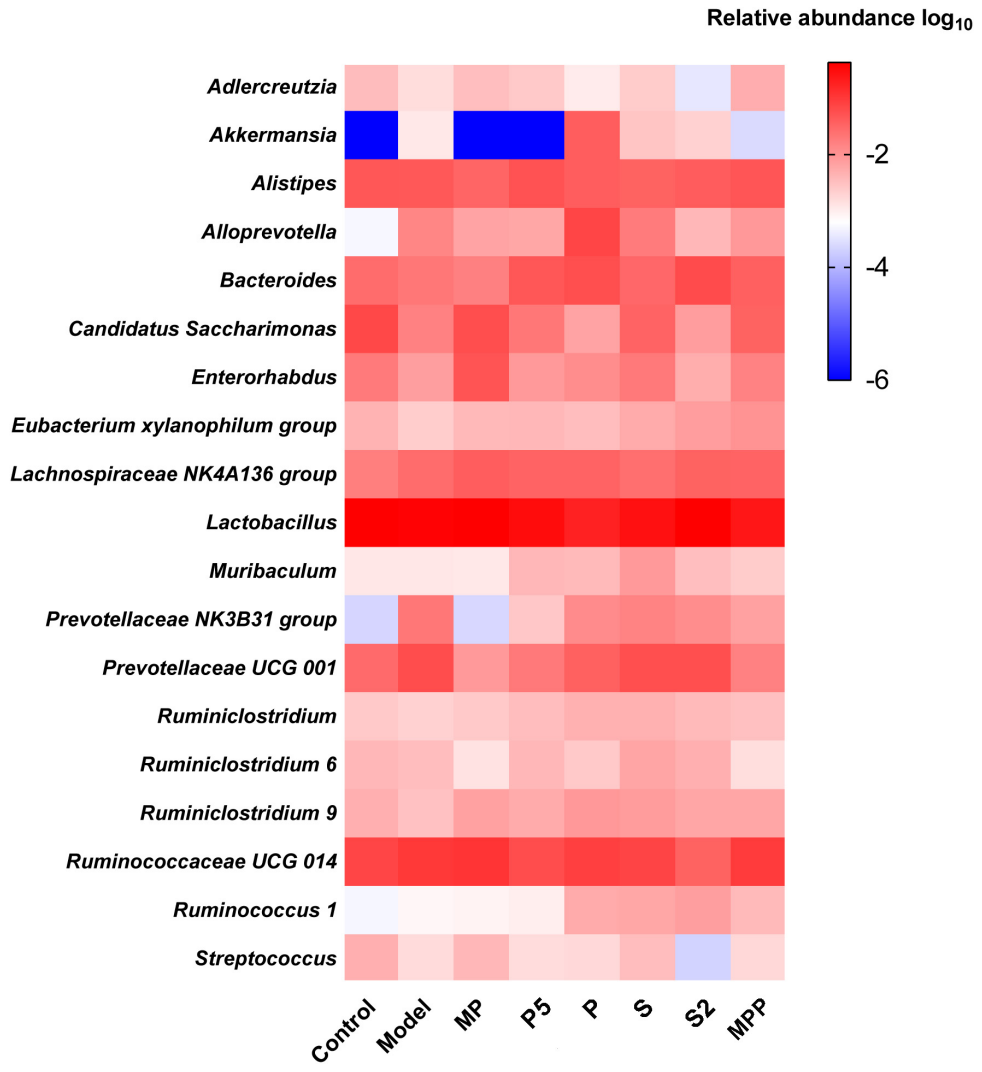

FIGURE 5
Heatmap of the top 20 fecal microbial genera among groups.

model group, while Firmicutes decreased. A significant increase in Actinobacteria was observed in S and MPP groups.

No significant change was observed between the control and model groups from the alpha-diversity index, including Chao1, Simpson, Shannon, as well as observed OTUs (Figures 4A–D). Treatments other than the synbiotics increased the Chao1 index and observed OTUs in mice (Figures 4A,B). Mice in the treated groups except for MP and S2 groups exhibited an obvious increase in Shannon and Simpson indexes (Figures 4C,D).

At the genus level, no apparent difference was found between the model and control groups except the increased Akkermansia in the model group (Figure 5). Ruminiclostridium 6, Ruminiclostridium 9, and Eubacterium xylanophilum group were more abundant in MP and MPP groups, in comparison with the model group, while the abundance of Alistipes was much lower (Figure 5). There was a rise in Ruminiclostridium 6, Ruminiclostridium 9, Ruminococcus 1, Ruminiclostridium, and Bacteroides, as well as a decrease in Alistipes in the P, P5, S, and S2 groups compared with the model group (Figure 5).

The synbiotics changed fecal short-chain fatty acids concentration in mice

The concentration of fecal SCFA is an important implication of intestinal motility. As shown in Table 3, loperamide administration decreased the level of fecal acetate in mice, and this decrease was reversed in the MP, P5, S, S2, and MPP groups. While the decline in fecal propionate was restored in all these groups. Butyrate in stool was less in the model group than in

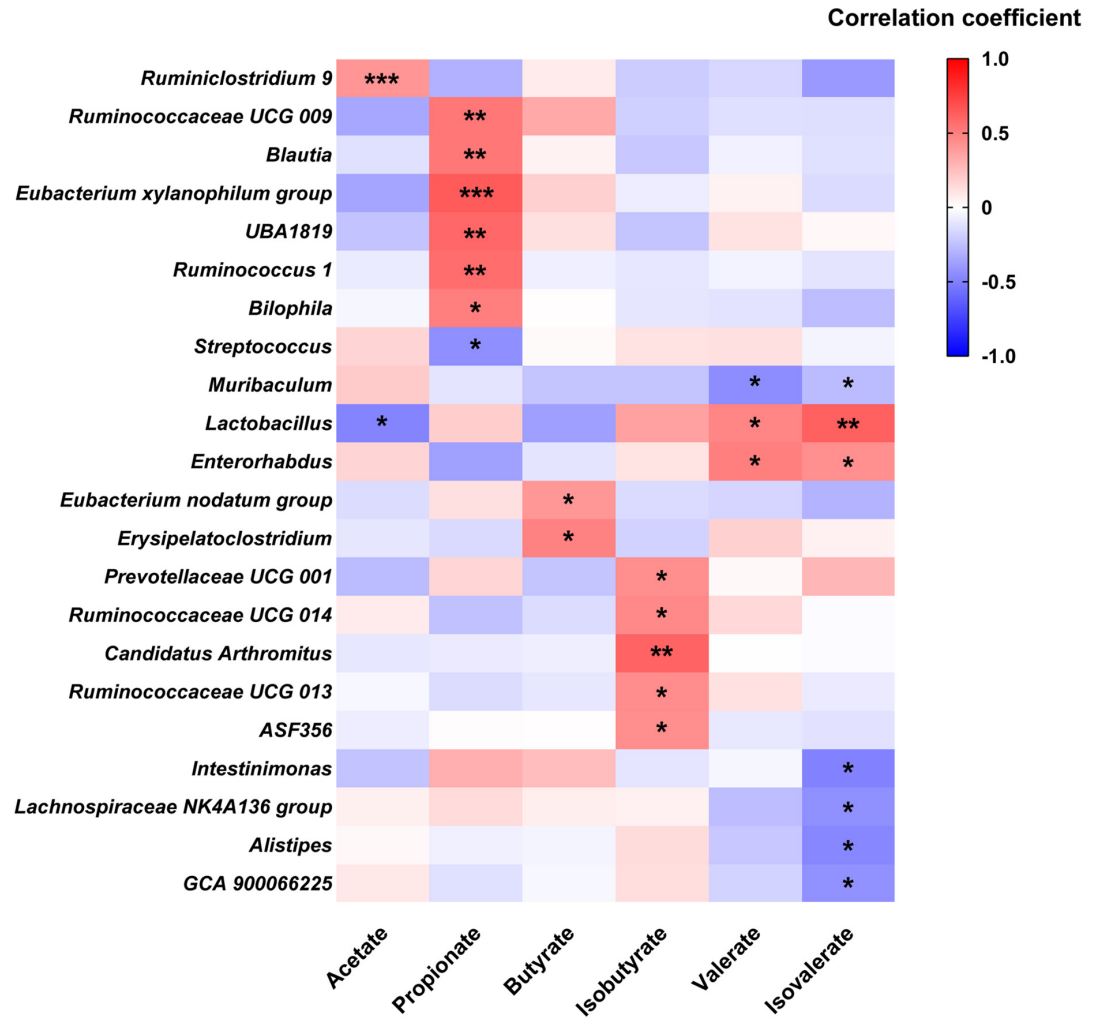

FIGURE 6
Heatmap of Pearson's correlation analysis between SCFA and fecal microbial genera. *$p < 0.05$, ** $p < 0.01$, *** $p < 0.001$ statistical significance of Pearson's correlation analysis.

the control group, which was reversed in the MP, P5, S, and S2 groups. A significant decrease in fecal valerate could be found in the model group, and this reduction was reversed by MP, S2, and MPP treatments. No obvious difference in fecal isobutyrate and isovalerate was observed between the control and model groups. Meanwhile, the level of isovalerate in stool increased in the MP, S, and S2 groups.

To explore the relationship between fecal SCFA and gut microbial genera, Pearson's correlation analysis was carried out. As shown in Figure 6, fecal acetate was positively correlated with Ruminiclostridium 9 and negatively associated with Lactobacillus. Fecal propionate level was positively related to six genera, including Ruminococcus 1 and Blautia, while negatively correlated with Streptococcus. Butyrate was just positively associated with Eubacterium nodatum group and Erysipelatoclostridium, while isobutyrate was positively correlated with five genera like Prevotellaceae UCG 001, Ruminococcaceae UCG 013, and Ruminococcaceae UCG 014. In contrast, valerate was positively related to Lactobacillus and Enterorhabdus, while negatively associated with Muribaculum. A positive correlation was observed between isovalerate and two genera: Lactobacillus and Enterorhabdus, while a negative one was recorded between isovalerate and five genera, including Muribaculum, Intestinimonas, Lachnospiraceae NK4A136 group, Alistipes, and GCA 900066225, respectively.

Linear regression analysis was applied to analyze the correlation between serum motilin and fecal SCFA. Among these SCFA, acetate, propionate, butyrate, valerate, and isovalerate exhibited positive correlations with serum motilin levels, while isobutyrate was not statistically correlated with that (Figure 7).

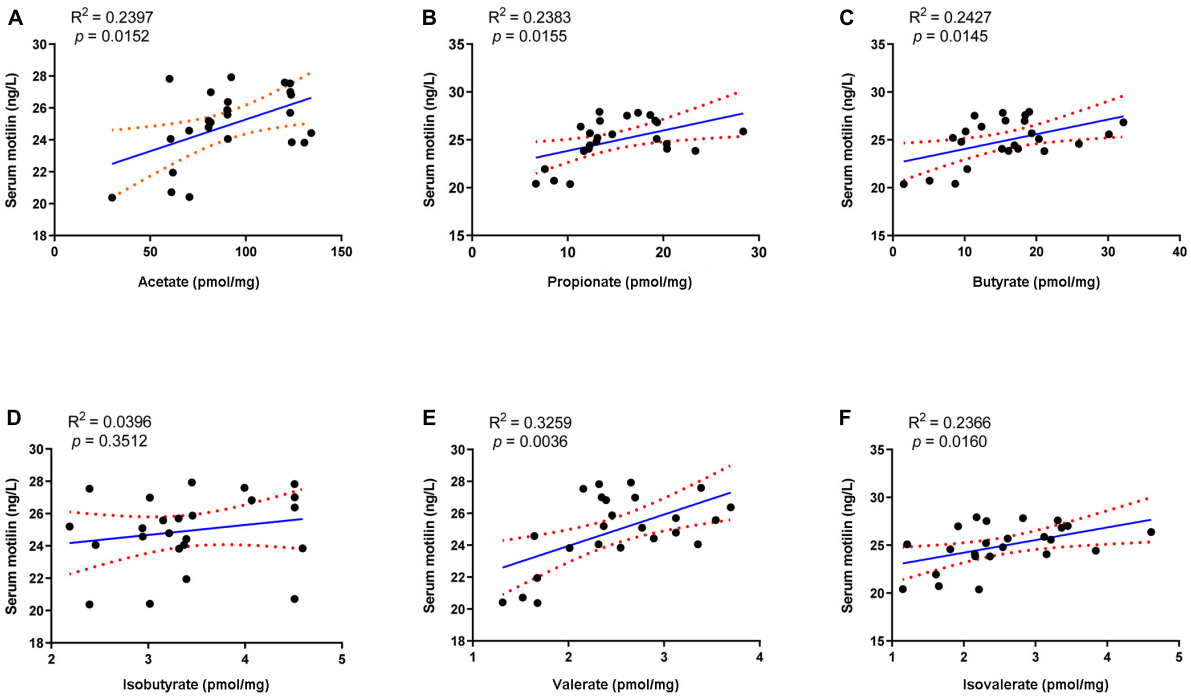

FIGURE 7
Linear regression analysis between serum motilin level and **(A)** acetate, **(B)** propionate, **(C)** butyrate, **(D)** isobutyrate, **(E)** valerate, and **(F)** isovalerate.

Discussion

Constipation is a functional GI disorder that is conventionally recognized by a decrease in defecation frequency, fecal water content, as well as GI motility. In recent years, the strategies based on gut microecological regulation, such as the supplementation of probiotics, prebiotics, and synbiotics, have drawn more attention. In this study, the effects of probiotics, postbiotics, and synbiotics were investigated in a mice model of spastic constipation, which was induced by loperamide administration (Salminen et al., 1998).

Loperamide, an agonist of μ-opioid receptors, prevents the release of acetylcholine and prostaglandin, thus inhibiting intestinal peristalsis and leading to prolonged retention of intestinal contents (Wang et al., 2017b). Our results showed that loperamide treatment caused typical symptoms of constipation, including an apparent increase in the time to the first black stool defecation and an obvious decrease in fecal water content. Administration of MP, P5, S, S2, and MPP treatments shortened the time to the first black stool and increased fecal water content in loperamide-treated mice, suggesting alleviations of these interventions. Constipation in mice was further confirmed by the decrease in intestinal propulsion rate. These treatments promoted intestinal propulsion rate in constipated mice, indicating an improvement in GI motility. In contrast, P treatment slightly improved fecal water content and GI motility but failed to shorten the time to the first black stool. Therefore, P treatment was less potent in relieving constipation than P5, and this might be due to the differences in dose.

Motilin is secreted by endocrine cells in the duodenum, jejunum, and antrum (Polak et al., 1975), and plays an important role in maintaining GI motility by stimulating its receptors (Kamerling et al., 2003). In this study, a significant decrease in serum motilin was recorded in constipated mice in contrast to healthy mice. This helped to explain the reduction in GI motility in this mice model. All interventions except for P restored serum motilin levels in constipated mice. Thus, MP, P5, S, S2, and MPP treatments might contribute to the stability of intestinal motility by sustaining motilin levels.

Alterations in the fecal microbiome were detected in constipated control mice, including the decreased Actinobacteria and Patescibacteria as well as the raised Bacteroidetes at the phylum level, suggesting gut microbial alterations due to loperamide treatment. Treatment with MP upregulated Firmicutes and downregulated Bacteroidetes in constipated mice. It was previously reported that increased Bacteroidetes and decreased Firmicutes were associated with constipation in rodents (Wang et al., 2017b). Thus, the probiotics applied in this study might help to reduce the risk of constipation by regulating the ratio of Firmicutes to Bacteroidetes. As for diversity, treatments increased different

alpha-diversity indicators, suggesting that these interventions contribute to stabilizing the gut microbiome in the host.

Apart from regulating gut microbiota, probiotics, prebiotics, and synbiotics can influence the fermentation products in the gut, such as SCFA (Wang et al., 2017b; Lan et al., 2020). SCFA is mainly formed by the bacterial fermentation of indigestible carbohydrates in the large intestine and can stimulate intestine contraction, thereby promoting GI motility (Niwa et al., 2002). Previous studies revealed an association between improved constipation and fecal SCFA concentration, especially those using microbial regulating strategies like supplementation of probiotics (Wang et al., 2017b), prebiotics (Lan et al., 2020), and dietary fiber (Niwa et al., 2002; Zhuang et al., 2019). Our results showed that fecal acetate, propionate, butyrate, and valerate decreased after loperamide treatment, and these decreases were inverted by the administration of MP (**Table 3**). MPP treatment restored the changes in acetate, propionate, and valerate during constipation. Both S and S2 treatments restored the reduction in acetate, propionate, and butyrate, and increased isovalerate in the feces, while S2 upregulated fecal valerate in constipated mice. In contrast, P5 treatment raised acetate, propionate, and butyrate in stool, while P treatment failed to change fecal SCFA profile in constipated mice. Meanwhile, the correlation analysis showed that the SCFA other than isobutyrate was positively correlated with serum motilin, indicating that increased intestinal SCFA may contribute to upregulated motilin synthesis. Therefore, the alterations in SCFA in the gut after the interventions except for P might contribute to promoting GI motility and alleviating constipation.

Alterations in gut microbial genera probably lead to changes in fecal SCFA profile. In this study, the relative abundances of *Ruminiclostridium 9* and *Eubacterium xylanophilum group* were increased after MPP administration, respectively, while *Alistipes* was reduced. Pearson's correlation analysis suggested that fecal acetate concentration was positively associated with *Ruminiclostridium* 9, and propionate was positively associated with the *Eubacterium xylanophilum group*, while *Alistipes* negatively related to isovalerate. *Ruminiclostridium 9* and the *Eubacterium xylanophilum group* were previously reported to be SCFA producers in the gut (Guo et al., 2018). Hence, the rise in these two genera in the gut might be favorable for improving SCFA production, thus promoting intestinal movement after MPP intervention. Treatments with P, P5, S, and S2 upregulated genera *Ruminiclostridium 9*, *Ruminiclostridium*, *Ruminococcus 1*, and *Bacteroides* in feces. *Ruminococcus 1*, which was identified as an SCFA producer (Louis and Flint, 2017), positively correlated with propionate in our results. According to Jacobson et al., upregulation of *Bacteroides* may help to raise propionate production, although fecal propionate did not show a significant correlation in this study (Jacobson et al., 2018). Accordingly, increases in *Ruminiclostridium 9*, *Ruminiclostridium*, *Ruminococcus 1*, and *Bacteroides* induced by P, P5, S, and S2 administrations might contribute to stimulating GI motility and ameliorating constipation.

Conclusion

The present study showed that the MP, P5, S, S2, and MPP treatments shortened the time to the first black stool, increased fecal water content and GI motility, and raised serum motilin levels in mice. Meanwhile, these interventions changed the gut microbial structure and increased fecal SCFA concentration, which contributed to their alleviating effects on constipation.

Data availability statement

The original contributions presented in this study are publicly available. This data can be found here: https://www.ncbi.nlm.nih.gov/bioproject/PRJNA842449; accession number: PRJNA842449.

Ethics statement

The animal study was reviewed and approved by the Ethics Committee of Jiangnan University [JN. No. 20201130b0720301 (355)].

Author contributions

YQZ conceived the project. YMZ completed the experiments and wrote the manuscript. QL and YH edited the manuscript. All authors contributed to the article and approved the submitted version.

Funding

This work was funded by Hyproca Nutrition Co., Ltd.

Acknowledgments

We would like to acknowledge Hyproca Nutrition Co., Ltd (Hunan, China) for funding this study.

Conflict of interest

All authors were employed by Hyproca Nutrition Co. Ltd. The authors declare that this study received funding from Hyproca Nutrition Co. Ltd. The funder was involved with study design.

Publisher's note

References

Black, C. J., and Ford, A. C. (2018). Chronic idiopathic constipation in adults: Epidemiology, pathophysiology, diagnosis and clinical management. *Med. J. Aust.* 209, 86–91. doi: 10.5694/mja18.00241

Cao, H., Liu, X., An, Y., Zhou, G., Liu, Y., Xu, M., et al. (2017). Dysbiosis contributes to chronic constipation development *via* regulation of serotonin transporter in the intestine. *Sci. Rep.* 7:10322. doi: 10.1038/s41598-017-10835-8

Chu, J. R., Kang, S. Y., Kim, S. E., Lee, S. J., Lee, Y. C., and Sung, M. K. (2019). Prebiotic UG1601 mitigates constipation-related events in association with gut microbiota: A randomized placebo-controlled intervention study. *World J. Gastroenterol.* 25, 6129–6144. doi: 10.3748/wjg.v25.i40.6129

Corazziari, E. (1999). Need of the ideal drug for the treatment of chronic constipation. *Ital. J. Gastroenterol. Hepatol.* 31, S232–S233.

Dimidi, E., Christodoulides, S., Fragkos, K. C., Scott, S. M., and Whelan, K. (2014). The effect of probiotics on functional constipation in adults: A systematic review and meta-analysis of randomized controlled trials. *Am. J. Clin. Nutr.* 100, 1075–1084. doi: 10.3945/ajcn.114.089151

Guo, J. R., Dong, X. F., Liu, S., and Tong, J. M. (2018). High-throughput sequencing reveals the effect of Bacillus subtilis CGMCC 1.921 on the cecal microbiota and gene expression in ileum mucosa of laying hens. *Poult. Sci.* 97, 2543–2556. doi: 10.3382/ps/pey112

Huang, L., Zhu, Q., Qu, X., and Qin, H. (2018). Microbial treatment in chronic constipation. *Sci. China Life Sci.* 61, 744–752. doi: 10.1007/s11427-017-9220-7

Inatomi, T., and Honma, M. (2021). Effects of probiotics on loperamide-induced constipation in rats. *Sci. Rep.* 11:24098. doi: 10.1038/s41598-021-02931-7

Jacobson, A., Lam, L., Rajendram, M., Tamburini, F., Honeycutt, J., Pham, T., et al. (2018). A gut commensal-produced metabolite mediates colonization resistance to salmonella infection. *Cell Host Microbe* 24, 296–307.e7. doi: 10.1016/j.chom.2018.07.002

Kamerling, I. M., Van Haarst, A. D., Burggraaf, J., Schoemaker, R. C., Biemond, I., Heinzerling, H., et al. (2003). Motilin effects on the proximal stomach in patients with functional dyspepsia and healthy volunteers. *Am. J. Physiol. Gastrointest. Liver Physiol.* 284, G776–G781. doi: 10.1152/ajpgi.00456.2002

Kamiński, M., Skonieczna-Żydecka, K., Łoniewski, I., Koulaouzidis, A., and Marlicz, W. (2020). Are probiotics useful in the treatment of chronic idiopathic constipation in adults? A review of existing systematic reviews, meta-analyses, and recommendations. *Prz. Gastroenterol.* 15, 103–118. doi: 10.5114/pg.2019.86747

Kandeel, W. A., Meguid, N. A., Bjørklund, G., Eid, E. M., Farid, M., Mohamed, S. K., et al. (2020). Impact of Clostridium Bacteria in Children with Autism Spectrum Disorder and Their Anthropometric Measurements. *J. Mol. Neurosci.* 70, 897–907. doi: 10.1007/s12031-020-01482-2

Lan, J., Wang, K., Chen, G., Cao, G., and Yang, C. (2020). Effects of inulin and isomalto-oligosaccharide on diphenoxylate-induced constipation, gastrointestinal motility-related hormones, short-chain fatty acids, and the intestinal flora in rats. *Food Funct.* 11, 9216–9225. doi: 10.1039/d0fo00865f

Lee, H. Y., Kim, J. H., Jeung, H. W., Lee, C. U., Kim, D. S., Li, B., et al. (2012). Effects of Ficus carica paste on loperamide-induced constipation in rats. *Food Chem. Toxicol.* 50, 895–902. doi: 10.1016/j.fct.2011.12.001

Louis, P., and Flint, H. J. (2017). Formation of propionate and butyrate by the human colonic microbiota. *Environ. Microbiol.* 19, 29–41. doi: 10.1111/1462-2920.13589

Martinez-Martinez, M. I., Calabuig-Tolsa, R., and Cauli, O. (2017). The effect of probiotics as a treatment for constipation in elderly people: A systematic review. *Arch. Gerontol. Geriatr.* 71, 142–149. doi: 10.1016/j.archger.2017.04.004

Mearin, F., Lacy, B. E., Chang, L., Chey, W. D., Lembo, A. J., Simren, M., et al. (2016). Bowel disorders. *Gastroenterology* [Epub ahead of print]. doi: 10.1053/j.gastro.2016.02.031

Mitrea, L., Nemeş, S. A., Szabo, K., Teleky, B. E., and Vodnar, D. C. (2022). Guts imbalance imbalances the brain: A review of gut microbiota association with neurological and psychiatric disorders. *Front. Med.* 9:813204. doi: 10.3389/fmed.2022.813204

Niwa, T., Nakao, M., Hoshi, S., Yamada, K., Inagaki, K., Nishida, M., et al. (2002). Effect of dietary fiber on morphine-induced constipation in rats. *Biosci. Biotechnol. Biochem.* 66, 1233–1240. doi: 10.1271/bbb.66.1233

Polak, J. M., Pearse, A. G., and Heath, C. M. (1975). Complete identification of endocrine cells in the gastrointestinal tract using semithin-thin sections to identify motilin cells in human and animal intestine. *Gut* 16, 225–229. doi: 10.1136/gut.16.3.225

Sabahi, S., Homayouni Rad, A., Aghebati-Maleki, L., Sangtarash, N., Ozma, M. A., Karimi, A., et al. (2022). Postbiotics as the new frontier in food and pharmaceutical research. *Crit. Rev. Food Sci. Nutr.* 29, 1–28. doi: 10.1080/10408398.2022.2056727

Sadeghifard, N., Salari, M. H., Ghassemi, M. R., Eshraghi, S., and Amin Harati, F. (2010). The incidence of nosocomial toxigenic clostridium difficile associated diarrhea in Tehran tertiary medical centers. *Acta Med. Iran.* 48, 320–325.

Salminen, S., Bouley, C., Boutron-Ruault, M. C., Cummings, J. H., Franck, A., Gibson, G. R., et al. (1998). Functional food science and gastrointestinal physiology and function. *Br. J. Nutr.* 80, S147–S171. doi: 10.1079/bjn19980108

Sekirov, I., Russell, S. L., Antunes, L. C., and Finlay, B. B. (2010). Gut microbiota in health and disease. *Physiol. Rev.* 90, 859–904. doi: 10.1152/physrev.00045.2009

Sharma, A., and Rao, S. (2017). Constipation: Pathophysiology and current therapeutic approaches. *Handb. Exp. Pharmacol.* 239, 59–74. doi: 10.1007/164_2016_111

Shin, A., Preidis, G. A., Shulman, R., and Kashyap, P. C. (2019). The gut microbiome in adult and pediatric functional gastrointestinal disorders. *Clin. Gastroenterol. Hepatol.* 17, 256–274. doi: 10.1016/j.cgh.2018.08.054

Simon, E., Călinoiu, L. F., Mitrea, L., and Vodnar, D. C. (2021). Probiotics, prebiotics, and synbiotics: Implications and beneficial effects against irritable bowel syndrome. *Nutrients* 13:2112. doi: 10.3390/nu13062112

Smith, B. (1973). Pathologic changes in the colon produced by anthraquinone purgatives. *Dis. Colon Rectum* 16, 455–458. doi: 10.1007/BF02588868

Ştefănuţ, C., Mitrea, L., and Ognean, L. (2015). Effects of probiotics, prebiotics and synbiotics on some hematological and microbiological parameters in laboratory mice. *Bull. Univ. Agric. Sci. Vet. Med. Cluj. Napoca.* 72, 301–305. doi: 10.15835/buasvmcn-vm:11435

Verdu, E. F., Bercik, P., and Collins, S. M. (2009). Effect of probiotics on gastrointestinal function: Evidence from animal models. *Therap. Adv. Gastroenterol.* 2, 31–35. doi: 10.1177/1756283X09337645

Wang, G., Yang, S., Sun, S., Si, Q., Wang, L., Zhang, Q., et al. (2020). *Lactobacillus rhamnosus* strains relieve loperamide-induced constipation *via* different pathways independent of short-chain fatty acids. *Front. Cell. Infect. Microbiol.* 10:423. doi: 10.3389/fcimb.2020.00423

Wang, L. E., Cui, X. Y., Cui, S. Y., Cao, J. X., Zhang, J., Zhang, Y. H., et al. (2010). Potentiating effect of spinosin, a C-glycoside flavonoid of Semen Ziziphi spinosae, on pentobarbital-induced sleep may be related to postsynaptic 5-HT(1A) receptors. *Phytomedicine* 17, 404–409. doi: 10.1016/j.phymed.2010.01.014

Wang, L., Hu, L., Xu, Q., Jiang, T., Fang, S., Wang, G., et al. (2017a). Bifidobacteria exert species-specific effects on constipation in BALB/c mice. *Food Funct.* 8, 3587–3600. doi: 10.1039/c6fo01641c

Wang, L., Hu, L., Xu, Q., Yin, B., Fang, D., Wang, G., et al. (2017b). Bifidobacterium adolescentis exerts strain-specific effects on constipation induced by loperamide in balb/c mice. *Int. J. Mol. Sci.* 18:318. doi: 10.3390/ijms18020318

Wang, R., Sun, J., Li, G., Zhang, M., Niu, T., Kang, X., et al. (2021). Effect of *Bifidobacterium animalis* subsp. lactis MN-Gup on constipation and the

composition of gut microbiota. *Benef. Microbes.* 12, 31–42. doi: 10.3920/BM2020.0023

Wang, Y. Y., Lu, R. Y., Shi, J., Zhao, S., Jiang, X., and Gu, X. (2021). CircORC2 is involved in the pathogenesis of slow transit constipation *via* modulating the signalling of miR-19a and neurotensin/motilin. *J. Cell. Mol. Med.* 25, 3754–3764. doi: 10.1111/jcmm.16211

Yi, R., Peng, P., Zhang, J., Du, M., Lan, L., Qian, Y., et al. (2019). *Lactobacillus plantarum* CQPC02-fermented soybean milk improves loperamide-induced constipation in mice. *J. Med. Food* 22, 1208–1221. doi: 10.1089/jmf.2019.4467

Yu, T., Zheng, Y. P., Tan, J. C., Xiong, W. J., Wang, Y., and Lin, L. (2017). Effects of prebiotics and synbiotics on functional constipation. *Am. J. Med. Sci.* 353, 282–292. doi: 10.1016/j.amjms.2016.09.014

Zhao, J., Tian, F., Yan, S., Zhai, Q., Zhang, H., and Chen, W. (2018). *Lactobacillus plantarum* CCFM10 alleviating oxidative stress and restoring the gut microbiota in d-galactose-induced aging mice. *Food Funct.* 9, 917–924. doi: 10.1039/c7fo01574g

Zhu, L., Liu, W., Alkhouri, R., Baker, R. D., Bard, J. E., Quigley, E. M., et al. (2014). Structural changes in the gut microbiome of constipated patients. *Physiol. Genomics* 46, 679–686. doi: 10.1152/physiolgenomics.00082.2014

Zhuang, M., Shang, W., Ma, Q., Strappe, P., and Zhou, Z. (2019). Abundance of probiotics and butyrate-production microbiome manages constipation *via* short-chain fatty acids production and hormones secretion. *Mol. Nutr. Food Res.* 63:e1801187. doi: 10.1002/mnfr.201801187

Zoppi, G., Cinquetti, M., Luciano, A., Benini, A., Muner, A., and Bertazzoni Minelli, E. (1998). The intestinal ecosystem in chronic functional constipation. *Acta Paediatr.* 87, 836–841. doi: 10.1080/080352598750013590

frontiers | Frontiers in Microbiology

TYPE Original Research
PUBLISHED 26 August 2022
DOI 10.3389/fmicb.2022.1001313

OPEN ACCESS

EDITED BY
Wenyi Zhang,
Inner Mongolia Agricultural University, China

REVIEWED BY
Chaoxin Man,
Northeast Agricultural University, China
Shuo Wu,
Chinese Academy of Medical Sciences, China

*CORRESPONDENCE
Wenwei Lu
luwenwei@jiangnan.edu.cn

SPECIALTY SECTION
This article was submitted to Food Microbiology, a section of the journal Frontiers in Microbiology

RECEIVED 23 July 2022
ACCEPTED 08 August 2022
PUBLISHED 26 August 2022

CITATION
Wang Q, Fang Z, Li L, Wang H, Zhu J, Zhang P, Lee Y-k, Zhao J, Zhang H, Lu W and Chen W (2022) *Lactobacillus mucosae* exerted different antiviral effects on respiratory syncytial virus infection in mice.
Front. Microbiol. 13:1001313.
doi: 10.3389/fmicb.2022.1001313

Lactobacillus mucosae exerted different antiviral effects on respiratory syncytial virus infection in mice

Qianwen Wang[1,2], Zhifeng Fang[1,2], Lingzhi Li[1,2], Hongchao Wang[1,2], Jinlin Zhu[1,2], Pinghu Zhang[3], Yuan-kun Lee[4,5], Jianxin Zhao[1,2], Hao Zhang[1,2,6,7,8], Wenwei Lu[1,2,5,6,7]* and Wei Chen[1,2,6]

[1]State Key Laboratory of Food Science and Technology, Jiangnan University, Wuxi, China, [2]School of Food Science and Technology, Jiangnan University, Wuxi, China, [3]Institute of Translational Medicine and Jiangsu Key Laboratory of Integrated Traditional Chinese and Western Medicine for Prevention and Treatment of Senile Diseases, Medical College, Yangzhou University, Yangzhou, China, [4]Department of Microbiology and Immunology, Yong Loo Lin School of Medicine, National University of Singapore, Singapore, Singapore, [5]International Joint Research Laboratory for Pharmabiotics and Antibiotic Resistance, Jiangnan University, Wuxi, China, [6]National Engineering Research Center for Functional Food, Jiangnan University, Wuxi, China, [7]Institute of Food Biotechnology, Jiangnan University, Yangzhou, China, [8]Wuxi Translational Medicine Research Center and Jiangsu Translational Medicine Research, Institute Wuxi Branch, Wuxi, China

Respiratory syncytial virus (RSV) infection is a constant threat to the health of young children, and this is mainly attributed to the lack of effective prevention strategies. This study aimed to determine whether *Lactobacillus* (*L.*) *mucosae*, a potential probiotic, could protect against respiratory viral infection in a mouse model. Naive 3–4-week-old BALB/c mice were orally administered with three *L. mucosae* strains (2.5×10^8CFU/mouse) 7days before RSV infection (10^5 $TCID_{50}$/mouse). Results showed that all three strains inhibited RSV replication and reduced the proportions of inflammatory cells, including granulocytes and monocytes in the blood. The *L. mucosae* M104R01L3 treatment maintained stable weight in mice and increased interferon (IFN)-β and tumor necrosis factor (TNF)-α levels. The *L. mucosae* DCC1HL5 treatment increased interleukin (IL)-1β and IL-10 levels. Moreover, the M104R01L3 and DCC1HL5 strains increased the proportions of *Akkermansia*, *Alistipes*, and *Anaeroplasma* which contributed to the advantageous modulation of the gut microbiota. Besides, *L. mucosae* affected the gut levels of short-chain fatty acids (SCFAs) that are important for the antiviral response. *L. mucosae* 1,025 increased acetate, propionate, and butyrate levels, whereas *L. mucosae* M104R01L3 increased the level of acetate in the gut. *L. mucosae* M104R01L3 may protect against viral infection by upregulating the IFN-β levels in the lungs and its antiviral effect may be related to the increase of acetate levels in the gut. In conclusion, the three *L. mucosae* strains exerted antiviral effects against RSV infection by differentially regulating immune responses and intestinal micro-ecological balance. This study can provide a reference for studying the mechanisms underlying the antiviral effects of *L. mucosae*.

KEYWORDS

respiratory syncytial virus, *Lactobacillus mucosae*, immune response, gut microbiota, short-chain fatty acid

Introduction

Respiratory syncytial virus (RSV) is an RNA virus of the Paramyxovirus family that causes diseases of variable severity with little systemic symptoms (Openshaw et al., 2017). This virus is responsible for most deaths due to lower respiratory viral infections in young children. In 2015, RSV caused lower respiratory tract infection in approximately 33.1 million children and over 100,000 deaths worldwide (Shi et al., 2017). RSV also threatens the health of individuals who are immunodeficient as a result of aging or lung transplantation (William et al., 2003; Burrows et al., 2015). Although a single RSV infection cannot cause severe disease, compelling evidence suggests that it may result in a secondary bacterial infection that induces more serious lung damage (Damasio et al., 2015). Moreover, RSV reinfection easily occurs because of immune escape even though primary infection induces both humoral and cellular immune responses (Kikkert, 2020). For example, the nonstructural protein NS1 of RSV contributes to immune escape by inhibiting the antiviral type I interferon (IFN) pathway (Hijano et al., 2019). At present, no effective prophylactic measures can protect against RSV infections. Therefore, a safe, universal, and cost-effective prophylactic approach is needed to reduce RSV infections early in life.

The intestinal microbe has recently attracted research interest because it relieves the symptoms of respiratory diseases, including asthma and bacterial and viral infections (Wypych et al., 2019). Previous investigations suggest that the lung health and intestinal micro-ecological balance (Tulic et al., 2016). The intestinal microbiota diversity in mouse models of respiratory viral infection is significantly altered, with increased Bacteroidetes and decreased Firmicutes (Groves et al., 2018) Particularly, RSV infection increases the abundance of *Muribaculaceae*, *Clostridiales*, *Odoribacteraceae*, and *Actinomyces* (Groves et al., 2018, 2020) and reduces that of short-chain fatty acids (SCFA)-producing bacteria, such as *Lachnospiraceae* (Harding et al., 2020). Gut microbes also affect lung health. Viral clearance is delayed, and antiviral immune responses are impaired in mice infected with the influenza virus and treated with antibiotics (Abt et al., 2012). According to present research, there are two main pathways for intestinal microbe to influence lung health. Firstly, toll-like receptors (TLRs) can recognize bacterial components and activate the nuclear factor-kappa B (NF-κB) transcription factor that is a prerequisite for the expression of genes associated with innate immunity and inflammation (Tsay et al., 2011). The intestinal microbe can regulate the toll-like receptors7 signaling pathway to protect against influenza (Wu et al., 2013). Meanwhile, intestinal bacterial metabolites are important to prevent respiratory viral infection. For instance, desaminotyrosine, produced in the gut by *Clostridium orbiscindens*, protects hosts from influenza infection (Steed et al., 2017). SCFAs are common metabolites of the intestinal microbiota that play an important role in protecting against respiratory infections. Influenza infection contributes to bacterial superinfection by reducing the production of SCFAs (Sencio et al., 2020). Especially acetate produced by gut microbiota protects against RSV infection by activating the type I IFN response (Antunes et al., 2019). SCFAs can regulate the balance of T cells and the immune responses (Trompette et al., 2014, 2018).

Lactobacillus (*L.*) *mucosae* is a common species of intestinal microbe that produces acetate, and *L. mucosae* 1,025 protects mice against infection with influenza A virus (Lu et al., 2021). Therefore, we hypothesize that *L. mucosae* may have antiviral effects on RSV infection in mice through regulating the gut microbiota and metabolites. The present study explored the antiviral effects of three *L. mucosae* strains in a mouse model infected with the RSV Long strain. The prophylactic effect of the three strains on RSV infection was evaluated by analyzing the clinical symptoms, immune responses, and gut microbiota composition. This study will contribute to explore the mechanisms of *L. mucosae* to protect against RSV infection.

Materials and methods

Bacterial strain propagation

Lactobacillus mucosae 1,025, *L. mucosae* M104R01L3, and *L. mucosae* DCC1HL5 strains were stored at the Culture Collection of Food Microbiology (CCFM) owned by Jiangnan University. The strains were cultured in De Man, Rogosa, and Sharpe medium (MRS) containing 0.05% (w/v) L-cysteine-HCl at 37°C for 24 h in an anaerobic incubator (AW500SG, Electrotek Scientific Ltd., Shipley, United Kingdom). The mice were orally administered with 2.5×10^8 CFU of the bacterial strain suspension (200 μl).

Treatments and RSV infection

The animal study was reviewed and approved by the Ethics Committee of Yangzhou University (Approval No. 202011004). Female 3–4-week-old BALB/c mice (Charles River Co., Ltd., Beijing, China) were kept in a facility with a controlled light cycle (12/12 h light/dark), temperature (25 ± 2°C), and humidity level (50%). Mice were fed standard commercial chow and water *ad libitum*. Mice were acclimated for 10 days, then randomly assigned to blank, RSV, positive control, and strain groups ($n = 8$ each).

Animal model of mice with RSV infection was established by intranasal instillation of 10^5 $TCID_{50}$ RSV Long strain (Key Laboratory of Avian Infectious Diseases, Yangzhou University, Yangzhou, China), and mice achieved a weight loss more than 3% of body weight in 5 days post-infection (Antunes et al., 2019). For 1 week before infection, all mice in the three bacterial strain groups were administered with 2.5×10^8 CFU of bacterial suspension (200 µl) daily (Kei et al., 2019). The blank and RSV groups were administered with an equal volume of sterile saline. All groups except the blank were intranasally infected with RSV on day 17. After infection, mice were continually administered with 200 µl of bacterial suspension or sterile saline for 5 days, until sacrificed after anesthesia on day 22 (Figure 1A). The positive controls were intraperitoneally injected with ribavirin on the day after infection. The mice were weighed daily after RSV infection to assess changes.

Routine blood analysis

Blood was collected from the sacrificed mice into anticoagulation tubes containing ethylenediaminetetraacetic acid (EDTA)-K2 at room temperature. Blood samples were evaluated using a BC-5000 Vet automated hematology analyzer (Shenzhen Mindray Biomedical Electronics Co., Ltd., Shenzhen, China).

Protein content in bronchoalveolar lavage fluid

Mouse lungs were lavaged three times with 0.8 ml phosphate-buffered saline to obtain bronchoalveolar lavage fluid (BALF). The protein content in BALF was measured using Enhanced BCA Protein Assay Kits (Beyotime Biotechnology Co., Ltd., Shanghai China).

Histopathological analysis of lung tissue

The left lobes of the lungs were fixed in 4% paraformaldehyde and embedded in paraffin blocks that were cut into 5-µm sections and stained with hematoxylin and eosin (HE). The stained sections were visualized using a Pannoramic MIDI digital scanner

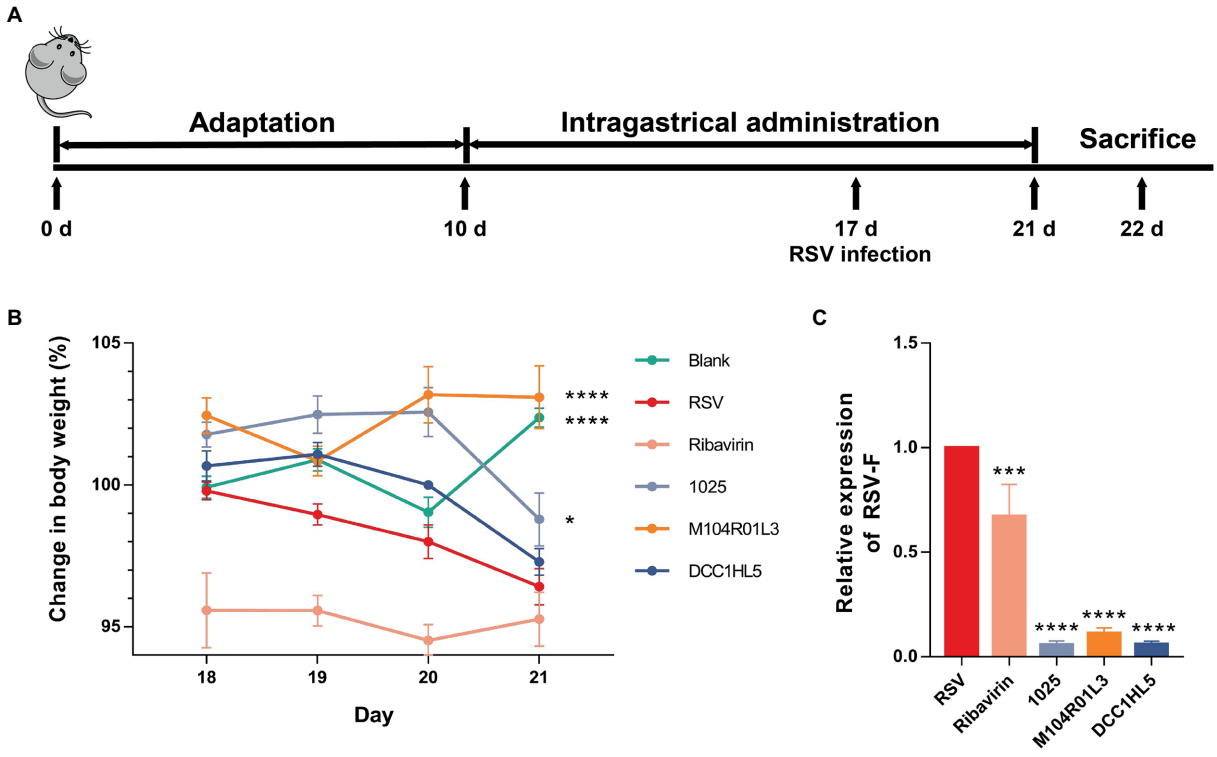

FIGURE 1
Effects of three *Lactobacillus mucosae* strains on weight loss and viral load in a mouse model of respiratory syncytial virus (RSV) infection. **(A)** Timeline of administering three *L. mucosae* strains to mouse models and infecting them with RSV. **(B)** Changes in body weight of mice. The calculation of the weight change of each mouse was taken their weight of Day 17 as the baseline. **(C)** Viral load in lung tissues (n=8; *p<0.05, ***p<0.001, ****p<0.0001 vs. RSV group). Error bars indicate the means ± standard error of the mean (SEM). Differences were compared using one-way ANOVA, followed by Fisher's LSD tests. P-values were adjusted using a false discovery rate. Blank, not infected with RSV. RSV, infected with respiratory syncytial virus and untreated.

TABLE 1 Primer sequences for qRT-PCR.

Primers	Forward/ reverse	Sequence (5′ to 3′)
GAPDH	Forward	AATGGTGAAGGTCGGTGTGAAC
	Reverse	GCCTTGACTGTGCCGTTGAA
RSV-F	Forward	GCAACCAACAATCGAGCCAG
	Reverse	GGCGATTGCAGATCCAACAC

TABLE 2 Primer sequences for *16S* rRNA.

Primers	Forward/ reverse	Sequence (5′ to 3′)
341F	Forward	CCTAYGGGRBGCASCAG
806R	Reverse	GGACTACNNGGGTATCTAAT

(3DHistech Ltd., Budapest, Hungary). The degree of histological damage to the lungs of four mice per group was scored on a scale of 0–3 (Jeffrey et al., 1991).

Viral load

Total RNA was extracted from lung tissues using the FastPure® Cell/Tissue Total RNA Isolation Kit (Vazyme Biotech Co., Ltd., Nanjing, China). First-strand cDNA was synthesized from total RNA using HiScript® III SuperMix for qPCR (Vazyme Biotech Co., Ltd., Nanjing, China). Real-time quantitative reverse transcription polymerase chain reaction (qRT-PCR) analysis was performed using iTaq Master SYBR Green Super Mix (Bio-Rad Laboratories Inc., Hercules, CA, United States) and a CFX96 Thermal Cycler (Bio-Rad Laboratories Inc.). The relative expression of genes was normalized to that of GAPDH and calculated using the $2^{-\Delta\Delta CT}$ method (Livak and Schmittgen, 2001). Table 1 shows the primer sequences.

Analysis of cytokine concentrations

Lung tissues were homogenized in RIPA Lysis Buffer (200 μl/20 mg tissue; Beyotime Biotechnology Co., Ltd., Shanghai China) containing a protease and phosphatase inhibitor cocktail (Beyotime Biotechnology Co., Ltd., Shanghai China). The homogenates were clarified using centrifugation at 4°C, and the cytokines IFN-β, tumor necrosis factor (TNF)-α, interleukin (IL)-1β, and IL-10 were quantified using the respective ELISA kits (SenBeiJia Co., Ltd., Nanjing, China). Protein results are expressed as BSA equivalents.

Gut microbial profiling

Fecal samples were collected using sterile tubes on day 21. DNA was extracted from fecal samples (frozen at −80°C) using the Fast DNA SPIN Kit for Feces (MP Biomedicals; Carlsbad, CA, United States), and the 16S rRNA gene was amplified *via* PCR using the specific primers (341F and 806R) for bacterial rRNA. Table 2 shows the primer sequences. The PCR products were purified using DNA Gel/PCR Purification Miniprep Kits (Beiwo Meditech Co., Ltd., Hangzhou, China). Libraries were constructed using a Library Prep Kit for Illumina (Illumina, San Diego, CA, United States) as described by the manufacturer. Index-coded samples were clustered on a cBot Cluster Generation System (Illumina) as described by the manufacturer. The libraries were sequenced using an Illumina MiSeq high-flux sequencing platform (Illumina), and paired-end reads were generated. Finally, *16S* rRNA sequence data were processed as previously described (Caporaso et al., 2010). Bioinformatics analyses included community diversity profiles and taxonomic differences between microbial communities.

Analysis of SCFA

SCFAs levels in cecal contents were measured using a GCMS-QP2010 Ultra gas chromatograph-mass spectrometer (Shimadzu Corp., Kyoto, Japan) according to a previously described external standard method (Moreau et al., 2003). Briefly, after acidification with sulfuric acid, SCFAs were extracted with ether and dehydrated with anhydrous sodium sulfate. The supernatant was analyzed using gas chromatography–mass spectrometry (GC–MS).

Statistical analysis

Differences were compared using one-way analysis of variance (ANOVA), followed by Fisher's least significant difference (LSD) tests. p values were adjusted using the false discovery rate. The error bars of the data indicate the means ± standard error of the mean (SEM). Gut microbial analysis was performed at online web.[1]

Results

Lactobacillus mucosae exerted antiviral effects on RSV infection

After infection, body weight of mice in the RSV group significantly decreased, whereas *L. mucosae* M104R01L3 and 1,025 strains improved weight loss (Figure 1B). Particularly, *L. mucosae* M104R01L3 maintained stable weight in mice. And the impact of DCC1HL5 treatment on body weight was limited. The positive controls injected with ribavirin weighed less than the RSV group throughout the infection period. Moreover, all

1 https://www.bioincloud.tech/

L. mucosae strains significantly ($p < 0.0001$) suppressed the viral load (expressed relative to levels of the RSV F protein) in lung tissue homogenates on day 5 post-infection and were more effective than ribavirin therapy (Figure 1C). These results indicated that all three *L. mucosae* improved RSV infection, particularly the M104R01L3 strain, which maintained body weight.

Lactobacillus mucosae exerted anti-inflammatory effect on systemic inflammatory responses

The effects of *L. mucosae* on systemic inflammatory responses were explored by quantifying changes in blood cell levels *via* routine blood tests. There were no significant changes in the proportion of lymphocytes (lymph%) between the RSV group and the blank group (Figure 2A). The number of lymphocytes was significantly ($p < 0.01$) increased in the DCC1HL5 group (Figure 2A), whereas the M104R01L3 treatment significantly ($p < 0.01$) reduced the lymph%. RSV infection significantly ($p < 0.01$) increased the proportion of monocytes (mon%) in the RSV group. However, the mon% were decreased in the positive control and *L. mucosae* groups, compared with RSV group (Figure 2B). The proportion of neutrophilic granulocytes (gran%) was higher in the RSV group. Like ribavirin in the positive controls, three *L. mucosae* treatments reduced the gran%. It is gratifying that *L. mucosae* 1,025 and DCC1HL5 treatment recovered gran% to normal (Figure 2C). RSV infection did not affect platelet (PLT) counts in the blood, whereas counts increased in the positive control and *L. mucosae* groups (Figure 2D).

Overall, *L. mucosae* strains recovered blood levels of granulocytes and monocytes but increased the numbers of PLTs. *L. mucosae* M104R01L3 treatment significantly reduced the lymphocyte proportions in the blood.

Lactobacillus mucosae exerted different effects on damage and inflammation in the lungs

The extent of the damage was expressed using total protein in BALF. And the effects of *L. mucosae* on lung inflammation were explored by quantifying cytokines and histologically assessing HE-stained lung sections.

The levels of total protein were significantly higher in BALF from the RSV group than the blank group ($p < 0.0001$), indicating lung damage in the infected mice. The protein content in BALF was significantly decreased in the positive control group ($p < 0.01$), whereas *L. mucosae* did not improve this index (Figure 3A).

TNF-α and IL-1β are the pro-inflammatory cytokines. RSV infection increased their expression in the lungs. *L. mucosae* regulated the expression of these cytokines in lung tissues. The *L. mucosae* 1,025 treatment exhibited a downward trend in the levels of pro-inflammatory cytokines, whereas the M104R01L3 treatment increased the levels of TNF-α and the DCC1HL5 treatment increased the levels of IL-1β in the lung tissues. However, ribavirin noticeably downregulated the expression of these pro-inflammatory cytokines (Figures 3B,C). IL-10 is an anti-inflammatory cytokine. RSV infection did not affect the levels of this cytokine. The concentrations of IL-10 were significantly increased in the 1,025 and DCC1HL5 groups (Figure 3D).

The levels of the major antiviral mediator, IFN-β, were in quantified lung homogenates. RSV infection did not activate the IFN-β response or change its concentration compared with that of the blank group. *L. mucosae* strains increased the levels of IFN-β. Particularly, this cytokine was significantly increased in the M104R01L3 group (Figure 3E).

Histological section is an important indicator to assess the damage and inflammation in the lungs. The sections histologically assessed the effects of *L. mucosae* treatments on pathological lung symptoms. The results showed perivascular infiltration of inflammatory cells after RSV infection compared with the blank. However, *L. mucosae* alleviated the inflammatory infiltration induced by viral infection. In particular, the inflammation score was lower for the M104R01L3 group than that of the 1,025 and DCC1HL5 groups (Figures 3F,G).

Hence, *L. mucosae* exerted different effects on host inflammation in the lungs. *L. mucosae* 1,025 strain reduced the expression of the pro-inflammatory cytokines and increased the levels of the anti-inflammatory cytokine. Specifically, IFN-β levels increased in the M104R01L3 group. According to histological sections and inflammation score, *L. mucosae* M104R01L3 exhibited the best improvement in the lungs.

Lactobacillus mucosae altered the gut microbiota composition

Alpha-diversity indices were analyzed to determine the diversity of the gut microbiota among the groups. The Chao1 index did not significantly differ among the groups (Figure 4A). According to the Shannon and observed operational taxonomic unit (OTU) indices (Figures 4B,C), RSV infection did not obviously change the diversity of the gut microbiota. However, these indices were significantly ($p < 0.01$) increased in the M104R01L3 group but not in the other groups. The Faith's phylogenetic diversity (faith_pd) index of the M104R01L3 and DCC1HL5 groups was significantly higher than that of the RSV group (Figure 4D).

According to the beta-diversity analysis, RSV infection minimally affected the gut microbiota diversity, whereas *L. mucosae* altered the beta diversity of the gut microbiota (Supplementary Figure 1). The composition of the gut microbiota was analyzed at the phylum level to determine changes. The relative abundance of Bacteroidetes was higher in the 1,025 and M104R01L3 groups (Supplementary Figure 2A), whereas M104R01L3 treatment decreased the abundance of Firmicutes (Supplementary Figure 2B),

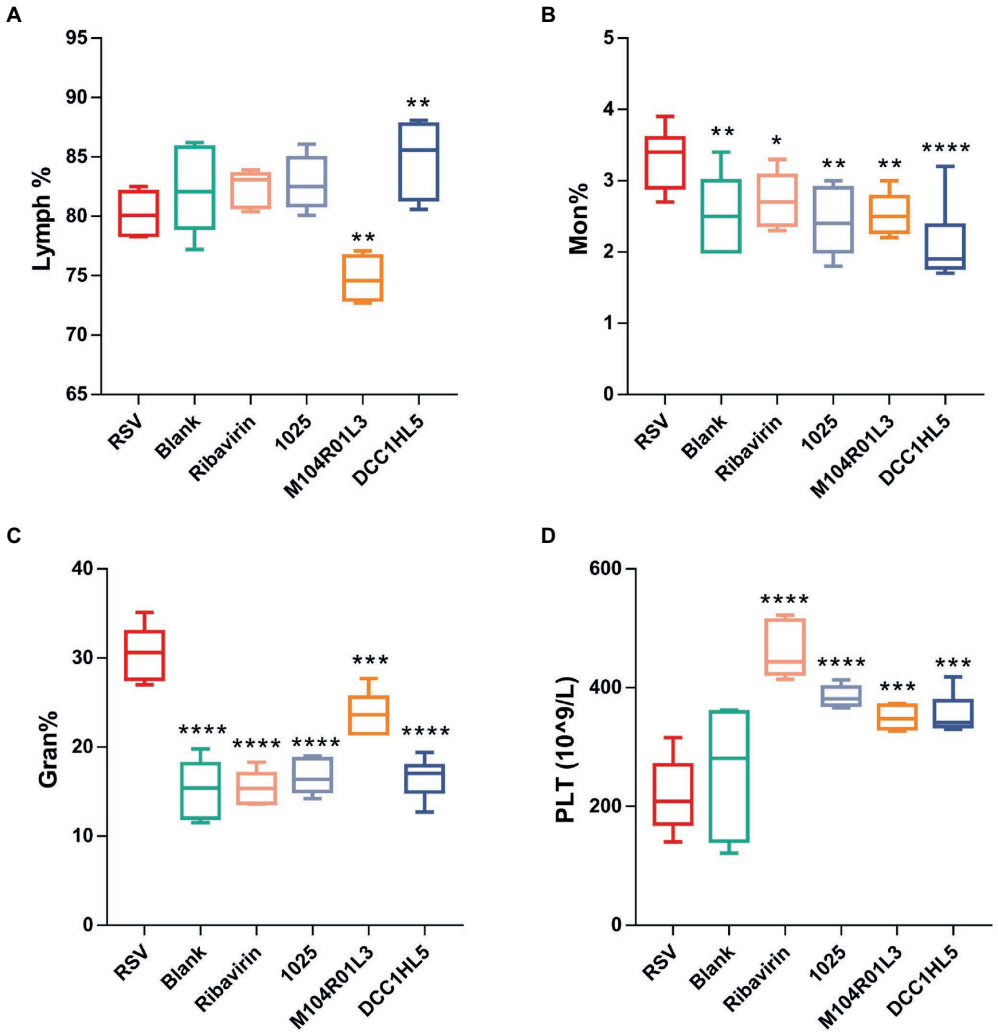

FIGURE 2
Changes in systemic immune responses. Proportions of **(A)** lymphocytes (Lymph%), **(B)** monocytes (Mon%), and **(C)** granulocytes (Gran%). **(D)** Platelets (PLTs) in blood (n=8; *p<0.05, **p<0.01, ***p<0.001, ****p<0.0001 vs. RSV group). Differences were compared using one-way ANOVA, followed by Fisher's LSD test. P-values were adjusted using false discovery rate. Blank, not infected with RSV. RSV, infected with respiratory syncytial virus and untreated.

and *L. mucosae* treatments had no effect on the abundance of Proteobacteria (Supplementary Figure 2C). DCC1HL5 treatment increased the relative abundance of the Verrucomicrobia family (Supplementary Figure 2D). Actinobacteria were more abundant in the RSV group than that of the blank group (Supplementary Figure 2E). The *L. mucosae* strains exerted different effects on gut microbiota composition at the family level using linear discriminant analysis effect size (LEfSe) analysis (Supplementary Figure 3A). At the family level, all of them increased the relative abundance of *Erysipelotrichaceae* (Supplementary Figures 3C–E). The abundance of *Muribaculaceae* (S24-7) was significantly higher in the 1,025 and M104R01L3 groups (Supplementary Figures 3C,D). The relative abundance of *Akkermansiaceae* was increased in the DCC1HL5 group (Supplementary Figure 3E).

The composition of the gut microbiota was analyzed at the genus level using LEfSe analysis. RSV infection altered the relative abundance of genera associated with SCFA production, including decreased *Lachnoclostridium* and *Butyricimonas*. And the abundances of *Alloprevotella* and *Prevotellaceae* NK3B31 group were higher than the blank group (Figure 5A). However, all *L. mucosae* groups increased the abundance of *Butyricimonas*, compared with RSV group (Figures 5B–D). Except for *Butyricimonas*, the *L. mucosae* 1,025 group had a higher abundance of *Ruminococcaceae* UCG-010, as well as that in the *L. mucosae* M104R01L3 group (Figures 5B,C). *L. mucosae* 1,025 treatment specially reduced the levels of *Prevotellaceae* NK3B31 group (Figure 5B). Furthermore, M104R01L3 and DCC1HL5 strains exerted similar effects on gut microbiota composition; they increased the relative abundance of *Akkermansia*, *Clostridium*

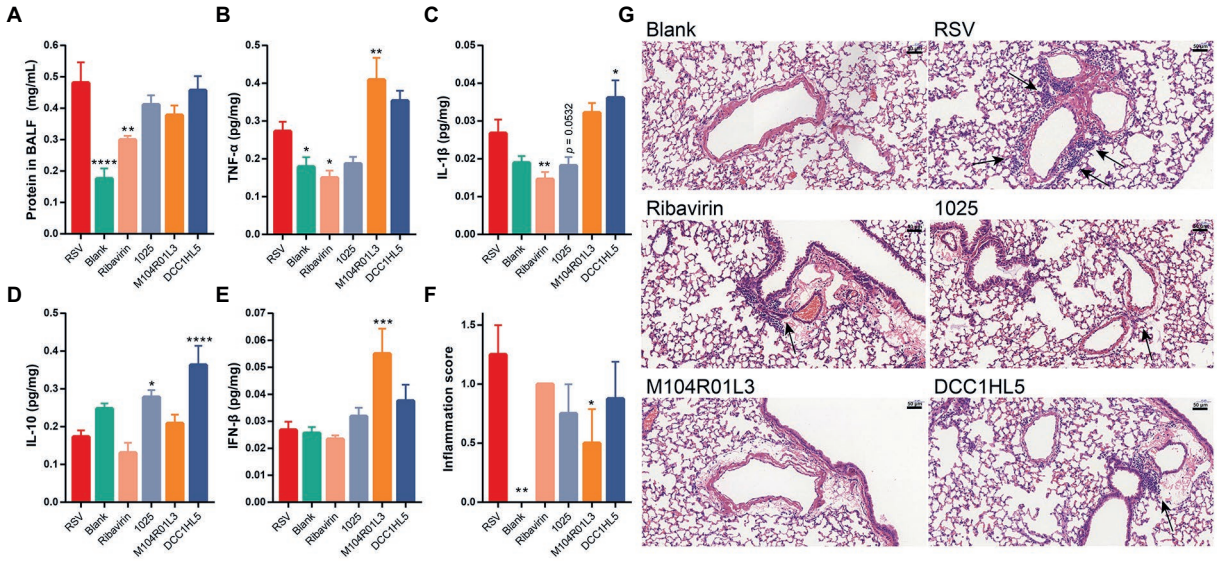

FIGURE 3
Impact of three *Lactobacillus mucosae* strains on cytokine levels and lung damage. Levels of **(A)** total protein in BALF, **(B)** TNF-α in lung tissues, **(C)** IL-1β in lung tissues, **(D)** IL-10 in lung tissues, and **(E)** IFN-β in lung tissues. **(F)** Inflammation scores of lung tissues (n=4). **(G)** Lung sections stained with hematoxylin and eosin. Arrows, perivascular inflammatory infiltration. Original magnification ×400. (n=8, except (F); *p<0.05, **p<0.01, ***p<0.001, ****p<0.0001 vs. RSV group). Error bars show the means ± standard error of the mean (SEM). Differences were compared using one-way ANOVA, followed by Fisher's LSD test. P-values were adjusted using a false discovery rate. Blank, not infected with RSV. RSV, infected with respiratory syncytial virus and untreated.

sensu stricto 1, *Rikenellaceae* RC9, *Turicibacter*, and *Ruminiclostridium* 9. Notably, the DCC1HL5 strain enriched the gut microbiota of mice with *Adlercreutzia* spp. The M104R01L3 treatment resulted in a higher abundance of *Alistipes* and Anaeroplasma (Figures 5C,D). These results indicated that *L. mucosae* strains modulated gut microbiota differently at the genus level.

Correlation analysis were performed between the gut microbiota and cytokines, using Spearman's rank correlation coefficient, to determine the impact of the gut microbiota on host inflammatory cytokines to RSV infection. The levels of TNF-α, IL-1β, and IFN-β were positively correlated with the abundances of *Clostridium sensu stricto* 1, *Faecalibaculum*, *Turicibacter*, *Lactococcus*, and *Escherichia-Shigella*. The abundances of *Prevotellaceae* NK3B31 were positively correlated with the levels of TNF-α and IL-1β. However, the abundances of *Lachnospira* and *Bacteroides* were negatively correlated with the levels of these pro-inflammatory cytokines. In addition, the abundances of *Catabacter*, *Akkermansia*, and *Rikenellaceae* RC9 were positively associated with increased TNF-α expression. The abundances of *Enterococcus* and *Alistipes* were positively correlated with the levels of IL-1β. And the TNF-α levels were negatively correlated with the levels of *Muribaculum*, *Ralstonia*, and *Coprococcus* 2. In particular, the abundances of *Angelakisella* were positively correlated with the IFN-β level and the abundances of *Lachnospira* were negatively correlated with this cytokine. The IL-10 levels were positively correlated with *Ruminococcaceae* UCG-014 and *Intestinimonas*, while it was negatively correlated with *Oscillibacter*, *Lachnospiraceae* UCG-006, *Acetatifactor*, A2, and *Harryflintia* (Figure 5E). To sum up, the upregulations of pro-inflammatory cytokines were positively correlated with the abundances of *Clostridium sensu stricto* 1, *Faecalibaculum*, *Turicibacter*, *Prevotellaceae* NK2B31, *Lactococcus*, *Catabacter*, *Akkermansia*, *Rikenellaceae* RC9, *Enterococcus*, and *Alistipes*. And the abundances of *Lachnospira*, *Bacteroides*, *Muribaculum*, *Ralstonia*, and *Coprococcus* 2 were negatively correlated with the levels of these cytokines. The levels of anti-inflammatory cytokine were positively correlated with *Ruminococcaceae* UCG-014 and *Intestinimonas*; negatively correlated with *Oscillibacter*, *Lachnospiraceae* UCG-006, *Acetatifactor*, A2, and *Harryflintia*.

Lactobacillus mucosae strains affected SCFA production

SCFAs are effective intestinal metabolites for alleviating respiratory diseases, including viral infections (Antunes et al., 2019). The levels of acetate, propionate, and butyrate were measured in cecal contents using GC–MS. RSV infection decreased all the levels of SCFAs, especially acetate and butyrate (Figures 6A–C). The results showed that 1,025 and M104R01L3 strains increased the concentrations of SCFAs, particularly acetate (Figure 6A). Acetate levels were higher in the M104R01L3 group than that in the other groups. And the 1,025 strain significantly increased the levels of propionate (Figure 6B). Furthermore, the 1,025 strain generated the most butyrate among all groups,

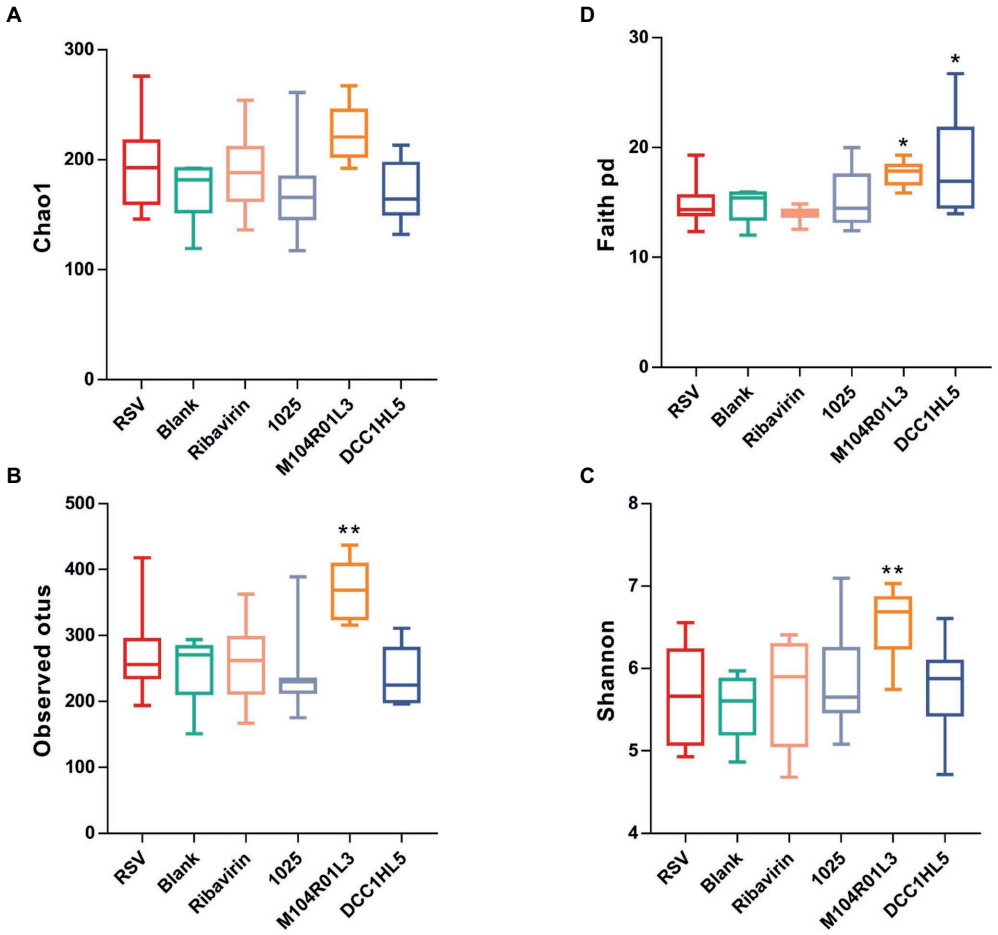

FIGURE 4
Impact of three *Lactobacillus mucosae* strains on the alpha-diversity of the gut microbiota. **(A)** Chao1, **(B)** observed operational taxonomic units (OTUs), **(C)** Shannon, and **(D)** Faith's phylogenetic diversity indices. (n=8; *p<0.05, **p<0.01 vs. RSV group). Differences were compared using one-way ANOVA, followed by Fisher's LSD test. p values were adjusted using a false discovery rate. Blank, not infected with RSV. RSV, infected with respiratory syncytial virus and untreated.

although other strains also triggered increased butyrate production (Figure 6C). Particularly, 1,025 strains significantly increased all the levels of SCFAs.

Discussion

Gut microbiota and probiotics exert preventive and alleviating effects on respiratory diseases, including viral and bacterial infections; however, the mechanisms are still not completely understood. According to the gut–lung axis theory, the gut microbiota influences lung health by generating soluble microbial components and metabolites that are transported *via* circulation (Wypych et al., 2019). Therefore, understanding gut microbial alterations that protect against respiratory diseases could contribute to the clinical applications of probiotics. *L. mucosae* modulates immune system tone (Ryan et al., 2019), and strain 1,025 significantly protects against influenza A infection (Lu et al., 2021). The present study investigated the prophylactic effects of three *L. mucosae* strains against infection with RSV Long strain. The results showed that all three strains significantly decreased viral load in the lungs, through different effects on cytokine levels and routine blood parameters. It is indicated that *L. mucosae* have various mechanisms to inhibit RSV replication and exert prophylactic effects against RSV infection.

The antiviral mechanisms of three strains of *L. mucosae* were explored by evaluating IFN-β levels as an indicator of the type I IFN response. Type I IFNs are major antiviral effectors that mediate antiviral responses, including the Mx GTPase pathway and the 2′,5′-oligoadenylate synthetase-directed ribonuclease L pathway (Sadler and Williams, 2008). Proteins of RSV may be an important means of inhibiting antiviral type I IFN expression through multiple pathways, thus promoting viral replication (Hijano et al., 2019). RSV does not induce strong, long-term immunity because of innate immune evasion; this leads to recurrent infections with the same or

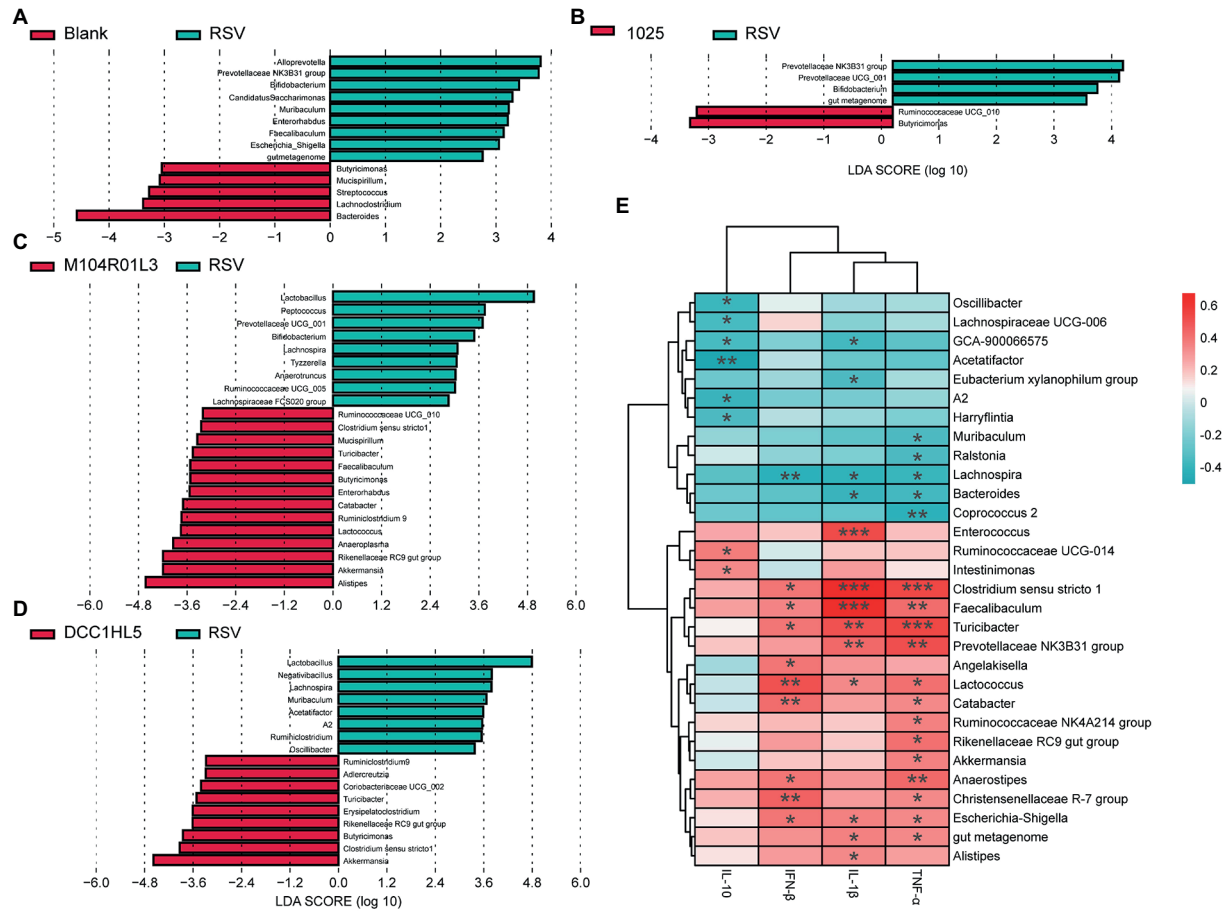

FIGURE 5
Impact of three *Lactobacillus mucosae* strains on the relative abundance of bacterial genera and correlation analysis. Linear discriminant analysis effect size (LEfSe) comparison of gut microbes at the genus level between **(A)** blank and RSV groups, **(B)** 1,025 and RSV groups, **(C)** M104R01L3 and RSV groups, and **(D)** DCC1HL5 and RSV groups. **(E)** Correlations between cytokines and gut microbiota. (n=8; *p<0.05, **p<0.01, ***p<0.001). Blank, not infected RSV. RSV, infected with respiratory syncytial virus and untreated.

different strains of RSV (Paul et al., 2006). In the present study, RSV infection did not increase IFN-β expression in the lungs. However, M104R01L3 treatment, but neither 1,025 nor DCC1HL5 treatments, significantly increased IFN-β levels. This indicated that M104R01L3 treatment could activate type I IFN expression in the lungs to inhibit viral replication. Moreover, both M104R01L3 and DCC1HL5 treatments increased the levels of TNF-α in the lungs. This pro-inflammatory cytokine has been regarded as a factor that exacerbates illness. However, TNF-α plays a protective role against RSV infection (Neuzil et al., 1996). It enhances the expression of the TLR and retinoic acid-inducible gene I (RIG-I) signaling pathways, which stimulate more cytokine and chemokine production in lung epithelial cells (Matikainen et al., 2006). Infants infected with RSV have less TNF-α synthesis than healthy infants, implying an impaired early innate immune response (Kreso et al., 2010). Anti-TNF-α treatment leads to a higher RSV lung viral load compared with that in the controls (Groves et al., 2020). According to these results, M104R01L3 and DCC1HL5 treatment may protect against RSV infection through a TNF-α-dependent pathway.

Based on the IL-1β concentrations in the lungs, it was speculated that DCC1HL5 treatment may induce the expression of TNF-α associated with IL-1β, which is a pro-inflammatory cytokine involved in innate immunity. Moreover, IL-1β induces TNF-α-mediated inflammatory responses in lung epithelial cells by improving TNF receptor surface expression in epithelial cells (Saperstein et al., 2009). IL-1β indirectly influences viral clearance by activating the TLR7 signaling pathway (Abdul-Cader et al., 2018). The small hydrophobic (SH) protein of RSV inhibits TNF signaling, and recombinant RSV without an SH gene increases the levels of IL-1β and TNF (Russell et al., 2015). In terms of DCC1HL5 treatment, IL-1β might be a critical factor for regulating immunity and protecting against RSV infection. Probiotics increase the levels of inflammatory cytokines in the lungs when they inhibit RSV replication. A regulated inflammatory response is necessary for pathogen elimination. Probiotics might regulate the expression of pro- and

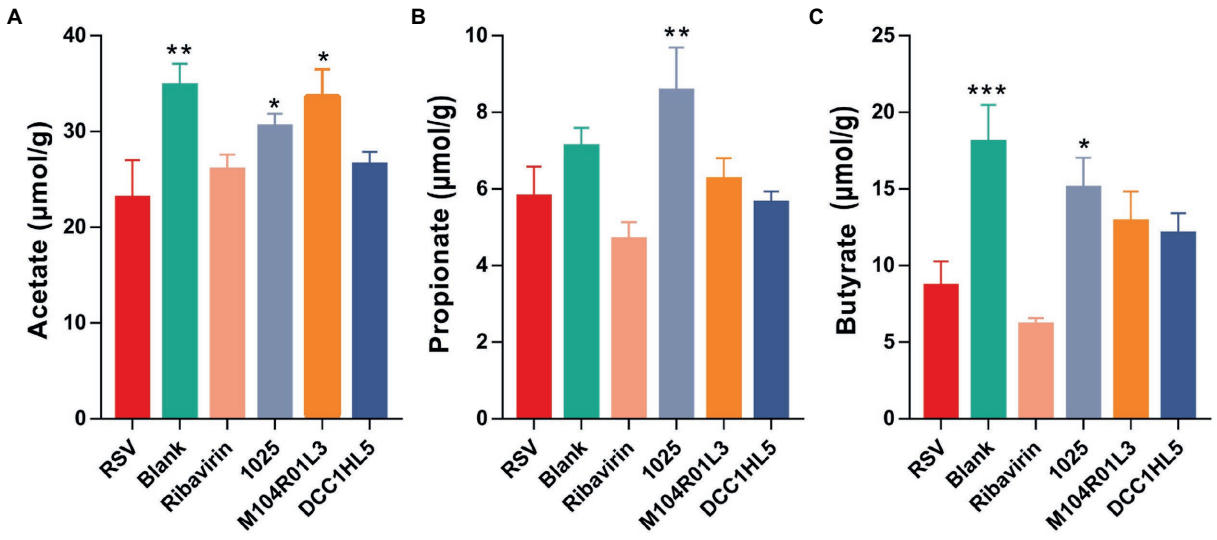

FIGURE 6
Levels of SCFAs in mouse ceca. **(A)** Acetate. **(B)** Butyrate. **(C)** Propionate (n=8. *p<0.05, **p<0.01, ***p<0.001 vs. RSV group). Error bars indicate the means ± standard error of the mean (SEM). Differences were compared using one-way ANOVA followed by Fisher's LSD test. p values were adjusted using a false discovery rate. Blank, not infected with RSV. RSV, infected with respiratory syncytial virus and untreated.

anti-inflammatory factors to balance immune responses. For example, treatment with *L. rhamnosus* CRL1505 induces TNF-α production while increasing IL-10 levels, leading to an effective and safe response against RSV infection (Yohsuke et al., 2013). In this study, DCC1HL5 treatment upregulated IL-10 secretion in the lungs, but not M104R01L3; M104R01L3 treatment might regulate this balance through different pathways. Moreover, the regulation of pro- and anti-inflammatory factors is not synchronous, which unliked *L. rhamnosus* CRL1505. M104R01L3 and DCC1HL5 treatments protect against RSV infection by activating inflammatory responses. In contrast, *L. mucosae* 1,025, a potential anti-inflammatory probiotic, decreased and increased the levels of pro- and anti-inflammatory cytokines, respectively. Surprisingly, *L. mucosae* 1,025 did not induce IFN-β expression. These results suggested that the antiviral mechanism of *L. mucosae* 1,025 is independent of both type I IFN and inflammatory responses. The mechanism by which *L. mucosae* 1,025 inhibits viral replication remains unknown and requires further investigation.

In the present study, RSV infection led to low lymphocyte counts in the blood with no significant difference. RSV infection restrains the development of cytotoxic responses, such as the induction of lymphocyte apoptosis (Roe et al., 2004) and alteration in dendritic cell function (Guerrero-Plata et al., 2006). The mechanism of apoptosis induced by RSV is responsible for the low lymphocyte counts. Lymphopenia during measles infection is thought to induce T cell immunosuppression, like RSV infection (O'Donnell and Carrington, 2002). T cell proliferative responses, the development of CD8+ T cell memory, and CD8+ T cell infiltration might be inhibited by RSV (Chang and Braciale, 2002). The increased lymphocyte levels in the DCC1HL5 group suggested that it might activate the systemic immune response. However, this requires further investigation. Interestingly, M104R01L3 treatment significantly decreased lymphocyte levels, which might be the result of redistribution in the lungs (Smith et al., 2001). Whether M104R01L3 treatment affects lymphocytes in accordance with this hypothesis requires further investigation. Neutrophils are critical effector cells of the innate immune system and are the predominant inflammatory cells recruited to the respiratory tract (Galani and Andreakos, 2015). They are also associated with disease severity in RSV infections (Kozo et al., 2005). Although neutrophils possess various defensive strategies that protect against pathogens, they may also cause collateral damage to host tissue (Cortjens et al., 2016). In the present study, all treatments, except for M104R01L3, observably decreased and recovered the level of neutrophilic granulocytes to the normal level. Appropriate neutrophil apoptosis is important for the resolution of inflammation (Driss and Filep, 2010). Platelets have a variety of transmembrane receptors, including TLRs and TNF receptors, which might be associated with the regulation of immune responses (Zamani-Rarani et al., 2022). During COVID-19, platelets play an important role in the host's antiviral responses (Trugilho et al., 2022). Interestingly, the levels of blood platelets significantly increased after ribavirin and *L. mucosae* strains treatments. The activation of platelets might contribute to damage repair and increase antiviral responses. Besides, the alteration of platelets might be due to the change in gut microbiota composition (Joseph et al., 2021). Future studies are needed to explore the mechanisms of increasing platelets in *L. mucosae* treatments.

This study indicated that *L. mucosae* can modulate systemic immune responses to alleviate inflammation induced by RSV infection.

The gut microbiota plays a critical role in protecting against pathogen infection through modulating the innate and adaptive immune responses. According to the gut–lung axis theory, RSV infection alters gut microbiota and metabolites. The alpha diversity is lower, and beta diversity significantly differs in the gut microbiota of patients with severe disease after RSV infection compared with that in the controls (Harding et al., 2020). However, RSV infection did not markedly affect either alpha or beta diversity in this study. The M104R01L3 and DCC1HL5 strains changed the composition of the gut microbiota, but *L. mucosae* 1,025 had little effect. Our analysis of the gut microbiota also suggested that the distinct immunoregulatory and antiviral activities mediated by *L. mucosae* during RSV infection might be associated with distinct bacterial genera. The abundance of *Butyricimonas*, which converts carbohydrates to butyrate, plays an important role in maintaining a beneficial gut environment during RSV infection. The three *L. mucosae* strains restored the abundance of *Butyricimonas*. In the *L. mucosae 1,025* group, the abundance of *Butyricimonas* might have been a major factor that resisted RSV infection when the strain supplement also increased the abundance of *Ruminococcaceae* UCG-010. *Butyricimonas* was negatively correlated with the IL-1β and IL-6 levels but positively correlated with those of TNF-α and IL-10 (Lee et al., 2018; An et al., 2021). In this study, the levels of pro-inflammatory cytokines were negatively correlated with the abundances of *Prevotellaceae* NK3B31, which were reduced in the *L. mucosae* 1,025 group compared with the RSV group. The anti-inflammatory mechanism of *L. mucosae* 1,025 may be associated with the enrichment of both *Butyricimonas* and *Ruminococcaceae* UCG-010 and the decrease of *Prevotellaceae* NK3B31. Although the abundances of *Butyricimonas* and *Ruminococcaceae* UCG-010 also increased in the M104R01L3 and DCC1HL5 groups, other genera may play a greater role in modulating inflammation and resisting viral infections. M104R01L3 and DCC1HL5 treatments increased the abundances of *Turicibacter* and *Clostridium sensu stricto* 1, which are considered pro-inflammatory taxa (Wang et al., 2017; Ma et al., 2018). The results of the correlation analysis indicated that enriched *Turicibacter* and *Clostridium sensu stricto* 1 might contribute to the increased levels of IL-1β and TNF-α in the M104R01L3 and DCC1HL5 groups. *Turicibacter* might be associated with bile acid metabolism (Kemis et al., 2019), while RSV infection downregulates the metabolism of primary and secondary bile acids (Groves et al., 2020). In addition, *Akkermansia*, a promising probiotic candidate, increased in M104R01L3 and DCC1HL5 groups. This genus exerted beneficial effects during H7N9 infection (Hu et al., 2020). In the present study, *Akkermansia* might play a beneficial role in protecting mice against RSV infection by inducing TNF-α expression. These results suggested that these strains might help the host fight off virus infection by increasing the abundance of *Akkermansia*. Except these genera, M104R01L3 characteristically increased the abundances of *Alistipes* and *Anaeroplasma*, which are prime candidates for effective anti-inflammatory probiotics (Beller et al., 2020; Parker et al., 2020). The increase of *Alistipes* might be associated with the increased levels of blood platelets (Joseph et al., 2021). In addition, *Faecalibaculum*, *Lactococcus*, and *Catabacter* were increased in the M104R01L3 group, which might have contributed to the upregulated IFN-β. The DCC1HL5 treatment increased the abundance of *Adlercreutzia*, an equol-producing bacteria (Bian et al., 2017). *Adlercreutzia* and its metabolites can increase anti-inflammatory capacity in the host (Wei et al., 2018). Our results suggested that *L. mucosae* protected the host from RSV infection associated with alteration of the gut microbiota composition.

The host interacts with microbiota-derived metabolites that are important for protection against pathogens. SCFAs, produced by the gut microbiota, regulate immune and antiviral responses that protect the host against respiratory infections. In the present study, RSV infection reduced the levels of SCFAs, especially acetate and butyrate. *L. mucosae* treatment significantly increased SCFA concentrations after RSV infection. Combined with the gut microbiota findings, the modulation of SCFA-producing bacteria contributed to the changes in cecal SCFAs. Unmetabolized SCFAs enter the lungs *via* the peripheral circulation (Wypych et al., 2019; Sencio et al., 2020). The antiviral mechanisms of the type I IFN response in lung tissues may be overcome by SCFAs in different ways. Probiotics protect against RSV-induced pathology through IFN-β derived from alveolar macrophages, which is attributed to increased acetate level (Ji et al., 2021). Acetate also exerts its effects on epithelial cells (Antunes et al., 2019). In addition to acetate, butyrate can induce a type I IFN response (Patel et al., 2012), and this correlates with the production of desaminotyrosine (Bastiaan et al., 2018), which is associated with the activation of type I IFN signaling that ameliorates influenza infection (Steed et al., 2017). Based on the upregulation of IFN-β expression in lung tissues, M104R01L3 treatment might recover the type I IFN response to protect against RSV infection by increasing gut levels of acetate. Furthermore, SCFAs also enter the bone marrow, which is the main site of immune cell development (Dang and Marsland, 2019). As RSV evades the adaptive immune response by skewing the balance of T helper type 1 (Th1)/Th2 toward a Th2-specific immune response (Becker, 2006), recovering the balance of T cells might inhibit RSV replication. Circulatory SCFAs can modulate dendritic cell hematopoiesis and functionality in the bone marrow and impair Th2 differentiation (Trompette et al., 2014). Moreover, SCFAs improve the host response to influenza infection by dampening deleterious neutrophil-dependent immunopathology with antiviral CD8+ T cell responses enhanced by increasing T cell metabolism. SCFAs can prevent neutrophil influx into the airways by retaining them in the bone marrow (Trompette et al., 2018). Based on these previous studies, this research indicates that *L. mucosae* may restore SCFAs levels to decrease neutrophil levels in the blood. Besides, Butyrate and propionate induce peripheral forkhead box protein P3 (FoxP3+) regulatory T cells, which promote influenza-specific T follicular helper. Butyrate

is an immune-suppressant *via* reducing the expression of co-stimulatory surface molecules and impairs T cell activation (Stricker et al., 2022). And the increased levels of SCFAs might inhibit the production of pro-inflammatory cytokines (Kruk et al., 2022). In the *L. mucosae* 1,025 group, butyrate and propionate might contribute to the anti-inflammatory and antiviral effects (Anderson and Reiter, 2020).

According to the gut–lung axis theory, *L. mucosae* M104R01L3 might activate the type I IFN responses by increasing the levels of acetate in the gut to inhibit the virus replication. The microbiota-derived acetate might activate the antiviral activity in the pulmonary epithelial cells *via* the peripheral circulation. *L. mucosae* 1,025 might decrease the inflammation by increasing the levels of butyrate and propionate that were transported *via* circulation. However, L. mucosae DCC1HL5 exerted fewer effects on SCFAs levels, its mechanisms of protecting against RSV infection might associated with the increase of *Turicibacter* and *Clostridium sensu stricto* 1 in the gut.

Conclusion

Three *L. mucosae* strains exerted antiviral effects on RSV infection by regulating the host immune responses and gut microbiota composition. Among the three strains, *L. mucosae* 1,025 treatment exhibited anti-inflammatory effects during RSV infection. M104R01L3 treatment induced the type I IFN response to protect against viral infection, whereas DCC1HL5 regulated the balance between anti- and pro-inflammatory cytokine levels. This study showed that *L. mucosae* prevent respiratory viral infection *via* various mechanisms, and gut microbiota and metabolites play essential roles. The findings of the present study can contribute to the future development of probiotics as prophylactic agents for RSV infections.

Data availability statement

The datasets presented in this study can be found in online repositories. The names of the repository/repositories and accession number(s) can be found at: https://www.ncbi.nlm.nih.gov/, PRJNA861107.

Ethics statement

The animal study was reviewed and approved by the Ethics Committee of Yangzhou University.

Author contributions

QW and WL: conceptualization. QW, WL, LL, and ZF: methodology. ZF and QW: software. QW, ZF, LL, and WL: validation. QW, HW, and JZhu: formal analysis. QW: investigation and writing—review and editing. JZha and WC: resources. QW, Y-kL, and JZhu: data curation. QW and LL: writing—original draft preparation. QW, ZF, and Y-kL: visualization. PZ, WL, and WC: supervision. PZ and WL: project administration. HZ and WC: funding acquisition. All authors contributed to the article and approved the submitted version.

Funding

This research was supported by the National Natural Science Foundation of China (Grant No. 31820103010 and 32021005) and 111 Project (no. BP0719028).

Acknowledgments

Thanks for the help from the Collaborative innovation center of food safety and quality control in Jiangsu Province.

Conflict of interest

The authors declare that the research was conducted in the absence of any commercial or financial relationships that could be construed as a potential conflict of interest.

Publisher's note

Supplementary material

The Supplementary material for this article can be found online at: https://www.frontiersin.org/articles/10.3389/fmicb.2022.1001313/full#supplementary-material

References

Abdul-Cader, M. S., Senapathi, U. S., Nagy, E., Sharif, S., and Abdul-Careem, M. F. (2018). Antiviral response elicited against avian influenza virus infection following activation of toll-like receptor (TLR)7 signaling pathway is attributable to interleukin (IL)-1β production. *BMC. Res. Notes* 11:859. doi: 10.1186/s13104-018-3975-4

Abt, M. C., Osborne, L. C., Monticelli, L. A., Doering, T. A., Alenghat, T., Sonnenberg, G. F., et al. (2012). Commensal bacteria calibrate the activation threshold of innate antiviral immunity. *Immunity* 37, 158–170. doi: 10.1016/j.immuni.2012.04.011

An, J., Lee, H., Lee, S., Song, Y., Kim, J., Park, I. H., et al. (2021). Modulation of pro-inflammatory and anti-inflammatory cytokines in the fat by an aloe gel-based formula, QDMC, is correlated with altered gut microbiota. *Immune Netw.* 21:e15. doi: 10.4110/in.2021.21.e15

Anderson, G., and Reiter, R. J. (2020). Melatonin: roles in influenza, Covid-19, and other viral infections. *Rev. Med. Virol.* 30:e2109. doi: 10.1002/rmv.2109

Antunes, K. H., Fachi, J. L., de Paula, R., da Silva, E. F., Pral, L. P., Dos Santos, A. Á., et al. (2019). Microbiota-derived acetate protects against respiratory syncytial virus infection through a GPR43-type 1 interferon response. *Nat. Commun.* 10:3273. doi: 10.1038/s41467-019-11152-6

Bastiaan, W. H., Eric, R. L., Jean-Luc, C., Amanda, J. P., Emily, F., Fatima, A., et al. (2018). Impact of gut colonization with butyrate-producing microbiota on respiratory viral infection following Allo-HCT. *Blood* 131, 2978–2986. doi: 10.1182/blood-2018-01-828996

Becker, Y. (2006). Respiratory syncytial virus (RSV) evades the human adaptive immune system by skewing the Th1/Th2 cytokine balance toward increased levels of Th2 cytokines and IgE, markers of allergy—a review. *Virus Genes* 33, 235–252. doi: 10.1007/s11262-006-0064-x

Beller, A., Kruglov, A., Durek, P., Goetze, V., Werner, K., Heinz, G. A., et al. (2020). Specific microbiota enhances intestinal IgA levels by inducing TGF-β in T follicular helper cells of Peyer's patches in mice. *Eur. J. Immunol.* 50, 783–794. doi: 10.1002/eji.201948474

Bian, X., Tu, P., Chi, L., Gao, B., Ru, H., and Lu, K. (2017). Saccharin induced liver inflammation in mice by altering the gut microbiota and its metabolic functions. *Food Chem. Toxicol.* 107, 530–539. doi: 10.1016/j.fct.2017.04.045

Burrows, F. S., Carlos, L. M., Benzimra, M., Marriott, D. J. E., Havryk, A. P., Plit, M. L., et al. (2015). Oral ribavirin for respiratory syncytial virus infection after lung transplantation: efficacy and cost-efficiency. *J. Heart Lung Transplant.* 34, 958–962. doi: 10.1016/j.healun.2015.01.009

Caporaso, J. G., Kuczynski, J., Stombaugh, J., Bittinger, K., Bushman, F. D., Costello, E. K., et al. (2010). QIIME allows analysis of high-throughput community sequencing data. *Nat. Methods* 7, 335–336. doi: 10.1038/nmeth.f.303

Chang, J., and Braciale, T. J. (2002). Respiratory syncytial virus infection suppresses lung CD8+ T cell effector activity and peripheral CD8+ Tcell memory in the respiratory tract. *Nat. Med.* 8, 54–60. doi: 10.1038/nm0102-54

Cortjens, B., Boer, O. J., Jong, R., Antonis, A. F., Sabogal Piñeros, Y. S., Lutter, R., et al. (2016). Neutrophil extracellular traps cause airway obstruction during respiratory syncytial virus disease. *J. Pathol.* 238, 401–411. doi: 10.1002/path.4660

Damasio, G. A. C., Pereira, L. A., Moreira, S. D. R., Duarte-dos-Santos, C. N., Dalla-Costa, L. M., and Raboni, S. M. (2015). Does virus-bacteria coinfection increase the clinical severity of acute respiratory infection? *J. Med. Virol.* 87, 1456–1461. doi: 10.1002/jmv.24210

Dang, A. T., and Marsland, B. J. (2019). Microbes, metabolites, and the gut-lung axis. *Mucosal Immunol.* 12, 843–850. doi: 10.1038/s41385-019-0160-6

Driss, E. K., and Filep, J. G. (2010). Role of neutrophil apoptosis in the resolution of inflammation. *Sci. World J.* 10, 1731–1748. doi: 10.1100/tsw.2010.169

Galani, I. E., and Andreakos, E. (2015). Neutrophils in viral infections: current concepts and caveats. *J. Leukoc. Biol.* 98, 557–564. doi: 10.1189/jlb.4VMR1114-555R

Groves, H. T., Cuthbertson, L., James, P., Moffatt, M. F., Cox, M. J., and Tregoning, J. S. (2018). Respiratory disease following viral lung infection alters the murine gut microbiota. *Front. Immunol.* 9:182. doi: 10.3389/fimmu.2018.00182

Groves, H. T., Higham, S. L., Moffatt, M. F., Cox, M. J., and Tregoning, J. S. (2020). Respiratory viral infection alters the gut microbiota by inducing Inappetence. *MBio* 11:11. doi: 10.1128/mBio.03236-19

Guerrero-Plata, A., Casola, A., Suarez, G., Yu, X., Spetch, L., Peeples, M. E., et al. (2006). Differential response of dendritic cells to human metapneumovirus and respiratory syncytial virus. *Am. J. Respir. Cell Mol. Biol.* 34, 320–329. doi: 10.1165/rcmb.2005-0287OC

Harding, J. N., Siefker, D., Vu, L., You, D., DeVincenzo, J., Pierre, J. F., et al. (2020). Altered gut microbiota in infants is associated with respiratory syncytial virus disease severity. *BMC Microbiol.* 20:140. doi: 10.1186/s12866-020-01816-5

Hijano, D. R., Vu, L. D., Kauvar, L. M., Tripp, R. A., Polack, F. P., and Cormier, S. A. (2019). Role of type I interferon (IFN) in the respiratory syncytial virus (RSV) immune response and disease severity. *Front. Immunol.* 10:566. doi: 10.3389/fimmu.2019.00566

Hu, X., Zhao, Y., Yang, Y., Gong, W., Sun, X., Yang, L., et al. (2020). *Akkermansia muciniphila* improves host defense Against influenza virus infection. *Front. Microbiol.* 11:586476. doi: 10.3389/fmicb.2020.586476

Jeffrey, L. C., Patricia, K. B., Martha, L. W., and Benfer, H. (1991). Requirement of CD4-positive T cells for cellular recruitment to the lungs of mice in response to a particulate Intratracheal antigen. *J. Clin. Invest.* 88, 1244–1254. doi: 10.1172/jci115428

Ji, J.-J., Sun, Q.-M., Nie, D.-Y., Wang, Q., Zhang, H., Qin, F.-F., et al. (2021). Probiotics protect against RSV infection by modulating the microbiota-alveolar-macrophage axis. *Acta Pharmacol. Sin.* 42, 1630–1641. doi: 10.1038/s41401-020-00573-5

Joseph, H. O., Caitlin, W. E., Scott, G. D., Lidiya, D., Michael, S., Kyle, B., et al. (2021). Pediatric patients with immune thrombocytopenic Purpura have a Dysbiotic gut microbiome at time of diagnosis. *Blood* 138, 3169–3170. doi: 10.1182/blood-2021-154180

Kei, E., Naoki, F., Hisako, N., and Tadaaki, M. (2019). Prevention of respiratory syncytial virus infection with probiotic lactic acid bacterium lactobacillus gasseri SBT2055. *Sci. Rep.* 9:4812. doi: 10.1038/s41598-019-39602-7

Kemis, J. H., Linke, V., Barrett, K. L., Boehm, F. J., Traeger, L. L., Keller, M. P., et al. (2019). Genetic determinants of gut microbiota composition and bile acid profiles in mice. *PLoS Genet.* 15:e1008073. doi: 10.1371/journal.pgen.1008073

Kikkert, M. (2020). Innate immune evasion by human respiratory RNA viruses. *J. Innate Immun.* 12, 4–20. doi: 10.1159/000503030

Kozo, Y., Atsushi, B., Yasushi, I., Tetsuo, K., Kohki, A., Tetsuo, M., et al. (2005). Neutrophil-mediated inflammation in respiratory syncytial viral bronchiolitis. *Pediatr. Int.* 47, 190–195. doi: 10.1111/j.1442-200x.2005.02039.x

Kreso, B., Valerija, V., Neda, A., Jasna, C.-B., Alenka, G., Gordana, M.-G., et al. (2010). Decreased toll-like receptor 8 expression and lower TNF-alpha synthesis in infants with acute RSV infection. *Respir. Res.* 11:143. doi: 10.1186/1465-9921-11-143

Kruk, A., Granica, S., Popowski, D., Malinowska, N., and Piwowarski, J. P. (2022). Tiliae flos metabolites and their beneficial influence on human gut microbiota biodiversity ex vivo. *J. Ethnopharmacol.* 294:115355. doi: 10.1016/j.jep.2022.115355

Lee, H., Lee, Y., Kim, J., An, J., Lee, S., Kong, H., et al. (2018). Modulation of the gut microbiota by metformin improves metabolic profiles in aged obese mice. *Gut Microbes* 9, 155–165. doi: 10.1080/19490976.2017.1405209

Livak, K. J., and Schmittgen, T. D. (2001). Analysis of relative gene expression data using real-time quantitative PCR and the 2(-Delta Delta C(T)) method. *Methods* 25, 402–408. doi: 10.1006/meth.2001.1262

Lu, W., Fang, Z., Liu, X., Li, L., Zhang, P., Zhao, J., et al. (2021). The potential role of probiotics in protection against influenza a virus infection in mice. *Foods* 10:902. doi: 10.3390/foods10040902

Ma, D., Wang, A. C., Parikh, I., Green, S. J., Hoffman, J. D., Chlipala, G., et al. (2018). Ketogenic diet enhances neurovascular function with altered gut microbiome in young healthy mice. *Sci. Rep.* 8:6670. doi: 10.1038/s41598-018-25190-5

Matikainen, S., Sirén, J., Tissari, J., Veckman, V., Pirhonen, J., Severa, M., et al. (2006). Tumor necrosis factor alpha enhances influenza A virus-induced expression of antiviral cytokines by activating RIG-I gene expression. *J. Virol.* 80, 3515–3522. doi: 10.1128/JVI.80.7.3515-3522.2006

Moreau, N. M., Goupry, S. M., Antignac, J. P., Monteau, F. J., Bizec, B. J., Champ, M. M., et al. (2003). Simultaneous measurement of plasma concentrations and 13C-enrichment of short-chain fatty acids, lactic acid and ketone bodies by gas chromatography coupled to mass spectrometry. *J. Chromatogr. B* 784, 395–403. doi: 10.1016/S1570-0232(02)00827-9

Neuzil, K. M., Tang, Y.-W., and Graham, B. S. (1996). Protective role of TNF-α in respiratory syncytial virus infection In vitro and In vivo. *Am. J. Med. Sci.* 311, 201–204. doi: 10.1016/S0002-9629(15)41695-7

O'Donnell, D. R., and Carrington, D. (2002). Peripheral blood lymphopenia and neutrophilia in children with severe respiratory syncytial virus disease. *Pediatr. Pulmonol.* 34, 128–130. doi: 10.1002/ppul.10140

Openshaw, P. J. M., Chiu, C., Culley, F. J., and Johansson, C. (2017). Protective and harmful immunity to RSV infection. *Annu. Rev. Immunol.* 35, 501–532. doi: 10.1146/annurev-immunol-051116-052206

Parker, B. J., Wearsch, P. A., Veloo, A. C. M., and Rodriguez-Palacios, A. (2020). The genus *Alistipes*: gut bacteria with emerging implications to inflammation, cancer, and mental health. *Front. Immunol.* 11:906. doi: 10.3389/fimmu.2020.00906

Patel, D. A., Patel, A. C., Nolan, W. C., Zhang, Y., and Holtzman, M. J. (2012). High throughput screening for small molecule enhancers of the interferon signaling pathway to drive next-generation antiviral drug discovery. *PLoS One* 7:e36594. doi: 10.1371/journal.pone.0036594

Paul, D. S., Rachel, O., Mwanajuma, N., Emelda, A. O., James Nokes, D., Graham, F. M., et al. (2006). Molecular analysis of respiratory syncytial virus reinfections in infants from coastal Kenya. *J Infect Dis* 193, 59–67. doi: 10.1086/498246

Roe, M. F. E., Bloxham, D. M., White, D. K., Ross-Russell, R. I., Tasker, R. T. C., and O'Donnell, D. R. (2004). Lymphocyte apoptosis in acute respiratory syncytial virus bronchiolitis. *Clin. Exp. Immunol.* 137, 139–145. doi: 10.1111/j.1365-2249.2004.02512.x

Russell, R. F., McDonald, J. U., Ivanova, M., Zhong, Z., Bukreyev, A., and Tregoning, J. S. (2015). Partial attenuation of respiratory syncytial virus with a

deletion of a small hydrophobic gene is associated with elevated interleukin-1β responses. *J. Virol.* 89, 8974–8981. doi: 10.1128/JVI.01070-15

Ryan, P. M., Stolte, E. H., London, L. E. E., Wells, J. M., Long, S. L., Joyce, S. A., et al. (2019). *Lactobacillus mucosae* DPC 6426 as a bile-modifying and immunomodulatory microbe. *BMC Microbiol.* 19:33. doi: 10.1186/s12866-019-1403-0

Sadler, A. J., and Williams, B. R. G. (2008). Interferon-inducible antiviral effectors. *Nat. Rev. Immunol.* 8, 559–568. doi: 10.1038/nri2314

Saperstein, S., Chen, L., Oakes, D., Pryhuber, G., and Finkelstein, J. (2009). IL-1beta augments TNF-alpha-mediated inflammatory responses from lung epithelial cells. *J. Interferon Cytokine Res.* 29, 273–284. doi: 10.1089/jir.2008.0076

Sencio, V., Barthelemy, A., Tavares, L. P., Machado, M. G., Soulard, D., Cuinat, C., et al. (2020). Gut Dysbiosis during influenza contributes to pulmonary pneumococcal Superinfection through altered short-chain fatty acid production. *Cell Rep.* 30, 2934–2947.e6. doi: 10.1016/j.celrep.2020.02.013

Shi, T., McAllister, D. A., O'Brien, K. L., Simoes, E. A. F., Madhi, S. A., Gessner, B. D., et al. (2017). Global, regional, and national disease burden estimates of acute lower respiratory infections due to respiratory syncytial virus in young children in 2015: a systematic review and modelling study. *Lancet* 390, 946–958. doi: 10.1016/S0140-6736(17)30938-8

Smith, P. K., Wang, S. Z., Dowling, K. D., and Forsyth, K. (2001). Leucocyte populations in respiratory syncytial virus-induced bronchiolitis. *J. Paediatr. Child Health* 37, 146–151. doi: 10.1046/j.1440-1754.2001.00618.x

Steed, A. L., Christophi, G. P., Kaiko, G. E., Sun, L., Goodwin, V. M., Jain, U., et al. (2017). The microbial metabolite desaminotyrosine protects from influenza through type I interferon. *Science* 357, 498–502. doi: 10.1126/science.aam5336

Stricker, S., Hain, T., Chao, C.-M., and Rudloff, S. (2022). Respiratory and intestinal microbiota in pediatric lung diseases-current evidence of the gut-lung Axis. *Int. J. Mol. Sci.* 23:12. doi: 10.3390/ijms23126791

Trompette, A., Gollwitzer, E. S., Pattaroni, C., Lopez-Mejia, I. C., Riva, E., Pernot, J., et al. (2018). Dietary fiber confers protection against flu by shaping Ly6c-patrolling monocyte hematopoiesis and CD8+ T cell metabolism. *Immunity* 48, 992–1005.e8. doi: 10.1016/j.immuni.2018.04.022

Trompette, A., Gollwitzer, E. S., Yadava, K., Sichelstiel, A. K., Sprenger, N., Ngom-Bru, C., et al. (2014). Gut microbiota metabolism of dietary fiber influences allergic airway disease and hematopoiesis. *Nat. Med.* 20, 159–166. doi: 10.1038/nm.3444

Trugilho, M. R. O., Azevedo-Quintanilha, I. G., Gesto, J. S. M., Moraes, E. C. S., Mandacaru, S. C., Campos, M. M., et al. (2022). Platelet proteome reveals features of cell death, antiviral response and viral replication in covid-19. *Cell Death Discov.* 8:324. doi: 10.1038/s41420-022-01122-1

Tsay, T.-B., Yang, M.-C., Chen, P.-H., Hsu, C.-M., and Chen, L.-W. (2011). Gut flora enhance bacterial clearance in lung through toll-like receptors 4. *J. Biomed. Sci.* 18:68. doi: 10.1186/1423-0127-18-68

Tulic, M. K., Piche, T., and Verhasselt, V. (2016). Lung-gut cross-talk: evidence, mechanisms and implications for the mucosal inflammatory diseases. *Clin. Exp. Allergy* 46, 519–528. doi: 10.1111/cea.12723

Wang, Y., Xu, L., Liu, J., Zhu, W., and Mao, S. (2017). A high grain diet dynamically shifted the composition of mucosa-associated microbiota and induced mucosal injuries in the colon of sheep. *Front. Microbiol.* 8:2080. doi: 10.3389/fmicb.2017.02080

Wei, X., Tao, J., Xiao, S., Jiang, S., Shang, E., Zhu, Z., et al. (2018). Xiexin Tang improves the symptom of type 2 diabetic rats by modulation of the gut microbiota. *Sci. Rep.* 8:3685. doi: 10.1038/s41598-018-22094-2

William, W. T., David, K. S., Eric, W., Lynnette, B., Nancy, C., Larry, J. A., et al. (2003). Mortality associated with influenza and respiratory syncytial virus in the United States. *JAMA* 289, 179–186. doi: 10.1001/jama.289.2.179

Wu, S., Jiang, Z.-Y., Sun, Y.-F., Yu, B., Chen, J., Dai, C.-Q., et al. (2013). Microbiota regulates the TLR7 signaling pathway against respiratory tract influenza A virus infection. *Curr. Microbiol.* 67, 414–422. doi: 10.1007/s00284-013-0380-z

Wypych, T. P., Wickramasinghe, L. C., and Marsland, B. J. (2019). The influence of the microbiome on respiratory health. *Nat. Immunol.* 20, 1279–1290. doi: 10.1038/s41590-019-0451-9

Yohsuke, T., Eriko, C., Hortensia, Z., Takuya, T., Kohichiro, T., Haruki, K., et al. (2013). Nasally administered *lactobacillus rhamnosus* strains differentially modulate respiratory antibiral immune responses and induce protection against respiratory syncytial virus infection. *BMC Immunol.* 14:40. doi: 10.1186/1471-2172-14-40

Zamani-Rarani, F., Zamani-Rarani, M., Hamblin, M. R., Rashidi, B., Hashemian, S. M. R., and Mirzaei, H. (2022). Comprehensive overview of COVID-19-related respiratory failure: focus on cellular interactions. *Cell. Mol. Biol. Lett.* 27:63. doi: 10.1186/s11658-022-00363-3

frontiers | Frontiers in Microbiology

TYPE Original Research
PUBLISHED 26 September 2022
DOI 10.3389/fmicb.2022.1015270

OPEN ACCESS

EDITED BY
Wenyi Zhang,
Inner Mongolia Agricultural University, China

REVIEWED BY
Junrui Wu,
Shenyang Agricultural University, China
Yanlong Jiang,
Jilin Agricultural University, China

*CORRESPONDENCE
Ruiping Du
duruiping1989@163.com
Xiao Wang
wangxiao@imu.edu.cn

†These authors have contributed equally to this work

SPECIALTY SECTION
This article was submitted to Food Microbiology, a section of the journal Frontiers in Microbiology

RECEIVED 09 August 2022
ACCEPTED 30 August 2022
PUBLISHED 26 September 2022

CITATION
Sheng S, Fu Y, Pan N, Zhang H, Xiu L, Liang Y, Liu Y, Liu B, Ma C, Du R and Wang X (2022) Novel exopolysaccharide derived from probiotic *Lactobacillus pantheris* TCP102 strain with immune-enhancing and anticancer activities.
Front. Microbiol. 13:1015270.
doi: 10.3389/fmicb.2022.1015270

Novel exopolysaccharide derived from probiotic *Lactobacillus pantheris* TCP102 strain with immune-enhancing and anticancer activities

Shouxin Sheng[1†], Yubing Fu[2†], Na Pan[1], Haochi Zhang[1], Lei Xiu[1], Yanchen Liang[1], Yang Liu[1], Bohui Liu[1], Cheng Ma[1], Ruiping Du[3]* and Xiao Wang[1]*

[1]State Key Laboratory of Reproductive Regulation & Breeding of Grassland Livestock, School of Life Sciences, Inner Mongolia University, Hohhot, China, [2]School of Life Sciences, Faculty of Medicine and Life Sciences, State Key Laboratory of Cellular Stress Biology, Xiamen University, Xiamen, China, [3]Animal Nutrition Institute, Agriculture and Animal Husbandry Academy of Inner Mongolia, Hohhot, China

Probiotics are gaining attention due to their functions of regulating the intestinal barrier and promoting human health. The production of exopolysaccharide (EPS) is one of the important factors for probiotics to exert beneficial properties. This study aimed to screen exopolysaccharides-producing lactic acid bacteria (LAB) and evaluate the probiotic potential. we obtained three exopolysaccharide fractions (EPS1, EPS2, and EPS3) from *Lactobacillus pantheris* TCP102 and purified by a combination of ion-exchange chromatography and gel permeation chromatography. The structures of the fractions were characterized by FT-IR, UV, HPLC, and scanning electron microscopy (SEM) analysis. The Mw of EPS1, EPS2, and EPS3 were approximately 20.3, 23.0, and 19.3 kDa, and were mainly composed of galactose, glucose, and mannose, with approximate molar ratios of 2.86:1:1.48, 1.26:1:1, 1.58:1.80:1, respectively. Furthermore, SEM analysis demonstrated that the three polysaccharide fractions differ in microstructure and surface morphology. Additionally, preliminary results for immune-enhancing and anticancer activities reveal that these EPSs significantly induced the production of nitric oxide (NO), TNF-α, and IL-6 in Ana-1 cells and peritoneal macrophage cells. Meanwhile, the EPSs also significantly suppressed the proliferation of HCT-116, BCG-803, and particularly A-2780 cells. The results suggest that the three novel EPSs isolated from *Lactobacillus pantheris* TCP102 can be regarded as potential application value in functional food and natural antitumor drugs.

KEYWORDS

exopolysaccharide, probiotic, *Lactobacillus pantheris*, immune-enhancing activity, anticancer activity

Introduction

Probiotics, which the WHO defines as "live microorganisms when administered in adequate quantities confer a health profit to the host cell," play important roles in preventing disease and promoting health of the host (Ouwehand, 2017). Most probiotics are bacteria belonging mainly to the genera *Lactobacillus* and *Bifidobacterium*. Probiotics have been shown to be effective in mitigating gastrointestinal inflammatory conditions such as inflammatory bowel disease, irritable bowel syndrome, certain respiratory conditions, and allergies (Quigley, 2013; Butel, 2014; Plaza-Diaz et al., 2014). In addition to regulating intestinal epithelial homeostasis and immune responses, certain probiotics have been reported to have anticancer activity through different mechanisms (Chong, 2014; Thomas et al., 2014; Kayama and Takeda, 2016). Furthermore, research indicates that certain probiotic functions are related to bacterial secretions (Shida et al., 2011).

Various genera of lactic acid bacteria (LAB) are capable of synthesizing exopolysaccharide (EPS) that are either attached to the cell surface or are found in the extracellular medium as slime (Nwodo et al., 2012; Patel et al., 2012; Zannini et al., 2016). EPS is widely used in the biotechnology, health, and pharmaceutical industries and is widely accepted as food products. Many reports have indicated that EPS has various potential physiological functions and biological activities. For example, various EPSs are known to have antioxidant, anticancer, immune-enhancing, antibacterial, hypoglycemic, and antihypertensive activities (Sengül et al., 2011; Nácher-Vázquez et al., 2015; El-Deeb et al., 2018). The therapeutic activity of polysaccharides depends on their structural features such as molecular weight, chemical structure, and the conformation and configuration of the glycosidic linkages. These features, in turn, are dependent on various biotic and abiotic factors such as biomass morphology, pH, oxygen, fermentation time, temperature, stirring, carbon and nitrogen contents, and the C/N ratio of the culture medium (Champagne et al., 2006; Ruhmkorf et al., 2012; Ma et al., 2014). The structure-function relationship of EPS remains a major research topic (Surayot et al., 2014; Gentès et al., 2015).

An increasing number of researchers are investigating the use of EPS with macrophage immune-enhancing activity. Macrophages are an important part of the innate immune system. They interact and coordinate with adaptive immune responses through the production of cytokines and phagocytosis of pathogens. A hallmark of macrophage activation is the release of cytokines and NO. For example, microbial exopolysaccharides can increase the activities of IL-2 in the supernatant of murine splenocytes and IL-6 and TNF-α in the supernatant of murine macrophages, by promoting the expression of the mRNAs of these cytokines (Chen et al., 2006; Ren et al., 2016; Wang et al., 2016). In addition, EPS has been reported to exhibit intense antitumor activities. EPS treatment observably altered the cell morphology and even damaged the human cancer cell lines HepG-2, BGC-823, and HT-29, and could induce cancer cell apoptosis (Chen et al., 2013; Li et al., 2014b, 2015).

In the present study, we evaluated the probiotic potential of 18 strains of lactic acid bacteria isolated from tomato pomace in our laboratory. As basic properties of probiotics, acid resistance, bile salt tolerance, and adhesion ability were investigated. We isolated three different polysaccharides named EPS1, EPS2, and EPS3 from a TCP102 culture. The chemical structure and physicochemical properties of the purified EPSs were characterized by high performance liquid chromatography (HPLC), ultraviolet (UV) and Fourier transform infrared spectroscopy (FT-IR), and scanning electron microscopy (SEM). This research aimed to isolate lactic acid bacteria from tomato pomace to assess their potential probiotic properties and provide information on the structure-function relationship between the characteristics of the EPSs and their potential bioactivities, such as immune-enhancing activity in murine macrophages and antiproliferative effects with three human cancer cells. This study will provide the scientific reference for further systematic investigation and application in immune-enhancing functional food and natural antitumor drugs of lactic acid bacteria polysaccharides.

Materials and methods

Strains and culture condition

Eighteen strains of lactic acid bacteria were isolated from tomato pomace by our laboratory. The strains were maintained at −80°C in MRS broth (Guangdong Huankai, China) containing 30% (v/v) glycerinum (Sinopharm Chemical Reagent Co., Ltd, China). The strain was propagated successively in MRS agar then in MRS broth at 37°C for 18 h, prior to the experiments. A batch fermentation was performed for 30 h at 37°C under anaerobic conditions. All strains were identified based on cell morphology, biophysical and biochemical tests, and 16S rRNA gene sequence analysis. Strains TCP001, TCP004, TCP007, TCP008, TCP009, TCP015, TCP016, TCP017, TCP024, TCP029, TCP037, TCP045, TCP050, TCP063, TCP071, TCP073, TCP080, and TCP102 were unambiguously identified as *Lactobacillus harbinensis*, *Lactobacillus paracasei subsp. paracasei*, *Lactobacillus fermentum*, *Lactobacillus plantarum*, *Lactobacillus rhamnosus*, *Lactobacillus coryniformis subsp. torquens*, *Lactobacillus buchneri*, *Lactobacillus manihotivorans*, *Lactobacillus parafarraginis*, *Lactobacillus camelliae*, *Lactobacillus rapi*, *Lactobacillus pontis*, *Lactobacillus helveticus*, *Lactobacillus vaginalis*, *Lactobacillus amylovorus*, *Lactobacillus hilgardii*, *Lactobacillus panis*, and *Lactobacillus pantheris*.

The indicator bacteria of antibacterial experiment were *Escherichia coli* CMCC 44102 and *Staphylococcus aureus* ATCC 27543, which were purchased from Beijing Nanolink Biotechnology Research Institute and American Culture Collection Center. The indicator strains were cultivated in LB broth (Guangdong Huankai, China) with shaking at 37°C for 24 h.

The evaluation of probiotic properties of lactic acid bacteria

Bile salt tolerance

The ability of isolates to grow in presence of bile salt was measured. This was carried out with 0.3% w/v oxgall, 0.5% w/v oxgall, 1.0% w/v oxgall and control was maintained employing MRS broth. The samples were inoculated at 37°C for 24 h and OD_{600} of samples was measured to check the viability of cells. The oxgall resistance was determined by the following equation: Survival Rate (%): [OD (After treatment)/OD (Before treatment)] × 100%.

Gastric tolerance

The resistance of strains to gastric was measured as described by Wang et al. (2021), with minor modifications. Lactic acid bacteria that were frozen at −80°C were activated and inoculated into MRS broth. Take 5 ml of bacterial liquid and centrifuge at 3,000 rpm for 10 min to discard the supernatant. Add 5 ml of sterile saline and mix to make the bacterial suspension. Take 1 ml of bacterial suspension and mix with 9 ml of artificial gastric juice, respectively. The samples were inoculated at 37°C for 0 h and 3 h, and calculate the survival rate by serial dilution and plating, three replicates for each strain. The survival rate was calculated using the following equation: Survival Rate (%): [OD (After treatment)/OD (Before treatment)] × 100%.

Adhesion to Caco-2 cells

The ability of the tested bacteria to adhere to the Caco-2 cell layer was investigated according to the previously published method (Sałański et al., 2022) with minor modifications. For this purpose, Caco-2 cells were cultured in RPMI medium supplemented with 10% heat-inactivated fetal bovine serum and 1% penicillin–streptomycin blend and cells were refined on 24-well tissue culture plates and incubated at 37°C in 5% CO_2 under a relatively humidified atmosphere until a confluent monolayer was formed. Sometime recently the attachment measure, the media within the wells containing a Caco-2 cell monolayer were evacuated and supplanted with new antibiotic-free RPMI. From that point, 1×10^8 CFU/mL of isolates was included to each well with a add up to volume of 1 mL and after that incubated for 3 h at 37°C under an atmosphere of 5% (v/v) CO_2. The wells were washed twice with a sterile pre-warmed PBS solution to evacuate non-attached bacterial cells. 1 mL of 1% (v/v) Triton X-100 was included to each well to withdraw the cells from the wells and the blend was mixed for 10 min. To measure the viable cell count, the cell suspension was plated onto MRS agar and hatched at 37°C. Each experiment was made at least in three independent biological replicates with triplicate technical repetitions.

Antimicrobial activity

The antimicrobial features of isolates were performed by agar well diffusion assay.

In this method, plates containing *Escherichia coli* and *Staphylococcus aureus* agar medium impregnated with different indicator bacteria was used. The oxford cup was used to create wells in medium. Finally, 100 μL supernatants of isolates were placed inside each well and plates were then incubated at 37°C for 24 h. After incubation time, the measured inhibition halo zone diameters were statistically analyzed.

Extraction, isolation, and purification of exopolysaccharide

Culture medium of lactic acid bacteria was heated in boiling water for 10 min to inactivate enzymes, cooled down to 25°C centrifuged (20 min, 5,500 rpm, 4°C) to remove cells and coagulated proteins, and then the supernatant was collected. Trichloroacetic acid (80%, w/v) was added to the supernatant to a final concentration of 4% (w/v) with gentle stirring and the solution was kept at 4°C for 10 h. The precipitated proteins were removed by centrifugation (15 min, 10,000 rpm, 4°C), and the supernatant was precipitated by slowly adding four volumes of prechilled absolute ethyl alcohol and incubating at 4°C overnight (Ai et al., 2008; Wang et al., 2014). The EPS was collected by centrifugation at the same conditions as described above (15 min, 10,000 rpm, 4°C). The precipitates were dialyzed (Mw cut-off: 8,000-14,000 Da) with three changes of water per day for 3 days. The dialysate was then lyophilized, and collected as crude EPS.

The crude EPS was purified by a two-step process. Samples were first applied to a DEAE-Sepharose Fast Flow (GE, USA) ion exchange column (26 mm × 400 mm), and eluted with Tris-HCl buffer (55 mM, pH 7.5–7.8), followed by and a linear gradient of 0–1 M NaCl buffer. The eluate fractions were collected at a rate of 6 mL per tube using a fraction collector (Ai et al., 2008). The yield and total sugar content of EPS were measured by the phenol-sulfuric acid method using 0–200 mg/L of glucose as a standard (Matsuzaki et al., 2015). One polysaccharide fraction named EPS1 was obtained during the elution using Tris–HCl buffer, while another two fractions, named EPS2 and EPS3, were eluted using the linear gradient of NaCl. EPS fractions were dialyzed against deionized water with three changes of water per day for 3 days at 4°C, and then lyophilized. The three fractions were further purified on a Sepharose CL-6B (GE, USA)

gel column (16 mm × 1,000 mm). Each fraction was eluted with 55 mM Tris–HCl buffer (pH 7.6–7.8) at a flow rate of 0.5 mL/min, collecting 6 mL of eluate per tube. The eluates with EPS were detected, collected, dialyzed against deionized water with three changes of water every day for 3 days at 4°C. The dialysates were lyophilized, and the resulting products consisted of the major purified fractions that were used for further study. The total carbohydrate content of each fraction was measured using the phenol-sulfuric acid method with glucose as standard (Matsuzaki et al., 2015).

Estimation of homogeneity and apparent molecular weight

To estimate the homogeneity and apparent molecular weight of purified TCP102 EPSs, samples were separated on a BRT105-104-102 (Shimadzu) tandem gel column (8 mm × 300 mm). The samples were eluted isostatically with ultrapure water (vacuum-filtered through 0.22 μm membrane filter and degassed), at 40°C and a flow rate of 0.8 mL/min. Aqueous standards and EPS fractions (5 mg/mL and 10 μL, respectively) were filtered through 0.22 μm cellulose acetate filters (Análisis Vínicos, Tomelloso, Toledo, Spain) and injected (20 μL) into the HPLC. The system was calibrated with glucan molecular weight standards (1,152, 11,600, 23,800, 48,600, 80,900, 148,000, 273,000, and 409,800 Da). Peaks were detected using a refractive index detector (RI) (Waters).

Monosaccharide composition analysis

To determine the monosaccharide composition of purified TCP102 EPS, a 10 mg sample was hydrolyzed with 4 mL of 4 mol/L trifluoroacetic acid (TFA) at 120°C for 2 h under a N_2 environment. The hydrolysates were dried under a stream of N_2 and dissolved with 10 mL ultrapure water. The IC (ion chromatography) system used was a Dionex ICS3000 equipped with a conductivity detector and a Carbo PacTMPA20 analytical column (3 mm × 150 mm) and running at a flow rate of 0.5 mL/min at 35°C. Peaks were assigned based on peak retention times of a standard. The diluted samples were filtered through a 0.22 μm syringe filter prior to injection.

Ultraviolet and Fourier transform infrared spectroscopy spectrometric analysis

Ultraviolet–visible (UV–vis) spectroscopy was combined with HPLC (GE, USA). The EPS solution was prepared for HPLC by suspending a sample in distilled water to a concentration of 500 μg/mL. Spectroscopy was conducted within the wavelength range of 190–400 nm.

The GPC system included a surveyor pump, Surveyor Autosampler (Themo Electron Corporation, Waltham, MA, USA), a Surveyor Photodiode Array Detector, two columns (Ultrahydrogel 500 and Ultrahydrogel 250 column, 7.8 mm × 300 mm) connected serially. The mobile phase was an isocratic solvent system consisting of acetic acid and sodium acetate (sodium acetate 18 g, acetic acid 9.8 mL, plus ultrapure water to 1 L) running at a flow rate of 0.9 mL/min. The temperature of column was 45°C. Solutions were filtered through a 0.22 μm filter and degassed prior to use.

The various functional groups of EPS fractions were determined using a Fourier transform infrared spectrophotometer (Thorlabs Inc, Newton, NJ, USA). The purified EPS samples (1–2 mg) were ground with 100–200 mg KBr powder and pressed into pellets prior to FTIR measurements in the frequency range of 4,000–400 cm^{-1}.

Scanning electron microscopy analysis

The microstructure and surface morphology of the three purified EPS fractions were investigated using an S-4800 scanning electron microscope (Hitachi, Japan) at an accelerating voltage of 10.0 kV. Purified EPS samples were glued onto SEM stubs and gold-coated before analysis.

Immune-enhancing activity of exopolysaccharide

The mouse macrophage cell line Ana-1 was purchased from the Type Culture Collection of the Chinese Academy of Sciences (Shanghai, China). Peritoneal macrophage cells were obtained from the lateral wall of the peritoneum of Ana-1 mice. Cells were cultured in RPMI-1640 medium (GE Healthcare Life Sciences, Hy Clone Laboratories, Utah, USA) containing 100 μg/mL penicillin, 100 μg/mL streptomycin, 2 mM L-glutamine, and 10% fetal bovine serum (FBS; GE Hy Clone). The 75-cm^2 culture flasks were incubated at 37°C in a 5% CO_2 atmosphere. The cell suspension was then pipetted into the wells of a 96-well plate at the rate of 200 μL/well (2×10^5 cells/mL). Cells were preincubated for 4 h, then treated with 200 μL of different concentrations of EPS (0, 31.25, 62.5, 125, 250, and 500 μg/mL) suspended in RPMI-1640 medium for 24 h. LPS (1 μg/mL) was used as the positive control.

NO production was measured using a Griess reagent kit (Promega Corporation, Beijing, China) following the manufacturer's protocol. The absorbance was monitored at 540 nm with a microplate reader (Thermo Fisher Scientific, Shanghai, China). Following NO measurements, the culture supernatants of macrophage cells were collected to estimate the

amount of secreted TNF-α and IL-6 reagent (R&D Systems, Minneapolis, USA) using ELISA.

Anticancer activity

The human colon cancer, ovarian cancer, and gastric cancer cell lines HCT-116, A-2780, and BCG-803, respectively (all cancer cell lines were purchased from the ATCC, Manassas, VA, USA), were cultured using DMEM (GE, Hy Clone) containing 100 μg/mL penicillin, 100 μg/mL streptomycin, 2 mM L-glutamine, and 10% FBS in 75-cm^2 culture flasks at 37°C under a 5% CO_2 atmosphere. To measure the inhibitory rates of EPS on the growth of cancer cells, the cell suspensions were pipetted into a 96-well plate at the rate of 200 μL/well (2×10^5 cells/mL). After 4 hours, the cancer cells were treated with 200 μL of various concentrations of purified EPS (0, 31.25, 62.5, 125, 250, and 500 μg/mL) and 5-FU (5-fluorouracil, 50 μg/mL) for 24, 48, and 72 h. At the end of each treatment, MTS reagent (Promega Corporation, Beijing, China) was added to each well (20 μL/well), and the plates were incubated at 37°C for 2 hours in a humidified, 5% CO_2 atmosphere. The absorbance at 490 nm was measured using a 96-well plate reader. The inhibitory rate was calculated using the following equation:

$$\text{Inhibitory Rate (\%)} = [1 - (A_{sample} - A_{blank})/(A_{control} - A_{blank})] \times 100\%$$

where A_{sample} is the absorbance of the reagent mixture with EPS or 5-FU, A_{blank} is the absorbance of the reagent mixture with medium, and $A_{control}$ is the absorbance of the reagent mixture without EPS and 5-FU.

Statistical analysis

All experiments were repeated thrice. Results were expressed as the mean ± SD of triplicate analyses. Statistical significance was analyzed by one-way ANOVA using SPSS16.0 software. Asterisks indicate the P values of the comparison between treatment means versus the control group, where *, **, and *** indicate $P < 0.05$, $P < 0.01$, and $P < 0.001$, respectively.

Results

Identification of strains

The 16S-rRNA gene sequencing was used to validate the phenotypic characterization of the selected lactic acid bacteria isolates. The PCR-amplified 1,544 bp fragments of the 16S-rRNA gene of the isolates were sequenced and blasted with the sequences deposited in GenBank. Amplification of the 16S-rRNA genes of 18 LAB isolates confirmed that all of which

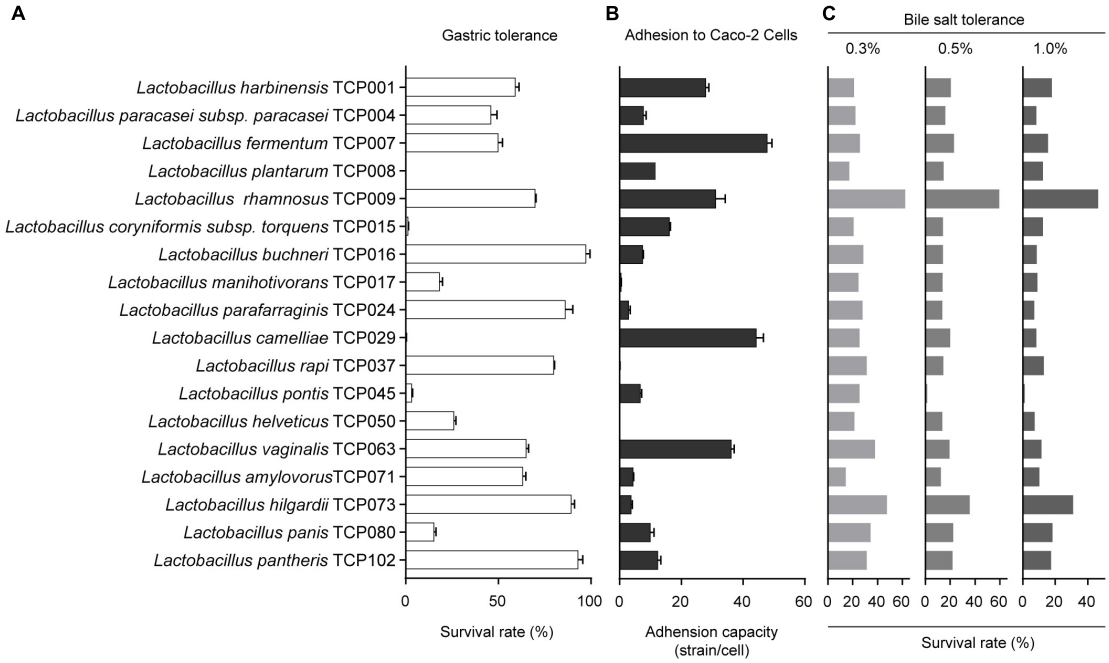

FIGURE 1
The evaluation of probiotic properties of lactic acid bacteria. **(A)** The results of the tolerance of 18 lactic acid bacteria strains to artificial gastric juice. **(B)** The adhesion results of 18 lactic acid bacteria strains to Caco-2 cells. **(C)** The results of bile salts tolerance of 18 lactic acid bacteria strains.

belonged to the genus *Lactobacillus*, which had been identified in our previous study. In addition, the nucleotide sequences of the 16S rRNA gene had been deposited with GenBank (Wu et al., 2014).

Acid resistance

The results of the tolerance of 18 lactic acid bacteria strains to artificial gastric juice are shown in Figure 1A. The strains of TCP015, TCP029, and TCP045 could hardly survive in gastric juice, and the survival rate of strains of TCP016, TCP024, TCP073, TCP102, and TCP037 in artificial gastric juice was greater than 80%. The survival rate of TCP001, TCP007, TCP071, TCP063, and TCP009 was between 50 and 80%, in addition, the survival rate of TCP008 and TCP050 was between 20 and 50%, and the survival rate of TCP016, TCP017 and TCP080 was between 10 and 20%. The results showed that the survival rate of most lactic acid bacteria in gastric juice was above 10%, which could tolerate the environment of gastric acid.

Adhesion assay

The adhesion results of 18 lactic acid bacteria strains to Caco-2 cells are shown in Figure 1B. The results showed that the adhesion ability of different lactic acid bacteria to Caco-2 cells was very different, among which TCP017, TCP050, and TCP037 had almost no adhesion ability. The strains of TCP004, TCP016, TCP024, TCP045, TCP071, and TCP073 adhered to an average of 3-10 bacteria per cell, and the strains of TCP008, TCP015, TCP102, and TCP080 adhered 10-20 bacteria per cell. In addition, the five strains of TCP001, TCP007, TCP029, TCP063, and TCP009 had strong adhesion ability, with an average of 28–48 bacteria adhered to each cell.

Bile salt tolerance

The survival rates of 18 isolates in 0.3, 0.5, and 1.0% oxgall are indicated in Figure 1C, and these bacteria have a certain tolerance to 0.3, 0.5, 1.0% oxgll, despite variations in the degree of viability. Among them, TCP009 had the highest tolerance to all concentrations of bile salts, and was significantly different from other strains. The five strains TCP073, TCP102, TCP080, TCP063, and TCP037 had a high tolerance to 0.3% bile salts, ranging from 30% to 50%, except for TCP008 and TCP071, which had a tolerance to 0.3% bile salts. Except for 10–20%, the rest of the strains were between 20% and 30%. The tolerance to 0.5 and 1.0% bile salts was the highest among TCP073 and TCP009. Except for TCP045, which was extremely low, the rest of the strains were almost between 10 and 20%.

TABLE 1 The results of antibacterial activity for the strains against various pathogens.

Indicator bacteria	Zone diameter (mm)																	
	TCP 001	TCP 004	TCP 007	TCP 008	TCP 009	TCP 015	TCP 016	TCP 017	TCP 024	TCP 029	TCP 037	TCP 045	TCP 050	TCP 063	TCP 71	TCP 073	TCP 080	TCP 102
Escherichia coli	12.00 ± 0.20	14.00 ± 0.10	12.00 ± 0.22	16.00 ± 0.24	21.00 ± 0.10	12.40 ± 0.30	6.50 ± 0.10	11.80 ± 0.10	0.00 ± 0.00	0.00 ± 0.00	8.50 ± 0.10	17.40 ± 0.10	0.00 ± 0.00	17.40 ± 0.10	16.50 ± 0.10	13.50 ± 0.10	11.50 ± 0.10	5.40 ± 0.20
Staphylococcus aureus	18.30 ± 0.10	21.60 ± 0.10	15.50 ± 0.10	15.50 ± 0.10	21.60 ± 0.10	20.30 ± 0.20	19.60 ± 0.10	21.70 ± 0.10	16.40 ± 0.10	18.50 ± 0.10	19.60 ± 0.10	19.60 ± 0.10	24.40 ± 0.20	17.40 ± 0.20	17.60 ± 0.10	20.50 ± 0.10	20.70 ± 0.20	18.60 ± 0.10

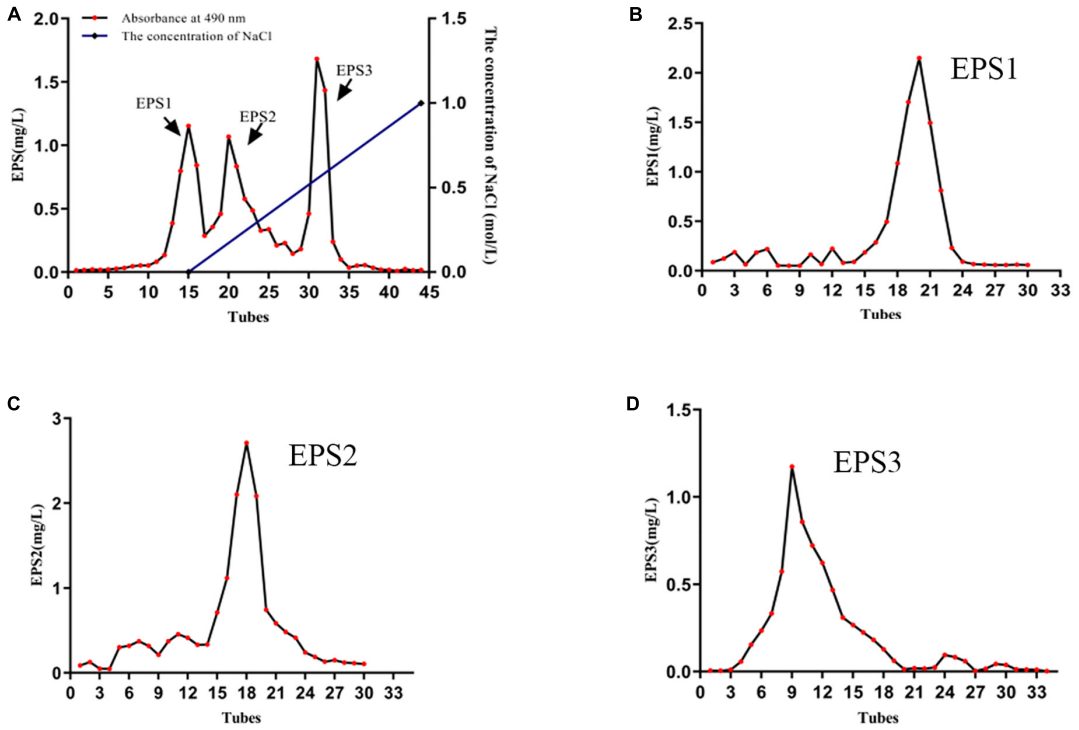

FIGURE 2
The characterization of EPSs. **(A)** Elution profile of EPSs produced by strain *L. pantheris* TCP102 on DEAE-Sepharose fast flow column. Elution profiles of **(B)** EPS1, **(C)** EPS2, and **(D)** EPS3 on Sepharose CL-6B gel columns.

Antimicrobial activity

The bacteriostatic results of 18 strains against *Escherichia coli* and *Staphylococcus aureus* are shown in **Table 1**. The results showed that these 18 strains had stronger bacteriostatic effect on *Staphylococcus aureus* than *Escherichia coli*. TCP009, TCP008, TCP045, TCP071, TCP063, and TCP004 had strong antibacterial effects on *Escherichia coli*. In addition, TCP009, TCP004, TCP015, TCP017, TCP050, TCP073, and TCP080 had the strongest antibacterial effect on *Staphylococcus aureus*.

Extraction and purification of exopolysaccharide

The results showed that 11 lactic acid bacteria strains including TCP001, TCP004, TCP007, TCP008, TCP009, TCP016, TCP063, TCP071, TCP073, TCP080, and TCP102 had probiotic potential. Next, we selected the TCP102 strain with probiotic properties as a further study strain. **Supplementary Figures 1A,B** showed the smooth and whitish colony appearance of strain TCP102 on MRS agar. Colonies were round and medium-sized. The morphological characteristics and 16S rRNA gene sequence analysis identified strain TCP102 as *Lactobacillus pantheris*. The yield of crude exopolysaccharide was 525 mg/L based on analysis of MRS fermentation broth. Three homogeneous exopolysaccharides, designated EPS1, EPS2, and EPS3, were obtained after a two-step isolation and purification process. First, the crude EPS solution was separated through anion-exchange chromatography using DEAE-Sepharose Fast Flow. The resulting three elution peaks were detected by the phenol-sulfuric acid assay. EPS1 was eluted with Tris-HCl buffer, and was thus a neutral polysaccharide. EPS2 and EPS3 were eluted with Tris-HCl and a high ionic strength NaCl solution, which were acidic polysaccharides (**Figure 2A**). The three exopolysaccharides were purified using a Sepharose CL-6B gel column (**Figures 2B–D**), resulting in a single and relatively symmetrical peak on the elution profile for each fraction. The total sugar contents of EPS1, EPS2, and EPS3 were approximately 92.36, 95.75, and 93.24%, respectively, and all purified exopolysaccharides were colorless powders. Each of fractions were collected, dialyzed, and lyophilized for the following analysis.

Molecular weight and monosaccharide composition of exopolysaccharide

A GPC system was used to determine the purity and molecular weights (Mw) of the EPSs, that the chromatogram

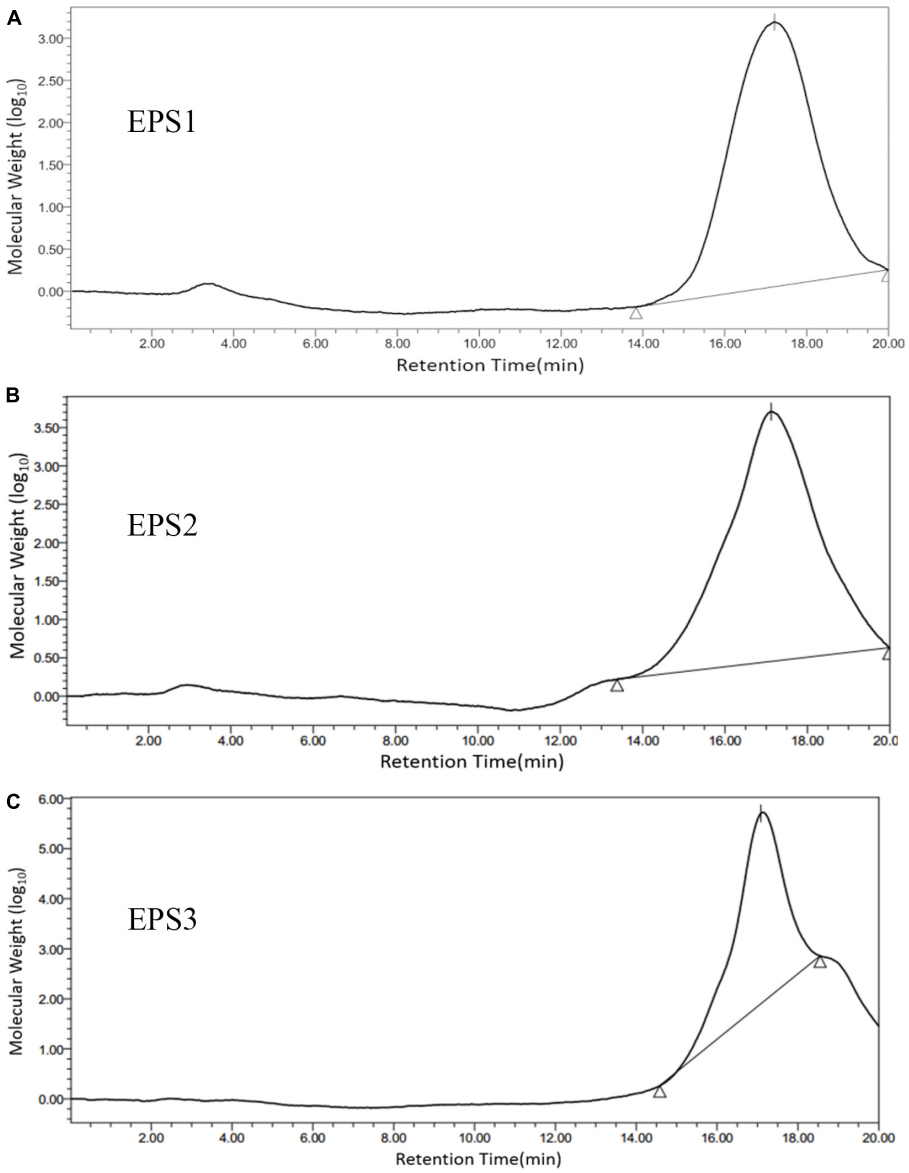

FIGURE 3
Molecular weight distribution of **(A)** EPS1, **(B)** EPS2, and **(C)** EPS3 on high performance gel permeation chromatogram (HPGPC). The samples were applied to a BRT105-104-102 system with a tandem gel column (8 mm × 300 mm, 8 μm) and eluted with 0.1 M ultrapure water at 0.8 mL/min and a column temperature of 40°C.

shows only one symmetrical peak corresponding to EPS1, EPS2, and EPS3 (**Figure 3**), indicating that the polysaccharides are homogeneous. The molecular weights of EPS1, EPS2, and EPS3 were estimated to be 20.3, 23.0, and 19.3 kDa, respectively, suggesting similar molecular weight distributions among the three purified polysaccharide fractions. The molecular weights of the three polysaccharides are lower than those of *Nitratireductor* sp. PRIM-31 (90 kDa) (Priyanka et al., 2016), *Tolypocladium* sp. fungus (40 kDa) (Yan et al., 2010), and *L. curvatus* DPPMA10 (100 kDa) EPSs (Minervini et al., 2010). In general, polysaccharides with lower molecular weights are more water soluble, with a relatively expanded chain conformation, which are associated with more bioactive molecules (Shi et al., 2016).

Monosaccharide composition analysis (**Figure 4**) shows the presence mainly of galactose, glucose, and mannose with approximate molar ratios of 2.86:1:1.48, 1.26:1:1, and 1.58:1.80:1 in EPS1, EPS2, and EPS3, respectively. Furthermore, all the EPSs contain trace amounts of galacturonic acid and glucuronic acid. The analysis also yielded one unknown monosaccharide, which we designated as "n.a.". Similar results were reported by Li et al., who found glucose, mannose, and galactose as the

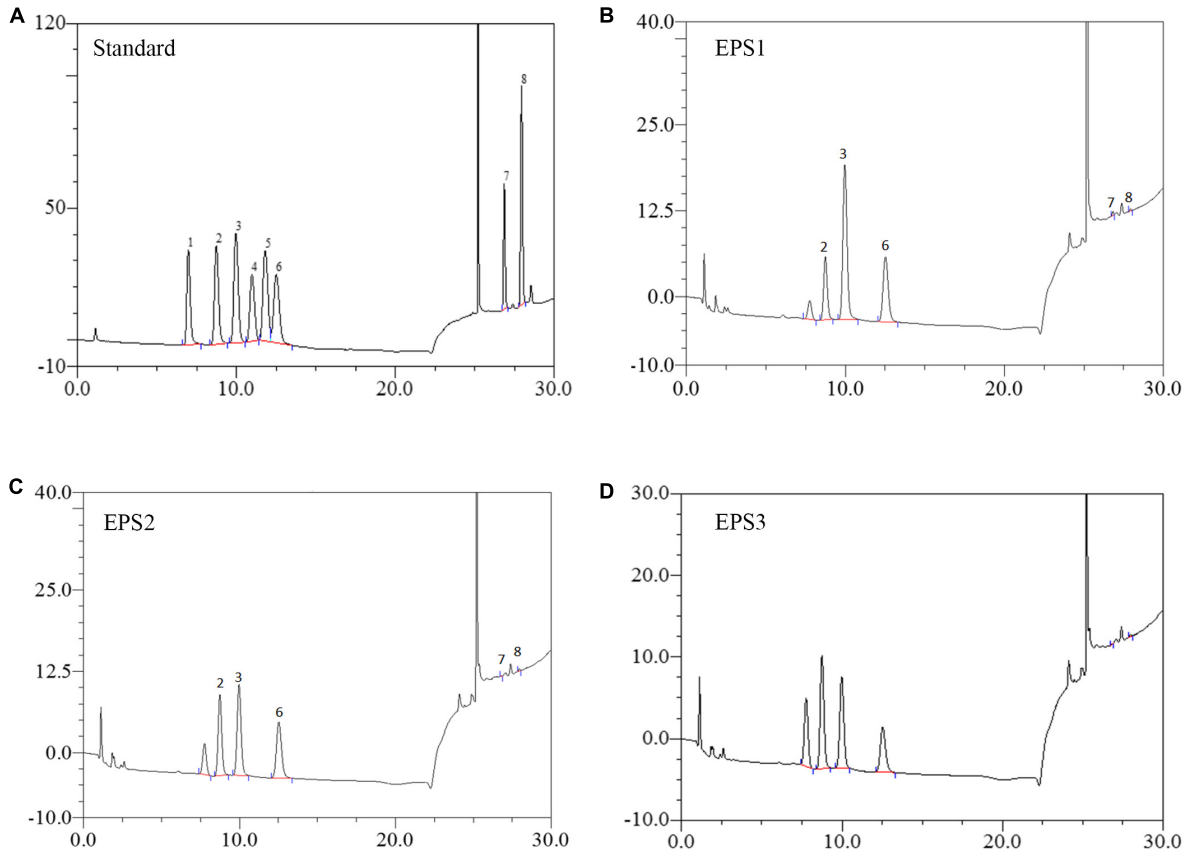

FIGURE 4
HPLC chromatogram of the monosaccharide components of EPSs from *L. pantheris* TCP102. **(A)** Monosaccharide standard, the peak values of 1–8 represent arabinose, galactose, glucose, xylose, mannose, ribose, galacturonic acid, and glucuronic acid, respectively. **(B)** EPS1, **(C)** EP2, and **(D)** EPS3.

predominant components of the EPS of *Lactobacillus helveticus* MB2-1 (Li et al., 2014a). Moreover, glucose and mannose are also the primary components of the EPS of *Bifidobacterium animalis* RH and *Streptococcus thermophilus* 05–34 (Shang et al., 2013; Li et al., 2016).

Ultraviolet and Fourier transform infrared spectroscopy analysis

An analysis of the ultraviolet scan spectrum of the EPSs is shown in **Figure 5A**. No absorption peaks were found at 260 and 280 nm, indicating an absence of proteins and nucleic acids. In the infrared wavelengths, the EPSs exhibit properties characteristic of polysaccharides. Specifically, the FT-IR spectrum (**Figure 5B**) shows common characteristic bands among EPS1, EPS2, and EPS3, the bands at 3,374, 3,375 and 3,371 cm^{-1} indicate the stretching vibration of the O-H group. The signals at 2,914, 2,914 and 2,920 cm^{-1} are attributed to the stretching vibration of the C-H bond (Liu et al., 2009). Meanwhile, the stronger absorption signals at 1,637, 1,640, and 1,637 cm^{-1} in the FT-IR spectra of EPSs indicate the dominance of the C = O stretching group (Shuhong et al., 2014). All above mentioned characteristic bonds are typical groups of polysaccharides. Furthermore, the peaks at 2,850 cm^{-1} are usually defined as the N-H bending of amides, and it couldn't be found among EPS1, EPS2, and EPS3 in **Figure 5B**, which confirms that the protein was basically eliminated during the purification process. This statement is consistent with the results of UV spectrum in **Figure 5A**. EPS-1, EPS-2 and EPS-3 had no absorption peak near 1,730 cm^{-1}, indicating that they were neutral polysaccharides. Moreover, the strong absorption signals at 1,058, 1,030, 1,041, and 1,036 cm^{-1} indicate the dominance of the pyran rings, especially signals at 1,058 cm^{-1} could be attributed to the α-(1→6) glycosidic bond in the main chain (Wu et al., 2009; Shuhong et al., 2014). The absorption signals at 864, 881, and 877 cm^{-1} in the IR spectra are characteristic of the β-anomeric configuration. In addition, the strong absorption signals at 798, 801, and 801 cm^{-1} indicate the presence of the α-anomeric configuration of mannose units, which agree with the results of monosaccharide composition of EPS

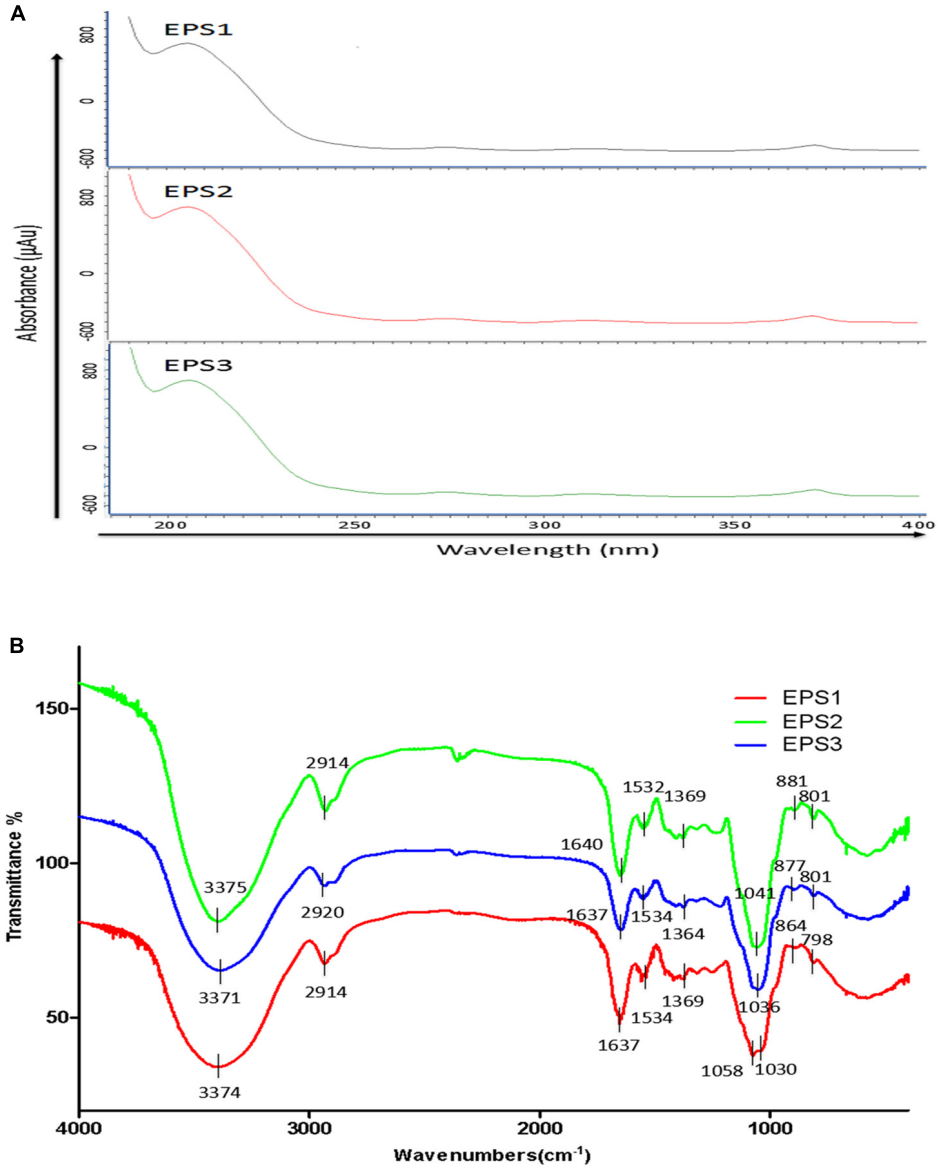

FIGURE 5
UV and FT-IR spectrometric analysis. **(A)** UV spectra of EPSs in the range of 180–540 nm. **(B)** FT-IR spectra of EPSs in the range of 600–4,000 cm^{-1}.

(Mathlouthi and Koenig, 1987). These results suggest that all the three EPSs may be neutral polysaccharide with both α- and β-anomeric configuration, with the existence of α-(1→6) glycosidic bond.

Scanning electron microscopy analysis

Scanning electron microscopy has been widely used to characterize the surface morphology and the microstructure of polysaccharides. SEM images of EPS1, EPS2, and EPS3 are shown in **Figure 6**. EPS1 (**Figure 6A**) appears as a smooth sheet structure with many homogeneous rod-shaped lumps. Meanwhile, EPS2 (**Figure 6B**) is characterized by flakes piling over a compact structure with a rough surface. Lastly, EPS3 (**Figure 6C**) displays inner filaments composed of irregularly shaped particles, which is associated with greater viscosity, film forming properties, and water retention performance. In *L. plantarum* KX041, SEM micrographs of EPS shows an irregular, highly porous web-like structure, and an uneven surface (Xu et al., 2019). The EPS from *Lactobacillus pentosus* LZ-R-17 also displays a web-like structure, but its smooth surface probably improves its viscosity and water holding capacity (You et al., 2020). It should be noted that while EPS

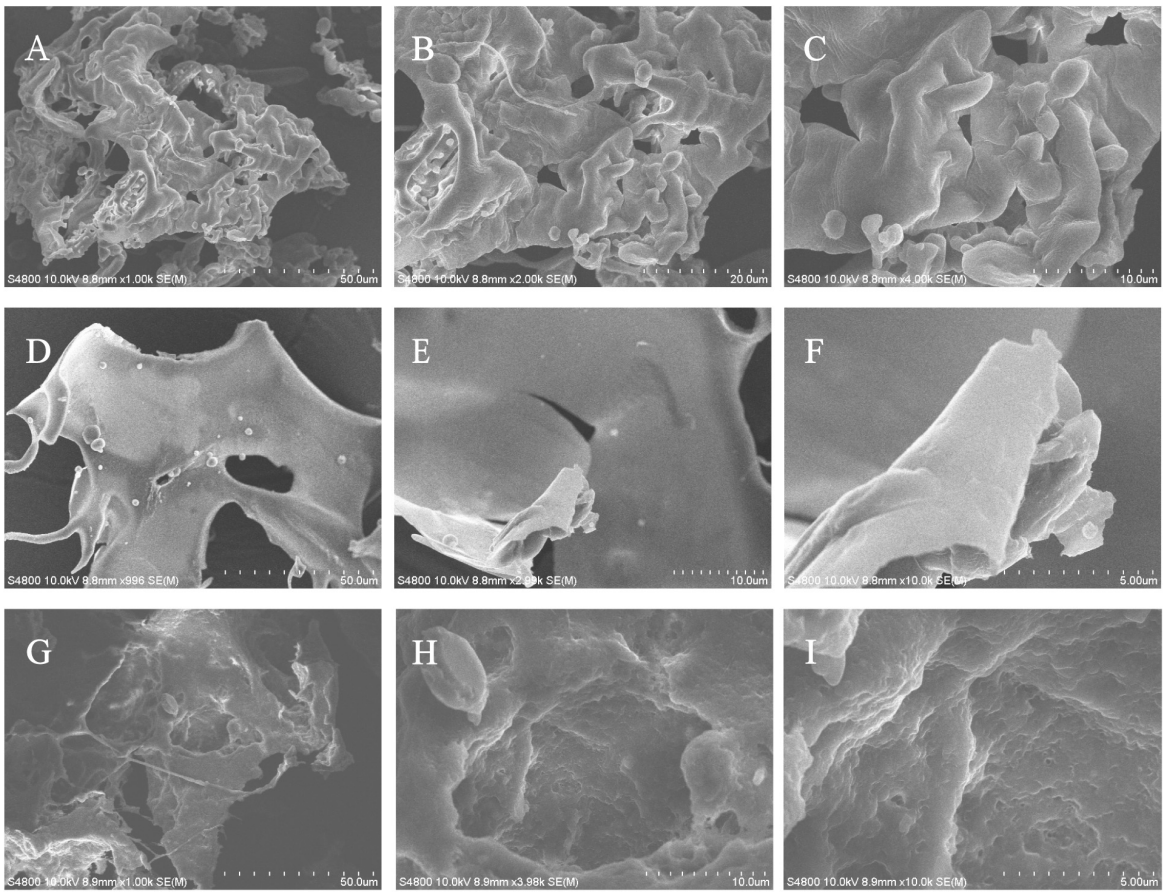

FIGURE 6
The microstructure and surface morphology of purified EPS fractions observed by SEM analysis. **(A)** SEM image of EPS1 in the scale bar of 50 μm. **(B)** SEM image of EPS1 in the scale bar of 10 μm. **(C)** SEM image of EPS1 in the scale bar of 5 μm. **(D)** SEM image of EPS2 in the scale bar of 50 μm. **(E)** SEM image of EPS2 in the scale bar of 10 μm. **(F)** SEM image of EPS2 in the scale bar of 5 μm. **(G)** SEM image of EPS3 in the scale bar of 50 μm. **(H)** SEM image of EPS3 in the scale bar of 10 μm. **(I)** SEM image of EPS3 in the scale bar of 5 μm.

composition and structure can determine the its microstructure and surface morphology, many difference are most likely due to the different methods of sample extraction, preparation, and purification (Kanamarlapudi and Muddada, 2017).

Immune-enhancing effect

Effect of exopolysaccharide on the production of nitric oxide

Activated macrophages catalyze the generation of inducible NO synthase (iNOS), which results in the production of a large amount of NO from L-arginine and molecular oxygen (Alderton et al., 2001). NO is an important intracellular messenger molecule in living organisms as it is involved in killing microorganisms and tumor cells (Feng et al., 2002; Kleinert et al., 2003). Thus, we investigated the macrophage stimulating activities of the EPSs by measuring their ability to induce the release of NO from mouse macrophages. NO was quantified by measuring its stable breakdown product, nitrite. Because LPS significantly stimulates NO production, we included this as a positive control (**Figure 7**). EPS-induced NO production levels in Ana-1 and peritoneal macrophage cells were significantly increased in a dose-dependent manner. The results show significant differences among all concentrations of EPS (except for EPS1 at the concentration of 31.25 μg/mL), which suggested that these polysaccharides enhanced the ability of Ana-1 macrophages to secrete NO. EPS1 treatments did not differ significantly from untreated control (**Figure 7A**). However, EPS2 (125, 250, and 500 μg/mL) and EPS3 [125, 250, and 500 μg/mL ($P < 0.001$), 62.5 μg/mL ($P < 0.01$), 31.25 μg/mL ($P < 0.05$)] promoted NO production of macrophages considerably, when compared to the untreated cells (**Figures 7B,C**). The phagocytic effect of Ana-1 cells treated with higher concentrations of EPS (500 μg/mL) exhibited significant difference with that of positive control ($P < 0.001$). In addition, 62.5–500 μg/mL of all EPSs significantly increased the viability of peritoneal macrophage cells in a dose-dependent

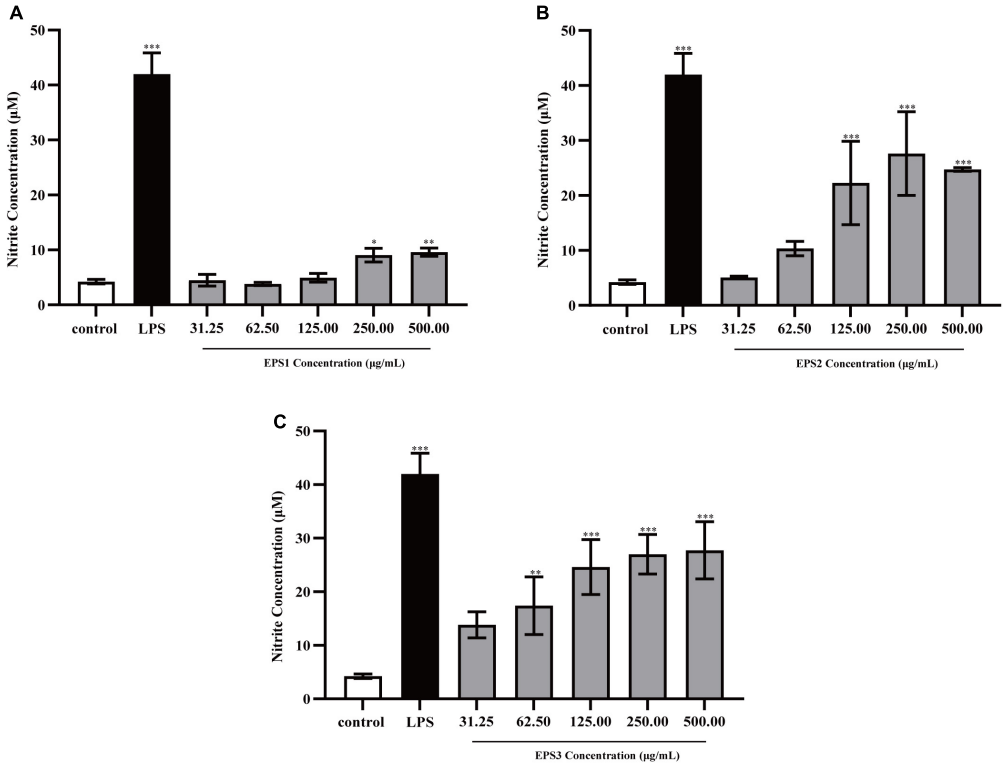

FIGURE 7
Production of NO from Ana-1 cells treated with **(A)** EPS1, **(B)** EPS2, and **(C)** EPS3 from *L. pantheris* TCP102. Data are expressed as the mean ± standard error ($n = 6$). $^{*}P < 0.05$, $^{**}P < 0.01$, $^{***}P < 0.001$, compared to untreated control. Error bars represent ± SD.

manner, compared to the blank control ($P < 0.05$) (Figure 8). Since the overproduction of NO can cause apoptosis in macrophages, the above results suggest that the macrophage activation of these three EPSs are more moderate than that of LPS.

Effect of exopolysaccharide on the production of cytokines

Cytokines are complex molecules that stimulate immune macrophages and play vital role in cell proliferation, intercellular interactions, and other functions (Kanamarlapudi and Muddada, 2017). IL-6 and TNF-α are the most important pro-inflammatory cytokines (Yuan et al., 2015). TNF-α induces the expression of many other immunoregulatory and inflammatory mediators and inhibits tumorigenesis. Meanwhile, IL-6 mediates the immune-enhancing activity by initiating the immunologic cascade during the induction of the acute phase protein response. In general, activated macrophages secrete cytokines, including TNF-α and IL-6 that are directly involved in inhibiting the growth of a wide range of invading substances as part of the immune-enhancing activity.

TNF-α and IL-6 levels in the culture supernatants of Ana-1 and peritoneal macrophage cells treated with purified EPSs were measured by ELISA (Figure 9). Various concentrations (31.25–500 μg/mL) of EPS1 (Figure 9A), EPS2 (Figure 9B), and EPS3 (Figure 9C) groups significantly ($P < 0.001$) increased the expression of TNF-α and IL-6 compared with the untreated cells, except for EPS1 at 31.25 and 62.5 μg/mL. Untreated cells secreted negligible amounts of these cytokines. In peritoneal macrophage cells treated with purified EPSs (Figure 10), all polysaccharides significantly induced the secretion of TNF-α (Figures 10A–C) and IL-6 (Figures 10D–F) in a dose-dependent manner. Compared with the control, all concentrations (from 31.25 to 500 μg/mL) of EPS1, EPS2, and EPS3 significantly increased the production of TNF-α and IL-6 ($P < 0.05$). These results demonstrate that EPSs secreted by *Lactobacillus pantheris* TCP102 could exert immune-enhancing activity by stimulating the release of TNF-α, IL-6 and NO in macrophages, which are essential for killing pathogens, microorganisms, and coordinating various biological activities as intracellular messenger molecules.

Antitumor activity

Human colon cancer (HCT-116), ovarian cancer (A-2780), and gastric cancer (BCG-803) cell lines, are commonly used models in research on cancer cell proliferation.

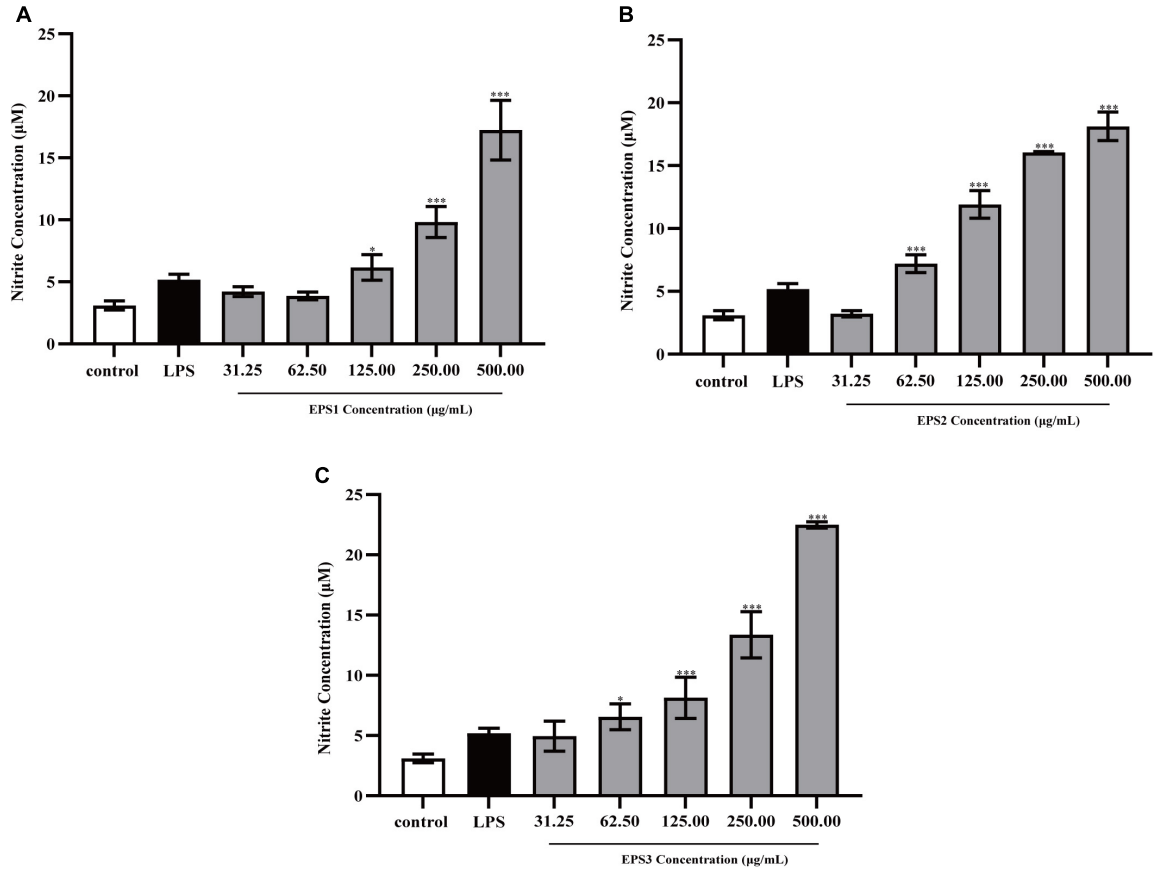

FIGURE 8
Production of NO from peritoneal macrophage cells treated with purified **(A)** EPS1, **(B)** EPS2, and **(C)** EPS3 from *L. pantheris* TCP102. Data are expressed as the mean ± standard error of the mean ($n = 6$). $^{*}P < 0.05$, $^{***}P < 0.001$, compared to untreated control. Error bars represent ± SD.

Figure 11 shows that all three EPSs inhibit the proliferation of HCT-116, A-2780, and BCG-803 cells in concentration- and time-dependent manners. After 72 h of treatment, EPS3 exhibited the strongest antiproliferative activity against all cancer cell lines. At a dose of 500 μg/mL, HCT-116, A-2780, and BCG-803 cells were inhibited at rates of 45.68, 71.55, and 54.50%, respectively (Figures 11C,F,I). These results follow a similar as those of 5-FU (63.68, 88.77, and 66.04%). The antiproliferative effect of EPS2 against all three cancer cells was also time- and dosage-dependent (Figures 11B,E,H). After 72 h of incubation, HCT-116, A-2780, and BCG-803 were inhibited by 500 μg/mL of EPS2 at rates of 44.15, 56.61, and 45.33%, respectively. EPS1 inhibited the three tumor cells at rates lower than those of EPS2 and EPS3 under the same conditions (Figures 11A,D,G). Specifically, 500 μg/mL of EPS1 inhibited HCT-116, A-2780, and BCG-803 cells at rates of rates were 28.62, 50.17, and 43.05%, after 72 h of treatment. At concentrations of 31.25 and 62.5 μg/mL and 24 h of treatment, the antiproliferative activity of EPS1 ranged from low to no effected. Altogether, these results show that EPSs isolated from *L. pantheris* TCP102 have antitumor activities against HCT-116, A-2780 and BCG-803 cells ranging from moderate to strong (e.g., EPS3 against A-2780 cells). EPS3 has the strongest antiproliferative activity.

Discussion

LAB strains such as *Lactobacilli* are the most common microorganisms which are considered as probiotic. There are several criteria for bacteria to recognize as probiotic. The main features for selecting highly potent probiotic species are their tolerance to acidic conditions and bile salts, ability to adhere to the intestinal cells, antibiotic resistance, survival in the GI-tract, and especially antimicrobial activity against pathogens (Mojgani et al., 2007).

In this work, the probiotic potential of 18 strains of lactic acid bacteria isolated from tomato pomace were evaluated by our laboratory, resistance to 0.3,0.5, and 1% bile salts, adherence to Caco-2 cells, and antagonism against some enteric pathogens. Our observations indicated that 11 isolated *Lactobacilli* (TCP001, TCP004, TCP007, TCP008, TCP009,

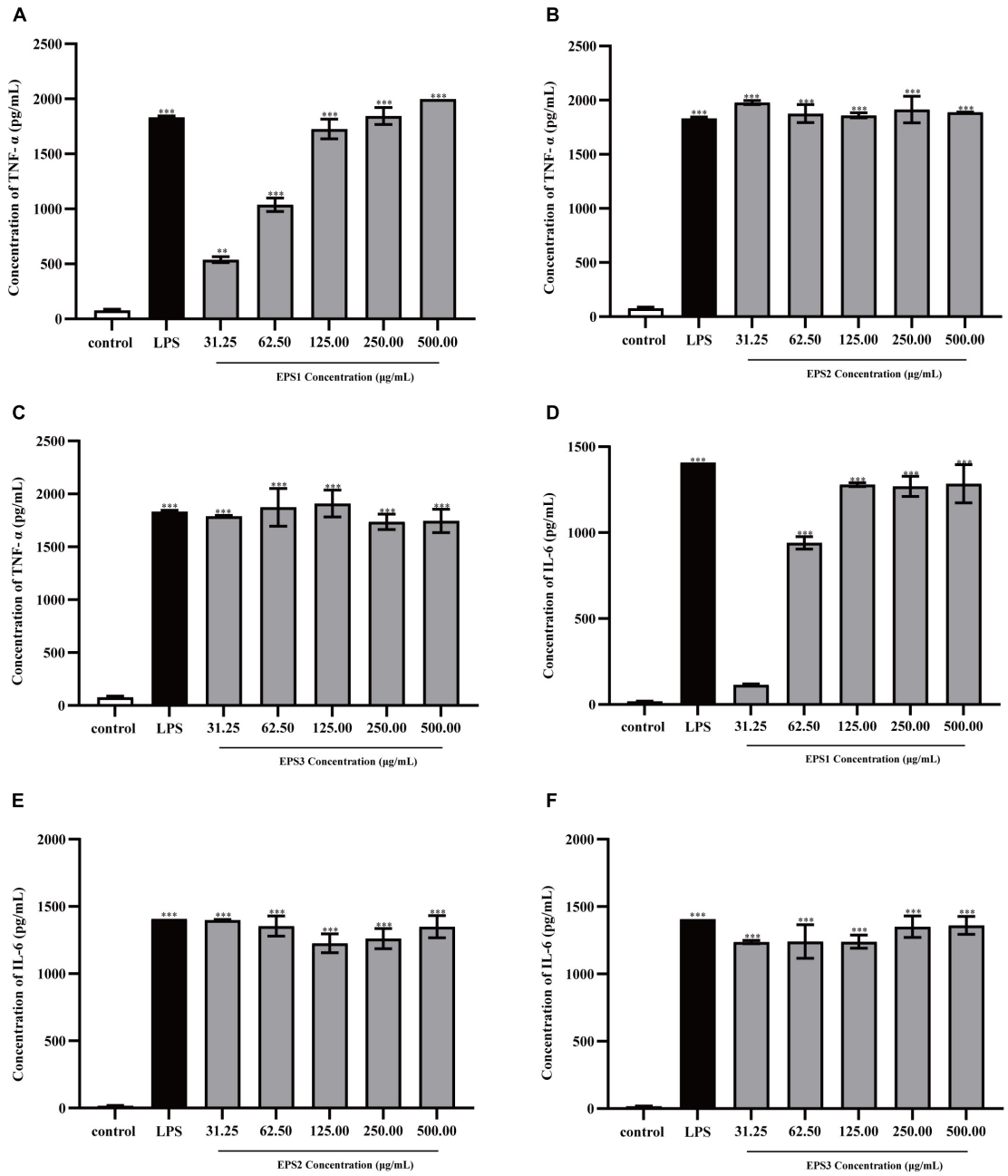

FIGURE 9
Production of the cytokines TNF-α by Ana-1 cells treated with purified **(A)** EPS1, **(B)** EPS2, and **(C)** EPS3. IL-6 production by Ana-1 cells treated with **(D)** EPS1, **(E)** EPS2, and **(F)** EPS3. Data are expressed as the mean ± standard error of the mean ($n = 6$). $^{**}P < 0.01$, $^{***}P < 0.001$, compared to untreated control. Error bars represent ± SD.

TCP016, TCP063, TCP071, TCP073, TCP080, and TCP102) were resistant to gastric acid and 0.3, 0.5 and 1% bile salt, and exhibited good adhesion to Caco-2 cells. This study reveals that most isolates are more resistant to acidic condition than the control strain, which agrees with the previous report from Malaysia (Shokryazdan et al., 2014). In addition, the results show that these 18 strains have stronger bacteriostatic effect on *Staphylococcus aureus* than *Escherichia coli* which is in agreement with previous reports (Shokryazdan et al., 2014; Halimi and Mirsalehian, 2016). Antimicrobial activity is another criterion for selecting probiotic bacteria. Application of lactic acid bacteria as bio preservatives has been confirmed in various previous studies, due to their antagonistic effects against common foodborne bacteria (Jomehzadeh et al., 2020).

10.3389/fmicb.2022.1015270

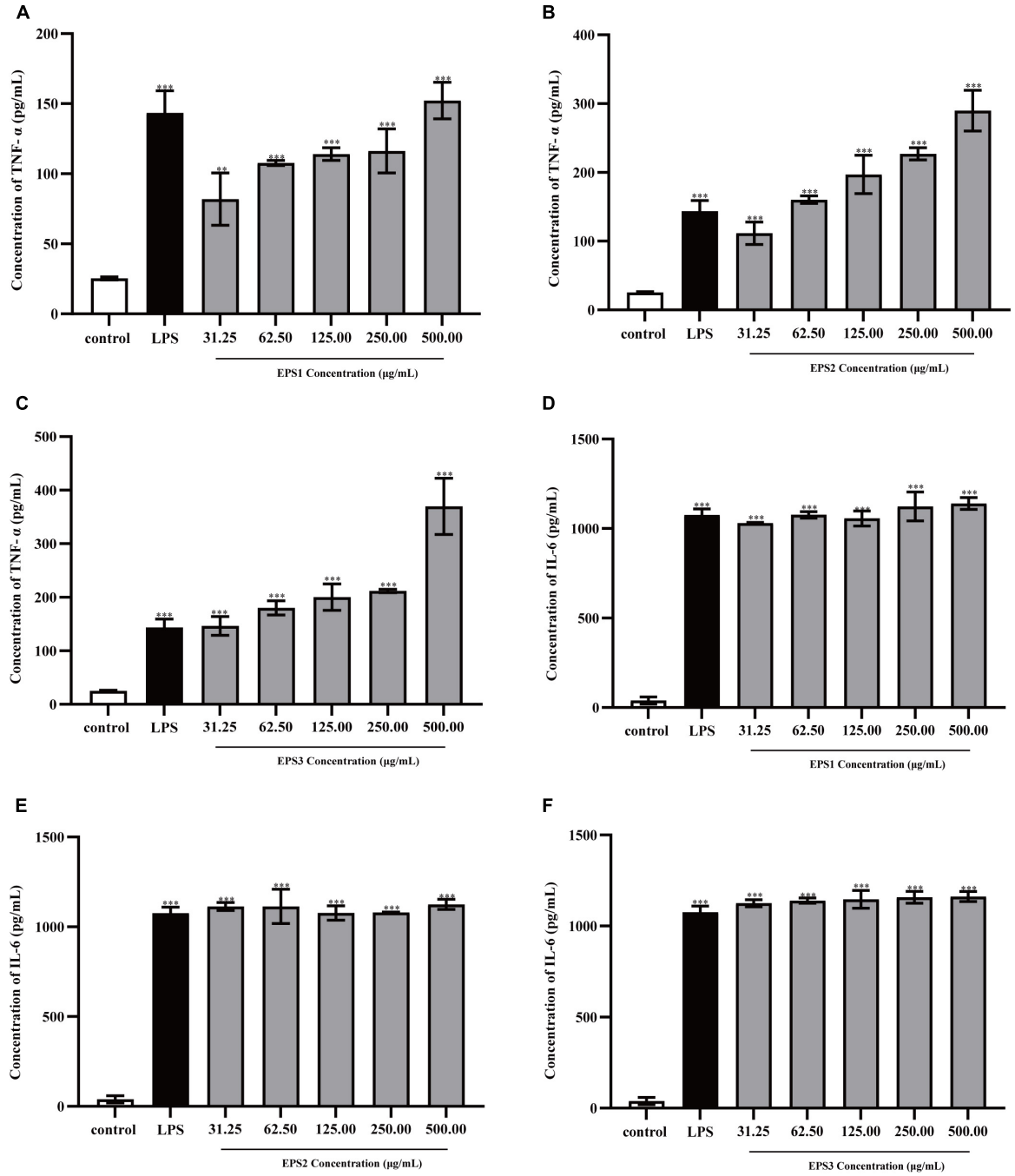

FIGURE 10
Production of the cytokines TNF-α by peritoneal macrophage cells treated with purified **(A)** EPS1, **(B)** EPS2, and **(C)** EPS3. Production of cytokine IL-6 by peritoneal macrophage cells treated with **(D)** EPS1, **(E)** EPS2, and **(F)** EPS3. Data are expressed as the mean ± standard error of the mean ($n = 6$). $^{**}P < 0.01$, $^{***}P < 0.001$, compared to untreated control. Error bars represent ± SD.

Recent studies show that various derived polysaccharides could stimulate NO and cytokines secretion in macrophages (Li et al., 2018), thereby stimulating the immune-enhancing activity. In this study, the three EPSs could exert immune-enhancing activity by stimulating the release of TNF-α, IL-6 and NO in Ana-1 and peritoneal macrophage cells. Previous studies show that the molecular structure, monosaccharide composition, chain conformation, and stereochemistry configuration of EPSs affect their immune-enhancing and anticancer activities (Ruas-Madiedo et al., 2002;

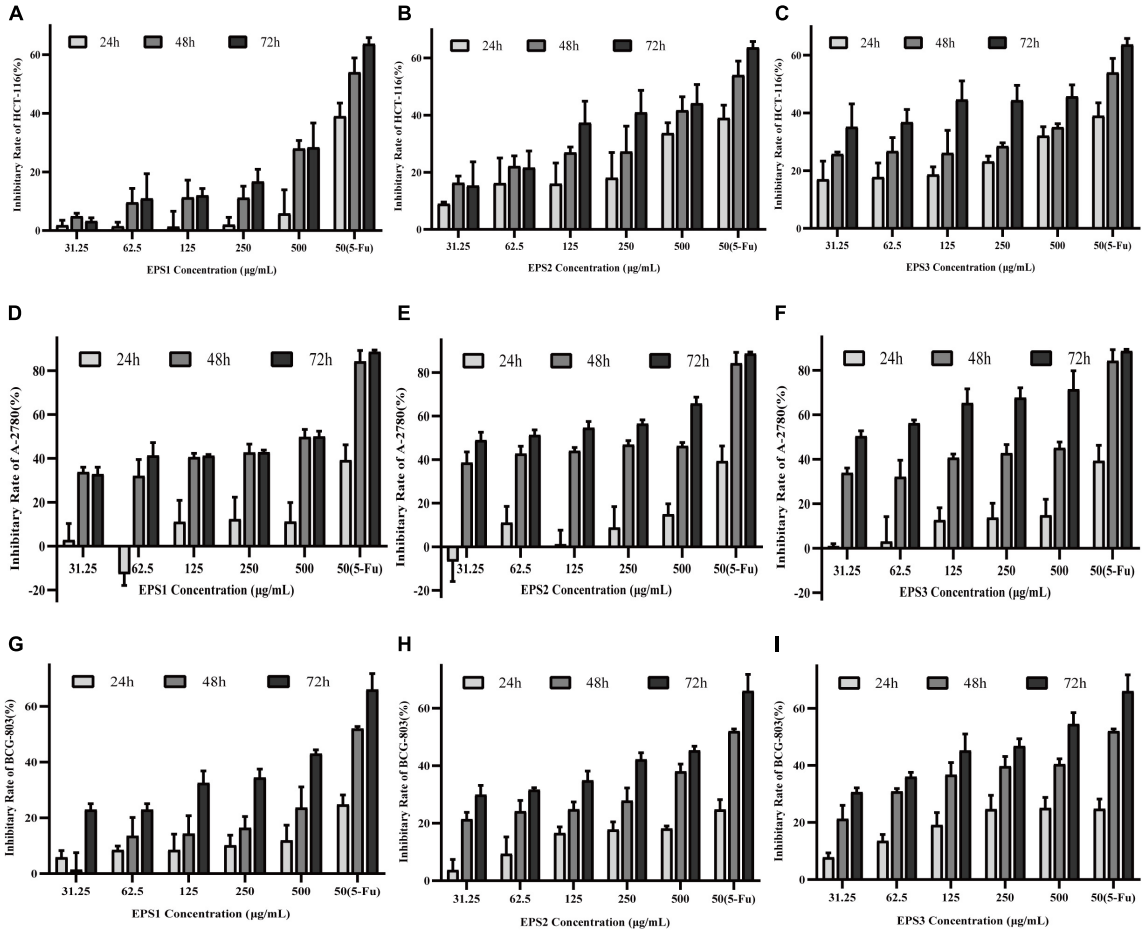

FIGURE 11
The effects of the purified EPS1, EPS2, and EPS3 from *L. pantheris* TCP102 and 5-fluorouracil on human colon cancer (HCT-116), ovarian cancer (A-2780), and gastric cancer (BCG-803) cell lines. Effect of **(A)** Effect of EPS1, **(B)** EPS2, and **(C)** EPS3 on HCT-116 at 24, 48, and 72 h treatment. Effect of **(D)** EPS1, **(E)** EPS2, and **(F)** EPS3 on A-2780 after 24, 48, and 72 h of treatment. Effect of **(G)** EPS1, **(H)** EPS2, and **(I)** EPS3 on BCG-803 after 24, 48, and 72 h of treatment. Data are expressed as the mean ± standard error of the mean ($n = 6$). Error bars represent ± SD.

Jung et al., 2015; Uzum et al., 2015). In the present study, we performed the first isolation and purification of EPS from the fermentation medium of *Lactobacillus pantheris* TCP102, resulting in three homogeneous exopolysaccharides, EPS1, EPS2, and EPS3. Purified EPS1, EPS2, and EPS3 have similar Mw, 20.3, 23.0, and 19.3 kDa, respectively, which are lighter than many other exopolysaccharides, such as EPS from *L. curvatus* DPPMA10, *L. plantarum* YW32, and *S. thermophiles* (Minervini et al., 2010; Wang et al., 2015; Ren et al., 2016). Polysaccharides with Mw between 10^4 and 10^6 Da, including galactose, glucose, and mannose, they are always related to immune-enhancing activity (Lee et al., 2018). Results from HPLC analysis indicate that EPS1, EPS2, and EPS3 are homogenized polysaccharides. EPS1, EPS2, and EPS3 are mainly composed of galactose, glucose, and mannose, at approximate molar ratios of 2.86:1:1.48, 1.26:1:1, 1.58:1.80:1, respectively. Therefore, the chemical composition and structure of the three EPSs were significantly beneficial for the immune-enhancing activity of polysaccharides. However, we only evaluate the immune-enhancing activity of EPSs on macrophages. Therefore, it is necessary to further probe the immune-enhancing activity mechanisms in the activation of macrophages by TCP102 EPS in the future. Furthermore, the EPSs isolated from *L. pantheris* TCP102 have antitumor activity against HCT-116, A-2780 and BCG-803 cells ranging from moderate to strong (e.g., EPS3 against A-2780 cells). EPS3 has the strongest antiproliferative activity. Other physicochemical properties of polysaccharides, such as the presence of uronic acid, pyranose, glucose, and β-type glycosidic linkages, are also conducive to increasing their anticancer activity (Ma et al., 2013). The differences in antitumor activities between them might be relating to their monosaccharide composition, Mw, and linkage types of glycosidic bond. The research on these factors affecting the immune-enhancing and

antitumor activities of polysaccharides is not very in-depth, nor systematic, which needs further in-depth study. However, this study would provide scientific reference for further systematic investigation on the structure–bioactivity relationship of lactic acid bacteria polysaccharide.

Conclusion

In conclusion, several isolates evaluated in this study showed potential probiotic properties, the majority of evaluated isolates showed high antimicrobial activities against potentially *Escherichia coli* and *Staphylococcus aureus*. In addition, the preparation, purification, structural characterization of polysaccharides, the immune-enhancing and antitumor activities of polysaccharides from *Lactobacillus pantheris* TCP102 were evaluated. The Mw of EPS1, EPS2 and EPS3 were estimated to be 20.3, 23.0, and 19.3 kDa, respectively. EPS1, EPS2 and EPS3 had the similar structure, and composed of galactose, glucose, and mannose, with molar ratios of 2.86:1:1.48, 1.26:1:1, 1.58:1.80:1, respectively. SEM results indicated the three polysaccharide fractions differ in microstructure and surface morphology. In addition, these EPSs significantly induced the production of nitric oxide (NO), TNF-α, and IL-6 in Ana-1 cells and peritoneal macrophage cells. Meanwhile, The EPSs also significantly suppressed the proliferation of HCT-116, BCG-803, and particularly A-2780 cells. Collectively, these findings indicate that EPSs from *Lactobacillus pantheris* TCP102 can be exploited as a potential immune-enhancing functional food and tumor-inhibiting drug.

Data availability statement

The 16S-rRNA sequencing raw data are deposited in the online repositories. The names of the repository and accession number(s) can be found at: https://www.ncbi.nlm.nih.gov/, KF312693, KF312677–KF312692, and KF318727 for the strains TCP001, TCP007, TCP004, TCP008, TCP015–TCP017, TCP050, TCP029, TCP024, TCP045, TCP071, TCP073, TCP102, TCP080, TCP063, TCP037, and TCP009, respectively.

Author contributions

SS and YF: conceptualization, investigation, formal analysis, and writing—original draft and preparation. NP, HZ, and LX: writing—review and editing. YLia, YLiu, BL, and CM: technical support. RD and XW: conceptualization, resources, supervision, funding acquisition, project administration, and writing—review and editing. All authors contributed to the article and approved the submitted version.

Funding

This research was funded by the Science and Technology Major Project of the Inner Mongolia Autonomous Region of China (Grant number 2021ZD0013), Key Scientific and Tech-non-logical Research Program of Inner Mongolia Autonomous Region (Grant number 2021GG0156), and the National Natural Science Foundation of China (Grant number 32060800).

Conflict of interest

The authors declare that the research was conducted in the absence of any commercial or financial relationships that could be construed as a potential conflict of interest.

Publisher's note

All claims expressed in this article are solely those of the authors and do not necessarily represent those of their affiliated organizations, or those of the publisher, the editors and the reviewers. Any product that may be evaluated in this article, or claim that may be made by its manufacturer, is not guaranteed or endorsed by the publisher.

Supplementary material

The Supplementary Material for this article can be found online at: https://www.frontiersin.org/articles/10.3389/fmicb.2022.1015270/full#supplementary-material

References

Ai, L., Zhang, H., Guo, B., Chen, W., Wu, Z., and Wu, Y. (2008). Preparation, partial characterization and bioactivity of exopolysaccharides from *Lactobacillus casei* LC2W. *Carbohydr. Polym.* 74, 353–357. doi: 10.1016/j.carbpol.2008.03.004

Alderton, W. K., Cooper, C. E., and Knowles, R. G. (2001). Nitric oxide synthases: Structure, function and inhibition. *Biochem. J.* 357, 593–615. doi: 10.1042/0264-6021:3570593

Butel, M. J. (2014). Probiotics, gut microbiota and health. *Med. Mal. Infect.* 44, 1–8. doi: 10.1016/j.medmal.2013.10.002

Champagne, C. P., Barrette, J., Roy, D., and Rodrigue, N. (2006). Fresh-cheesemilk formulation fermented by a combination of freeze-dried citrate-positive cultures and exopolysaccharide-producing lactobacilli with liquid lactococcal starters. *Food Res. Int.* 39, 651–659. doi: 10.1016/j.foodres.2006.01.002

Chen, N.-Y., Hsu, T.-H., Lin, F.-Y., Lai, H.-H., and Wu, J.-Y. (2006). Effects on cytokine-stimulating activities of EPS from *Tremella mesenterica* with various carbon sources. *Food Chem.* 99, 92–97. doi: 10.1016/j.foodchem.2005.07.023

Chen, Y. T., Yuan, Q., Shan, L. T., Lin, M. A., Cheng, D. Q., and Li, C. Y. (2013). Antitumor activity of bacterial exopolysaccharides from the endophyte *Bacillus amyloliquefaciens* sp. isolated from *Ophiopogon japonicus*. *Oncol. Lett.* 5, 1787–1792. doi: 10.3892/ol.2013.1284

Chong, E. S. (2014). A potential role of probiotics in colorectal cancer prevention: Review of possible mechanisms of action. *World J. Microbiol. Biotechnol.* 30, 351–374. doi: 10.1007/s11274-013-1499-6

El-Deeb, N. M., Yassin, A. M., Al-Madboly, L. A., and El-Hawiet, A. (2018). A novel purified *Lactobacillus acidophilus* 20079 exopolysaccharide, LA-EPS-20079, molecularly regulates both apoptotic and NF-κB inflammatory pathways in human colon cancer. *Microb. Cell Fact.* 17:29. doi: 10.1186/s12934-018-0877-z

Feng, X., Guo, Z., Nourbakhsh, M., Hauser, H., Ganster, R., Shao, L., et al. (2002). Identification of a negative response element in the human inducible nitric-oxide synthase (hiNOS) promoter: The role of NF-kappa B-repressing factor (NRF) in basal repression of the hiNOS gene. *Proc. Natl. Acad. Sci. U.S.A.* 99, 14212–14217. doi: 10.1073/pnas.212306199

Gentès, M. C., Turgeon, S. L., and St-Gelais, D. J. I. D. J. (2015). Impact of starch and exopolysaccharide-producing lactic acid bacteria on the properties of set and stirred yoghurts. *Int. Dairy J.* 55, 79–86. doi: 10.1016/j.idairyj.2015.12.006

Halimi, S., and Mirsalehian, A. (2016). Assessment and comparison of probiotic potential of four *Lactobacillus* species isolated from feces samples of Iranian infants. *Microbiol. Immunol.* 60, 73–81. doi: 10.1111/1348-0421.12352

Jomehzadeh, N., Javaherizadeh, H., Amin, M., Saki, M., Al-Ouqaili, M. T. S., Hamidi, H., et al. (2020). Isolation and identification of potential probiotic *Lactobacillus* species from feces of infants in southwest Iran. *Int. J. Infect. Dis.* 96, 524–530. doi: 10.1016/j.ijid.2020.05.034

Jung, J. Y., Shin, J. S., Rhee, Y. K., Cho, C. W., Lee, M. K., Hong, H. D., et al. (2015). In vitro and in vivo immunostimulatory activity of an exopolysaccharide-enriched fraction from *Bacillus subtilis*. *J. Appl. Microbiol.* 118, 739–752. doi: 10.1111/jam.12742

Kanamarlapudi, S., and Muddada, S. (2017). Characterization of exopolysaccharide produced by *Streptococcus thermophilus* CC30. *Biomed. Res. Int.* 2017:4201809. doi: 10.1155/2017/4201809

Kayama, H., and Takeda, K. (2016). Functions of innate immune cells and commensal bacteria in gut homeostasis. *J. Biochem.* 159, 141–149. doi: 10.1093/jb/mvv119

Kleinert, H., Schwarz, P. M., and Forstermann, U. (2003). Regulation of the expression of inducible nitric oxide synthase. *Biol. Chem.* 384, 1343–1364. doi: 10.1515/BC.2003.152

Lee, J., Li, C., Surayot, U., Yelithao, K., Lee, S., Park, W., et al. (2018). Molecular structures, chemical properties and biological activities of polysaccharide from *Smilax glabra* rhizome. *Int. J. Biol. Macromol.* 120, 1726–1733. doi: 10.1016/j.ijbiomac.2018.09.138

Li, D., Li, J., Zhao, F., Wang, G., Qin, Q., and Hao, Y. (2016). The influence of fermentation condition on production and molecular mass of EPS produced by *Streptococcus thermophilus* 05-34 in milk-based medium. *Food Chem.* 197, 367–372. doi: 10.1016/j.foodchem.2015.10.129

Li, H., Dong, Z., Liu, X., Chen, H., and Zhang, M. J. (2018). Structure characterization of two novel polysaccharides from *Colocasia esculenta* (taro) and a comparative study of their immunomodulatory activities. *J. Funct. Foods* 42, 47–57. doi: 10.1016/j.jff.2017.12.067

Li, W., Ji, J., Tang, W., Rui, X., Chen, X., Jiang, M., et al. (2014b). Characterization of an antiproliferative exopolysaccharide (LHEPS-2) from *Lactobacillus helveticus* MB2-1. *Carbohydr. Polym.* 105, 334–340. doi: 10.1016/j.carbpol.2014.01.093

Li, W., Ji, J., Chen, X., Jiang, M., Rui, X., and Dong, M. (2014a). Structural elucidation and antioxidant activities of exopolysaccharides from *Lactobacillus helveticus* MB2-1. *Carbohydr. Polym.* 102, 351–359. doi: 10.1016/j.carbpol.2013.11.053

Li, W., Xia, X., Tang, W., Ji, J., Rui, X., Chen, X., et al. (2015). Structural characterization and anticancer activity of cell-bound exopolysaccharide from *Lactobacillus helveticus* MB2-1. *J. Agric. Food Chem.* 63, 3454–3463.

Liu, J., Luo, J., Ye, H., Sun, Y., Lu, Z., and Zeng, X. (2009). Production, characterization and antioxidant activities in vitro of exopolysaccharides from endophytic bacterium *Paenibacillus polymyxa* EJS-3. *Carbohydr. Polym.* 78, 275–281. doi: 10.1016/j.carbpol.2009.03.046

Ma, L., Qin, C., Wang, M., Gan, D., Cao, L., Ye, H., et al. (2013). Preparation, preliminary characterization and inhibitory effect on human colon cancer HT-29 cells of an acidic polysaccharide fraction from *Stachys floridana* Schuttl. ex Benth. *Food Chem. Toxicol.* 60, 269–276. doi: 10.1016/j.fct.2013.07.060

Ma, X. K., Zhang, H., Peterson, E. C., and Chen, L. (2014). Enhancing exopolysaccharide antioxidant formation and yield from *Phellinus* species through medium optimization studies. *Carbohydr. Polym.* 107, 214–220. doi: 10.1016/j.carbpol.2014.02.077

Mathlouthi, M., and Koenig, J. L. (1987). Vibrational spectra of carbohydrates. *Adv. Chem. Phys.* 44, 7–89. doi: 10.1016/s0065-2318(08)60077-3

Matsuzaki, C., Hayakawa, A., Matsumoto, K., Katoh, T., Yamamoto, K., and Hisa, K. (2015). Exopolysaccharides produced by *Leuconostoc mesenteroides* strain NTM048 as an immunostimulant to enhance the mucosal barrier and influence the systemic immune response. *J. Agric. Food Chem.* 63, 7009–7015. doi: 10.1021/acs.jafc.5b01960

Minervini, F., De Angelis, M., Surico, R. F., Di Cagno, R., Ganzle, M., and Gobbetti, M. (2010). Highly efficient synthesis of exopolysaccharides by *Lactobacillus curvatus* DPPMA10 during growth in hydrolyzed wheat flour agar. *Int. J. Food Microbiol.* 141, 130–135. doi: 10.1016/j.ijfoodmicro.2010.03.014

Mojgani, N., Torshizi, M., and Rahimi, S. (2007). Screening of locally isolated lactic acid bacteria for use as probiotics in poultry in Iran. *Poult. Sci.* 44, 357–365. doi: 10.2141/jpsa.44.357

Nácher-Vázquez, M., Ballesteros, N., Canales, Á, Rodríguez Saint-Jean, S., Pérez-Prieto, S. I., Prieto, A., et al. (2015). Dextrans produced by lactic acid bacteria exhibit antiviral and immunomodulatory activity against salmonid viruses. *Carbohydr. Polym.* 124, 292–301. doi: 10.1016/j.carbpol.2015.02.020

Nwodo, U. U., Green, E., and Okoh, A. I. (2012). Bacterial exopolysaccharides: Functionality and prospects. *Int. J. Mol. Sci.* 13, 14002–14015. doi: 10.3390/ijms131114002

Ouwehand, A. C. (2017). A review of dose-responses of probiotics in human studies. *Benef. Microbes* 8, 143–151. doi: 10.3920/bm2016.0140

Patel, S., Majumder, A., and Goyal, A. (2012). Potentials of exopolysaccharides from lactic Acid bacteria. *Indian J. Microbiol.* 52, 3–12. doi: 10.1007/s12088-011-0148-8

Plaza-Diaz, J., Gomez-Llorente, C., Fontana, L., and Gil, A. (2014). Modulation of immunity and inflammatory gene expression in the gut, in inflammatory diseases of the gut and in the liver by probiotics. *World J. Gastroenterol.* 20, 15632–15649. doi: 10.3748/wjg.v20.i42.15632

Priyanka, P., Arun, A. B., Ashwini, P., and Rekha, P. D. (2016). Functional and cell proliferative properties of an exopolysaccharide produced by *Nitratireductor* sp. PRIM-31. *Int. J. Biol. Macromol.* 85, 400–404. doi: 10.1016/j.ijbiomac.2015.12.091

Quigley, E. M. (2013). Gut bacteria in health and disease. *Gastroenterol. Hepatol.* 9, 560–569.

Ren, W., Xia, Y., Wang, G., Zhang, H., Zhu, S., and Ai, L. (2016). Bioactive exopolysaccharides from a *S. thermophilus* strain: Screening, purification and characterization. *Int. J. Biol. Macromol.* 86, 402–407. doi: 10.1016/j.ijbiomac.2016.01.085

Ruas-Madiedo, P., Hugenholtz, J., and Zoon, P. (2002). An overview of the functionality of exopolysaccharides produced by lactic acid bacteria. *Int. Dairy J.* 12, 163–171.

Ruhmkorf, C., Jungkunz, S., Wagner, M., and Vogel, R. F. (2012). Optimization of homoexopolysaccharide formation by lactobacilli in gluten-free sourdoughs. *Food Microbiol.* 32, 286–294. doi: 10.1016/j.fm.2012.07.002

Sałański, P., Kowalczyk, M., Bardowski, J. K., and Szczepankowska, A. K. (2022). Health-promoting nature of *Lactococcus lactis* IBB109 and *Lactococcus lactis* IBB417 strains exhibiting proliferation inhibition and stimulation of interleukin-18 expression in colorectal cancer cells. *Front. Microbiol.* 13:822912. doi: 10.3389/fmicb.2022.822912

Sengül, N., Işık, S., Aslım, B., Uçar, G., and Demirbağ, A. E. (2011). The effect of exopolysaccharide-producing probiotic strains on gut oxidative damage in experimental colitis. *Dig. Dis. Sci.* 56, 707–714. doi: 10.1007/s10620-010-1362-7

Shang, N., Xu, R., and Li, P. (2013). Structure characterization of an exopolysaccharide produced by *Bifidobacterium animalis* RH. *Carbohydr. Polym.* 91, 128–134. doi: 10.1016/j.carbpol.2012.08.012

Shi, Y., Xiong, Q., Wang, X., Li, X., Yu, C., Wu, J., et al. (2016). Characterization of a novel purified polysaccharide from the flesh of *Cipangopaludina chinensis*. *Carbohydr. Polym.* 136, 875–883. doi: 10.1016/j.carbpol.2015.09.062

Shida, K., Nanno, M., and Nagata, S. (2011). Flexible cytokine production by macrophages and T cells in response to probiotic bacteria: A possible mechanism by which probiotics exert multifunctional immune regulatory activities. *Gut Microbes* 2, 109–114. doi: 10.4161/gmic.2.2.15661

Shokryazdan, P., Sieo, C. C., Kalavathy, R., Liang, J. B., Alitheen, N. B., Faseleh Jahromi, M., et al. (2014). Probiotic potential of *Lactobacillus* strains with antimicrobial activity against some human pathogenic strains. *Biomed. Res. Int.* 2014:927268. doi: 10.1155/2014/927268

Shuhong, Y., Meiping, Z., Hong, Y., Han, W., Shan, X., Yan, L., et al. (2014). Biosorption of Cu(2+), Pb(2+) and Cr(6+) by a novel exopolysaccharide from *Arthrobacter* ps-5. *Carbohydr. Polym.* 101, 50–56. doi: 10.1016/j.carbpol.2013.09.021

Surayot, U., Wang, J., Seesuriyachan, P., Kuntiya, A., Tabarsa, M., Lee, Y., et al. (2014). Exopolysaccharides from lactic acid bacteria: Structural analysis, molecular weight effect on immunomodulation. *Int. J. Biol. Macromol.* 68, 233–240. doi: 10.1016/j.ijbiomac.2014.05.005

Thomas, L. V., Ockhuizen, T., and Suzuki, K. (2014). Exploring the influence of the gut microbiota and probiotics on health: A symposium report. *Br. J. Nutr.* 112, S1–S18. doi: 10.1017/S0007114514001275

Uzum, Z., Silipo, A., Lackner, G., De Felice, A., Molinaro, A., and Hertweck, C. (2015). Structure, genetics and function of an exopolysaccharide produced by a bacterium living within fungal hyphae. *Chembiochem* 16, 387–392. doi: 10.1002/cbic.201402488

Wang, G., Zhu, L., Yu, B., Chen, K., Liu, B., Liu, J., et al. (2016). Exopolysaccharide from *Trichoderma pseudokoningii* induces macrophage activation. *Carbohydr. Polym.* 149, 112–120. doi: 10.1016/j.carbpol.2016.04.093

Wang, J., Zhao, X., Yang, Y., Zhao, A., and Yang, Z. (2015). Characterization and bioactivities of an exopolysaccharide produced by *Lactobacillus plantarum* YW32. *Int. J. Biol. Macromol.* 74, 119–126. doi: 10.1016/j.ijbiomac.2014.12.006

Wang, K., Li, W., Rui, X., Chen, X., Jiang, M., and Dong, M. (2014). Structural characterization and bioactivity of released exopolysaccharides from *Lactobacillus plantarum* 70810. *Int. J. Biol. Macromol.* 67, 71–78. doi: 10.1016/j.ijbiomac.2014.02.056

Wang, Y., Tian, Y., Zhang, N., Li, X., Wang, X., Wang, W., et al. (2021). *Pediococcus pentosaceus* PP04 improves high-fat diet-induced liver injury by the modulation of gut inflammation and intestinal microbiota in C57BL/6N mice. *Food Funct.* 12, 6851–6862. doi: 10.1039/D2FO01347A

Wu, J.-J., Du, R.-P., Gao, M., Sui, Y.-Q., Xiu, L., and Wang, X. (2014). Naturally occurring lactic acid bacteria isolated from tomato pomace silage. *Asian Austral. J. Anim. Sci.* 27, 648–657. doi: 10.5713/ajas.2013.13670

Wu, M., Wu, Y., Zhou, J., and Pan, Y. (2009). Structural characterisation of a water-soluble polysaccharide with high branches from the leaves of *Taxus chinensis* var. mairei. *Food Chem.* 113, 1020–1024. doi: 10.1016/j.foodchem.2008.08.055

Xu, Y., Cui, Y., Wang, X., Yue, F., Shan, Y., Liu, B., et al. (2019). Purification, characterization and bioactivity of exopolysaccharides produced by *Lactobacillus plantarum* KX041. *Int. J. Biol. Macromol.* 128, 480–492. doi: 10.1016/j.ijbiomac.2019.01.117

Yan, J.-K., Li, L., Wang, Z.-M., and Wu, J.-Y. (2010). Structural elucidation of an exopolysaccharide from mycelial fermentation of a *Tolypocladium* sp. fungus isolated from wild *Cordyceps sinensis*. *Carbohydr. Polym.* 79, 125–130. doi: 10.1016/j.carbpol.2009.07.047

You, X., Yang, L., Zhao, X., Ma, K., Chen, X., Zhang, C., et al. (2020). Isolation, purification, characterization and immunostimulatory activity of an exopolysaccharide produced by *Lactobacillus pentosus* LZ-R-17 isolated from Tibetan kefir. *Int. J. Biol. Macromol.* 158, 408–419. doi: 10.1016/j.ijbiomac.2020.05.027

Yuan, Q., Zhao, L., Cha, Q., Sun, Y., Ye, H., Zeng, X. J., et al. (2015). Structural characterization and immunostimulatory activity of a homogeneous polysaccharide from *Sinonovacula constricta*. *J. Agric. Food Chem.* 36, 7986–7994. doi: 10.1021/acs.jafc.5b01086

Zannini, E., Waters, D. M., Coffey, A., and Arendt, E. K. (2016). Production, properties, and industrial food application of lactic acid bacteria-derived exopolysaccharides. *Appl. Microbiol. Biotechnol.* 100, 1121–1135. doi: 10.1007/s00253-015-7172-2

frontiers | Frontiers in Microbiology

TYPE Review
PUBLISHED 14 December 2022
DOI 10.3389/fmicb.2022.1044820

OPEN ACCESS

EDITED BY
Taotao Li,
South China Botanical Garden (CAS), China

REVIEWED BY
Gianfranco Pannella,
University of Molise, Italy
Huang Yan-yan,
Foshan University, China

*CORRESPONDENCE
Rina Wu
wrn6956@163.com
Junrui Wu
junruiwu@126.com

SPECIALTY SECTION
This article was submitted to Food Microbiology, a section of the journal Frontiers in Microbiology

RECEIVED 15 September 2022
ACCEPTED 23 November 2022
PUBLISHED 14 December 2022

CITATION
Shi H, An F, Lin H, Li M, Wu J and Wu R (2022) Advances in fermented foods revealed by multi-omics: A new direction toward precisely clarifying the roles of microorganisms. *Front. Microbiol.* 13:1044820. doi: 10.3389/fmicb.2022.1044820

Advances in fermented foods revealed by multi-omics: A new direction toward precisely clarifying the roles of microorganisms

Haisu Shi[1,2,3], Feiyu An[1], Hao Lin[1], Mo Li[1], Junrui Wu[1,2,3]* and Rina Wu[1,2,3]*

[1]College of Food Science, Shenyang Agricultural University, Shenyang, China, [2]Liaoning Engineering Research Center of Food Fermentation Technology, Shenyang Agricultural University, Shenyang, China, [3]Shenyang Key Laboratory of Microbial Fermentation Technology Innovation, Shenyang Agricultural University, Shenyang, China

Fermented foods generally comprise a complex micro-ecosystem with beneficial microbiota, functional products, and special flavors and qualities that are welcomed globally. Single-omics analysis allows for a comprehensive characterization of the main microbial factors influencing the function, flavor, and quality of fermented foods. However, the species, relative abundance, viability, growth patterns, and metabolic processes of microorganisms vary with changes in processing and environmental conditions during fermentation. Furthermore, the mechanisms underlying the complex interaction among microorganisms are still difficult to completely understand and analyze. Recently, multi-omics analysis and the integration of multiple types of omics data allowed researchers to more comprehensively explore microbial communities and understand the precise relationship between fermented foods and their functions, flavors, and qualities. Multi-omics approaches might help clarify the mechanisms underpinning the fermentation processes, metabolites, and functional components of these communities. This review clarified the recent advances in the roles of microorganisms in fermented foods based on multi-omics data. Current research achievements may allow for the precise control of the whole industrial processing technology of fermented foods, meeting consumers' expectations of healthy products.

KEYWORDS

multi-omics, fermented foods, exploration of microbial communities, health, fermentation mechanisms, flavor

Introduction

With the current increasing demand of consumers for healthy foods, fermented foods with beneficial microbiota, nutrients, and healthy functions have attracted increasing attention. The consumption of fermented foods has had a long history and has spread worldwide. Although many kinds of fermented foods exist, industrialized fermented products are limited; however, with the development of the fermentation theory, meta-omics technology, and the integration of multiple types of omics data, the mysterious world of microbes can be revealed.

The application of multi-omics in fermented foods may offer an opportunity to precisely discover the changes in the microbiota during fermentation, the interactions involved, the link between microorganisms and functional components, flavor substances, and deleterious inhibition, among other aspects. The key points of the processing control of fermented foods include the types of starter cultures, the microbial communities at each fermentation stage, and various operational conditions. The application of multi-omics replaces the single-cell omics approach for the analysis of microbial communities, allowing for a comprehensive understanding of the dynamic microbial changes in the food fermentation process. It is helpful to characterize the microbial community and species succession during different fermentation stages, evaluating the influence of the external environment on the microbial community, ultimately enhancing the fermentation conditions. Understanding the directional selection of a microbial community is helpful in finding ways to improve the function and added value of fermented foods. In addition, the multi-omics approach can allow for accurate analysis of the mechanism underlying the complex interactions among microorganisms, which is conducive to improving the quality, flavor, and safety of fermented foods and boosting bioactive metabolite levels essential for human health. Furthermore, the multi-omics approach has potential application for unraveling the relationship between the quality and safety of fermented food products as it involves cell data acquisition and the identification of specific genes and proteins of harmful microorganisms. Moreover, preferential starter cultures can be ascertained in the industrial process of fermented foods using the multi-omics approach. In summary, multi-omics will serve as a comprehensive processing technology, helping produce healthy fermented foods that meet consumers' demands.

Herein, the roles of microbial communities in fermented foods were clarified *via* multi-omics strategies. Then, the relationship between fermented foods composed of complex microorganisms and their functions, flavors, and qualities was revealed using a multi-omics approach. Furthermore, the mechanism underlying the fermentation process, metabolites, and functional components was analyzed. Finally, innovation of the industrialized production mode of fermented foods was prospected based on multi-omics insights.

The roles of microorganisms in fermented foods by multi-omics

Disadvantages of single-omics approaches

Single-omics analysis can only describe a certain biological process and cannot analyze microbial metabolic differences or the complex mechanisms underlying their interactions during fermentation. It represents a single result at the nucleic acid, protein, or metabolite levels and cannot fully represent proteomes or metabolomes under different transcriptional conditions (Kaster and Sobol, 2020). In addition, it cannot identify low-abundance microorganisms or their roles in fermented foods, even obscuring certain interactions between microbial communities (Afshari et al., 2020a). There is a lack of effective data supporting the signal transductions, interaction networks, growth regulations, inter-species interactions, and phenotypic predictions of diverse microorganisms in naturally fermented foods. For instance, important coding genes or the enrichment of pathways discovered by metagenomics do not necessarily contribute to the changes in corresponding functional molecules. At the same time, single-omics analysis, such as metagenomics, cannot distinguish between living and dead cells, thus interfering with subsequent analyses of the effects of microbial interactions on cell metabolites (Kaster and Sobol, 2020). Moreover, metagenomics based on gene sequencing has inherent limitations, including the inability to directly determine the functional activity of microorganisms and the difficulty in identifying molecules performing critical functions (Franzosa et al., 2014). Finally, single-omics analysis cannot bypass the issue of whether whole microbial communities are equivalent to the microorganisms that produce active components during fermentation. For example, transcriptomics analyzes gene expression levels, whereas proteomics aims to explore the functions and key enzymes of microorganisms at the protein level, neither of which can fully yield integrated data on the relationship between microbial communities and the effects thereof on active components (Yang et al., 2020).

Advantages of multi-omics application

Multi-omics can span the multi-layer analysis of gene and protein expression, as well as metabolite differences of all microorganisms in the environment, consequently yielding a large amount of data (**Figure 1**). It is well-known that in systems biology, multi-omics jointly "open

up" multiple levels of analysis, allowing an exploration of the development, differentiation, signal transduction, and interaction network between cells in response to environmental changes. Furthermore, multi-omics can provide effective regulatory targets for stress disturbance in response to environmental changes, including the regulation of the internal metabolic pathways of the host (Kopczynski et al., 2017). Specifically, multi-omics is applied to fermented foods research: culturology separates living bacteria from traditional fermented foods; genomics, transcriptomics, and proteomics analyze the structure, regulation, and expression of microbial functional genes in traditional fermented foods; macrogenomics and metabolomics clarify the diversity of microbial functional genes and their metabolites. Multi-omics analysis can integrate multi-level analyses and has a multiplier effect on the screening, evolutionary succession, functional gene screening, expression, and metabolic network mining of microbes in fermented foods.

Multi-omics is regarded as the mainstream way of analyzing fermented food microorganisms and has marked advantages of "$1 + 1 > 2$" in analyzing microbial succession, determining functional genes, and exploring the metabolic network of active components (**Figure 1**). However, research on microbial succession and metabolic mechanisms of fermented foods using multi-omics is still in its infancy. On the one hand, differences in the production process of traditional fermented foods, spatial heterogeneity, dynamic variability in the fermentation environment, and uneven distribution in the microbial communities lead to the evolution of microorganisms at different growth points due to the interaction of different mechanisms, resulting in a variety of phenotypes, implying the lack of representativeness of multi-omics approaches. On the other hand, the speed of the research and development on sequencing and mass spectrometry exceeds the development of analysis software or databases, resulting in a large amount of data that cannot yet be fully analyzed.

Multi-omics-based exploration of microbial communities in fermented foods

The production of fermented foods needs the coordinated action of a plethora of microbial communities. The analysis of species, metabolic pathways, and interactive relationships of these microbial communities is conducive to the directional control of microbial species in the fermentation process, therefore improving production efficiency and the flavor of fermented foods, as well as ensuring the safety thereof.

The coordination of the microbial communities of fermented foods can be achieved by multi-omics from virtually every dimension (**Figure 1**). It can provide an overall view of which microorganisms are present in a community, how they behave, interact, and what the phenotypic manifestations of this complex arena are, which is conducive to studying traditional microbiology in the fermented food industry. From 2011 to 2021 (**Supplementary Figure 1**), the number of studies published on the application of multi-omics in fermented foods increased, indicating a growing interest in multi-omics-based research on fermented foods. This is because multi-omics can help researchers systematically analyze changes in the factors that regulate the whole fermentation process. This includes the exploration of all microorganisms involved in fermentation to master and control the regularity of dynamic changes in the microbiota at each point of fermentation. Another goal is to unearth the mechanisms underlying the effects of microbial communities on the quality, flavor, and safety of fermented foods under various fermentation conditions.

Multi-omics approaches have far-reaching implications for fully exploring food microbial resources and improving the quality of fermented foods. In the past, owing to technological limitations, researchers thought that fermented foods were products of fermentation by a single or several strains. However, with the recent development of multi-omics, numerous studies have focused on food microbial communities. Accordingly, a large number of new and previously unknown microbial communities have been discovered in fermented foods (**Supplementary Table 1**). The source classification and geographical distribution of microorganisms in food fermentation in different countries are shown in **Supplementary Figure 2**. A total of 33 countries were found as source countries. There were 17 countries with more than 15 species, accounting for 52% of the total identified species. India, Korea, Nepal, China, Indonesia, Pakistan, Japan, and Bangladesh were the top eight source countries.

The exploration of microbial communities has played a fundamental role in food fermentation, in which complex microbial communities are inherently involved in the quality, as well as safety, of the product (Bokulich et al., 2016). Using metaproteomics, Xie et al. (2019a,b) found 1,415 microbial protein clusters in soybean paste; their Illumina MiSeq results showed a high diversity of microbial communities in soybean paste. Alcohol dehydrogenase produced by *Tetragenococcus* sp., and family Lactobacillaceae, genus *Leuconostoc* sp., was highly abundant in naturally fermented soybean paste. The strains of the species thereof played a key role in forming alcohol flavor components, as evidenced by a combination of metaproteomics and metabonomics (Xie et al., 2019a,b). Lee et al. (2020) revealed that metagenomic, metatranscriptomic, and metabolomic analyses provided information on the preferred carbon sources of individual microorganisms, including the various genes and intermediate metabolites involved in the kimchi fermentation using these carbon sources. Afshari et al. (2020b) reported that metagenomic and metabolome analyses revealed qualitative and semi-quantitative differences in microbiota metabolites between different types of cheese. They also found that the presence of two compounds (3-hydroxypropanoic acid and

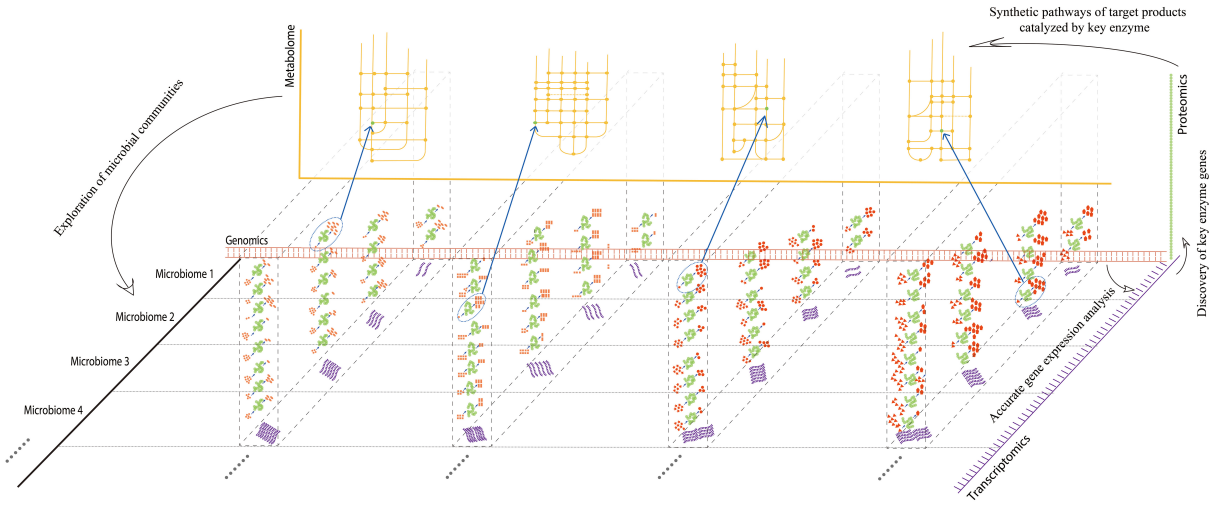

FIGURE 1
Advantages of multi-omics analysis at multi-dimensions. Red double-chain structures indicated "genomics," while purple single-chain structures indicated "transcriptomics," originating from different microorganisms split by a horizontal dotted line. In each microbiome, the transcription level of the corresponding gene may be different. Proteins or enzymes (green) translated by RNA at different transcriptional levels may have different activities, catalyzing different substrates for products (red). The bottom left corner of each enzyme indicated the substrate, and the top right-hand corner indicated the product. The numbers of substrates and products indicated different catalytic activities for each enzyme. The enzymes with the highest activities, which participated in the corresponding pathways, were circled by dotted ellipses. Synthetic pathways (yellow) of target products can be analyzed by key enzymes discovered at the metabolic level. Exploration of microbial communities can be achieved by each omic from every dimension.

O-methoxycatechol-*O*-sulfate) in artisanal cheese had not previously been reported in any type of cheese. Their integrative analysis of multi-omics datasets revealed that highly similar cheeses, identical in age and appearance, could be distinctively clustered according to the cheese type and brand (Afshari et al., 2020b). The above results reveal that multi-omics can enhance the understanding of which microbes are present in the fermentation process, as well as improve the understanding of the complex interactions among microbes and overall microbial activities.

Multi-omics insights into microbial succession at different fermentation stages

The microbial succession of fermented food plays a key role in its quality and safety. In the early stage of food fermentation, bacteria are in the growth phase, and the number of microbial species is relatively small. However, the number of microbial species greatly increases during the middle and late fermentation stages, when harmful bacteria, such as *Staphylococcus aureus*, *Listeria monocytogenes*, and *Staphylococcus equorum*, also begin to proliferate (**Supplementary Table 2**). However, there is still a lack of systematic research on the regulation of microbial succession and its mechanism in fermented food.

Multi-omics data can reveal microbial succession in different fermentation stages. Dugat-Bony et al. (2015) reported that metagenomics and macro transcriptomics could be combined to reveal the dominant microbial species in the cheese fermentation process, including the effect of their interactions on milk-based product degradation. On day one of their study, *Lactococcus delbrueckii* subsp., lactis and *Kluyveromyces lactis* were the most active species, both of which consumed lactose quickly during their early stage of maturity; the produced lactic acid was rapidly consumed by *Debaryomyces hansenii* [lactose consumption increased from day 1 (1%) to day 14 (9%)] and *Geotrichum candidum* (the dominant strain on day 7) (Dugat-Bony et al., 2015). *Corynebacterium casei* and *Hafnia alvei* were detected on day 31. In the first 2 weeks of maturation, the dominant species, *L. lactis* and *K. lactis*, were gradually replaced by *C. casei* (Dugat-Bony et al., 2015). According to Bertuzzi et al. (2018) metagenomics and metabolomics could be combined to confirm that *D. hansenii* and *G. candidum* were the dominant strains during the first mature stage of surface-ripened cheese. However, they were replaced by *Brevibacterium linens* and *Glutamicibacter arilaitensis* during a later stage (Bertuzzi et al., 2018). Ruggirello et al. (2018) using Illumina HiSeq sequencing and gas chromatography-mass spectrometry (GC-MS), found that *L delbrueckii* subsp., lactis was the most abundant microorganism during cheese production and early ripening but began to decline significantly after 30 days of ripening and was later no longer detected. He et al. (2020) found that the microbial communities of Chinese sauerkraut

were dominated by the *Serratia* and *Pseudomonas* genera during the early stages of fermentation and by the family Lactobacillaceae, genus *Lactobacillus* during the later stages. He et al. (2020) also detected a total of 86 volatile compounds in sauerkraut samples using genomics and metabonomics. Of these compounds, 13 were significantly positively correlated with lactic acid bacteria, whereas 11 were significantly negatively correlated with *Pseudomonas* sp. (He et al., 2020). These studies analyzed microbial succession using multi-omics, which can further reveal the flavor profiles, functional components, and their regulation in fermented food at each fermentation stage.

Multi-omics insights into the relationship between fermented foods composed of complex microorganisms and their function, flavor, and quality

Function

Some unique components contained in functional fermented foods are generally considered bioactive compounds produced by microorganisms, which positively improve human health and physical function. At present, single-omics analysis is mainly used to reveal the relationship between the functionality of fermented foods and their microbial communities; however, most results are unsatisfactory. Applying the principles of multi-omics can improve the identification of bioactive compounds in fermented foods, as well as their safety and reliability. Sugahara et al. (2017) analyzed the differences between live and heat-inactivated *Bifidobacterium breve* in regulating host immunity, intestinal metabolism, and intestinal gene expression using transcriptomics and metabolomics. They believed that both cells had the potential to regulate immunity, inhibit the production of pro-inflammatory cytokines in splenocytes, and affect intestinal metabolism. Nonetheless, these functions were presented more significantly in living cells than the inactivated ones (Sugahara et al., 2017). The combination of omics enables the detection of specific genes that produce specific active constituents in fermented foods, in turn improving the functions of fermented foods (Cocolin et al., 2018). Previous studies have shown that complex biozone systems cannot be accurately identified by single-omics analyses, such as genomics, which explains the changes in gene abundance and interactions between microbial colonies, but not the potential links to phenotypes (Amer and Baidoo, 2021; Ferrocino et al., 2022). Therefore, a multi-omics approach is adopted to systematically track specific genes that produce specific active constituents in fermented foods (Cocolin et al., 2018); these data are then combined with the final phenotype using transcriptomes and proteomes, further enhancing the understanding of fermented food systems. Wang et al. (2023) established a murine model of hyperuricemia to explore the effective treatment ability of *Bacillus subtilis*-fermented *Astragalus* using a multi-omics approach, which revealed that the abundance of butyrate-producing bacteria (*Odoribacter splanchnicus* and *Collinsella tanakaei*) and probiotics (*Lactobacillus enterocolitica* and *Bacillus mycoides*) increased significantly during fermentation, thereby effectively reducing kidney inflammation and regulating the expression of uric acid transporters to treat hyperuricemia. Using a multi-omics approach, it is more affordable to identify genes and gene products responsible for the functional metabolites in fermented foods, yielding highly active metabolites for human health (Lee et al., 2021).

Flavor

The formation mechanism of characteristic flavor components in fermented food can be revealed by multi-omics, and functional microorganisms are screened to guide the production process of fermented foods. *Via* the analysis of the differences in microecological diversity, genes, and metabolic levels by multi-omics, the transcription and expression of microbial genes related to the formation of characteristic flavor components can be clarified, and key biomarkers for the metabolic regulation of fermentation flavor components are characterized. Wu et al. (2022) analyzed the regulatory relationship between differential genes and secondary metabolite biosynthesis in fermented soybean by transcriptomics, proteomics, and metabolomics. They found a total of 130 upregulated metabolites and 160 downregulated proteins related to fermented soybean flavor (Wu et al., 2022). Multi-omics can greatly promote the understanding of microbial evolution, physiology, and metabolic pathways in fermented foods, as well as predict the formation of expected and undesired flavors according to conditions of flavor formation, which are affected by each strain. Multi-omics can also explain the influence of microorganisms on the flavor of fermented foods *via* the catalysis of enzyme–substrates and their interaction at the species level. Karaduman et al. (2017) and Lu et al. (2018) used proteomics and metabolomics as powerful methods for real-time *in situ* detection and quantitative analysis of colony metabolites. By doing so, they could detect and guide the real-time changes of microorganisms and metabolites in fermented dairy products (Karaduman et al., 2017; Lu et al., 2018). Hu et al. (2021) clarified the relationship between fungal communities and non-volatile flavor compounds during solid-state batch fermentation of green tea using genomics and metabolomics. The dominant fungal strain in green tea fermentation was *Aspergillus*, which can produce abundant hydrolases that hydrolyze cellulose, pectin, and protein in

the tea cell wall, forming soluble carbohydrates, amino acids, soluble pectins, and other compounds conducive to the taste and organoleptic properties of green tea (Hu et al., 2021). Applying a combination of genomics and metabolomics, Unno et al. (2021) found that lactic acid was positively distributed and accounted for 41% of the total variance on surface-ripened mold cheeses and smear cheese. Notably, 47.7% of ketones and alcohols were produced by specific bacteria (*Pseudoalteromonas* sp. and *Marinomonas* sp.) (Unno et al., 2021).

Quality

There are individual metabolic differences and complex interactions in microbial communities in fermented food, which cannot ensure the stable quality and food safety of final fermented products (Montel et al., 2014). Multi-omics can systematically and deeply analyze the beneficial, pathogenic, and spoilage-related strains during fermentation. Fermented foods are less likely to be spoiled under fermentation conditions, mainly due to the correct control of the reproduction of pathogens by factors such as fresh food materials, fermentation time, and pH. Song et al. (2020) divided kimchi into two groups: one cultured using a starter culture of kimchi, sauerkraut, and garlic was successfully fermented; the other cultured using a starter culture of ginger and red pepper could not support fermentation, revealing that different starter sources significantly differ in terms of dominant microbes and their metabolites. Thus, the microbial communities determined the final quality of fermented food (Song et al., 2020). Medina et al. (2016) indicated that the quality of natural green olive was better during the early and middle stages of fermentation, but spoilage microorganisms such as *Pseudomonas*, *Propionibacterium*, *Modestobacter*, *Rhodovibrio*, and *Salinibacter* appeared during a later fermentation stage. Wu et al. (2019) combined proteomics and transcriptomics, revealing that the decrease of milk pH (pH 5.5) during fermentation inhibited the expression of glutamate differential proteins by 0.43-fold. In contrast, it upregulated the expression of two key proteins (locus: T303-05420 and T303-05425) involved in cysteine catabolism by 4.25- and 7.26-fold, respectively, thus affecting the milk quality (Wu et al., 2019).

Multi-omics insights into the mechanism underlying the fermentation process, metabolites, and functional components

Traditionally, in fermented foods, the main contribution of bacteria is to produce flavor compounds; yeast produces alcohol and low levels of flavor compounds, and mold decomposes macromolecules. Although this understanding is reasonable, it should also be noted that this understanding is based on the physiological and metabolic characteristics of some single-cultured microorganisms. There is a serious lack of understanding of the functions of non-isolated cultured microorganisms. More importantly, there is a lack of a systematic analysis of the mechanism underlying microbial interaction in complex fermentation systems and its effect on fermentation processes, metabolites, and functional components.

Multi-omics can be used as the main way of analyzing the correlation between microbial communities, gene metabolites, and the interaction mechanism in fermented foods, and characterize the regulation mechanism underlying microbial communities of fermented foods during fermentation as well as the metabolites and functional components thereof at multiple levels (Sattin et al., 2016). Multi-omics is bound to become the main research field of fermented foods to build a predictive model of microbial communities by monitoring the dynamic changes of microorganisms, their differential gene expressions, and their metabolite compositions in real-time. Zhang et al. (2020) revealed the functional microorganisms during the first stage of Pixian soybean paste fermentation by amplicon sequencing and proteomics. They found three strains secreting peptidase and producing amino acids, which can induce polypeptide degradation in hypertonic fermentation (Zhang et al., 2020). Hu et al. (2021) used genomics and metabolomics to explore the effect of fungal succession on the content of various non-volatile flavor compounds in fermented dry green tea. The alkaloid level decreased by 37.50%, and the catechin level decreased from 7969.98 ± 346.36 to 233.98 ± 20.29 μg/g (Hu et al., 2021). Settachaimongkon et al. (2016) used headspace solid phase microextraction (SPME)-GC/MS and metabonomics to reveal the significant effect of sublethal precultured *Lactiplantibacillus plantarum* WCFS1 on the metabolite spectrum of yogurt. The addition of precultured *L. plantarum* impaired the survival of *Lactobacillus delbrueckii* (Settachaimongkon et al., 2016). Piddocke et al. (2011) clarified the effect that the addition of multicomponent protease had on the metabolism of brewer's yeast *via* transcriptomic and metabolomic analysis. In addition, environmental factors are considered in the multi-omics analysis to predict the physiological characteristics and microbial succession in a specific environment so that it can more objectively reveal the interactions of microbial communities in fermented foods. Stellato et al. (2015) believed that there were differences in metabolic pathways between environmental samples from surfaces and tools, and the different types of cheese samples produced by the same factory. The persistence of microorganisms in the environment may resist the development of potentially harmful species that

may contaminate cheese and adversely impact product quality (Stellato et al., 2015).

Multi-omics has gradually gained popularity in the field of the fermentation mechanisms of various fermented foods. However, many hindrances appear at present. The primary problem for the mechanisms underlying the fermentation process, metabolites, and functional components to characterize microbial communities of fermented foods includes how to analyze and explore a large amount of multi-omics data and how to effectively use the results thereof to objectively form the fermentation system. Secondly, multi-omics are comprehensively used to analyze the assembly mechanism of microbial communities in fermented foods and reveal the influencing factors of community assembly and its effect on later fermentation. In addition, the establishment of supporting databases and multivariate statistical analysis models also need to be timely followed up on for a large amount of obtained multi-omics data. Finally, traditional isolation and culture of microbes is the most intuitive way to verify the prediction of microecological communities by multi-omics data, which is necessary for the annotation of new genes, as well as the functional characterization and physiological identification of species. The results of multi-omics combined with traditional isolation and culture are currently still missing a link in systems biology (Jansson and Baker, 2016).

Innovation of industrialized production mode of fermented food *via* multi-omics

The Multi-omics Database of Microbes in Fermented Foods (MDMFF) should be further developed for application in the fermented foods industry (Lee et al., 2020). Microbial resources are the core to updating the industrial production mode of future fermented foods. The establishment of fermented food culture collection can protect and preserve beneficial strains, effectively avoiding their extinction and inheriting the valuable microbial resources known for thousands of years in the traditional fermentation of foods. Furthermore, MDMFF can offer quality genomes, metataxonomes, metagenomes, metatranscriptome sequences, metaproteomes, and associated metabolome information of fermented food-associated bacteria, archaea, and eukaryotic microorganisms. Furthermore, the database will include several analytical tools for multi-omics analyses by an input query in the database. Lee et al. (2020) recently developed an Omics Database of Fermentative Microbes, integrating comprehensive omics information from fermentative microorganisms at the World Institute of Kimchi. It provides basic information to evaluate microbial strains isolated from fermented foods as candidate starter cultures in terms of the fermentation processes, qualities, flavors, and sensory properties. Moreover, multi-omics can couple the interactions between microorganisms in fermented foods with their quality and safety, helping promote healthy production management at the industrial level (Ferrocino et al., 2022). Siren et al. (2019) used genomics, proteomics, and metabolomics to explore the interactions between microbial communities and the factory environment during wine fermentation by *Saccharomyces cerevisiae* and *Oenococcus oeni*. Suitable probiotics were also used to promote the formation of specific aromas, which was conducive to the production of industrial wine (Siren et al., 2019).

Fermented food production should be standardized to predict and control the fermentation process using these multi-omics data. Multi-omics can be used to accurately select the cultures required for the formation of qualities, flavors, and sensor properties of fermented foods. By connecting genomic characteristics with phenotypic output and exploring the metabolic diversity of starter cultures, the impact of a single strain on the qualities, flavors, sensor properties, and metabolic pathways of fermented food can be understood to customize the starter mixture to meet the needs of specific fermented foods in the industry. Multi-omics can also be used to optimize the control of fermented foods under different processing and storage conditions to accurately determine the detailed parameters of various processes in each fermentation stage and ensure the optimal quality, flavor, aroma, nutrition, and safety of fermented foods. Janssen et al. (2020) and Franciosa et al. (2021) conducted multi-omics analyses of fermented sausages, revealing the role of microbial communities in the production chain during fermentation. These studies identified specific metabolic pathways during sausage fermentation and provided a basis for the growth of local microbiomes, thereby improving and controlling the industrial fermentation process and enhancing product quality. Alessandria et al. (2016) used genomics and proteomics to explore the microbial communities of Italian hard cheese, analyze the mechanism underlying the antagonism and coexistence between starter lactic acid bacteria and microbial colonies, and explain the taste, aroma, and texture of that cheese, so as to promote safe production in the cheese industry. These processes are particularly helpful for developing high-quality starter cultures and new products with higher qualities, improved sensor properties, unique flavors, and specific functions for the future fermented food market.

Conclusion

The roles of microorganisms profoundly affect the quality, flavor, and safety of fermented foods. More microbial communities can be investigated using multi-omics, rather than single-omics, to reveal new findings between fermented foods composed of complex microorganisms and their functions,

flavors, and qualities. Analyzing the mechanism underlying the fermentation process, metabolites, and functional components using multi-omics provides in-depth technical support for the industrialized production mode of fermented food.

Author contributions

HS: conceptualization and roles/writing – original draft. FA: investigation, data curation, and resources. HL: software and formal analysis. ML: validation. JW: project administration. RW: supervision, writing – review and editing, and funding acquisition. All authors contributed to the article and approved the submitted version.

Funding

This work was supported by the National Natural Science Foundation of China (Nos. 31801567, 31972047, and 31871831) and Shenyang Science and Technology Innovation Platform Project (21-103-0-14 and 21-104-0-28).

Conflict of interest

The authors declare that the research was conducted in the absence of any commercial or financial relationships that could be construed as a potential conflict of interest.

Publisher's note

All claims expressed in this article are solely those of the authors and do not necessarily represent those of their affiliated organizations, or those of the publisher, the editors and the reviewers. Any product that may be evaluated in this article, or claim that may be made by its manufacturer, is not guaranteed or endorsed by the publisher.

Supplementary material

The Supplementary Material for this article can be found online at: https://www.frontiersin.org/articles/10.3389/fmicb.2022.1044820/full#supplementary-material

References

Afshari, R., Pillidge, C. J., Dias, D. A., Osborn, A. M., and Gill, H. (2020a). Cheesomics: the future pathway to understanding cheese flavour and quality. *Crit. Rev. Food Sci. Nutr.* 60, 33–47. doi: 10.1080/10408398.2018.1512471

Afshari, R., Pillidge, C. J., Read, E., Rochfort, S., Dias, D. A., Osborn, A. M., et al. (2020b). New insights into cheddar cheese microbiota-metabolome relationships revealed by integrative analysis of multi-omics data. *Sci. Rep.* 10:3164. doi: 10.1038/s41598-020-59617-9

Alessandria, V., Ferrocino, I., De Filippis, F., Fontana, M., Rantsiou, K., Ercolini, D., et al. (2016). Microbiota of an italian grana-like cheese during manufacture and ripening, unraveled by 16S rRNA-based approaches. *Appl. Environ. Microbiol.* 82, 3988–3995. doi: 10.1128/AEM.00999-16

Amer, B., and Baidoo, E. E. K. (2021). Omics-driven biotechnology for industrial applications. *Front. Bioeng. Biotechnol.* 9:613307. doi: 10.3389/fbioe.2021.613307

Bertuzzi, A. S., Walsh, A. M., Sheehan, J. J., Cotter, P. D., Crispie, F., McSweeney, P. L. H., et al. (2018). Omics-based insights into flavor development and microbial succession within surface-ripened cheese. *mSystems* 3:e00211-17. doi: 10.1128/mSystems.00211-17

Bokulich, N. A., Lewis, Z. T., Boundy-Mills, K., and Mills, D. A. (2016). A new perspective on microbial landscapes within food production. *Curr. Opin. Biotechnol.* 37, 182–189. doi: 10.1016/j.copbio.2015.12.008

Cocolin, L., Mataragas, M., Bourdichon, F., Doulgeraki, A., Pilet, M. F., Jagadeesan, B., et al. (2018). Next generation microbiological risk assessment meta-omics: the next need for integration. *Int. J. Food Microbiol.* 287, 10–17. doi: 10.1016/j.ijfoodmicro.2017.11.008

Dugat-Bony, E., Straub, C., Teissandier, A., Onesime, D., Loux, V., Monnet, C., et al. (2015). Overview of a surface-ripened cheese community functioning by meta-omics analyses. *PLoS One* 10:e0124360. doi: 10.1371/journal.pone.0124360

Ferrocino, I., Rantsiou, K., and Cocolin, L. (2022). Microbiome and -omics application in food industry. *Int. J. Food Microbiol.* 377:109781.

Franciosa, I., Ferrocino, I., Giordano, M., Mounier, J., Rantsiou, K., and Cocolin, L. (2021). Specific metagenomic asset drives the spontaneous fermentation of Italian sausages. *Food Res. Int.* 144:110379. doi: 10.1016/j.foodres.2021.110379

Franzosa, E. A., Morgan, X. C., Segata, N., Waldron, L., Reyes, J., Earl, A. M., et al. (2014). Relating the metatranscriptome and metagenome of the human gut. *Proc. Natl. Acad. Sci. U.S.A.* 111, E2329–E2338. doi: 10.1073/pnas.1319284111

He, Z., Chen, H., Wang, X., Lin, X., Ji, C., Li, S., et al. (2020). Effects of different temperatures on bacterial diversity and volatile flavor compounds during the fermentation of suancai, a traditional fermented vegetable food from northeastern China. *LWT* 118:108773.

Hu, S., He, C., Li, Y., Yu, Z., Chen, Y., Wang, Y., et al. (2021). Changes of fungal community and non-volatile metabolites during pile-fermentation of dark green tea. *Food Res. Int.* 147:110472. doi: 10.1016/j.foodres.2021.110472

Janssen, D., Dworschak, L., Ludwig, C., Ehrmann, M. A., and Vogel, R. F. (2020). Interspecies assertiveness of *Lactobacillus curvatus* and *Lactobacillus sakei* in sausage fermentations. *Int. J. Food Microbiol.* 331:108689.

Jansson, J. K., and Baker, E. S. (2016). A multi-omic future for microbiome studies. *Nat. Microbiol.* 1:16049. doi: 10.1038/nmicrobiol.2016.49

Karaduman, A., Ozaslan, M. O., Kilic, I. H., Bayil-Oguzkan, S., Kurt, B. S., and Erdogan, N. (2017). Identification by using MALDI-TOF mass spectrometry of lactic acid bacteria isolated from non-commercial yogurts in southern Anatolia, Turkey. *Int. Microbiol.* 20, 25–30. doi: 10.2436/20.1501.01.282

Kaster, A. K., and Sobol, M. S. (2020). Microbial single-cell omics: the crux of the matter. *Appl. Microbiol. Biotechnol.* 104, 8209–8220. doi: 10.1007/s00253-020-10844-0

Kopczynski, D., Coman, C., Zahedi, R. P., Lorenz, K., Sickmann, A., and Ahrends, R. (2017). Multi-OMICS: a critical technical perspective on integrative lipidomics approaches. *Biochim. Biophys. Acta Mol. Cell Biol. Lipids* 1862, 808–811. doi: 10.1016/j.bbalip.2017.02.003

Lee, S. H., Whon, T. W., Roh, S. W., and Che, O. J. (2020). Unraveling microbial fermentation features in kimchi: from classical to meta-omics approaches. *Appl. Microbiol. Biotechnol.* 104, 7731–7744.

Lee, S. J., Jeon, H. S., Yoo, J. Y., and Kim, J. H. (2021). Some important metabolites produced by lactic acid bacteria originated from kimchi. *Foods* 10:2148. doi: 10.3390/foods10092148

Lu, Y., Ishikawa, H., Kwon, Y., Hu, F., Miyakawa, T., and Tanokura, M. (2018). Real-time monitoring of chemical changes in three kinds of fermented milk products during fermentation using quantitative difference nuclear magnetic resonance spectroscopy. *J. Agric. Food Chem.* 66, 1479–1487. doi: 10.1021/acs.jafc.7b05279

Medina, E., Ruiz-Bellido, M. A., Romero-Gil, V., Rodríguez-Gómez, F., Montes-Borrego, M., Landa, B. B., et al. (2016). Assessment of the bacterial community in directly brined Alorea de Málaga table olive fermentations by metagenetic analysis. *Int. J. Food Microbiol.* 236, 47–55.

Montel, M.-C., Buchin, S., Mallet, A., Delbes-Paus, C., Vuitton, D. A., Desmasures, N., et al. (2014). Traditional cheeses: rich and diverse microbiota with associated benefits. *Int. J. Food Microbiol.* 177, 136–154. doi: 10.1016/j.ijfoodmicro.2014.02.019

Piddocke, M. P., Fazio, A., Vongsangnak, W., Wong, M. L., Heldt-Hansen, H. P., Workman, C., et al. (2011). Revealing the beneficial effect of protease supplementation to high gravity beer fermentations using "-omics" techniques. *Microb. Cell Fact.* 10:27. doi: 10.1186/1475-2859-10-27

Ruggirello, M., Giordano, M., Bertolino, M., Ferrocino, I., Cocolin, L., and Dolci, P. (2018). Study of Lactococcus lactis during advanced ripening stages of model cheeses characterized by GC-MS. *Food Microbiol.* 74, 132–142. doi: 10.1016/j.fm.2018.03.012

Sattin, E., Andreani, N. A., Carraro, L., Lucchini, R., Fasolato, L., Telatin, A., et al. (2016). A multi-omics approach to evaluate the quality of milk whey used in ricotta cheese production. *Front. Microbiol.* 7:1272. doi: 10.3389/fmicb.2016.01272

Settachaimongkon, S., van Valenberg, H. J. F., Gazi, I., Nout, M. J. R., van Hooijdonk, T. C. M., Zwietering, M. H., et al. (2016). Influence of Lactobacillus plantarum WCFS1 on post-acidification, metabolite formation and survival of starter bacteria in set-yoghurt. *Food Microbiol.* 59, 14–22. doi: 10.1016/j.fm.2016.04.008

Siren, K., Mak, S. S. T., Fischer, U., Hansen, L. H., and Gilbert, M. T. P. (2019). Multi-omics and potential applications in wine production. *Curr. Opin. Biotechnol.* 56, 172–178. doi: 10.1016/j.copbio.2018.11.014

Song, H. S., Whon, T. W., Kim, J., Lee, S. H., Kim, J. Y., Kim, Y. B., et al. (2020). Microbial niches in raw ingredients determine microbial community assembly during kimchi fermentation. *Food Chem.* 318:126481. doi: 10.1016/j.foodchem.2020.126481

Stellato, G., De Filippis, F., La Storia, A., and Ercolini, D. (2015). Coexistence of lactic acid bacteria and potential spoilage microbiota in a dairy processing environment. *Appl. Environ. Microbiol.* 81, 7893–7904. doi: 10.1128/aem.02294-15

Sugahara, H., Yao, R., Odamaki, T., and Xiao, J. Z. (2017). Differences between live and heat-killed bifidobacteria in the regulation of immune function and the intestinal environment. *Benef. Microb.* 8, 463–472. doi: 10.3920/bm2016.0158

Unno, R., Suzuki, T., Matsutani, M., and Ishikawa, M. (2021). Evaluation of the relationships between microbiota and metabolites in soft-type ripened cheese using an integrated omics approach. *Front. Microbiol.* 12:681185. doi: 10.3389/fmicb.2021.681185

Wang, R., Lin, F., Ye, C., Aihemaitijiang, S., Halimulati, M., Huang, X., et al. (2023). Multi-omics analysis reveals therapeutic effects of Bacillus subtilis-fermented *Astragalus membranaceus* in hyperuricemia via modulation of gut microbiota. *Food Chem.* 399:133993. doi: 10.1016/j.foodchem.2022.133993

Wu, Q., Chu, H., Padmanabhan, A., and Shah, N. P. (2019). Functional genomic analyses of exopolysaccharide-producing *Streptococcus thermophilus* ASCC 1275 in response to milk fermentation conditions. *Front. Microbiol.* 10:1975. doi: 10.3389/fmicb.2019.01975

Wu, Y., Tao, Y., Jin, J., Tong, S., Li, S., and Zhang, L. (2022). Multi-omics analyses of the mechanism for the formation of soy sauce-like and soybean flavor in *Bacillus subtilis* BJ3-2. *BMC Microbiol.* 22:142. doi: 10.1186/s12866-022-02555-5

Xie, M., An, F., Yue, X., Liu, Y., Shi, H., Yang, M., et al. (2019a). Characterization and comparison of metaproteomes in traditional and commercial dajiang, a fermented soybean paste in northeast China. *Food Chem.* 301:125270. doi: 10.1016/j.foodchem.2019.125270

Xie, M., Wu, J., An, F., Yue, X., Tao, D., Wu, R., et al. (2019b). An integrated metagenomic/metaproteomic investigation of microbiota in dajiang-meju, a traditional fermented soybean product in Northeast China. *Food Res. Int.* 115, 414–424. doi: 10.1016/j.foodres.2018.10.076

Yang, L., Fan, W., and Xu, Y. (2020). Metaproteomics insights into traditional fermented foods and beverages. *Compr. Rev. Food Sci. Food Saf.* 19, 2506–2529. doi: 10.1111/1541-4337.12601

Zhang, L., Bao, Y., Chen, H., Huang, J., and Xu, Y. (2020). Functional microbiota for polypeptide degradation during hypertonic moromi-fermentation of pixian broad bean paste. *Foods* 9:930. doi: 10.3390/foods9070930

Frontiers in Microbiology

Explores the habitable world and the potential of microbial life

The largest and most cited microbiology journal which advances our understanding of the role microbes play in addressing global challenges such as healthcare, food security, and climate change.

Discover the latest Research Topics

See more →

Frontiers

Avenue du Tribunal-Fédéral 34
1005 Lausanne, Switzerland
frontiersin.org

Contact us

+41 (0)21 510 17 00
frontiersin.org/about/contact